The chiral cyclobutane motif in foldamers, peptidic organogelators and host-guest chemistry

Sergi Celis Rodríguez

2013

PhD Thesis

Programa de Doctorat en Química
Departament de Química, Facultat de Ciències
Universitat Autònoma de Barcelona

Supervised by Prof. Rosa M. Ortuño Mingarro and Dr. Ona Illa Soler

This PhD Thesis is presented for graduation as Doctor by **Sergi Celis Rodríguez**

Read and approved,

Prof. Rosa M. Ortuño Mingarro **Dr. Ona Illa Soler**

Cerdanyola del Vallès, 27th May 2013

ACKNOWLEDGEMENTS

The present PhD Thesis has been carried out in the Chemistry Department at the *Universitat Autònoma de Barcelona* (UAB) under the direction of Professor Rosa Maria Ortuño and Doctor Ona Illa. I really would like to thank Rosa the chance she gave me to work in her group and participate in several projects that resulted in this thesis, as well as the financial support in the neediest moments. I want to thank both of them for the support, confidence placed in me and the excellent supervision they have done within this work.

Thank the *Universitat Autònoma de Barcelona* for the financial support through a grant for Research Training Staff (PIF), without which the realization of this thesis would have not been possible.

I want to thank Professor Vicenç Branchadell for his collaboration in the projects contributing with interesting computational studies. Don't forget about the huge help received from Dr. Pau Nolis from the *SeRMN* at UAB on carrying out structural studies as well as the valuable training in the equipment manipulation. I would also like to mention Dr. Judith Oró, from the *Instituto de Ciencia de Materiales de Barcelona* (ICMAB), for her help in SEM analysis and Dr. Michael Haynes, from the National University of Ireland, for his assistance in the use of the WinEQNMR2 program.

Special mention for all the lab mates who helped me with everything and the really nice moments we all had together, inside and out of the laboratory, making it all more than a professional project.

I get thrilled mentioning my friends Edu, Mitzzi, EduDlrg, Fabián, Paul, Arhamis, Sara, Jean-Marc, Víctor, Alicia, Cristóbal...for their true support and the VBM in my life.

Finally, I can not finish my acknowledgments without giving very special thanks to my parents and family for their motivation and incessant support in all.

Thank you all very much!

A mis padres,

Part of the results reported in this PhD Thesis has been published in the following scientific articles:

- **Low-molecular-weight gelators consisting of hybrid cyclobutane-based peptides.**

Celis, S.; Nolis, P.; Illa, O.; Branchadell, V.; Ortuño, R. M.

Org. Biomol. Chem. **2013**, *11*, 2839-2846.

- **Secondary Structure of Short β-Peptides as the Chiral Expression of Monomeric Building Units: A Rational and Predictive Model.**

Gorrea, E.; Pohl, G.; Nolis, P.; Celis, S.; Burusco, K. K.; Branchadell, V.; Perczel, A.; Ortuño, R. M. *J. Org. Chem.* **2012**, *77*, 9795-9806.

- **Designing hybrid foldamers: the effect on the peptide conformational bias of β- versus α- and γ-linear residues in alternation with (1R,2S)-2-aminocyclobutane-1-carboxylic acid.**

Celis, S.; Gorrea, E.; Nolis, P.; Illa, O.; Ortuno, R. M.

Org. Biomol. Chem. **2012**, *10*, 861-868.

ABBREVIATIONS

ACBC: 2-Amino-1-cyclobutanecarboxylic acid

ACHC: 2-Amino-1-cyclohexanecarboxylic acid

ACPC: 2-Amino-1-cyclopentanecarboxylic acid

ADP: Adenosine diphosphate

AFM: Atomic force microscopy

Aib: 2-Aminoisobutyric acid

Ala: Alanine

AMP: Adenosine monophosphate

ATP: Adenosine triphosphate

ATR: Attenuated total reflectance

AUDA: 11-Aminoundecanoic acid

B3LYP: Becke, three-parameter, Lee-Yang-Parr

Bn: Benzyl

Boc: *tert*-Butyl carbamate

BOP: Benzotriazol-1-yloxy)tris(dimethylamino)phosphonium hexafluorophosphate

BPLED: Bipolar longitudinal eddy current delay

CBP: Cyclobutane-containing peptides

Cbu: Cyclobutane

Cbz: Benzyl carbamate

CCP: Cell-penetrating peptides

CD: Circular dichroism

CF: 5(6)-Carboxyfluoresceine

CIS: Complexation-induced shift

COSY: Correlation spectroscopy

CPA: Carboxypeptidase A

CPB: Carboxypeptidase B

CS-AFM: Current-sensing atomic force microscopy

DBU: 1,8-Diazabicyclo[5.4.0]undec-7-ene

DFT: Density functional theory

DIPEA: *N*,*N*-Diisopropylethylamine

DMF: *N*,*N*-Dimethylformamide

DMSO: Dimethylsulfoxide

DNA: Deoxyribonucleic acid

DPPA: Diphenylphosphoryl azide

EDAC: 1-Ethyl-3-(3-dimethylaminopropyl)carbodiimide

ee: enantiomeric excess

ESI: Electrospray ionization

FDPP: Pentafluorophenyl diphenylphosphinate

GABA: Gamma-aminobutyric acid

GAGA: Gly-Ala-Gly-Ala

GB/SA: Generalized born/surface area

GC: Gas chromatography

Gly: Glycine

HATU: *O*-(7-Azabenzotriazol-1-yl)-*N*,*N*,*N*′,*N*′-tetramethyluronium hexafluorophosphate

HBTU: *O*-BenzoTriazole-*N*,*N*,*N*′,*N*′-tetramethyluronium hexafluorophosphate

HMBC: Heteronuclear multiple-bond correlation

HMPA: Hexamethylphosphoramide

HOBt: *N*-Hydroxybenzotriazole

HOMO: Highest occupied molecular orbital

HOPG: Highly oriented pyrolytic graphite

HPLC: High-performance liquid chromatography

HRMS: High Resolution Mass Spectroscopy

HSQC: Heteronuclear single quantum correlation

IR: Infrared

LMOG: Low molecular-mass organic gelator

LMWG: Low molecular weight gelator

LRMS: Low resolution mass spectroscopy

MCP: Metallocarboxypeptidases

mgc: Minimum gelation concentration

MMFF: Merck molecular force field

MO: Molecular orbital

MTT: 3-(4,5-Dimethylthiazol-2-yl)-2,5-diphenyltetrazolium bromide

NMR: Nuclear magnetic resonance

NOE: Nuclear Overhauser effect

NOESY: Nuclear Overhauser enhancement spectroscopy

NTA : Nitrilotriacetic acid

NTP: Nitrilotripropionic acid

PEG: Polyethylene glycol

Phe: Phenylalanine

PLE: Pig liver esterase

ppm: Parts per million

PyBOP: Benzotriazol-1-yl-oxytripyrrolidinophosphonium hexafluorophosphate

QM: Quantum mechanics

ROE: Rotating-frame nuclear Overhauser effect

ROESY: rotating-frame nuclear Overhauser effect correlation spectroscopy

SAFIN: self-assembled fibrillar networks

SEM: Scanning electron microscopy

SMD: Single molecule dilution

SP: Surface potential

SPFM: Scanning polarization force microscopy

TBA: Tetrabutyl ammonium

TEM: Transmission electron microscopy

TFA: Trifluoroacetic acid

THF: Tetrahydrofurane

TOCSY: Total correlated spectroscopy

tren: 2, 2’,2’’-tris-(2-Aminoethyl)amine

TTF: Tetrathiafulvalene

UV: Ultraviolet

Val: Valine

WAXD: Wide-angle X-ray diffraction

NUMBERING AND STRUCTURAL DESCRIPTION

1. The numbering of the molecules is established according to their order of appearance.

- Amines from a unique compound, in both free (-NH_2) or salt forms (-NH_2·HCl, -NH_2·TFA), are considered the same product and therefore a unique number for the molecule is designated.

2. The numbering of atoms in the molecules is established according to the following criteria:

- Linear or cyclic amino acids and linear, cyclic or mixed peptides and pseudotripeptides (-NHMe *C*-terminated derivatives) are numbered from the *N*-terminus to the *C*-terminus following the longest hydrocarbonated chain.
- For all compounds, from dipeptides to hexapeptides and pseudopeptides, with deprotected amine as free form or as salt form, the orthogonally protected peptide numbering is kept. For the amino acids, deprotected amine compounds are renumbered starting from the *N*-terminus.
- Cyclobutene pseudopeptides are numbered from one *C*-terminus to the other *C*-terminus arbitrarily (from top to bottom side).
- Other molecules are numbered according to SI nomenclature.

3. Structural description of ^{1}H and ^{13}C NMR spectra for amino acids, peptides and pseudopeptides is assigned with the corresponding number given to the molecules. For SI-named compounds, assignation of signals is done by functional or characteristic *R* groups, highlighting with *italic* the specific parts of these groups when confusion is possible.

NOMENCLATURE

In order to facilitate the writing of this work, an own nomenclature for the amino acids and related peptides has been adopted. Only when more than one enantiomer of a compound has been used, the absolute configuration has been indicated.

Compounds that are not amino acids, peptides or pseudopeptides are named as stated by SI nomenclature or traditional nomenclature.

All amino acids, peptides and pseudopeptides are named using the following abbreviations for each amino acid:

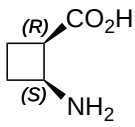

(S,R)-βCbu

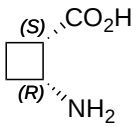

(R,S)-βCbu

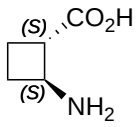

(S,S)-βCbu

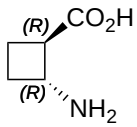

(R,R)-βCbu

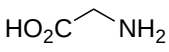

Gly

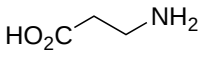

βAla

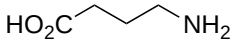

GABA

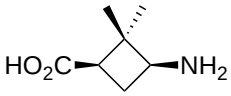

γCbu

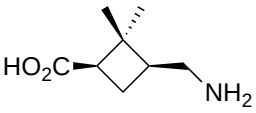

δCbu

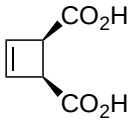

βdehydroCbu

‣ Absolute configuration of amino acids and peptides is only given for the 1,2-cyclobutane derivatives, from the *N*-terminus to the *C*-terminus. In the case of cyclobutene pseudopeptides absolute configuration of amino acids is kept although molecules have no *N*-terminus to start with. For the polycyclobutane pseudotripeptides it is given as their precursor dipeptides.

‣ Indeed, no numbering is used for the absolute configuration because numbering is different and specified in each compound.

‣ Protecting *N*- and *C*-terminus groups are expressed before and after the amino acid abbreviation, respectively. Some illustrative examples:

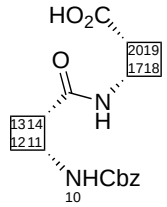

N-Cbz-*(R,S)*-βCbu-*(S,R)*-βCbu

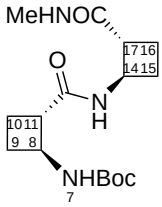

N-Boc-*(S,S)*-βCbu-*(R,R)*-βCbu-NHMe

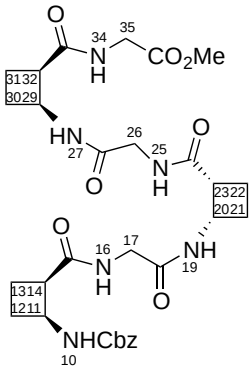

N-Cbz-[*(S,R)*-βCbu-Gly]$_3$-OMe

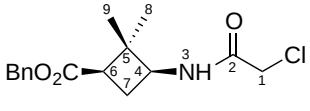

ClCH$_2$CO-γCbu-OBn

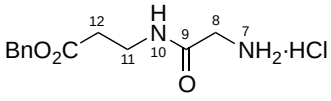

HCl·[Gly]$_2$-OBn

TABLE OF CONTENTS

GENERAL INTRODUCTION

During the past years the number of publications concerning peptides and related molecules has increased exponentially. Their interest has raised due to the importance of secondary and tertiary structures in the functions of proteins, what has enhanced their study through the use of peptidomimetics or peptoids for instance. Thus, description of the interactions in the arrangements in both molecular and supramolecular levels has been crucial for the understanding of many biological processes. Ultimately, the rationalization between the amino acid sequences and the resulting properties would provide key instructions for the design and synthesis of compounds exhibiting specific functionalities. In the current PhD Thesis, structure and recognition are the two main fields in which the prepared compounds find applications.

• By means of natural and non-natural amino acids, stereodivergent synthesis has been used to prepare chiral cyclobutane intermediates. Through diverse strategies and coupling methodologies, such scaffolds have been used to synthesize several families of α-, β- or γ-peptides and pseudopeptides. Some of them contain intercalated linear fragments, what has resulted in hybrid peptidomimetics with different conformational freedom degrees. On the other hand, amino acid-based tripodal amides around a nitrilotriacetic acid (NTA) core have been synthesized as anion hosts.

• The conformational analysis in solution and the supramolecular study of gel aggregates and host-guest complexes by the use of spectroscopic, microscopic and computational techniques is also exposed. The inherent rigidity of the cyclobutane moiety together with the flexibility of linear residues, demonstrates their determinant structural effect, providing molecules with a wide range of properties, from good low molecular weight organogelators to selective receptors towards fluoride anion.

CHAPTER I

Precedents in the Research Group

1.1. INTRODUCTION

The importance of proteins and their complex structures for life has prompted their interest in chemistry, among other sciences, which in our research group has been focused in the study of amino acids, peptides and related compounds. Diversity of proteins structures has been extensively catalogued, establishing that the polypeptide backbone can be induced to adopt a very large range of compact folded conformations. In natural proteins, the structural diversity is provided by 20 chemically different α-amino acids along the length of the polypeptide chains. Local folding patterns are determined by backbone conformational preferences of individual residues, which depend principally on short-range interactions which involve intermolecular forces, from the discrete Van der Waals to the crucial and whimsical hydrogen bonds. Many proteins effectively consist of short pieces of regular secondary structures like helices and β-strands, connected by irregular segments generally denoted as loops. The association of extended strands by interstrand hydrogen-bonding results in the formation of sheets. Herein, the structural basis to construct proteins, closely related to life, were stated to the world about 50 years ago, when the crystal structure of myoglobin was determined.[1]

Since then, a new vision to the field of biomimetic structures has been introduced, by Seebach *et al.*, through the recognition that the variety of polypeptide foldings can be greatly achieved by the creation of structures that incorporate backbone homologated amino acids, synthetically accessible from the proteinogenic amino acids.[2-5] A step forward was taken by Gellman *et al.*, whose studies of model peptides containing covalently constrained β-amino acids led to the realization that new classes of folded polyamide structures, the foldamers, could be generated in sequences containing backbone expanded amino acids.[6,7]

With the aim of being a part of the global contribution to the establishment of the rules that govern the foldamers, the study of cyclobutane containing amino acids, peptides and related compounds has been carried out in our research group. These compounds, used as basic scaffolds for the construction of the representative oligomers, are presented as β- and γ-amino acids mainly, although α- and δ-moieties are synthesized or incorporated sometimes. The synthetic part of β-amino acids is going to be explained in the next chapter while the structural, in solution and in the solid state, and the supramolecular studies are highlighted in the present one. Reference to the synthetic strategies of other compounds will be simply described, emphasizing the structural properties too.

1.1.1. Structural study in solution and the solid state of β-cyclobutane containing amino acids, peptides, ureas and thioureas

The structural study in solution is commonly covered by high-resolution NMR experiments and computational calculations. Moreover, correlation between them is a useful and decisive tool to reach reliable conclusions. Other techniques such as Circular Dichroism and IR spectroscopy can help in the elucidation of a determined structure. In the solid state the analysis of the structure is made by X-ray crystallography.

In 1998, the first enantioselective synthesis of the (1*R*,2*S*)-2-aminocyclobutane-1-carboxylic acid was reported by our group.[8] Notwithstanding, sole amino acids do not provide representative folding patterns, so the synthesis of longer oligomers was necessary and easily achieved by the combination of the same compound through peptide synthesis. From this approach, a series of polycyclobutane β-peptides was afforded, which ranged from di- to octapeptides, where all the residues had the same absolute configuration. The structural study revealed a clear preference for a β-strand type secondary structure, with an intra-residue 6-membered hydrogen-bonding pattern, attributable to all the members of the series (Figure **1**).[9]

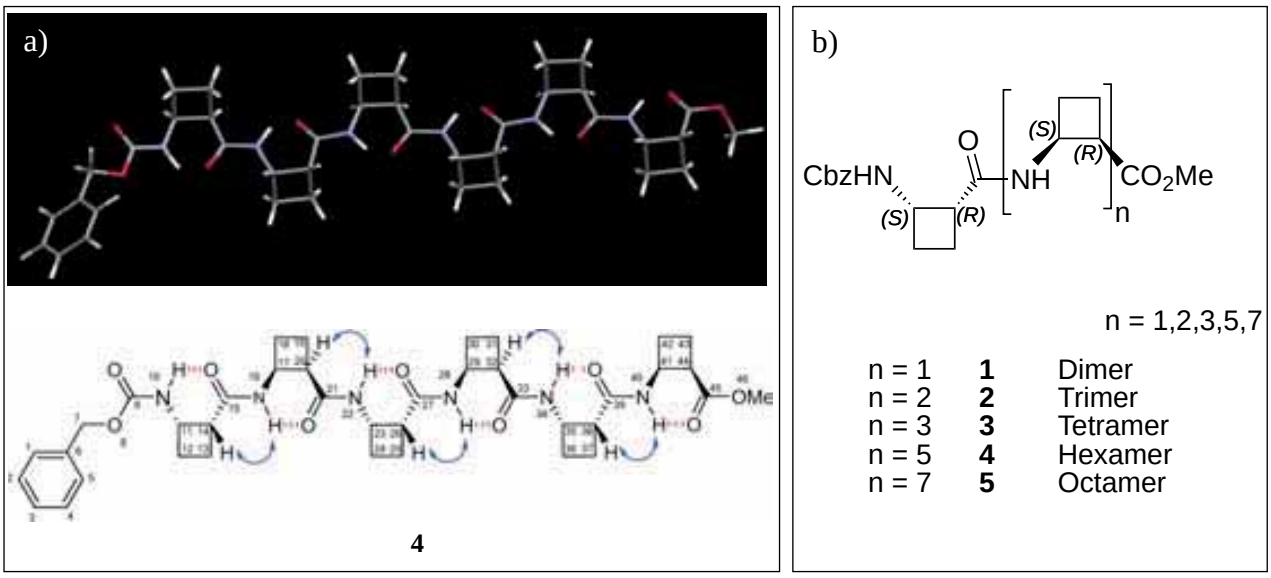

Figure **1**. a) Strand-type conformation for hexamer, as representative example, in MD calculation (*top*) and in $CDCl_3$ solution (NMR results, *bottom*). Blue arrows show inter-residue $H\alpha_i$ and NH_{i+1} NOE contacts while red-dashed lines the hydrogen bonds. b) Skeletal formula for the homochiral polycyclobutane β-peptides series.

CD spectra were recorded in MeOH solutions for some of the oligomers, exhibiting the same preferential conformation. Comparison of tetramers with both benzyl and *tert*-butyl carbamate protections at *N*-terminus showed no significant changes on the CD spectra for 0.5 mM solutions in methanol. Alternatively, comparison within the same NHCbz series resulted in an increasing intensity from dimer to octamer, according to the increasing number of chromophores, although the

band for the octamer and tetramer were similar in this aspect. On the other side, if normalized (per residue) CD spectra are compared, very close intensities are observed for all the peptides except for the octamer, what is explained because of its greater flexibility than shorter oligomers (Figure **2**).

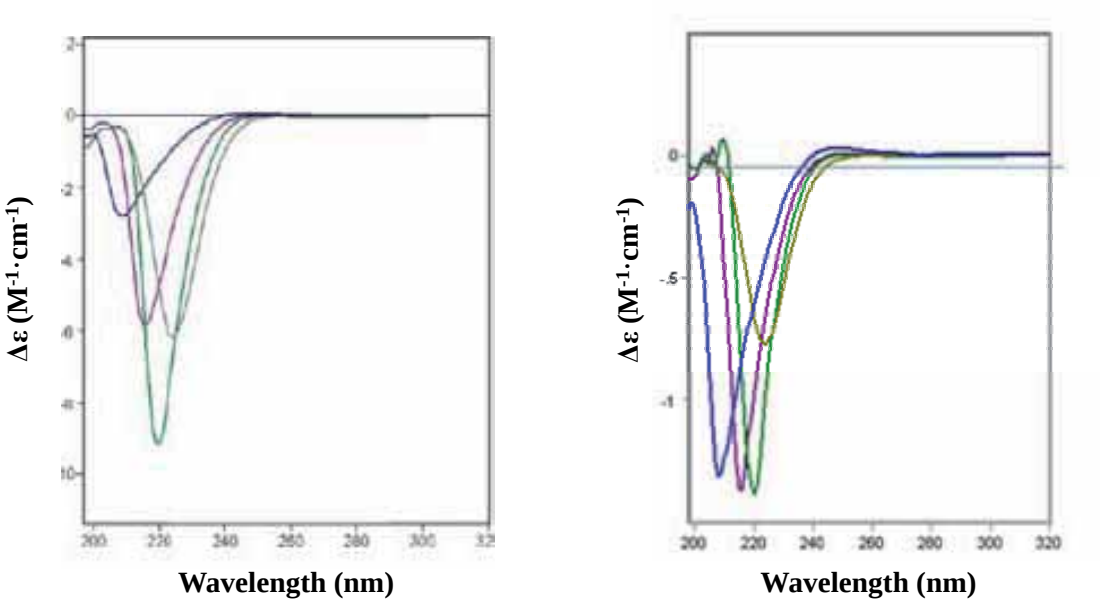

Figure **2**. CD spectra (*left*) and normalized CD spectra (molar ellipticity is normalized per residue)(*right*) of 0.5 mM methanol solutions of **(***S*,*R*,*S*,*R*)-**1** (blue), (*S*,*R*,*S*,*R*,*S*,*R*,*S*,*R*)-**3** (violet), **4** (green) and **5** (grey-light green).

The next customary step, keeping the same backbone, was to introduce the same cyclobutane β-amino acid but with other absolute configurations, in order to find out the structural changes due to the different chirality. Preliminary studies led to the comparison of three new dipeptides with the previously synthesized (*S*,*R*,*S*,*R*)-**6** (Figure **3**).[10]

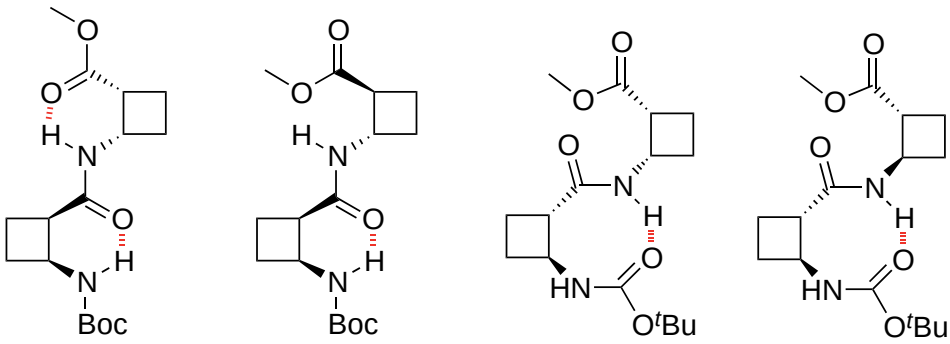

Figure **3**. Preferred conformation for the three β-dipeptides compared to the all *cis* one (*S*,*R*,*S*,*R*)-**6**.

These conformations were determined by 1D selective NOE NMR experiments and DFT optimization calculations at the B3LYP/6d31G(d) level of theory. The conclusion was that

dipeptides in which the *N*-terminus presented *cis* relative configuration, adopted conformations involving 6-membered hydrogen bonds, while when the relative configuration on the *N*-terminus residue was *trans* they preferred 8-membered hydrogen bonds.

Some years before the X-ray diffraction structure of several bis-cyclobutane dipeptides was solved. For (*S*,*R*,*S*,*R*)-**6** dipeptide it was concluded that inter-residual hydrogen bonds were also present in the solid state. Three-dimensional packing of the molecules to become the crystal is organized by infinite chains of molecules linked by hydrogen bonds involving amide groups (Figure **4**).[9a]

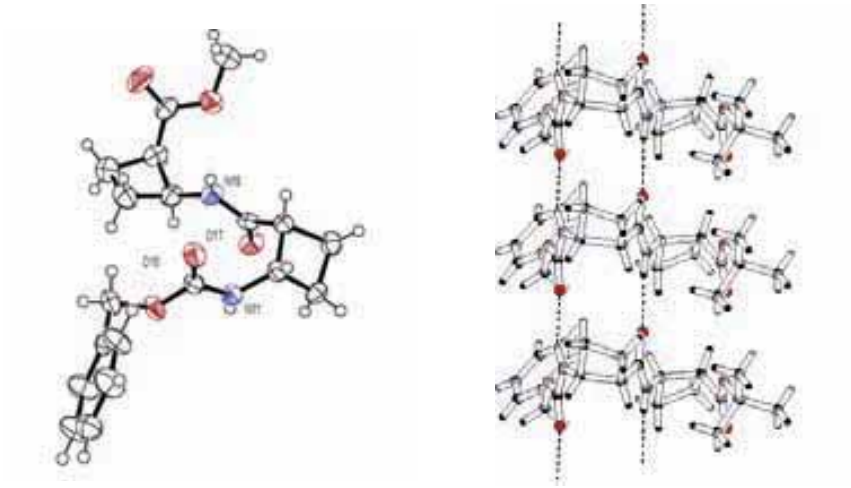

Figure **4**. Dipeptide (*S*,*R*,*S*,*R*)-**6**: Molecular structure as obtained from X-ray diffraction analysis (*left*) and intermolecular hydrogen bonds forming infinite chains in the crystal structure (*right*). Red spheres: O atoms, blue spheres: N atoms.

Therefore, the question of 'how would the chirality of single monomers affect the whole structure' came to our minds. Since then, subsequent studies concerning β-oligomers containing cyclobutane amino acids with alternated chirality were carried out, and constitute the chapter 2 in the present thesis.

At that point, the strong influence of the conformationally constrained cyclobutane ring was obvious and critical for the achievement of foldamers with fixed secondary structures, in the same way as the chirality of the cyclobutane moiety, as shown in the preliminary results. Then, to broaden ours horizons, it was decided to study the combination of cyclobutane β-amino acids of a unique chirality (the easiest and readiest synthetically accessible) with linear unbranched amino acids. From this work, the β,β-hybrid tetrapeptide **7** was obtained, which presented two β-alanine moieties alternating between two cyclobutane residues. The structural analysis in solution, assessed by NMR experiments and theoretical calculations too, concluded that this backbone change, which increased the flexibility, allowed the molecule to adopt a 14-helix conformation in $CDCl_3$, a completely different structure from the strand-type one (Figure **5**).[11]

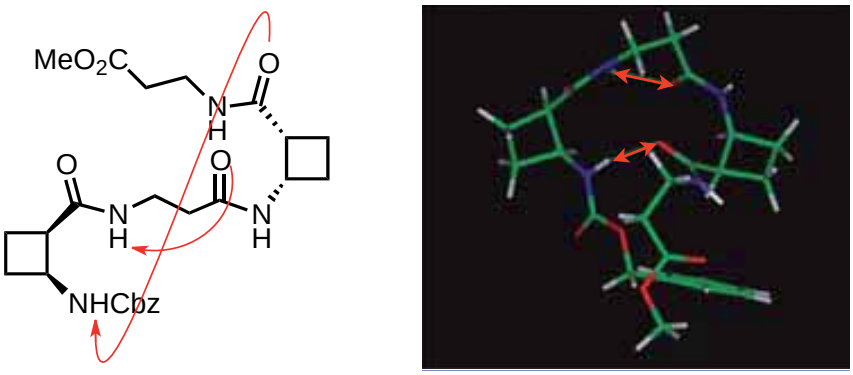

Figure **5**. Skeletal structure (*left*) and computational structure optimized at the B3LYP/6-31G(d) level of theory (*right*) of compound **7**, showing 14-helical conformation. Red arrows represent the hydrogen bonds.

This shocking result opened the door to a new series of foldamers, consisting of the alternation of β-cyclobutane residues with linear amino acids. Besides the β-alanine, glycine and GABA amino acids were used to obtain a homologated series of α,β-, β,β- and β,γ-hybrid peptides, what constitutes the chapter 3 of the current thesis.

Ureas and thioureas are related cyclobutane containing compounds which can derive from β-amino acids. The ones synthesized in the group contain two cyclobutane rings and they are achieved by an enantioselective strategy, starting from the recurring common chiral precursor (*S*,*R*)-**8** (Scheme **1**).

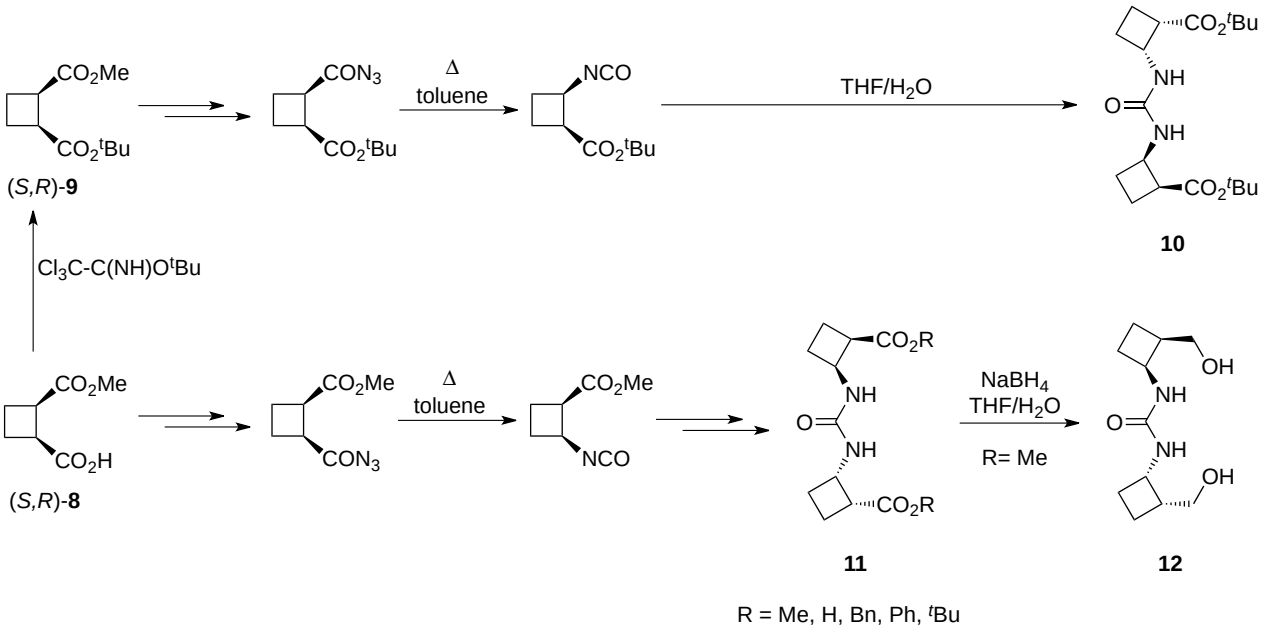

Scheme **1**. Synthesis of bis-cyclobutane ureas *via* an enantioselective strategy.

Structural studies of such ureas were carried out by X-ray crystallography, since some of them formed crystals easily in common solvents. The X-ray analysis showed that the R substituent was critical for the adoption of the tertiary structure (Figure **6**).

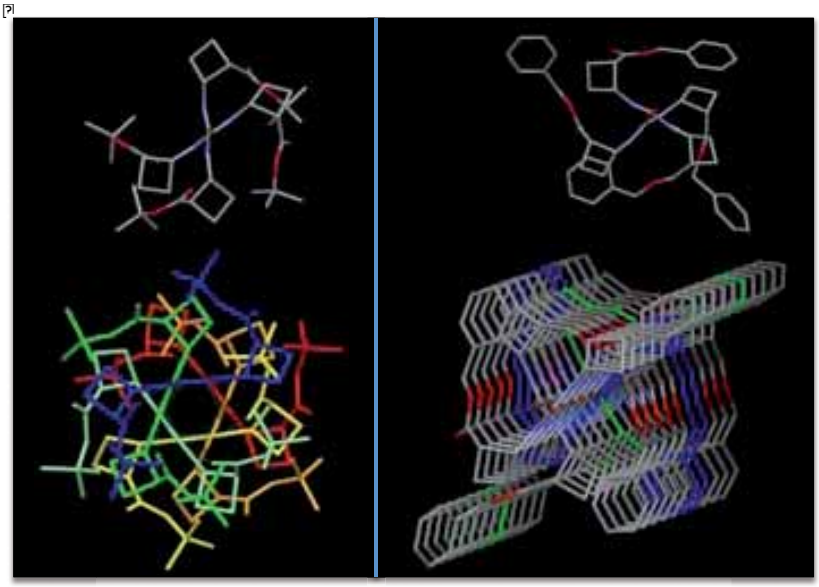

Figure **6**. Crystal packing of urea **10** (*left*) and urea **11** (R=Bn) (*right*).

Other ureas were obtained by serendipity when cyclobutane β-peptides were being synthesized. Nevertheless, later on, a stereoselective and efficient synthetic route was developed to afford chiral *cis*-fused *N*-monoprotected bicyclic ureas (*S,R*)-**13**, (*S,R*)-**14** and (*R,S*)-**14**. Proper chemical transformations, on both functional groups of the chiral precursor (*S,R*)-**11**, were necessary to direct the syntheses to three key stereoisomers, which underwent an intramolecular Curtius rearrangement, in the presence of diphenylphosphoryl azide (DPPA) and Et_3N, giving the corresponding ureas in one-pot reactions in 70-80% yield (Scheme **2**).[12]

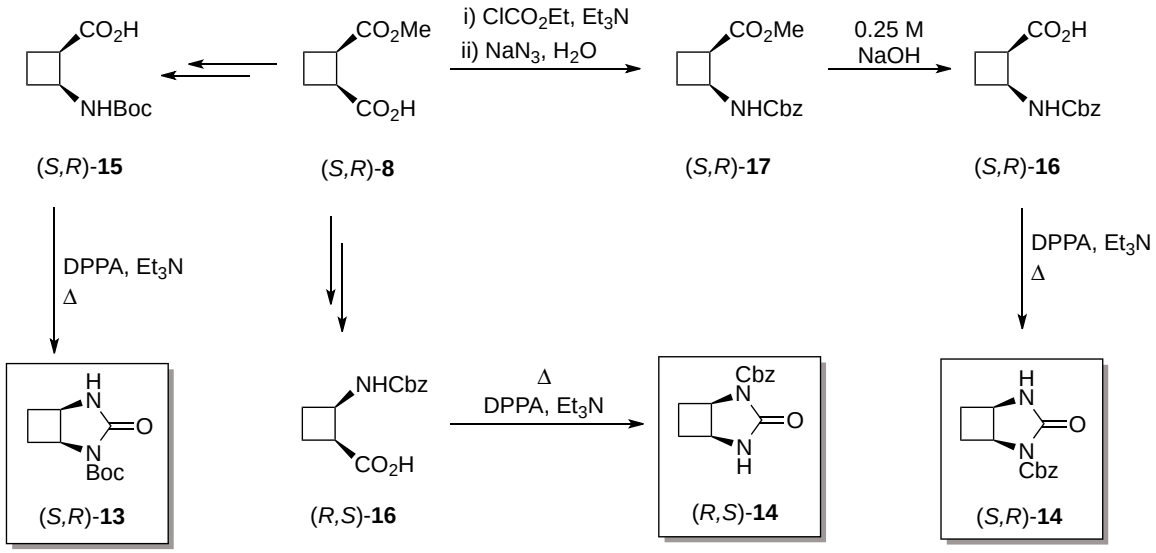

Scheme **2**. Synthesis of chiral *cis*-fused *N*-monoprotected cyclobutane bicyclic ureas *via* a stereoselective strategy.

Both structural studies in solution and in the solid state revealed a great tendency of these ureas to form ordered aggregates. NMR, IR and TEM techniques showed that ureas interacted through hydrogen bonds to form fibrillar assemblies in solution, while X-ray analysis presented two urea molecules interacting *via* only one hydrogen bond, which yielded infinite chains (Figure **7**). Moreover, the coplanarity of both carbamate and urea groups led the crystal packing to a parallel molecular arrangement. Theoretical calculations supported this last result, reproducing well the geometry and predicting favourable energies for the formation of tetramers and higher aggregates.

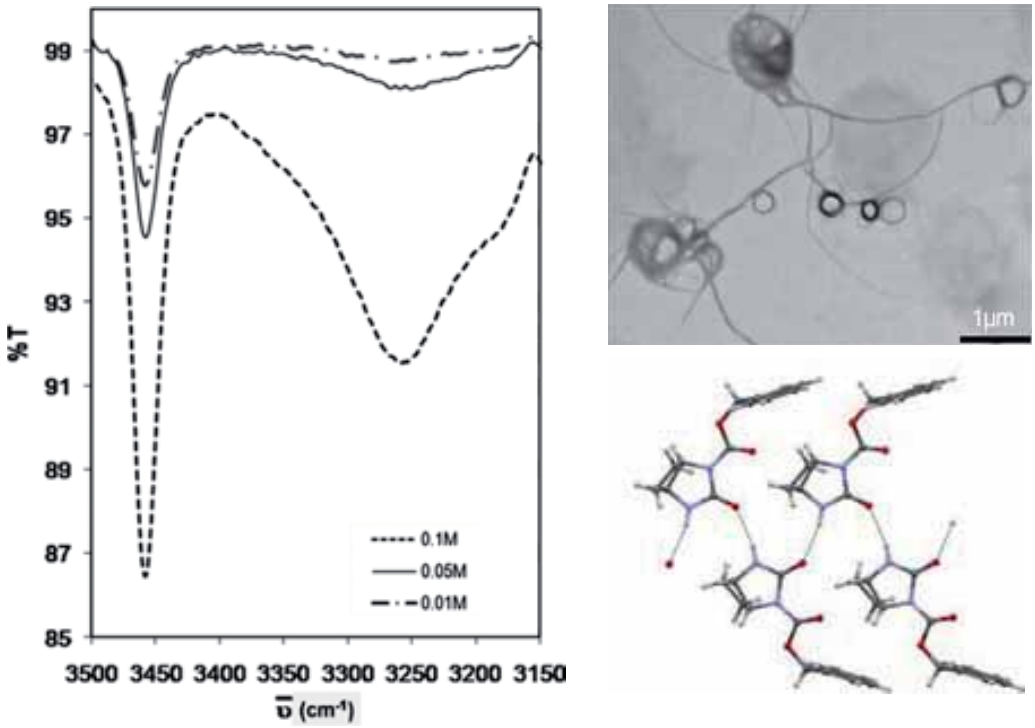

Figure **7**. Urea (*R,S*)-**14**: IR spectra at the NH stretching region in $CDCl_3$ (*left*); TEM image of fibres formed from 5 mM solutions in MeOH (*right-top*); view of infinite chains parallel to the crystallographic *a* axis (*right-bottom*). Dashed lines represent hydrogen bonds**.**

Cyclobutane-containing thioureas, alternatively, have been reported as organocatalysts. Starting from the same hemiester (*S,R*)-**8**, *cis*- and *trans*-cyclobutane containing 1,3-diamines and 1,3-amino alcohols were synthesized in a stereocontrolled manner. Afterwards, efficient functionalization *via* Curtius rearrangement afforded the desired thioureas (Scheme **3**).[13]

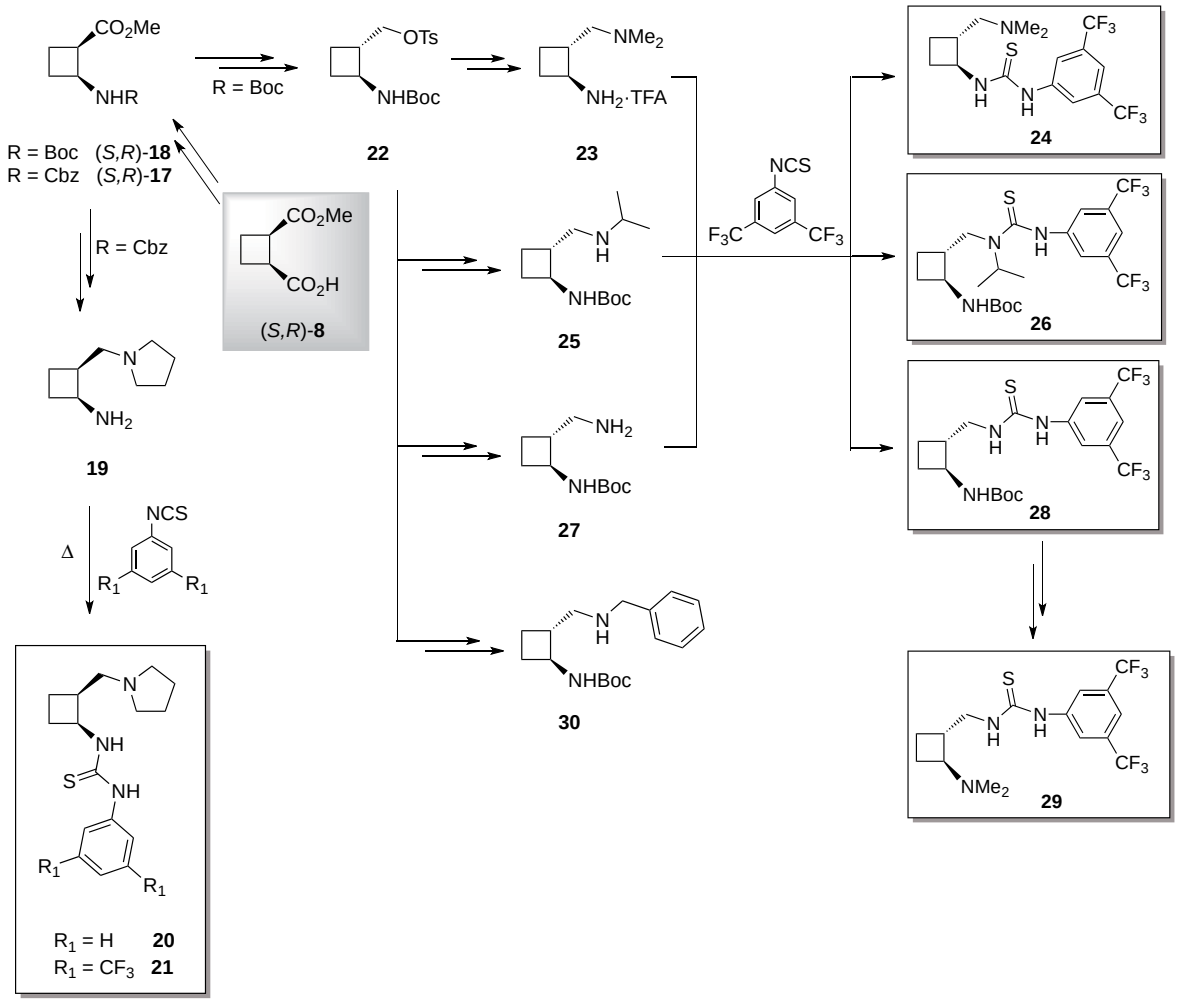

Scheme **3**. Diastereodivergent synthesis of chiral *vic*-disubstituted-cyclobutane scaffolds: 1,3-diamines and 1,3-amino alcohols. Further functionalization into thioureas.

In order to better understand how the stereochemical features of **21** influenced its mode of catalyze, its conformation in the solid state was studied through X-ray diffraction analysis of single crystals. The structure showed the *E*-conformation for the thiourea NH protons and, the intramolecular hydrogen bonding between the pyrrolidine nitrogen atom and the neighbouring (C=S)NH (Figure **8**).

Figure **8**. Structure of **21** as obtained from X-ray diffraction analysis. Red-dashed line represents the hydrogen bond.

1.1.2. Supramolecular study on β-cyclobutane containing oligomers

In many cases, the directing capacity of the cyclobutane-containing scaffolds to give defined and ordered secondary structures is transmitted to the supramolecular level. The foldamers self-assemble into higher structures to result in aggregates or materials with defined morphology, size and other physico-chemical properties. The techniques employed for the description of such properties often cover many types of microscopies (TEM, SEM, AFM...) besides the usual spectroscopic techniques (NMR, IR, CD...) and theoretical calculations, which prove their usefulness in elucidating the self-assembly interactions or processes, for instance. Physically, the supramolecular chemistry of our β-oligomers has been translated into materials as gels and aggregates as fibres or vesicles. Their behaviour is really dependent on the solvents and the concentrations used.

For the homochiral series of polycyclobutane β-peptides, from dimer to octamer, their ability to form nano-sized fibres in more or less regular and ordered patterns was demonstrated, as observed *via* TEM (Figure **9**). Critical concentration dependence was showed by the octapeptide, which formed homogeneous vesicles at 0.5 mM concentration after 1 day of incubation, and they remained unaltered for 2 weeks at room temperature. However, when the concentration of the sample was 1 mM, such vesicles self-organized into fibres after 1 week of incubation. Hence, the concentration influenced the morphology of the aggregates as much as the length of the peptide.[9b,c]

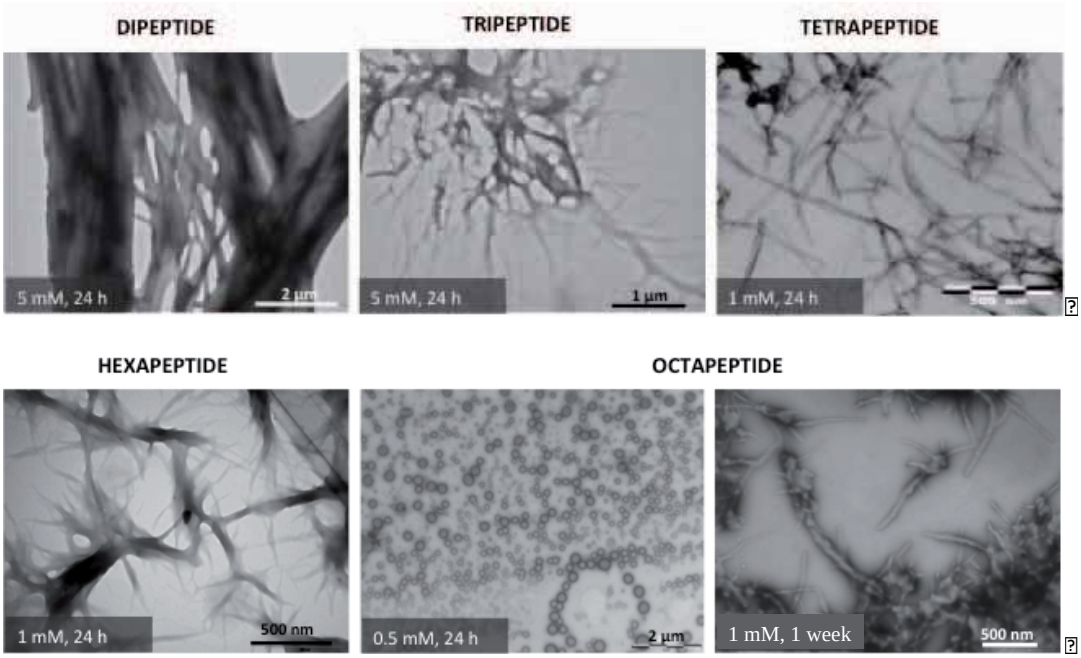

Figure **9**. TEM images of β-peptide samples, recorded from solutions at different concentration and after 1 day or 1 week of incubation.

AFM allowed to determine the height of the aggregates (monolayers that after long periods of time piled themselves into multilayer structures) formed by the tetrapeptide **3**, when depositing it onto a mica surface (Figure **10**). The heights measured ranged from 6.4 to 8.8 (±0.2) nm, in agreement with the results suggested by theoretical calculations of the dipole moment. At the B3LYP/6-31G(d) level of calculation, the dipole moment showed to be 11.1 D, with the positive pole on the *C*-terminus, proposing the arrangement depicted in Figure **10c**.[9b] Scanning Polarization Force Microscopy (SPFM) was used to determine the local charge distribution of the nano-sized fibres. It was concluded that the surface potential (SP) of the fibrils increased with the size of the self-assemblies (Figure **10b**).

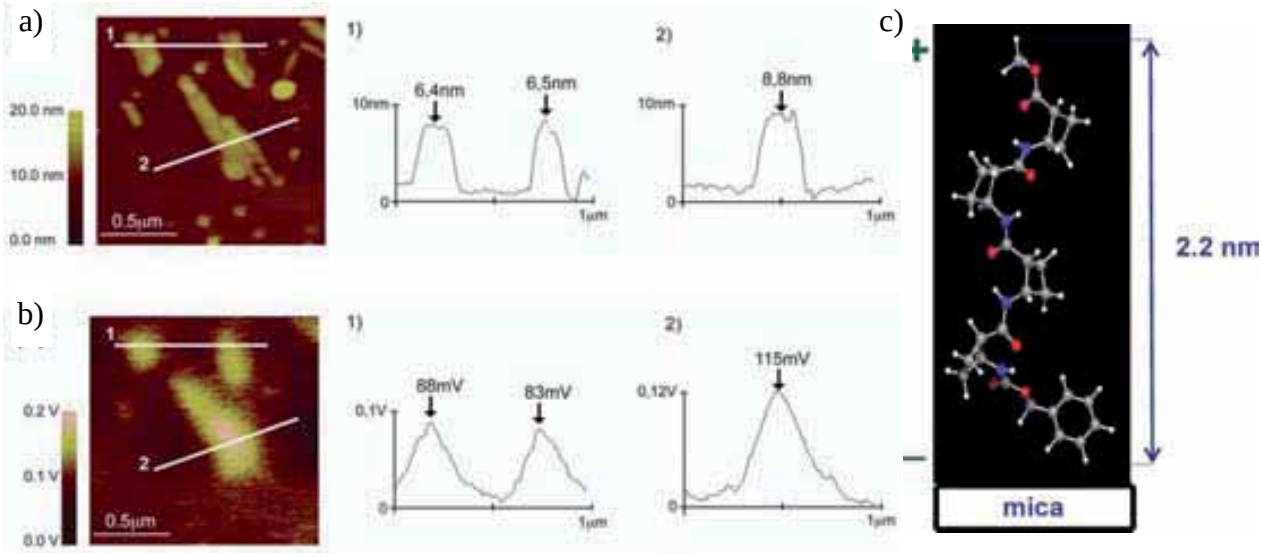

Figure **10**. Tetrapeptide **3**: a) Topographic image of molecules deposited onto a freshly cleaved mica substrate. Heights range from 6.4-8.8 nm. b) Surface potential image at the same conditions. SP measurements range from 83-115 mV. c) Modelled vertical arrangement of molecules in the assemblies.

Moreover, both *N*-Boc and *N*-Cbz protections of tetrapeptide **3** formed organogels when dissolved in 1:3 CH_2Cl_2/pentane (5.8 mM) and 3:2 EtOAc/hexane (1 mM), respectively. These organogels remain unaltered for several days at room temperature (Figure **11**).

Figure **11**. Gel formed from a 1:3 dichloromethane/pentane 5.8 mM solution of the *N*-Boc protected tetrapeptide **3**.

Molecular modelling, together with all the rest of techniques, allowed the assignation of a preferred model for the arrangement of the molecules in a parallel manner, showing conformations in agreement with the ones in solution (Figure **12**). Both hydrogen bonding and hydrophobic interactions are the driving forces responsible of the aggregation.[9c]

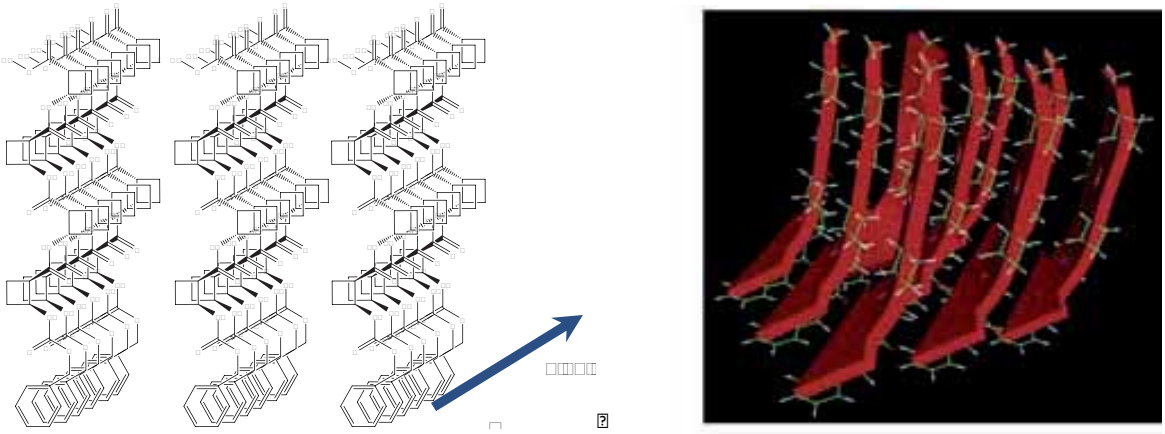

Figure **12**. Two representations of the proposed model for the assembly of tetramer **3**, based on TEM, AFM, SPFM and theoretical studies. Parallel arrangement is more favourable than the alternate disposition.

In solution, the structural effect due to the introduction of *trans*-residues in β-dipeptides was demonstrated. Using the same techniques, such as NMR, TEM, AFM, IR, CD and computational calculations along with others like SEM and X-ray powder diffraction, (*S*,*S*,*S*,*R*)-**6** (*trans*,*cis*) and (*S*,*S*,*S*,*S*)-**6** (*trans*,*trans*) dipeptides were investigated, exhibiting some key differences with respect to the all-*cis*-polycyclobutane β-oligomers. Both dipeptides formed gels in toluene, so this solvent was employed to perform the main experiments (Figure **13**).[14]

Figure **13**. Gels from 40 mM solutions of dipeptides (*S*,*S*,*S*,*S*)-**6** (*left*) (1) and (*S*,*S*,*S*,*R*)-**6** (*right*) in toluene.

TEM and SEM images showed well-defined fibrillar aggregates for both samples, besides the evident differences of the resulting images concerning each technique and their different preparation procedures. TEM images presented more dispersed fibrils, while images of the surface of xerogels obtained by SEM consisted in intertwined fibres and bundles of variable width. In addition, AFM images afforded the heights of aggregates, which could also pile themselves (Figure **14**).

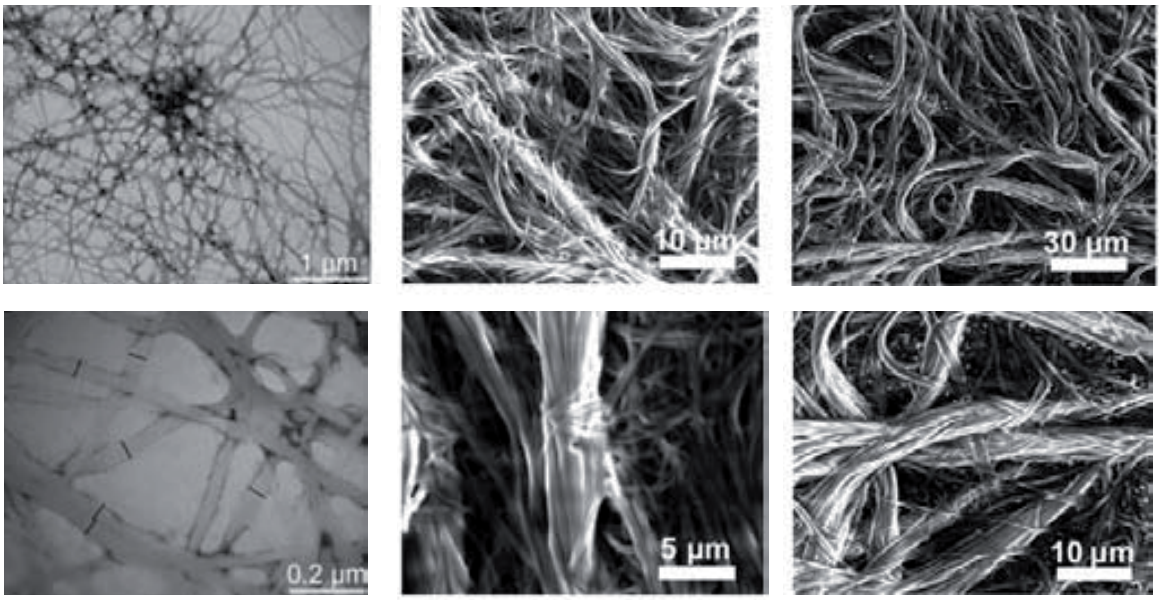

Figure **14**. TEM images of the fibrils formed from 5 mM solution of (*S*,*S*,*S*,*S*)-**6** in MeOH after 1 day of incubation (*left*). SEM images of (*S*,*S*,*S*,*S*)-**6** (*centre*) and (*S*,*S*,*S*,*R*)-**6** (*right*)as xerogels (from toluene) on graphite at 60 Pa.

NMR experiments on 40 mM solutions of (*S*,*S*,*S*,*R*)-**6** and (*S*,*S*,*S*,*S*)-**6** in toluene-d_8 determined their temperature of gelation at three different concentrations. Gelation processes were monitored by variable-temperature ^{1}H-NMR experiments; the representation of normalized integrals *vs.* temperature showed a hydrogen-bond fixing and a sample gelation subprocesses, which converged at the gelation temperatures (T_{gel}) (Figure **15**). Furthermore, some different behaviour could be detected between the *trans*,*cis*- and the *trans*,*trans*-dipeptides, because some NH shielding during the gelation process and some NOE patterns at low temperature differed significantly from one another.

Compound	T_{gel} [K]		
	at 7.5 mM	at 15 mM	at 40 mM
(*S*,*S*,*S*,*S*)-**6**	266	273	295
(*S*,*S*,*S*,*R*)-**6**	260	269	284

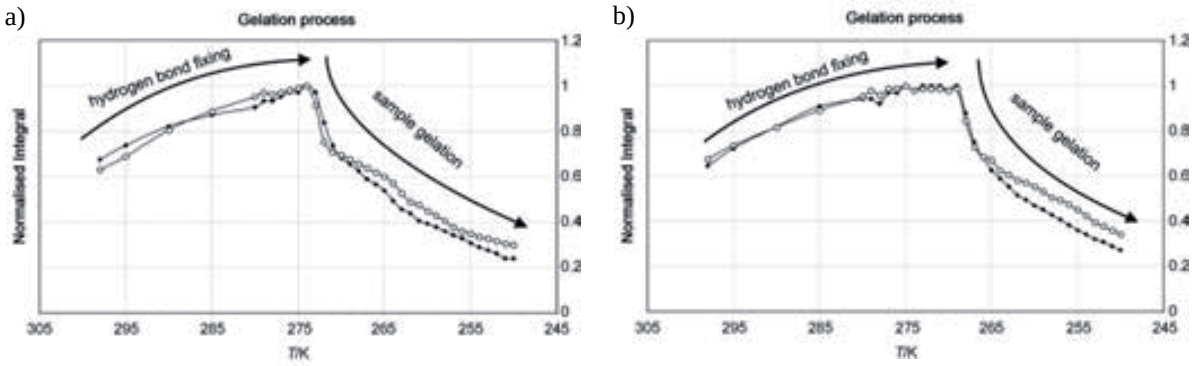

Figure **15**. Graphical representation of the normalized NH proton integrals NH_4 (○) and NH_{10} (♦) during the gelation process for 15 mM solutions of a) (*S*,*S*,*S*,*S*)-**6** and b) (*S*,*S*,*S*,*R*)-**6** in toluene-d_8. Table of concentration dependence of T_{gel} is also displayed.

Regarding the self-assembly of the fibres, CD, wide-angle X-ray diffraction (WAXD) and theoretical studies suggested two different models of aggregation for each one of the samples. The self-assembly of octameric aggregates was studied computationally in order to find out the most favourable model of self-organization: two molecules can arrange themselves in a head-to-head (h-h) or a head-to-tail (h-t) disposition. Calculations concluded that for the *trans*,*cis*-**6** dipeptide the h-t disposition was the most favourable, unlike for the *trans*,*trans*-**6**, where the h-h disposition is more favourable instead (Figure **16**). This result was in good agreement with the NMR observations aforementioned, and conclusions could be extrapolated for both toluene and chloroform solvents.

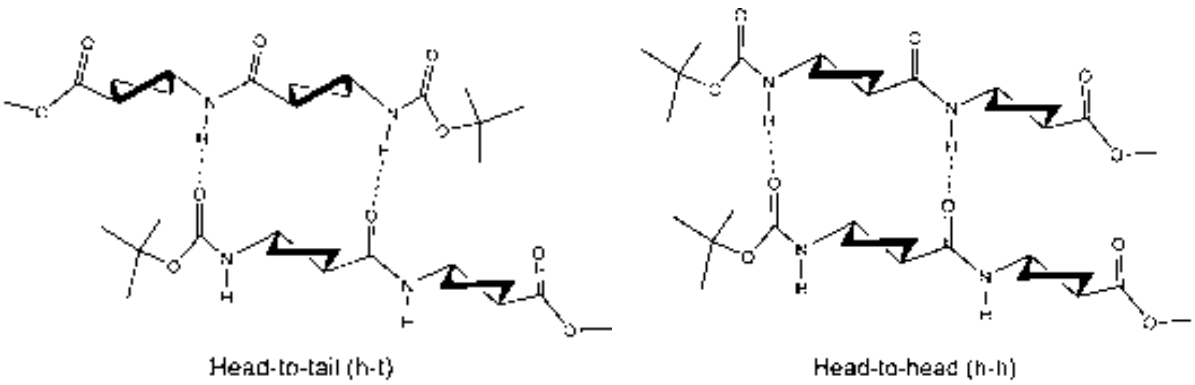

Figure **16**. The arrangements of two molecules of (*S*,*S*,*S*,*S*)-**6** through two intermolecular hydrogen bonds.

Solid CD of the xerogels from toluene (30 mM in KBr) exhibited similar bands to those of the peptides in MeOH solutions, proving the existence of helical assemblies. They just differed on the signal magnitude, attributable to the distinct degree of twisted conformation, higher in non-assembled molecules in solution. Such helical supramolecular organization was in accordance with theoretical results at the MMFF level of theory for hexadecameric aggregates of both dipeptides in $CDCl_3$. In turn, data from WAXD diffractograms, which showed low-angle sharp signals at 5 and 10 Å, fit well to distances between consecutive and alternate dipeptide molecules within a hydrogen-bonded single chain, as described by calculations (Figure **17**).

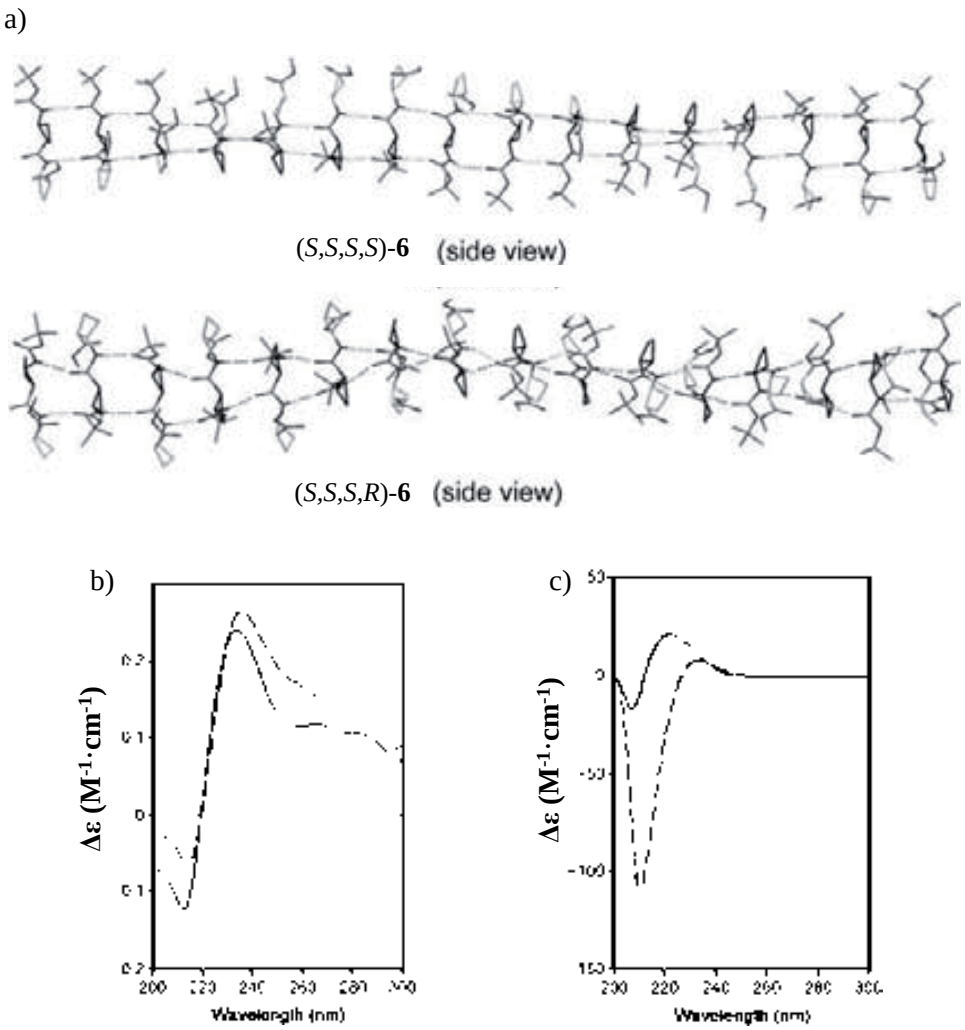

Figure **17**. a) Side views of hexadecameric aggregates of (*S*,*S*,*S*,*S*)-**6** and (*S*,*S*,*S*,*R*)-**6** optimised in $CDCl_3$. Non-acidic hydrogens have been omitted for clarity. b) CD spectra of xerogels from toluene at 30 mM in KBr. c) CD spectra of 0.5 mM MeOH solutions, for (*S*,*S*,*S*,*S*)-**6** (—) and (*S*,*S*,*S*,*R*)-**6** (---), based on TEM, AFM, SPFM and theoretical studies. Parallel arrangement is more favourable than the alternate disposition.

1.1.3. Synthesis and structural study in solution of cyclobutane containing γ-amino acids and γ-peptides

The other line of investigation in our group that deals with cyclobutane containing compounds has been developing interesting γ-amino acids and γ-peptides derived from (-)-verbenone, among other possible derivatizations resulting in hybrid peptides, dendrimers and polyfunctional platforms, for instance. Starting from this bicyclic monoterpenic natural product, efficient and stereodivergent synthetic approaches were optimized for achieving enantiomerically pure γ-amino acids. However, such compounds could contain the cyclobutane ring as a part of the γ-amino acid backbone skeleton (cyclobutane amino acids) or contrarily, the cyclobutane ring could be a side group of the linear γ-amino acid chain instead (cyclobutyl amino acids) (Figure **18**).

Cyclobutyl γ-amino acid Cyclobutane γ-amino acid

Figure **18**. Types of γ-amino acids containing a cyclobutane ring. Difference lies in if the amino acid backbone chain involves or not the cyclobutane moiety.

On one side, several cyclobutyl γ-amino acids were synthesized to reach branched scaffolds, in order to prepare polyfunctional platforms, where the cyclobutane ring plays a central role. The synthesis went through a reactive aldehyde, transformed into an olefin by a Wittig reaction; over this substrate, the Michael type addition of nitromethane afforded the key intermediate in a totally diastereoselective way. From this, proper selective functionalization allowed the synthesis of the corresponding orthogonally protected peptides (Scheme **4**).[15]

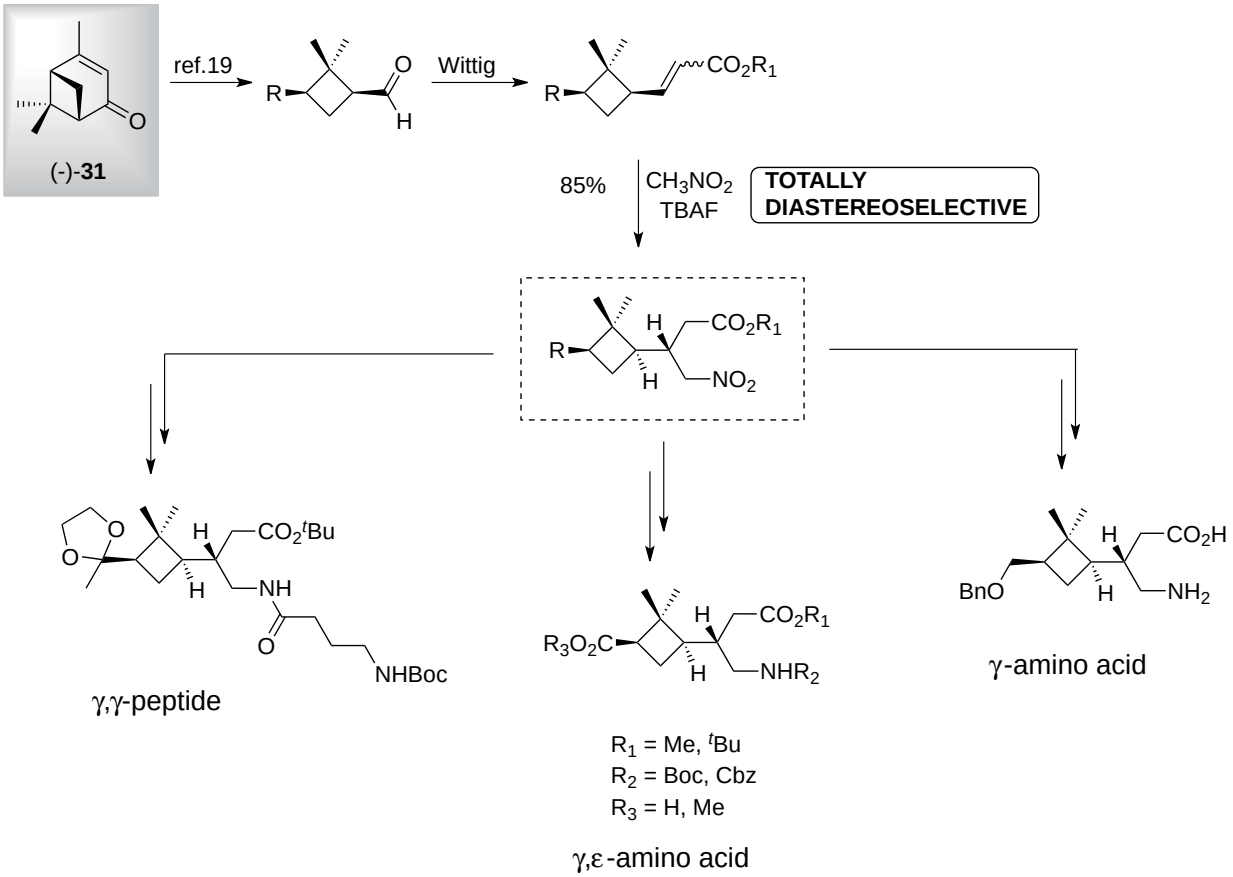

Scheme **4**. Diastereoselective synthetic approaches to prepare cyclobutyl γ-amino acids leading to branched peptides with a cyclobutane core.

On the other side, the simple oxidation of (-)-verbenone (-)-**31** led to the (-)-*cis*-pinononic acid (-)-**32** without epimerization, which after the appropriate transformations involving Curtius rearrangements afforded the enantiomeric pair of cyclobutane γ-amino acids. Combination of such compounds with themselves[16] or other amino acids as *cis*-4-amino-*L*-proline[17,18] or GABA[16] was performed in order to obtain homo or hybrid γ,γ-peptides (Scheme **5**). Their structural study, aiming a similar promotion of compact foldings as in β-cyclobutane peptides, did not show any particular structure induced by long distance hydrogen bondings as expected. On the contrary, extended or β-sheet-like conformations were observed as preliminary results, probably owing to the bulkiness of the 2,2-dimethyl substitution in the *cis*-3-aminocyclobutanecarboxylic acid. For the proline derivatives, promising biological applications as cell-penetrating agents have been recently reported.[18]

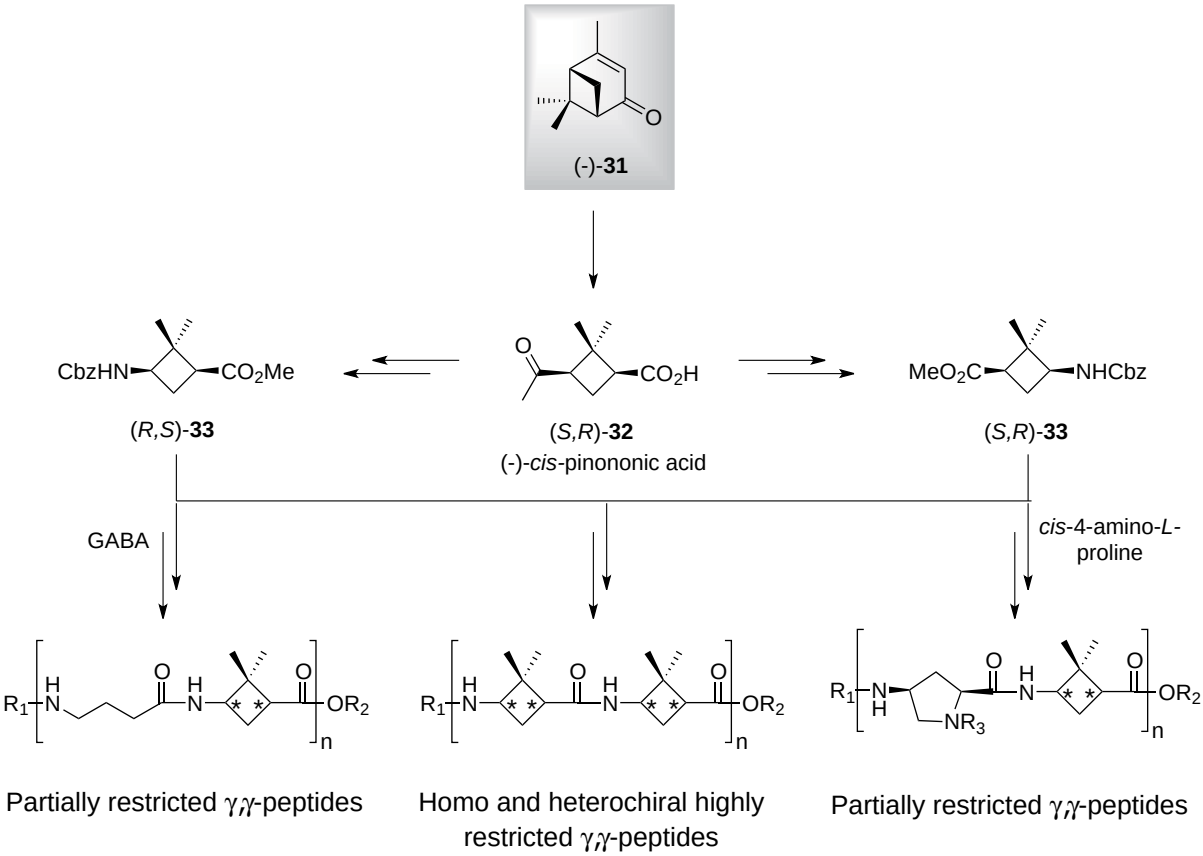

Scheme **X**. Enantioselective synthetic approaches to prepare cyclobutane γ-amino acids and pure and hybrid γ,γ-peptides.

The resulting molecules of alternated introduction of *cis*-4-amino-*L*-proline into the backbone of cyclobutane γ-peptides were studied by NMR experiments and theoretical calculations in chloroform, which rationalized the influence of both cyclic residues. A series of diastereomeric hybrid γ,γ-peptides, from dimer to hexamer, was synthesized by solution peptide coupling methodology, through selective deprotection of the amine and carboxylic acids and using PyBOP as coupling agent (Figure **19**). Nevertheless, the chirality of the cyclobutane residue did not have a relevant role in the preferred foldings.

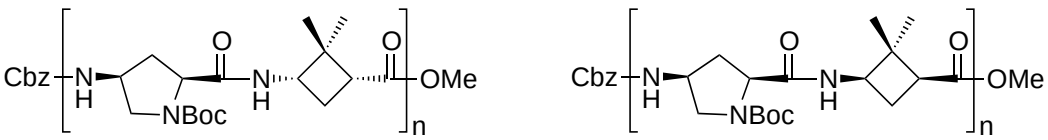

n= 1 **34**
n= 2 **35**
n= 3 **36**

n= 1 **37**
n= 2 **38**
n= 3 **39**

Figure **19**. Diastereomeric series of cyclobutane-proline hybrid γ,γ-peptides, from dimers to hexamers.

The structural study in solution was first performed for the proline compound only, considering the absence of relative data in the literature, and then for the hybrid peptides, showing interesting results according to the driving force of the cyclobutane moiety about inducing major conformations. ^{1}H-NMR spectrum of proline compound showed split resonances in most of the signals. This was due to the existence of both *cis/trans* conformers, because of the slow dynamic rotation of the conjugated N-C bond in Boc group within the NMR time scale. Both conformers were almost equally populated (Figure **20**).

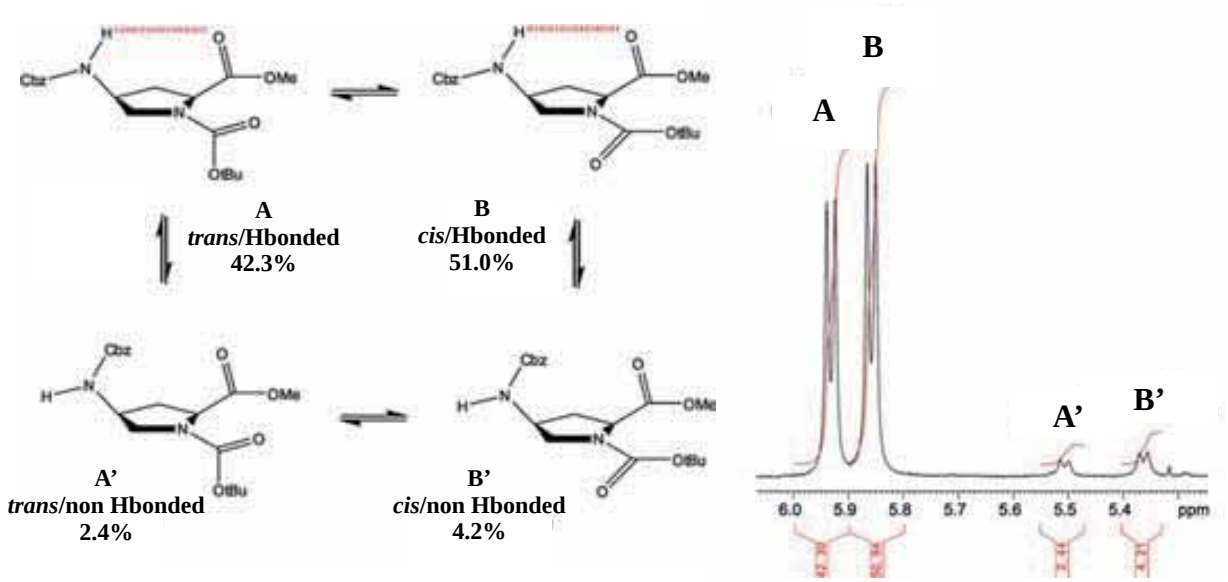

Figure **20**. Zoom of the NH area from the ^{1}H-NMR spectrum of *cis*-4-amino-*L*-proline at 273 K, and detailed conformations.

Then, when the cyclobutane amino acids were introduced, a major conformation could be observed (among the minor ones), corroborating the restricting structural motif that this dimethyl cyclobutane ring is. For all the hybrid γ,γ-peptides, similar extended conformations were determined, in which the key feature lied on the hydrogen bonding between the carbonyl of the N(Boc) group and the fixed NH amide proton (adjacent to the cyclobutane ring), avoiding the aforementioned dynamic rotation of the Boc group. NOE and ROE connections along with *J* couplings became key parameters to reach this conclusion (Figure **21**).

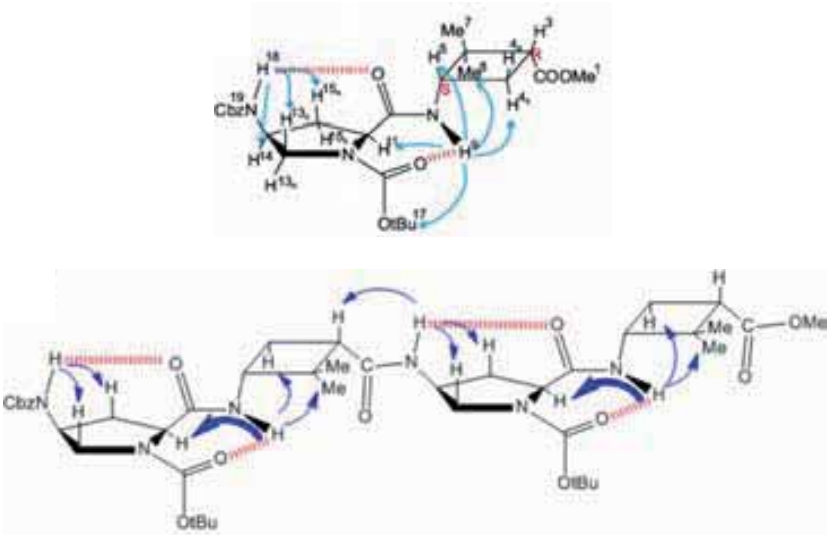

Figure **21**. Main conformation for dipeptide **34** and tetrapeptide **38** deduced from NOE and *J* couplings for the former and ROE and $^{3}J_{NHCH}$ couplings for the latter. NOEs (blue thin arrows), ROEs (bold blue arrows) H-bonds (dashed red lines).

CD spectra of both diastereomeric series showed opposite signature and defined Cotton effects for the larger peptides. This result was in agreement with NMR observations, which showed different splitting and NH proton shielding between the comparable pair of peptides of each diastereomeric series (Figure **22**).

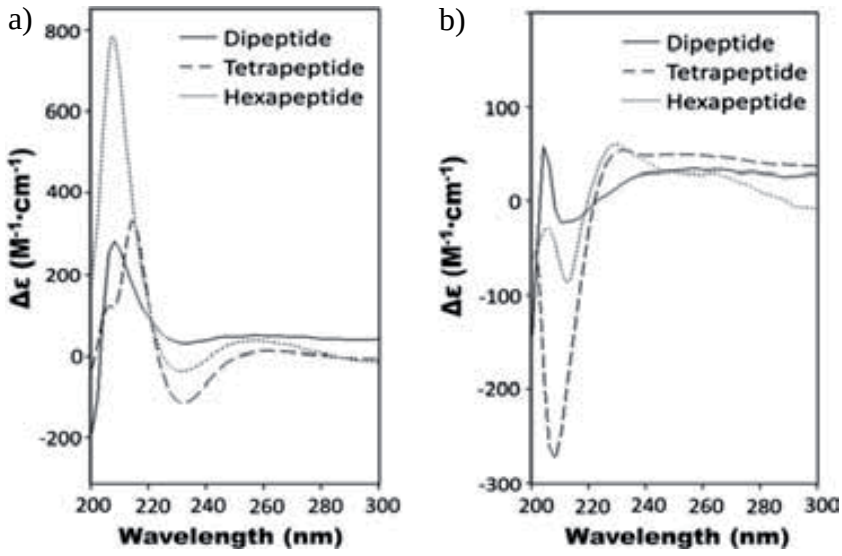

Figure **22**. CD spectra of γ,γ-peptides a) **37-39** and b) **34-36** in 0.01 mM MeOH solutions.

A computational study was carried out with the aim of discovering differences between the two diastereomeric series. Molecular Dynamic calculations were performed for tetrapeptides in chloroform and for hexapeptides in gas phase, resulting in comparable structural trends. Comparing hexamers **36** and **39**, some crucial differences were observed. The inter-residue hydrogen bonds and

the proline intra-residue ones are always present in both hexamers, whereas the cyclobutane intra-residue H-bonds are only present in **39** (4 in total). From these, the interior cyclobutane residues presented bifurcated hydrogen bonds from the same NH of the cyclobutane, which also constitute the inter-residue ones. This fact leads the hexamer **36** to have a more twisted conformation (Figure **23**).

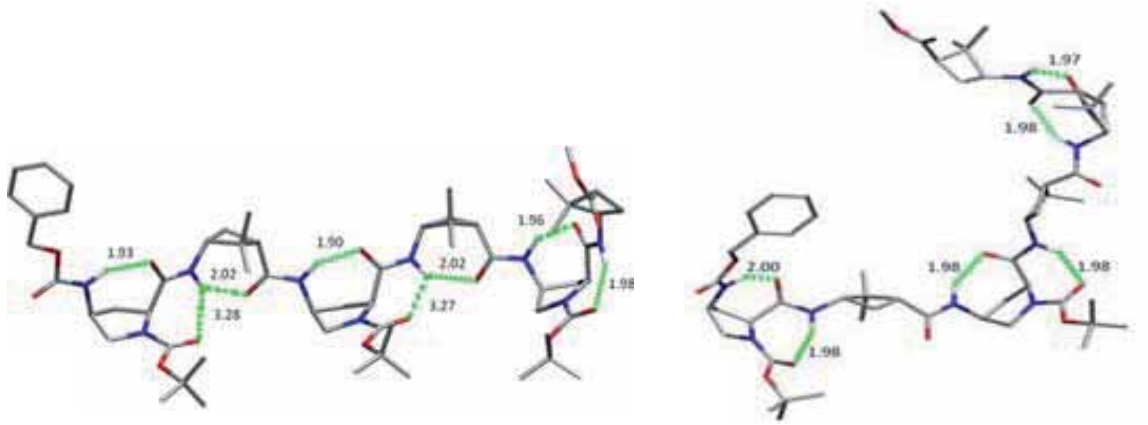

Figure **23**. Preferred conformations for hybrid hexapeptides **39** (*left*) and **36** (*right*) as obtained at B3LYP/ 6-31G(d) level of theory in gas phase. H-bonds (dashed green lines) distances in Å. Non-acidic protons have been omitted for clarity.

Incubation of all the peptides in 2 mM MeOH solutions afforded nano-sized well-defined vesicles, observed by TEM micrographs, demonstrating the ability of hybrid cyclobutane-proline γ,γ-peptides to self-assemble (Figure **24**).

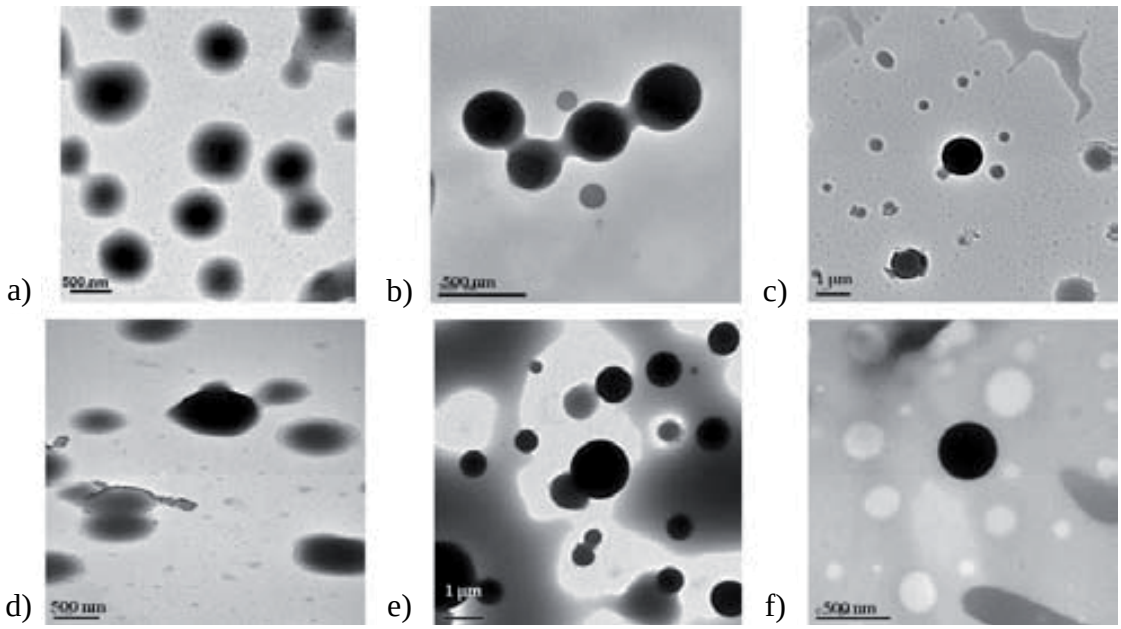

Figure **24**. TEM images of the vesicles formed by a) dipeptide **37**, b) tetrapeptide **38**, c) hexapeptide **39**, d) dipeptide **34**, e) tetrapeptide **35**, f) hexapeptide **36** from 2 mM solutions in MeOH (1 day incubation for a, b, d, e and 4 days incubation for c, f) placed onto a carbon-film coated copper grid.

1.1.4. Applications

1.1.4.1. Inhibitors of the metallocarboxypeptidases (MCP) A and B

Peptidomimetics containing non hydrolyzable bonds have been widely exploited in the design of potent protease inhibitors. Cyclobutane containing peptides (CBPs) are good candidates for such purpose since their biological properties are scarcely explored compared to other cycloalkyl derivatives and, they are easy to synthesize and of a low molecular weight, which are common properties with the α-peptides substrates of MCPs. Moreover, the cyclobutyl moiety provides a rigid scaffold that enhances the proper binding to them. Selected cyclobutane-containing β-peptides were computationally docked to the enzymes and their binding properties analysed in depth. As a result of this work, a novel class of MCP inhibitors was synthesized and tested (Figure **25**).[19]

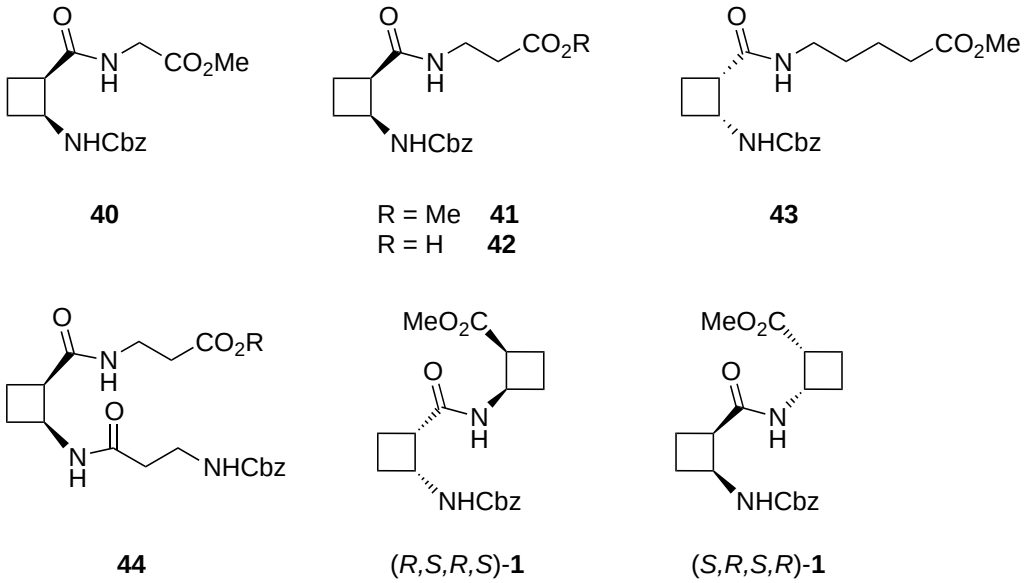

Figure **25**. Cyclobutane-containing di- and tripeptides tested as MCPs inhibitors.

All the CBPs showed activity against both prototypical MCPs, CPA and CPB, in the micromolar range (Table **1**).

Table **1**. Biological activity of CBPs

Compound	K_i[a] (μM)	
	CPA	CPB
40	550 (100)	500 (95)
41	180 (30)	400 (70)
42	70 (12)	43.0 (7.5)
43	72.5 (9.5)	410 (80)
44	70 (15)	165 (55)
(*R*,*S*,*R*,*S*)-**1**	67 (10)	70 (10)
(*S*,*R*,*S*,*R*)-**1**	95 (18)	275 (45)

[a] Values inside parentheses indicate the standard error of the mean (SEM).

The lower K_i value, the higher inhibitory activity, so the conclusion was that peptide **42** was the most potent compound, specially against CPB, while peptide **43** presented a preference to inhibit CPA. Targeting to CPB was optimized because of the presence of a β-alanine linear chain and free carboxylic acid, whereas longer chains or methyl carboxylates did not cause such effect. Best inhibition of CPA was achieved by using longer alkyl chains (four -CH_2- units) and a methyl blocked carboxylate. Both (*R*,*S*,*R*,*S*)-**1** and (*S*,*R*,*S*,*R*)-**1** enantiomers showed moderate biological activity towards the target proteins and their docked structures suggested similar binding modes.

On the other hand, analysis of **42** binding showed that the inhibitor backbone was bent at the cyclobutane ring, due to the inherent conformational rigidity of it and the strong interactions with the residues at the active site of the protein. In the case of inhibitor **43**, the important role of phenolic aromatic rings of the protein facilitated its binding (Figure **26**).

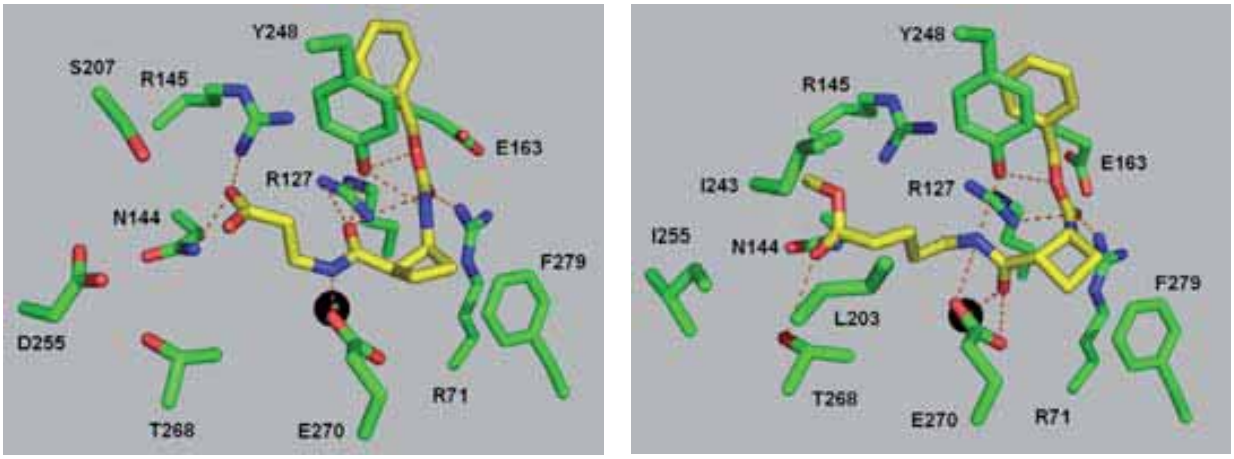

Figure **26**. Predicted binding of compound **42** to human CPB structure (*left*) and compound **43** to CPA structure (*right*). The ligand (yellow carbons) and selected CPB side-chains (green carbons) are shown in sticks model. Other atoms are coloured blue (nitrogen) and red (oxygen). Intermolecular interactions are as dashed orange lines. The catalytic zinc ion is shown as a black sphere.

1.1.4.2. Conductive materials

Self-assembly of polycyclobutane peptides derived from ACBA has been widely proved. Therefore, the incorporation of a bis-cyclobutane β-peptide in the side-chains of a functional molecular unit could enhance its capability of organization in ordered aggregates.[20] This combination resulted in compound **45**, synthesized by the coupling of dipeptide (*R*,*S*,*R*,*S*)-**46** and the π-electron-rich tetrathiafulvalene (TTF) unit (Scheme **6**). Cyclobutane containing moiety would provide chirality and rigidity to the final compound whereas the TTF moiety would afford the conducting properties.

This proposal was approached on the basis of previous simple amide derivatives of TTF, which self-assembled into nanoscopic fibres.

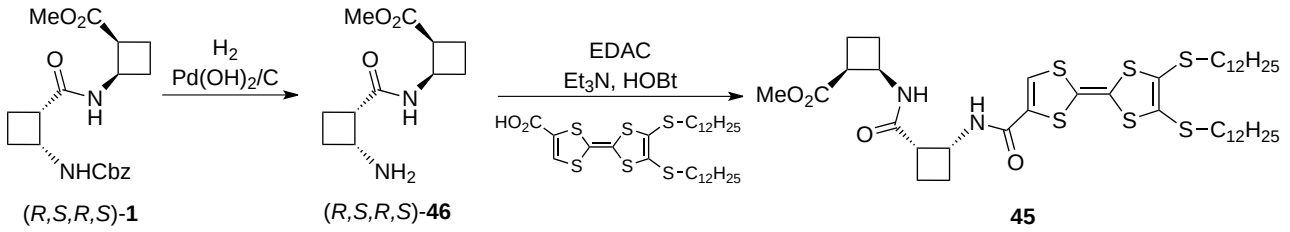

Scheme **6**. Synthesis of compound **45**.

The interest of such a material lies on the gaining of a fibrous system capable of conducting electricity, once doped (oxidized) to produce a conduction pathway. The product was obtained by simple reaction of the amide derivative from the dipeptide and the acid derivative from TTF, using EDAC/HOBt coupling agents. The compound was not stable for long periods of time, apparently because of the cleavage of the TTF-amide linkage, but it could be stored in air for several days.

Characterization was performed *via* NMR, IR and Mass spectroscopies. Circular dichroism spectra of methanol solutions for compounds (*R,S,R,S*)-**1** and **45** presented Cotton effects at around 205 nm, what suggested a similar strand-type secondary structure for both, as in polycyclobutane β-oligomers, and proved the optical activity of **45** (Figure **27**). No self-aggregation of the hybrid compound was observed due to the absence of temperature dependence at the concentrations used for the mentioned experiments.

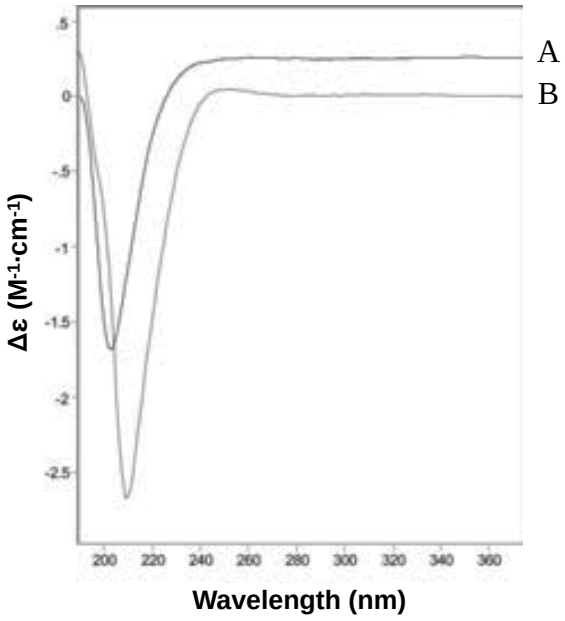

Figure **X**. Superimposed CD spectra of compound **48** (A) and dipeptide (*R,S,R,S*)-**1** (B) in methanol at 20 ºC.

To check the ability of compound **45** to form a fibrous material, TEM and AFM were employed. TEM images revealed the formation of a complex network of fibres of width about 10-15 nm, which could be organized into wider bundles. However, no regular chirality was detected on these fibres despite the chiral nature of the molecule. However, when they were studied by AFM, a highly oriented pyrolytic graphite (HOPG) was used. Two concentrations of **45** were tested and chirality could be observed in the formation of twisted bilayers in some parts of the surface, as well as fibres providing an interwoven network with spaces between them. Head-to-head bilayer-type structure was observed in the bundles, of 8 nm of height and 100-200 nm of width (Figure **28**).

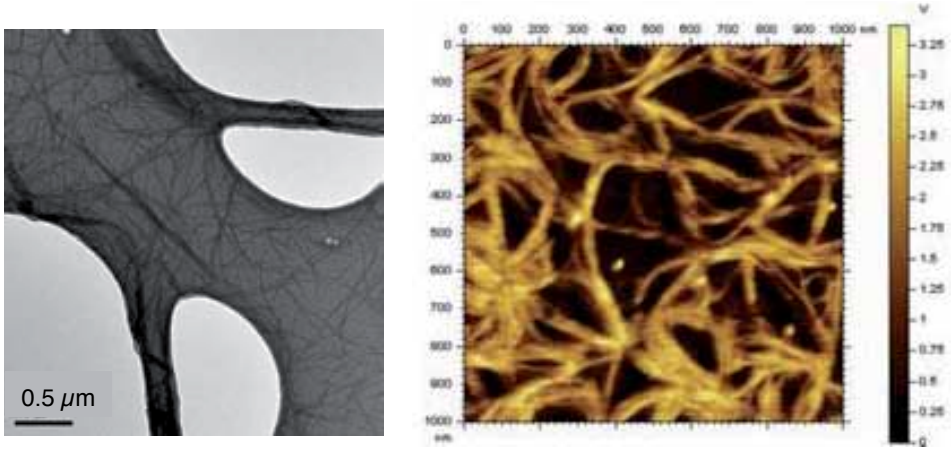

Figure **28**. TEM image of a sample of **45** deposited onto a holey carbon grid (*left*) and AFM image, by casting a 28 μM chloroform solution of **45** onto HOPG, revealing the interwoven nature of the fibril network (*right*).

Conductivity could be probed when charge carriers were introduced by doping the films of **45** with iodine vapour. Current-sensing atomic force microscopy (CS-AFM) was used to explore the films on HOPG and the conductivity was appreciated from the current-potential curve performed with the tip of the microscope. Such conductivity was uniform over hundreds of square nanometers, an important aspect of these materials for further applications (Figure **29**).

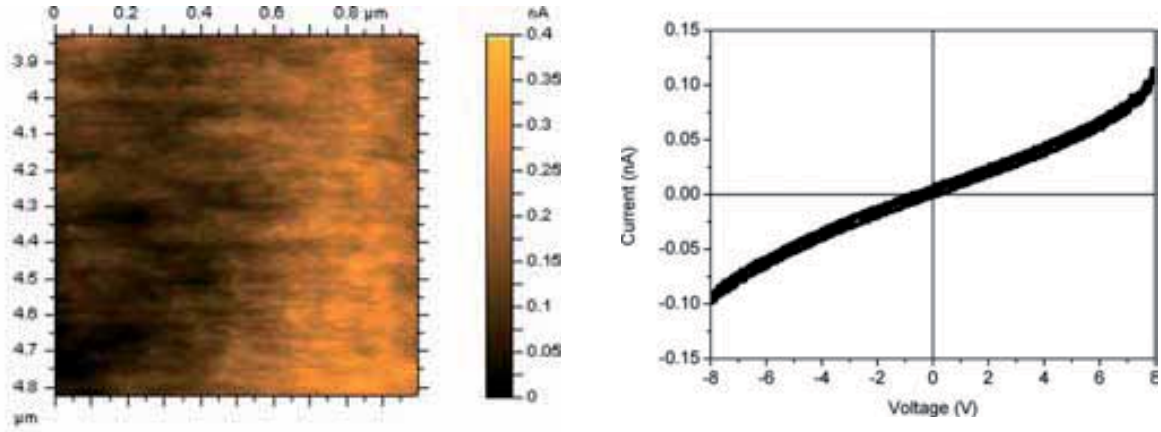

Figure **29**. CS-AFM image (at 5 V applied potential) of a doped film of **45** on HOPG (*left*) and a representative spectroscopy curve (*right*).

1.1.4.3. Cell-penetrating peptides (CPPs)

Two diastereomeric series of hybrid cyclobutane-proline γ,γ-peptides were successfully synthesized as a first generation by a solution phase procedure. Study of the capacity of these peptides to act as CPPs needed the introduction of 5(6)-carboxyfluoresceine (CF) by a coupling reaction too. Toxicity was firstly tested for these groups of di-, tetra- and hexapeptides by MTT assay, showing they were non-toxic. Cell-uptake properties were investigated using HeLa cells but unfortunately they showed poor penetration into the cells. Chirality of the cyclobutane moieties did not affect significantly on these properties.[18]

Therefore, it was decided to prepare a second generation of γ,γ-hexapeptides by solid phase methodology. These peptides consisted in the same backbone from the most synthetically accessible diastereomeric series, but with the *C*- and *N*-terminus interchanged. Their derivatives would differ in the groups attached to the secondary *N* atom of the proline residues, expecting a better cell-uptake because of the balance between hydrophobicity and positive charge (Figure **30**).

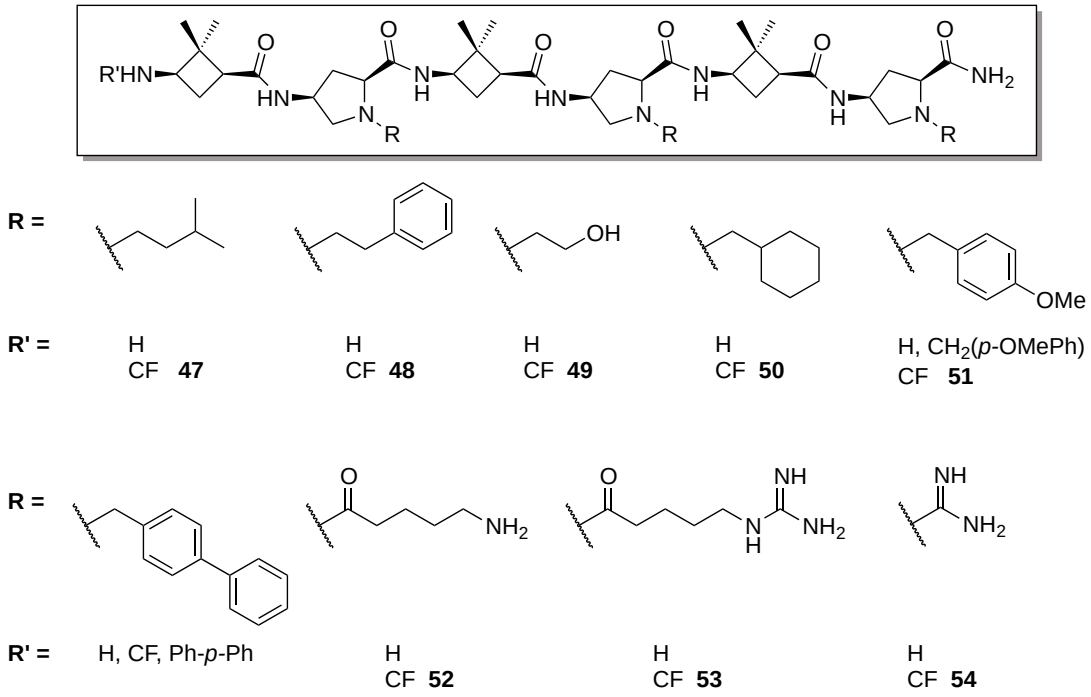

Figure **30**. Chemical structure of the second generation of hybrid γ,γ-proline-cyclobutane hexapeptides synthesized.

Toxicity tests, performed in similar conditions to the first generation, showed comparable and low toxicities towards de HeLa cells. In contrast, penetration into the cells was different and particular for each peptide, corroborating the crucial effect of the R group. The best cell-uptake properties were observed for the peptide **53**, containing a guanidinium group in the side chains within its sequence, that in the cell environment would be protonated. Comparing both guanidinium containing peptides **53** and **54**, one could state the important role of the spacer, the flexibility of

which would dispose the guanidinium groups more accessible to the cell membranes, enhancing the peptide penetration (Figure **31**).

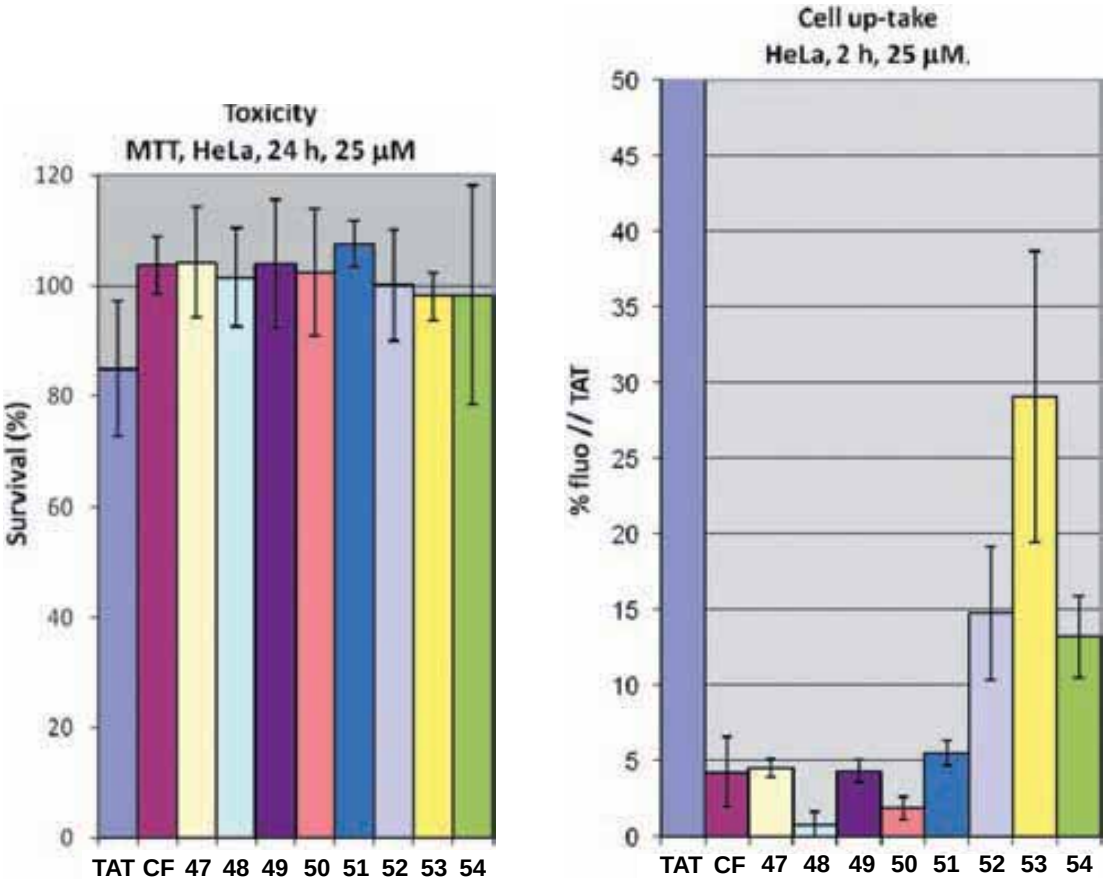

Figure **31**. a) Cytotoxicity of the γ,γ-hexapeptides as monitored in HeLa cell lines. Cell death was quantified using MTT assay after 24 h of incubation and 25 µM peptide concentration. b) Flow cytometry quantification of the cellular uptake of γ,γ-hexapeptides in HeLa cells. Cells were incubated with 25 µM peptide concentration for 2 h at 37 ºC; graph has been cut at 50% of fluorescence for clearness (TAT = 100%). Errors bars represent standard deviation of three independent experiments.

1.1.4.4. Organocatalysts

Some of the thioureas aforementioned were used as bifunctional organocatalysts to assist a Michael reaction, resulting in good yields and moderate enantioselectivities (Figure **32**, Table **2**).[13]

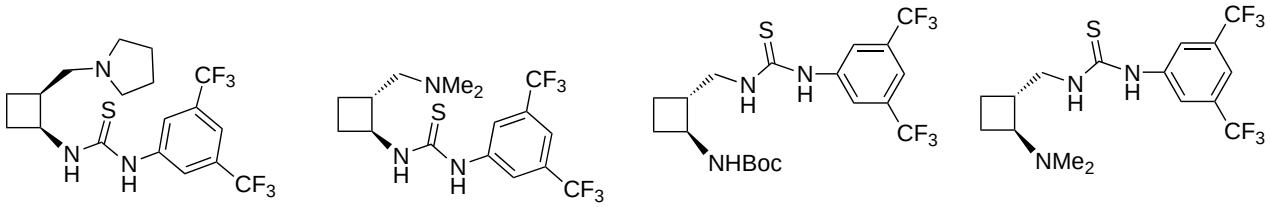

Figure **32**. Thioureas employed as bifunctional organocatalysts for the Michael addition reaction.

Nevertheless, information about the influence of stereochemical features on the reaction acceleration and the asymmetric induction was gained in order to complete the studies. The best result in terms of conversion and enantioselectivity was obtained for thiourea **21** using toluene at room temperature for 24 h (Table **2**, Entry 6). Otherwise, it appeared that the *cis* stereochemistry of the cyclobutane moiety induced better enantioselectivity for such reactions than did the *trans* configuration, as deduced from comparison of Entries 5 and 6 with Entries 11 and 12. Moreover, the use of prepared amino alcohols and diamines to afford candidates for metal ligands and for new chiral surfactants is under active investigation in our laboratories.

Table **2**. Conjugate addition of diethyl malonate to (*E*)-β-nitrostyrene catalyzed by **21, 24**, **28** and **29**.

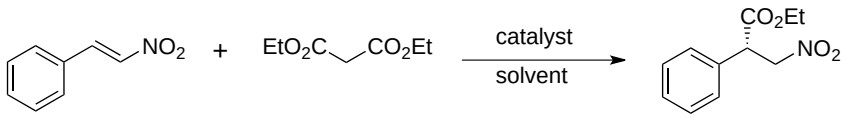

Entry	Cat.	mol[%]	Solvent	*T*[°C]	*t*[h]	Yield[%]	*e.r.*[*S*/*R*][a]
1	**21**	10	CH_3CN	25	24	42[b]	60:40
2	**21**	10	diglime	25	24	68[b]	68:32
3	**21**	10	dioxane	25	24	65[b]	62:38
4	**21**	10	THF	25	24	65[b]	63:37
5	**21**	10	CH_2Cl_2	25	24	42[b]	68:32
6	**21**	10	toluene	25	24	85[b]	74:26
7	**21**	15	toluene	25	24	59[b]	69:31
8	**21**	5	toluene	25	24	45[b]	71:29
9	**21**	10	toluene	0	48	60[b]	73:27
10	**21**	10	toluene	–25	48	61[b]	75:25
11	**24**	10	CH_2Cl_2	25	24	88[b]	52:48
12	**24**	10	toluene	25	24	75[b]	60:40
13	**29**	10	CH_2Cl_2	25	24	61[b]	59:41
14	**29**	10	toluene	25	24	67[b]	64:36
15	**28**	10	CH_2Cl_2	25	48	< 5[c]	60:40
16	**28**	10	toluene	25	48	< 5[c]	–

[a] Determined by chiral HPLC analysis of the reaction mixture. [b] Isolated yield. [c] Conversion determined by GC of the reaction mixture.

CHAPTER II

Folding of Short Polycyclobutane β-Peptides as the Chiral Expression of Monomeric Building Units

2.1. INTRODUCTION

The imitation of the well know secondary structures that are only naturally occurring in α-peptides is one of the most studied areas in peptide chemistry. β-Sheets, β-turns and α-helices are the most common structural motifs found in proteins, and their mimicry through synthetic foldamers one of the scientific hits. Their successful application is due in part to their non-proteinogenic nature, what makes them to be biocompatible but not so biodegradable by peptidases in biological systems. Hence, peptidomimetics can be used as potential scaffolds for therapeutics while they keep in equilibrium some decisive factors as stability, affinity, specificity and efficacy. They can be made from cyclic peptides, *N*-alkylated peptides to conformationally restricted peptides, as the β-amino acids. The most striking finding of the early work on oligomeric β-peptides is the observation of regular helical structures with hydrogen bonding patterns, which run in both directions, with respect to the polypeptide chain. These are the 14-,[21-25] 12-,[26-28] 12/10-,[23,29-31] 10-[32,33] and 8-helix[34,35], which have been experimentally prepared or theoretically postulated for β-oligomers and have emerged from the main investigation of Gellman, Seebach and Fleet (Figure **33**).

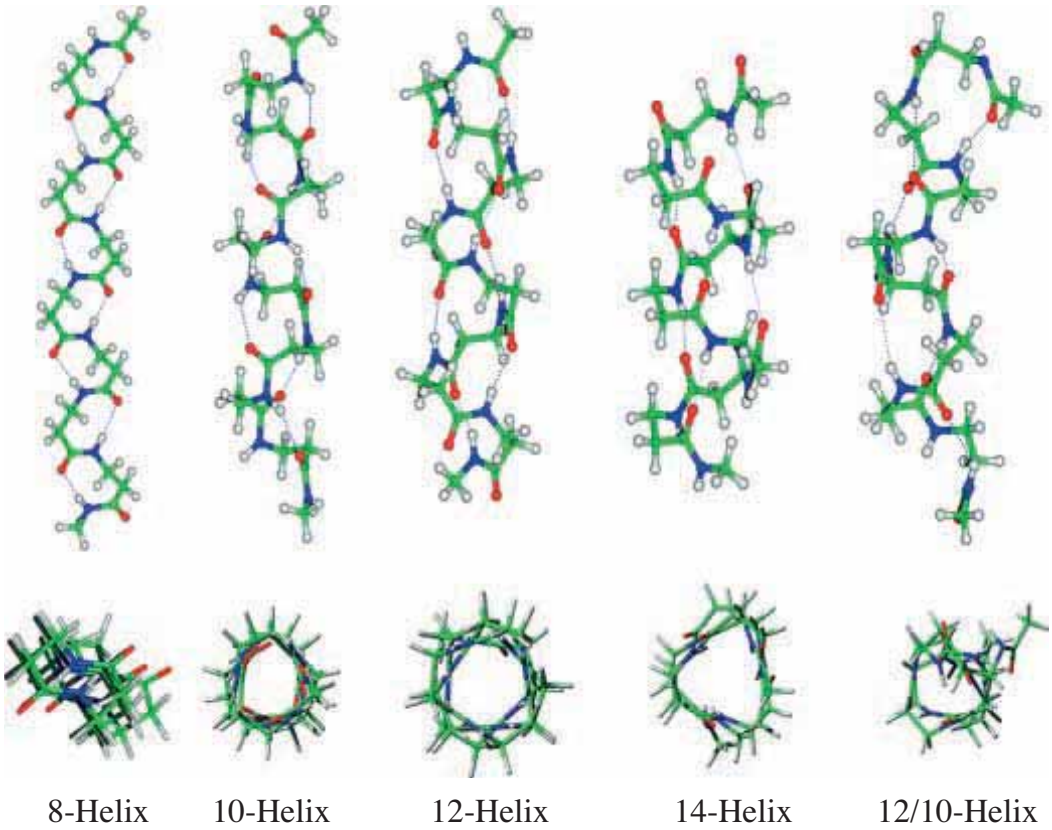

Figure **33**. Novel helices formed by oligo-β-peptides. The structures have been generated using insight II program using theoretically or experimentally determined backbone torsion angles. Views obtained perpendicular to the helix axis and down the helix axis are shown. Figure extracted from reference 36

Nevertheless, extended arrangements can be also found in α-peptides and proteins. Short polypeptide segments (from 2 to 5 residues) that form chain reversals facilitate registry of antiparallel strands stabilized by cross strand hydrogen bonds. Parallel strands can also self-assemble and therefore, the formation of a β-hairpin or a β-sheet secondary structure, if the unit is periodically repeated along the polypeptide chain, takes place (Figure **34**). While some conformational restricted cyclic β-amino acids in homo-peptides have led to ribbon-type structures,[9b] other poly-β-peptides, constructed with β-alanine[37,38] or poly(α-isobutyl-*L*-aspartate)[39,40] resulted in β-sheets.[41-44]

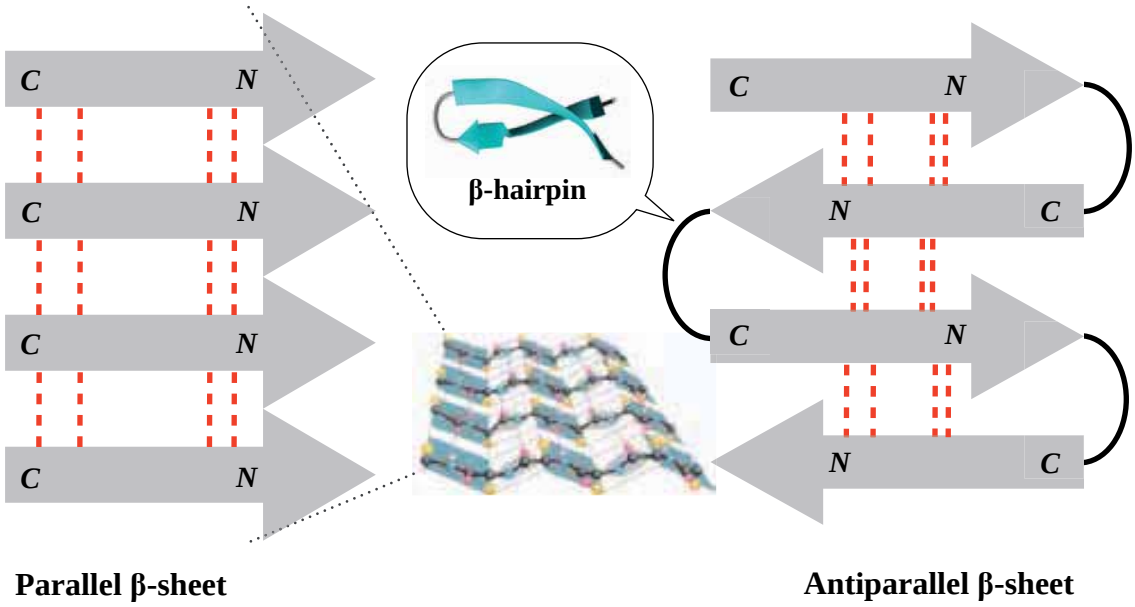

Figure **34**. Parallel (*left*) and antiparallel (*right*) β-sheet foldings with inter-strand hydrogen bonds in red-dashed lines. β-Hairpin turn, a structural inductor of antiparallel β-sheets. β-Hairpin figure is extracted from reference 45; parallel sheet figure extracted from reference 46

ω-Amino acid is a term used to refer to the entire family of these residues generated by homologation of the backbone of an α-amino acid, which are employed in the preparation of new foldamers. Ten years ago, among these ω-residues, an increasing interest on the synthesis of cyclic β-amino acids emerged. Since they had shown to present interesting biological activity,[19,47-49] application for the design of peptidomimetics[50] and the construction of molecular scaffolds exhibiting strong self-organization, the demand of new synthetic procedures was raised. Publications regarding cyclic β-amino acids were mostly related to cyclopropane,[51,52] cyclopentane[28,53-56] and cyclohexane[54,58-60] derivatives but poor research had been developed for amino acids and peptides based on the cyclobutane ring.

2.1.1. Synthesis of cyclobutane β-amino acids and β-peptides

From then on, several synthetic approaches have appeared to solve this matter and two leading strategies can be established.

On one side, the synthesis can be tackled starting from simple and *meso*-molecules with little functionalization (without N atoms for instance), which are desymmetrized in the first stages. Afterwards, functionalization to the protected amino acids takes the rest of the synthetic work. On the other side, starting from non-necessarily symmetric molecules, the synthesis goes through racemic compounds which are further separated from some diastereoisomeric compound.

The first work on the synthesis of cyclobutane β-amino acids is attributed to Kennewell *et al.*, who reported it in a racemic way; from the cyclobutane-1,2-dicarboxylic acids, *cis*- and (±)-*trans*-2-amino-1-cyclobutanecarboxylic acid (ACBC) were achieved by a series of selective transformations after chemical desymmetrization.[61] In our group, a similar strategy was adopted to gain access to the first enantionselective synthesis of the orthogonally protected *cis*-amino acid (*S,R*)-**55** (Scheme **7**).[8,62] The key step was the desymmetrization of *meso*-diester **56** *via* a catalytic enantioselective hydrolysis of the *pro*S chiral carbon atom using *PLE*, which provided the chiral hemiester (*S,R*)-**8** with >97% *ee*.

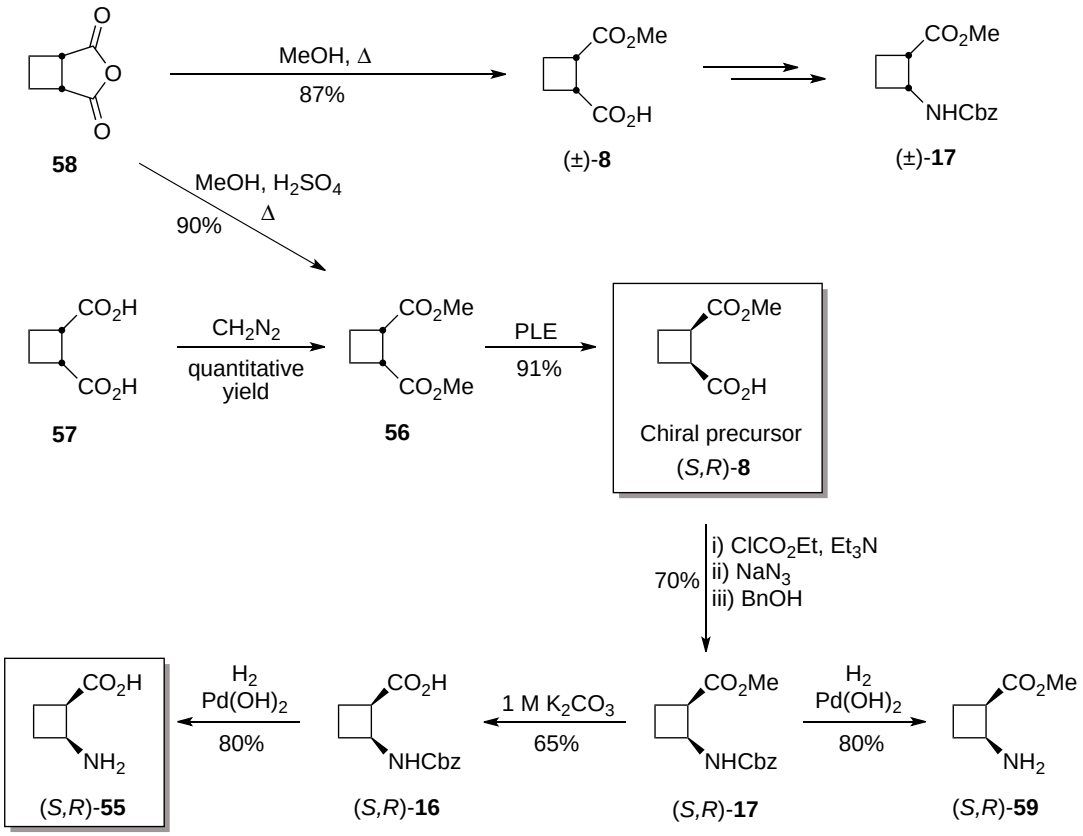

Scheme **7**. First enantioselective synthesis of a β-amino acid derived from ACBC.

From the publication of this work in 1998, the procedure has been optimized. The main change refers to the starting material: while first approaches employed commercially available cyclobutane diacid **57** or cyclobutane anhydride **58**, later approximations have used [2+2] photochemical reactions to synthesize the cyclobutane ring. During some time, cycloaddition reaction was performed between a mixture of *cis*-/*trans*-1,2-dichloroethylene but it was then substituted by ethylene, so the required hydrogenation step to eliminate chlorine atoms was avoided (Scheme **8**).[9c]

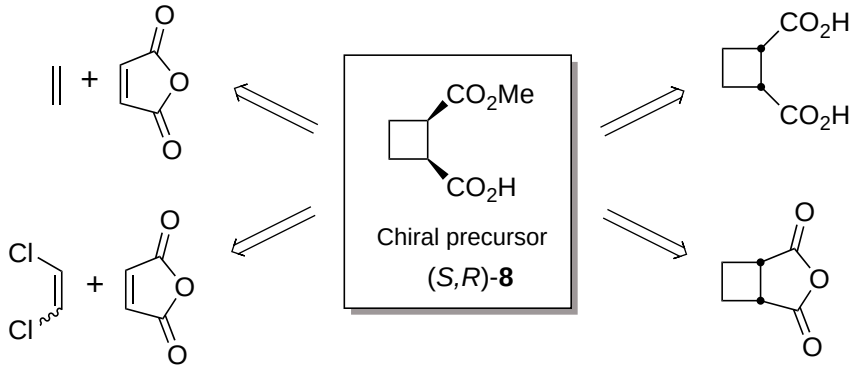

Scheme **8**. Retrosynthetic approach for the common chiral precursor (*S*,*R*)-**8**, showing all the starting materials tested.

The complete synthetic pathway to achieve all the four orthogonally protected enantiomers of ACBC is fully described, step by step, in section **2.3.1.1.**

However, Bolm[63,64] *et al.* later described a different methodology to the enzymatic one, which was adapted from that of Jones and Sabbioni.[65] They desymmetrized cycloalkyl *meso*-anhydrides through an alkaloid-mediated opening in the presence of alcohols, to afford both enantiomeric hemiesters with very good *ee*s and yields (Scheme **9**).

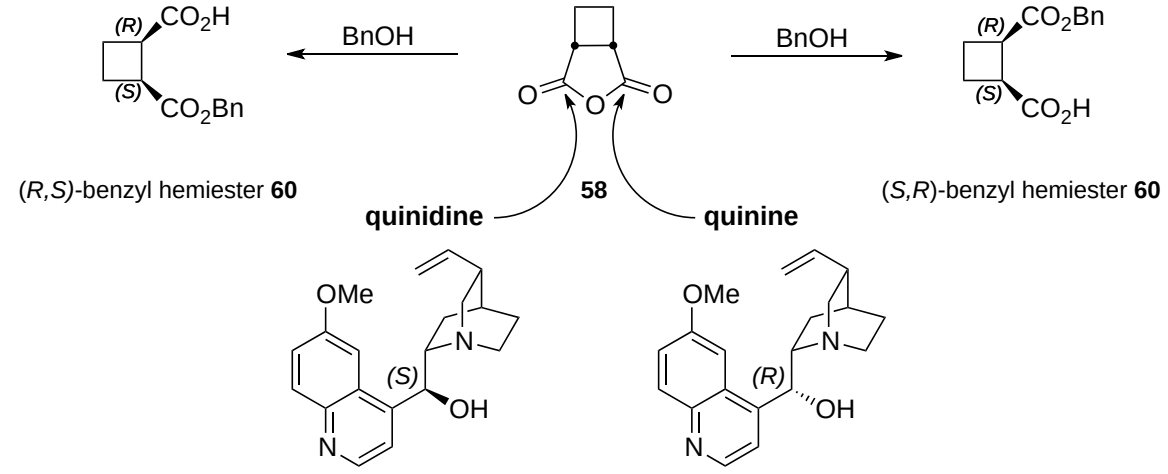

Scheme **9**. Quinidine- and quinine-mediated opening of cyclobutane anhydride in the presence of BnOH.[63,64]

This alkaloid covers both stereoisomers of the cinchona (or quina) enantiomeric pair, quinine and quinidine, which assisted on the nucleophilic opening of the anhydrides. Auxiliary quinine directs the ring opening to the *pro*R carbon whereas the quinidine does it on the *pro*S (Scheme **9**). For example, the cyclobutane anhydride **58** was derivatized using benzyl alcohol into (*R*,*S*)-**60** and (*S*,*R*)-**60**, with 93% *ee* (90% yield) and 90% *ee* (85% yield) respectively. Then, successive functional transformations led to obtain both *N*-Boc protected *cis*-amino acids.

On the other side, Aitken and his group have been developing an alternative synthetic route to prepare enantiomerically pure ACBCs, using the [2+2] photocycloaddition reaction of ethylene with uracil for the construction of the 4-membered ring.[66-72] From 2002 to 2011 they have been refining the route by the optimization of some key steps in order to gain access to the four enantiomers of the *N*-Boc-2-aminocyclobutane-1-carboxylic acid. This strategy is interesting since they reached the *N*-Boc amino acid (±)-**15** in 3 steps, in 65% overall yield, although in the racemic form. Anyway, this was not a drawback because further chiral resolution allowed to separate both corresponding diastereomers **61** and **62**, in 46% and 44% yield respectively (Scheme **10**).

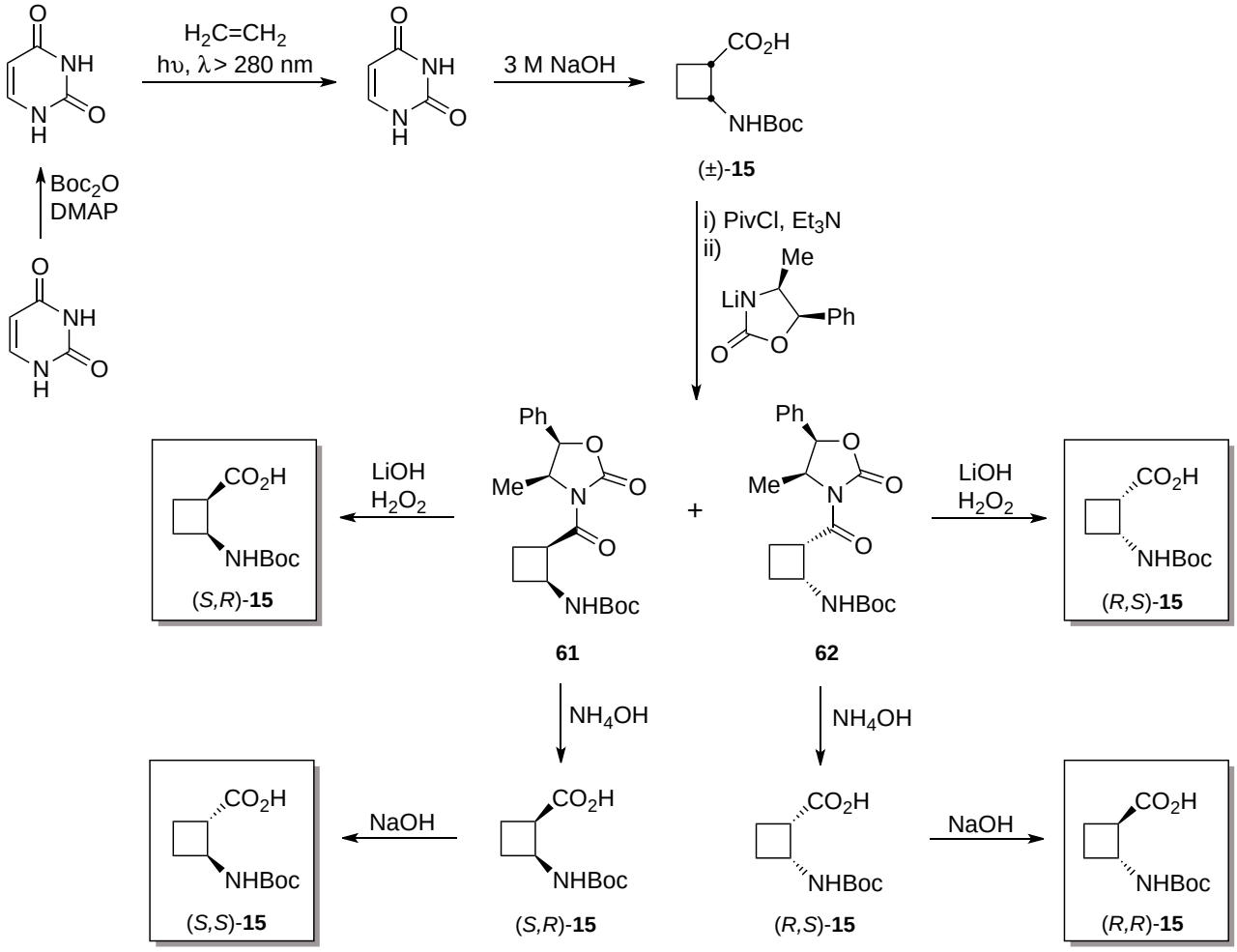

Scheme **10**. Synthetic alternative route proposed by Aitken and collaborators.

Next, selective hydrolysis of the chiral resolving complexes afforded both *cis* enantiomers, while the ammonolysis *via* ammonium hydroxide led to primary amides, which were subsequently epimerizated under strong basic conditions. This epimerization employs a useful and novel protocol for the synthesis of *trans* conformers from the *cis* ones (Scheme **10**).

2.1.2. Study of the secondary structure in non proteinogenic β-amino acids and β-peptides

In the area of foldamer science, oligomers of cycloalkane β-amino acids have shown a great propensity to adopt preferred conformations. From cyclohexane to cyclopropane, going through cyclopentane and cyclobutane, many regular foldings can be observed leading to secondary structures involving all kind of turns, helices, hairpins and β-sheets, which were firstly attributed only to the biologic peptides and proteins formed by the natural α-amino acids.

For instance, small oligomers of *trans*-2-aminocyclohexanecarboxylic acid (*trans*-ACHC) are known to adopt a 14-helix conformation,[57,73] while oligomers of *trans*-cyclopentane derivative (*trans*-ACPC) prefer a 12-helix conformation.[55] In contrast, their corresponding *cis* oligomers (*cis*-ACPC) adopt a strand-like structure.[74] However, small ring β-amino acids have had less contribution to the field and it is, to a large extent, because of the intrinsic instability of the cyclopropane and cyclobutane rings. Indeed, 2-aminocyclopropanecarboxylic acid does not exist because the vicinal push–pull substituent system facilitates rapid and irreversible ring opening.[75] The cyclobutane analogues also undergo ring openings, not so easily but, it usually occurs when the deprotection of the amine takes place, enhancing the push-pull event. Depending on the conditions in which the cleavage is carried out and on the reactant, open chain dicarbonylic compounds[68,76] or open chain amino acids[9a] are obtained as byproducts. Nevertheless, when such small ring amino acids are incorporated into oligomers of just two residues, the deprotection of *N*-terminus does not affect the ring stability, allowing the elongation of the peptides successfully (Scheme **11**).

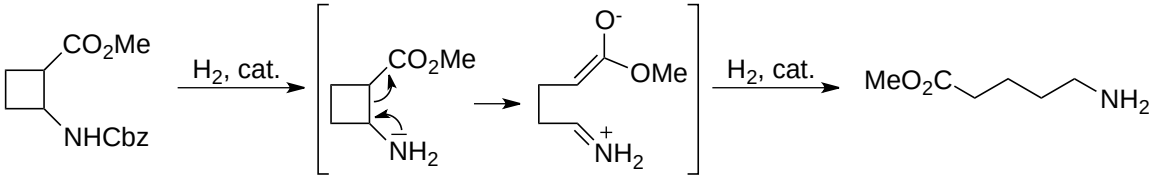

Scheme **11**. Ring-opening reaction on cyclobutane compounds by push-pull effect.

Another possibility concerns the mixing of different backbone β-amino acids. Hybrid peptides in which ACHC or ACPC have been combined with other β-amino acids may retain a propensity for some folding.[77-82] Similarly, a variety of helical structures have been demonstrated for mixed α/β-peptides with heterogeneous backbones in which ACHC or ACPC has been combined with α-amino acids.[81,82] In fact, this methodology is used in the next chapter, where the *cis*-ACBC is mixed with linear α-, β- and γ-amino acids to obtain a homologated series of α,β- β,β- and β,γ-peptides. Specific foldings have been determined in each case, demonstrating the inherent capacity of these compounds to afford novel and smart foldamers.

2.1.2.1. Techniques for the conformational study of peptides

The structural study of peptides mainly involves the determination of their most stable conformations through hydrogen bond interactions in solution or in the solid state. Nevertheless, although protein or peptide crystallization can afford crucial information in the solid state, usually by X-ray methods, the conformational study in solution (in aqueous solutions mainly) is more interesting due to its analogy with the biologic systems. Moreover, function of proteins also belongs to the structural study area.

Many techniques can be used for the conformational determination in solution but, some of them usually require previous detailed study in order to apply them in a reproducible manner. Circular Dichroism (CD) or Infrared spectroscopy (IR) belong to such group of techniques, which usually give qualitative information in a supramolecular or molecular level. Among the other techniques, which are able to state more specifically the interactions taking place from the atomic scale to the secondary structures, the most used are Nuclear Magnetic Resonance (NMR) spectroscopy and Theoretical and Computational Calculations. In addition, the degree of agreement between both increases the reliability of the conclusions achieved.

NMR spectroscopy

NMR spectroscopy is the main tool used for studying the secondary conformational structure of proteins and peptides in solution. Once the structural elucidation is achieved, the NMR experiment which directly gives more information about the spatial disposition of the atoms, and hence the conformation, is the determination of NOEs. This experiment can be mono- or bi-dimensional and is usually applied for ^{1}H nuclei; it allows to determine the couplings between non-adjacent atoms so they are called space couplings. Many publications can be found in the literature about the use of

NMR experiments on determining the presence of hydrogen bonds on secondary structures, so that the resolution of which type of secondary structure is involved has been achieved.

For instance, Gellman and coworkers have a wide experience on the use of this technique. In 2010, they published a 12-helix secondary structure by means of crystallographic data and NOE contacts (Figure **35**).[83]

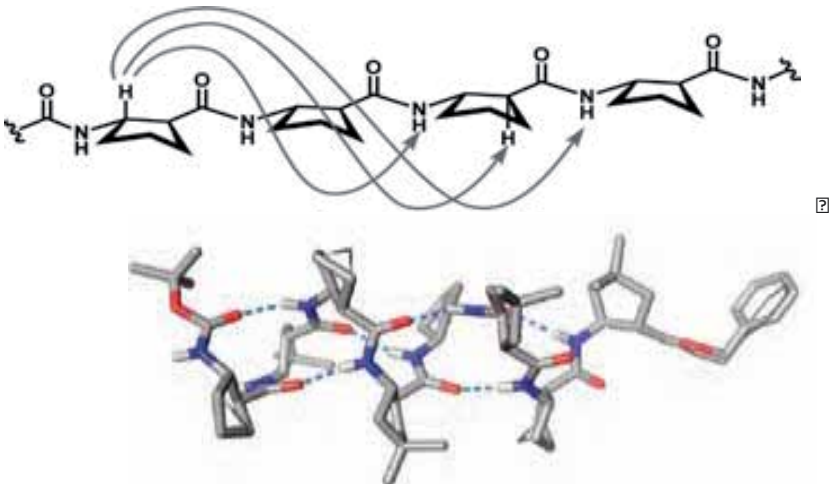

Figure **35**. Medium-range NOE patterns observed for 12-helical β-peptides described by Gellman.

A similar foldamer has been recently reported by Aitken and his collaborators, who prepared oligomers constituted of *trans*-1,2-cyclobutane amino acids (Figure **36**).[84] The hexamer and octamer were studied by computational calculations and in pyridine-d_5 solution, the only solvent in which the compounds were soluble, showing to adopt a 12-helix secondary structure. NOE contacts helped on the determination of this conformation.

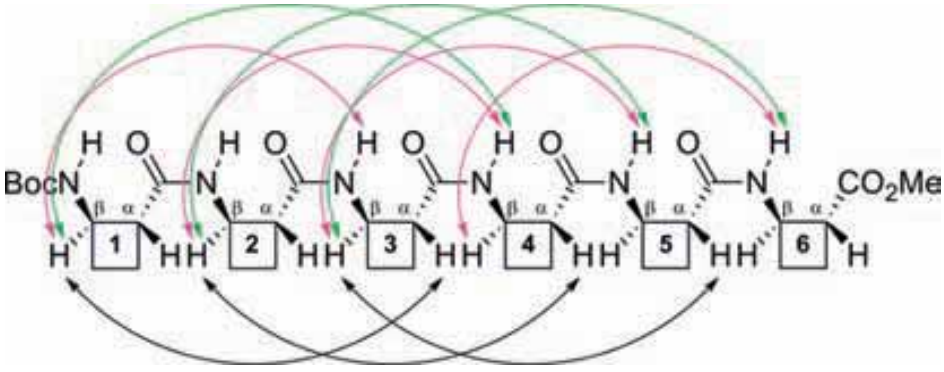

Figure **36**. Graphical representation of the observed NOEs described by Aitken for the all-*trans* hexamer.

In addition to NOE experiments, experiments of solvent exchange can be performed in order to define if a NH proton is fixed or not. This fixation can be caused by the presence of protecting groups or because of the formation of hydrogen bonds. The weaker the proton exchange with the

solvent is, the more fixed it is, being the hydrogen bond more stable and strong at once. Water is the common solvent used for such analysis although methanol can be a good alternative too. Thus, given the fact that all amide protons are easily interchangeable with water, if the experiment shows that the intensity distribution of the NH protons decays faster than any non-exchangeable proton of the molecule, it means that such proton is not involved in the formation of any hydrogen bond. Conversely, if the intensity of such proton falls with the same proportion as the rest, that would mean that there is not any exchange with the solvent and so, the proton is fixed and probably involved in a hydrogen bond. It is noteworthy that these experiments are carried out in a concentration in which the self-aggregation of the peptides is not possible, so the hydrogen bond interactions which take place are unequivocally considered of intramolecular nature.

Theoretical and Computational Calculations

Theoretical studies are also a useful tool for the determination of the prevalent secondary structures on peptides or proteins. Mostly, theoretical calculations arise to complete experimental results so they can be corroborated, using some basic experimental data or just running the calculation with no experimental restrictions. On the other hand, they can be employed before any experimental job, as a predicting tool to start an approach to a hitherto unknown chemical problem. For instance, and as the way it has been used in the present chapter, when the experimental development involves a lot of laboratory work or the compounds are highly insoluble, computational studies become really helpful and appropriate, allowing to save time, money and materials. Moreover, proper command of the computational chemistry grants access to some structural and physicochemical information (distances, dihedral angles, absolute and relative interaction energies, electronic charge distributions, dipoles and higher multipole moments, vibrational frequencies, reactivity or other spectroscopic quantities, etc.), which would be hardly obtained empirically in most of cases. These cases to be studied can be from simple little molecules to complex systems, so here arises the necessity from.

One example is the synthesis and theoretical study of a novel family of oxanorbornene β-peptides described by Klein and collaborators (Figure **37**).[34] Density Functional Theory (DFT) computations of the tridimensional structure and ^{1}H-NMR chemical shifts, predicted that the dimer and trimer formed consecutive 8-membered hydrogen bonded ring helices, which was supported with experimental solution NMR data. This kind of 8-helix interaction was not often observed before, although it was later detected on the study of peptides reported in the current thesis.

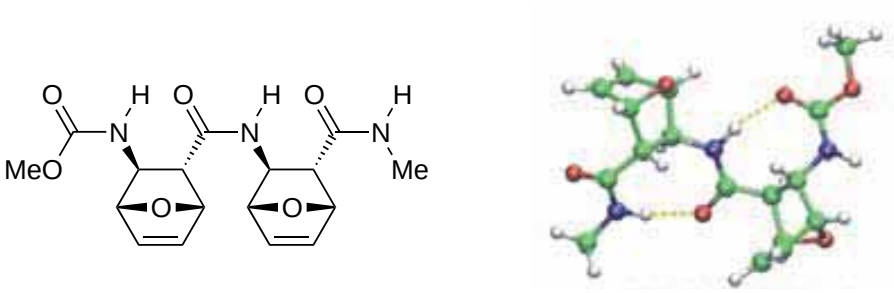

Figure **37**. Molecular structure of the dimer and its most stable conformation. 8-Hydrogen bonds are in yellow.

Perczel and co-workers published a complete theoretical study on β-peptides.[85] Intrinsic conformational characteristics of β-peptides, built up from simple achiral and chiral β-amino acids residues were studied using quantum chemical calculations, a method based on simulation of forces to find stationary points on the energy surface as the position of the nuclei is varied. To display the folding preference, the relative stability of selected conformers as functionp of the length of the polypeptide chain was determined.

In addition, by means of the four different backbone folds common in the secondary structure elements of β-peptides, they established a conformer-based systematic and uniform nomenclature to differentiate all the possible conformations (Figure **38**).

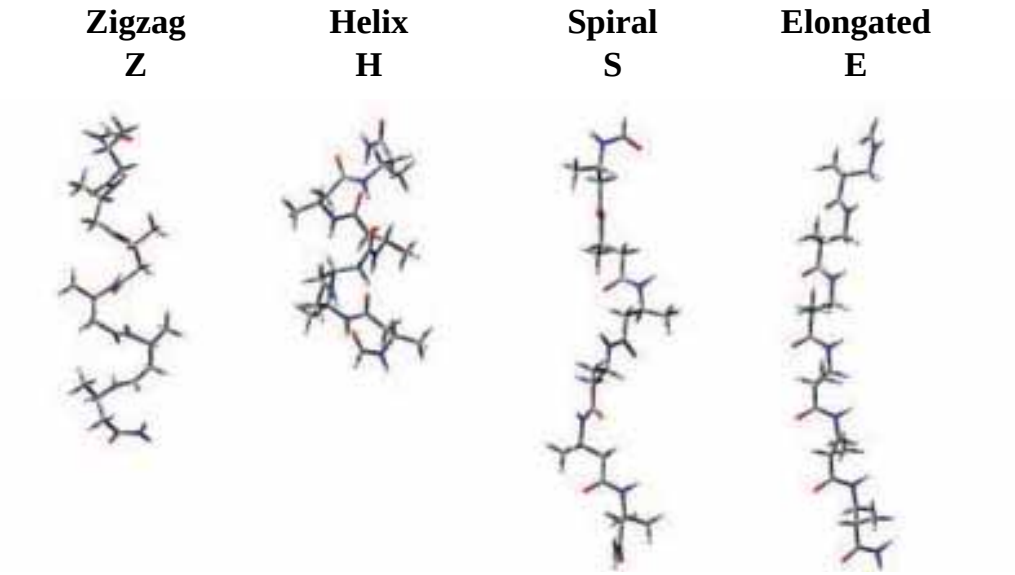

Figure **38**. Four different backbone folds common in secondary structure elements of β-peptides.

This division was made depending on the three φ, ψ and μ torsion angles, primarily related as *gauche plus*, *anti* and *gauche minus*, to finally be assigned as the corresponding conformation (Figure **39**).

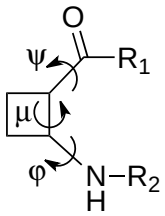

Figure **39**. β-Cyclobutane amino acid ψ, φ and μ torsion angles.

Then, Zn, Hn, Sn and En means zigzag, helical, spiral and elongated conformations, respectively, in which *n* is the number of atoms involved in the hydrogen bonding interaction. Depending on the folding direction, P indicates plus (or clockwise) and M is minus (or counterclockwise) twist or helicity. Moreover, the 27 possible conformations described for β-peptides could be represented in the appropriate 3D Ramachandran Cube, which is a way to visualize backbone dihedral angles of amino acid residues in protein structure (Figure **40**).

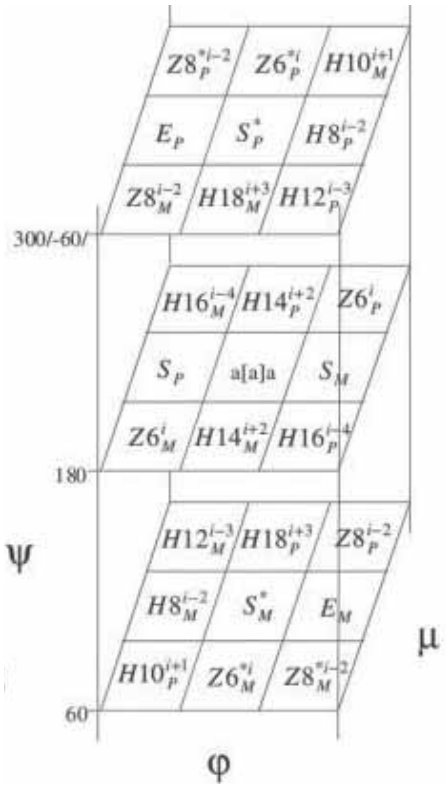

Figure **40**. General 3D Ramachandran cube described by Beke *et al*. for β-peptides.[85]

2.2. OBJECTIVES

Since the chirality of the amino acids, forming oligomers and peptides, has been experimentally observed to give different and specific foldings, the interest on the rationalization of such chirality-structure relationship has grown up in the last few years. Thus, the following aims were proposed to shed light on it:

• Design of a theoretical model to predict secondary structures of β-polycyclobutane peptides on the basis of the conformational energies of their respective containing monomers.

• Synthesis of some selected dipeptides, pseudotripeptides and tetrapeptides as a representative group of oligomers, in order to prove the validity of the model by studying their structure by NMR experiments.

2.3. RESULTS AND DISCUSSION

Precedents in our research group, where all-*cis* polycyclobutane-β-peptides (from di- to octapeptides) presented β-strand like conformations due to the presence of a six-membered hydrogen bond pattern, were shown in the introduction.[9c] Such intra-residual interactions are mainly promoted by the *cis* relative configuration of the substituents in the monomers, *cis*-(*S*,*R*) and *cis*-(*R*,*S*) (Figure **41**). When the *trans*-(*S*,*S*) monomer was combined with some of the *cis*-residues the resulting dipeptides showed significant changes on their structure because of the formation of an eight-membered hydrogen bond.[10] Nevertheless, these results could not lead to a general conclusion which defined the influence of the chirality in such secondary structures, given the fact that the *trans*-(*R*,*R*) unit and the multiple combinations between all of them were not considered.

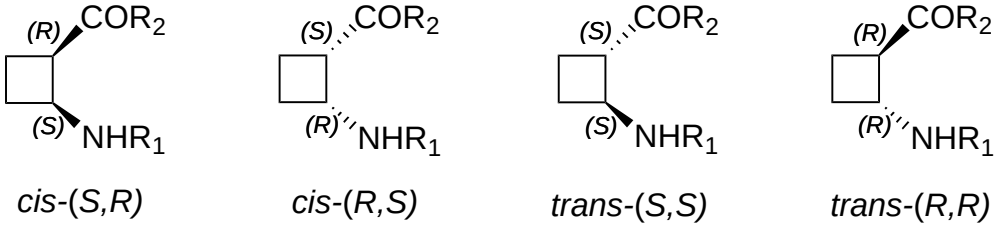

Figure **41**. 1,2-disubstituted cyclobutane monomers.

These combinations give a total number of 16 (4^2) dimers and 256 (4^4) tetramers to be studied, what is a great number of compounds. By symmetry effect, the total number is reduced to 8 dimers and 128 tetramers, respectively, what still is a lot of work to carry out.

Therefore, it was decided to perform a computational study that would allow to predict all the foldameric structures without the need of synthesizing and studying each of the possible β-peptides. However, with the aim of validating the theoretical model presented herein we synthesized some selected molecules, and studied them by high-resolution NMR.

2.3.1. Synthesis of cyclobutane β-amino acids and β-peptides

In the interest of having representative dimers and tetramers to validate the model, the four enantiomerically pure 1,2-disubstituted cyclobutane amino acids were prepared. Four is the number of total stereoisomers but other functionalizations led to more orthogonally protected amino acids. Through the experience gained in our laboratory, the four stereoisomers were prepared as both benzyl or *tert*-butyl carbamates at the *N*-terminus and as methyl esters at the *C*-terminus (Figure **42**).

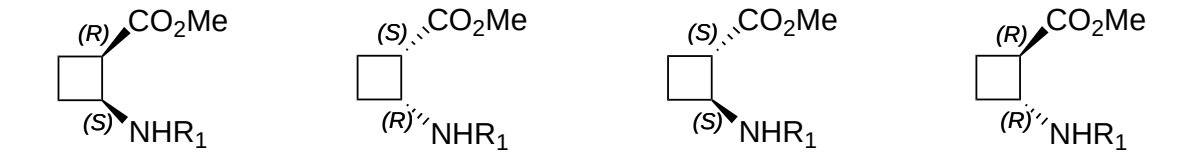

R_1= Boc (*S*,*R*)-**18** R_1= Boc (*R*,*S*)-**18** R_1= Boc (*S*,*S*)-**18** R_1= Boc (*R*,*R*)-**18**
Cbz (S,R)-**17** Cbz (*S*,*S*)-**17**

Figure **42**. The four stereoisomers of the 1,2-disubstituted cyclobutane amino acids to be synthesized.

Then, the corresponding dipeptides, pseudotripeptides and tetrapeptides to be studied by NMR were synthesized employing phosphorus derived coupling agents.

2.3.1.1. Synthesis of the four enantiomers of the orthogonally protected 1,2-aminocyclobutanecarboxylic acid

The synthesis of the four diastereomers starts with the preparation of *cis*-(*S*,*R*)-**18** and *cis*-(*R*,*S*)-**18** amino acids, from which the *trans* monomers can be achieved. In turn, both *cis* enantiomeric compounds (avoiding differences in their protecting groups) derive from a common chiral precursor, the (1*R*,2*S*)-2-(methoxycarbonyl)cyclobutanecarboxylic acid or hemiester (*S*,*R*)-**8** (see Scheme **12**).

To reach the first enantiomerically pure compound of the series, a photochemical reaction was performed between maleic anhydride and ethylene at low temperature in acetone. The [2+2] cycloaddition afforded the cyclobutane anhydride **58** quantitatively, so the cyclobutane moiety was built in the first step. Anhydride opening with methanol under acid catalysis and mild conditions led to the symmetric diester **59**. Desymmetrization of the *meso* compound was achieved by an enzymatic methodology, consisting in the enantioselective hydrolysis of the prochiral *S* centre by *PLE* in an aqueous buffer solution at pH 7 and room temperature. The chiral precursor (*S*,*R*)-**8** was then quantitatively obtained.

Direct derivatization of (*S*,*R*)-**8** through a Curtius reaction in the presence of benzyl or *tert*-butyl alcohols, with the required previous activation step of the mixed anhydride formation, led to the orthogonally protected amino acids (*S*,*R*)-**17** and (*R*,*S*)-**18** with maximum yields of 67% and 60%, respectively, after two steps. Later, saponification of (*S*,*R*)-**17** and (*R*,*S*)-**18**, respectively, gave the corresponding carboxylic acids (*S*,*R*)-**16** and (*R*,*S*)-**15** quantitatively.

On the other hand, to afford the enantiomeric series *tert*-butyl ester formation using *tert*-butyl-2,2,2-trichloroacetimidate was firstly needed to obtain the chiral diester (*S*,*R*)-**9**, which under

saponification led to the carboxylic acid (*R*,*S*)-**63** in 75% yield. Curtius rearrangement in the presence of BnOH allowed to obtain amino acid (*R*,*S*)-**64**, which was further deprotected on the *C*-terminus to afford free carboxylic acid (*R*,*S*)-**16**. This could be later methylated with excess of diazomethane to obtain (*R*,*S*)-**17** (Scheme **12**).

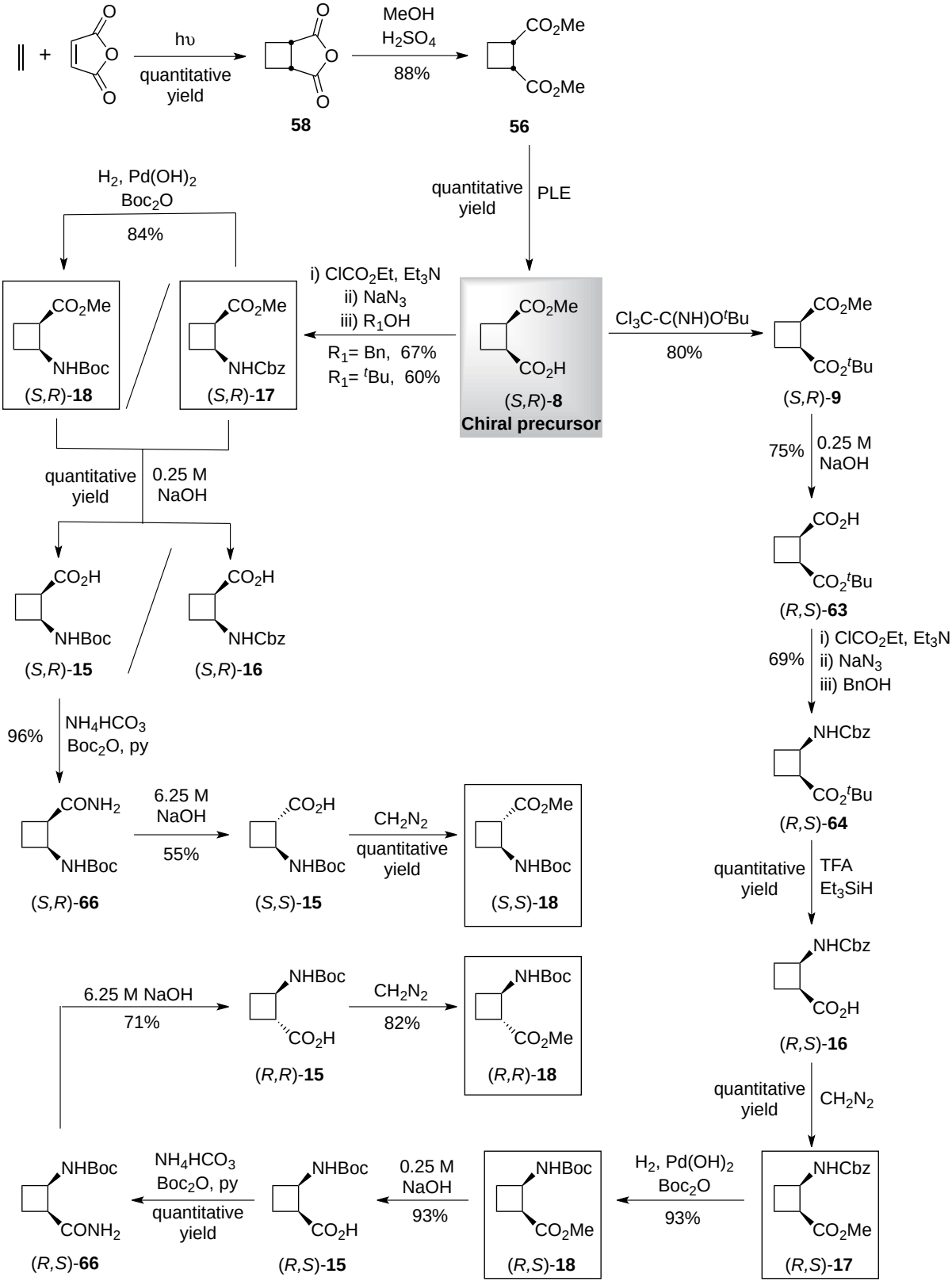

Scheme **12**. Synthesis of the four orthogonally *N*-Boc protected amino acids (*S*,*R*)-**21**, (*R*,*S*)-**21**, (*S*,*R*)-**66** and (*R*,*S*)-**66**. The *N*-Cbz *cis*-derivatives were also synthesized to afford *cis*-amines for the coupling reactions.

In order to achieve *trans* monomers, it was necessary to have the *tert*-butyl carbamate protection. Since the Curtius reaction using BnOH worked better most of the times, a one-pot transformation from benzyl to *tert*-butyl carbamate was optimized: catalytic hydrogenation of (*S*,*R*)-**17** or (*R*,*S*)-**17** in the presence of Boc_2O resulted in the compound (*S*,*R*)-**18** or (*R*,*S*)-**18** with 84% and 93% yield, respectively. On the other side, a two-step alternative route was tried through compound (*R*,*S*)-**65** but it was not finally applied. It consisted in a first *tert*-butyl and benzyl double carbamate formation and a subsequent catalytic hydrogenation. The double carbamate was obtained with a 38% yield so this option was not longer considered (Scheme **13**).

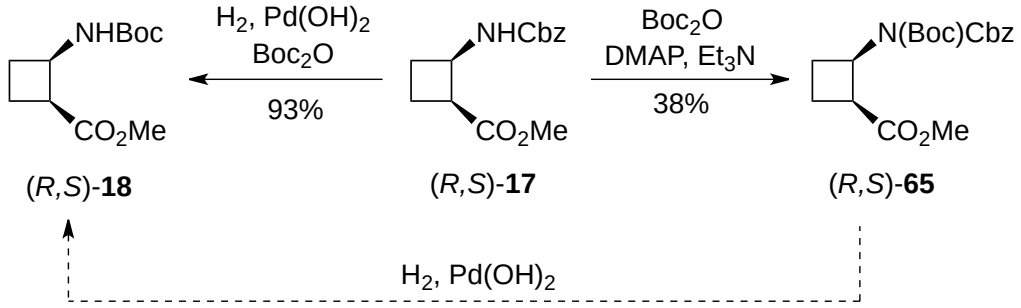

Scheme **13**. Two synthetic approaches to afford the orthogonally protected amino acid (*R*,*S*)-**18**.

The crucial step was the *cis* to *trans* isomerization and, although in our group it was firstly tried through an epimerization using NaOMe,[86] the methodology reported by Aitken *et al.*[72] resulted to work better. In parallel, both free carboxylic acids (*S*,*R*)-**15** or (*R*,*S*)-**15** were initially transformed into primary amides (*S*,*R*)-**66** or (*R*,*S*)-**66**, in a one-pot reaction where Boc_2O, pyridine and NH_4HCO_3 were added and stirred for 4 hours. Next, epimerization on the *C*-terminus occurred under strong basic media and reflux, affording the two free carboxylic acids *trans*-(*S*,*S*)-**15** and *trans*-(*R*,*R*)-**15**, respectively (Scheme **12**).

2.3.1.2. Synthesis of the building units

The building units used for the development of the theoretical model were defined as *N*-Ac and *C*-NHMe for simplicity. Dr. Esther Gorrea prepared them as described in Scheme **14**.

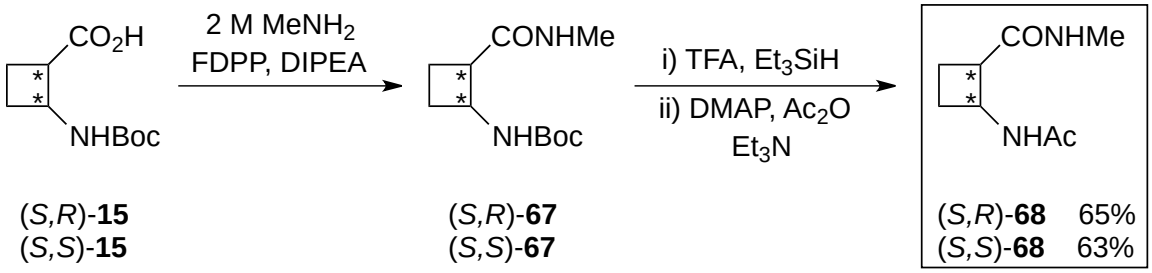

Scheme **14**. General synthesis of the building units prepared by Dr. Gorrea.

Two diastereomers were chosen because of the complementarity inside every pair of enantiomers. Starting from *N*-Boc amino acids (*S*,*R*)-**15** and (*R*,*S*)-**15**, a coupling reaction with methylamine was performed to afford both pseudodipeptides. Next, they were *N*-deprotected by strong acidolysis and subsequently acetylated. Both (*S*,*R*)-**68** and (*R*,*S*)-**68** building units were produced in 65% and 63% overall yield after three steps, respectively.

2.3.1.3. Synthesis of the dipeptides, pseudotripeptides and tetrapeptides

In collaboration with Dr. Esther Gorrea, who presented this complete study in her PhD Thesis, the peptides and pseudotripeptides containing cyclobutane residues with the same, alternate or random absolute configurations were prepared. The synthetic work was divided between Dr. Gorrea and myself and their further structural study by NMR experiments allowed to corroborate the viability of the predicting model.

Once we had the key amino acids (Figure **42**), the synthesis of dipeptides was achieved *via* a succession of amine and carboxylic acid deprotections so their derivatives could be coupled using P-containing coupling agents. Then, to obtain their corresponding *C*-NHMe derivatives, saponification followed by methylamidation were carried out. Such pseudotripeptides were synthesized due to their similarity with the buildings units aforementioned. The selected dipeptides and pseudotripeptides to be synthesized and studied were the ones in Figure **43**.

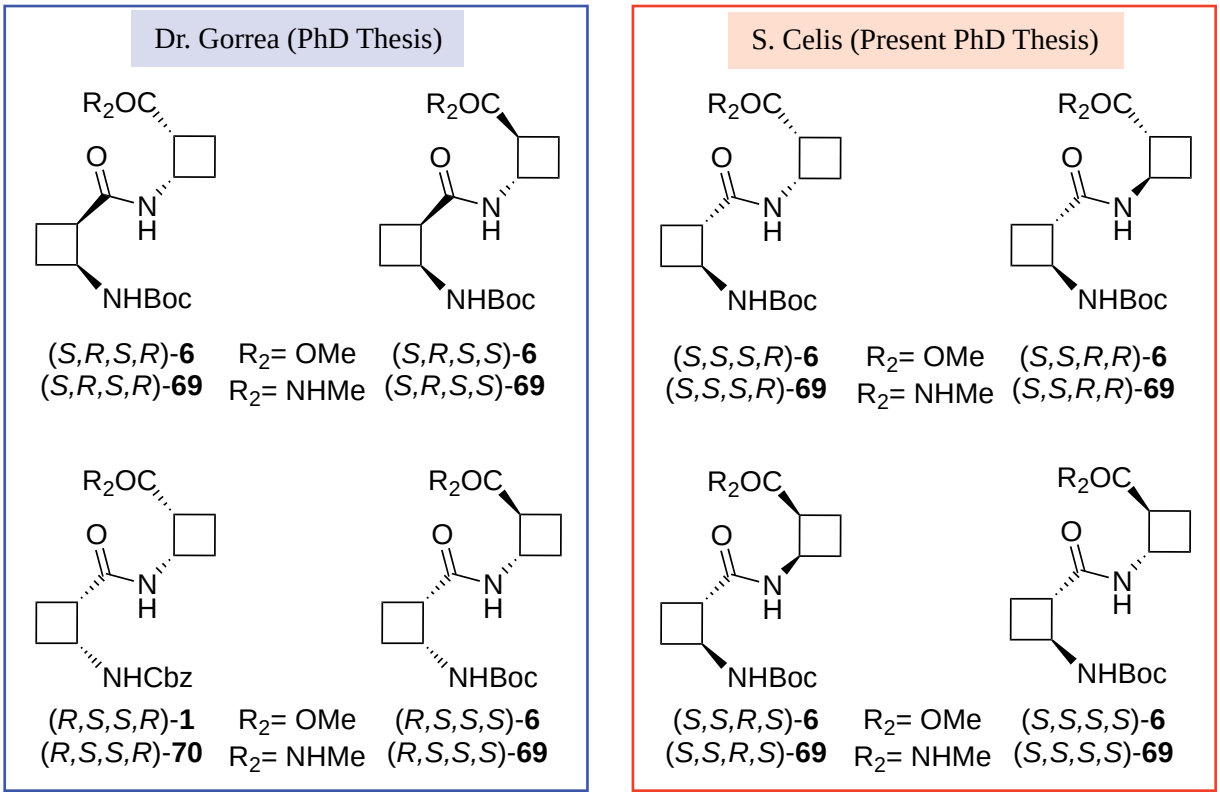

Figure **43**. Dipeptides and pseudotripeptides to be synthesized and studied.

All these products were synthesized according to the methodology shown in Scheme **15**.

On one side, saponification of the orthogonally protected monomers under mild conditions led to carboxylic acids. The free amines were obtained by selective cleavages using catalytic hydrogenation in the presence of TFA acid when *N*-Cbz or acydolisis with TFA and triethylsilane when *N*-Boc. Both ways led to trifluoroacetate salts of the amines, which were *in situ* neutralized by the DIPEA added in the coupling reaction. Such amide formation was assisted by coupling agents such as FDPP or PyBOP, both providing the dipeptides with yields from poor to excellent.

To reach the methylamine containing compounds, prior saponification using the same procedure as before was required and then, methylamidation on the carboxylic acids was subsequently achieved by a second coupling reaction employing similar conditions and a 2 M solution of $MeNH_2$ in THF. Yields were also between poor and excellent, depending on the particular chirality of each peptide.

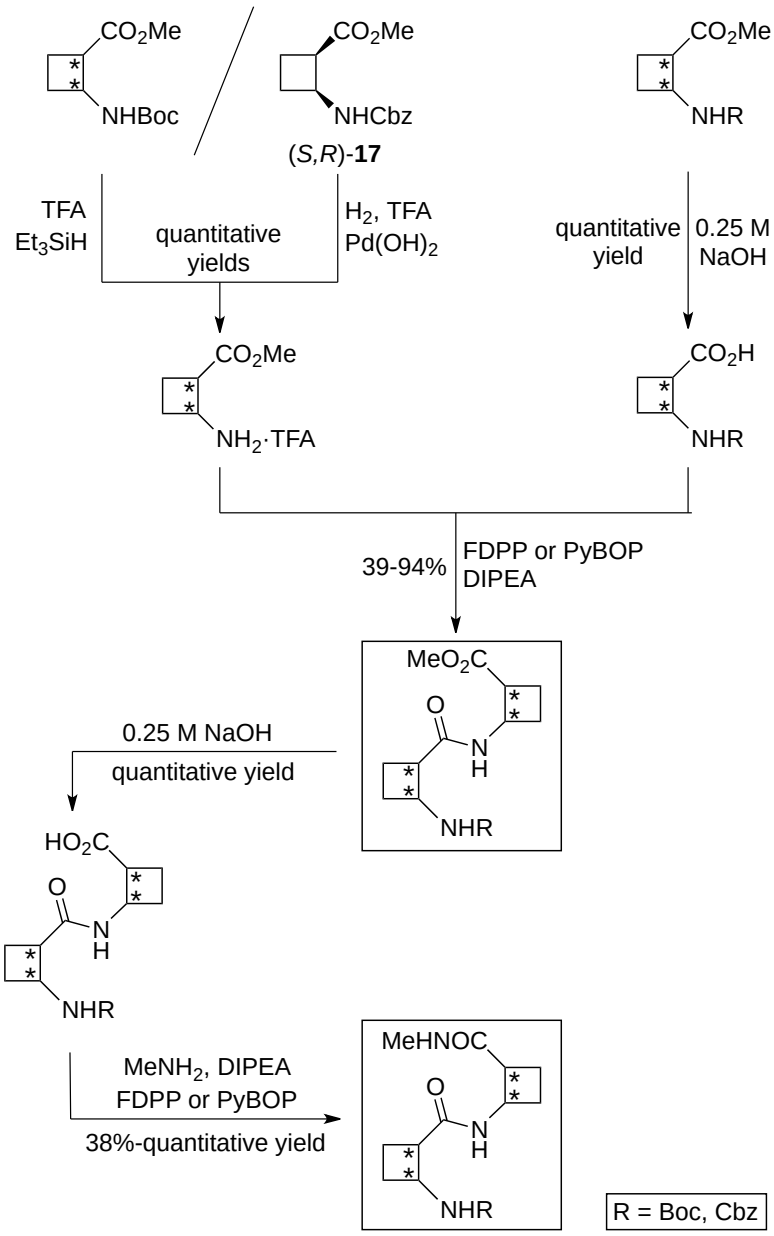

Scheme **15**. Synthesis of dipeptides and pseudotripeptides prepared by S. Celis and Dr. Gorrea.

Dr. Gorrea applied the same strategy for the synthesis of tetramers. Some selected tetrapeptides and one pseudopentapeptide were chosen as representative diastereomers, with the expectation that they would show singular secondary structures in solution according to their specific chirality. Selective *C*-OMe and *N*-Boc/Cbz deprotections and the coupling reactions were achieved by the same methodology aforedescribed.

2.3.2. Structural study in solution of the β-amino acids and β-peptides

High-resolution NMR experiments were carried out for all of them in $CDCl_3$, a solvent of low dielectric constant ($\varepsilon < 5$), suitable for conformational analysis and comparable to the results obtained by theoretical calculations and other β-oligomers investigated in our group.[9c,10,14,20] The concentrations employed were in the order of 5-10 mM so the self-aggregation was avoided. These compounds were not soluble in protic solvents like water or methanol, which in case they were, acidic protons of such solvents could affect to the conformations because they would compete in the formation of hydrogen bonds.

In collaboration with Dr. Pau Nolis, from the NMR Service of the UAB, the following NMR experiments were acquired for each of the selected compounds:

^{1}H-NMR spectrum.

^{13}C-NMR spectrum.

COSY NMR spectrum.

NOESY NMR spectrum.

HSQC NMR spectrum.

HMBC NMR spectrum.

1D selective TOCSY experiments.

1D selective NOESY experiments.

First of all, standard 1D and 2D high-resolution correlation NMR spectra allowed to do the total atomic assignation of the molecules; in addition, ^{1}H-^{1}H NOESY experiments provided intra- and inter-residual H-bond connectivities. Both NOE contacts and H-H scalar coupling constants, $^{3}J_{H\text{-}H}$, confirmed the *trans* stereochemistry of all the amide bonds within the major conformer of each peptide.

As an example of the followed procedure, experiments and results for dimer (*S,R,S,S*)-**69** are exposed and discussed in Annex section **2.5.1.**

These results were further used to computationally represent the experimental structures in order to compare them with the theoretically calculated conformations.

On one side, the NOE enhancements were chemically translated into distances between hydrogen atoms, NH_i and other H in this case. The NOE intensities were categorized as very-strong, strong, medium, medium-weak and weak signals, and their intensities were correlated to a specific distance being 2.0, 2.5, 3.0, 3.5, 4.0 and 4.5 Å, respectively. In order to give a certain degree of flexibility, a ± 0.5 Å interval was added for each distance.

On the other side, ^3J(NHCH) coupling values were related to dihedral angles and their translation was performed *via* the Karplus type curve for H-N-C_α-H_α torsion angles in peptides, proposed by Ludvingsen.[87] Here, the angle mobility was achieved by means of ± 20º interval.

Afterwards, both NOE and *J* couplings experimental NMR parameters were employed to restrain internuclear distances and dihedral angles. The iterative conformational search led to structures representing real conformers, which could be compared to the theoretical ones. The MacroModel energy minimization calculation was carried out using the molecule with the restraints described.

For example, for pseudotripeptide (*S*,*R*,*S*,*S*)-**69**, the results pointed out the presence of two possible conformers, which corresponded to $Z6_PH8_P$ and $Z8_PH8_P$, as also determined by DFT theoretical calculations (Figure **44**).

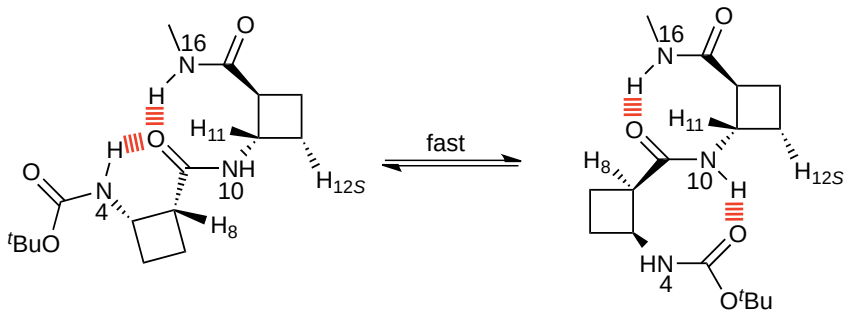

$Z6_PH8_P$ **$Z8_PH8_P$**

Figure **44**. Fast equilibrium between Z8H8 and Z6H8 conformation for pseudotripeptide (*S*,*R*,*S*,*S*)-**69**.

Trying to relate the NOE enhancements with the resulting structures, it was clearly seen that the strongest one between NH_{16}-H_{11} was explainable from both conformers, because in both of them NH_{16} was forming a stable 8-membered hydrogen bond with the carbonyl of the amide group in the middle. The NH_{10} proton had an interesting NOE enhancement because it is in the middle part of the molecule and as NH_4, could be formally forming or not a hydrogen bond. Its high fixation was compatible with both conformers although intensity of NOE was highest with H_8 than H_{12S}, what

meant a slight displacement of the equilibrium towards the Z6PH8P conformer. Nevertheless, both conformers were so similar that the results fitted well with Z8PH8P conformer too.

Comparison of experimental and theoretical dihedral angles suggested a mixture of both conformations, but also with a slightly higher population for the Z6PH8P one. However, NH_{10} did not exchange with water, what led us to think that it was involved in some hydrogen bonding or anyway protected from the solvent, which displaced the equilibrium to the Z8PH8P conformer.

So, according to all the conclusions reached from comparing experimental and theoretical results, one can state that both Z6PH8P and Z8PH8P conformers are present for (*S*,*R*,*S*,*S*)-**69** dipeptide in rather similar populations, exhibiting a fast exchange in the NMR time scale.

These NMR experiments described in detail were performed on the rest of monomers, peptides and pseudopeptides to be studied. The prevalent structures, as a cause of intramolecular red-dashed hydrogen bonds, for the monomers dipeptides and pseudotripeptides are shown in Figure **45**.

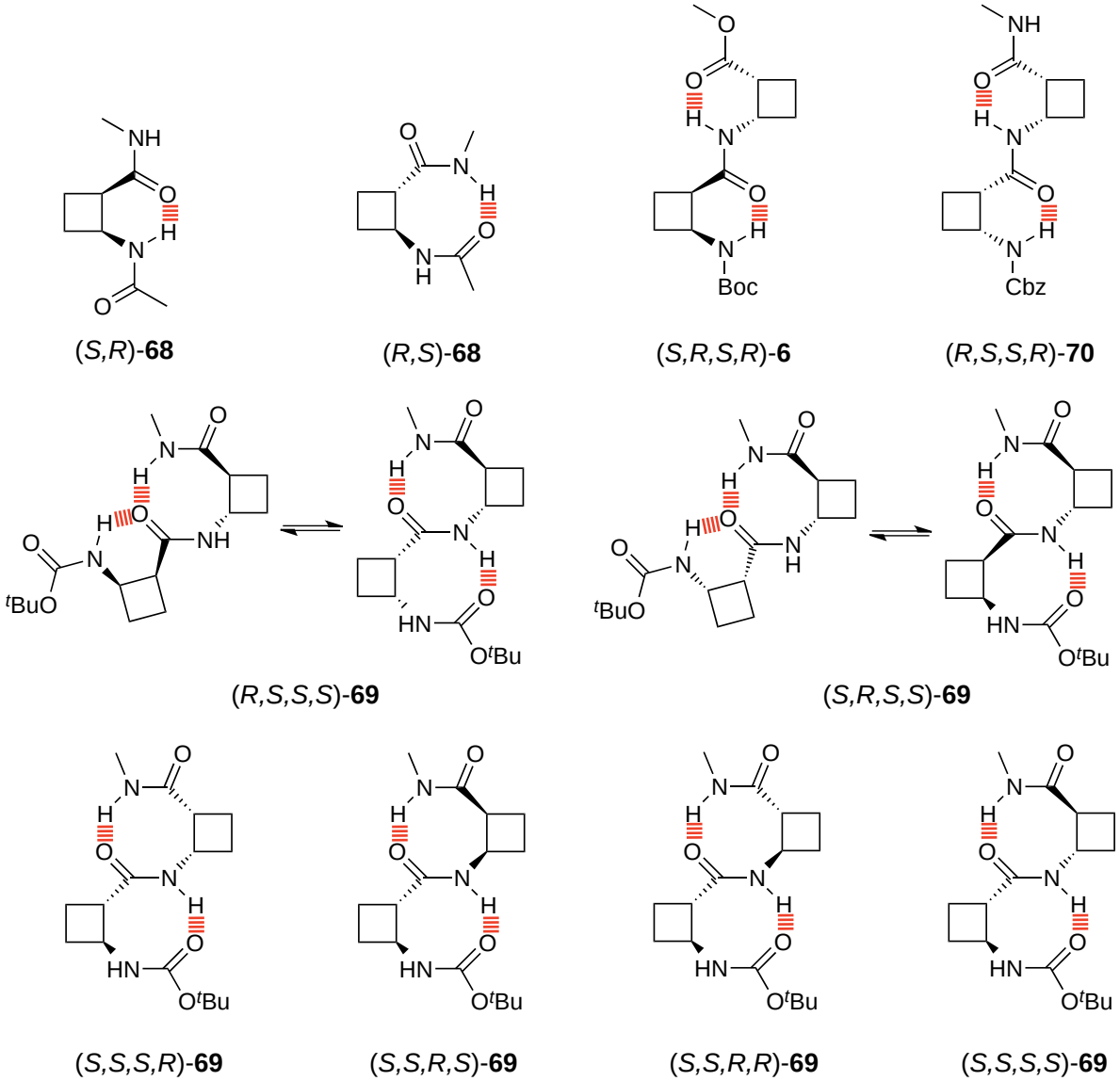

Figure **45**. Prevalent molecular structures of synthesized monomers, dipeptides and pseudotripeptides predicted by QM calculations and verified by ^{1}H-NMR experiments. Dashed red lines are for H-bonds.

Therefore, the conformation study was completed on tetramers depicted in Figure **46**, where the most stable structures are represented too. Note that as pseudopentapeptide (*S*,*R*,*S*,*R*,*S*,*R*,*S*,*S*)-**72** was insoluble in $CDCl_3$ it was studied in DMSO-d_6.

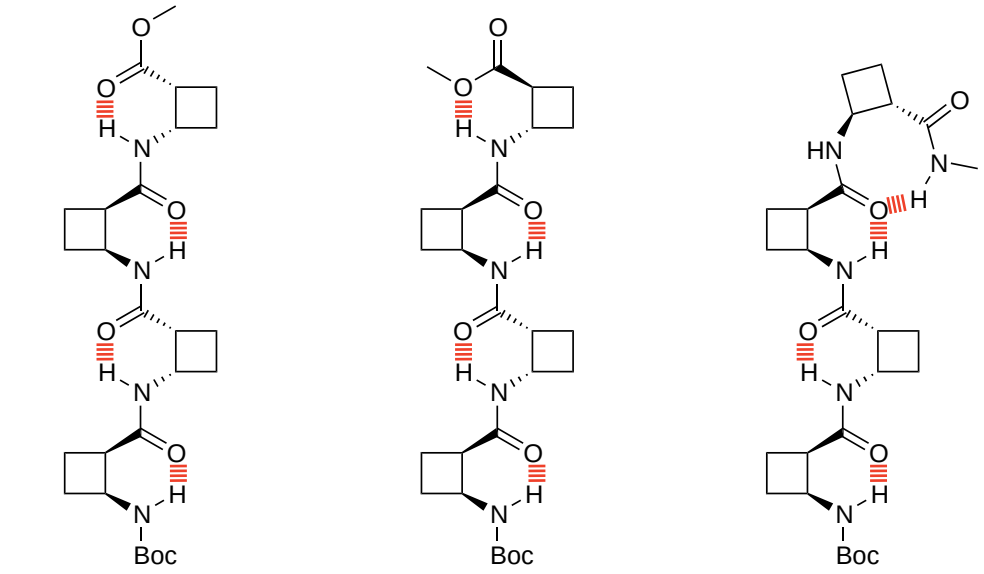

(*S*,*R*,*S*,*R*,*S*,*R*,*S*,*R*)-**71** (*S*,*R*,*S*,*R*,*S*,*R*,*S*,*S*)-**71** (*S*,*R*,*S*,*R*,*S*,*R*,*S*,*S*)-**72**

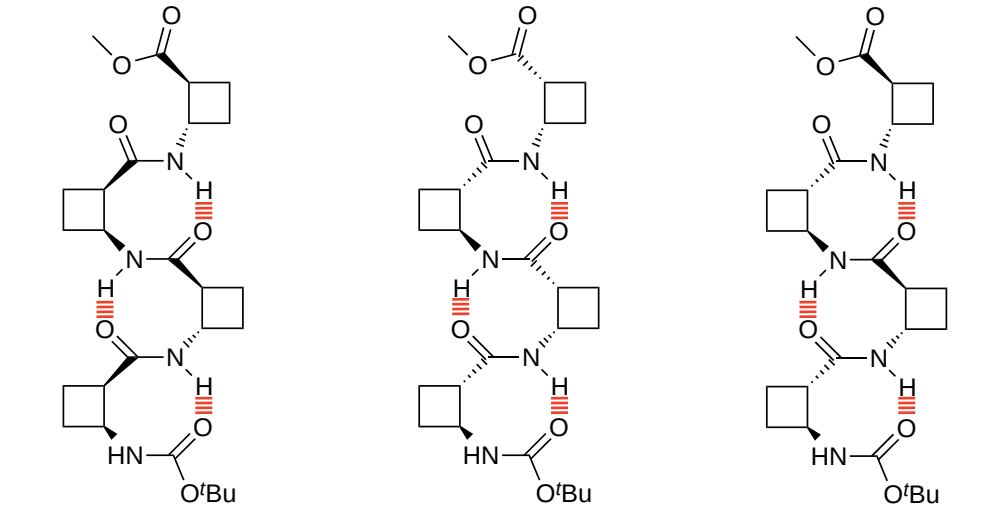

(*S*,*R*,*S*,*S*,*S*,*R*,*S*,*S*)-**71** (*S*,*S*,*S*,*R*,*S*,*S*,*S*,*R*)-**71** (*S*,*S*,*S*,*S*,*S*,*S*,*S*,*S*)-**71**

Figure **46**. Prevalent molecular structures of synthesized tetrapeptides and pseudopentapeptide predicted by QM calculations and verified by ^{1}H-NMR experiments. Dashed red lines are for H-bonds.

2.3.3. Design of the theoretical model

In collaboration with Prof. András Perczel and Dr. Gábor Pohl, from the laboratory of Structural Chemistry and Biology at the Eótvós Loránd University, Dr. Esther Gorrea, from our research group, set up this theoretical model during her stay in Budapest, Hungary.

A simple approach based on computational calculations was proposed to demonstrate that the chirality of the four 1,2-cyclobutane monomers is the responsible and controls the main overall conformation of short cyclobutane-β-peptides. Monomeric units were initially constructed with *N*-Ac and *C*-NHMe protecting groups in order to minimize and simplify the calculations, instead of using benzyl or *tert*-butyl carbamates and methyl carboxylic esters (Figure **47**).

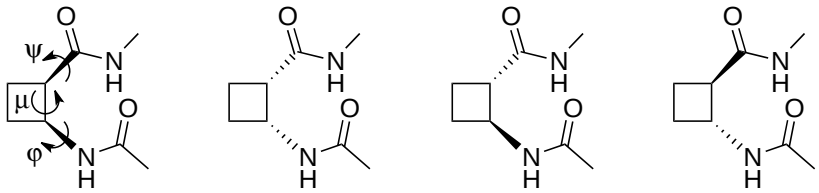

Figure **47**. Structure of the four stereoisomers representing the building units. ψ, φ and μ torsion angles are shown.

An optimization and a potential energy scanning was performed on the four monomers, resulting in 3D Ramachandran surfaces that showed energy minima. The enantiomeric conformers had opposite potential surfaces so their representative conformations were shared, as expected. These energy-minima structures were extracted and their relative stabilities were recalculated for each compound in chloroform, since further NMR experiments were going to be carried out in deuterated chloroform. Table **3** shows the energy values obtained and the Boltzmann distribution too.

Table **3**. Calculated relative stabilities of the *cis* and *trans* monomeric building units as computed at the B3LYP/ 6-31G8d) level of theory.

Compound	**Conformation**	**Compound**	**Conformation**	**ΔG[a] (% population)[b]**	
				vacuum	**$CHCl_3$**
(*S,R*)-68	$Z8_P$	**(*R,S*)-68**	$Z8_M$	8.3[c]	8.1[c]
	$Z6_P$		$Z6_M$	1.6 (79%)	1.7 (77%)
	$Z8_P$		$Z8_M$	2.4 (21%)	2.4 (23%)
	$H12_M$		$H12_P$	10.2[c]	8.4[c]
(*S,S*)-68	$H8_P$	**(*R,R*)-68**	$H8_M$	0.0	0.0 (96%)
	$H6_M$		$H6_P$	3.2[c]	1.9 (4%)

[a] Units: kcal·mol^{-1}. [b] Relative abundance values from the Boltzmann-distribution at 298.15 K.
[c] Relative abundance is < 1% of population.

As expected, the Gibbs energy values were the same for both pair of enantiomers, and so were the Boltzmann distributions too. The resulting conformations were also shared with a unique difference on the chirality, P or M. Note that the Gibbs energy values considering the solvent effect were not significantly different from the ones in the gas phase.

The geometry scans showed that the *trans* isomers, (*S*,*S*) and (*R*,*R*) stereoisomers of the monomeric building units, had more constrained structures. This fact led both monomers to mainly adopt a H8 conformation (96% of population) from the two possible ones. Those of *cis* configuration had four minima, but only two were representative, the Z6 (77%) and the Z8 (23%) (Figure **48**).

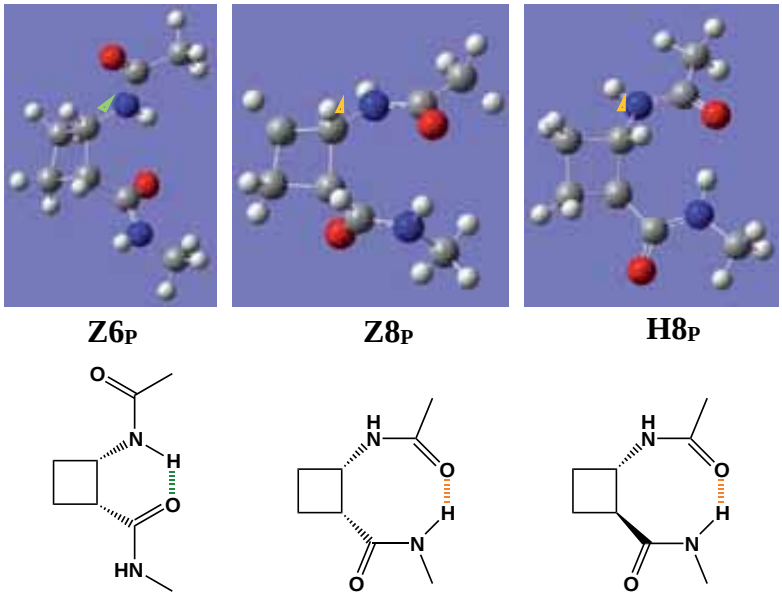

Figure **48**. Most stable conformations of the *cis*-(*S*,*R*) monomer (*left* & *middle*) and *trans*-(*S*,*S*) monomer (*right*) at the B3LYP/6-31G(d) level of theory.

Once the most stable conformations for each monomeric unit were established, the combination of four minima for the *cis* and two for the *trans* allowed the construction of all the possible structures for the dimeric and tetrameric compounds. In parallel, the predicting model was tested: by summing up the energies of the corresponding building units, a good agreement between the stabilities of the conformations obtained by the computed and the predicted calculations was observed, proving the viability of this methodology in the design of well defined foldamers.

From the last results, the formation of a novel foldamer was detected: when a *trans* and a *cis* building block were combined, a transitional Z6H8-Z8H8 conformation, both with almost equal stability, was observed (Figure **49**). The reason relied on a bifurcated hydrogen bond involving the *C*-terminal carbonyl group of the first residue and the first and third NH hydrogen atoms, which gave this (*S*,*R*,*S*,*S*) and (*R*,*S*,*S*,*S*) flipping conformation. On the other hand, dimers (*S*,*S*,*S*,*R*) and (*S*,*S*,*R*,*S*) formed only the H8Z8 structure as a major conformation because the carbonyl group is

not accessible to the first NH group aforementioned, resulting in a single hydrogen bond. Then, except the novel conformations, it was demonstrated that all the dipeptides had a unique conformer as the most stable one, among all the possible combinations. For the all-*cis* dipeptides, structures with six-membered hydrogen bonds were predominant whereas for the all *trans* compounds, the eight-membered hydrogen bonds tend to be much more present, even when they were combined with *cis* units.

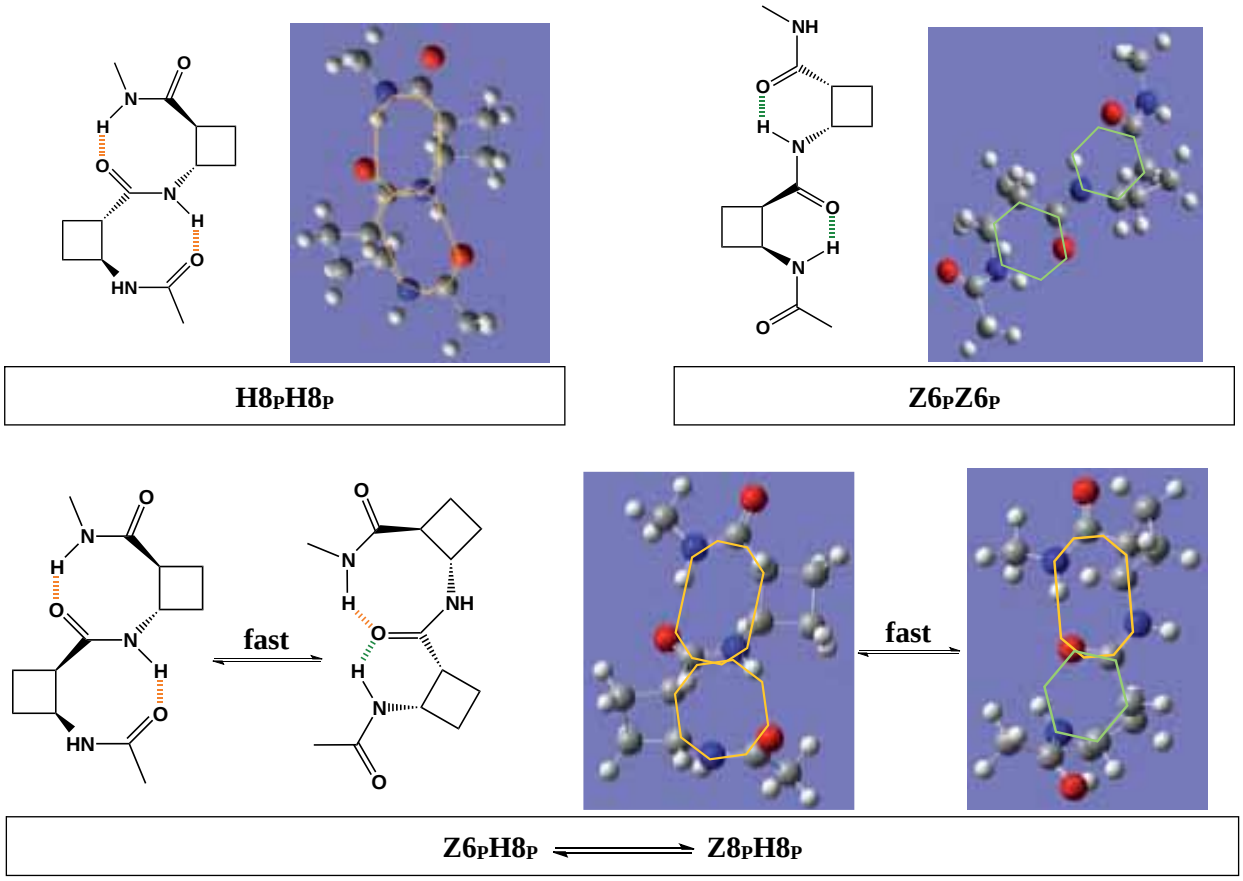

Figure **49**. Most stable structures of some representative dimers: (*S*,*S*,*S*,*S*) (*left-top*), (*S*,*R*,*S*,*R*) (*right-top*), (*S*,*R*,*S*,*S*) (*bottom*) obtained at the B3LYP/6-31G(d) level of theory.

Therefore, it can be affirmed that an evident conformational restriction exists due to the presence of the cyclobutane moiety, considering the fact that for each foldamer formed by two building units a total of 81 (9^2) conformers could have been expected.

The application of the model (summing up the energies of the monomers) to predict the most stable conformations of tetramers gave predicted energy values with a minimum error respect to the calculated values (calculation of the whole molecule), making the model to be highly reliable. In addition, predicted energy values were summed up also considering dimers as building units of tetramers (Table **4**). A tendency on the tetramers with a *cis*-residue on the *N*-terminus was observed, so that when this occurred, the tetramers presented more than a unique possible conformation with

notable relative population. This was caused again by the flipping structure Z6H8 ⇌ Z8H8, which appeared when the *N*-terminus was a (*S*,*R*) or (*R*,*S*) cyclobutane moiety. Anyway, the exception that proves the rule, was the case when all the residues were *cis* and then the most stable conformation was Z6Z6Z6Z6, as previously reported by our group.[17]

Table **4**. Conformer relative stabilities of selected tetramers as predicted from monomers, dimers and as computed at the B3LYP/6-31G8d) level of theory.

Compound	**Conformation**	**ΔG[a]**		
		Predicted[c]		**Calculated[b]**
		from monomers	**from dimers**	
(*S*,*R*,*S*,*R*,*S*,*S*,*S*,*S*)	Z6ᵖZ6ᵖH8ᵖH8ᵖ	3.2	4.4	7.6
	Z6ᵖZ8ᵖH8ᵖH8ᵖ	4.0	5.7	8.0
	Z8ᵖZ8ᵖH8ᵖH8ᵖ	4.8	6.6	7.3
(*S*,*R*,*S*,*R*,*S*,*R*,*S*,*S*)	Z6ᵖZ6ᵖZ8ᵖH8ᵖ	5.6	7.9	10.7
	Z6ᵖZ6ᵖZ6ᵖH8ᵖ	4.8	7.8	9.4
	Z8ᵖZ8ᵖZ8ᵖH8ᵖ	7.2	10.1	11.0
	Z6ᵖZ8ᵖZ8ᵖH8ᵖ	6.4	9.2	11.0
(*S*,*R*,*S*,*S*,*S*,*S*,*S*,*S*)	Z8ᵖH8ᵖH8ᵖH8ᵖ	2.4	3.5	3.8
	Z6ᵖH8ᵖH8ᵖH8ᵖ	1.6	3.4	4.5
(*S*,*S*,*S*,*S*,*S*,*S*,*S*,*S*)	H8ᵖH8ᵖH8ᵖH8ᵖ	0.0	0.0	0.0
(*S*,*R*,*S*,*R*,*S*,*R*,*S*,*R*)	Z6ᵖZ6ᵖZ6ᵖZ6ᵖ	6.4	8.8	9.3

[a] Units: kcal·mol^{-1}.
[b] Calculated Gibbs energy computed at the B3LYP/6-31G8d) level of theory.
[c] Predicted Gibbs energy by addition of single building units' energies.

Thus, the model employs a simple and good methodology to predict the most stable structures adopted by short β-peptides, with a maximum of four cyclobutane residues. This stands to reason because longer β-peptides could give non-predictable foldings such as 10-, 12- and 14-helices. However, to make sure that these conformations were not stable for short systems, the three of them were constructed and calculated for some representative tetramers and, all of them resulted in much more unstable structures than the Z6 and H8.

In the comparative study, φ, ψ and μ torsion angles were determined by a computational method and extracted from the experimental data of the prepared molecules. Their comparison led us to

conclude the good agreement between both theoretical and experimental conformations, confirming the validity of the theoretical model, from which the design of foldamers can be achieved by simple combination of the buildings units, what reminds of a lego game (Figure **50**).

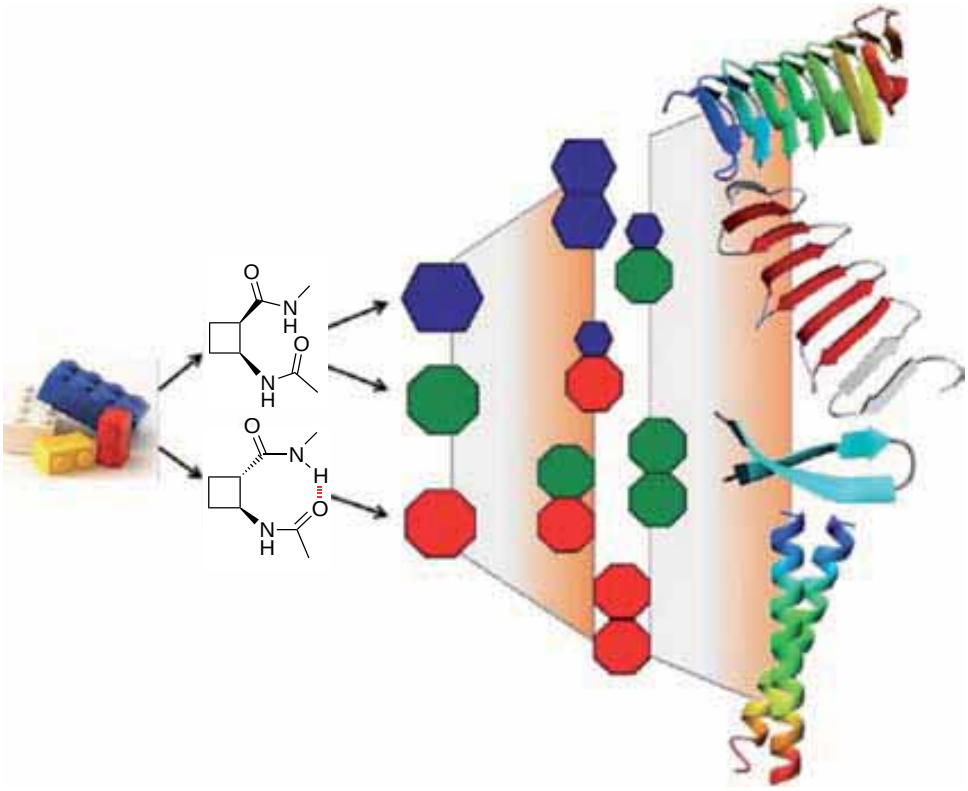

Figure **50**. The rational design of any short new β-peptide with a defined folding becomes possible by simply combing the appropriate lego conformational building units.

2.4. SUMMARY AND CONCLUSIONS

A new theoretical model for the prediction and design of foldamers, constituted of polycyclobutane β-peptides up to tetramers, has been satisfactorily developed. For this objective, the stability of all the possible conformations for the monomeric building units forming the peptides was calculated. *cis*-Monomers preferred intraresidual 6-membered ring linear hydrogen bonds (Z6) while the *trans*-units adopted 8-membered ring twisted hydrogen bonds (H8), with greater stability. By summing the conformational energies of the units, in order to construct dimers and tetramers, their conformations could be easily predicted unequivocally, allowing the preparation of any foldamer with a previously designed structure.

The validation, consisting in the conformational study in $CDCl_3$ using high-resolution NMR, was performed for selected monomers, dimers and tetramers. Most of them were new compounds, synthesized in their enantiomerically pure form and were fully characterized. By means of NMR experiments, the adoption of a secondary structure was determined in all cases. Quantum mechanics calculations were carried out employing NMR data as structural restrictions and, the resulting structures were fully comparable with the calculated molecules, so validating the theoretical model.

Thus, based on the structural properties of a given protein fragment, epitope, or subunit to be mimicked by foldamers, the right combination of the appropriate ACBC stereoisomer subunits makes feasible the unambiguous design and subsequent synthesis of new cyclobutane β-peptides presenting solely the desired secondary structural form. Biologically active foldamers of almost any kind can now be issued by simply condensing the correct sequence of lego elements.

CHAPTER III

Spacer-containing Hybrid Cyclobutane Peptides as Foldamers and Low Molecular Weight Gelators

3.1. INTRODUCTION

ω-Amino acids and their use for the synthesis of novel foldamers reproducing helical or extended foldings has been clearly demonstrated in the previous chapter, in which the synthesis and study of polycyclobutane β-peptides has been tackled. The combination of the residues, that could differ or not in their stereochemistry, showed a great effect in the secondary structures adopted by the corresponding oligomers. However, their backbone structure was homogeneous, so totally formed by cyclobutane amino acids.

3.1.1. The role of hybrid peptides

An alternative approach to prepare peptidomimetics is to strategically replace α-amino acids from a peptide sequence with closely related β-amino acids.[88] However, single approaches do not assure a proper peptidomimetic because when some factors are optimized other can be threatened. In a theoretical assumption for instance, in a sequence of ten amino acids, if only one is replaced by a homologated analog, the corresponding peptidomimetic might be still cleaved by proteases. Moreover, in an α,β-peptidomimetic of eleven amino acids (Boc-Val-Ala-Phe-Aib-β-Val-β-Phe-Aib-Val-Ala-Phe-Aib-OMe), the helical folding of the homo-α-peptide was maintained. Although a bit expanded, Roy and co-workers concluded that the helix was not disturbed despite the insertion of an homologated β,β-spacer.[89]

Thus, if novel foldings are desired to be obtained, other approaches may be entailed. The combination of amino acids of different peptide backbone, this is to say, synthesizing α,ω-peptides with less proportion of α-amino acids and totally unnatural ω,ω-peptides, could be a good solution. The backbone of the resulting peptides would be heterogeneous and therefore, they would be hybrid peptides. A definition given by Karle *et al.* says that hybrid polypeptides are heteropolymers composed of diverse ω-amino acids, and they are of special interest in attempts to mimic all α-peptide backbones, using sequences containing non-proteinogenic amino acids.[90]

With the intention of addressing the latter proposals, a different strategy from the changeable stereochemistry for the study of secondary structures was applied. Taking homogeneous poly(*cis*-cyclobutane) β-peptides, various α- and γ-spacers were alternatively introduced in order to observe and determine if any structural effects were involved.

Almost all the α-induced structural motifs (helices, β-turns, β-sheets...) have been demonstrated to be generated also by hybrid peptides. Regarding the extended foldings, Gellman, for instance, reported compound **73** in which two alanine residues in alternation with a *D*-proline glycolate

afforded antiparallel β-sheet-like structure. The change in the peptide chain orientation was caused by the proline-based residue, which adopted a β-turn-like conformation. Further transformations playing with different substituted alanine residues proved their influence in providing more or less β-sheet character to the extended strands of the molecule. When the *D*-proline glycolate was replaced by an heterochiral β-dipeptide analogue of nipecotic acid, the resulting structure **74** kept its β-sheet conformation. The new spacer, introduced between the β-alanine residues resulting in a hybrid β,β-tetrapeptide, also induced a β-turn (Figure **51**).

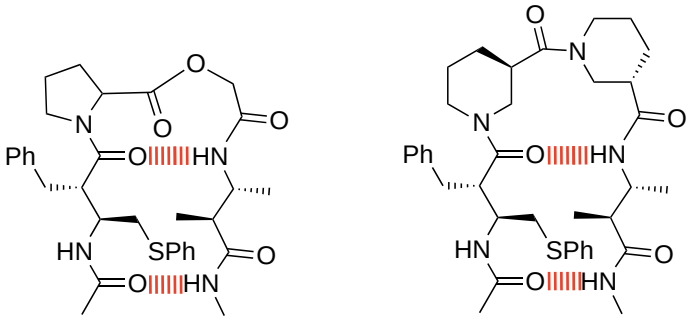

73 **74**

Figure **54**. Two β-alanine-containing peptidomimetics **73** and **74** constituting part of a β-sheet-like structure.

All these β-sheet-like foldings were self-assembled in antiparallel orientation, corroborating the affirmation of some authors.[91-94] They state that polar (antiparallel) sheet formation is a property of ω-amino acids with an even number of backbone atoms between the NH and CO groups. In account to that, if our α- and γ-amino acid-containing hybrid peptides gave sheet-like structures, their orientation would be in a parallel-non-polar way.

On the other hand, our group firstly reported a hybrid β-alanine-containing β,β-tetrapeptide in which a helical structure was found to prevail in chloroform solution.[11]

It should be noted that if the number of backbone atoms are considered, correspondence may be obtained between α,ω- and ω,ω-sequences and a stretch of α-residues. For instance, this equivalence, since hydrogen-bonding patterns are directly associated to specific structural motives, could be a good approach to custom-designed hybrid foldamers. Hence, n-membered hydrogen bonds could be constructed as suggested by the following hybrid dipeptide sequences (Figure **52**).

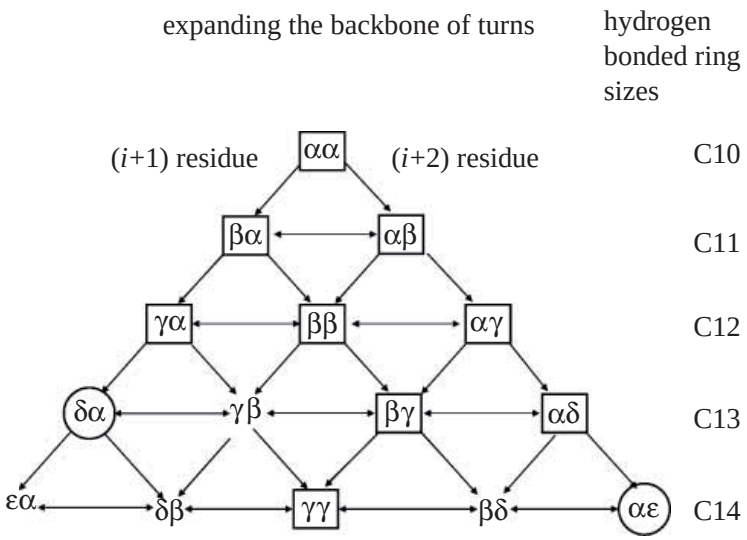

Figure **52**. Hydrogen-bonded ring sizes that can be generated in principle from hybrid dipeptide sequences, the hydrogen- bond directionality being the same as in normal all a- polypeptide structures. Turns encircled with rectangles have been characterized in single crystals by X-ray diffraction. Turns established only by NMR are indicated with circles. Figure extracted from reference 95.

Moreover, some structural equivalences have been determined. γ-Turn (C_7), based on an α-residue, can be provided by a β-alanine residue, resulting in an expanded γ-turn (C_8), while two β-alanine residues (C_{12}) can act like a expanded β-turn of two α-residues (C_{10}). When β- and γ-amino acids are combined in a dipeptide (C_{13}), α-turn (C_{13}) can be analogously mimicked (Figure **53**).[95,96] Applying this to the peptides to be studied, the cyclobutane moiety could act as a γ-turn inductor itself. On the contrary, it would participate, in units constituted with one or both of the α- or γ-linear residues in each side, in other structural motifs.

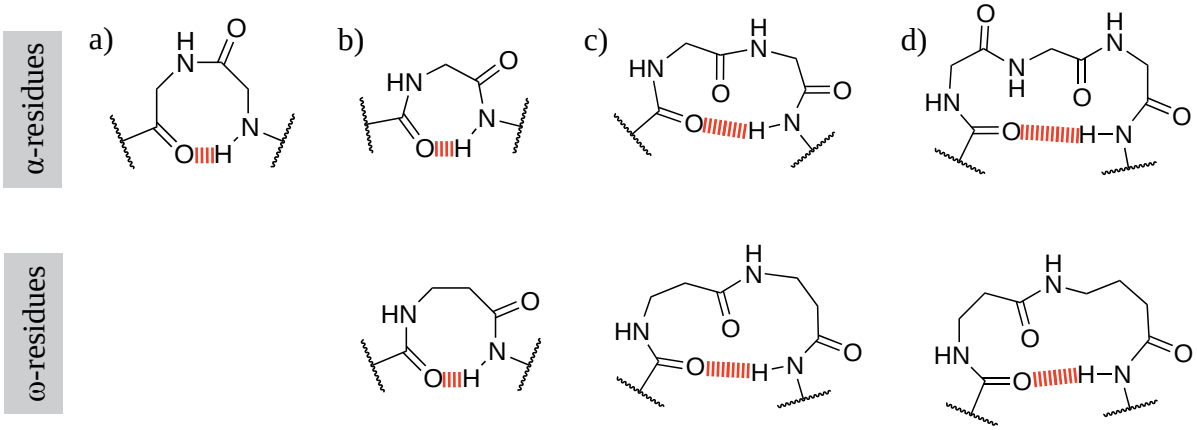

Figure **53**. Schematic illustration of turns in all α-residue segments (*top*) and their equivalence in ω-residues (*bottom*). a) δ-turn (C_8). b) γ-turn (C_7). c) β-turn (C_{10}). d) α-turn (C_{13}). Red-dashed lines represent hydrogen bonds.

From this modified heterogeneous new peptides, structural effects can be studied particularly and relationships between spacer and effect can be stated, so requested foldings can be achieved by strategically designing hybrid peptide sequences.

3.1.2. Low Molecular Weight Gelators (LMWGs)

Gels have always arisen curiosity since they are soft materials with particular properties between the liquid and solid states. However, a gel is a material easier to recognise than define.[97] Many definitions are given but in general, gels are colloidal materials with components arranging into 3D self-assembled fibrillar networks (SAFINs) which immobilise the flow of the bulk 'liquid-like' solvent phase in which is formed. Thus, two components, the gelator and the solvent, are arranged in a supramolecular phenomenon inside a medium with a density close to liquids but with a structure more similar to solids.[98,99]

A general description of a material like a gel needs of several parameters to be determined:[100-102]

1. Rheology-morphology properties to prove the new soft material is a gel *per se*:
   - Reproducible *Tube Inversion Test* is the common way to evaluate the jelly nature of a new material. When turning upside down the vial where the gel has been prepared gravity proves its resistance to drop.
   - Viscosity defines a weak or a strong gel in terms of consistency.
   - Turbidity is related to the light that the material allows to pass through, being classified as transparent or opaque gels. Coloured gels can be obtained too.

2. Thermodynamic properties:
   - Thermoreversibility: once the gel is formed (usually by changes in temperature), its heating and posterior cooling should provide the gel again. Mechanical reversibility is found in some soft materials too.
   - Temperatures of gelation (T_{gel}) can be determined for both solution-gel (cooling) or gel-solution (heating) processes.

3. Structural/self-assembly properties can be studied by:
   - IR spectroscopy (NH and CO, comparison between solid, solution and gel states)
   - NMR
   - CD
   - TEM, SEM and cryo-SEM
   - Theoretical calculations

4. Minimum gelation concentration (*mgc*) is the minimum quantity of gelator necessary to gel a solvent at specified experimental conditions.

An excellent organogel is that one containing the minimum quantity of gelator, what means that the gel *mgc* must be below 1-2 mg per mL of solvent. Hence, this little proportion of the gelator has to present three main powerful characteristics:

- Strong and directional intermolecular interactions.
- Capability to form interwined aggregates between the 1D fibrils.
- Presence of factors preventing neat crystallization of the gelator molecules.

3.1.2.1. Classification of gels

A simple classification of gels is based on the bonds responsible for the supramolecular self-assembly of the gelator molecules. When these bonds are covalently attached one can find the chemical gels, in general constituted by polymers (polyamides, polyesters, etc.). On the other hand, when the 3D network is self-assembled by non-covalent interactions, the resulting gels are classified as supramolecular or physical gels.[98,99]

Inside them, and depending on the media where they are formed, a subdivision can be displayed. If the solvent is aqueous or organic, hydrogels and organogels can be defined respectively. Ambidextrous gels are rare but also exist, having the capability of gelling both aqueous and organic solvents, and when the solvent has been replaced by gas, one can have aerogels, with interesting properties like very low density, porosity and high thermal insulation. Finally, in the xerogels, which are usually employed for the supramolecular studies of the respective gels, the solvent has been fully removed by drying. Among the supramolecular gels, the most common gelators are the Low Molecular Weight Gelators (LMWGs) or the Low Molecular Mass Organic Gelators (LMOGs), in which the supramolecular gelator is a small organic molecule, typically with molecular mass < 3000. A wide range of organic molecules including long chain hydrocarbons,[103,104] saccharides,[105,106] amides,[107-110] ureas,[101,111-113] steroid derivatives,[114-116] multi-component systems[117-120] and others[121-123] can act as LMOGs.

Gels were initially discovered by serendipity and the Aromatic-Linker-Steroid (ALS) is an example. Although gelation can be also caused by any of the three components of ALS individually, twenty years ago Weiss and Lin found out the gelation properties of CAB (Figure **54**). This was constituted by the ALS structure and was one of the first reported LMOGs.[124,125] From then on, many ALS-based molecular approaches were investigated with the aim of creating new gelators.

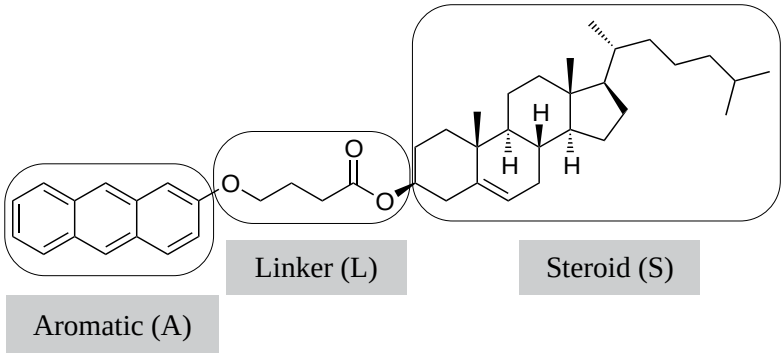

Figure **54**. Chemical structure of cholesteryl 4-(2-anthryloxy)butyrate, CAB.

A miscellaneous group includes different types of LMOGs as dendrimers,[127,128] macrocycles,[129,130] sugar derivatives[131-135] and salt-based gelators,[136-138] which can not be classified in other groups because their specific structure is equal or more important than their chemical bond nature or their gelation ability. In recent years, organometallic compounds have also attracted interest in this field. Organogels constituted of metal complexes can be useful for catalytic, or not, organic synthesis, providing new functionalizable material supports.[139-141]

Nevertheless, since the hydrogen bonds are a useful tool to form stable supramolecular assemblies, peptides and oligopeptides are, together with amides, carbamates and ureas, one of the most used scaffolds for the preparation of gels.

3.1.2.2. Peptide and amide-based LMWGs

Hydrogen bonds are amongst the most important elements to give hierarchical arrangements in nature. In fact, they participate from the formation of DNA double helix to the aggregation of β-amyloid deposits, causing Alzheimer disease. This is possible because the formation of amide-amide hydrogen bonds is favoured in the hydrophilic biological media by entropy.[142,143] In the hydrogels field, the diversity of amino acid side chains, combined with the stability of amide bond, and their pH-dependent chemistry, opens a variety of applications in tissue engineering,[144-146] molecular electronics[147,148] or drug delivery[149] for instance, in a race towards the maximum biocompatibility with the biological systems. On the other hand, in the lipophilic media, amide-amide hydrogen bond is enthalpy driven amounting to a negative Gibbs energy change ΔG of -6.7 ± 1 kcal/mol. Low molecular weight peptides, often incorporating hydrophobic amino acids, have been widely employed as organogelators.[150-155] Peptides aggregate through hydrogen bonding whereas the apolar groups maintain the solubility in the organic solvent and avoid the precipitation. The crucial role of solubility in LMWGs was reported by Smith, Miravet and collaborators.[156] Their investigation highlighted that the minimum gelation concentration and the macroscopic thermal

stability (T_{gel}) could be rationalized in terms of solubility and a cooperative self-assembly model. Indeed, peptide gels are an elegant example of supramolecular assemblies, where numbers of small molecules self-assemble into 1D fibrous arrangements in most cases.[157] These fibrous microstructures entangle among themselves through surface tension and capillary forces entrapping the solvent, with the consequent loss of fluidity.[158]

Some examples of LMWGs are going to be mentioned as an outlook of the different kind of amide-based structures with gelating capability. Probably, the most simple amide gelators are monoamides and monocarbamates. Employing tris(alkoxy)benzamide scaffold or linear derivatives of the 11-aminoundecanoic acid (AUDA), LMOGs were prepared, some of them showing great capabilities of gelating both very polar aprotic solvents as DMF and apolar solvents as *n*-decane.[159,160] Diamides have been also reported, being the derivatives of *trans*-diaminocyclohexane one of the most studied scaffolds. Hanabusa prepared good organogelators by derivatising the cyclic diamine with long alkyl lipophilic chains or alkyl chains with terminal functional groups. Nevertheless, the cyclic triamides published by Hanabusa and Shirota are widely known in this field. Both authors worked with the trimesic acid, functionalizing it with alkyl amines. Short alkyl amines or methyl substitution of the amide protons resulted in compounds incapable of gelating the solvents.[161,162] Much more efficient triamide gelators were the ones based on *cis*-1,3,5-cyclohexanetricarboxylic acid and long alkylamines, which derivative with seventeen -CH_2- groups had promising applications as an electrochromic material (Figure **55**).[100]

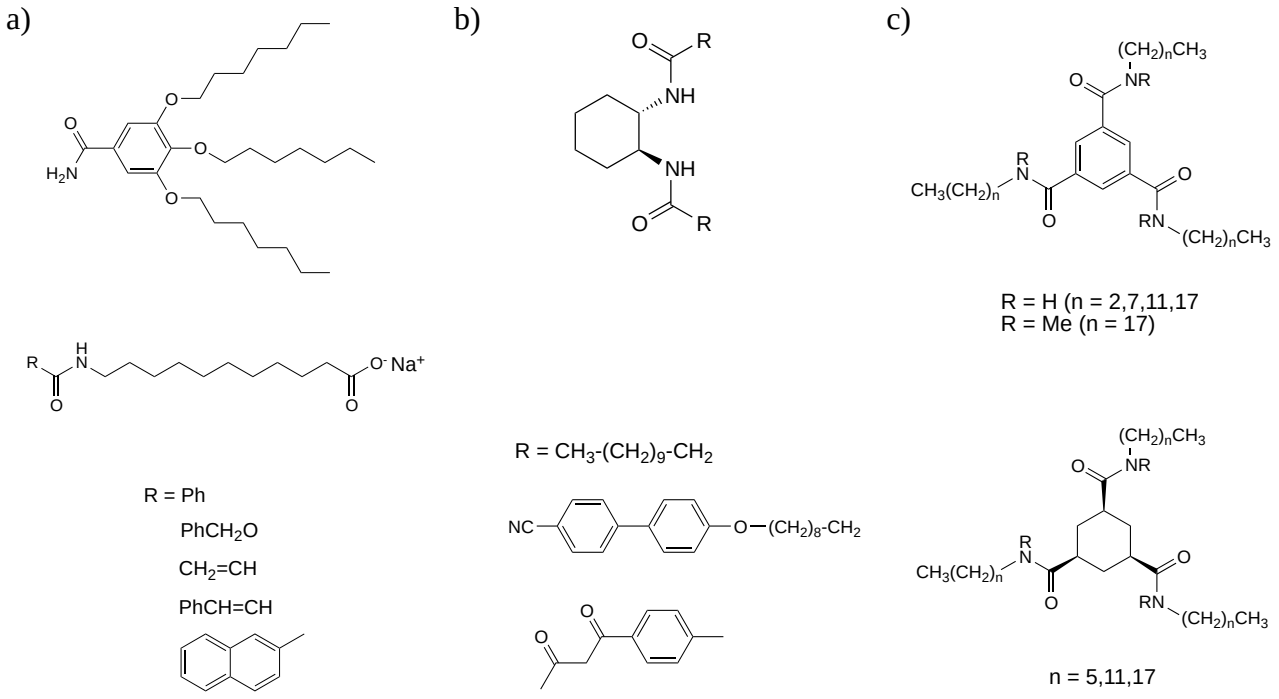

Figure **55**. Some examples of amide-based organogelators. a) Mono-amides. b) *trans*-Cyclohexanediamines. c) Benzene-1,3.5-tricarboxamides (*top*) and cyclohexane-1,3,5-tricarboxamides (*bottom*).

Although they reported hydrogelators, it is interesting to make reference to Feringa and van Esch, [163,164] who on the contrary, used lipophilic amino acids with the same cyclohexane scaffold. Their compounds, presenting acidic or basic terminal groups, exhibited impressively efficient gelation of water at *mgc* of 0.3 to 0.8 mg/mL. In fact, the employment of amino acids for preparing LMWGs has provided a wide range of compounds, and their intrinsic amphiphilic nature makes unavoidable to mention the hydrogelators. Combination with long alkyl chains enlarges their applications in gelating both aqueous and organic solvents. Indeed, *N*-lauroyl-*L*-Ala compound was found to efficiently gelate various higher-alkane and aromatic solvents, including fuels, at *mgc* values between 2 and 12 mg/mL, even in the presence of water. If two phasic fuel-water systems are tested the gelator selectively gelates the oil phase, revealing a potential use in sea oil transport accidents. Recently, its methyl ester derivative led to gels with applications in drug delivery systems.[149] Another amphiphilic gelators are the bolaamphiphiles or bola-type gelators, with a structure in which two polar groups are separated by a lipophilic group, usually a long alkyl chain.[150,165,166] Nevertheless, they have been also prepared without alkyl spacers.[167] Among the cyclic amino acid LMOGs, Escuder and Miravet synthesized peptidomimetic cyclophanes based on *m*-phenylene and two identical amino acid units bridged by diaminopolymethylenes of variable length. These compounds showed good gelation of aromatic solvents in the range of 3-5 mg/mL (Figure **56**).[129,168]

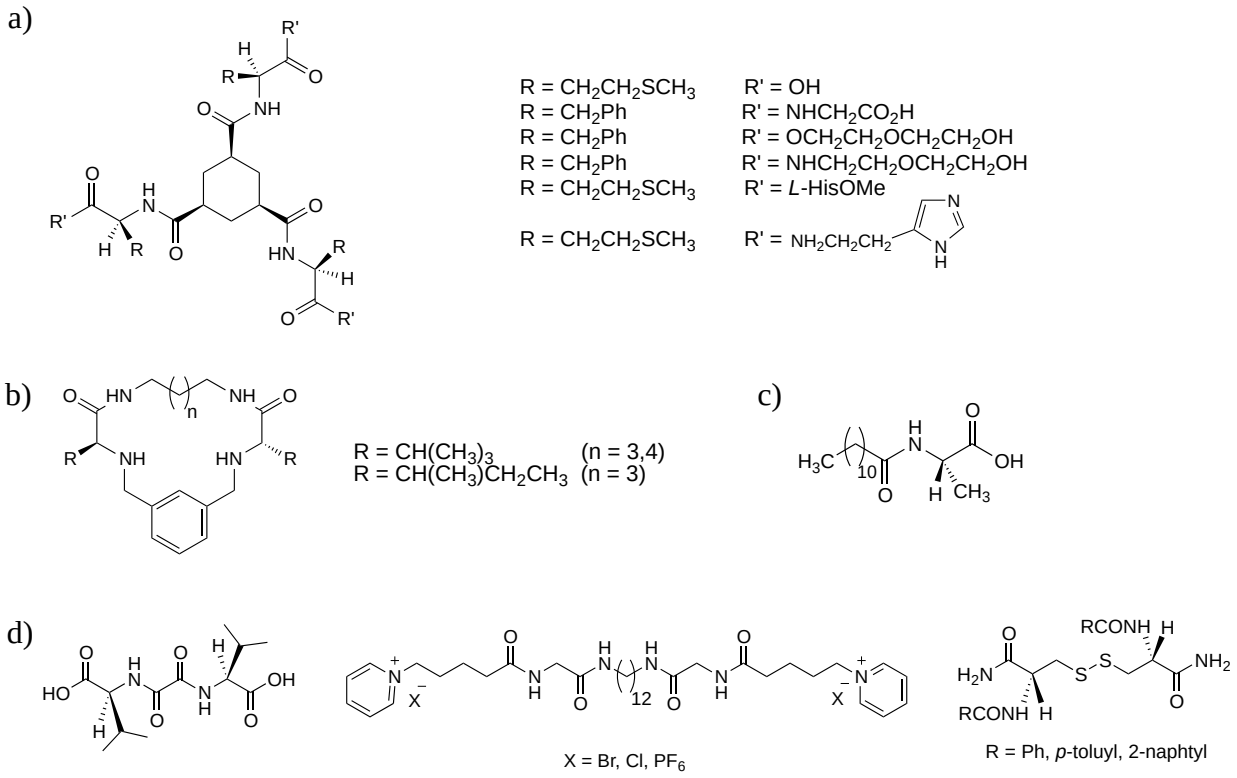

Figure **56**. Some examples of amino acid-based LMWGs. a) Hydrogelators based on *cis*-1,3,5-cyclohexanetricarboxylic acid. b) Cyclic gelator reported by Val and Ile. c) *N*-lauroyl-*L*-ala selective organogelator. d) Bola-type gelators.

Small peptidic gelators are also directed towards the creation of biomaterials and therefore they are investigated to provide hydrogelating properties. However, LMOGs can be achieved with simple peptide structures of just few amino acids (Figure **57**). Tripeptides **75** and **76**, differing only in one of the three amino acids, exhibited different supramolecular arrangement.[169] While **75**, containing 2-aminoisobutyric acid (Aib) showed a β-turn motif, causing gelation of some apolar solvents, compound **76**, constituted by glycine instead of Aib, showed an extended conformation which led to antiparallel β-sheets, that did not provide gels but crystals. Escuder and Miravet reported the LMOG **77** synthesized by inspiration of natural silk, Gly-Ala-Gly-Ala (GAGA).[170] The supramolecular study revealed an antiparallel β-sheet self-assembly too. In a search for an accurate model of amyloid fibrils, related to Alzheimer diseases, the amphiphilic tripeptides **78**, **79**, **80** and **81** were investigated.[171,172] Their novelty lies on the particular behaviour in solvents of opposite polarity and very different dielectric constants. They could gelate solvents of low polarity like benzene, cyclohexane and CCl_4, in which they formed inversed bilayers with the alkyl chains pointing out of the aggregates. In medium polarity solvents as $CHCl_3$ they did not form aggregates and in water, on the contrary, they gave translucent dispersions formed by bilayers with the polar groups pointing outwards (Figure **57**). Working for similar goals, Atkins reported a compound based on oxidized glutathione, which exhibited antiparallel β-sheet-like arrangements in polar solvents as DMSO and in H_2O/DMF and H_2O/MeOH mixtures.[173]

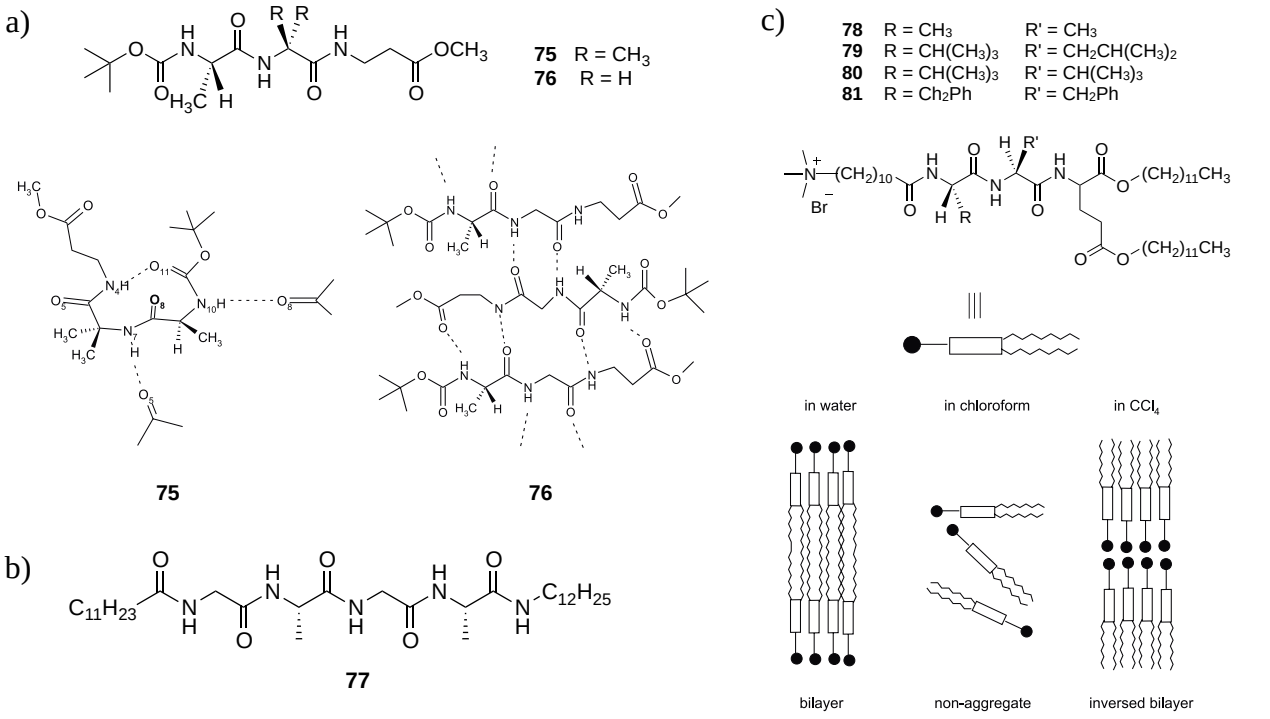

Figure **57**. Amino acid-based LMWGs showing β-sheet-like assemblies. a) Replacement of Aib (**75**) by Gly (**76**) showed different arrangement. b) Silk-inspired LMOG. c) Amphiphilic gelator with switchable folding by solvent polarity.

Cyclobutane-containing LMOGs

Besides the gels obtained in our group with homo-[9b] and heterochiral[14] oligopeptides as mentioned in the general introduction, in the literature, very little examples where the cyclobutane moiety forms part of gelator are found. Dastidar uses organic salt gelators, the supramolecular self-assembly of which is based on strong and directional hydrogen bonding, as well as stronger but less directional electrostatic interactions.[138,158,174] In all his reported publications, he employs the cyclobutane 1,1-dicarboxylic acid in its anionic form and different amines as cations as a two-component organogelator. In fact, this special case of multi-components LMOGs are interesting because they afford materials with highly tuneable microscopic and macroscopic properties, due in part to their salt nature, that results in very defined supramolecular structures (Figure **58**).

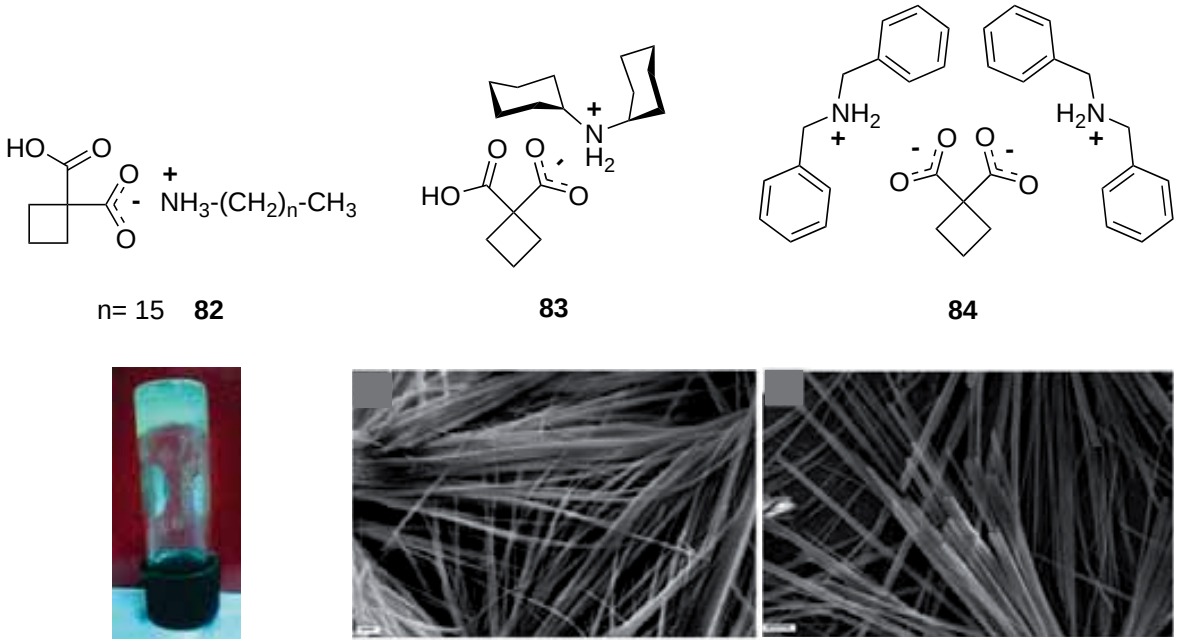

Figure **58**. Some examples of two-components LMOGs containing the cyclobutane motif. Compound **82** forms a stable gel in nitrobenzene at 2 mg/mL concentration (*left*). Compounds **83** and **84** form needle-like supramolecular structures observed by SEM (*middle* and *right*).

The amines constitute the positive-charged component of the gelator, being of alkyl, cycloalkyl, or aromatic nature or even imidazolidine cationic derivatives. For instance, compound **82** forms a very stable gel with nitrobenzene at a very low concentration, under 2 mg/mL (5 mM). A series of primary ammonium salts with n-alkyl amines were studied as a function of alkyl chain length. While salts with $n < 11$ did not show any gelation ability, salts with $n > 11$ could gelate many solvents, specially for the compound with n=15 (Figure **58**).

3.2. OBJECTIVES

Since the influence of the cyclobutane ring stereochemistry has been successfully proved, other possibilities have been considered in order to disrupt the folding of poly(*cis*-cyclobutane) β-peptides. To provoke that effect and promote new foldings some spacers have been introduced between the cyclobutane residues, considering both rigid and flexible units. In addition, the utility of the cyclobutane motif in hybrid systems to enhance gel formation was investigated. In order to achieve this purpose the following goals were proposed:

• Synthesis of a pseudodipeptide and a pseudotetrapeptide, as a result of combining a cyclobutene diacid with (1*R*,2*S*)-methyl 2-aminocyclobutanecarboxylate (*S*,*R*)-**59** and its corresponding homogeneous dipeptide (*S*,*R*,*S*,*R*)-**46**, respectively.

• Synthesis of a homologated series of hybrid peptides, from dimers to octamers, as a result of the combination of β-cyclobutane and α-, β- and γ-linear amino acids. Glycine, β-alanine or GABA units are intercalated between (1*R*,2*S*)-2-aminocyclobutanecarboxylic acid residues providing heterogeneous-backbone peptides with increasing degrees of freedom, respectively.

• Structural study, by NMR experiments and theoretical calculations, of some selected hybrid pseudopeptides and peptides as a representative group of all the series, in order to state the spacer effect in the the secondary structure.

• Gelation study of some cyclobutane-linear-containing tetrapeptides, with the aim of proving their Low Molecular Weight Gelator ability in common solvents. A supramolecular study is carried out on some selected gels.

3.3. RESULTS AND DISCUSSION

The introduction of spacers into the sequence of poly(*cis*-cyclobutane) β-peptides, which show a defined β-ribbon-like secondary structure, was expected to have some crucial structural effect regarding their different backbone. Such introduction would disrupt the hierarchical hydrogen-bond pattern of intraresidual six-membered rings in the way that new interactions would take place or not, providing new or same/distorted foldings respectively (Figure **59**).

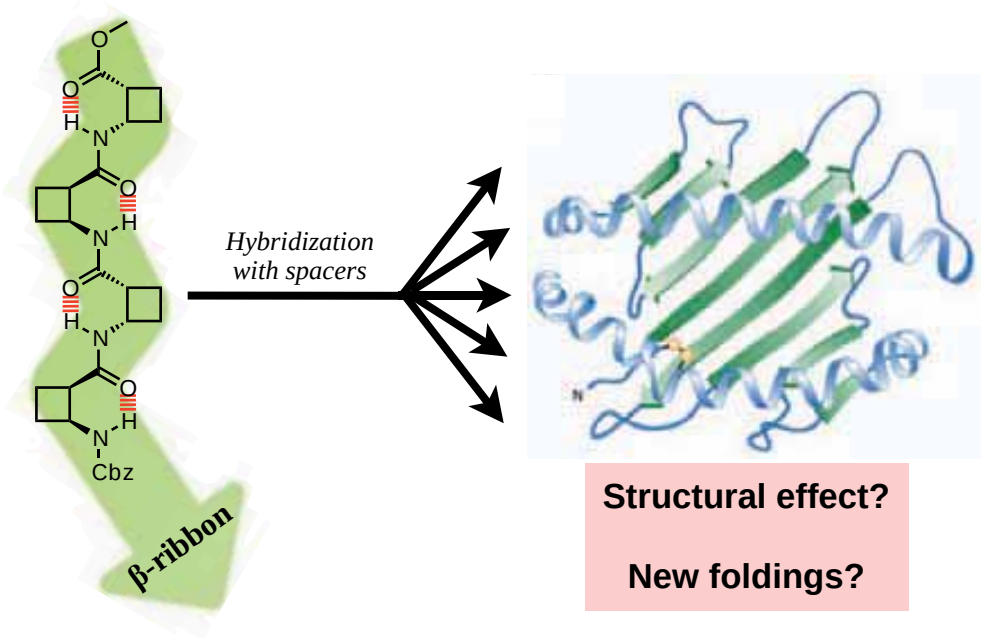

Figure **59**. By means of introducing distinct backbone spacers into homochiral polycyclobutane peptides, which show β-ribbon secondary structure, the associated structural effect was studied aiming for spacer-induced new foldings.

Using the (1*R*,2*S*)-2-aminocyclobutanecarboxylic acid (*S*,*R*)-**59** as the common rigid structural base, spacers have been intercalated between the cyclobutane residues. The rigid intercalator was proposed to be a cyclobutene ring while the flexible one would be a linear amino acid. Within the flexible intercalator, three spacers differing in their length have been tested.

3.3.1. Synthesis of cyclobutene-containing hybrid peptides

The synthesis of cyclobutene-containing hybrid peptides was firstly approached as the preparation of a dipeptide in which one of the cyclobutane rings was additionally constrained by a double bond. A cyclobutene-cyclobutane hybrid dipeptide was tried to be synthesized but, no isolation of the required cyclobutene amino acid precursor was found because of its intrinsic instability. Although the synthesis of *cis*-cyclobutene β-amino acid was not successful, their open-chain derivatives and other related compounds were obtained. Therefore, the cyclobutene moiety was decided to be

introduced as a cyclobutene diacid **85**, which combined with cyclobutane amino acids would provide hybrid pseudopeptides (Scheme **16**).

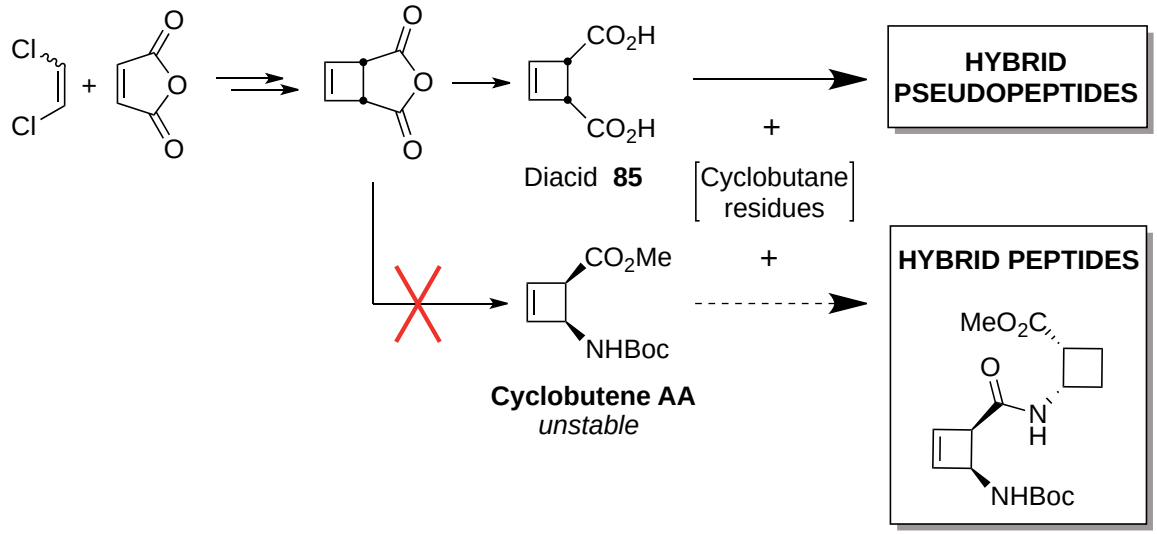

Scheme **16**. Synthetic approaches towards hybrid pseudopeptides and peptides.

3.3.1.1. Synthetic studies of cyclobutene amino acids and derivatives

A photochemical reaction between maleic anhydride **86** and *cis*-/*trans*-1,2-dichloroethylene **87** at -40 ºC afforded quantitatively a mixture of dichloro-cycloadducts **88a**, **88b** and **88c**. This reaction was performed as described by Dr. Esther Gorrea in her PhD Thesis.[175] Then, reductive elimination of the chlorides was optimized and carried out following the methodology reported by Huet *et al*.[176] Distillation under reduced pressure (1 mbar, 70-85 ºC), afforded the cyclobutene anhydride **89** as a white crystalline solid in 51% of isolated yield (Scheme **17**).

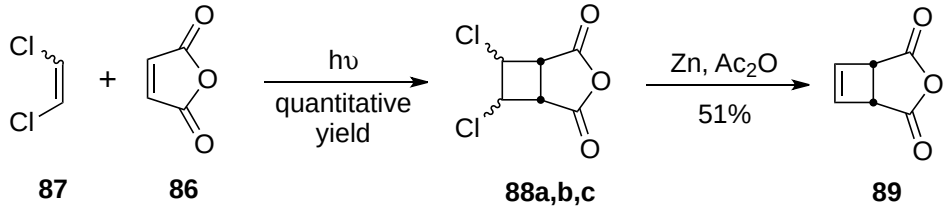

Scheme **17**. Synthesis of cyclobutene anhydride **X** in two steps.

Sometime, byproducts were identified during the reduction reaction with Zn. As a result of bad anhydrizing/drying of the reactants/solvents or the presence of prior unreacted starting materials, cyclobutene diacid **85** and succinic anhydride **90** were observed in some mixtures (Scheme **18**).

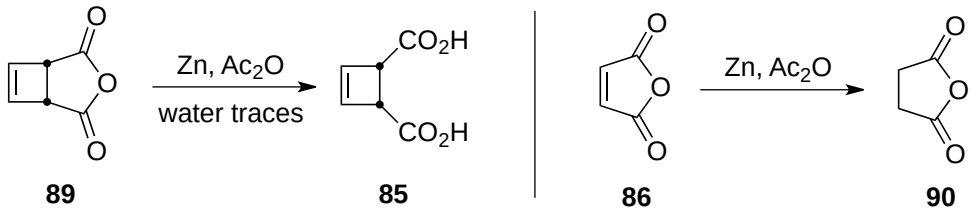

Scheme **18**. Side reactions during the preparation of cyclobutene anhydride **89**.

The anhydride ring-opening by acid-catalyzed methanolysis was primarily carried out at 50 ºC during 5 hours but (2*Z*,4*E*)-dimethyl hexa-2,4-dienedioate **91** was the major product in the mixture instead of cyclobutene compound **92** (Scheme **19**).

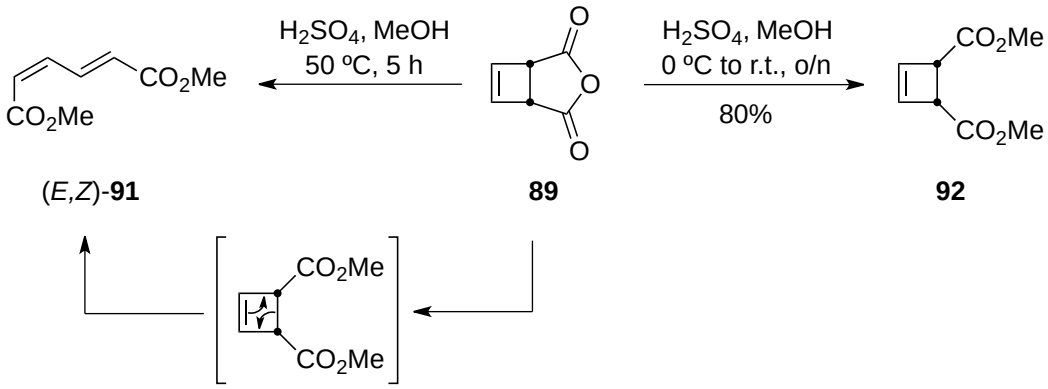

Scheme **19**. Both experimental conditions tested for the synthesis of diester **92**.

This thermal isomerization was already described by Hess *et al.*[177] so the experimental conditions had to be optimized. In order to avoid ring-opening, sulfuric acid was added to the ice-cooled solution of the reactants and the reaction was stirred overnight at room temperature.[178] Distillation at 1 mbar of pressure and between 40 and 65 ºC afforded cyclobutene diester **92** in 80% yield. Nevertheless, first attempts of distillation resulted in open-chain side-products too; the critical thermal isomerization temperature was found to be 65 ºC at 1 mbar of pressure.

As the Woodward-Hoffmann Molecular Orbital (MO) theory rules predict, in the electrocyclic reactions, cycloadditions or cycloreversions a *principle of conservation of the orbitals symmetry* exists. Such reactions can take place by both thermal or photochemical activation; in the thermal ones, the symmetry of the cyclobutene HOMO orbital determines the process.[179,180] In order to keep symmetry the ring-opening bonds involving 4 π electrons have to turn conrotatorily.[181] This movement can take place in both directions but, as the starting cyclobutene is in its *meso* form, just the (*E*,*Z*) isomer was obtained at the given temperature, displaying the stereospecificity of the reaction.

On the other side, trying to optimize the synthetic route, Zn reduction to obtain the cyclobutene diester **92** was carried out on the mixture of cyclobutane diesters **93a,b,c** (Scheme **20**). However, the desired product was not obtained.

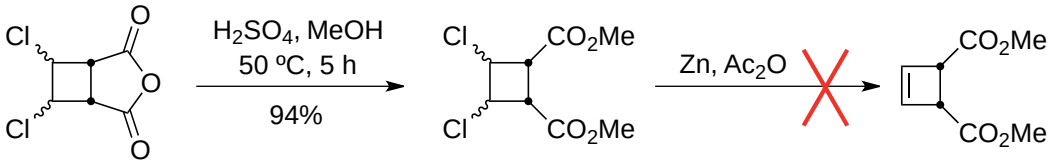

88a,b,c **93a,b,c** **92**

Scheme **20**. Alternative approach for the synthesis of cyclobutene diester **92**.

The asymmetric induction to provide the chiral hemiester (*S,R)*-**94** was carried out following two methodologies:

a) Enzymatic methodology was applied as for the saturated cyclobutane series: using *PLE*, the prochiral-*S* centre was hydrolyzed following the same procedure, also reported by Crout *et al.*,[182] with a 86% *ee*. In order to confirm that the enantiomer obtained was the (1*S*,2*R*)-**94**, the specific rotation was determined in acetone as $[\alpha]_D$= +11.34, in good agreement with the value $[\alpha]_D$= +11.08 found in literature.[178] The best yield obtained for this reaction was 70% without needing further purification (Scheme **21**).

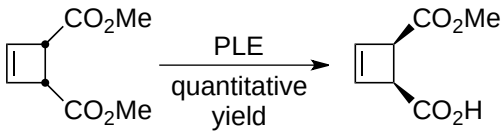

92 (*S,R*)-**94**

Scheme **21**. Enzymatic desymmetrization for the synthesis of cyclobutene hemiester (*S,R*)-**94**.

b) Chiral auxiliary methodology: using quinine and quinidine, desymmetrization of *meso* anhydrides in the presence of alcohols was reported by Bolm.[63,64] The procedure is an alcoholysis in which the chiral assistant opens the anhydride attacking one or the other prochiral centre, as explained in section **2.1.1**. Therefore, this methodology was tried to be performed using methanol and quinine, due to our objective of obtaining the (1*S*,2*R*)-**94** enantiomer. However, the reaction was tried three times with quinidine and once with quinine: in all cases hemiesters (*S,R*)-**94** and (*R,S*)-**94** were observed by NMR, respectively (their absolute

configuration was supposed to be the one according to the stereospecificity of chiral auxiliaries), but it only was possible to isolate some product from an experiment performed with quinidine and distilled starting cyclobutene anhydride **89**, obtaining 4% of hemiester (*R*,*S*)-**94** (Scheme **22**). The reaction needs special equipment for a slow drop-by-drop addition of the alcohol into a solution containing the anhydride and the auxiliary at -55 ºC. Regarding these results, it was decided to continue through the enzymatic methodology.

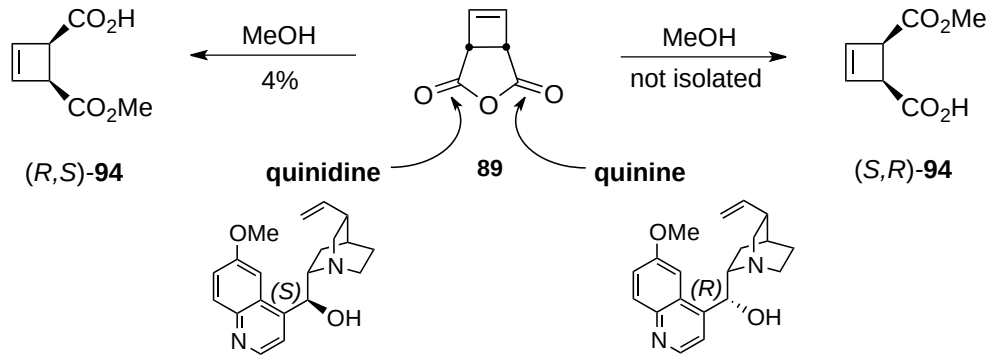

Scheme **22**. Quinine- and quinidine-mediated synthesis of the cyclobutene hemiester (*S*,*R*)-**94** and its enantiomer (*R*,*S*)-**94**.

Finally, the synthesis of the cyclobutene amino acid **95** was attempted: first, the preparation of the azide derivative was easily solved by activation of the free carboxylic acid in hemiester (*S*,*R*)-**94**, and subsequent substitution of the mixed anhydride employing NaN_3. Next, the Curtius reaction was performed but, as it needs high temperature (T ≃ 80 ºC), the production of the cyclic amino acid was supposed not to occur. In fact, column chromatography afforded the open-chain orthogonally protected amino acid (2*E*,4*E*)-**96**, in 6% isolated yield from the hemiester (Scheme **23**). Other unidentified byproducts were observed and several attempts more were carried out at lower temperatures (T < 80 ºC) without satisfactory results.

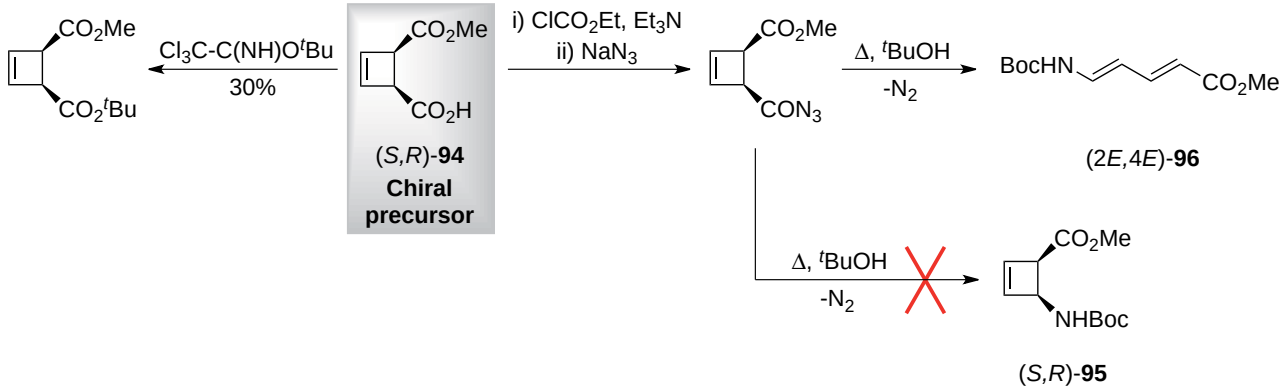

Scheme **23**. Synthesis approach towards the unstable cyclobutene amino acid (*S*,*R*)-**95** from the chiral hemiester**.** In this case, open-chain amino acid (2*E*,*4E*)-**96** was obtained.

On the other hand, an orthogonally protected diester was synthesized. Reaction of hemiester (*S*,*R*)-**94** with *tert*-butyl 2,2,2-trichloroacetimidate in anhydrous dichloromethane afforded methyl *tert*-butyl diester derivative in 30% yield, because some part of the product seemed to decompose during column chromatography. Next, due to the impossibility of obtaining cyclobutene amino acids observed in the enantiomeric series, this path was not further studied (Scheme **23**).

Similar ring-opening behaviour was found in the literature, where some authors stated that the synthesis of such compounds was not viable. Cyclic systems with a conformational tension as cyclobutane and even more the cyclobutene rings, undergo electrocyclic isomerization resulting in the ring opening because of the temperature. Huet and Gourdel-Martin,[183] in their study of analogues of Norcarbovir® antiretroviral drug, were not able to synthesize cyclobutene β-amino acid in Figure **60** (*left*). Other compounds also undergo partial ring opening even at room temperature. Moreover, their purification by column chromatography in silica-gel increases the final proportion of the open form (Figure **60**).

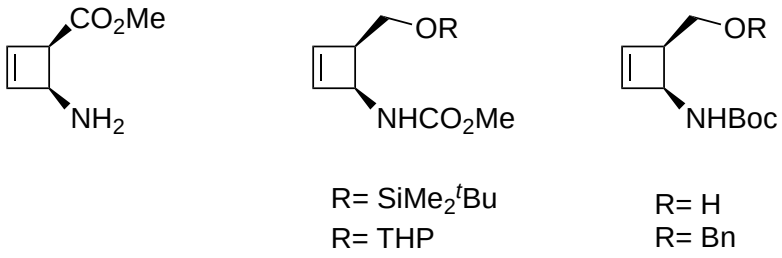

Figure **60**. Some examples of thermally unstable cyclobutene compounds. (1*R*,4*S*)-methyl 4-aminocyclobut-2-enecarboxylate (*left*) an other unstable cyclobutene compounds.

Huet and Gauvry,[184] in their work about the synthesis of dienamides from cyclobutene compounds, concluded that the lactam opening with LiOH and MeOH took place through the unstable cyclobutene intermediate (*S*,*R*)-**95**, which rapidly underwent the open diene form (2*E*,4*E*)-**96** (Scheme **24**). Considering that, as Woodward-Hoffmann rules state, the ring opening had to be with the conrotatory turn of the substituents, the major isomer to be formed would be the (*E*,*Z*). So, the fact that only isomer (*E*,*E*) was observed was explained by an additional isomerization of *Z* bond from *cis* to *trans* configuration, more thermodynamically stable, due to the basic medium, for which the authors reported that some precedents existed.

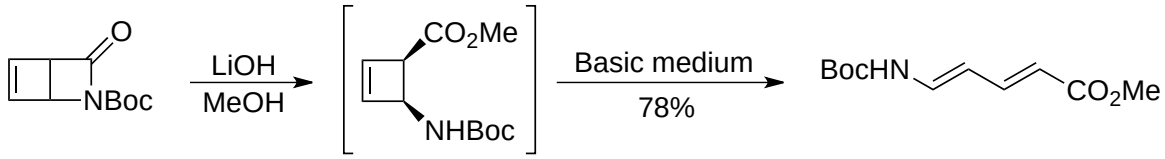

(*S*,*R*)-**95** (2*E*,4*E*)-**96**

Scheme **24**. Synthesis of open-chain amino acid (2*E*,4*E*)-**96** from the cyclobutene lactam**.** Authors suggested that the cyclobutene amino acid (*S*,*R*)-**95** was the unstable intermediate.

The more acceptable reasoning for our case, since basic medium was not possible, was the thermal isomerization of the (2*E*,4*Z*)-**96** to the (2*E*,4*E*)-**96** isomer, given that the Curtius reaction was carried out from 80 to 120 ºC. A mechanism for this transformation has been proposed, and although the ring-opening step has been considered to take place after the cyclobutene amino acid formation, it probably could happen during the Curtius rearrangement (Scheme **25**).

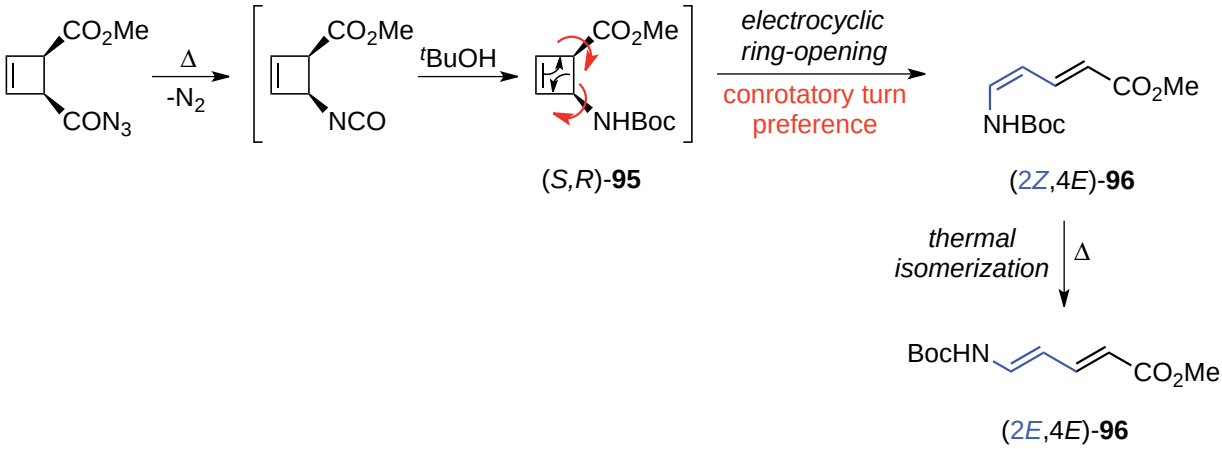

(*S*,*R*)-**95** (2*Z*,4*E*)-**96** (2*E*,4*E*)-**96**

Scheme **25**. Proposed mechanism for the synthesis of (2*E*,4*E*)-**96**. Cyclobutene amino acid (*S*,*R*)-**95** is suggested to be an unstable intermediate although prior ring-opening on isocianate or acylazide derivatives would be also possible.

In addition, theoretical studies performed by Houk's group affirm that the allylic substituents nature in the cyclobutene ring has a decisive effect in the velocity and stereoselectivity of conrotation. It is known that π-donor substituents (amines for instance) and π-acceptor substituents (carboxylic esters) have, in adjacent positions, a complementary conrotatory preference. This fact is explained by, besides the Woodward-Hoffmann theory, the energetic stabilization of the MOs because of the distinct overlapping with p_π atomic orbitals of the substituents, in the electrocyclic ring opening transition state. The stereoselectivity given by the turn preference in one or the other direction is named as torquoselectivity.[179]

At that point, compound (*E*,*E*)-**96** was fully characterized and the open form was corroborated by specific rotation, which showed a $[\alpha]_D$= +1.26 low value, comparable to zero. The (*E*,*E*) stereochemistry of double bonds was confirmed by comparison of the olefinic protons couplings to the ones reported by Huet and Gauvry.[184]

This is why our approach to cyclobutene-containing peptides was modified into a new proposal, in which cyclobutene diacid would act as rigid spacer between cyclobutane residues, what would result in highly conformationally restricted pseudopeptides.

3.3.1.2. Synthesis of pseudodipeptide 97 and pseudotetrapeptide 98

Since the amino and carboxyl groups in a β-position are not allowed to be in a cyclobutene ring, both carboxyl groups were proposed to be carried by a cyclobutene moiety whereas the amino groups, on the other side, would be provided by methyl (1*R*,2*S*)-2-aminocyclobutanecarboxylate and its corresponding amino-deprotected dipeptide (Figure **61**).

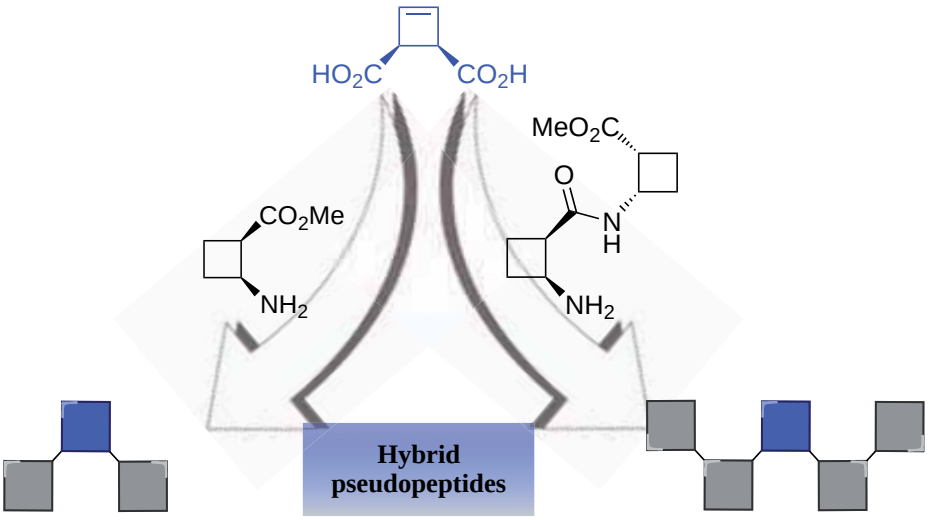

Figure **61**. Synthesis of cyclobutane-containing pseudopeptides in which the cyclobutene ring acts as structural spacer.

Cyclobutene *meso*-diacid **85** could be easily afforded by hydrolysis of cyclobutene anhydride **89**, the reaction of which was performed following a procedure reported by Novak.[185] This consisted in adding 10 eq. of H_2O into an anhydride solution in acetone and let it to be stirred at room temperature overnight (Scheme **26**). These conditions were mild and the unsaturated ring integrity was preserved. The work-up just required evaporation of solvent at room temperature. The diacid was obtained as a white solid in quantitative yield, and further purification was not necessary.

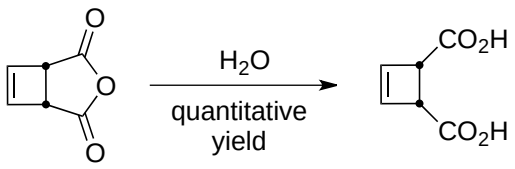

89 **85**

Scheme **26**. Hydrolysis of the cyclobutene anhydride to provide diacid **85**.

Synthesis of the pseudodipeptide was achieved by coupling diacid **85** with amino acid (*S*,*R*)-**59**, using DIPEA as base and FDPP as coupling agent, in anhydrous DMF and under nitrogen atmosphere (Scheme **27**). Pseudodipeptide **97** was obtained in 20% yield. Taking in account that two couplings took place in a one-pot reaction, the single yield for every coupling would be 45%. Nevertheless, low yield was mainly attributable to the easy electrocyclic ring opening of the cyclobutene ring, favoured in part by the purification in silica. Its longer analog was similarly prepared, but using bis-cyclobutane dipeptide (*S*,*R*,*S*,*R*)-**46** in its trifluoroacetate salt form. Two column chromatography purifications were also necessary, in EtOAc and MeOH, to provide pseudotetrapeptide **98** in 14% yield.

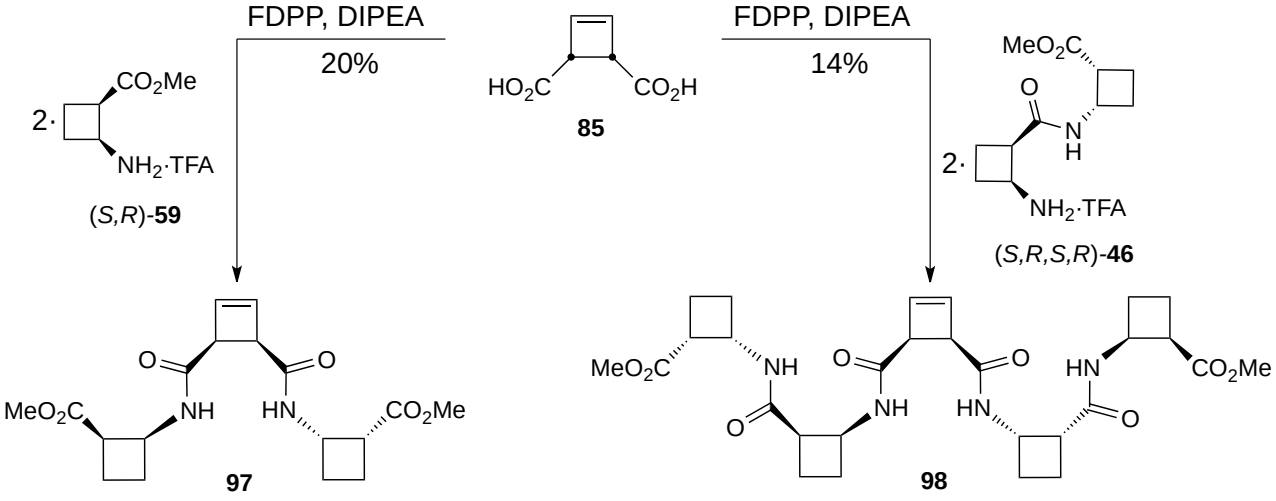

Scheme **27**. Synthesis of cyclobutane-containing pseudodipeptide **97** and pseudotetrapeptide **98** *via* FDPP.

It is noteworthy to remark that, although diacid **85** is a *meso*-compound, their corresponding pseudopeptides are not. However, ^{1}H-NMR spectra of both only showed clear differences in the chemical shifts for the NH protons and the olefinic protons, making obvious a certain symmetry degree as further as the atoms are from the central cyclobutene moiety.

3.3.1.3. Structural study in solution of cyclobutene-containing pseudopeptides

Full characterization of both pseudopeptides was performed through high-resolution NMR experiments. However, complete atomic assignation was not possible due to the aforementioned "symmetry" in the sides of the molecules, what results in overlapped signals. In the beginning, the presence of two cyclobutane or two bis-cyclobutane residues may remind of similar peptide chains formed by polycyclobutane oligomers. Hence, this would make one to think that their tendency to give β-ribbon-like structures would prevail, what would structurally suppose the conservation of the hydrogen-bonding pattern.

Anyway, and among the possible foldings in solution derived from them, two secondary structures were proposed for pseudodipeptide **97**: the cyclobutene spacer could affect the intra-residual hydrogen-bond pattern, making the NH protons to interact with some of the carbonyls of the cyclobutene moiety, or could not affect at all. In the first case, one of the residues could keep its six-membered hydrogen bond while the other could twist in the way that a new seven-membered interaction would be formed. In the case that the spacer did not have any structural effect, both residues would keep their "natural" intra-residual interactions in solution (Figure **62**).

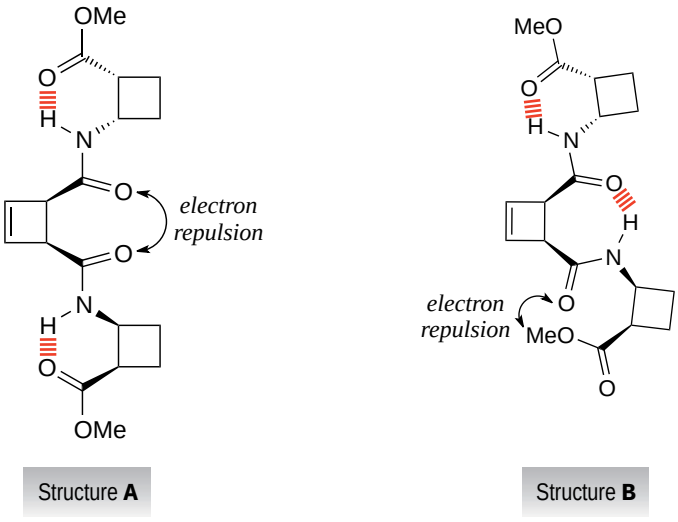

Figure **62**. Two possible proposed secondary structures for pseudodipeptide **97**.
Red-dashed lines represent hydrogen bonds.

The structural study was then started for the pseudodipeptide, and according to the results obtained, the study for the pseudotetrapeptide would be tackled. As usual, selective NMR experiments as TOCSY and NOESY were crucial for the secondary structure elucidation.

Pseudodipeptide 97

For pseudodipeptide **97,** 1D selective TOCSY experiments on both NH_8 and NH_{15} protons were carried out for its characterization. Both spectra showed the same pattern for the two cyclobutane residues, what is translated into having similar coupling networks throughout the ^1H-^1H connectivity. 1D selective NOESY also showed similar intra-residue patterns. See Annex section **3.5.1.1** for NMR spectra and details. As a preliminary result, TOCSY data and NOE contacts suggested the formation of similar six-membered hydrogen-bonded rings in every residue, as in the isolated monomers. Therefore, the structural effect of the intercalated cyclobutene unit seemed to be negligible.

In order to prove which of the two proposed structures was the most probable, the hydrogen bonding between NH protons and the extra carbonyl group in the cyclobutene moiety was investigated (Figure **63**).

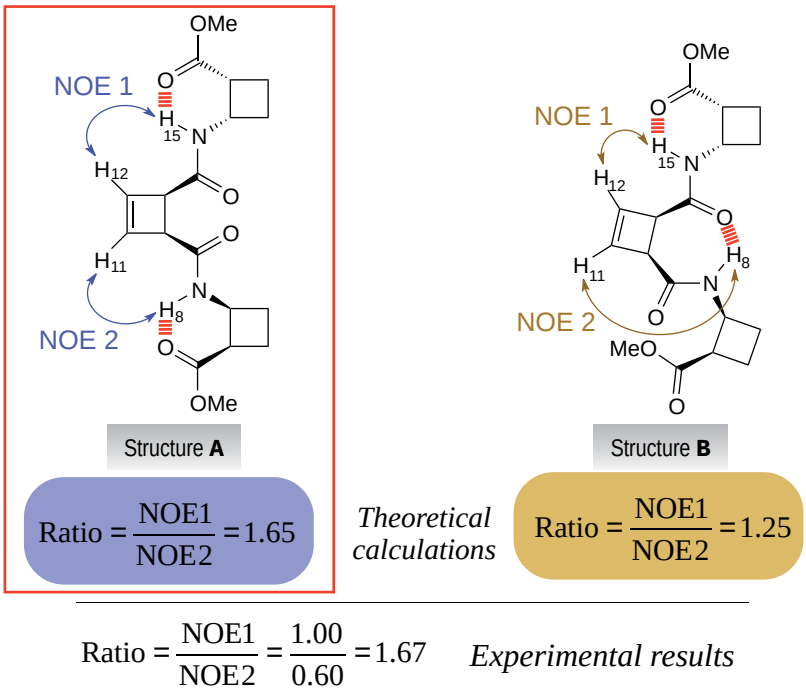

Figure **63**. Computational calculation of ratio between NOE1 (H_{12}-NH_{15}) and NOE2 (NH_8-NH_{11}) in both proposed structures A and B, showed that experimental ratio between same NOE contacts was in agreement with structure A. Thus, pseudodipeptide **X** presents a secondary structure consisting in two six-membered rings. Red-dashed lines represent hydrogen bonds and arrows represent NOE contacts.

The difference between both structures mainly relies on the presence or not, of a seven hydrogen-bonded ring, without regarding the residue where it takes place. Relative distances between atoms can be qualitatively extracted from NOE data integration. Thus, when the ratio between NH_8-H_{11} and H_{12}-NH_{15} was calculated it resulted in 1.67, which fitted nicely to the value 1.65, calculated by assuming the formation of two theoretical six-membered rings. On the contrary, calculations

considering one six- and one seven-membered ring afforded a ratio of 1.25, in clear discrepancy with the experimental value (Figure **63**).

Then, the negligible effect of a cyclobutene spacer introduced between two cyclobutane residues was corroborated. It would seem that the six-membered rings are more stable than a seven-membered ring, what results in a secondary structure very similar to that of the only cyclobutane-containing β-dipeptide (*S*,*R*,*S*,*R*)-**1**. The reason would be that the highly constrained conformation of the unsaturated ring does not significantly distort the orientation and distances of the atoms involved in the decisive hydrogen bonds.

Pseudotetrapeptide 98

For pseudotetrapeptide **98**, 1D selective TOCSY experiments showed two different pairs of NH-cyclobutane residues. In each pair, the two involved moieties were not completely distinguishable due to the presence of signal overlapping in most of the cyclobutane signals. Similarly to the pseudodipeptide, ROESY experiments were carried out in order to determine ROE contacts, which provide same ^{1}H-^{1}H space correlation as NOESY does. Strong inter-residue ROE contacts were observed between H$\alpha_{(i)}$ and NH$_{(i\pm1)}$ protons. See Annex section **3.5.1.2** for NMR spectra and details. These results suggested a similar secondary structure to that of the β-tetrapeptide exclusively made with saturated cyclobutane residues (Figure **64**).

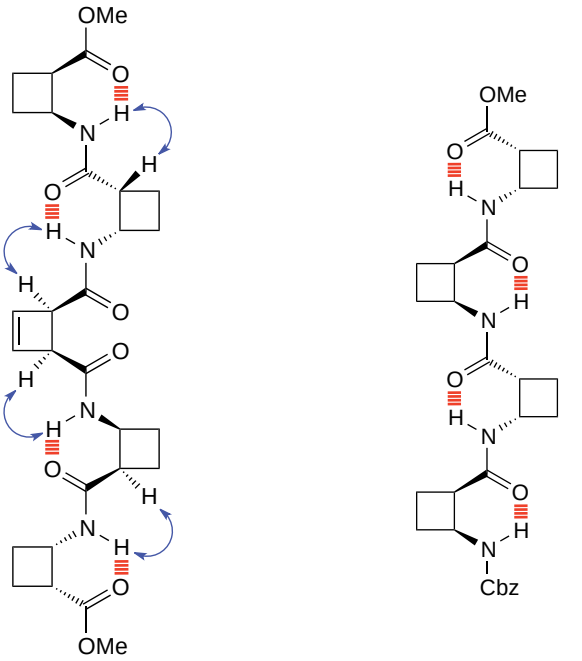

98 (*S*,*R*,*S*,*R*,*S*,*R*,*S*,*R*)-**3**

Figure **64**. NMR-suggested secondary structure of pseudotetrapeptide **98** in $CDCl_3$ (*left*), in comparison with the extended strand-type conformation shown by the all *cis*-cyclobutane β-tetrapeptide **3** (*right*). Red-dashed lines represent hydrogen bonds and blue arrows represent NOE contacts.

3.3.2. Synthesis of linear AA-containing hybrid peptides

Following the previous study published in our group of a hybrid cyclobutane-containing tetrapeptide with β-alanine residues joined in alternation,[11] the synthesis of the glycine and GABA derivatives was undertaken. By means of coupling reactions, cyclobutane and linear residues were combined in alternation to provide from mixed dipeptides to octapeptides (Figure **65**). All of them were designed to contain the first cyclobutane residue at the *N*-terminus protected as *N*-Cbz, so the *C*-terminus, on the contrary, was formed by the linear residue as *C*-OMe.

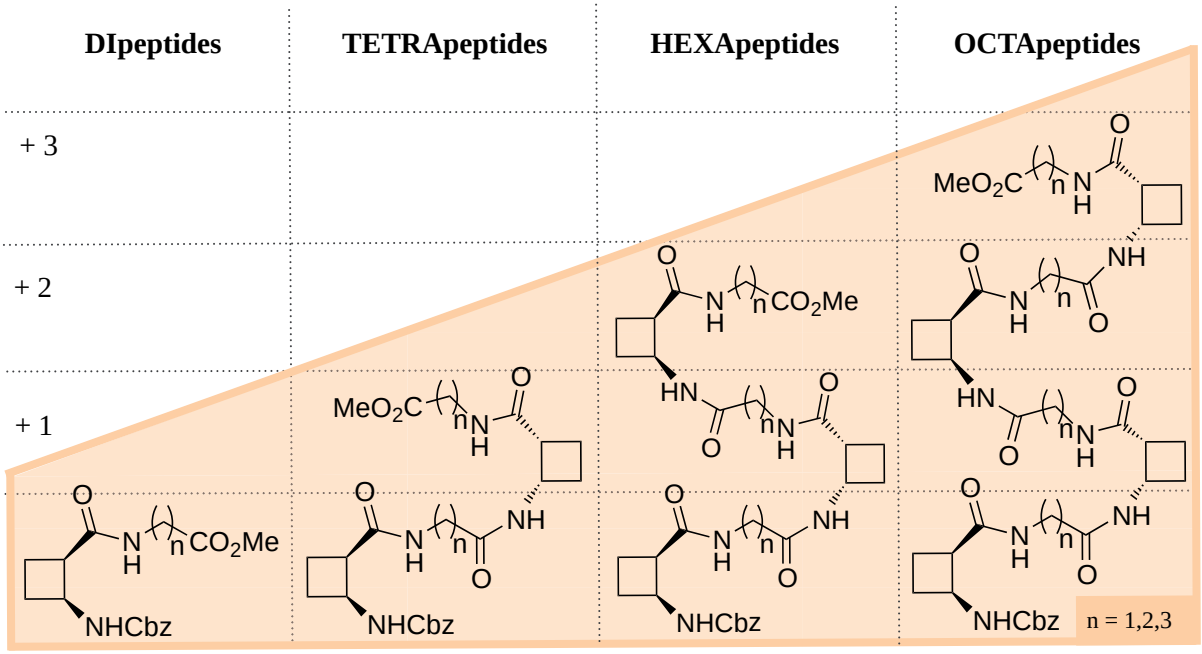

Figure **65**. Homologated series of cyclobutane-containing hybrid peptides.

The cyclobutane moiety used consisted of the most directly accessible *cis*-cyclobutane β-amino acid (*S*,*R*)-**17**, obtained by the enantioselective synthesis reported in our group and explained in detail in the previous chapter. This acid was coupled with methyl ester protected linear amino acids (Scheme **28**).

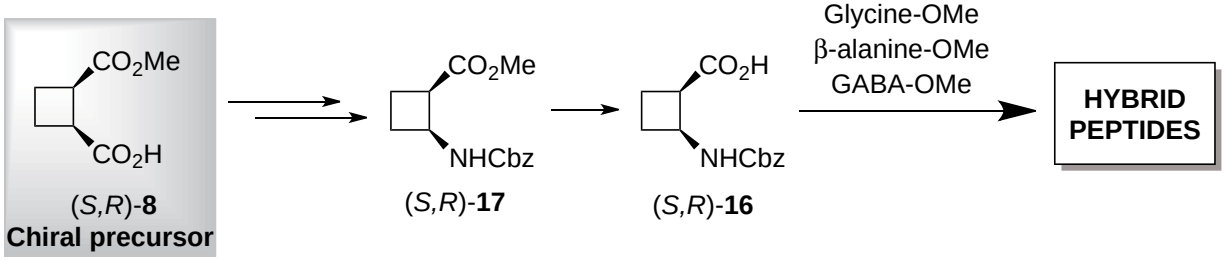

Scheme **28**. Synthesis of cyclobutane-containing hybrid peptides.

These amino acids are commercially available in the convenient protected form for their direct coupling (Gly and β-alanine) or in the free from, as GABA amino acid. The last one had to be properly functionalized as the methyl ester derivative (Scheme **29**). GABA **99** was benzylated on its *N*-terminus by reaction with CbzCl in aqueous basic medium affording acid **100** quantitatively. Methylation, using methyl iodide in a basic medium, gave the orthogonally protected amino acid **101**. In order to couple it, deprotection of the amine group required catalytic hydrogenation.

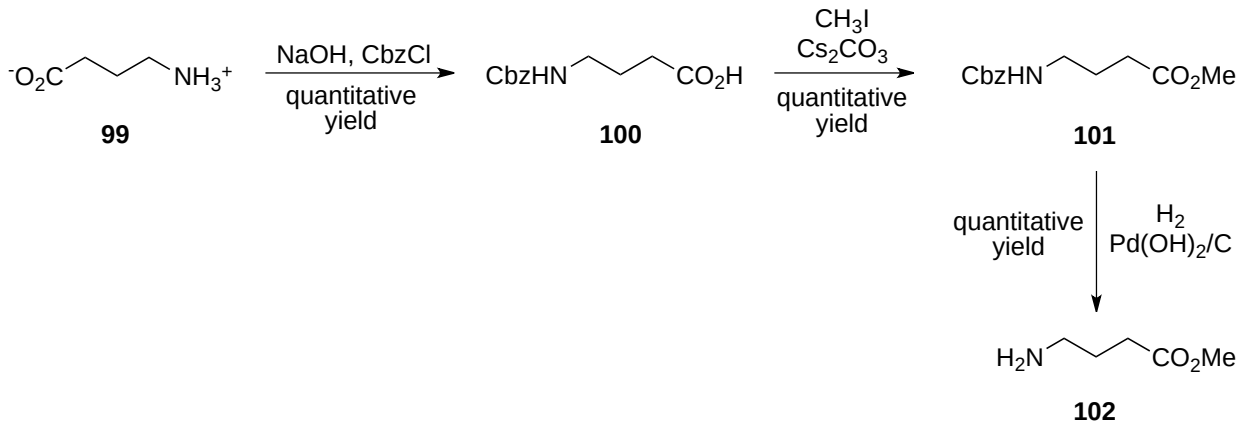

Scheme **29**. Synthesis of GABA-OMe **102**.

3.3.2.1. Synthesis of the homologated series of linear AA-containing hybrid peptides

The preparation of the hybrid dipeptide and tetrapeptide of β-alanine and the dipeptide of glycine was already reported in our group,[11,19] however their synthesis was necessary to achieve the rest of compounds. From here, the synthesis was tackled optimizing the procedure previously used and investigating other coupling agents like the phosphorous-based ones or the uronium reagents, which avoid the pre-activation of the carboxylic acids.

The synthetic approach to the hybrid peptides was based on the ensemble of couplings, selective deprotections and further couplings until the size of the desired peptide was reached. All the reactions were simple and easy to carry out, in poor to excellent yields, and the difficulties came mainly from the purification steps. In order to separate the peptides from the coupling agent residues, which showed comparable high polarities and sometimes low solubilities, silica-gel flash chromatography was not always useful, because the larger the peptides were the more insoluble they became. Finally, digestions and cold washes were found to be the best methodology for their precipitation and purification.

The synthetic procedure is described just for the glycine derivative as the rest of compounds were prepared in a similar way. Step-by-step synthetic route is shown in the next Scheme **30**.

Cyclobutane amino acid (*S*,*R*)-**16** was equimolarly coupled with HCl·Gly-OMe **103** in the presence of PyBOP and distilled DIPEA, in an anhydrous DMF medium at room temperature and during 1 hour. After purification, hybrid dipeptide **40** was obtained in 78% yield as white solid.

Saponification of **40**, dissolved in a THF/H_2O mixture, by adding a 0.25 M NaOH solution and stirring for 3 h from 0 ºC to room temperature, provided acid **104** quantitatively. This selective carboxylic acid deprotection was performed for an equimolar amount of dipeptide on one hand, whereas on the other equimolar amount, the selective cleavage was carried out on the amine group. Hydrogenation of a concentrated solution of **40** in EtOAc by the action of catalytic 20% $Pd(OH)_2/C$ and the presence of TFA, afforded amino salt **105** quantitatively after evaporation and lyophilization.

Then, coupling of **104** and **105** as before but using FDPP instead, resulted in a mixture which after cold ether washes provided the hybrid tetrapeptide **106** in 52% yield.

Saponification of **106** on one side and its TFA-free hydrogenation on the other, resulted in acid **107** and amine **108**, respectively.

Acid tetrapeptide **107**, coupled with amine salt dipeptide **105** using PyBOP, provided glycine hexapeptide **109** in 30% yield, after cold ether washes and silica-gel flash chromatography, employing CH_2Cl_2/MeOH (20:1) as eluent.

Finally, the coupling of acid tetrapeptide **107** with amine tetrapeptide **108** by the action of PyBOP, in an anhydrous CH_2Cl_2/DMF mixture and only after 1.5 hours, afforded octapeptide **110** in 32% yield after ether precipitation and washing.

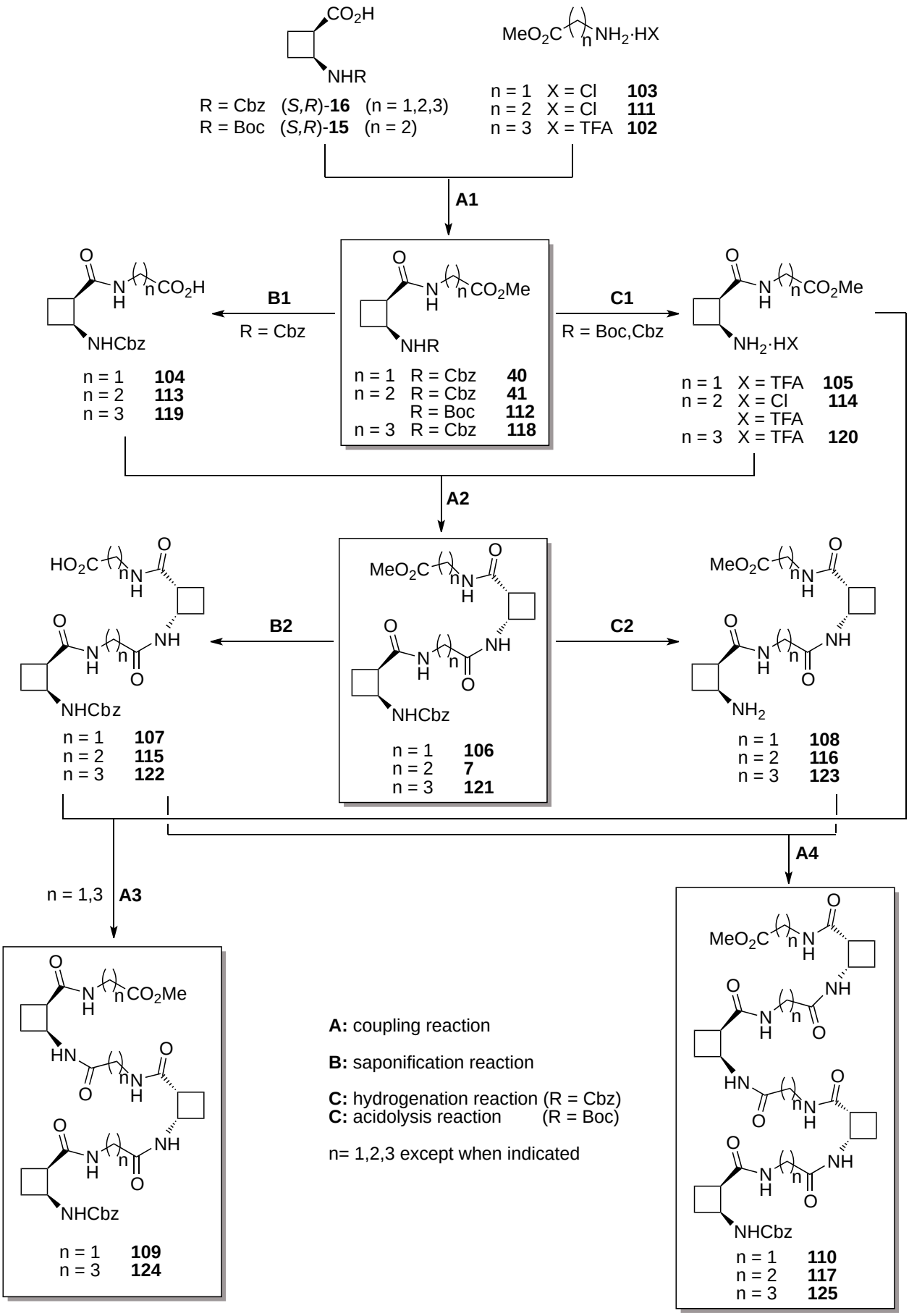

Scheme **30**. Synthetic procedure for the preparation of homologated series of cyclobutane-linear hybrid peptides.

Once the series were obtained and the structural study for tetrapeptides **106** and **121** was begun, a new compound was decided to be synthesized in order to contribute to the conformational elucidation of GABA tetrapeptide **121**.

Preliminary NMR experiments on **121** showed that the last carbonyl could be interacting with some NH of the molecule. Under this premise, the absence of CO_{31} would result in the lack of the $NH_x \cdots OC_{31}$ hydrogen bond, resulting in a reorganization of the NH_x to a new carbonyl or to a non-hydrogen-bonded form. This is why pseudotetrapeptide **126** was prepared, *n*-hexyl chain being the second linear residue, with the same number of chain-atoms as provided by GABA residue (Figure **66**).

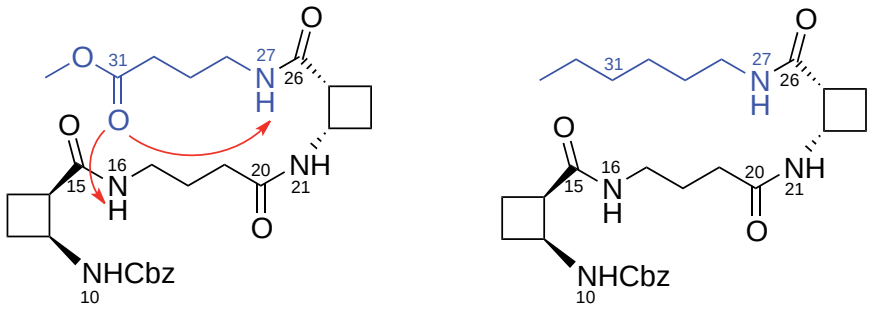

Figure **66**. Hybrid tetrapeptide **121** showing the two most probable hydrogen bonds (red arrows) of CO_{31} (*left*). The absence of carbonyl at position C_{31} of pseudotetrapeptide **126** would have to cause a change to be observed by NMR experiments.

Thus, the synthesis of **126** was approached following the same procedure as before with the only condition that the *n*-hexyl-containing precursor would have to be the amine to be coupled at some stage. Pseudodipeptide **127** was prepared, and after being hydrogenated in the presence of TFA or HCl was coupled to acid dipeptide **119**, affording pseudotetrapeptide **126** in 62% yield as the best result (Scheme **31**).

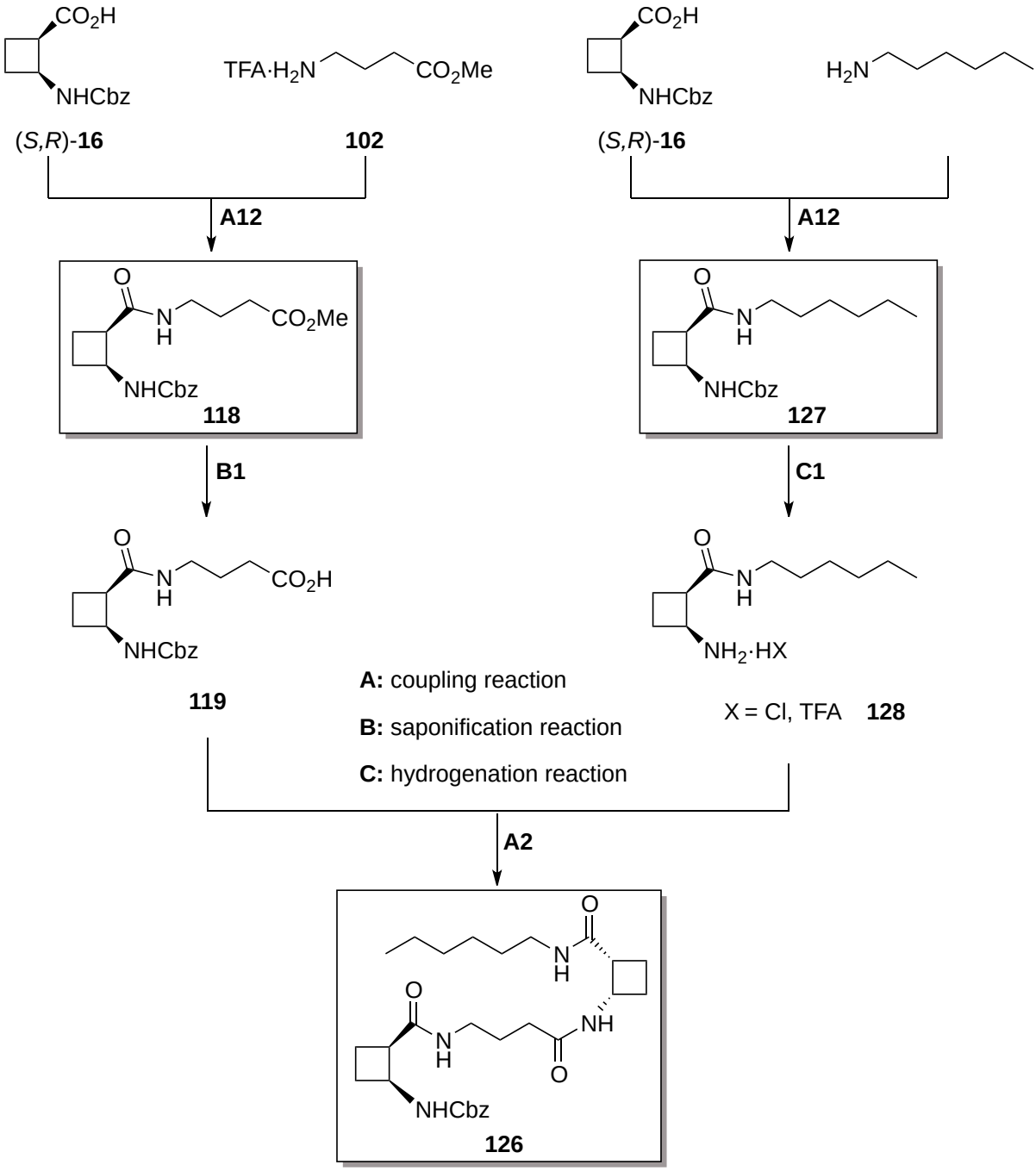

Scheme **31**. Synthetic procedure for the preparation of hybrid pseudotetrapeptide **126**.

Table **5** displays the reaction conditions tested in each case, for the synthesis of all the hybrid peptides, showing, in rough outlines, the yield-effect of the coupling agent.

Table **5**. Yields of reactions A, B and C for each linear amino acid derivative from Schemes **30** and **31**. For reaction A, the coupling agent is indicated as a crucial element of the resulting yield.

Reaction	**A: Coupling agent** **Yield (%)**				
	n = 1	**n = 2**	**n = 3**	**n = 3 (*n*-hexyl)**	
A1	PyBOP 78	PyBOP 90 (R = Cbz) 69 (R = Boc)	PyBOP 80	**A11** PyBOP 80	**A12** PyBOP 85
A2	FDPP 52	FDPP 60 (X = TFA^-) 48 (X = Cl^-)	FDPP 60	FDPP 62 (X = Cl^-) 52 (X = TFA^-)	
A3	PyBOP 30	--	HATU 36	--	
A4	PyBOP 32	PyBOP 27	HATU 62	--	
B1	96	93	91	91	
B2	79	94	quantitative	--	
C1	quantitative	quantitative (R = Boc,Cbz)	quantitative	quantitative (X = Cl^-,TFA^-)	
C2	quantitative	quantitative (R = Cbz)	98	--	

Three different coupling agents were used for carrying out the peptide couplings between the amine or amine salt and the corresponding carboxylic acids. PyBOP, FDPP and HATU were tested and some conclusions could be extracted from their application in the current synthesis, because although some generalizations can be stated form their use, no success is guaranteed until such coupling reagent has been tried. PyBOP appeared in the early 90s as a safer alternative of BOP reagent, avoiding the carcinogenic HMPA by-product (Figure 67).[186,187]

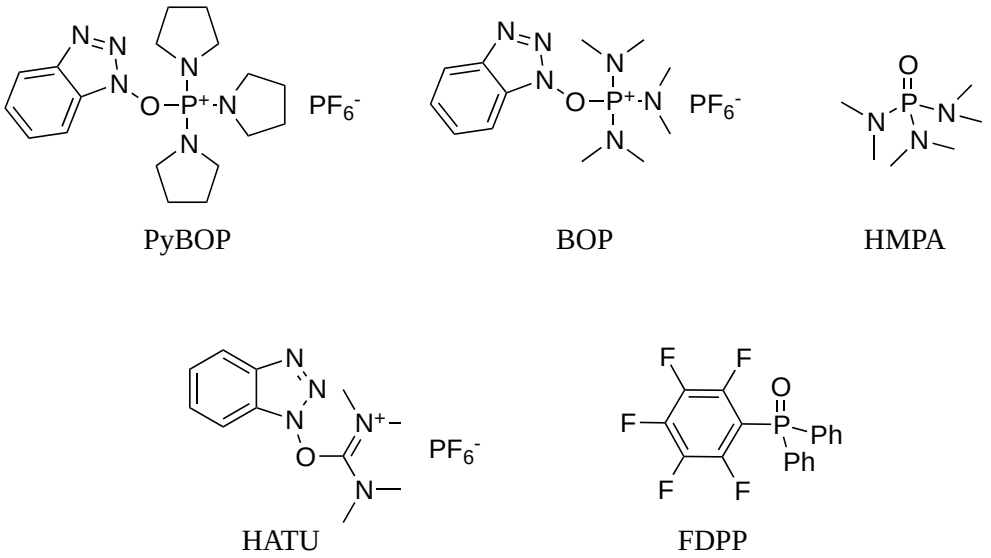

Figure 67. Structures of some coupling reagents and byproducts used for the synthesis of peptides.

This phosphonium reagent has the phosphorous atom substituted by pyrrolidine rings instead of dimethylamine groups, and the main advantage we found was the short reaction times (most of the times less than 2 h.), with good to excellent associated yields. So, we started employing it for the synthesis of hybrid dipeptides, mostly providing yields over 80%. When we applied them for the synthesis of tetrapeptides the conversion was also good, but purification was very difficult. Hybrid tetrapeptides and the tris(pyrrolidinophosphine) oxide, the solid by-product of PyBOP, showed similar polarity in silica-gel flash chromatography and solubility in solvents in which the tetrapeptide was poorly soluble were not found. Then, organophosphorous reagent FDPP was tested, as it gave good yields and low epimerization in other peptide synthesis in our group. Despite the good chemical conversions, purification by ether washes only provided the pure isolated compounds in yields between 50-60%. Uronium-based reagent HATU was previously used in our group for the synthesis of cyclobutane-containing tridentate dendrimers, because its known advantages in coupling sterically hindered *N*-alkylamines.[188] GABA hexa- and octapeptides were synthesized using it, what resulted in a better yield for the octamer.

TFA and 2 M HCl (Et_2O) were added to form the corresponding salts of the free amine on the hybrid dipeptides. Resulting salts were *in situ* neutralized by the action of DIPEA as general base in the coupling reactions.

3.3.2.2. Structural study of linear AA-containing hybrid peptides and pseudopeptides

The folding of peptides generally depends on some factors that can be directly custom designed. Among them are the length of the peptide chain, the nature and the conformational freedom of the amino acids and the solvents in which the structural studies are performed. These are crucial elements that determine the presence and quality of a recognizable secondary structure, and they are inter-dependent too. For instance, α-peptides in polar solvents like methanol or trifluoroethanol, require a minimum of 10-12 natural amino acids to form stables helices. Helical foldings in biopolymers are commonly length-dependent, showing significant helix formation after a critical chain length is reached. In order to improve the stability, whatever its type is, some changes can be introduced.[7]

The use of β-amino acids as good scaffolds for this purpose, because the formation of β-hydrogen bonds tends to be 1-2 kcal/mol more favourable than α-hydrogen bonds has been already discussed.[189-191] So, using β-peptides, the length of the amino acid sequence can be shortened to just few amino acids, depending on the conformational restriction. Cyclic β-amino acids formed by ACHC or ACPC have proved to give stable 14-helix and 12-helix with only six and four residues, respectively. On the other hand, the more polar and acidic the solvent is, the less stability has to be expected for such hydrogen-bond based structures.

Amongst the hybrid β-peptides here described, only tetra-, hexa- and octamers would be suitable since they are conformationally restricted by half of the residues they are formed by. However, the other half part is constituted by linear amino acids, with increasing conformational freedom from glycine to GABA. The drawback is that hexa- and octapeptides are little soluble in most of organic solvents except MeOH or DMSO, solvent which in its deuterated form was used for their ^{1}H- and ^{13}C-NMR characterization. Both solvents were refused to be employed in a structural study since their manipulation, residual solvent peaks and other properties were not appropriate for the NMR studies. Nevertheless, precedents in the determination of a 14-helix structure for the β-alanine tetrapeptide, proved the efficiency of $CDCl_3$ as a proper solvent for theoretical calculations and NMR experiments.[135] Moreover, $CDCl_3$ is a solvent that has been successfully used in the NMR conformational analysis of related cyclobutane peptides.[9a,9b,10]

Hence, $CDCl_3$ was used for the computational and NMR studies of glycine and GABA tetrapeptides. On the other hand, in order to prove the validity of the structural studies of tetramers and their extrapolation to the rest of the series, CD was performed for all of them in 0.5 mM solutions in methanol, exhibiting negative peaks (Figure **68**).

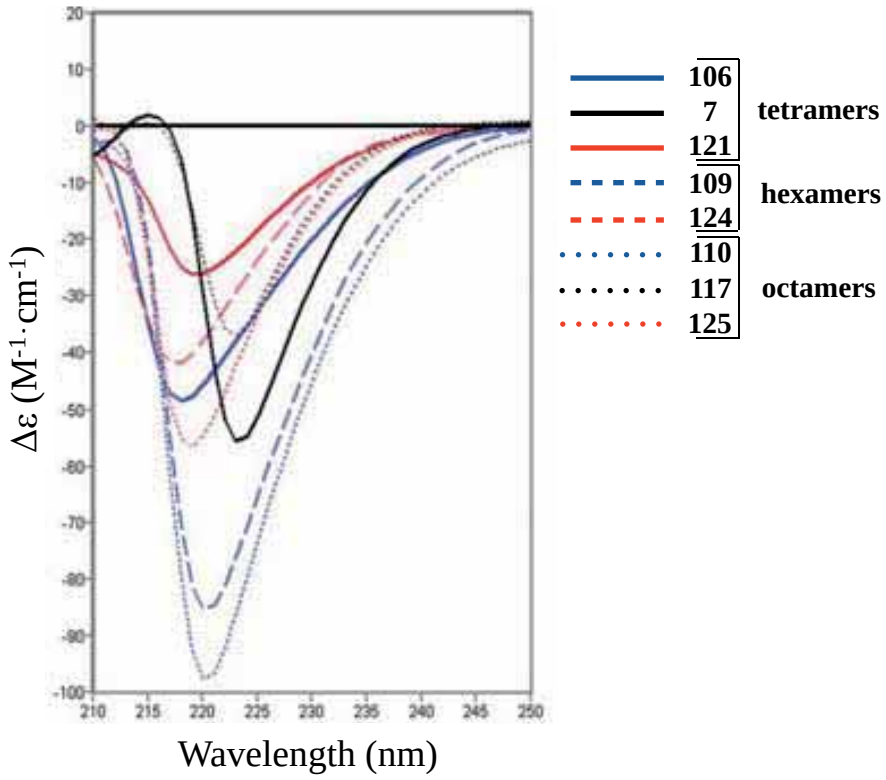

Figure **68**. CD spectra of 0.5 mM methanol solutions of hybrids of β-cyclobutane amino acids and glycine, β-alanine and GABA, respectively.

Minima peaks at 223 nm were found for tetramer **7** and octamer **117** in the β-alanine series. This excellent concordance allowed us to assume a helical conformational preference for octamer **117** in view of previous results.[9b]

An accurate coincidence in the CD signatures was also observed for tetra-, hexa- and octamers in glycine and GABA series, respectively, showing that both linear residues induce a similar preferred conformation in solution (Figure **68**). According to the literature, the presence in the spectrum of negative minima peaks at 217-219 nm would suggest a β-sheet-like structure.[192-195]

These observations were corroborated by NMR experiments, which mainly correlated protons through the space, in order to determine intra- or inter-residue disposition. In addition, it provided structural information to later perform computational calculations.

NMR study in solution

A detailed structural study was carried out on α,β- and β,γ-tetrapeptides **106** and **121**, respectively, which allowed to assign all protons and carbon atoms for each peptide. In the NH region of both ^{1}H-NMR spectra, additional signals were observed, which could be attributed to minor conformers. These minor signals were more appreciable in the GABA peptide derivative, due to its higher

flexibility on the linear residues. Specifically, 2D ^{1}H-^{1}H ROESY experiments, together with selective TOCSY experiments, permitted intra- and inter-residue ROE contacts to be established, contributing to define the spatial environment of NH protons. Some of these ROE contacts and H-H coupling constants confirmed the *trans* stereochemistry for all amide bonds in the major conformer for each peptide (Figure **69**).

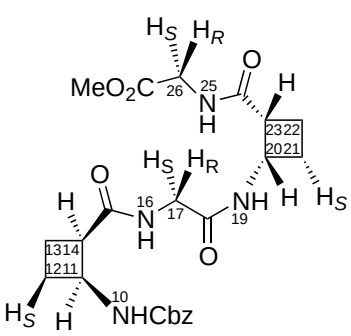

106

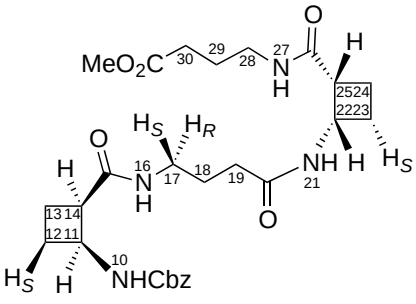

121

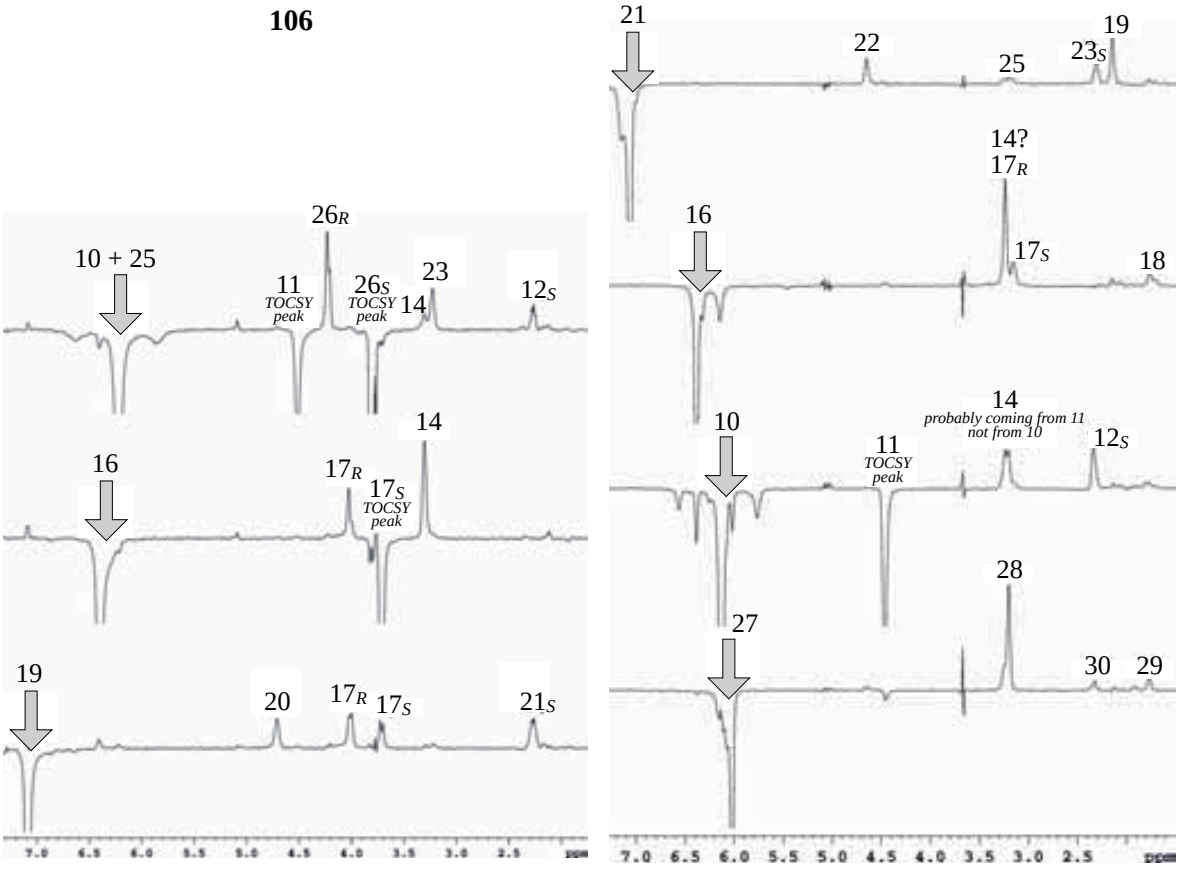

Figure **69**. 1D ROESY slices extracted from 2D spectrum for tetrapeptide **106** (*left*) and tetrapeptide **121** (*right*) in $CDCl_3$ recorded at 298 K (600 MHz).

Self-diffusion and MeOD exchange experiments were performed to give an idea of the fixation and, therefore, of the involvement of each NH proton in hydrogen bonds. For both tetrapeptides the self-diffusion experiments were recorded at 298 K and 270 K, showing similar patterns in which all the protons decayed approximately at the same rate. Experiments consisting in adding small amounts of

MeOD in the $CDCl_3$ sample solutions, also resulted in a similar decay of NH signals and, therefore, in a similar exchange of NH protons too (Figure **70**).

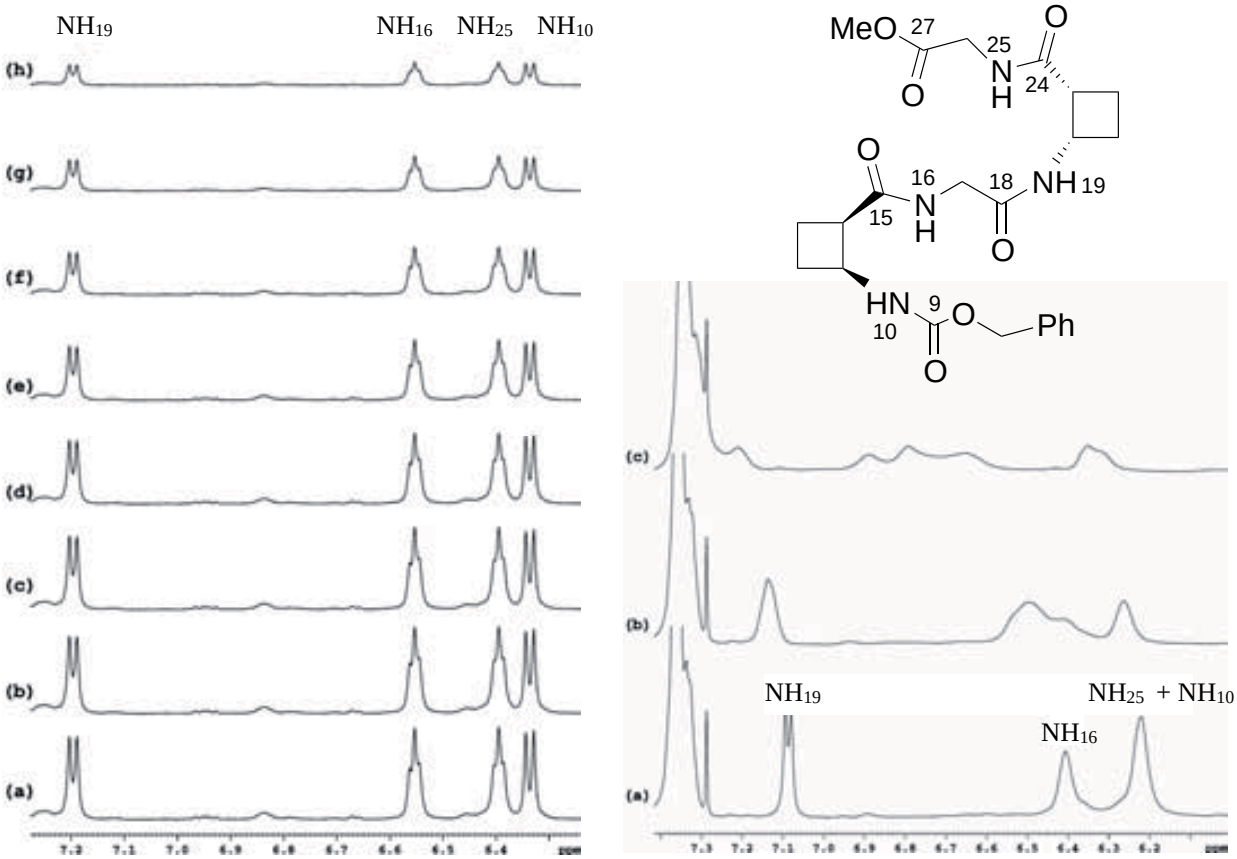

Figure **70**. Self-diffusion NMR studies in $CDCl_3$ of tetrapeptide **106** at 600 MHz at 270 K. BPLED spectra are recorded with a diffusion time of 20 ms, with a gradient duration of 0.5 ms and with a gradient strength from 2% to 95% in eight lineal steps from (a) to (h). All proton signals decay approximately at the same rate (*left*). MeOD exchange experiment for tetrapeptide **106** (*right*).

Moreover, variable temperature experiments were carried out to make these results more reliable. ^{1}H-NMR spectra were recorded from 260 K to 330 K every 5 K and temperature coefficients were calculated (Table **6**).

Table **6**. Temperature coefficients determined for the four NH protons of both hybrid tetrapeptides **106** and **121**.

Tetrapeptide 106		**Tetrapeptide 121**	
NH signal	**Temperature coefficient (ppb/K)**	**NH signal**	**Temperature coefficient (ppb/K)**
NH_{10}	-4.6	NH_{10}	-5.1
NH_{16}	-5.1	NH_{16}	-6.4
NH_{19}	-3.9	NH_{21}	-5.3
NH_{25}	-5.3	NH_{27}	-5.1

As it can be seen, temperature coefficients for NH protons of **121** are bigger than -5.1 ppb/K, whereas for peptide **106** all of them are below -5.3 ppb/K. It is commonly accepted that more negative values than -4.5 ppb/K correspond to non-hydrogen-bonded NH atom and more positive values describe the hydrogen-bonded NH protons. This reference value was determined on globular proteins so the strength of the hydrogen bonding is comparable up to a certain extent.[196] Hence, on the basis of these results, it can be concluded that all the NHs in each peptide presented approximately similar hydrogen-bonds in terms of fixation, although in the GABA tetrapeptide **121** lower temperature coefficients suggested a less fixed structure, as expected due to its higher flexibility caused by longer GABA spacers. Notwithstanding, it is noteworthy the fact that both cyclobutane intra-residue hydrogen bonds (both NH_{10}, and NH_{19} in **106** and NH_{21} in **121**) presented the lowest negative values, corroborating the cyclobutane driving force to provide more stable hydrogen bonds due to its rigidity. On the other side, inter-residue interactions, responsible for the β-sheet-like formations, showed to be less fixed.

For **106**, results strongly supported the formation of an anti-parallel β-sheet-type folding, with the two glycine residues facing each other, although, as usual in our group, theoretical calculations were required in order to support this secondary structure. As mentioned before, tetrapeptide **121** presented less rigidity so, to verify if the β-sheet formation was in the major conformer or, on the contrary, the terminal GABA segment was conformationally random, we synthesized and studied pseudopeptide **126**. Nevertheless, a little evidence from the 1D ROESY slice of NH_{27} in Figure **69** (*right*) pointed out that GABA segment coiled itself up. ROE contact between NH_{27}-H_{30}, although very small, would not support a β-sheet-type folding because this long-distance ROE contact would be more suitable for a coiled-up GABA fragment.

When hexyl group was introduced instead of the GABA residue, all the NH protons became less unshielded, indicating a loss of secondary structure (rigidity). However, not all the NH protons moved in the same proportion, which indicated that the loss of ordered structure only took place in a part of the molecule, surely at the *C*-terminus, as expected. Concretely, NH_{27} proton was the most shifted one, what suggested that it had mostly lost its hydrogen bond, presumably formed with the chemically removed CO_{31} (Figure **71**).

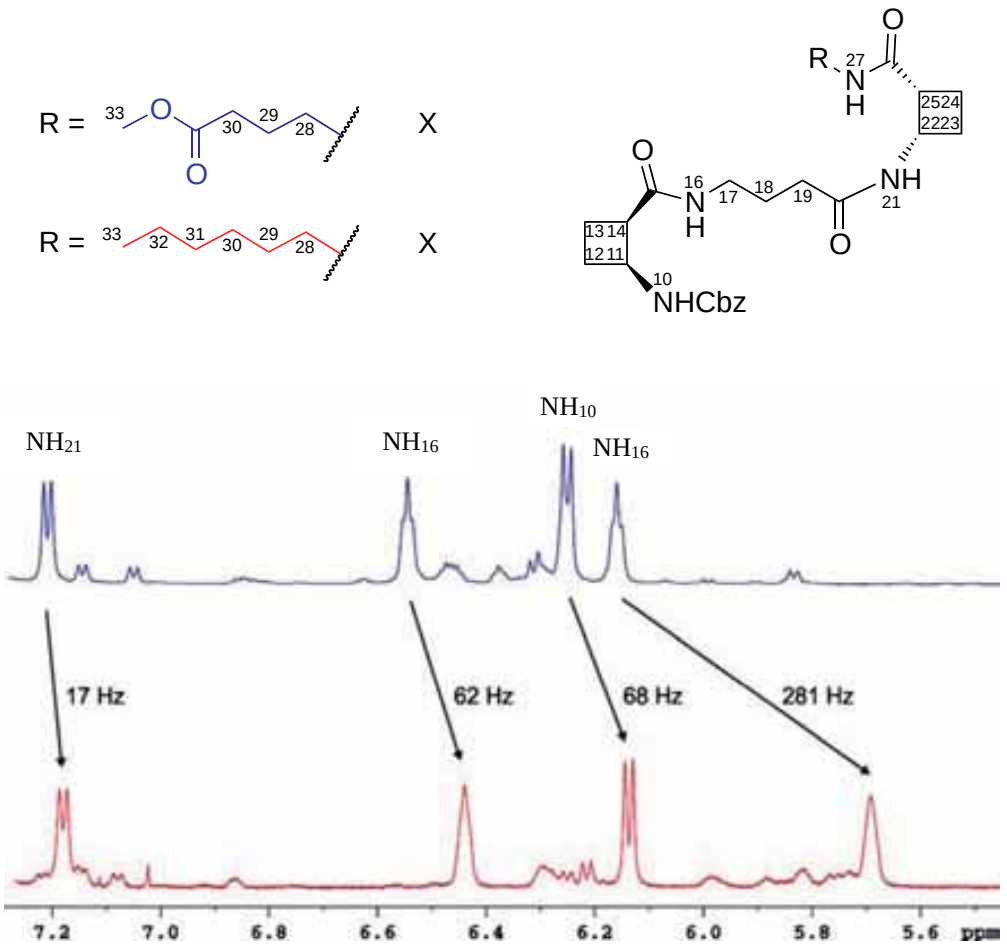

Figure **71**. Comparison of the NH region in the 600 MHz ^{1}H-NMR spectra in $CDCl_3$ of compounds **121** (blue) and **126** (red).

Surprisingly, NH_{16} proton did not shift too much compared to NH_{27}. Assuming that a β-sheet type structure was present, it was expected so because the interaction NH_{16}-OC_{31} was removed. Neither NH_{21} nor NH_{10} protons shifted too much (compared with NH_{27}), indicating they preserved most of the hydrogen bond character they had prior to the introduction of the hexyl moiety and, therefore, preserving the six-membered rings, as it was deduced from the temperature coefficients. Nevertheless, these experimental results were explained by computational calculations, which showed that the most stable conformation presents a stable intra-residue hydrogen bond between NH_{27}-OC_{31}.

The extracted conclusions with the tetrapeptides were extended to the corresponding hexa- and octapeptides in each series, according to CD results.

Theoretical calculations

To assess the feasibility of the conformations deduced by the NMR experiments for **106** and **121**, and confirm the suggested β-sheet type foldings, theoretical calculations were carried out. Because β-alanine tetrapeptide **7** had been studied previously,[8] the study was performed with the glycine and the GABA hybrid tetrapeptides. The calculation procedure was performed with restrictions extracted from NMR data.

1D Slices from 2D ^{1}H-^{1}H ROESY spectrum were employed for the correlation of the spatial contacts with bond distances. Hence, ROE contacts were used to define three groups of ^{1}H-^{1}H distances: 3, 4 and 5 Å, respectively, for strong, medium and weak signals. A margin of ± 0,5 Å was allowed for all distance restrictions. In addition, *J* coupling values were used to extract dihedral angles applying a Karplus-type equation.[87]

The computational method was applied following three steps:

1. **Conformational Search**. A mixed Monte-Carlo[197,198]/Low-Mode[199,200] conformational search was carried out using the MMFF (Merck Molecular Force Field)[201] force field implemented in the Macromodel 9.8 program.[202,203] The solvent effect was included using the GB/SA[204] method implemented in Macromodel with chloroform as solvent. For each of the starting geometries, if the number of structures computed within a 1 kcal/mol range was too big a second conformational search was carried out limiting the margin of the angles to ± 10º. If the number of structures obtained within 1 kcal/mol was too small, the conformers within 2 kcal/mol were also considered.

2. **Optimization**. After the conformational search was carried out, the selected structures within the defined energy range were grouped into different families if necessary, with the criteria of similar NH-OC interactions. The most stable structure (lowest energy) of each of these families was optimized at B3LYP[205]/6-31G(d) level of theory in gas phase with Gaussian09 package.[206]

3. **Frequency Calculation**. To ensure that the optimized structure was an energetic minimum, a frequency calculation was also run.

The detailed data for each computational step is displayed and discussed in Annex section **3.5.3.2.**

Hybrid Tetrapeptide 106

The most stable secondary structures A, B, C and D were finally obtained for glycine-tetrapeptide **106** (Figure **72)**.

A ΔG^0_{rel} = 0.0 kcal/mol	**B** ΔG^0_{rel} = 1.4 kcal/mol
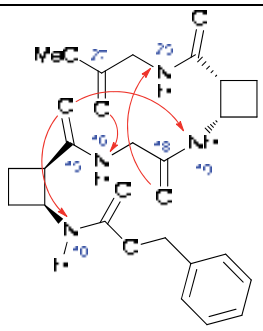	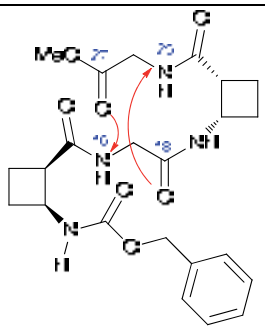
NH_{10}-CO_{15} : 2.53 Å NH_{16}-CO_{27}: 2.14 Å NH_{19}-CO_{15}: 2.08 Å NH_{25}-CO_{18}: 1.95 Å	NH_{16}-CO_{27}: 1.99 Å NH_{25}-CO_{18}: 2.04 Å
C ΔG^0_{rel} = 2.2 kcal/mol	**D** ΔG^0_{rel} = 2.4 kcal/mol
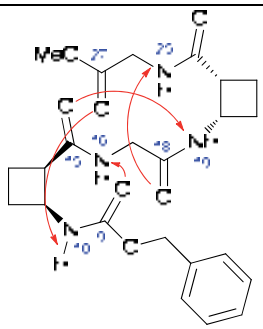	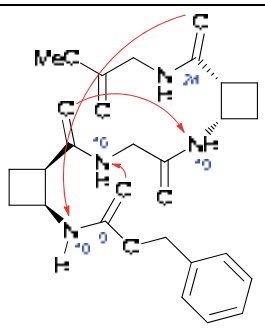
NH_{10}-CO_{27} : 1.82 Å NH_{16}-CO_{9}: 2.04 Å NH_{19}-CO_{15}: 1.94 Å NH_{25}-CO_{18}: 1.99 Å	NH_{10}-CO_{24} : 2.03 Å NH_{16}-CO_{9}: 2.04 Å NH_{19}-CO_{15}: 1.94 Å

Figure **72**. Structure of the 4 most stable conformers computed for tetrapeptide **106**.

The most stable calculated conformer A presents 4 possible hydrogen bonds between NH_{16}-OC_{27}, NH_{25}-OC_{18} and a bifurcated one between CO_{15} and NH_{10} and NH_{19}, respectively. The latter one is a common γ-turn typical belonging to α-residues. This structure fully agreed with the NMR data and represents an anti-parallel β-sheet-type folding, the two glycine residues facing each other and having the cyclobutane residue as a loop at the junction (Figure **73**). However, β-sheet is not

perfectly extended due to a tension induced by the formation of the NH_{18}–OC_{15} inter-residue hydrogen bond, which affords an extra fold to the peptide.

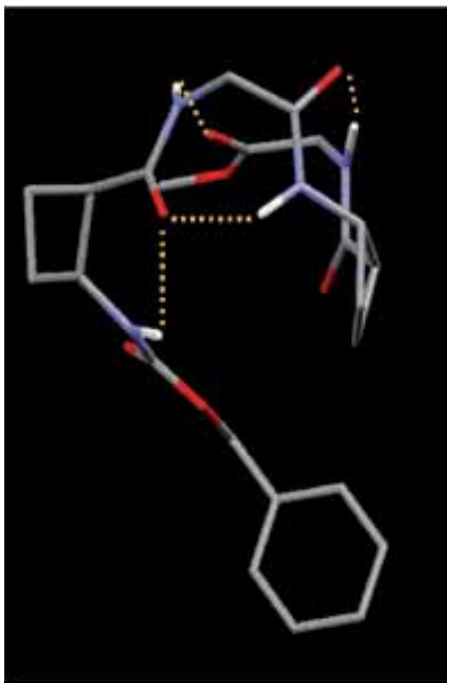

Figure **73**. Most stable conformer computed for tetrapeptide **106**.

Therefore, we can conclude that the introduction of glycine spacers in alternation with cyclobutane residues, providing α,β-peptides **106**, **109** and **110**, causes their folding into distorted β-sheets. Nevertheless, this proved ability competed with the propensity of poly(*cis*-cyclobutane) β-peptides to form intra-residue six-membered hydrogen-bonded rings. Thus, from computational calculations for tetrapeptide **106**, four structures emerged within ΔG^{o} values differing in less than 2.5 kcal/mol. If longer peptide segments of glycine units were introduced, it could be expected that the second cyclobutane residue would act like a β-hairpin, giving longer Gly-β-sheets.

Hybrid Tetrapeptide 121

As the conformational freedom of GABA residues prompted the existence of many conformations to be calculated, some extra restrictions were necessary (Annex section **3.5.3.2**).[207] Finally, the most stable secondary structures A, B, C and D were finally obtained for GABA-tetrapeptide **121** (Figure **74)**.

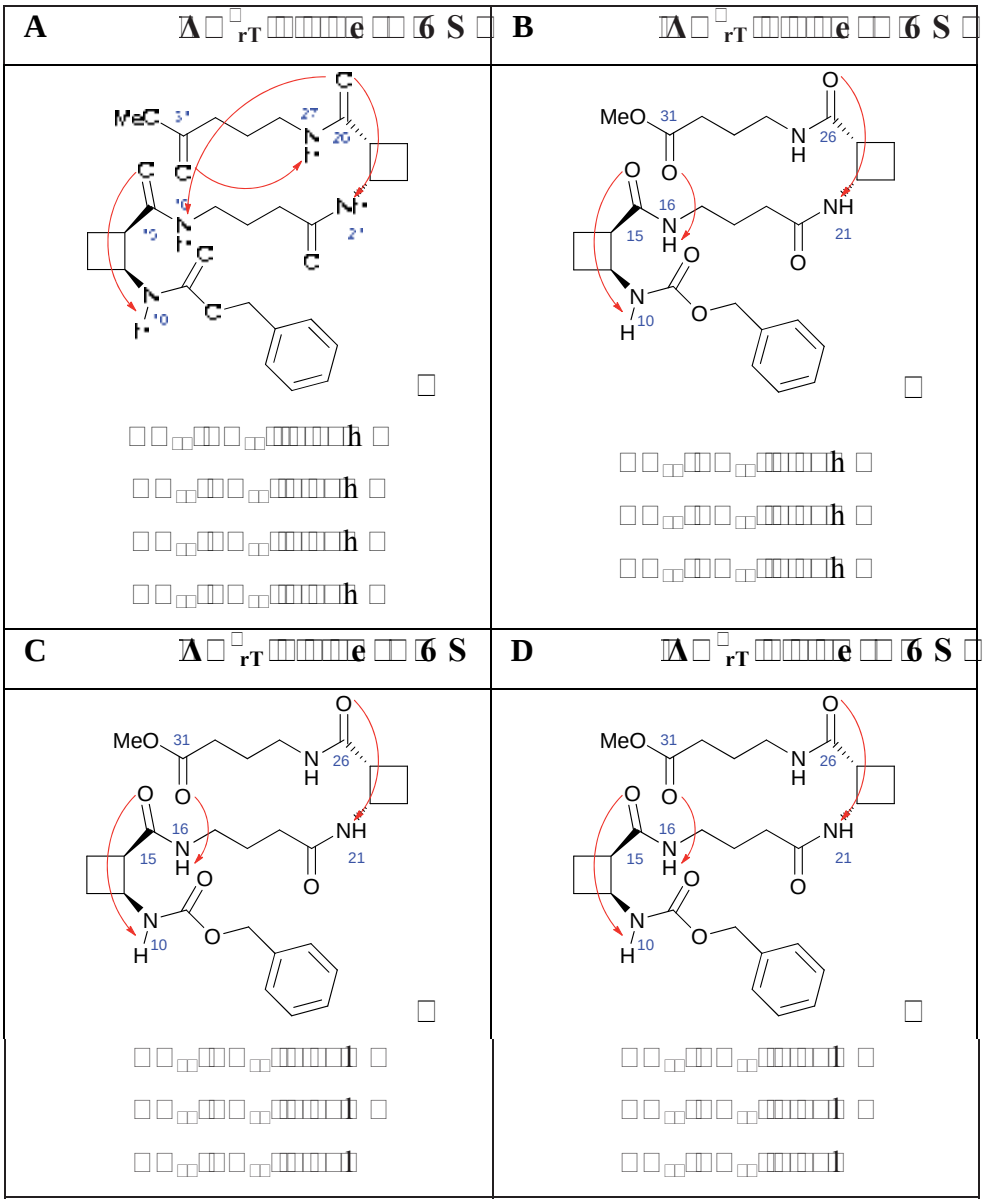

Figure **74**. Structure of the 4 most stable conformers computed for tetrapeptide **121**.

The most stable calculated conformer E presents 4 possible hydrogen bonds between NH_{10}-OC_{15}, NH_{27}-OC_{31} and a bifurcated one between CO_{26} and NH_{16} and NH_{21}, respectively. The CO_{26}-NH_{16} 11-membered hydrogen bond, which is constituted by the central γ,β-fragment, involves two residues therefore mimicking a δ-turn. This structure is consistent with the NMR data and represents a β-sheet type folding, although the arrangement is disrupted by the formation of the intra-residue NH_{27}–OC_{31} bond (Figure **75**). This interaction is in accordance with NMR

observations when comparing tetrapeptide **X** with pseudotetrapeptide **X**. Nevertheless, the expected inter-residue NH_{16}-OC_{31} is found in the second most stable structure with relative ΔG^o 1.9 kcal/mol higher.

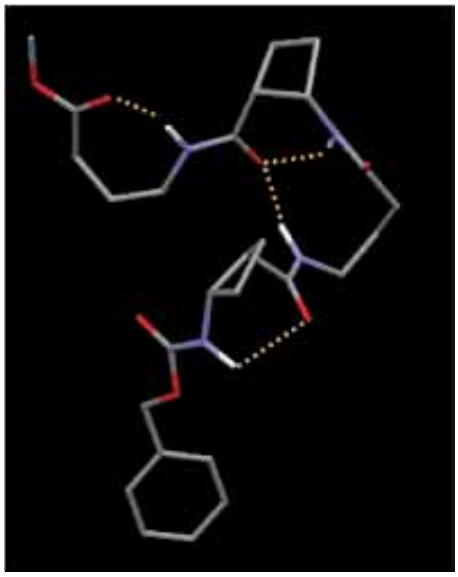

Figure **75**. Most stable conformer computed for tetrapeptide **121**.

So, as conclusion, β,γ-peptides **121**, **124** and **125** show more distorted β-sheet foldings, in part due to the more flexibility of the GABA spacer. In fact, the intra-residue NH_{10}-OC_{15} and NH_{21}-OC_{26} bonding in **121** resemble those observed in the cyclobutane monomer and in the poly(*cis*-cyclobutane) β-peptides[9c] and, probably, the resultant NMR structure displays an average between this bonding and the inter-residue interactions with the linear segments.

3.3.2.3. Linear AA-containing hybrid peptides as LMOGs. Gelation study

In the precedents of the group, the poly(*cis*-cyclobutane) β-tetrapeptide showed the ability to gelate some mixtures of organic solvents, materials which remained unaltered for several days at room temperature.[9c] Undoubtedly, the conformational restriction of the cyclobutane scaffold, which is moved to the NH groups, was critical. Such ability was expected to be maintained in the hybrid peptides, since their most stable structures in solution demonstrated that some the cyclobutane intra-residue hydrogen bonds were still prevalent (Figure **76**). Without going any further, during the manipulation of tetrapeptides their ability to gelate $CDCl_3$ was promptly seen, because in the preparation of the NMR samples for characterization they gelated the solvent.

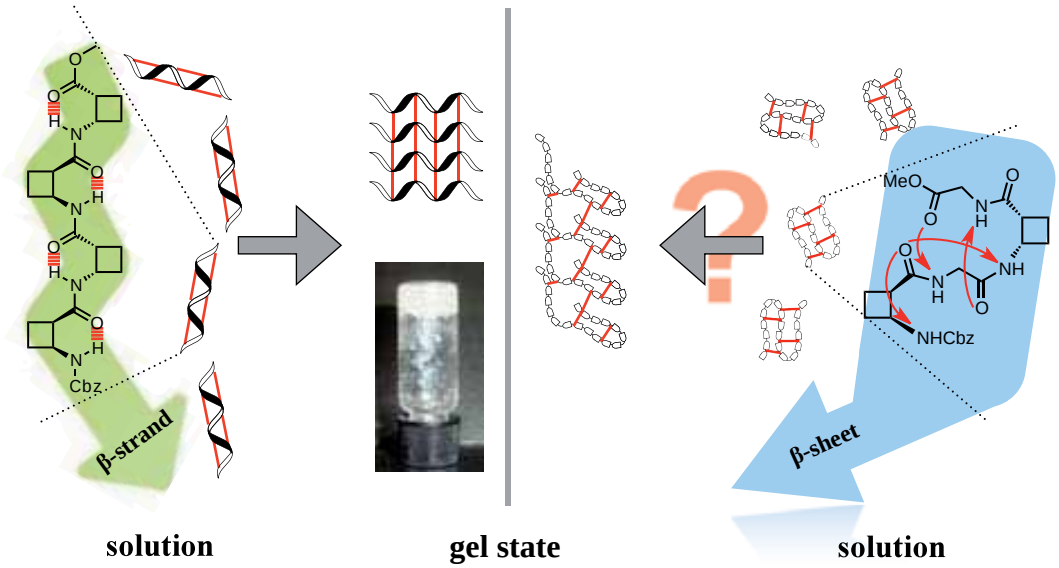

Figure **76**. Poly(*cis*-cyclobutane) β-peptides gelate some solvents and forms ordered nano-sized aggregates as observed by TEM.[9c] Will the cyclobutane-containing hybrid β-peptides have the ability?

Thus, it was decided to perform some quantitative-qualitative study of the gelating properties of some selected hybrid peptides. Hybrid dipeptides, containing only one cyclobutane residue, did not show to form any gel in organic solvents. On the contrary, biscyclobutane β-dipeptides containing *trans*-residues could form gels in toluene for instance.[14] Then, it was observed that the hybrid tetrapeptides presented some advantages with respect to the hexa- and octapeptides:

- Solubility in toluene and $CDCl_3$ for analysis and comparison with precedents.
- Solubility in a wide range of temperature to enhance gel formation.
- Proper size for computational short time calculations.
- Shorter synthetic approach.

So, tetrapeptides **106**, **7** and **121** and pseudotetrapeptide **126** were used as the compounds to be studied as LMOGs (Figure **77**).

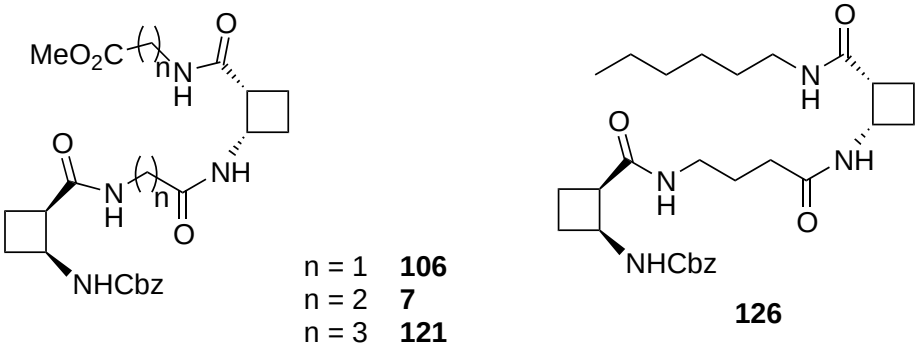

Figure **77**. Structure of cyclobutane-containing hybrid peptides subjected to the gelation study.

The preparation of the gels was achieved by a procedure described in the experimental part (see Annex section **5.1.5**).

Pure compounds **106**, **7** and **121** were quantitatively tested as LMOGs in solvents of different dielectric constant, and compound **126** was also considered in order to investigate the possible effect of the lipophilic alkyl chain in the gelation behaviour of theses type of products. Table **7** summarizes the results and Table **8** shows the appearance of such gels formed at the *mgc*.

Table **7**. Gelation behaviour of compounds **106**, **7**, **121** and **126** in common solvents.[a]

Compound	Solvent and minimum gelation concentration[b,c]													
	Pentane	**Toluene**	**1,2-dioxane**	**Et_2O**	**$CHCl_3$**	**EtOAc**	**THF**	**CH_2Cl_2**	***iso*-PrOH**	**Acetone**	**Ethanol**	**Methanol**	**MeCN**	**H_2O**
106	I	3 7	33 70	I	122 26	8 18	100 211	60 132	50 105	50 105	100 211	100 211	17 35	I
7	I	4 8	100 199	I	S	10 20	100 199	100 199	50 99	20 40	100 199	200 398	10 20	I
121	I	6 12	100 188	I	S	8 16	50 94	200 377	100 188	14 27	200 377	200 377	11 21	I
126	I	6 12	33 65	I	S	5 10	25 49	25 49	50 97	7 14	S	S	5 10	I

[a] Dielectric constant increases from left to right.
[b] Units: *mgc* in mg/mL (*top*) and mM (*bottom*).
[c] I: insoluble. S: soluble.

None of these compounds was soluble in water so they were not able to form hydrogels. Nevertheless, since some of the alcohols contained some residual water, a qualitative test in which the solvent was a mixture of alcohol and water was performed. Nice gels were obtained from *iso*-PrOH at 5-10 *mgc* for the four compounds so, in the same vials some water was added (<0.05 mL) making the gels to disappear slowly. Even when the gel was resolubilized by heating, in order to homogenize the mixture, sonicated and it was let to reach room temperature, the mixture did not gelate anymore. Therefore, water molecules destroy the gel network irrevocably, probably inserting between the peptide molecules. Tetrapeptides **106**, **7** and **121** formed gels in methanol and ethanol at rather high concentrations whereas compound **126**, which contains a C_6-alkyl chain at the *C*-end, was very soluble. In the other solvents, the behaviour of these four compounds was quite similar

although pseudotetrapeptide **126** required lower *mgc* in most cases, pointing out the influence of the lipophilic alkyl chain.

Table **8**. Pictures of the gels of compounds **106**, **7**, **121** and **126** in common solvents[a] at the *mgc*.

Compound	Solvent[b]													
	Pentane	**Toluene**	**1,2-dioxane**	**Et_2O**	**$CHCl_3$**	**EtOAc**	**THF**	**CH_2Cl_2**	***iso*-PrOH**	**Acetone**	**Ethanol**	**Methanol**	**MeCN**	**H_2O**
106	I			I										I
7	I			I	S									I
121	I			I	S									I
126	I			I	S							S	S	I

[a] Dielectric constant increases from left to right.
[b] I: insoluble. S: soluble.

A related behaviour based on a C_6-alkyl chain in low polar solvents was reported by Escuder and Miravet.[151] In a big family of linear tetrapeptides formed by glycine and alanine residues in alternation, crucial differences due to a C_6- or C_3-terminal substitution were observed.

Compound **129**, containing the C_6-alkyl chain, was able to gelate most of solvents tested from methanol to toluene but when it was C_3-substituted, the new compound **130** precipitated or did not form any gel in low-to-medium polarity solvents. This effect was attributed to the shorter chain in **130**, because in these solvents the polarity make the hydrogen-bonding to be more decisive and therefore, the alkyl chains may play a role in the solubilization of molecules by favourable interactions with the solvent (Figure **78**).

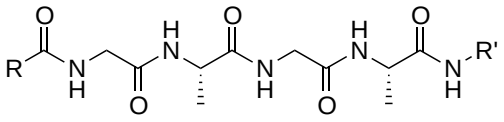

R= -CH_2-$(CH_2)_3$-CH_3 R'= -CH_2-$(CH_2)_4$-CH_3 **129**
R= -CH_2-CH_3 R'= -CH_2-CH_2-CH_3 **130**

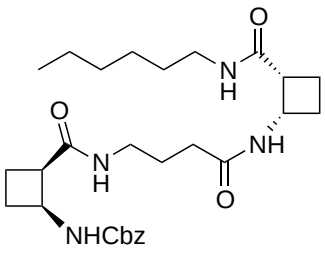

126

Figure 7**8**. For tetrapeptides **129** and **130**, reported by Escuder and Miravet, the length of the R' chain was found to be crucial in the gelation of low-to-medium polarity solvents, as observed in our pseudotetrapeptide **126**.

They were insoluble in pentane and diethyl ether, what could be also rationalized by the lack of long alkyl chains, and very soluble in chloroform, glycine tetrapeptide **106** being the only able to form a gel in this solvent at *mgc* = 122 mg/mL. Very nice gels were obtained in toluene in a 0.3-0.6 *mgc* range. Slightly higher *mgc* are required to form gels in ethyl acetate, acetonitrile and acetone and herein compound **126** required equal or slightly lower concentrations to form gels compared with tetrapeptides **106**, **7** and **121**. As observed qualitatively, the solvents in which the solubility of the peptides was low at room temperature but appropriate when heating, toluene, EtOAc or MeCN for instance, the *mgc* of the gels was lowered considerably compared to the rest of solvents. The importance of solubility with respect to the *mgc* had been accurately tackled by Smith, Miravet and co-workers for the first time in a joint publication.[156]

All the gels here described were stable at room temperature for weeks at their *mgc*. In addition, gels formed in toluene, CH_2Cl_2, $CHCl_3$ and MeCN were thermoreversible at concentrations beyond the *mgc* (15 mM approximately), while in oxygenated solvents as EtOAc, THF, 1,4-dioxane and the alcohols no evidences of thermoreversibility were found.

On the other hand, some qualitative experimental observations were stated during the preparation of the gels. All the gels formed by tetrapeptide **106** resulted to be the most opaque at the *mgc*, with the exception of the one in toluene, whereas the most transparent were the gels provided by pseudotetrapeptide **126**. In some cases, spontaneous gelation was observed for the organogelators **121** and **126** (see Annex section **3.5.2**).

In addition, hybrid hexapeptides **109** and **124** and octapeptide **125** were also tested, though their solubility and gelation abilities were restricted to alcohols. Only GABA-hexapeptide **124** was able to gelate some alcohols (see Annex section **3.5.2**).

Hydrogelation tests were also tried with some of the organogels provided by GABA hexapeptide **124** in the alcohols. Each vial contained 4 mg of **124**, the gel in only alcohol was formed and then deionized water was added. Subsequent mixing, heating and sonication did not afford any gel,

despite the solvents usually contain residual water, specially ethanol 96% (methanol and *iso*-propanol contained 0.017% and 0.1%, respectively). Results are summarized in Annex section **3.5.2**.

3.3.2.4. Supramolecular study of gels from hybrid tetrapeptides in toluene

The use of toluene as solvent to form the corresponding gels provided them in a good quality and an easy way. Its high boiling point allowed to solubilize completely the organogelators and made the time to reach room temperature to be longer, allowing a better homogenization. In addition, the *mgc* of the resulting gels was quite low and this solvent is appropriate to perform NMR experiments to gain insight into the sol-gel process. On the other hand, supramolecular studies with the aforementioned *trans*-cyclobutane-containing dipeptides were performed in toluene, which rendered satisfactory and reliable results.[14] Thus, the gels of tetrapeptides **106**, **7**, **121** and **126** in toluene were chosen for the following supramolecular study (Figure **79**).

Figure **79**. Toluene gels at 40 mM concentration used for the supramolecular study of tetrapeptides **106**, **7**, **121** and pseudotetrapeptide **126** (from *left* to *right*).

Their physical properties such as morphology, size and type of supramolecular arrangement were analyzed by using several techniques, including scanning electron microscopy (SEM), circular dichroism (CD) and IR spectroscopy. For some selected gels produced from β,α-tetrapeptide **106** in toluene, the self-assembly of the molecules was modelled to investigate their tridimensional arrangement. High-resolution NMR experiments were also carried out, with the aim of studying the dynamics of the sol-gel process.

Scanning Electron Microscopy

In collaboration with Dr. Judith Oró from the ICMAB, SEM experiments were carried out to investigate the morphology of the gels obtained from solutions in toluene. Wet gels were disposed on a carbon-film-coated copper grid and dried by standing for 30 minutes on the grid. The resulting xerogels (dry gels) were then introduced into the microscope chamber working at 70 Pa and 5 kV (Figure **80**).

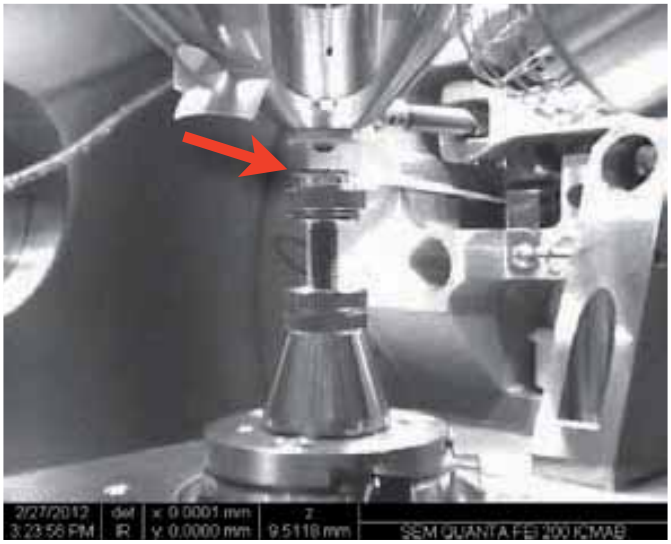

Figure **80**. Microscope interior chamber where the samples, previously deposited on a circular support, are placed to be analyzed.

Preliminary attempts were performed using gels from **106** at the *mgc* (7 mM), but SEM micrographs were poor in terms of image quality and quantity of material. Thus, other two concentrations, 15 mM and 40 mM, were tested, exhibiting that 40 mM solutions afforded more representative xerogels to be analyzed. Notwithstanding, the kind of material and aggregates in each case was proved to be the same or very similar, dismissing any sign of concentration-dependent morphology within these range (Figure **81**). Note that the micrographs are equally zoomed at 6000X magnifications.

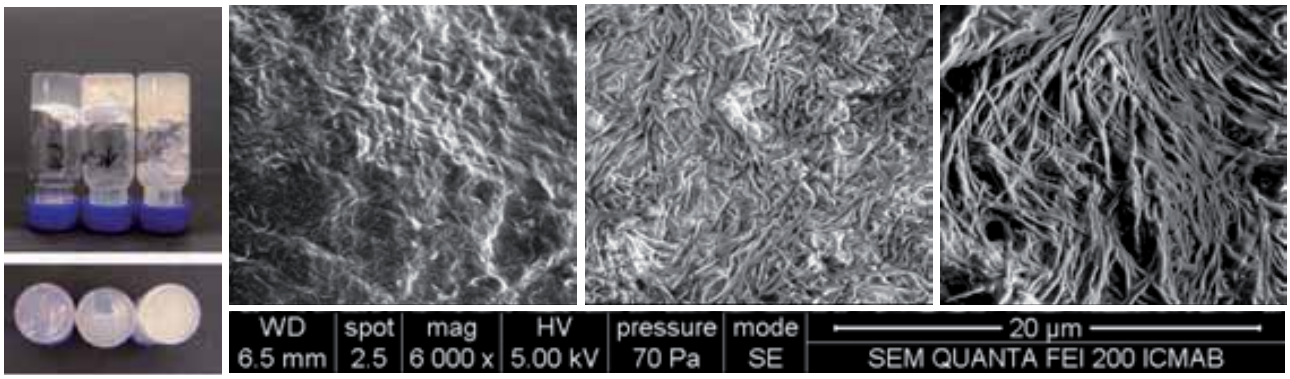

Figure **81**. Picture showing the gel of **106** in toluene at 7, 15 and 40 mM concentration from left to right. SEM micrographs of the xerogels from these gels at 7, 15 and 40 mM concentration from left to right. No significant structural differences were observed but better xerogels came from the 40 mM solutions.

Some selected SEM micrographs of the corresponding xerogels, from 40 mM gels in toluene, are shown in Figure **82**.

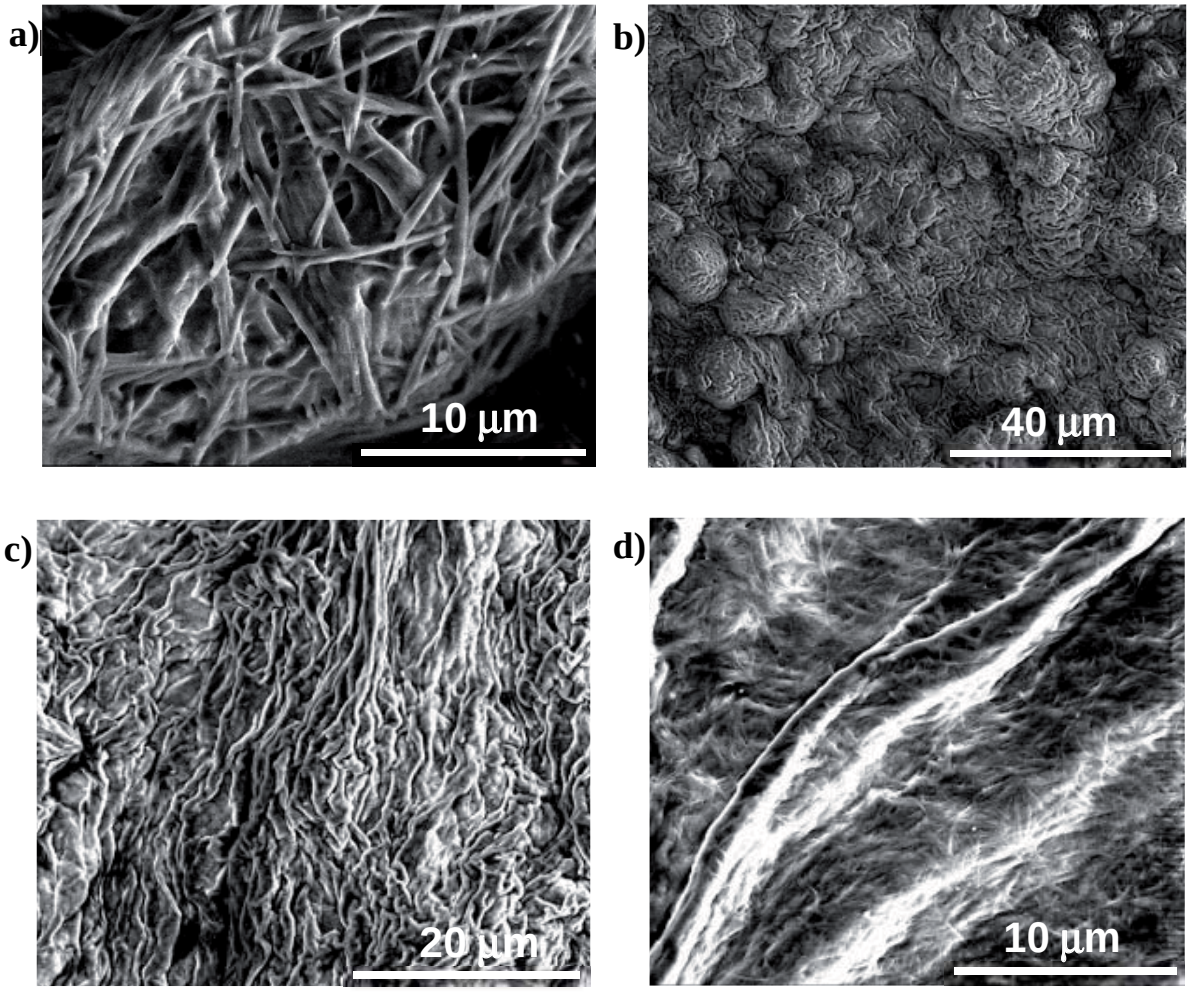

Figure **82**. SEM images of samples of **106** (a), **7** (b), **121** (c) and **126** (d) as xerogels (from toluene) on graphite at 70 Pa.

Tetrapeptide **106** exhibited the most defined structures, giving bundles of fibres with variable width (100-600 nm). **7** gave homogeneous and non defined structures with the appearance of rough spheres. Similar but more poorly defined and wider bundles were observed for tetrapeptide **121**, with respect to **106**. Compound **126** gave wide and undefined structures although it was possible to appreciate, inside the material, very small fibres that are intertwined with each other. This fits well with the higher molecular flexibility of **126** due to the absence of the ester group at the *C*-end, thus avoiding hydrogen bonds interactions. This fact accounts for the less ordered molecular and supramolecular structures observed. The different behaviour of tetrapeptide **7**, affording a spherulitic instead of a fibrillar network in the xerogel, was also evidenced in solution. Therein, a helical folding was observed while **106** and **121** presented β-sheet-type folding.

Furthermore, the definition of the supramolecular structures for **106**, **7** and **121** correlate well with the level of conformational order observed for the same molecules in solution. These properties emphasize the influence of the linear segment length connecting the cyclobutane moieties as much in the molecular as in the supramolecular level.

IR Spectroscopy

The N-H and C=O regions of the vibrational spectra of **106**, **7**, **121** and **126** in the solid state were investigated by IR spectroscopy, as were the corresponding bands for the xerogels from toluene (30 mM in KBr), in both cases using the ATR mode. Such data was also recorded in solution (5 mM in $CDCl_3$). Note that toluene was not used due to aggregation problems. Results are summarized in Table **9**.

Table **9**. N-H and C=O bands in the IR spectra of peptides **106**, **7**, **121** and **126** in solution, as xerogels from toluene and as solids.

Compound	NH[a]			CO[a]		
	Crystalline solid[b]	Xerogel[c]	Solution[d]	Crystalline solid[b]	Xerogel[c]	Solution[d]
106	3307	3305	3423	1703 1650	1759 1729 1686 1638	1739 1706 1662
7	3308	3305	3438	1734 1689 1642	1734 1689 1642	1712 1652
121	3308	3307	3439	1735 1668 1639	1733 1668 1640	1719 1656
126	3307	3307	3413 3310[e]	1688 1639	1690 1641	1703 1653

[a] In cm^{-1}.
[b] ATR.
[c] Xerogel from toluene gel at 30 mM in KBr.
[d] 5 mM solution in $CDCl_3$.
[e] Associated NH band.

No significant differences were observed between the spectra of the four xerogels. In chloroform solution, tetrapeptides **106**, **7** and **121** showed one band at about 3420-3440 cm^{-1} but bands

corresponding to associate N-H stretching were not observed in any case. In contrast, compound **126** showed two bands of comparable intensity at about 3440 and 3310 cm^{-1} (toluene) corresponding to free and associate N-H stretching, respectively. The N-H stretching bands were shifted to lower wave number and their intensity was slightly increased when passing from liquid solution to solid, in accordance with the formation of aggregates. Relevant features were not observed in the C=O region.

Since this technique did not allow to extract any applicable information to explain the self-aggregation of the tetrapeptides, CD was carried out.

Circular Dichroism Spectroscopy

CD spectroscopy in the solid state was used to obtain more information about the self assembly of the four compounds. The samples were prepared mixing the xerogels at 30 mM in KBr under an IR heating lamp. Next, thin films were made from the mixtures using a press and they were analyzed on a special set-up for this kind of samples.

The solid-state CD spectra of the xerogels displayed bisignate Cotton effects (Figure **83**). On one hand, they showed a negative Cotton effect at 224-226 nm, while a positive one at 242-251 nm was observed on the other hand. These CD signatures differed from the ones obtained of 0.5 mM solutions of these compounds in methanol, which indicated that the supramolecular arrangement in the xerogel was different from that in solution (section **3.3.2.2**).

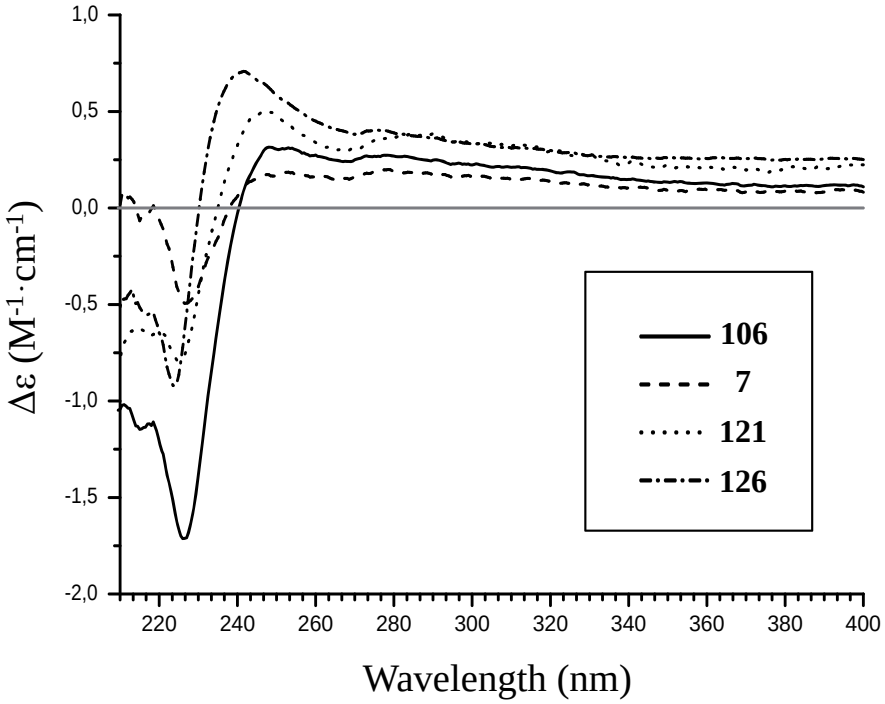

Figure **83**. CD spectra from xerogels from toluene in KBr, *c* = 30 mM.

According to data in the literature,[14,208-210] these values and intensities, especially for **106**, suggested that the molecules were organized in helical structures in the supramolecular aggregates.

Theoretical studies for tetrapeptide 106

In collaboration with Dr. Vicenç Branchadell, from the Chemistry Department of the *Universitat Autònoma de Barcelona*, computational calculations were performed on tetrapeptide **106**. Since it was the organogelator which gave more defined supramolecular structure, it was found interesting to determine how the molecules arranged themselves into the fibrils, observed by SEM in three of the compounds studied.

The self-assembly of the molecules was firstly tackled with the creation of an octameric aggregate, made by placing eight molecules of tetrapeptide **106** (from the most stable conformation in solution) one next to the other. Montecarlo conformational search[197,198] using the MMFF[211] force field implemented in the Macromodel program[212] was carried out for the octameric aggregate and the solvent effect was included through the GB/SA[204] method using chloroform. In the most stable structure was found that the molecules had been extended and the central ones interacted with each other through intermolecular hydrogen bonds involving **106**, whereas intramolecular hydrogen bonds prevailed in the terminal units (Figure **84**).

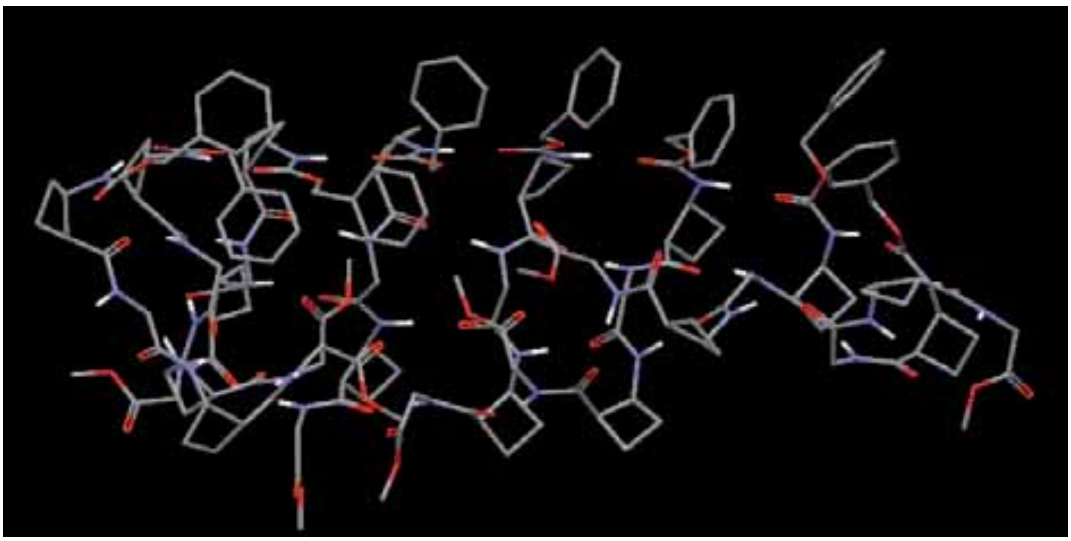

Figure **84**. Octameric aggregate resulting structure from first conformational search.

Next, from the interaction pattern between the central molecules, the structures of a dimeric (D), tetrameric (T) and hexameric (H) aggregates were constructed in a head-to-head (h-h) disposition and subsequently optimized at the M06-2X[211]/6-31G(d) level of calculation (Figure **85**).

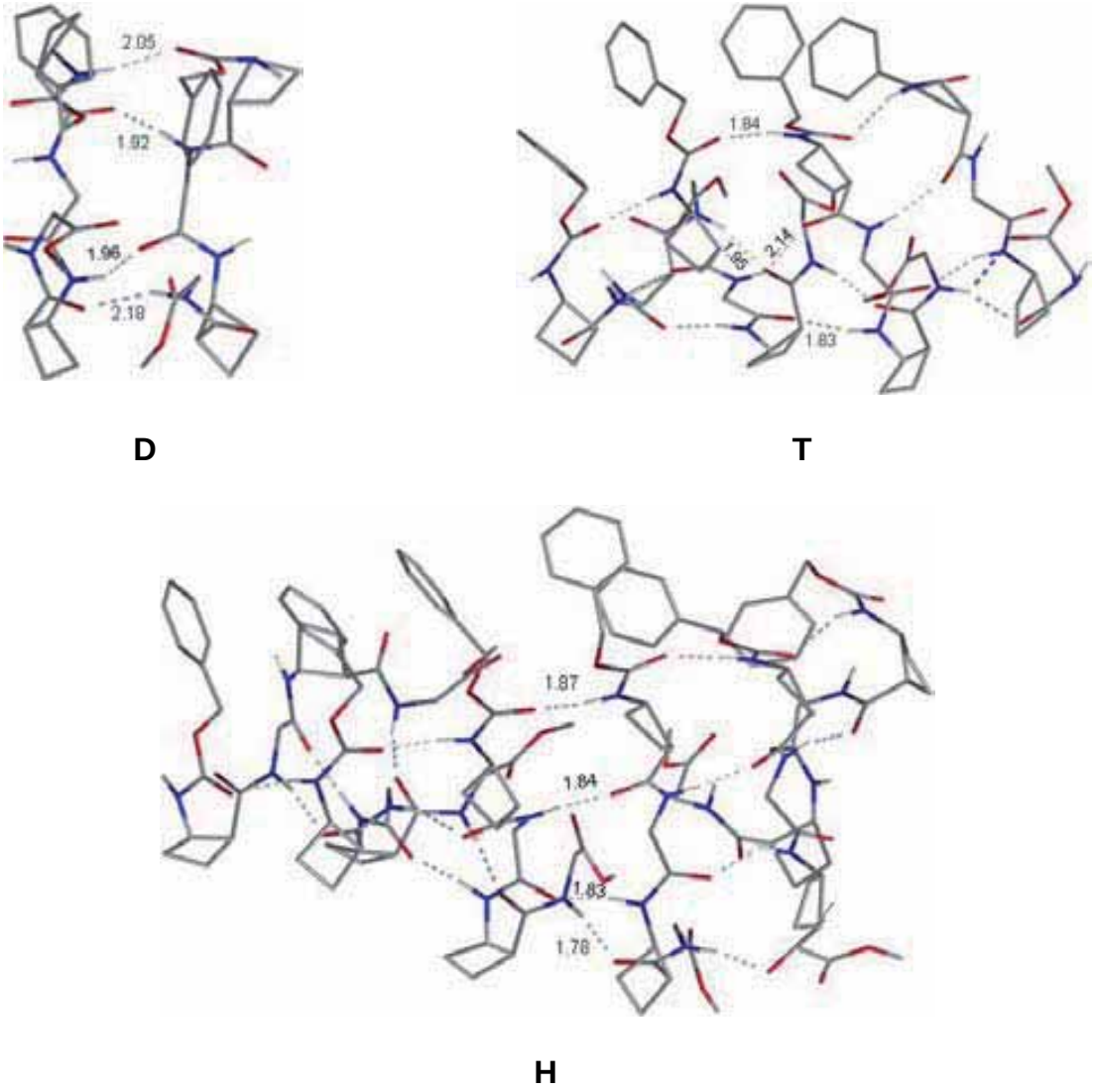

Figure **85**. Structures of dimeric (D), tetrameric (T) and hexameric (H) aggregates of peptide **106** optimized at the M06-2X/6-31G(d) level of calculation. Selected interatomic distances are in Å. Non polar hydrogen bonds were omitted for clarity.

Harmonic vibrational frequencies were computed for the structures of dimeric and tetrameric aggregates to ensure that they correspond to energy minima, all of them resulting in real frequencies. The energies of the obtained structures were recalculated at the same level of calculation with the 6-311+G(d,p) basis set in toluene solution using the SMD method.[212] These calculations were done using the Gaussian-09 program.[206]

In parallel, a head-to-tail alternative organization was considered for the dimeric and tetrameric aggregates but the corresponding structures were clearly unfavoured with respect to those shown in (Annex section **3.5.3.2**).

From these computed D, T and H structures, it could be observed that each tetrapeptide molecule was able to form up to eight intermolecular hydrogen bonds with its neighbours. These self-

assemblies showed that through the length of the aggregate the molecules were twirled one with respect to next other, exhibiting a tendency of tetrapeptide **106** to form helical aggregates. With regard to the hydrogen bond distances between the central molecules (see Annex section **3.5.3.2**), a tendency to strengthen the interactions as the number of molecules increased could be observed, a feature which was more evident in the central units. This fact could be confirmed when the aggregation energies were considered (Table **10**). As a matter of fact, the aggregation energy per molecule (ΔE/n) linearly increased, in absolute value, with the number of molecules, in such a way that there was a cooperative effect in the aggregation process.

Table **10**. Aggregation energies[a] computed for tetrapeptide **106**.

Structure	In *vacuo*[b]		In toluene[c]	
	ΔE	**ΔE/n**	**ΔE**	**ΔE/n**
D	-22.1	-11.0	-15.8	-7.9
T	-76.9	-19.2	-50.6	-12.6
H	-149.7	-8.8	-105.8	-17.6

[a] In kcal/mol. ΔE corresponds to the n **106** → (**106**)$_n$ process.
[b] M06-2X/6-31G(d) level of calculation.
[c] SMD-M06-2X/6-311+G(d,p)//M06-2X/6-31G(d) level of calculation.

From the central units of the hexameric aggregate H, idealized octameric (O) and hexadecameric (HD) aggregates were built and their structures were optimized at the MMFF level of calculation in chloroform solution. With this last calculation, the self-assembly of tetrapeptide **106** in a hexadecameric aggregate reflected, even more, the helical trend (Figure **86**). Aiming to situate the helical axis some approximate measures were taken, showing that the molecules were not completely parallel and they moved, one with respect to the others, in the three dimensions along the fibril. Although no repetition for a single molecule in the same position was found, 16 tetrapeptides was the average number of molecules per complete turn of the helix (Annex section **3.5.3.2**).

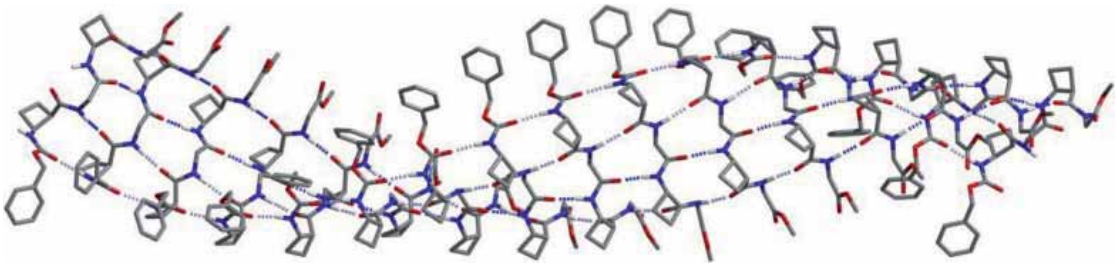

Side view

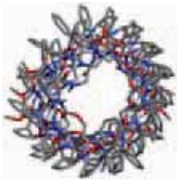

Top view

Figure **86**. Structure of the hexadecameric aggregate of peptide **106** optimized at the MMFF level of calculation in chloroform. Non polar hydrogen atoms have been omitted for clarity.

High-resolution NMR spectroscopy studies for tetrapeptide 106

In collaboration with Dr. Pau Nolis, from the NMR service at the *Universitat Autònoma de Barcelona*, high-resolution NMR experiments were carried out to complete the gelation study and determine the gelation temperature for the gel of tetrapeptide **106** in toluene (Figure **87**).

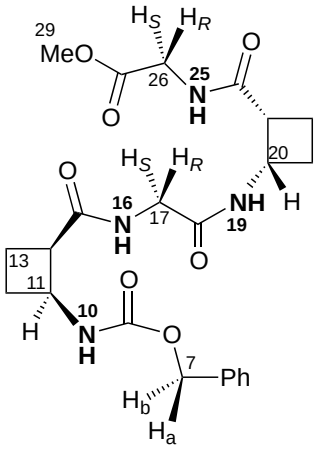

Figure **87**. Structure and numbering of tetrapeptide **106** for the NMR study, showing diastereotopic protons of glycine residues.

The gelation process of a solvent, in which the intermolecular interactions are enhanced by some external stimuli, reduces the mobility of the molecules. There are many gelation inductors but

change in the temperature is one of the most applied and adaptable to the NMR. Therefore, if the gelation is slow compared to the NMR time scale measurement, this dynamic event can be monitored by variable temperature ^{1}H-NMR experiments. In this specific study, a controlled cooling down regime was applied to a 30 mM sample. ^{1}H-NMR spectra were acquired in 5 K steps, starting from 375 K and lowering to 275 K (Figure **88**). An equilibration time of three minutes was used as sample thermal equilibration period.

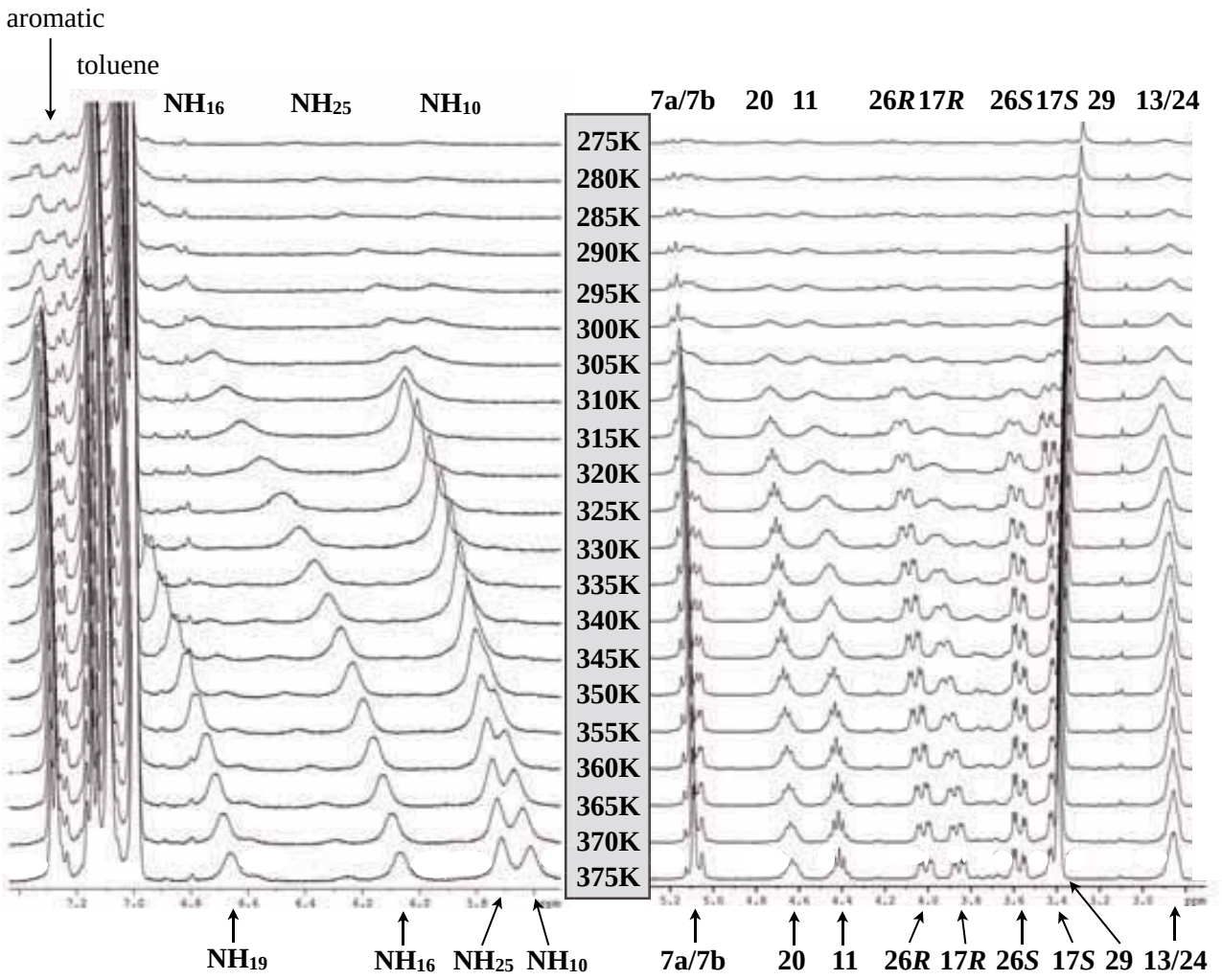

Figure **88**. Gelation process monitored by variable-temperature ^{1}H-NMR spectroscopy experiments in 30 mM solutions of **106** in toluene-*d8*. A 400 MHz Bruker Avance III spectrometer equipped with a cooling unit BCU-Xtreme was used. a) NH region from 5.6 ppm to 7.3 ppm. b) Aliphatic region from 2.8 ppm to 5.2 ppm.

Ordinary NMR experiments only permit the analysis of the electromagnetic radiation of the nuclei in the liquid part of the gel. Hence, by decreasing the temperature, a continuous signal line broadening was observed and finally a complete signal lost was produced due to the increasing "solid-like" part of the gel, which is not NMR-visible. Furthermore, since the gelation process was monitored in sufficient slow motion, a differential behaviour of similar signals was observed, which helped to better understand the gel-formation dynamic process. Adequate conditions of sample

concentration and appropriate cooling down gradient temperature were crucial in these experiments because gelation process strongly depends on both interdependent factors.

Regarding the experiment, two well distinguishable stages were observed during the cooling regime for all the protons. In the former, just prior to gelation, the intensity of signals increased and they became straighter. This was due to the molecule fixed positioning with a restricted conformational motion. In the second stage, signal intensities started to decay because the gelation process itself, in which the molecules become part of the solid-like material. It was noticeable that this occurred at slightly different temperatures for each NH proton (Figure **88**).

Graphical plots of normalized intensity and chemical shift were depicted for each, but some relevant cases are shown in here (Annex section **3.5.3.1**). Unfortunately, NH_{19} proton was overlapped by the toluene signal before disappearing and its complete behaviour could not be evidenced. Comparing the rest of NH signals, the fastest normalized intensity attenuation corresponded to NH_{16}, which started its signal decay at 350 K *vs* 340 K for the NH_{10} and NH_{25} protons (Figure 8**9**).

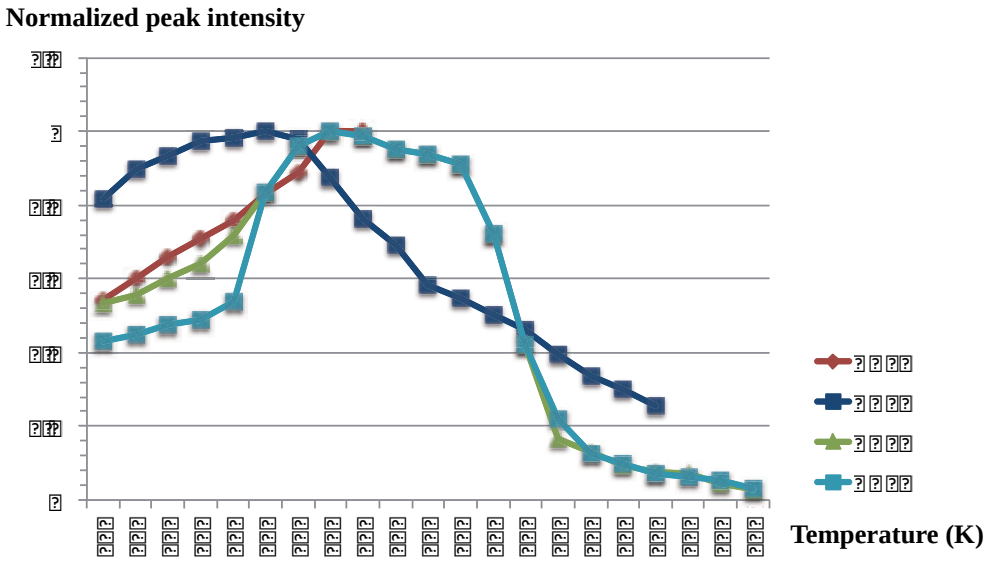

Figure 8**9**. Graphical plot of the normalized intensity of the four NH of peptide **106** during the gelation experiment from 375 K to 275 K (5 K step-wise).

This observation correlated satisfactorily with the performed calculations in the sense that NH_{16} is placed in central area of the gel structure, which is expected to be a more rigid region compared to both external sides (Figure **86**). The gelation temperature of a material is considered to be the temperature in which the gel is formed. However, as it is a dynamic process that involves a solution and a solid-like phases, this point is not usually a specific temperature. Thus, as the gelation of **106** takes place because of the hydrogen bonding from the four NH protons, the simultaneous intensity

decay of them was stated as the solution to gel temperature ($T_{sol\text{-}gel}$). This was considered to be about 350 K-340 K from a 30 mM solution of **106** in toluene-d_8 and for a cooling regime of 5 K step-wise from 375 K to 275 K. On the other hand, the global network gelation occurred at 310 K, in which the gel formation was suggested to be finished.

Another interesting feature about gel formation was observed in the aliphatic region (Figure **88b**). A quite noticeable differential behaviour of diastereotopic protons was observed during gelation process, both in terms of chemical displacement and gelation point. It should be highlighted that, to the best of our knowledge, this fact had not been reported before.

In Figure **90**, it can be observed that while H_{7a} proton started to attenuate at 330 K, H_{7b} attenuated at 350 K (their assignation was not possible). This indicated that gelation was being oriented in a direction that restrained the mobility of one of the diastereotopic protons. A more pronounced signal decay for both protons started at 310 K, which was attributed to the global network gelation. Moreover, a remarkable perturbation in the chemical shift displacement tendency of H_{7b} was observed at this point due to a conformational change to accommodate gelation. Finally, once the gel was totally formed, below 290 K, the same very low intensity was observed for both protons.

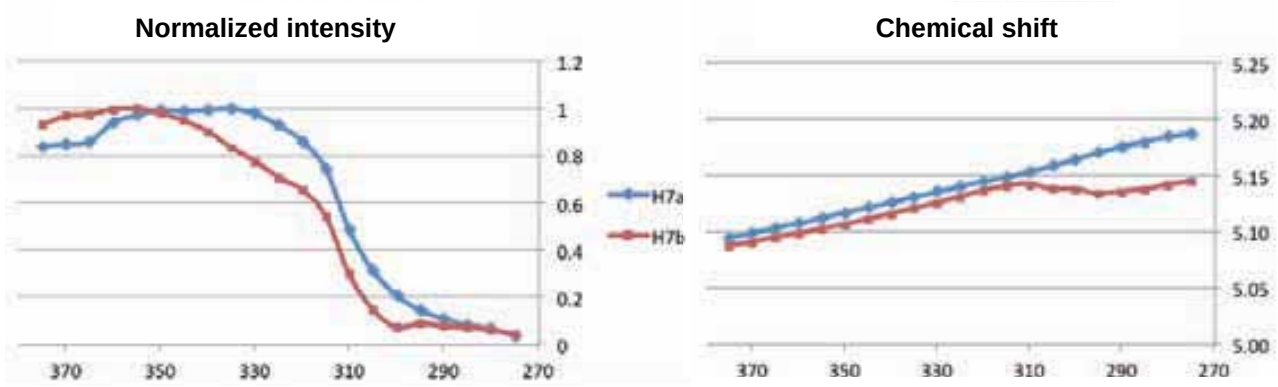

Figure **90**. Graphical plots of normalized intensity (*left*) and chemical shift (*right*) of protons H_{7a} and H_{7b}.

Similar differential behaviour was observed for H_{17} and H_{26} diastereotopic pairs of protons, although in a minor degree for the latter pair. This can be also explained by theoretical calculations, which suggested a structure for aggregates where the pro*R* H_{17} is in parallel to the hydrogen bonding direction, while pro*S* H_{17} is in a perpendicular position (Figure **91**). On the other hand, both pro*R* and pro*S* H_{26} protons are situated approximately at the same angle with respect the hydrogen bonding, therefore justifying their more similar behaviour.

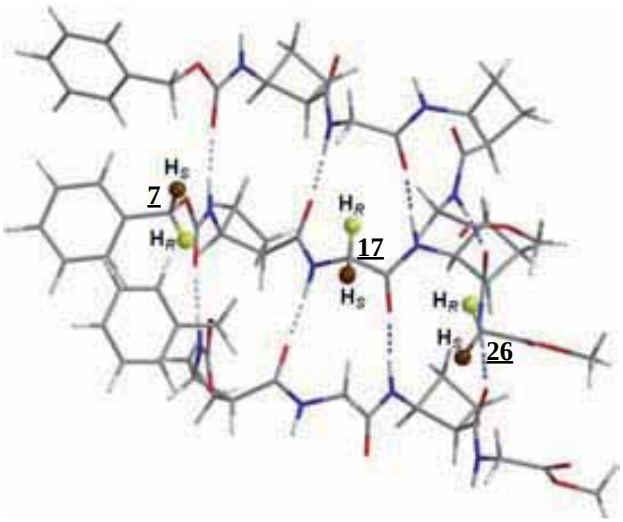

Figure **91**. Three consecutive peptide molecules from the hexadecameric aggregate of peptide **106** optimized at the MMFF level of calculation in chloroform. pro*R* and pro*S* hydrogen atoms of the central molecule are represented by yellow and brown spheres, respectively, and they correspond to H_7, H_{17} and H_{26} methylene protons from left to right.

Furthermore, cyclobutane H_{11}/H_{20} protons also showed this remarkable differential behaviour, being H_{11} the first proton to show signal attenuation due to gelation (Figure **91**). This fact was also in agreement with the structure from computational calculations because H_{11} is on the cyclobutane ring situated in the central area of the aggregate single-chain (Figure **86**). Comparatively, H_{20} attenuated later because it is on the cyclobutane placed in on of the external sides, which presumably is a more mobile area.

3.4. SUMMARY AND CONCLUSIONS

New hybrid peptides and pseudopeptides, consisting of chiral cyclobutane cyclic residues joined in alternation with C_2-C_4 linear residues and cyclobutene spacer, have been synthesized and studied. The intercalation of glycine, β-alanine and GABA with (*R,S*)-2-aminocyclobutane-1-carboxylic acid, providing hybrid α,β- β,β- and β,γ-peptides, respectively, modifies the secondary structure observed in homo poly(*cis*-cyclobutane) β-peptides, which show an extended ribbon-type conformation. On the contrary, this strong bonding is not disrupted by the incorporation of cyclic spacers, like in pseudopeptides **97** and **98**. The hybrid foldamers with linear segments allow conformational-bias tuning to β-sheet-like or helix-type motifs depending on the length of the spacer between the cyclic residues. The new conformations result from the production of inter-residue NH···OC interactions, which often are in rapid equilibrium with the intra-residue ones, affording the so-called bifurcated hydrogen bonds.

So, the propensity to helical folding previously reported in the literature[213-216] for other hybrid α,β-peptides switches to the formation of β-sheet-like structures due to the local flatness imposed by the *cis*-cyclobutane residues. In fact, neighbouring side-chain juxtapositions in the 14-helix are similar to those encountered in a β-sheet. CD and NMR spectroscopy suggest structures for β,γ-peptides similar to those of α,β-peptides. For GABA derivatives, NMR evidences the concurring presence of other related conformers, which can be explained by the higher flexibility of the C_4-fragment. In addition, some structural motifs present in proteins and α-peptides like γ- and δ-turns have been analogously found in the most stable hybrid structures.

The case of β-alanine seems to be special and the C_3-alternate fragment affords an appropriate scenario for a genuine helical folding. These results are relevant in the design of foldamers with well- defined and predictable conformations which currently are the object of active investigation in view of some possible applications in different fields.

The three hybrid α,β-, β,β- and β,γ-tetrapeptides and a β,γ-pseudotetrapeptide investigated have shown their capability to gelate several organic solvents, being toluene the one which required the lowest *mgc*. SEM has revealed that **106**, **121** and **126** present fibrillar networks in the xerogel while regarding **7** a spherulitic network is evidenced. The most defined and regular morphology is observed for **106**, fact that correlates the flexibility of tetrapeptides **106**, **7** and **121** with their ability to self assemble into ordered aggregates, as previously observed in solution.

Computational calculations performed on **106** suggest a helical arrangement of the self-assemblies in excellent agreement with CD and NMR spectroscopies. Moreover, NMR allows to conclude two interesting points: firstly, gel structure of **106** around the gelation point has two differentiated

regions concerning mobility. There is a more rigid central region and there are more flexible regions at the sides of the aggregate structure. Secondly, gelation occurs in such a way that a chiral supramolecular structure is produced and prochiral diastereotopic methylene protons are differentiated *during* the gelation process. This fact is strongly in agreement with a certain degree of chiral helicity in accordance with CD studies and also with computational calculations, as shown in Figure **92**.

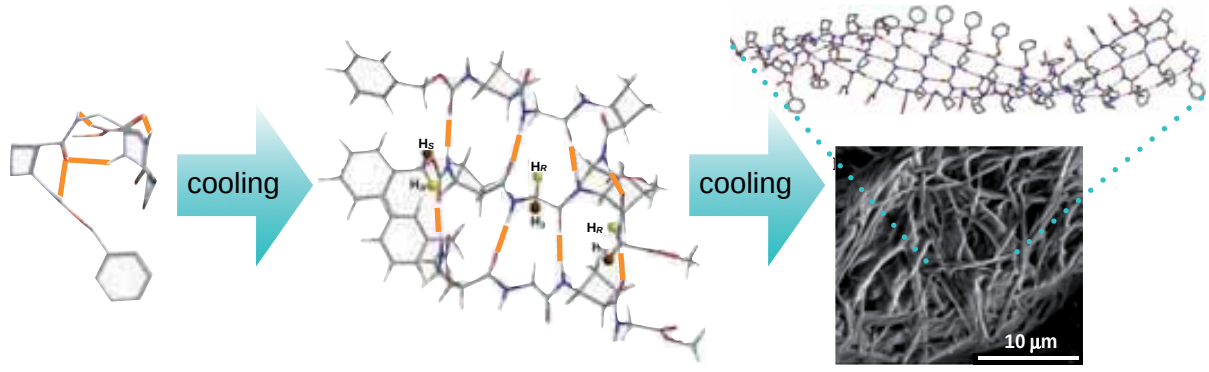

β-sheet-like
Solution conformation

1D Fiber self-assembly

Helical fibers
Supramolecular structure

Figure **92**. Gelation process suggested for the hybrid α,β-tetrapeptide **106**.

CHAPTER IV

NTA-based Tripodal Amides as Anion Receptors

4.1. INTRODUCTION

The discovery of crown ethers and their unique complexation properties in the 60s gave birth to a new field in coordination chemistry that is now called host-guest chemistry, all embraced in the broader concept of supramolecular chemistry. Host-guest chemistry describes the complexes formed by two or more units that hold together by non-covalent interactions. These bonds are represented by the common intermolecular interactions such as hydrogen bonds, ionic bonds, van der Waals forces and hydrophobic interactions. This kind of supramolecular chemistry involves the recognition of the host towards the guest in the way that the host molecules entraps, encapsulates or even just slightly retains the guest unit.

4.1.1. Host-guest chemistry: from origins to podands

About 50 years ago, some developments in macrocyclic chemistry started to motivate the field of supramolecular chemistry. In the early 50s, Donald Cram had worked on macrocyclic cyclophanes, spherands and carcerands trying to imitate naturally occurring macrocycles. In the mid-to-late 60s, Curtis, Busch and Jäger synthesized three imine hosts for cationic guests using a Schiff base condensation reaction. However, it was not until 1967, when C. J. Pedersen submitted a manuscript with the first series of crown ethers, that host-guest chemistry sprung up. He reported the by-now-classical 18-crown-6 **131**, and its ability to bind cations. In the same year C. H. Park and H. E. Simmons reported the first synthetic organic ligands of the bicyclic diammonium type or diazabicyclic, named *katapinands*, **132**, which were able to bind halide anions. Both were major contributions to the beginning of modern supramolecular chemistry (Figure **92**).[217,218]

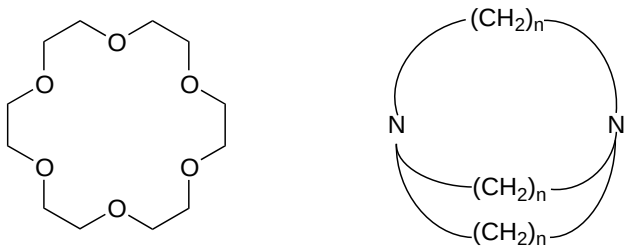

Figure **92**. First cation receptor 18-crown-6 **131** (*left*) and the first anion receptor *katapinand* **132** (*right*).

Pedersen's publication had a great impact and new ether-type complexating agents were swift to appear, whereas the diammonium bicyclic anion receptors of Park and Simmons were not so successful. So here, we can see that coordination chemistry of cations started to be extensively studied contrary to anion coordination.[217]

During the 70s and 80s, interest and developing in non-covalent anion coordination chemistry continued, with great contributions by F. P. Schimdtchen and J. M. Lehn, who previously synthesized them in the late 60s, mainly of cryptand type (analogues of *katapinands*).[218]

Anions play a variety of roles in both organic and mineral worlds. For example, 70-75% of enzyme substrates and cofactors engaged in biological processes are negatively charged species and very often phosphate residues (ADP^{3-}, ATP^{4-}) or inorganic phosphate ($H_2PO_4^-$).[219] Because of their intrinsic more complicated characteristics (i.e., solubility, hydration energy, large size and numerous geometries), anion recognition by synthetic receptors has not been developed as wide as has been done with cations. Nevertheless, their complexation of the anions by synthetic hosts has recently been stated as a new area of coordination chemistry.

Classification of supramolecular host-guest compounds is simple and provides two kind of complexes, irrevocably related to a host classification. *Cavitands* may be described as hosts with permanent and intrinsic intramolecular cavities and exist both in solution and in the solid state. On the other side, *clathrands* are hosts with extramolecular cavities, the cavity essentially represents a gap between two or more host molecules and it only exists in the solid state. Even so, these are wide-broad definitions and within the *cavitands* many hosts have molecular or ion recognition with no closed cavities, receptors which undergo conformational changes upon the guest presence. These models of binding, *lock and key* model and *induced-fit* model, were described for the enzyme-substrate complexes by E. Fischer in 1894 (Figure **93**).[218]

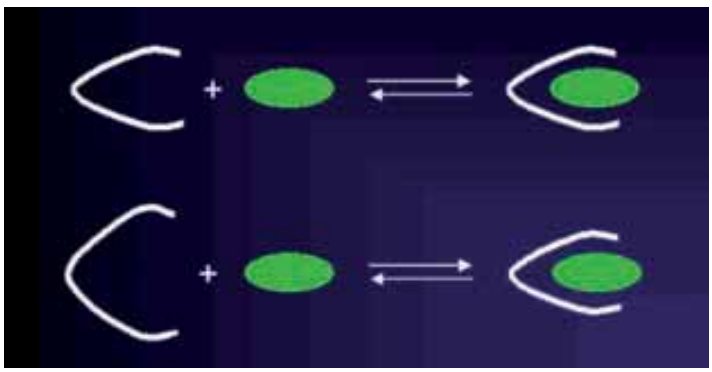

Figure **93**. Schematic representation of *lock and key* model (*top*) and the *induced-fit* model (*bottom*).[220]

Apart from parent-type crown ethers compounds, a wide range of monocyclic coronands or crown compounds, bi- and oligocryptands (spherands when they have spherical structure), cryptophands, hemicarcerands and carcerands and even more complex systems have appeared in the world of hosts (Figure **94**).

Anyway, many times, less is more. High selectivity and stability of complexation of complicated structures entails a high expenditure of preparation and low kinetics of complexation, so here, the evolution to the design of less-complicated structures has risen up.

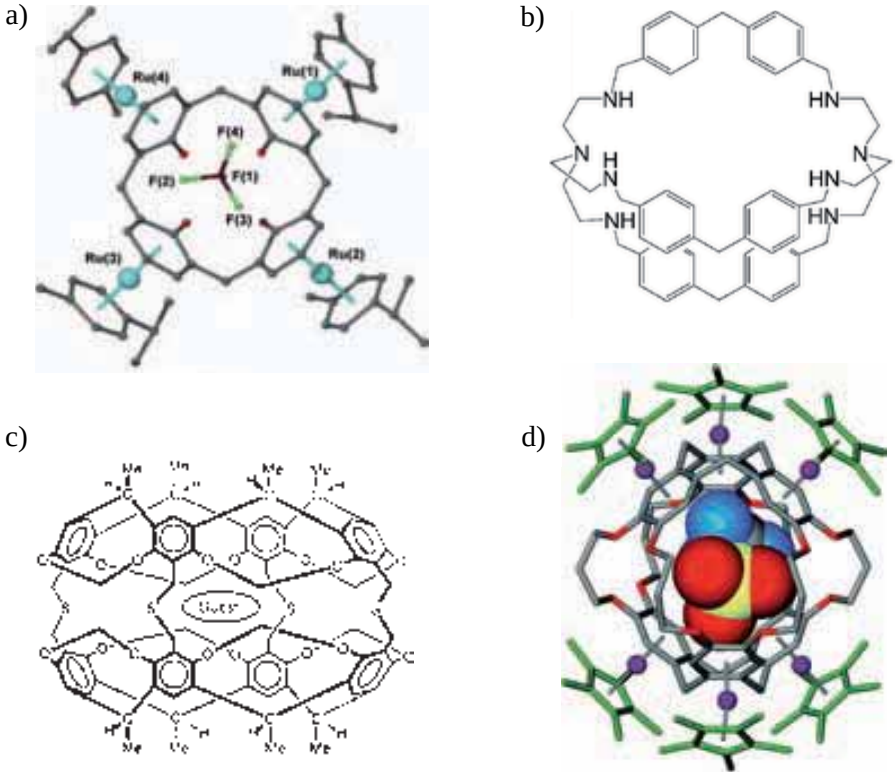

Figure **94**. a) Crystal structure of BF_4^- inclusion complex with Ru-metallated calixarene.[221] b) Bis-*tren* based cryptand able to bind dianionic terephthalate when hexaprotonated.[222] c) Carcerand or carceplex by combination/shell closure of two cavitands, where guest can be Cs^+, Ar, DMF, Bu_2O.[223] d) Triflate inclusion by Ru-metallated cryptophane.[224]

This process has led to podands, open-chained analogues of crown molecules and cryptands by definition. They were well known before host-guest chemistry was stated because their structural features are traditional in ligands such as oligoamines, salens, oligoglycols, etc. used in inorganic coordination chemistry, and in some natural cation-binding ionophores (i.e., antibiotics, siderophores). Indeed, many anion recognition events take place by the usage of cationic hosts, generally podal ligands previously attached, in several ways, to metal cations.[225]

The name podand comes from the Greek meaning foot but it is commonly referred as arm. This term was coined by Vögtle and Weber in 1979, whose work involved quinoline-terminated podands such as **133**, which are able to entrap several alkali cations giving crystalline solids (Figure **95**).[218]

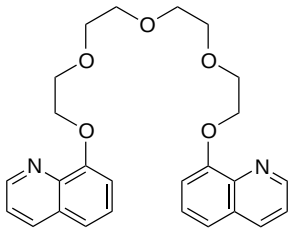

Figure **95**. Quinoline-terminated podand **133** developed by Vögtle and Weber.

Other definitions say that podands are multidentate organic ligands, host molecules with pendant binding sites[226] or multidonor-site host molecules and their characteristic structural feature is the alignment of donor atoms (D) in the open-chain backbone.[227] The arms are branched from an anchor group (A) and it usually is an aromatic or an oligovalent atom (often C, N, P but also B, S, As). The noncyclic backbone can be a simple line of atoms or a branched or multibranched arrangement (from mono-, di-, tri- to multipodands), and the most common bridging element connecting the donor atoms between them or with a common anchor group is ethylene unit, 1,2-phenylene and related groups, enhancing the overall preorganization of the podand as more rigid the spacer element is (Figure **96**). [228-230]

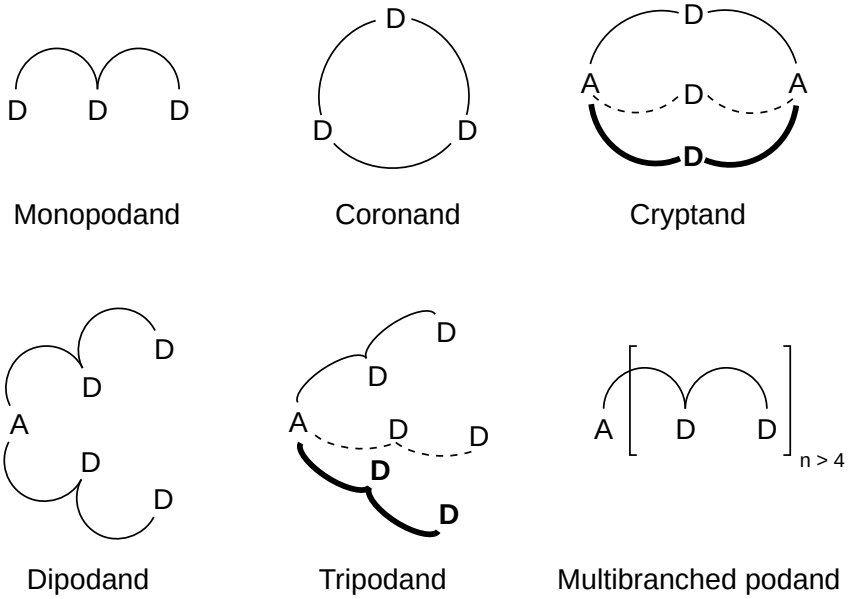

Figure **96**. General classification and nomenclature of podands.

Podands provide not only synthetically simpler receptors but they can display a wide scope of binding groups in their structure and they can modulate the flexibility degree with different levels of preorganization, allowing flexibility in host design to suit almost any analytical and sensing application. Probably, anion recognition is the major focus of work in the podand field at present.

4.1.2. Relationship of host structure and anion geometry

The evolution of anion coordination chemistry as time went by can be described, up to a certain point, by the increasing complexity of complexes in terms of geometry of the anions. So, spherical anions such as halides were the first to be studied. Ligands or receptors used were different types of macrocycles (*katapinands*, bicyclic, tricyclic) varying on their size, total charge and heteroatoms fitted in their hydrocarbonated structures. These heteroatoms are basically N atoms (in the form of secondary, tertiary o quaternary amines, mostly protonated), O atoms, and other atoms such as B, Sn, Si or Hg (Figure **97**).

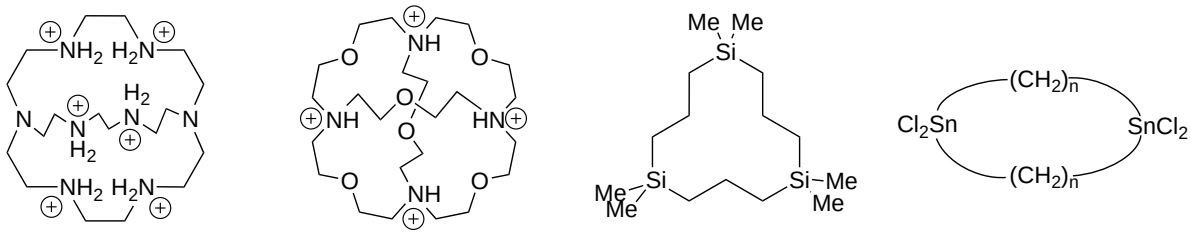

Figure **97**. Some examples of hosts for halide complexation. First bicyclic host binds F^- because of good complementarity between anion size and the ligand's cavity.[231] Macrotricyclic compound binds Cl^- with great affinity (logK > 4 in H_2O).[232] Silicon-containing host has shown to transport chloride and bromide across an organic layer.[233] Neutral receptor provided with Sn as Lewis acid forms 1:1 and 1:2 complexes with Cl^- in acetonitrile.[234]

Recognition on molecular anions with a linear geometry was first reported in the case of azide, bound by the hexaprotonated macrobicyclic receptor.[235,236]

The important recognition of planar trigonal carboxylate anion, owing to their fundamental biological roles, was widely reported (Figure **98**).[237] Its best-adapted unit of recognition is considered to be the guanidinium unit because it is able to form two zwitterionic hydrogen bonds and it has a high protonation constant, which makes the guanidinium to exist in a wide range of pH. Other receptors for carboxylate anions are based on azamacrocycles, quaternary ammonium, amide groups and diuranyl-containing metallomacrocycles, among others.

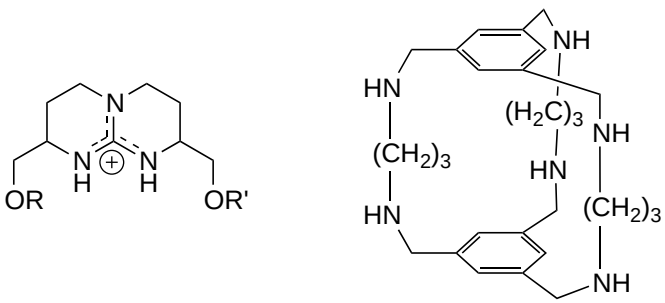

Figure **98**. Guanidinium-containing receptor has been largely used for carboxylate complexation (*left*). Hexaprotonated ligand has shown to form 1:1 complex with nitrate in solution but X-ray analysis revealed that anion was not located within the cavity (*right*).

Tetrahedral anions such as phosphate and their biological derivatives (AMP^{2-}, ADP^{3-}, ATP^{4-}) have been entrapped in complexes due to binding by guanidinium- and ammonium-containing receptors (Figure **99**).[238,239]

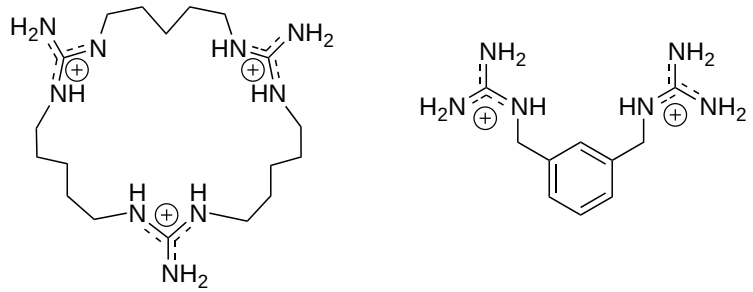

Figure **99**. Receptor containing three guanidinium units binds phosphate anion (*left*). Natural phosphate-containing nucleotides have been recognised by bis-guanidinium ligands (*right*).

Sulfate and perchlorate anions have been also complexed by protonated polyazamacrocycles.[240,241]

Square planar anions such as $PdCl_4^{2-}$ have been complexed by protonated macrocycles.[242]

Octahedral anions as SiF_6^{2-}, $Fe(CN)_6^{4-}$, $Fe(CN)_6^{3-}$ or $Ru(CN)_6^{4-}$ can also be entrapped inside big polyammonium macrocycles, so they become the second coordination sphere of transition metals (Figure **100**).[243]

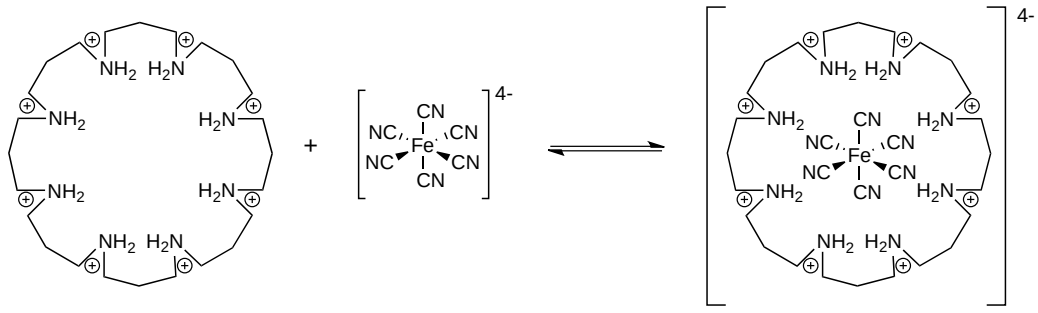

Figure **100**. Polyammonium macrocycles can host other anionic complexes as inorganic coordination compounds.

In the middle of the 90's, the concept of molecular recognition of the anions was used to construct large-size molecular assemblies where anions and cations were interconnected by intermolecular interactions such as hydrogen bonds or electrostatic forces. While this is not a formal recognition process novel molecular structures as rods, tapes[244] and sheets were obtained and they led to one dimensional solids. An example of those is the salt with two components: bisamidinium cation and the terephtalate as anion (Figure **101**).

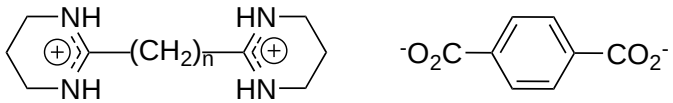

Figure **101**. Some diammonium molecules form rods and tapes when interacts with terephtalate dianion.

4.1.3. Amides and thioamides as binding sites in receptors

Although polyammonium hosts were more present in the area initially, in the 80s researchers started to focus on other H-bond donor groups, mainly including amide/thioamide, urea/thiourea[245,246] and sulfonamides. For example, Pascal and coworkers reported the amide-based cryptand **134**, which bound fluoride in DMSO-d_6.[247] Reinhoudt and coworkers published a *tren*-based amide **135**, which would become one of the most used tripodal scaffolds for the receptors with three branches.[248] Thioamides were not explored until the early 2000, when Yamamoto and Bowman-James groups almost simultaneously published the first thioamide-based receptors **136** and **137**, respectively (Figure **102**).[249,250]

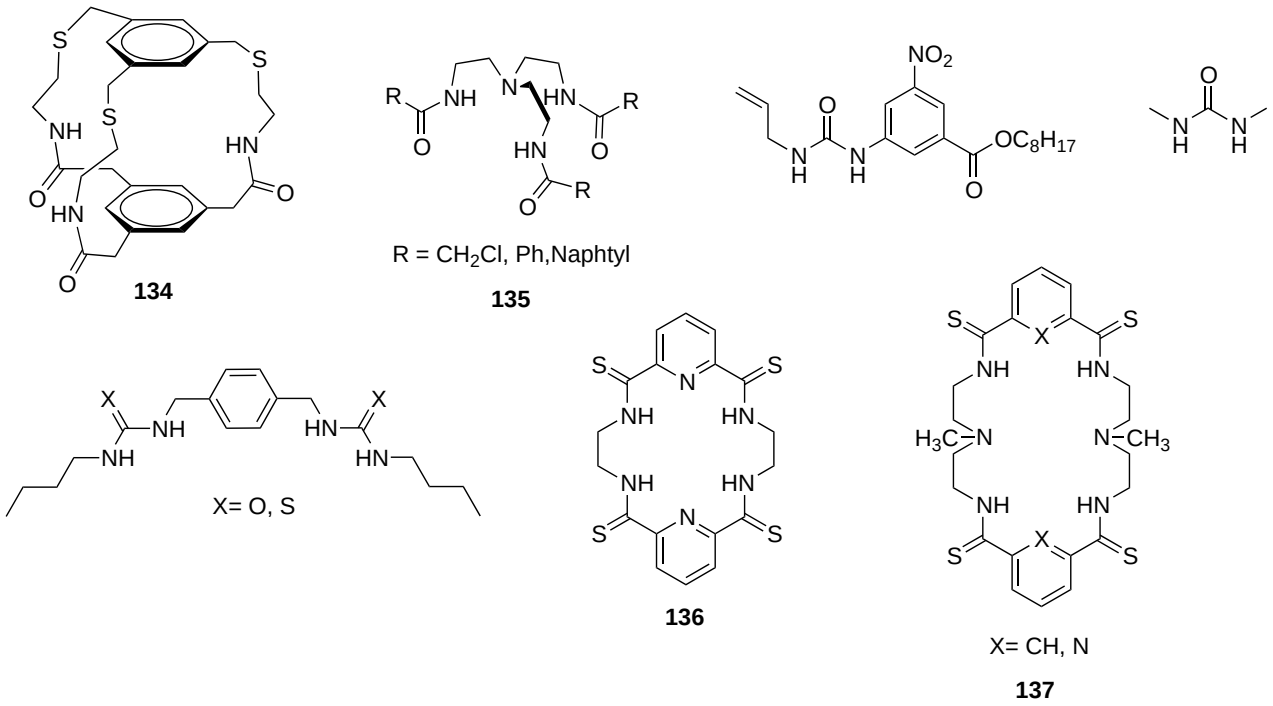

Figure **102**. Anionic hosts of different structure and based on amide, urea or thiourea binding sites.

Crabtree introduced diamide-based hosts **138** for halides Br^- and Cl^- (Figure **103**).[251] It was an important contribution, as the one by Beer, who reported a very good tripodal *tren*-amide-based receptor **139** for $H_2PO_4^-$, with an impressive binding constant of $K_a = 1.4 \cdot 10^4$ M^{-1} ($\log K_a = 4.2$) in acetonitrile despite its fundamentally flexible nature.[252] Such receptors have applications as redox sensors.

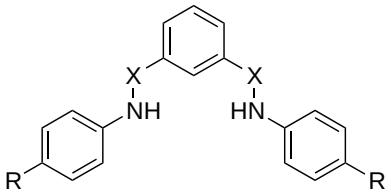

R= H, X= CO
R= *n*-Bu, X= CO
R= H, X, SO_2

138

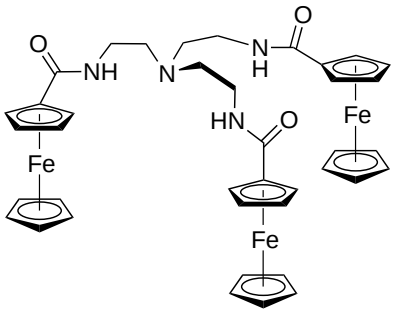

139

Figure **103**. Dipodand amide-based receptor selective for chloride and bromide (*left*) and tripodal amide-based metallated receptor with high affinity for dihydrogenphosphate anion (*right*).

Other *tren*-based receptors, are the ones reported by the Bowman-James group, which examined the influence of chain length on binding nitrate anion with the protonated host **140**, forming a lipid-bilayer-like complex (Figure **104**).[253] One of the amide carbonyl groups was observed to be intramolecularly H-bonded to an adjacent amide NH proton, which is a drawback that amide-based receptors sometimes have. Gosh and coworkers presented also a protonated *tren* derivated host **141** with nitro substituents in the aromatic rings.[254] Once more, the encapsulation of an anionic species, bromide anion in this case, is prevented by the same type of intramolecular hydrogen bond.

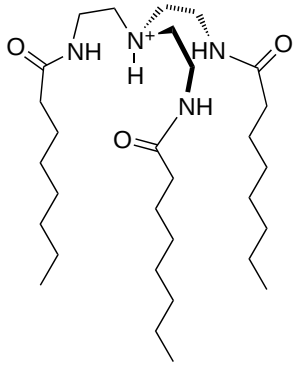

140

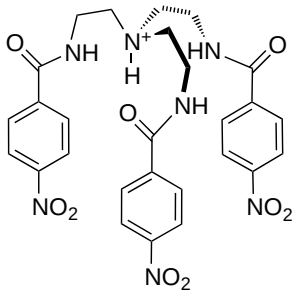

141

Figure **104**. Two C_3-symmetric tren-based receptors **140** and **141** in their protonated form on the apical N atom.

The interest of amides in host molecules is quite related to the structural analogy of the amides in proteins, able to form defined and stable secondary and tertiary structures. While amine hosts act as H-bonding donors mainly when they present the protonated form, amide-based receptors readily form H-bonds when neutral.[255] By adding a second NH group attached to the carbonyl of an amide, a urea is obtained, which interest is due to its directional and potentially chelating properties. When the oxygen atoms of an amide and a urea are replaced by sulfur atoms, giving a thioamide and a thiourea respectively, hydrogen bonding properties are improved because the more polarizable sulfur atom weakens the NH bond by about 10 kcal/mol.[256] That is to say that increases its acidity;

for example, in DMSO, the pKa of thiourea is 21.1 whereas pKa of urea is 26.9.[257] So they are an attractive subarea in the development of new receptors with high anion association.

Referred to this point, Zielinsky and Jurczak synthesized, using Lawesson's reagent, thioamide **142** from the corresponding amide **143** in THF (Scheme **32**). Association constants were determined to be K_a= 3.8 and 11.1 M^{-1} for chloride ion for **143** and **142**, respectively, by titrations in DMSO-d_6 with 0.5% of H_2O.[258]

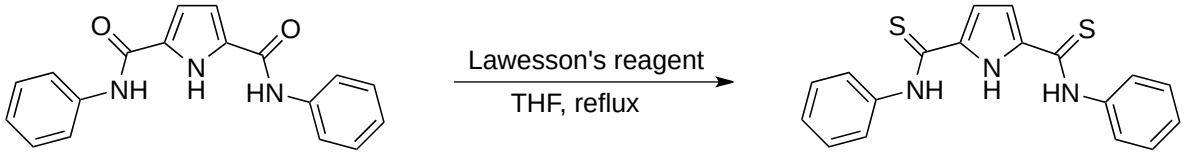

143 **142**

Scheme **32**. Transformation of the aromatic diamide **143** into the more Cl-selective thioamide **142**.

4.1.4. Synthesis of podands

Most of the conventional podands are well known because they were used in inorganic coordination chemistry before being used in host-guest chemistry. Most of them are industrial products (polyethyleneglycols, PEG monoalkyl ethers, glymes, nonoxynols, etc.)[259] usually obtained by polymerization of ethylene oxide and other synthetic units forming the final polymer. Nevertheless, polymerization gives mixtures of compounds, not useful when pure compounds are required. Other podands are natural ions receptors found in nature, for example carboxypeptidase A, phosphate and sulfate binding proteins, superoxide dismutase, siderophores found in some bacteria and fungi and the oxygen carrier metalloprotein in mammalians, hemoglobin.

In fact, the synthesis of podands is, by far, less problematic than the industrial polymers, macrocyclic crown compounds and other more complicated systems.[260] Hence, podands are generally obtained by using conventional synthetic methods among which we find the ether, sulfide, ester or amide bond formation.[228,229] However, some difficulties can arise from the synthesis of multibranched podands, as it occurs with dendrimers, with respect to the control of reactive sites.

It is also worth to take into account the concept that Vögtle and Weber developed within their work. They observed that flexibility of podands led to lower affinity because they adopt non-binding open conformations. This drawback can be corrected using more rigid anchor groups as aromatic cores but it can also be rectified by the "end-group" concept. This consists in adding rigidity at the end-groups of the arms of the podand and it is normally performed by derivatising them with functional groups (aromatic, ester, amide) capable of giving interbranched non-covalent interactions to reduce

the conformational freedom. In this way, the ordered end-groups become the trapdoor where the cation/anions pass through to the binding area of the podand.[218]

In order to deal with the global synthesis of the desired final hosts/receptors two strategies can be chosen. We have divergent or convergent synthetic strategies, which arise from the synthesis of dendrimers. Dendrimers are repetitively branched molecules with a central core from which one or several generations of functionalized branches are sprout. Therefore, the relationship of dendrimers with podands is clear; they have very similar structures because a podand is a dendrimer with a specific number of branches or arms. The clue is that in podands a repetitive moiety is not usually found until the end-group is reached, whereas in dendrimers there is a unit that is repeated until the dendron reaches the surface (Figure **105**). In dendrimers, all the iterated units at the same level or distance around the core are called generation. This definition reflects what Steed and Swinburne stated in their article: "The multiarmed podands lead naturally into the key concept of multivalency and they are the conceptual precursors of dendrimers".[255] From another point of view it could be said that podands are like dendrimers of first generation.

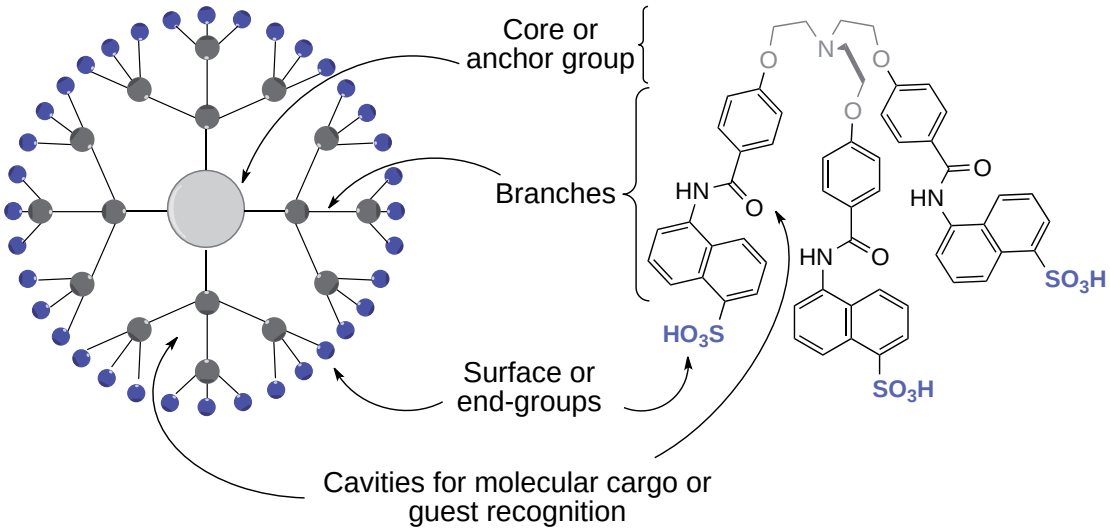

Figure **105**. Comparative illustration between dendrimers and podands structure.

Anyway, although the podands here described have no repetitive units, the concept of divergent and convergent synthesis can be applied:

- A divergent route is characterized by a branch *B* growth from the starting anchor group *A*. This growth is carried out on all the reactive sites of the core at the same time and in a one-pot reaction. For example, starting from *A* as a core with three reactive sites, three branches *B* can be assembled through a substitution reaction. The main problem related to this strategy is to remove impurities

of trailing compounds (uncompleted reactions could lead to mono- or di-substituted compounds) because their size and properties are very similar and this complicates the separation.

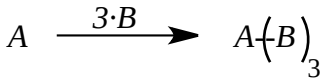

In dendrimers, more reactions could be performed on the peripheral groups until the desired generation was reached:

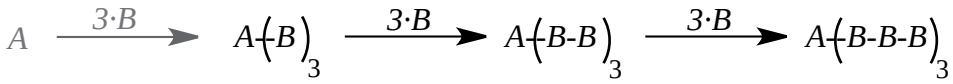

- A convergent route instead, is based on a first synthesis of one segment *A'-B*, where one branch *B* is already attached to a fraction of the anchor group *A*, called *A'*. In parallel, the other two branches *B* are attached to a second fraction *A"* to give two second segments *A"-B*. Then, and here the convergent step takes place, one segment *A'-B* is attached to two segments *A"-B*. The clue is that the core *A* is synthesized by the substitution reactions between the segments. The advantage of this strategy is a more controlled final composition and that purer compounds are obtained; anyhow, larger sizes are not possible because crowding around the anchor group is limited by steric effect.

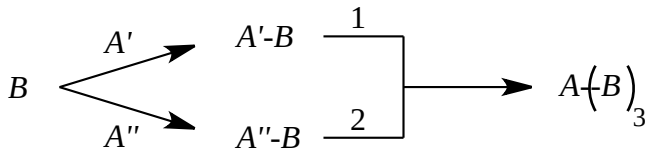

In the dendrimer analogy:

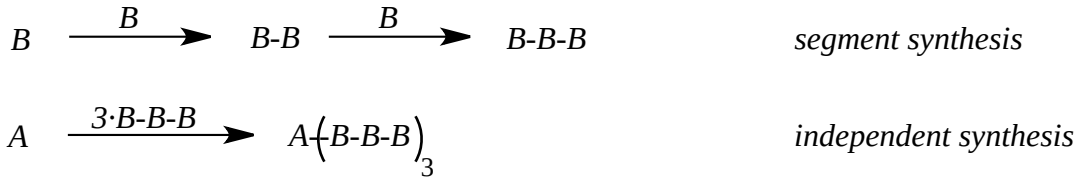

4.1.5. Analogues of tripodal 2,2',2"-nitrilotris(*N*-amides)

Podands have emerged as simple and effective receptors because of their easier synthesis and low cost compared to big macrocycles, which usually involve special and critical reaction conditions. It is important to remark that the term of podand refers to the number of branches sprouting from the anchor group, it is a simple atom or a molecule, that is different from the number of binding atoms in the whole molecule. In a host, the number of branches is specified by the *number prefix* +

podand and the number of binding atoms (coordination number) is usually expressed as the *number prefix* + *dentate*. For instance, Jurczak and collaborators reported dipodand **144** based on an isoindoline group, but the receptor binds benzoate anion in a tridentate manner, employing all three NH protons of the molecule (Figure **106**).[261]

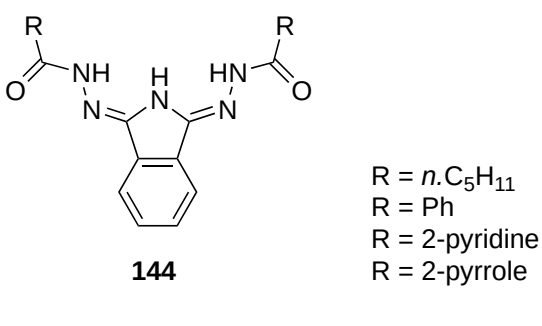

Figure **106**. Dipodand receptor molecular structure with an isoindoline core and various end-groups (*left*). Crystallographic structure of the host (R = Ph)-benzoate complex: dipodand host has a tridentate coordination to the anion (*right*).

Nowadays, among simplest podands, di- and tetrapodands have less presence in the literature than tripodands. Whereas dipodands appeared as an imitation of crown ethers, featuring an open-chain framework with alignment of oxygen atoms bridged *via* ethylene units,[262] tetrapodands have been less studied maybe because the chemistry of tetravalent atoms is partially focused on the synthesis of tripodal hosts.[263] Anyway, the use of calixarene[264-266] or aromatic platforms[267] and molecular tetrapodal arrangements[268] are good scaffolds for the development of tetrapodands (Figure **107**).

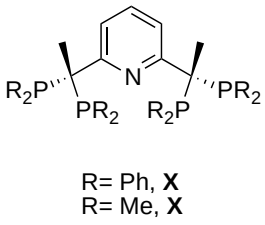

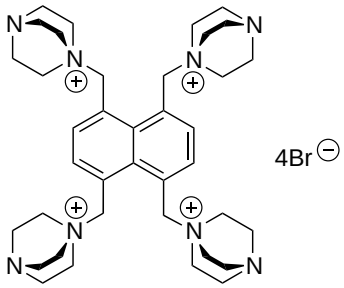

Figure **107**. Tetrapodal phosphane-based receptors for complexation of Co (II) and Ni (II) (*left*). Tetrapodand polyanionic host based on positive charged DABCO end-groups (*right*).

So, besides the use of tetravalent atoms, the N atom is the most useful trivalent atom to construct tripodal receptors. Its trigonal pyramidal geometry makes the branches to be in a flexible but well disposed conformation for guest recognition; indeed, this organization can be adjusted with more rigid frameworks or end-groups.

The most used commercially available *N*-tripodal scaffold is the tris(2-aminoethyl)amine, *tren*, that can be directly transformed into amides and ureas, and their respective thio-derivatives, or also into

imines.[269,270] Another anchor group used for tripodal hosts is the tris(2-hydroxyethyl)amine or 2, 2', 2''-nitrilotriethanol, which is readily converted into a trichloride derivative to further substitute alcohols like *para*-hydroxymethylbenzoate,[271] cresols[272] or benzimidazole-pyridine-carboxyamide units.[273]

Regarding to the analogues of the anion receptors developed in this PhD Thesis, the length of spacers between the apical N atom and the NH groups, the NH groups with the end-groups and also the relative position of amide *N* and *C* atoms inside the host have been considered (Figure **108**).

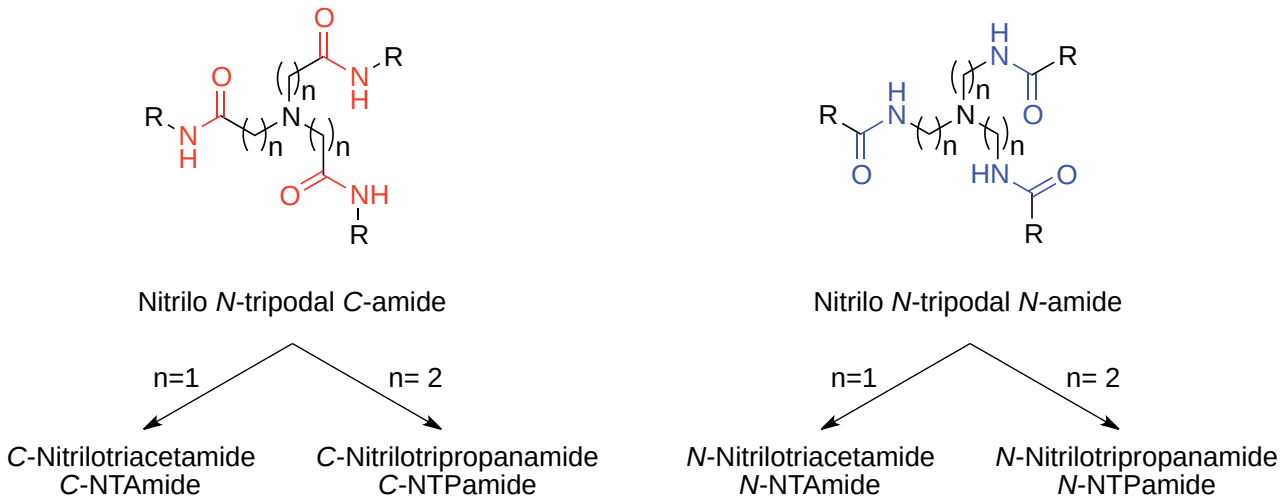

Figure **108**. Structure and nomenclature of four types of nitriloamide-based tripodal receptors.

For n= 2 the most studied compounds are the *tren*-based amides. These *N*-NTPamide compounds have been tested for anion recognition and present entrapping properties for several kinds of the anions, all of them monovalent (Figure **109**).

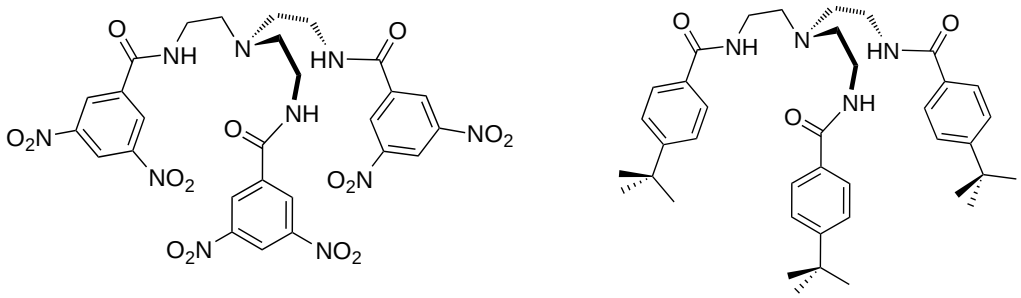

Figure **109**. Tripodal *tren*-based receptors differing in the aromatic end-group selective for fluoride (*left*)[274] and nitrate (*right*) ions.[275] Little changes in the aromatic substituents lead to distinct affinities.

The *C*-NTPamide derivatives are scarcely investigated, in contrast with the nitrilotriacetic amide derivatives, or *C*-NTAmide, which are usually investigated to coordinate metals.[276-280] The *N*-

NTAmide tripodands also appear in a very few occasions, and always referring to synthetic approaches.[281,282]

Notwithstanding, it is interesting to note that both *C*-NTAmide and *N*-NTPamide, the types of nitrilo receptors with more applications, have the binding acceptor atoms (amide NH protons) at the same distance from the apical N atom. Then, it is logic to think that *C*-NTAmide receptors will also point the NH hydrogen atoms in a similar way (Figure **109**).

The glycine derivative **144** was already achieved by Andrews and coworkers in 2008.[283] Starting from nitrilotriacetic acid they coupled benzyl or methyl ester protected amino acids using HBTU as coupling agent. However, although they were presented as chelating ligands, no host-guest chemistry was reported in this or other publications (Scheme **33**).

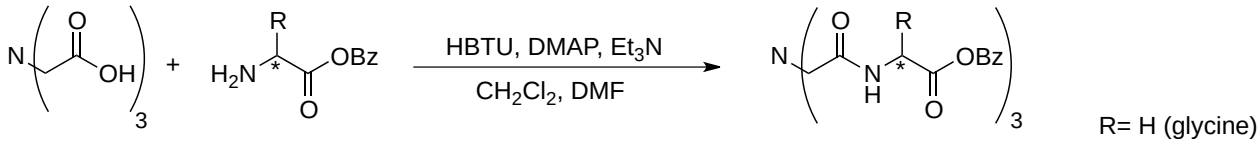

144

Scheme **33**. Synthesis of tripodal amide receptors with benzyl ester end-group reported by Andrews *et al.*

Two years later, Togrul and colleagues published a work where two NTA-based receptors recognised several anions, in their tetrabutylammonium salt form, in DMSO-d_6.[284] They compared the association constants and the anion scope of both, which differed in the aromatic end-group (Figure **110**).

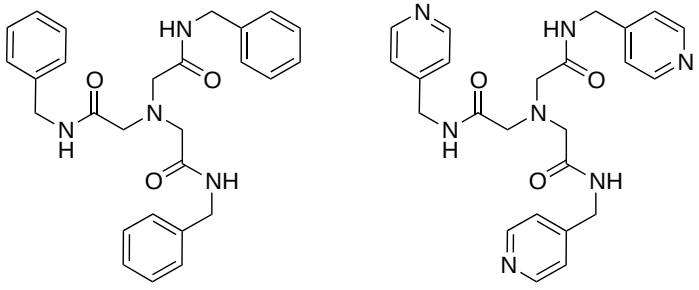

145 **146**

Figure **110**. Skeletal formula of both NTA-based tripodal amides reported by Togrul and coworkers, very similar to the ones to be developed in the current thesis.

On the other hand, the same receptors reported by Togrul have been used, by other authors, for the preparation of metal complexes with the lanthanides (III)[285] and Pb (II).[286] In this case, because of the opposite nature of cations, the complexation of the metal guest is done by donor atoms in the

ligand, that is, the carbonyl oxygen atoms and the apical nitrogen atom coordinate the cation (Figure **111**).

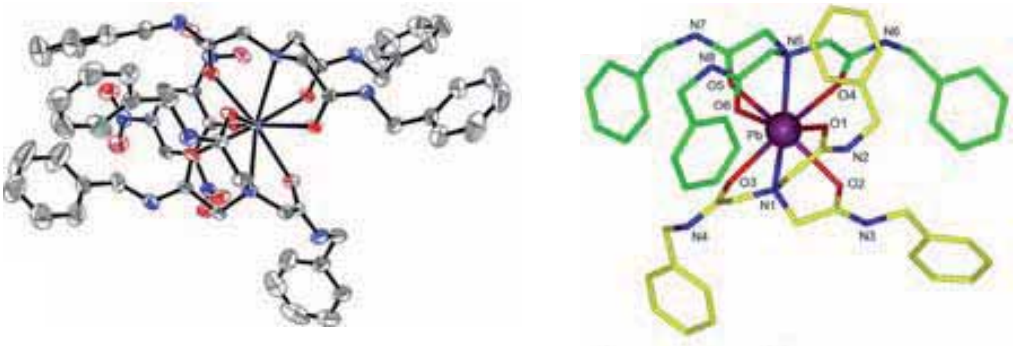

Figure **111**. a) Molecular structure of [Ln**145**$_2$](pic)$_2$ (purple: Pr or Nd ion, red: O, blue: N). b) Molecular structure of [Pb**145**$_2$](ClO$_4$)$_2$ · 3H$_2$O. Both diagrams are extracted from X-ray analysis of the corresponding solids. H atoms are omitted for clarity. Both complexes are in 2:1 stoichiometry (host:guest).

Some cases in the literature highlight the recognition capacity of this and related tripodal amide systems with cations. On the contrary, we directed the host:guest study towards anion complexation.

4.1.6. Study of the binding properties of the tripodal amide receptors

The host-guest event is a typical phenomenon in supramolecular chemistry and when it is given, the first question to be resolved is how strong the complex is. In thermodynamic terms, that is to determine the value of free energy (ΔG) of the reaction and, the most straightforward way of measuring this is through the equilibrium constant (K) of the system. Both parameters are related by equation (1):[255]

$$\Delta G = -R \cdot T \cdot \ln(K) \qquad (1)$$

Association constant (K_a) is a type of equilibrium constant and can be mentioned as binding constant, stability constant or, commonly in biological systems, as dissociation constant. All of them refer to the same thermodynamic parameter.[218] Nevertheless K_a is a general term that does not take into account the complex involved, or that can be used when only 1:1 complexes are formed. The thermodynamic constants are referred as $\beta_{11} = K_{11}$ when only a 1:1 complex formation takes place; $\beta_{12} = K_{11} \cdot K_{12}$, because the formation of a 1:2 complex involves 1:1 complex too; and so on. The complexation constants can be calculated from a mathematic equation of a specific order depending on the type of equilibrium, in reference to whether the stoichiometry of the complex is 1:1, 1:2, ... (host:guest).

Anion complexation leads, most of the time, to significant changes in some of the physicochemical properties of solutions. To start the investigation in these systems it is crucial to identify which species are formed in the host-guest event as well as to determine their association constants. To accomplish this, measurements of any physicochemical property, the magnitude of which significantly changes in the complexation event, may be used. A point to highlight from those descriptions is that the parameter to be measured must fulfil the following conditions, valid for any equilibrium study:[218]

i) The equation correlating the extent of the host-guest event and the parameter being measured must be known.

ii) The parameter has to change significantly with respect to the experimental error.

iii) Measurements have to be performed in a concentration range where the complex formation is significant but not complete.

Therefore, in principle, the same general techniques employed for determining stability constants of metal ion complexes can be applied. Such techniques have been extensively reviewed and described in several publications[217,218,230,255,287] but among them, there are four which are mainly employed for the experimental determination of binding constants: NMR, UV-vis, fluorescence and calorimetric titrations. Note that the three first ones are spectroscopic techniques, although other kind of techniques can be applied (Table **11**).[230]

Table **11**. Typical methods for stability constant determination. The most employed techniques are highlighted in light grey.

Spectroscopic	Electrochemical	Thermodynamic	Special
NMR spectroscopy	Potentiometry	Calorimetry	Reaction kinetics
UV/ visible spectroscopy	Polarography	Extraction/distribution	Competition methods
Fluorescence/phosphorescence spectroscopy	Ionic conductivity	Ion exchange	
CD spectroscopy	Ion selective electrode measurement	Solubility measurement	
Mass spectrometry		Partial pressure measurement	

While in biochemistry it is frequently possible to determine directly the concentration of the complex of interest, for example, by electrophoreses or filter-binding assays, this is not often possible in supramolecular chemistry, where main methods detect complexation indirectly. NMR is

one of the most employed in non-aqueous systems and it easily provides the association constants of interest with high reliability and reproducibility. This technique has the principal advantage that besides thermodynamic information it also evidences information at molecular level (sites of interaction, structural conformation, etc.) about the host-guest event. Moreover, the misinterpretations caused by impurities, which sometimes are important in the optical methods, can be avoided. In addition, NMR spectroscopy can supply various sets of signals to be followed for the independent evaluation of stability constants.[230]

When the NMR method is applied, two physical properties are mainly concerned, chemical shift (δ) and relaxation time (*T*). In order to use the chemical shift it is a requisite that at least one interacting site in both free and complexed host gives remarkably different chemical shifts. Such complexation-induced shift (CIS) in tripodal amides is frequently observed in NH protons or protons from other parts of the host near to the site of complexation.[230] Occasionally, molecular guests or anions with organic moieties or nonzero spin containing atoms, for example ^{19}F, ^{31}P or ^{35}Cl, can be used to determine the chemical shift variation (Δδ).

In order to facilitate the reading of the present chapter, details about the procedure to graphically or computationally determine thermodynamic parameters of complexes are explained in Annex section **4.5.1**.

4.2. OBJECTIVES

The importance of exploiting specific anion recognition systems and the relevance that this research area is having in the field of supramolecular chemistry, have promoted the following objectives:

- Synthesis of a series of new neutral C_3-symmetric tripodal amides based on a NTA core, using natural and synthetic amino acids as branches (cyclic-chiral or linear-achiral) and varying, for some derivatives, in their *C*-terminus carboxylic ester protecting end-groups.

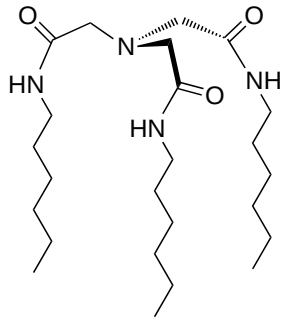

HHex, 147

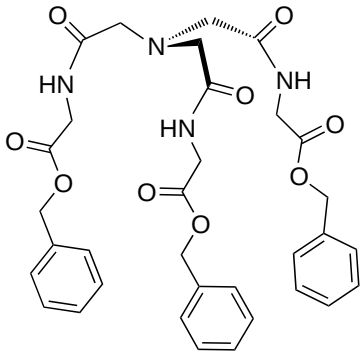

HαOBn, 144

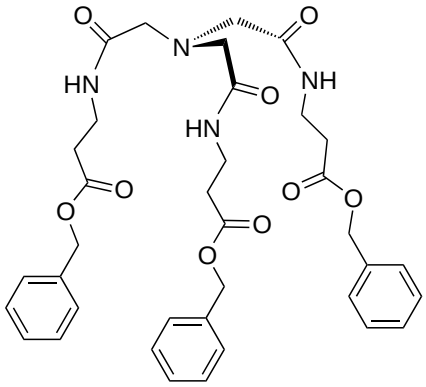

HβOBn, 148

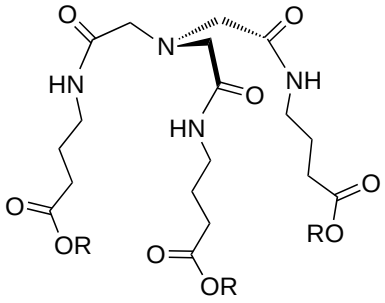

R= OBn **HγOBn, 149**

R= OMe **HγOMe, 150**

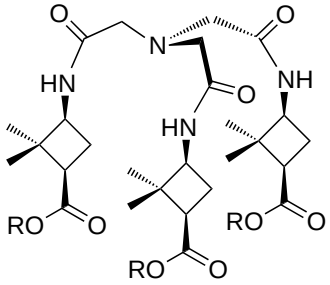

R= OBn **HγCbuOBn, 151**

R= OMe **HγCbuOMe, 152**

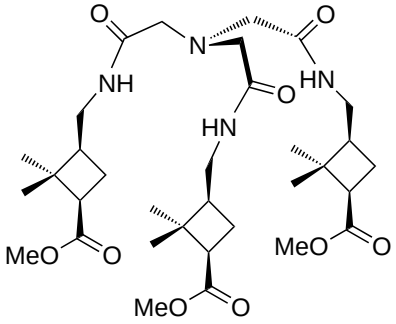

HδCbuOMe, 153

- Anion scope tests of these tripodal amides as receptors for several mono-anionic guests in DMSO-d_6, using the ^{1}H NMR spectroscopy technique. Study of the chain length effect, the linear-achiral vs. cyclic chiral influence and the end-group impact.

- Determination and comparison of stoichiometry and stability constants of some selected complexes, *via* high-resolution ^{1}H NMR experiments.

4.3. RESULTS AND DISCUSSION

Since few publications described anion binding of *C*-NTAmide hosts, our research in this area has been targeted to the synthesis and binding study of new tripodal amide anion hosts based on the nitrilotriacetic core. On the other side, *tren*-based tripodal amides have a noticeable presence in the field of anion recognition and it is exciting to complete the range of similar hosts and compare association properties with little changes in their structures, recalling the influence of the binding site environment in the selectivity and specificity.

Up to this point of the thesis, the new compounds synthesized were based on 2-aminocyclobutane-1-carboxylic acid (*S,R*)-**55** and their stereoisomers, one of them combined with α, β and γ simplest linear amino acids. In this chapter instead, we used 1,3-disubstituted 2,2-dimethylcyclobutane γ- and δ-amino acids, because they were supposed to be easily attached to a relative sterically hindered C_{3v}-symmetric NTA core. In addition, glycine, β-alanine and GABA amino acids were also employed for this new family of possible receptors. Benzyl and methyl ester *C*-terminus protection were employed and the linear *n*-hexylamine too.

The 1,3-substituted cyclobutane-containing γ- and δ-amino acids were provided from the natural chiral terpenoids (*S*)-(-)-verbenone **31** and (*S*)-(-)-α-pinene **154**, respectively (Scheme **34**). Linear α-, β- and γ-amino acids and *n*-hexylamine were used directly from commercial sources with little or no functional group transformations.

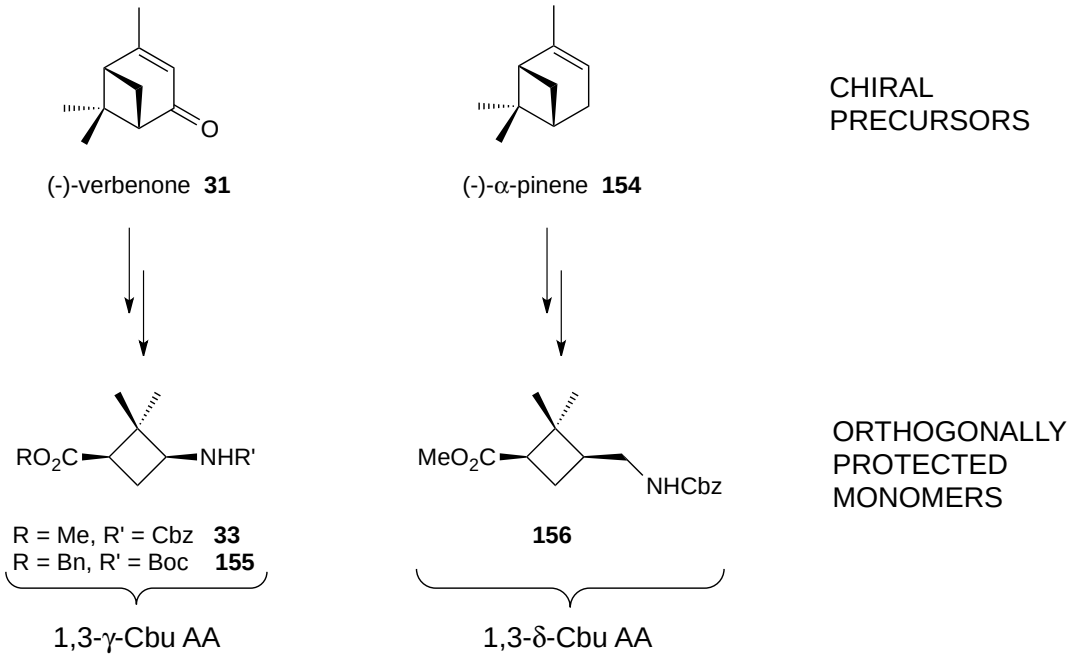

Scheme **34**. Orthogonally protected cyclobutane containing amino acids for the synthesis of non-natural peptides and their respective chiral precursors.

4.3.1. Synthesis of *C*-nitriloacetamide-based receptors

For the synthesis of 2,2-dimethylcyclobutane γ-derivatives a previous work in our research group has been followed to reach the γ-amino acid skeleton structure.[287-289]

On the other side, the synthesis of homologated analogs of 2,2-dimethylcyclobutane γ-derivatives to observe possible differences in their hosting behaviour was interesting. That is the reason why a series of new 2,2-dimethylcyclobutane δ-amino acids was synthesized for the first time. The only reference to this kind amino acids was done by Burgess and collaborators, who described the synthesis of one of the enantiomers obtained from (+)-α-pinene **154**.[290]

To afford the final tripodal amides properly functionalized two synthetic approaches were tested: a convergent route and a divergent route. In order to understand this it is necessary to take into account that the NTA group can be commercially sourced as a core itself or, it can be synthesized by a nucleophilic substitution reaction between branch-containing segments (Scheme **35**).

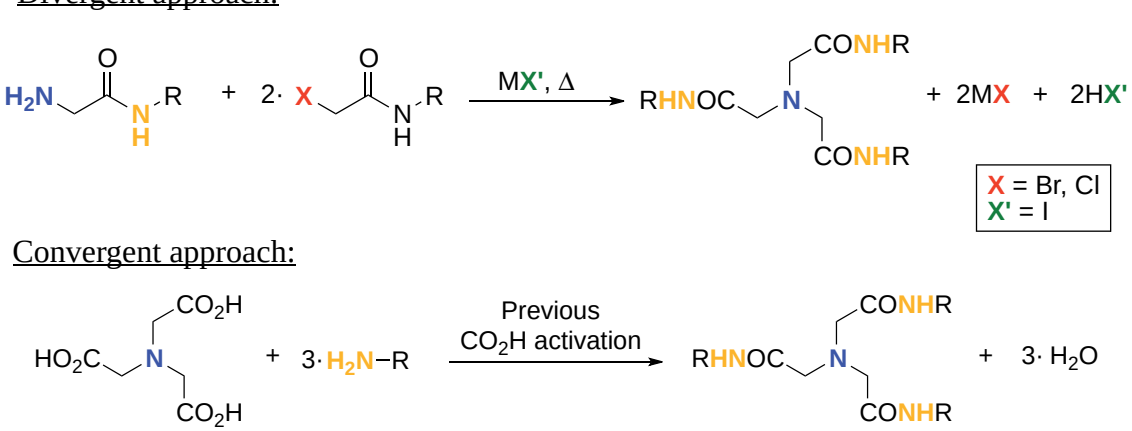

Scheme **35**. Divergent and convergent strategies are approached depending on the achievement of the NTA core.

So, each tripodal amide has been synthesized by one, the other or both methodologies (Figure **112**):

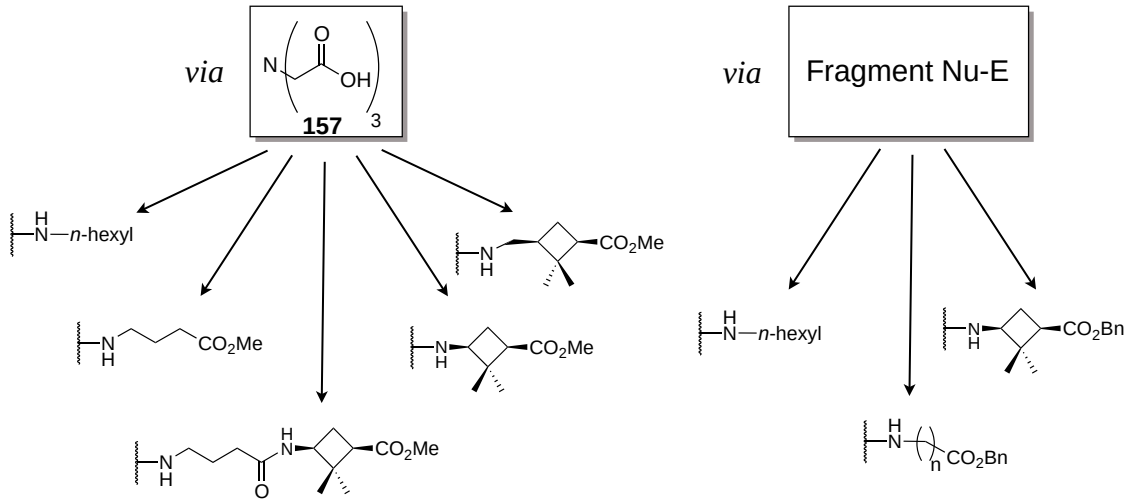

Figure **112**. General scheme showing which synthetic route was applied for the synthesis of every host.

It is worthy to mention that analysis of the reaction in order to check desired product formation was done by ^{1}H and ^{13}C-NMR experiments. Anyhow, since the methylene group forming the nitrilo or NTA core has a characteristic ^{13}C-NMR signal at about 60 ppm, this property would determine the successful formation of the tripodal amides. When some signals around 60 ppm appeared in the same sample, possible mixtures of final product and trailing compounds had to be considered.

4.3.1.1. Synthesis of the orthogonally protected γ-amino acids 33 and 155 and the γ,γ-dipeptides 164 and 165

Scheme **36** shows the synthesis of γ-amino acid **33** by a stereoselective strategy stated by our group, [16] which allowed its preparation with an overall yield of 47%.

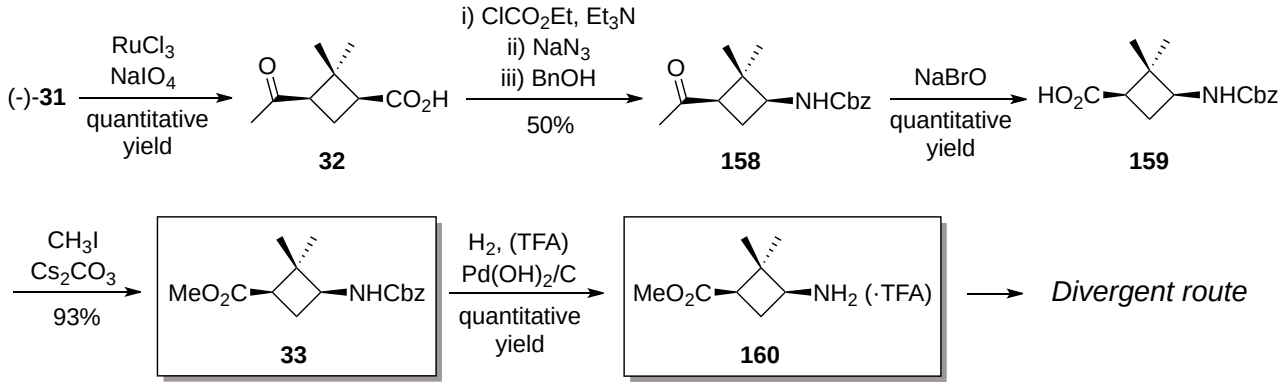

Scheme **36**. Preparation of orthogonally protected amino acid **33** and the corresponding amine **160** for the synthesis of cyclobutane-containing tripodands by divergent strategy.

For the synthesis of γ-amino acid **155**, catalytic hydrogenation on **33** in the presence of Boc_2O and a subsequent saponification under mild conditions were carried out to yield *N*-Boc protected amino acid **162**. The only new reaction to optimize was the benzylation of carboxylic acid (see Annex section **4.5.2.1** for experimental details). Benzylation of the free carboxylic acid during 65 hours, finally provided orthogonally protected γ-amino acid **155** in 74% yield over three steps.

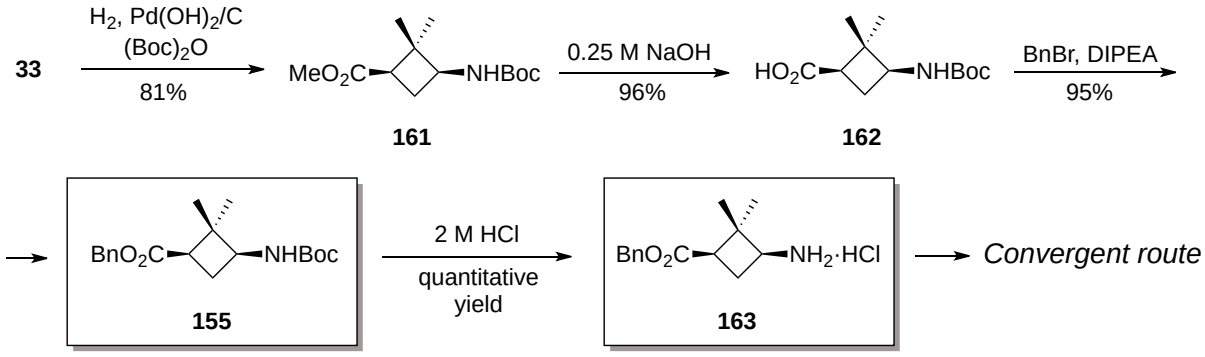

Scheme **37**. Preparation of orthogonally protected amino acid **155** and the corresponding amine **163** for the synthesis of cyclobutane-containing tripodands by convergent strategy.

Deprotection of both amines in **33** and **155** γ-amino acids afforded both free amines **160** and **163** quantitatively (Scheme **36** and Scheme **37**). Both key intermediates constitute the branches of their respective tripodal amides with different carboxylic ester end-groups.[291]

Since the combination of cyclobutane and linear monomers led to interesting conclusions within the hybrid peptides, a dipeptide-containing tripodal amide was synthesized. Dipeptides **164** and **165** were synthesized from the amino acid **160**, after deprotection of the amine and coupling reactions with properly protected GABA derivatives. For the final synthesis of the γ,γ-dipeptide containing tripodal amide, both compounds were selectively deprotected to give amine **166** (Scheme **38**).

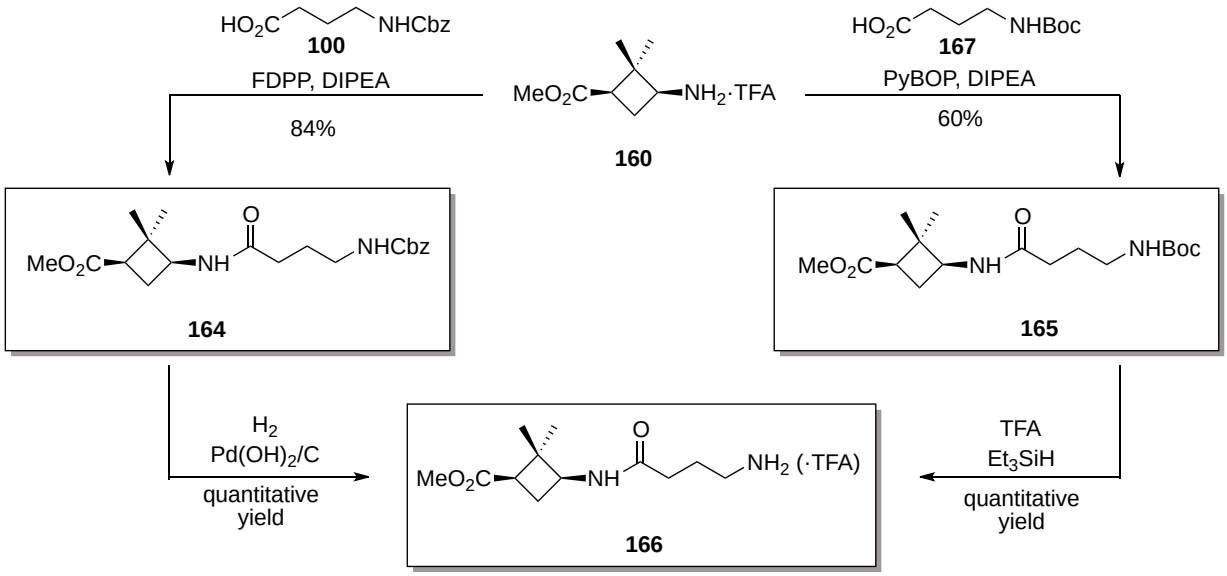

Scheme **38**. Synthetic route for the preparation of dipeptides **164**,**165** and **166**.

4.3.1.2. Synthesis of the orthogonally protected δ-amino acid 156

The same methodology for the synthesis of 2,2-dimethylcyclobutane γ-amino acids was applied for the enantioselective synthesis of 2,2-dimethylcyclobutane δ-amino acids (Scheme **39**).

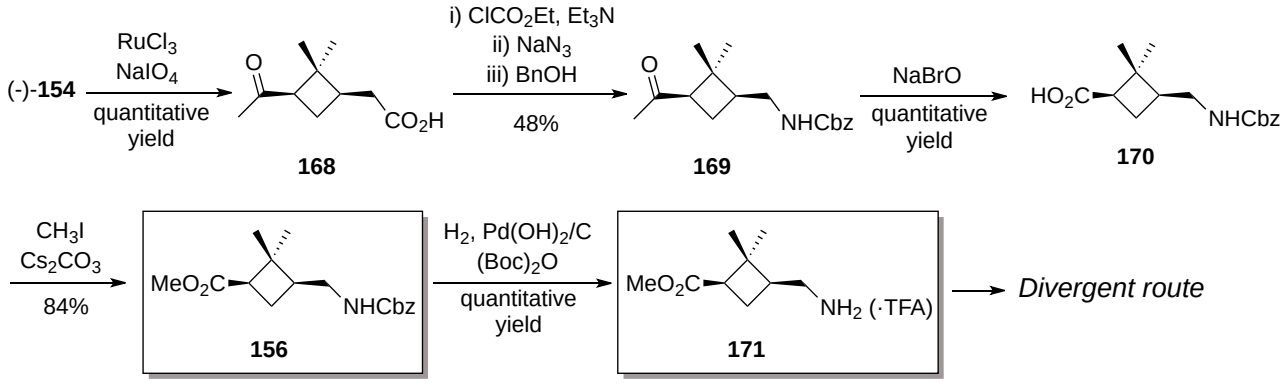

Scheme **39**. Synthetic path to achieve orthogonally protected amino acid **156** and its corresponding amine.

Monomer **156** was obtained in 40% overall yield. Compounds **169**, **170** and **156** are new products , the homologated analogues of the γ-derivatives and the presence of an extra methylene group make

them to be noticeably different. The δ-amino acids **170** and **156** for example, are both physically dense oils at room temperature whereas their γ-analogues are solids.

4.3.1.3. Synthesis of the orthogonally protected α,α-, α,β- and γ,α- linear dipeptides 176, 183, 188 and pseudodipeptides 177, 184 and 189

First host-guest preliminary experiments were carried out using host **152**, whose methyl ester end-group did not give noticeable anion recognition. Because of that and taking into account the end-group effect, it was decided to synthesize new hosts with a benzyl ester termination.

Thus, glycine, β-alanine and GABA amino acids were conveniently protected to be used in the synthesis of nucleophilic (**176**, **183**, **188**) and electrophilic species (**177**, **184**, **189**) for the substitution reactions (Scheme **40**, Table **12**).

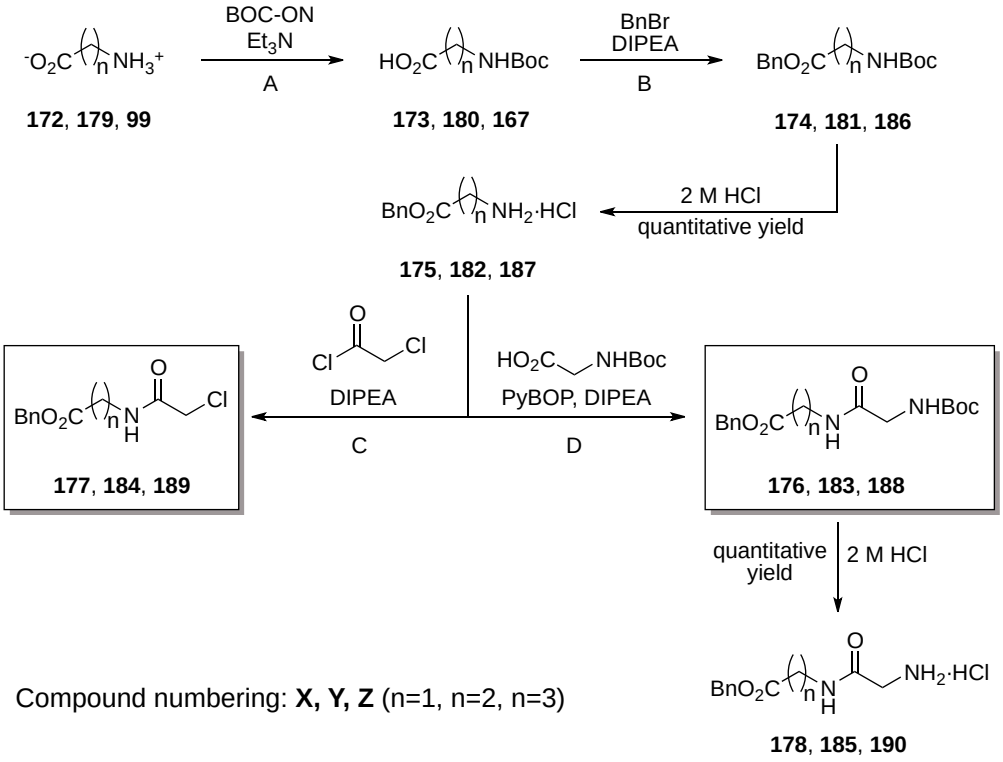

Scheme **40**. Synthetic route for the preparation of *C*-OBn linear amino acids.

Table **12**. Yields of reactions A, B, C and D for each amino acid derivative from the Scheme **40**. Rest of reactions are quantitatively yielded in all cases.

Reaction	Yield (%)		
	n = 1	n = 2	n = 3
A	93	quantitative	99
B	99	99	88
C	56	55	77
D	57	79	83

4.3.1.4. Divergent synthesis of tripodal amides 147, 150, 152, 153 and 191

Our experience in peptide synthesis has prompted us to use many coupling agents. In contrast, for the divergent synthesis of tripodal amides it was decided to use acid halide methodology because its derivatives are highly reactive and it has a relative low cost. Moreover, as we use a NTA acid core where three amines have to be coupled, this methodology is firmly recommended for steric hindrance motives (Scheme **41**).[292]

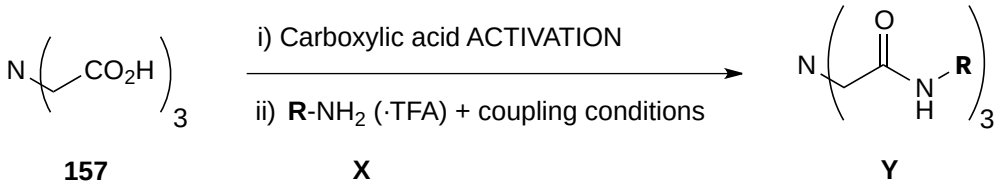

Scheme **41**. General reaction for the synthesis of tripodal amides by divergent strategy.

Table **13** summarizes the best results *via* the divergent path.

Table **13**. Best results obtained in the synthesis of tripodal amides by divergent strategy.

Entry	NTA acid activation	Coupling conditions	R		Yield[a]
			Amine X	Tripodand Y	
1	$(ClCO)_2$ anhyd. DMF drops anhyd. CH_2Cl_2 reflux, 1-2 h	reflux to r.t., 24 h 6 eq. Et_3N	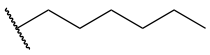		60%
			n-hexylamine	**147**	
2			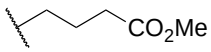		20%
			102	**150**	
3		r.t., 24 h 6 eq. DIPEA	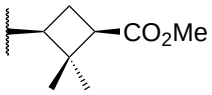		35%
			160	**152**	
4		reflux, 24 h 6 eq. Et_3N	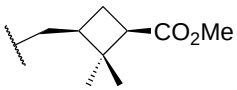		20%
			171	**153**	
5		reflux, 30 h 6 eq. Et_3N	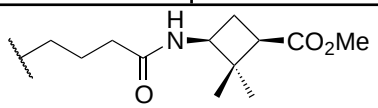		Not isolated
			166	**191**	

[a] Isolated yield after purification.

Other conditions for the acid activation and coupling conditions were tested. However, the use of PyBOP, HATU or $(ClCO)_2$ did not work as good as the acyl chloride activation. Variations in the temperature, time of reaction and solvent were also tried.

The acid halide methodology was also chosen because *a priori* involves easier purification, since no organic neutral byproducts are generated as it occurs using most coupling agents. The dark colour gained during the reaction, probably due to impurities from partial amine decomposition, was one of the problems of purification. Silica-gel flash chromatography was tried for the colour removal, although high polarity of triamides was a drawback, since they only eluted using some methanol. Heating a solution of some products with activated charcoal was performed without success. Despite the final ochre-coloured crude mixtures, product isolations were achieved by precipitation using apolar solvents such as diethyl ether, pentane and hexane.

Tripodal amide **150**, containing GABA-OMe branches, was also obtained by oxalyl chloride activation followed by addition of amine, what yielded the desired tripodand in 20%, with enough quantity and purity to perform the anion scope test.

Before the preparation of tripodal amide **153** we thought that it would be harder to attach 2,2-dimethylcyclobutane γ-amino acids to the NTA core than the respective δ-amino acids, due to the less hindered amine in the last ones. Nevertheless, this prediction was not later reflected on the reaction conversion (see Annex section **4.5.2.2**). Finally, the desired tripodand was isolated with a 20% yield.

In the synthesis of tripodand **191** the formation of the product was observed but it could not be isolated. Analysis of a fraction from the flash chromatography suggested a mixture of tripodand and trailing compounds (see Annex section **4.5.2.3**).

4.3.1.5. Convergent synthesis of tripodal amides 144, 147, 148, 149 and 151

Employing the convergent strategy, the tripodands were achieved by a bimolecular nucleophilic substitution reaction (S_N2), where the nucleophile and electrophile species had to contain the branches attached to a fraction of the NTA core.[293]

First attempts to synthesize the electrophile derivative were carried out using bromoacetic acid because bromide is a better leaving group, essential requirement for the S_N2 reaction (Scheme **42**). Such approach was carried out as reported by Huang *et al.*,[294] who also used a NTA core as multivalent unit to obtain NTA conjugates for analytical and drug delivery systems.

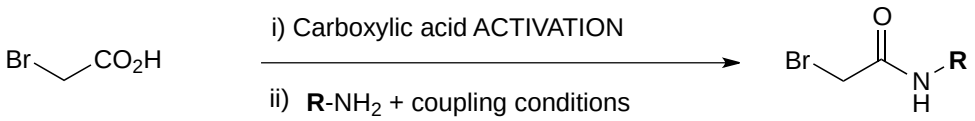

Scheme **42**. Coupling reaction to synthesize bromo-derivatives.

No reproducible results were achieved through this procedure: it was concluded that bromoacetic acid was so reactive from both the reactive sites, that no stable bromide derivative was easily obtained (see Annex section **4.5.2.4** for experimental details). Other similar reactions performed in our research group employing bromide derivatives for the synthesis of surfactants, gave similar drawbacks. For that reason, chloride derivatives were stated as the better alternative.

Convergent synthesis of tripodal amide 147

The $N(CH_2CO\text{-}Hex)_3$ tripodal amide **147** was obtained by the procedure in Scheme 4**3**. The last S_N2 reaction, involving two substitutions in a one-pot experiment, took place in 95% yield.

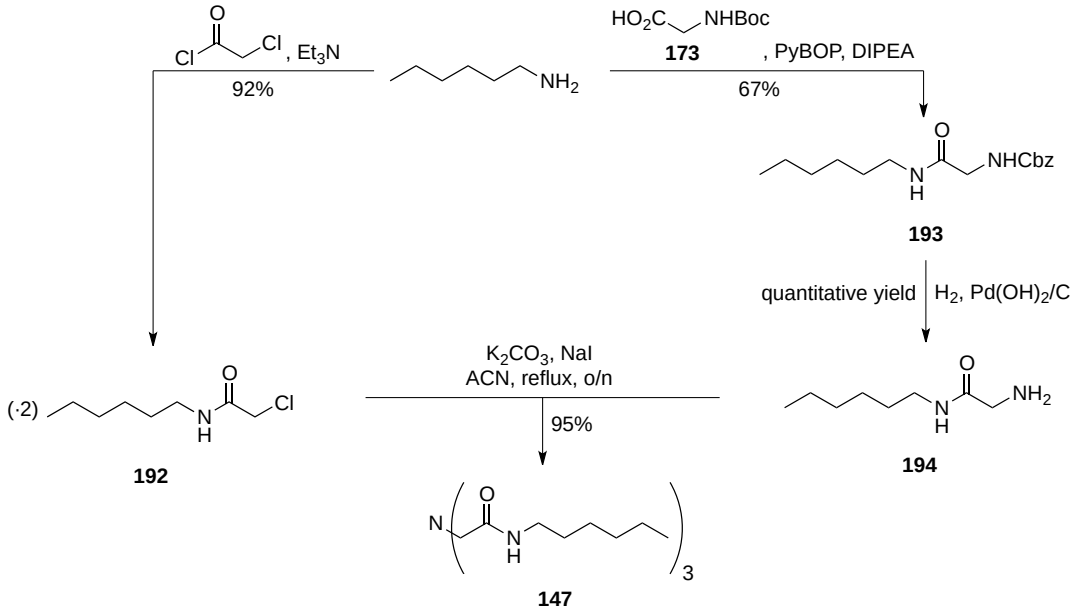

Scheme **43**. Synthesis of compound **147** through the convergent strategy.

The mechanism of the final reaction is a common S_N2 mechanism, where a nucleophile attacks an electrophile sustaining a good leaving group. However, experimental conditions involving the addition of NaI, make that two kind of substitutions take place: iodide firstly substitutes the chloride atom in the electrophilic molecule, so the leaving group becomes better and then, amine attacks the electrophilic carbon atom linked to the iodide. The second kind of S_N2 takes place twice, first to give a secondary amine (intermediate or trailing compound) and then a tertiary amine or tripodal amide (final product). Deprotonation of the secondary and tertiary amines by K_2CO_3 in the media

occurs after the S_N2 in each step (Scheme **44**). Note that this mechanism is the same in all the tripodands achieved by this methodology.

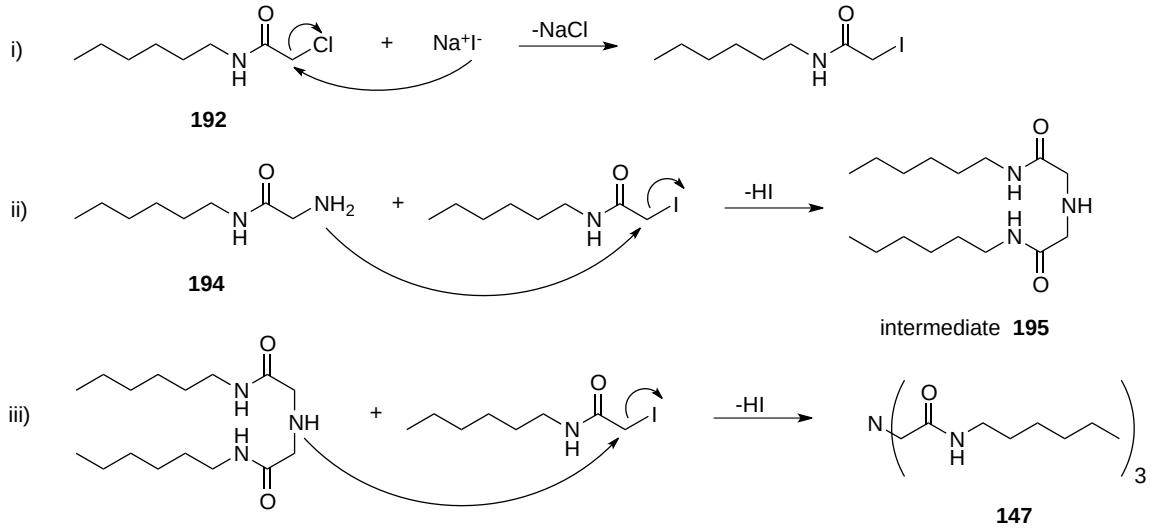

Scheme **44**. Mechanism of the double SN_2 reaction for the achievement of hexyl tripodal amide by convergent approach. This can be applied for the rest of compounds synthesized by this methodology.

The purification procedure following this methodology was less complicated than the one through the divergent route. To remove impurities in the form of secondary amines, 2 M aqueous HCl solution was used to wash a solution of the sample in EtOAc; pure desired product was ultimately isolated in 95% yield (Annex section **4.5.2.5**).

Convergent synthesis of tripodal amide 151

Tripodal amide **151** was synthesized following the same methodology aforedescribed (Scheme **45**).

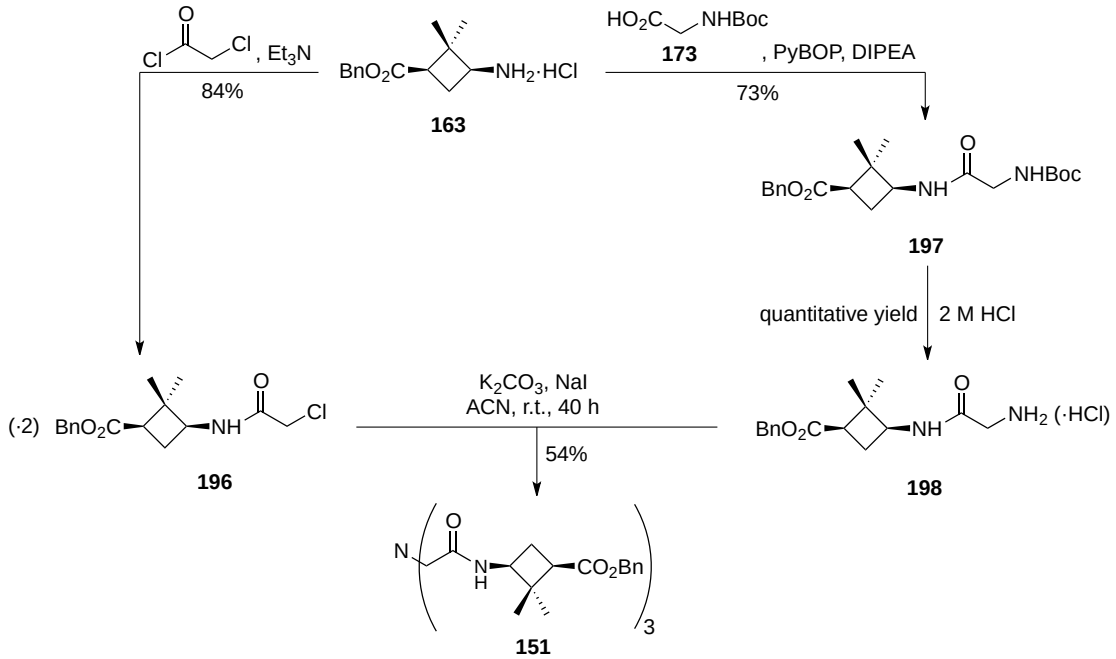

Scheme **45**. Synthesis of compound **151** through the convergent strategy.

The S_N2 reaction applied for this cyclobutane containing tripodal amide was carried out at room temperature. For the rest of compounds synthesized by the same methodology, the reaction was performed in refluxing acetonitrile because for the conversion of a S_N2 reaction heating is a promoter, as it is a good leaving group too. The inconvenient in this case was that, the 2,2-dimethylcyclobutane platform has two epimerizable centres, which could be affected by the presence of carbonate in the media and under the referred reflux conditions. Finally, the cyclobutane-containing tripodal host was obtained in 54% isolated yield.

Preparation of the bromide-containing electrophile was also tried but reaction did not work at all, probably because high reactivity of bromoacetic acid too. Chloride derivative formation was then optimized (see Annex section **4.5.2.6** for experimental details).

Alternatively, the tripodand synthesis was attempted through saponification of the previously synthesized methyl ester derivative **152** under mild conditions (Scheme **46**).

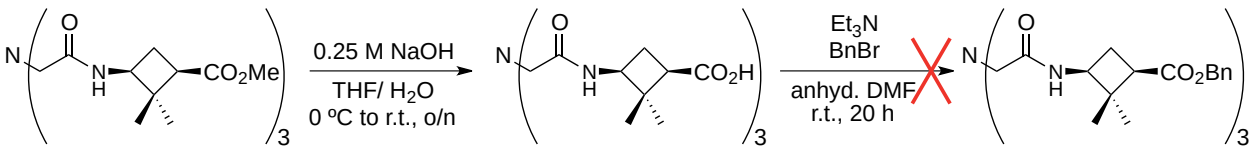

152 **199** **151**

Scheme **46**. Failed attempt to afford tripodand **151** by further functionalization from tripodand **199**.

It was possible to obtain triacid **199** for the first time, but subsequent benzylation failed during the final transformation into **151**.

Convergent synthesis of the N[CH_2CO-$(CH_2)_n$-OBn]$_3$ tripodal amides 144, 148 and 149

The synthesis of a new series of homologated (n = 1 to 3 carbon atoms) tripodands with a benzyl ester termination was developed *via* convergent approach. The reaction between the electrophiles and the nucleophiles of the tripodal amides was a S_N2 substitution carried out in the same way for all three cases (Scheme **47**).

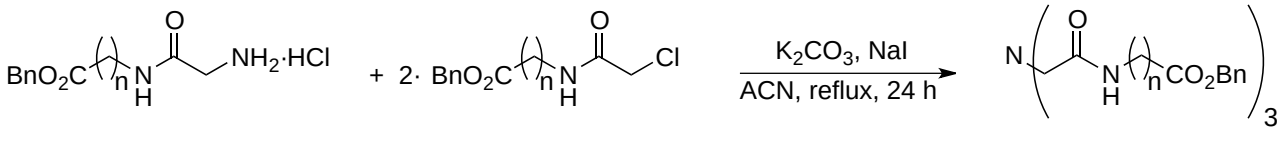

n= 1	**178**	n= 1	**177**	n= 1	**144**
n= 2	**185**	n= 2	**184**	n= 2	**148**
n= 3	**190**	n= 3	**189**	n= 3	**149**

Scheme **47**. Double SN_2 reaction to synthesize a homologated series of benzyl ester-terminated linear amino acid-containing tripodands (n = 1, 2, 3).

The yields obtained were moderate, in all cases below 50% (Table **14**). Nevertheless, two substitution reactions take place in a one-pot experiment so it can be considered that every reaction underwent with higher single yields.

Table **14**. Overall and single yields for the tripodal amides **144**, **148** and **149** synthesized by the double S_N2 reaction.

Reaction	Overall yield[a] (%)	Single yield[b] (%)
n = 1	39	62
n = 2	43	58
n = 3	34	66

[a]Yield after first purification stage.
[b]Single yield is calculated by square root of overall yield.

Purification of these compounds was achieved by flash chromatography but further cold digestions with apolar solvents were necessary to remove other impurities. Such digestions afforded manipulable white crystalline solid for Gly-OBn derivative but not for the rest of the series. Anyhow, enough quantities with acceptable purity were available for the host-guest studies.

4.3.2. Anion scope of receptors

Before starting the host-guest studies, some gelation tests were carried out in some tripodands in order to check their self-assembly properties. Taking into account the precedents of good LMOGs made of cyclobutane-containing hybrid tetrapeptides, **HγCbuOMe** and **HHex** tripodands were tested. However, both compounds were not able to gelate any of the common solvents tried (they were fully soluble up to 500 mg/mL).

In order to compare the anion affinity of each receptor with every anion, tables and spectra are displayed relating them by a relative shifting (see Annex section **4.5.3**). This chemical shift change has been expressed as a % value, for each anion with respect to each receptor, as a representation of the recognition event caused by the addition of the anion (10 eq.) to a solution of the free host. If one compares all the hosts, the 100% relative shifting value is the maximum shielding of the NH signal caused by fluoride when was added to **HγCbuOMe** ($\Delta\delta$ = 4.158 ppm). Table **15** summarizes and relates the relative affinity of all the receptors with respect to all the anions. On it, a red colour gradient is displayed to visually and qualitatively show the diverse degrees of association, being the redder ones the stronger recognitions.

Table **15**. Relative affinity of all the hosts synthesized towards all the anions tested.

	HHex 147	**HαOBn 144**	**HβOBn 148**	**HγOBn 149**	**HγOMe 150**	**HγCbuOBn 151**	**HγCbuOMe 152**	**HδCbuOMe 153**
Free H	0	0	0	0	0	0	0	0
PhS^-	3	7	2	2	2	0	0	2
$PhCO_2^-$	9	26	12	3	7	1	1	7
$CH_3CO_2^-$	13	30	21	11	13	1	1	12
$H_2PO_4^-$	10	46	28	15	17	1	1	8
HSO_4^-	0	0	0	0	0	0	0	0
IO_4^-	0	0	0	0	0	0	0	0
BF_4^-	0	0	0	0	0	0	0	0
I^-	0	0	0	0	0	0	0	0
Br^-	0	0	0	0	0	0	0	0
Cl^-	2	4	3	2	2	1	0	3
F^-	88	67	92	84	94	*	100	92

* No clear signal is observed (below 13 ppm). However, recognition takes place because NH resonance disappears completely.

Fluoride anion was selectively recognised by all the receptors except for **HαOBn** host, where $H_2PO_4^-$ anion competed the most together with $CH_3CO_2^-$ and $PhCO_2^-$. In the case of **HγCbuOBn**, the absence of a clear and only signal made it pointless determine a relative affinity value. Nevertheless, the disappearance of the NH resonance made clear there was a recognition event. The cyclobutane-containing receptors derived form (-)-verbenone, **151** and **152**, were highly selective to fluoride anion. Nevertheless, F^- is a basic anion, so there was a possibility that a second event, namely an acid-base reaction, took place. If this reaction occurred at a non-underestimating extent, the system would get complicated because it would stop being a simple complexation reaction.

These facts and the big shielding of NH signals to downfields (as very acidic protons), led one to think that the acid-base reaction could not be underrated. When the determination of the stoichiometry and K_a of the **[HαOBn][F]** complex was preliminarily carried out but, it was seen that titration experiments to obtain the Job's plot resulted in a non-gradual shielding of the NH signal and, even at 1:0.67 (HαOBn:F) molar ratio, the signal disappeared and also doubled, as occurred for **HγCbuOBn**.

Therefore, F^- anion is a special anion to be treated separately. Anyway, and for the six hosts with high and selective positive recognition of the anion, whatever process went on, it must be said that they are very sensitive receptors for fluoride anion.

For this reason, a new relative affinity Table **16** was set up recalculating relative affinities without taking into account fluoride titrations.

Table **16**. Recalculated relative affinity of all the hosts synthesized towards all the anions tested except F^-.

	HHex 147	**HαOBn 144**	**HβOBn 148**	**HγOBn 149**	**HγOMe 150**	**HγCbuOBn 151**	**HγCbuOMe 152**	**HδCbuOMe 153**
Free H	0	0	0	0	0	0	0	0
PhS^-	7	15	4	4	4	1	1	4
$PhCO_2^-$	19	56	25	7	14	1	2	15
$CH_3CO_2^-$	28	64	44	23	28	2	3	27
$H_2PO_4^-$	21	100	61	33	37	1	2	16
HSO_4^-	0	0	0	0	0	0	0	0
IO_4^-	0	1	0	1	1	0	0	1
BF_4^-	0	0	0	0	0	1	0	0
I^-	0	0	0	0	0	1	0	0
Br^-	1	1	0	1	1	1	0	1
Cl^-	5	8	7	5	5	1	1	5

Comparing all the hosts with all the anions it was clearly seen that **[HαOBn][H_2PO_4]** complex was formed with the highest relative affinity. Then, the next strongest complexes were also formed by **HαOBn** host, with $CH_3CO_2^-$ and $PhCO_2^-$ anions and the **HβOBn** with respect to the $H_2PO_4^-$ anion. On the other side, **HγCbuOBn** and **HγCbuOMe** receptors hardly interacted in a host:guest event with any less basic anion. The reason must lay on their structure, which may have a very hindered binding site because of the dimethylcyclobutyl moieties. The end-group effect had no influence here, because its expected preorganization was eclipsed by the steric effect.

Notwithstanding, when a methylene unit was attached between the amide nitrogen atom and the cyclobutane, as it happens in **HδCbuOMe** receptor, the affinities towards some anions were raised to acceptable relative values. Hence, the presence of bulky and conformationally restricted moieties, directly attached to the NH binding bond, obviously decreased or even cancelled the coordination of the anions, with the exception of fluoride, the basicity and little size of which made it behave differently. The methylene spacer played an important role allowing the access of bigger anions to the binding cavity, moving the bulky moieties away from the core.

In general, and leaving **HγCbuOR** (R= OBn, OMe) hosts aside, the most detected anions were both carboxylates and the dihydrogenphosphate. Chloride and thiophenolate were slightly bound by six of the eight reported receptors. Hence, the basicity of the anions is determinant in their recognition.

The supposed driving force of aromatic end-group effect was the motif to synthesize the benzyl ester terminated hosts. Nevertheless, in Table **16** it is demonstrated that such effect did not enforce the binding properties of comparable receptors **HγCbuOR** and **HγR** (R= OBn, OMe). For instance, in both GABA analogues, in principle, aromatic π-stacking interactions can give preorganization to the host and enhance their binding properties in contrast with the methyl esters. Then, for $H_2PO_4^-$ and $CH_3CO_2^-$ anions, both hosts bound them through a similar relative affinity but for $PhCO_2^-$ anion, the **HγOMe** receptor even presented double sensitivity. If one notice **HHex** receptor, it can be said that no functional end-group neither had a negative effect on the binding abilities of this hexyl tripodal amide under these conditions. The reason why the end-group had no longer effect is probably due to the chain length effect, more decisive than a hypothetical aryl end-group. Indeed, it would have been interesting to compare the **HαOBn** with a methyl ester terminated derivative, which should have shown similar behaviour.

Comparing the homologated series of benzyl ester terminated receptors, the three could recognise the same anions but in different grade. A clear tendency between them, with respect to the three anions towards which had more association, could be observed: the relative binding force decreased with the length of the linear chain and following this affinity order: $H_2PO_4^- > CH_3CO_2^- > PhCO_2^-$. Then, in a qualitative way, it can be stated that the chain length effect is quite important, probably due to the rigidity involving a specific coordination sphere, which would orient the NH bonds, up to a different extent, to the oxygen donor atoms of three anions. This same effect has been similarly observed before, when δ- and γ-Cbu-containing hosts were compared. Anyhow, it is supposed that the longer that spacer between NH and cyclobutane was (ε-derivatives for instance), the lower affinity the host would show.

The affinity towards aromatic anions did not depend on the aromatic terminations because PhS^- anion was less bound than $PhCO_2^-$, what means that carboxylate nature is the clue on such binding. Actually, **HHex** and **HγOMe**, with *n*-hexyl and methyl ester terminations, also bound thiophenolate.

Once the screening results came out it was decided which complexes were interesting to study quantitatively. Such studies consisted in the determination of the stoichiometry and association constant of these selected complexes.

4.3.3. HαOBn-AnionTBA complexes

From the beginning, and regarding our preceding structural studies, glycine derivative receptor was expected to give the best results in anion recognition. Its short molecular structure and, therefore, more rigid conformation is thought to be crucial in the definition of a binding cavity around the three amide bonds and the apical nitrogen atom (Figure **113**).

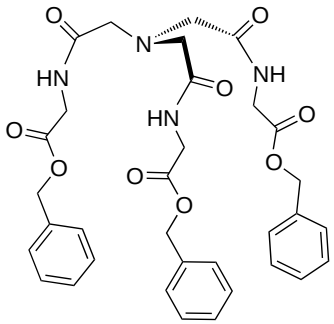

Figure **113**. The skeletal structure **HαOBn** host.

For this reason, and following the conclusions drawn through anion screening, the stoichiometry ratio and the K_a of the complexes **HαOBn** with five anions have been determined. Fluoride anion showed particular behaviour and it has been studied separately.

However, the first point to carry out was checking the self-aggregation behaviour of **HαOBn**. ^{1}H-NMR experiment was recorded covering a gradient of host concentration (Figure **114**).

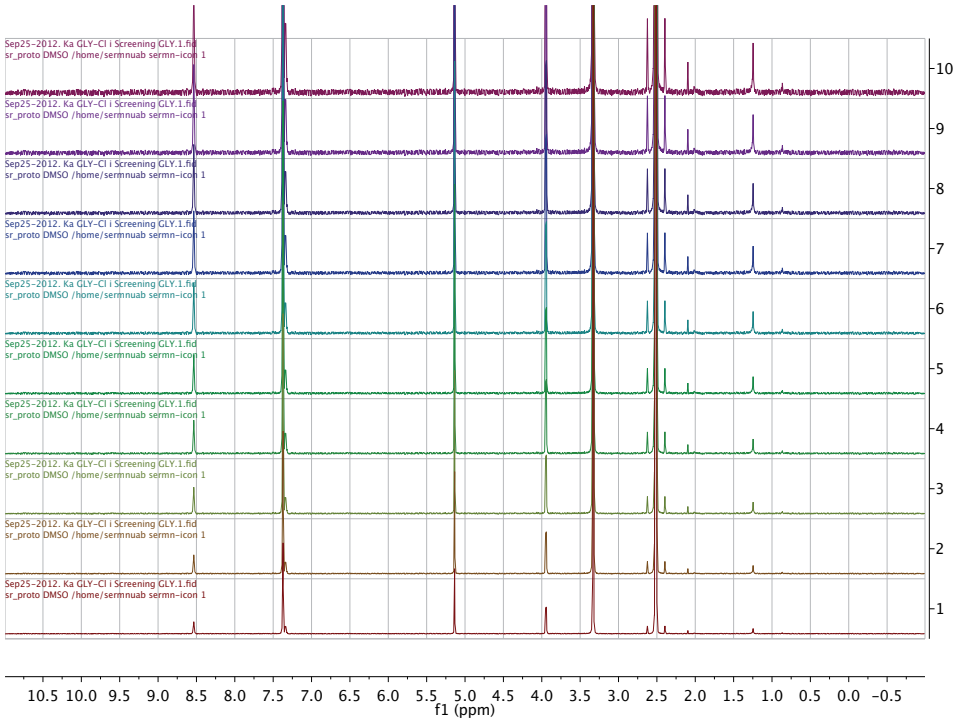

Figure **114**. ^{1}H-NMR spectra of the self-aggregation experiment for **HαOBn** receptor from [Host] = 4 mM (*top*) to [Host] = 0.2 mM (*bottom*). DMSO-d_6 (600 MHz).

If the compound showed any aggregate formation, the NH proton of the symmetric triamide would be shifted. As it can be observed in the spectra, no shielding of the proton signals occurred between 0.2 and 4 mM concentration of the host, so it was concluded that no self-aggregation took place for this receptor at such high concentration. Therefore, when signals experienced significant changes on their chemical shift (sometimes in their multiplicity too) in the presence of anionic species, the cause would surely be due to the anion recognition event. For none of the receptors used in the host-guest studies, self-aggregation under the same conditions was found.

For receptor **HαOBn**, the determination of stoichiometry and K_a of the complexes was carried out following the same procedure for $H_2PO_4^-$, $CH_3CO_2^-$, $PhCO_2^-$ and Cl^- anions. Equimolar 1:1 complexes were obtained for all the anions tested with this receptor in DMSO-d_6 so, only the procedure for the first case will be described in detail. The rest of data and spectra are shown in Annex section **4.5.4**.

As it will be seen in next section, F^- anion was also tested but the study of [**HOST][TBAF]** complexes was performed separately.

4.3.3.1. HαOBn complexes with $TBAH_2PO_4$, $TBACH_3CO_2$, $TBAC_6H_5CO_2$, TBACl anions

HαOBn-FTBA complex

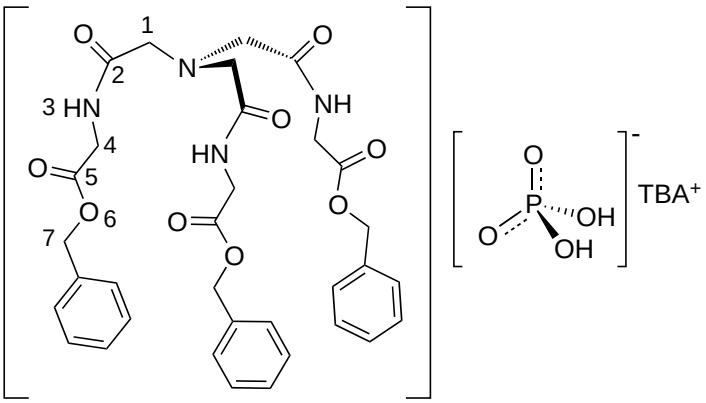

Stoichiometry

^{1}H-NMR spectra were recorded for the titration of $TBAH_2PO_4$ (Figure **115**).

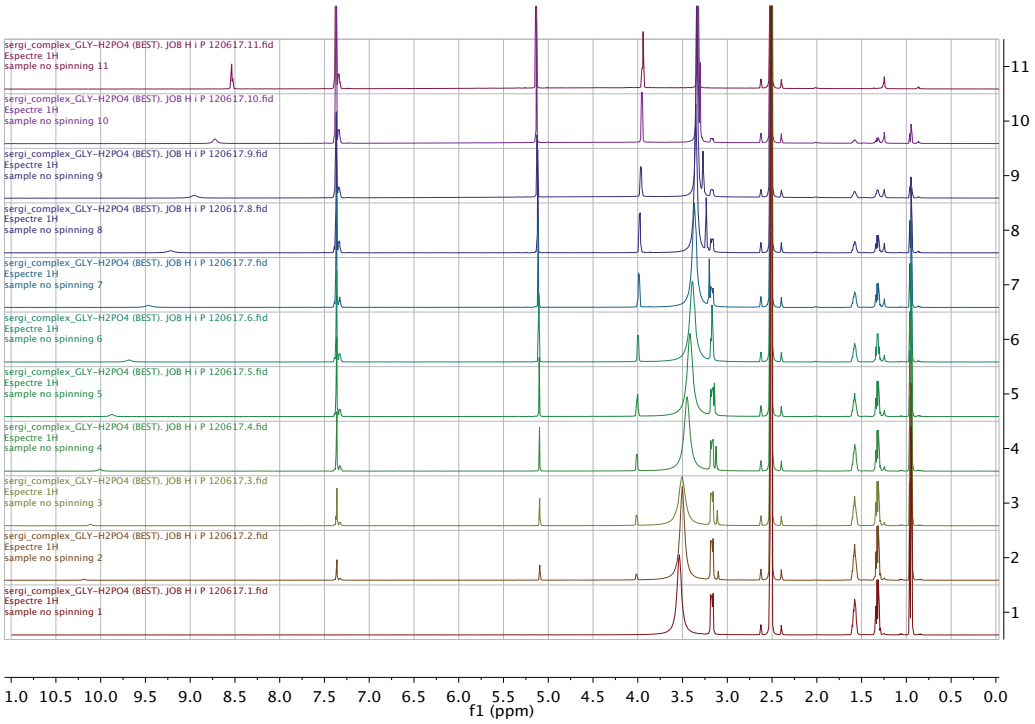

Figure **115**. ^{1}H-NMR spectra of **HαOBn** titration with **$TBAH_2PO_4$** to determine the stoichiometry of the complex. From X_{Host} = 1 (*top*) to X_{Host} = 0 (*bottom*) in ΔX = 0.1. DMSO-d_6 (600 MHz).

And close-up view of the NH area clearly showed the N-H_3 signal shielding towards downfields (Figure **116**).

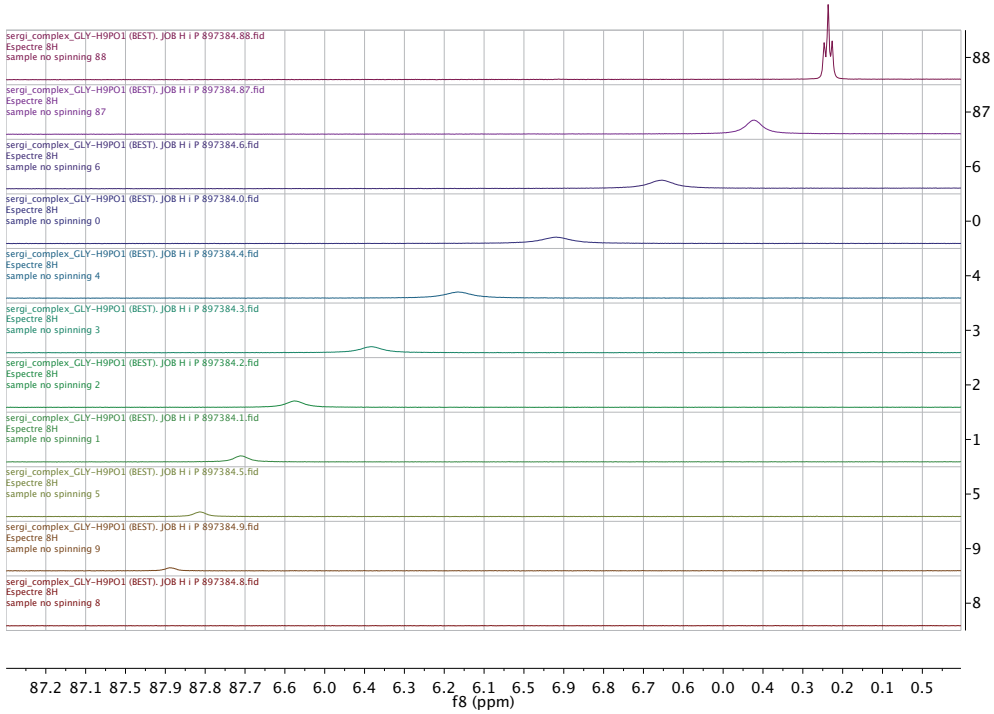

Figure **116**. Zoom of N-H_3 area from the ^{1}H-NMR spectra of **HαOBn** titration with **$TBAH_2PO_4$** to determine the stoichiometry of the complex. From X_{Host} = 1 (*top*) to X_{Host} = 0 (*bottom*) in ΔX = 0.1. DMSO-d_6 (600 MHz).

Although at lower extents, this behaviour was repeated for other four signals of the host suggesting a strong affinity towards the dihydrogenphosphate anion (Figure **117**).

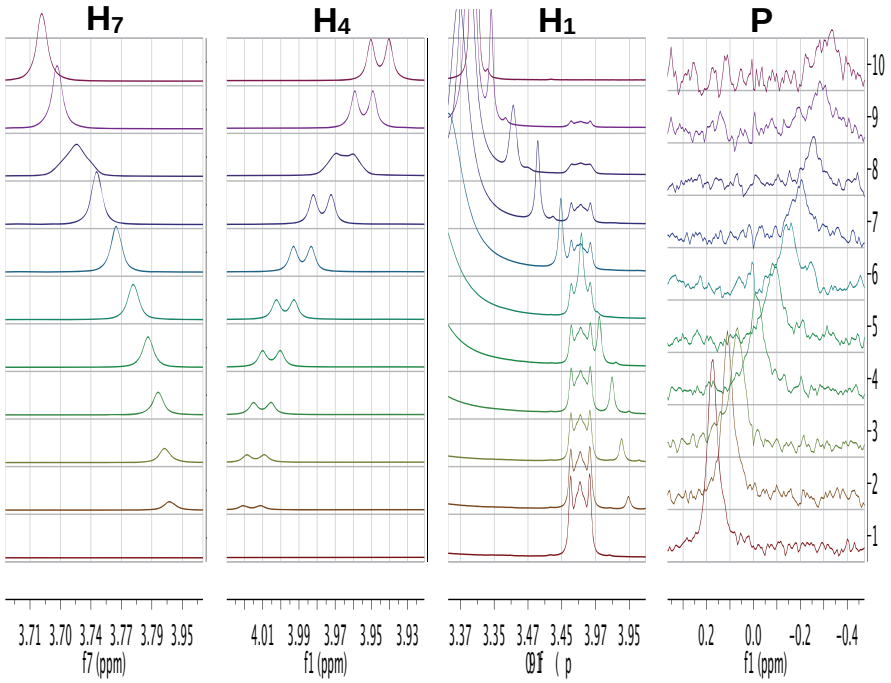

Figure **117**. Zoom of specific signals from the ^{1}H-NMR spectra of **HαOBn** titration with **TBAH$_2$PO$_4$** to determine the stoichiometry of the complex. From X_{Host} = 1 (*top*) to X_{Host} = 0 (*bottom*) in ΔX = 0.1. DMSO-d_6 (600 MHz).

Graphical representation of $\Delta\delta\cdot$[Host] *versus* X_{Guest} resulted in the Job's plots shown in Figure **118** and Figure **119**.

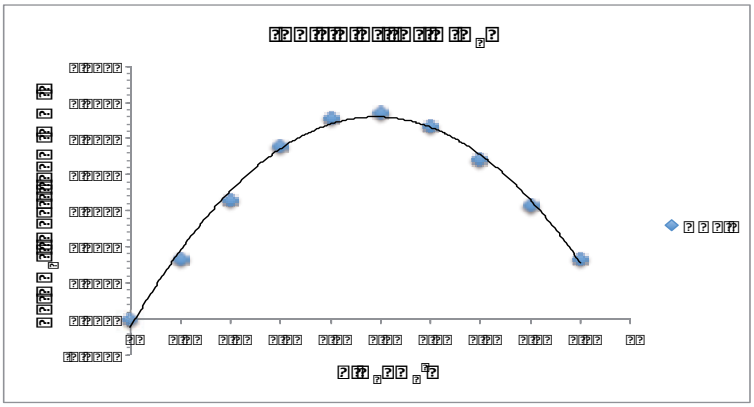

Figure **118**. Job's plot for **[HαOBn][H$_2$PO$_4$]** complex.

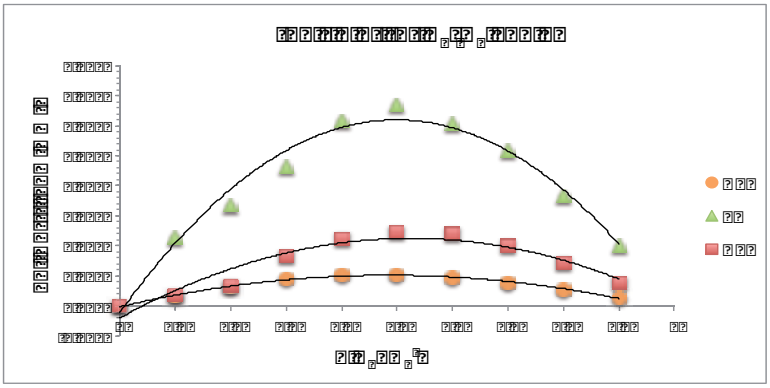

Figure **119**. Job's plots for **[HαOBn][H$_2$PO$_4$]** complex.

As it can be observed, the curves presented similar trends for N-H_3 and P signals while the other two plots for H_1 and H_4 exhibited broader curves because of the little shift variation. This prevented a reliable assignation of the stoichiometry through these two signals. However, the plots of N-H_3 and P signals were sharp enough to clearly point a maximum at molar fraction value of 0.5, suggesting a 1:1 stoichiometry for the complex **[HαOBn][H_2PO_4]**.

Association constant K_a

^{1}H-NMR spectra were recorded in an experiment in which the [Host] was constant (Figure **120**). Note that only 6 eq. in this experiment were enough to shift the N-H_3 signal up to 10.5 ppm, the same like adding 10 eq. in the screening tests (see Annex section **4.5.3**).

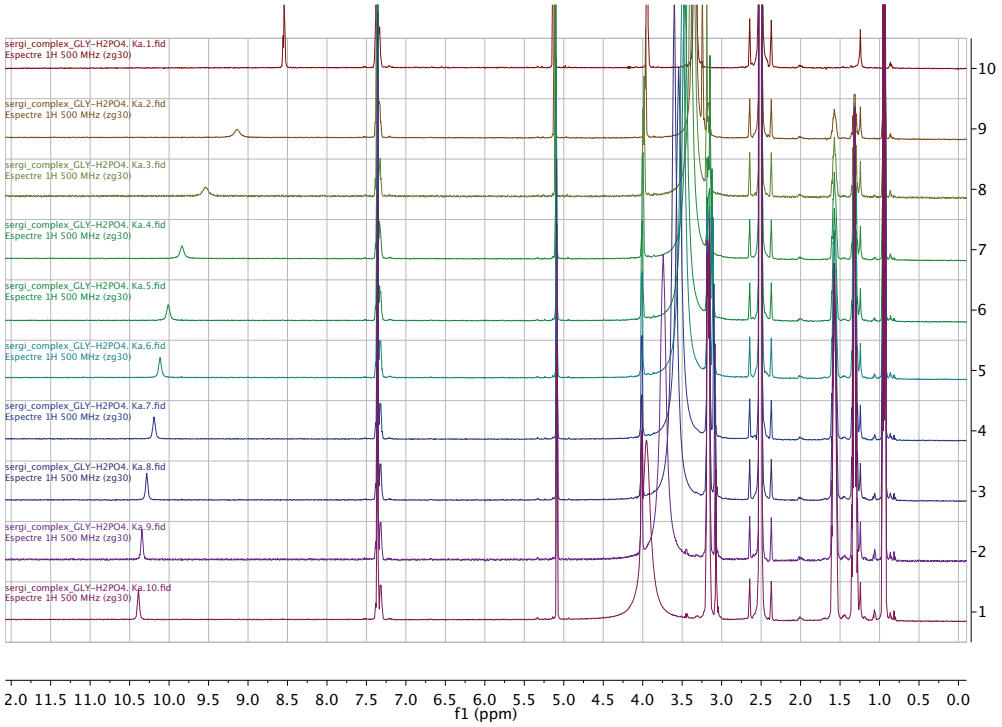

Figure **120**. ^{1}H-NMR spectra of **HαOBn** titration with **TBAH_2PO_4** to determine the K_a of the complex. From Eq. Guest = 0 (*top*) to Eq. Guest = 6 (*bottom*). DMSO-d_6 (600 MHz).

This titration showed a different shielding pattern for the N-H_3 signal, in which major variations took place before the stoichiometry of the complex was reached (Figure **121**).

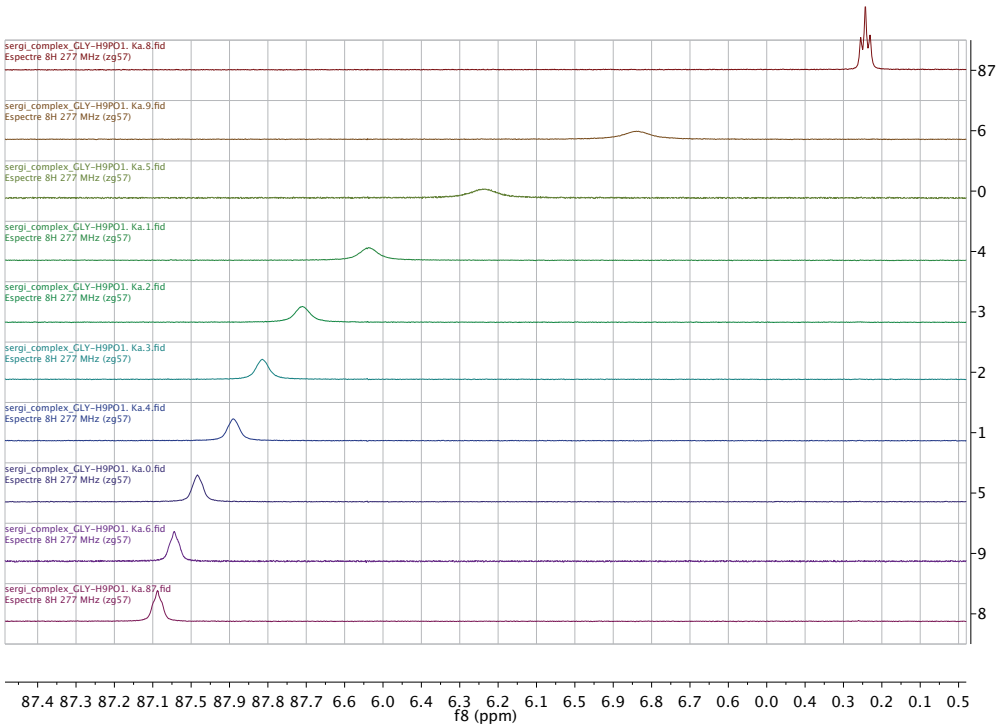

Figure **121**. Zoom of the N-H_3 area from the ^{1}H-NMR spectra of **HαOBn** titration with **TBAH$_2$PO$_4$** to determine the K_a of the complex. From Eq. Guest = 0 (*top*) to Eq. Guest = 6 (*bottom*). DMSO-d_6 (600 MHz).

Once the signals were assigned, the *x*- and *y*-coordinate parameters were calculated (Table **17**).

Table **17**. Calculated data to determine K_a of the complex **[HαOBn][H$_2$PO$_4$]** by linear regression of the represented data in light grey columns.

Tube	[Guest] = Eq. Guest	1/[Guest]	δ N-H_3	Δδ N-H_3	1/Δδ
1	0.0	--[a]	8.543	0.000	--[a]
2	0.5	2.00	9.134	0.591	1.692
3	1.0	1.00	9.534	0.991	1.009
4	1.5	0.67	9.834	1.291	0.775
5	2.0	0.50	10.01	1.467	0.682
6	2.5	0.40	10.11	1.567	0.638
7	3.0	0.33	10.19	1.647	0.607
8	4.0	0.25	10.28	1.737	0.576
9	5.0	0.20	10.34	1.797	0.556
10	6.0	0.17	10.39	1.847	0.541

[a] When [Guest] = 0 no useful data can be calculated, so it is not represented on the graphic.
Units:[Guest] (mM); 1/[G] (mM^{-1}); Δδ (ppm); 1/Δδ (ppm^{-1})

From the nine points to be represented only eight were taken so that the plot fitted better, exhibiting a $r^2 > 0.995$ (Figure **122**).

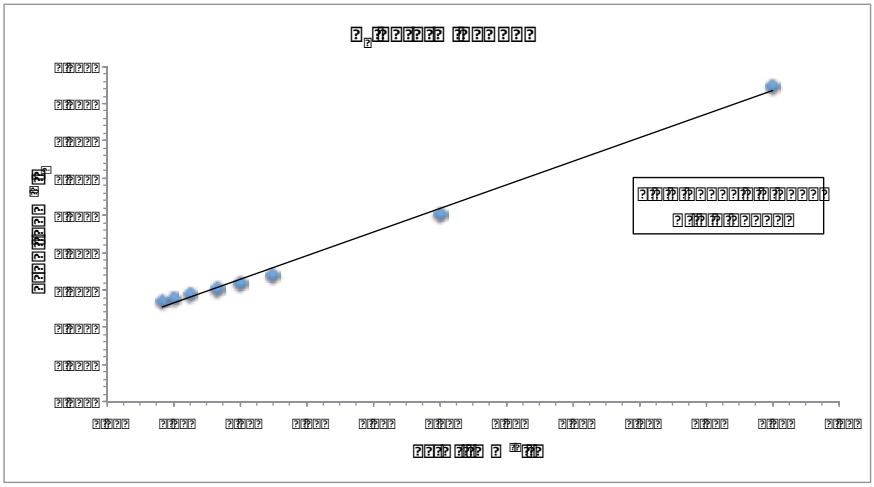

Figure **122**. Linear fitting of the data to determine the K_a of the **[HαOBn][H_2PO_4]** complex .

Next, parameters of the equation *y =slope·x + A* in Figure **122** were employed to calculate the association constant for the 1:1 **[HαOBn][H_2PO_4]** complex and its corresponding Gibbs energy (Table **18**).

Table **18**. Thermodynamic parameters K_a and ΔG^o determination for the **[HαOBn][H_2PO_4]** complex.

Equation	Calculation	Results
$K_a = \frac{A}{slope}$	$K_a = \frac{0.4038 ppm^{-1}}{0.6332 mM \cdot ppm^{-1}}$	$K_a = 0.6377 mM^{-1} = 638 M^{-1}$ $\log K_a = 2.80$
$\Delta G^\circ = -RT \ln K_a$	$\Delta G^\circ = -1.9 \frac{cal}{K \cdot mol} \cdot 298 K \cdot \ln(638 M^{-1})$	$\Delta G^\circ = -3656 \frac{cal}{mol} = -3.7 \frac{kcal}{mol}$

This procedure was carried out analogously for the rest of the anions aforementioned. All the complexes showed a 1:1 stoichiometry so their K_a could be determined using the graphical method. These constants (as decimal logarithm) were used as guide values for the calculation of more reliable K_a by WinEQNMR2 (Table **19**). See Annex section **4.5.1** for the description of the computational method procedure. See Annex section **4.5.4.5** for the statistics of the data fitting parameters and Annex section **4.5.4.6** for the input and output files and the *fitplots* and *concplots* of the **[HαOBn][H_2PO_4]** complex.

Table **19**. Logβ and ΔG° values for the four complexes formed by **HαOBn** host in DMSO-d_6.

		Anion sources and methods of determination of association constants[a] (*up*) and free energies[b] (*down*)							
HαOBn		**$TBAH_2PO_4$**		**$TBACH_3CO_2$**		**$TBAPhCO_2$**		**TBACl**	
		Graphical	**Win EQNMR2**	**Graphical**	**Win EQNMR2**	**Graphical**	**Win EQNMR2**	**Graphical**	**Win EQNMR2**
1:1	β_{11}	2.80	3.31 ± 0.023	2.32	2.37 ± 0.034	2.09	2.19 ± 0.020	1.83	1.65 ± 0.087
	ΔG	-3.66	-4.32 ± 0.03	-3.03	-3.08 ± 0.04	-2.72	-2.86 ± 0.03	-2.4	-2.15 ± 0.11
1:1 **1:2**	β_{11} β_{12} **ΔG**	--	3.70 ± 1.39 6.44 ± 2.64[c] -8.4 ± 3.4	--	2.56 ± 5.76 4.75 ± 7.04[c] -6.2 ± 9.2	--	2.70 ± 0.92 4.31 ± 2.36[c] -5.6 ± 3.1	--	1.12 ± 0.04 1.88 ± 4.04[c] -2.4 ± 5.3
1:1 **1:2** **2:2**	β_{11} β_{12} β_{22} **ΔG**	--	3.38 ± 0.60 5.50 ± 2.90 7.06 ± 9.65[c] -9.2 ± 13	--	2.62 ± 1.68 4.59 ± 4.89 7.72 ± 6.81[c] -10.1 ± 8.9	--	2.78 ± 2.06 4.49 ± 2.94 7.22 ± 9.57[c] -9.4 ± 12	--	1.30 ± 1.55 2.54 ± 2.90 4.70 ± 7.55[c] -6.1 ± 9.8

[a] Logβ: β_{11} (M^{-1}), β_{12} (M^{-2}), β_{22} (M^{-3}). [b] Units: kcal·mol^{-1}. [c] Good data fit but β errors are too big.

As it can be seen, **HαOBn** host formed 1:1 complexes with the four anions. The most stable complex was provided by dihydrogenphosphate anion, showing an association constant 100-fold bigger (in decimal logarithm values) than the rest of complexes at least. Linear regression approximation was appropriate for acetate, benzoate and chloride anions, which showed the most similar values of association constants, but not for dihydrogenphosphate. That is why systems 1:2 and 2:2, with the corresponding associated species, were tried to be fitted with the same NMR data, resulting in good statistics results. However, the corresponding errors associated to the given constants were too large, what made us refuse the possibility of the 1:2 and 2:2 systems. This was also carried out for the rest of the anions, showing similar results (Table **19**).

Dihydrogenphosphate: it has been widely used for the study of host-anion systems and its interest is usually related to the mimicry of active sites of phosphate-binding proteins, necessary for the ATP formation for instance. Its acidic properties together with the intrinsic basic ones from its anionic nature, make $H_2PO_4^-$ to be a versatile anion to be complexed in most cases. Moreover, the fact of having two hydrogen atoms susceptible of being coordinated by donor atoms, increases its attraction to many hosts. Sometimes, in the solid state, it has been observed that the presence of basic atoms in the host can cause deprotonation of acidic anions such as $H_2PO_4^-$ or HSO_4^-. However, and despite having a nitrogen atom in the apical position of the hosts, this behaviour was not observed for **144**, **148** or **149**.[250]

The acidic protons of the non-coordinated anion were not seen in the spectrum, just those from own of TBA counterion could be detected when the salt was added, even when the spectrum width

covered until 16 ppm. Only a single signal was detected in the titration process and therefore, the equilibrium between both coordinated and non-coordinated species was faster than the resonance frequency at which the spectrum was recorded (600 MHz). This behaviour was reproduced in all the tests except for the fluoride anion.

Acetate and benzoate: they are a common source of trigonal planar anion among the carboxylate anions, although acetate requires careful manipulation because it is very hygroscopic. Benzoate anion usually presents similar host-guest behaviour than acetate, although their differences normally raise from their distinct bulkiness in the binding sites of receptors. In our case, recognition of acetate was a bit stronger than for benzoate, although we thought that the aromatic moiety would enhance the stability of the complex by π-π stacking. Taking into account the A-values employed as a general representation of steric bulk for the determination of most stable conformations in a cyclohexane,[295] bulkiness of the methyl is lower than a phenyl ring so this would explain the higher stability of acetate anion complex. Moreover, benzoic acid is more acidic than acetic acid in both water and DMSO solvents so acetate anion is more basic, what also justifies its higher association constant [pKa(acetic acid, DMSO)=12.6;[296] pKa(benzoic acid, DMSO)=11.1].[297] A repetitive structural moiety that enforces the coordination of acetate anions is the presence of two NH amide groups linked by ethylene units as demonstrated by Schneider and Werner.[298-300]

Chloride: this anion is interesting since there are membrane transport agents for it in many biological systems. A key structural feature to bind chloride effectively is a cavity with the proper size to entrap it. The main reason is linked to the fact that spherical anions are not able to be bound by directionality of the negative charge density. Then, among amide-based receptors with affinity towards Cl^-, a lot of them are cyclic polyamides[301] or carcerands[302] for instance. In our case, the tripodal geometry of the binding site and the shape of chloride do not fit in a stable complex, although lower basicity of chloride also plays a determinant role.

Same host-guest study for **[HαOBn][H_2PO_4]** complex in $CDCl_3$ was also performed in contrast to DMSO-d_6. No self-aggregation was observed, but Job's plot experiment showed a rare behaviour of NH, being split or disappeared. The titration to determine the K_a resulted in spectra where two signals could be differentiated (Annex section **4.5.4.1**). Computational calculations employing H_7 shift data were done, showing that in $CDCl_3$ the same complex fitted the best for a 1:2 system (Table **20**).

Table **20**. Logβ and ΔGº values for the complexes formed by **HαOBn** host and dihydrogenphosphate anion in $CDCl_3$.

		Anion sources and methods of determination of association constants[a] (*up*) and free energies[b] (*down*)	
HαOBn		**$TBAH_2PO_4$ in $CDCl_3$**	
		Graphical	**Win EQNMR2**
1:1	**β_{11}**	No linear regression could be obtained from any of the H_1, H_4 and H_7 signals employed	3.01 ± 0.35[c]
	ΔG		-3.9 ± 0.5
1:1 **1:2**	**β_{11}** **β_{12}** **ΔG**	--	3.75 ± 0.98 8.47 ± 0.28 -11.0 ± 0.4
1:1 **2:1**	**β_{11}** **β_{21}** **ΔG**	--	3.85 ± 0.26 5.85 ± 2.97[c,d] -7.6 ± 3.9
1:1 **1:2** **2:2**	**β_{11}** **β_{12}** **β_{22}** **ΔG**	--	3.56 ± 0.52 5.10 ± 3.90 5.10 ± 0.06[c,d] -6.6 ± 0.1

[a] Logβ: β_{11} (M^{-1}), β_{12} and β_{21} (M^{-2}), β_{22} (M^{-3}). [b] Units: kcal·mol^{-1}. [c] Data does not fit as good as in a 1:2 system. [d] β errors are too big. [e] Regular data fit because some points were random.

For the statistics of the data fitting parameters see Annex section **4.5.4.1**.

Nevertheless, the observations on NMR spectra, together with the lower solubility of $TBAH_2PO_4$ salt and receptor, and the rapid evaporation of chloroform during the preparation of NMR tubes (which could vary the real concentrations) made us reject this solvent for the complexation studies.

Change in the complex's stoichiometry due to different solvents has been already reported in the literature.[303] On the other hand, association constants were higher because the solvent does not compete for the hydrogen bonds involved in the host-anion event, as expected. In fact, complexation of two dihydrogenphosphate anions resulted in a $\beta_{12} = 2.9 \cdot 10^8$ M^{-1}, a very high constant beyond the calculation limit by NMR methods.

4.3.3.2. HαOBn-FTBA complex

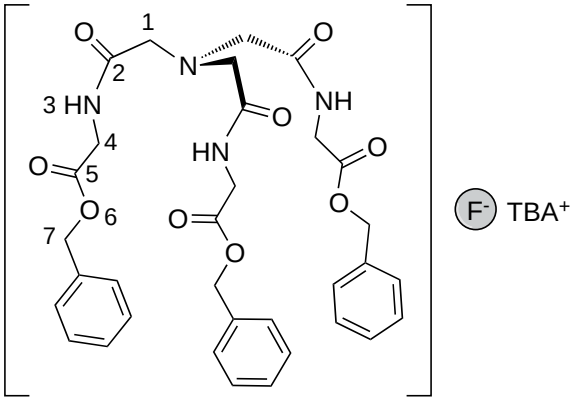

When the NMR experiments were carried out for the complex between **HαOBn** and fluoride anion the disappearance of N-H_3 signal was observed (Figure **123**).

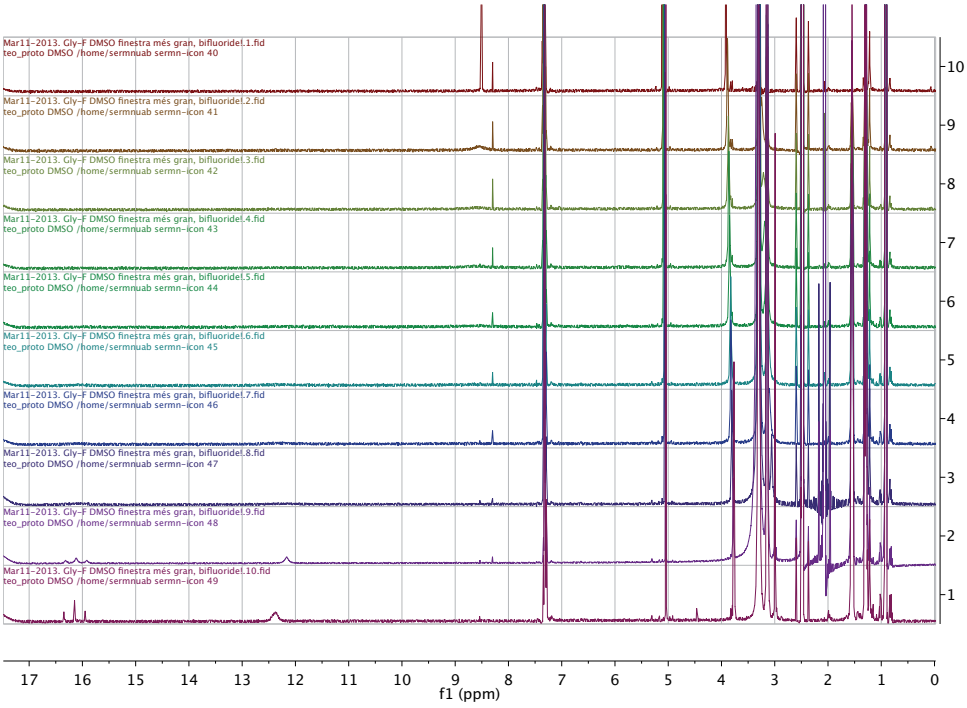

Figure **123**. ^{1}H-NMR spectra of **HαOBn** titration with **TBAF** to determine the K_a of the complex. From Eq. Guest = 0 (*top*) to Eq. Guest = 6 (*bottom*). DMSO-d_6 (600 MHz).

In the beginning, this made us think about a strong complex being formed, even in a polar solvent such as DMSO. The NH signal disappeared and at 2 eq. of TBAF split into two little intense signals, giving valuable information about the possible stoichiometry of the complex. Regarding the chemical shift of N-H_3 signal at the highest concentration of the anion (signal at about 12 ppm), the formation of a strong acid could be suspected, suggesting that fluoride coordination was so strong that the NH protons could be almost dissociated. Indeed, representation of chemical shifts *vs.* equivalents of TBAF exhibited a sigmoidal titration curve quite similar to those related to acid-base reactions (Figure **124**). One could discern a supposed acid-base equivalence point between 2 and 2.5 eq. of TBAF.

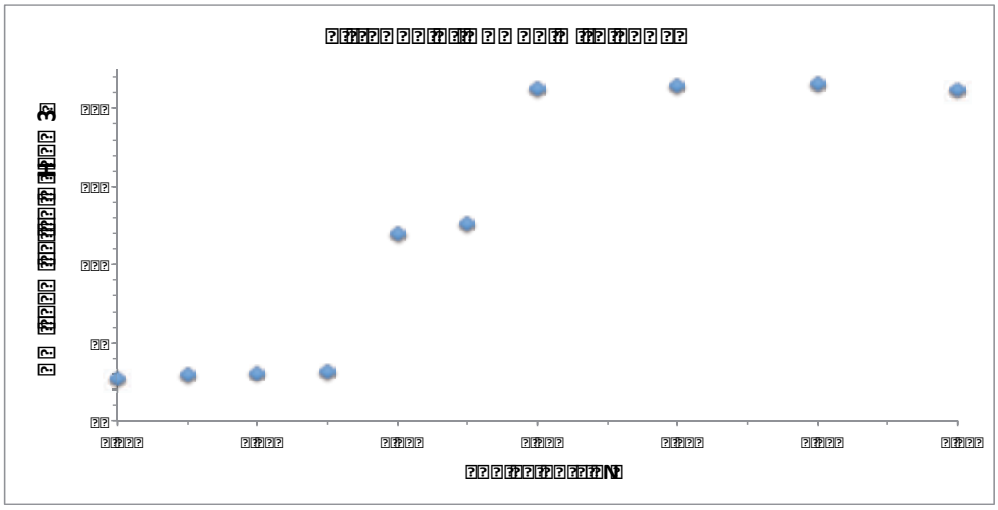

Figure **124**. Sigmoidal curve obtained by the titration of **HαOBn** with TBAF.

Moreover, an additional signal appeared about 16 ppm with a defined triplet multiplicity and a coupling constant of J = 120 Hz. This new signal must be related to the coupling of NH protons with fluoride anion because the J is too large for a ^{1}H-^{1}H coupling. A 1:2:1 triplet would mean that one proton is equivalently coupled to two fluorides, which also have a spin number of 1/2. In fact, this signal is typical of bifluoride anion (Figure **125**).[304] In addition, the total integral of signals at 16 ppm and 12 ppm adds up to about 1, what would correspond to the NH proton of the host, part in the form of bifluoride and part in the form of complexed NH. Note that integration of the host is made according to one of the three equivalent arms.

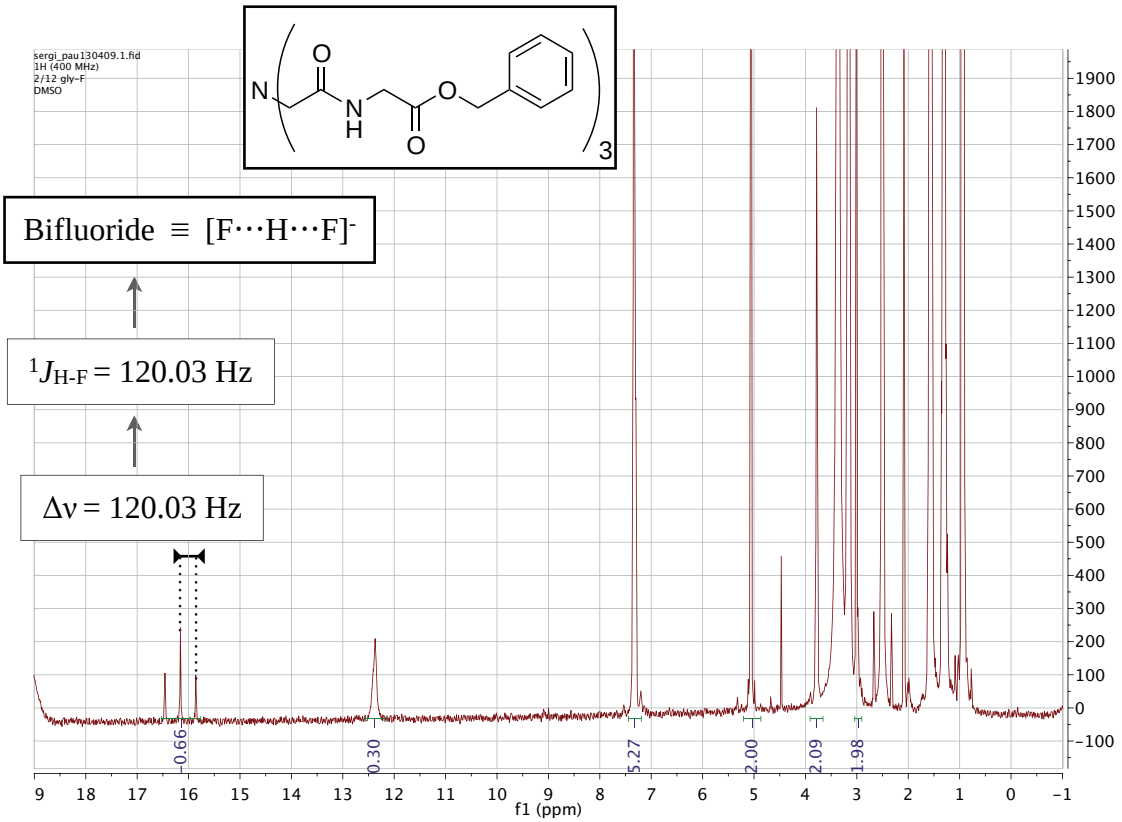

Figure **125**. ^{1}H-NMR spectrum of **HαOBn** (2 mM) with 6 eq. of **TBAF** (12 mM). DMSO-d_6 (400 MHz).

These observations have been mentioned in other cases, where authors justify the presence of bifluoride due to different reasons.[305,306] Fluoride is known as a strong base, able to abstract β-hydrogen atoms from tetra-*n*-butylammonium salts to yield 1-butene, tri-*n*-butylamine and tetra-*n*-butylammonium bifluoride. In the presence of more acidic protons, fluoride has been observed to abstract hydrogens from amide-based macrocycles[307] and cryptands,[308] as well as urea-,[309] thiourea-,[310] and pyrrole-based acyclic anion hosts,[311] often with the observation of bifluoride in the ^{1}H-NMR spectrum. Even some commercially available tetrabutylammonium fluoride salts contain bifluoride. To reject this latter possibility because the commercial salt we used was hydrated, a ^{1}H spectrum of our TBAF was performed from 0 to 20 ppm at 20 mM, showing the absence of bifluoride $(FHF)^-$ in the ^{1}H-NMR spectrum. However, in the ^{19}F-NMR spectrum, besides a singlet at -97 ppm corresponding to free fluoride, a 1:1:1 triplet with a J = 18 Hz was observed at about -143 ppm. These properties would suggest the presence of deuterium bifluoride $(FDF)^-$, since ^{1}H-decoupled and -coupled ^{19}F-NMR spectra showed the same multiplicity. This could be explained because basic fluoride is able to abstract of methyl D atoms from weak acids as DMSO-d_6 (see Annex section **4.5.4.7**).[312]

To get more insight about this issue, ^{19}F-NMR experiments were also carried out on a mixture of our glycine-containing host and fluoride (Figure **126** and Figure **127**).

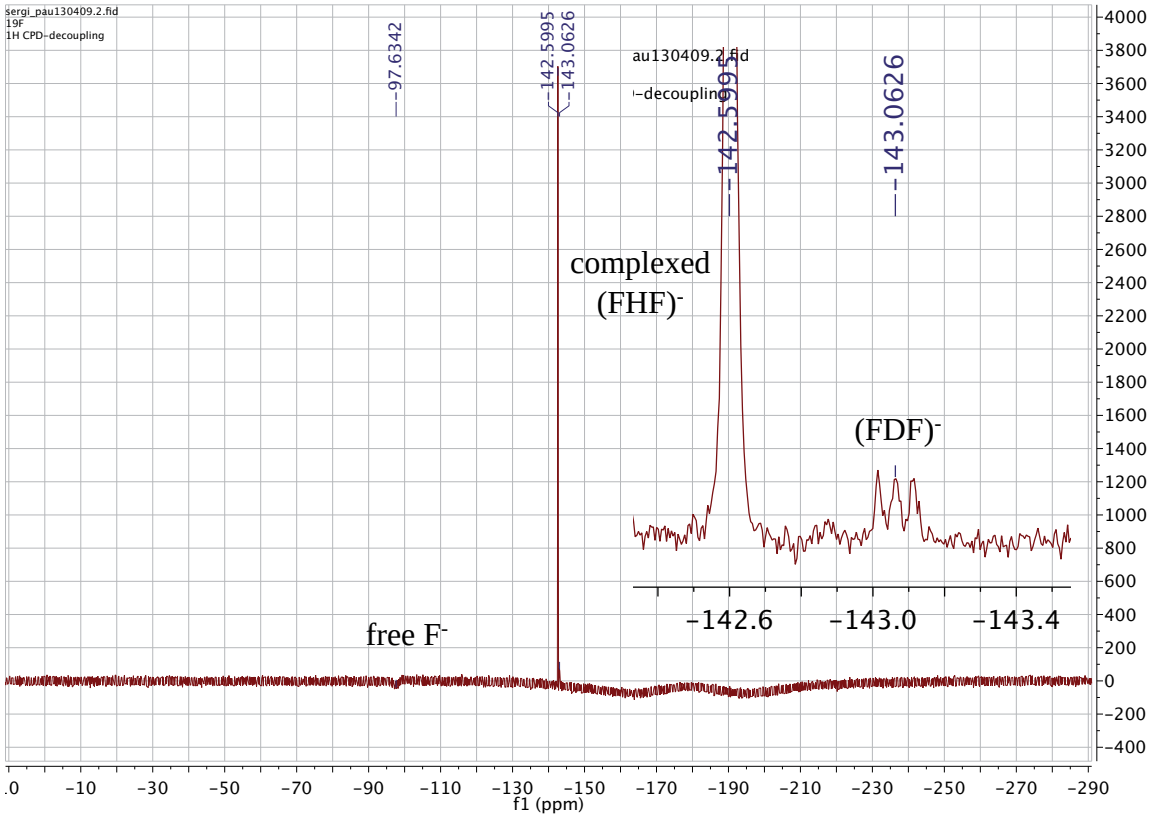

Figure **126**. ^{19}F-NMR ^{1}H-decoupled spectrum of **HαOBn** titration (2 mM) with TBAF (12 mM). DMSO-d_6 (400 MHz).

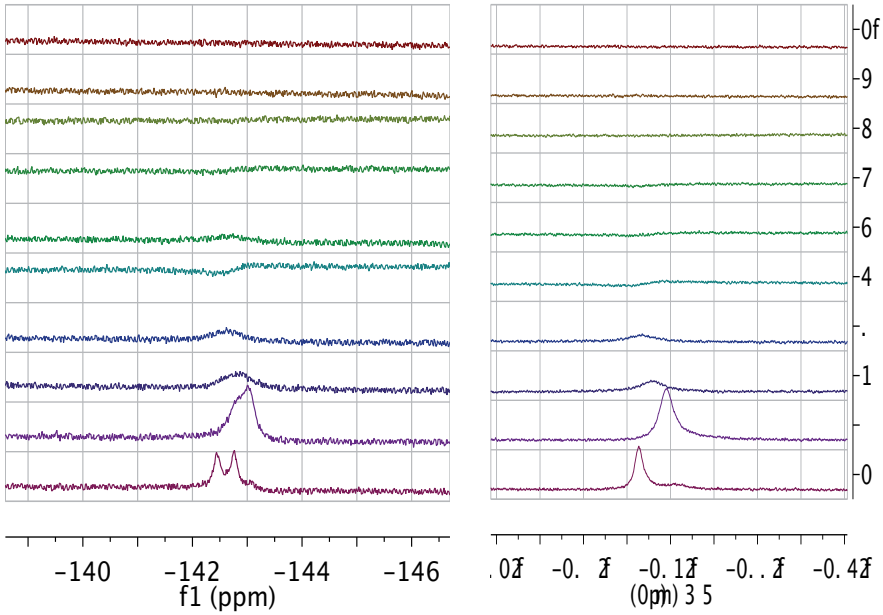

Figure **127**. Zoom of bifluoride area from the ^{19}F-NMR ^{1}H-coupled (*left*) and ^{19}F-NMR ^{1}H-decoupled (*right*) spectra of **HαOBn** titration with **TBAF** to determine the K_a of the complex. From Eq. Guest = 0 (*top*) to Eq. Guest = 6 (*bottom*). DMSO-d_6 (400 MHz).

After 2 equivalents of TBAF were added to **HαOBn** + F^- mixture (Figure **127**: 5th spectrum from above) a signal about -142 ppm appeared as a singlet in the ^{19}F-NMR ^{1}H-decoupled experiment. In the ^{19}F-NMR ^{1}H-coupled experiment, a doublet at the same chemical shift with a coupling constant of J = 122 Hz appeared at the highest concentrations of TBAF, what supported the *in situ* formation of bifluoride anion.

However, this chemical shift would correspond to non-complexed bifluoride anion as reported in the literature for the same solvent but a different host.[312] Otherwise, the same authors affirm that complexed bifluoride shows a triplet as above described in the ^{1}H-NMR spectrum (Figure **128**).

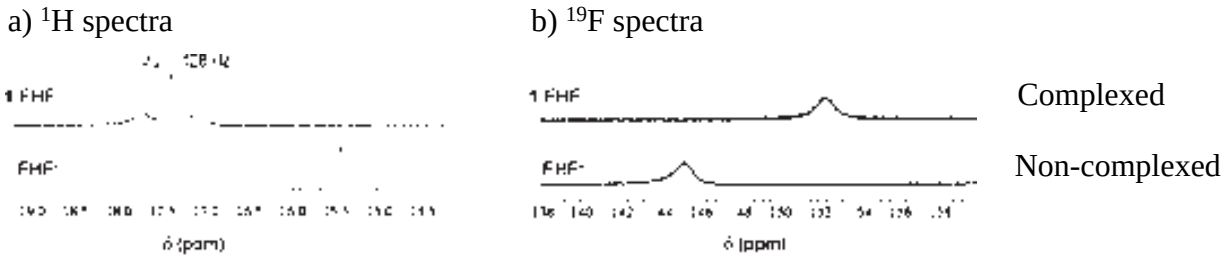

Figure **128**. ^{1}H-NMR and ^{19}F-NMR ^{1}H-decoupled spectra of [TBA][FHF] salt complexed and non-complexed. DMSO-d_6 (400 MHz).

On the other hand, no 1:1:1 triplet corresponding to deuterium bifluoride was significantly detected and the explanation lies on the fact that fluoride abstract NH more acidic protons instead of the less acidic methyl D atoms of DMSO-d_6 (Figure **127**).

Gale made a similar observation, in which the NH resonance also disappeared upon the addition of TBAF in DMSO-d_6 99.5%, fact that he attributed to some possible interchange. He proposed an

hypothesis of a three-step complexation process for the fluoride binding: 1) The initial equivalent of fluoride is coordinated, and a significant shift of the CH protons is observed; 2) With the second equivalent of fluoride, the pyrrole NH group is deprotonated, and bifluoride (FHF^-) is formed; 3) The third equivalent of fluoride is then coordinated.[311b,311c,313] Deprotonation was corroborated by X-ray diffraction, where two TBA counterions were detected (Figure **129**).

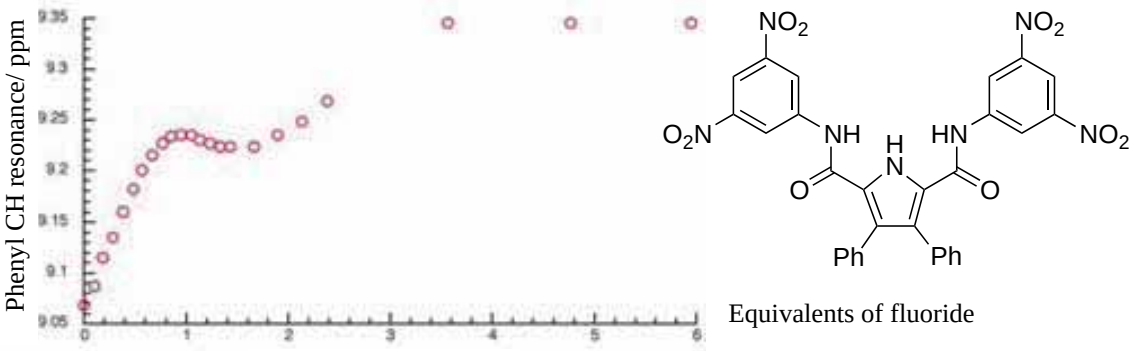

Figure **129**. NMR titration curve of pyrrole-based receptor (*right*) with TBAF in DMSO-d_6 with 0.5% of water.

Our experimental results instead, since the calculations of stability constants with WinEQNMR2 pointed out a 1:2 [**HαOBn][F]** complex (Table **21**, 5 pages below), suggested that bifluoride was coordinated as observed in the ^{1}H-NMR spectrum. In addition, after proton abstraction and subsequent formation of bifluoride, the coordination of two fluoride anions would not be so favoured because it would suppose three negative charges in a host, to be "neutralized" with three TBA counterions in a relatively close coordination sphere.

1D-selective ^{19}F-^{1}H NOE experiments were performed to find out any possible interaction between bifluoride and the host (Figure **130**).

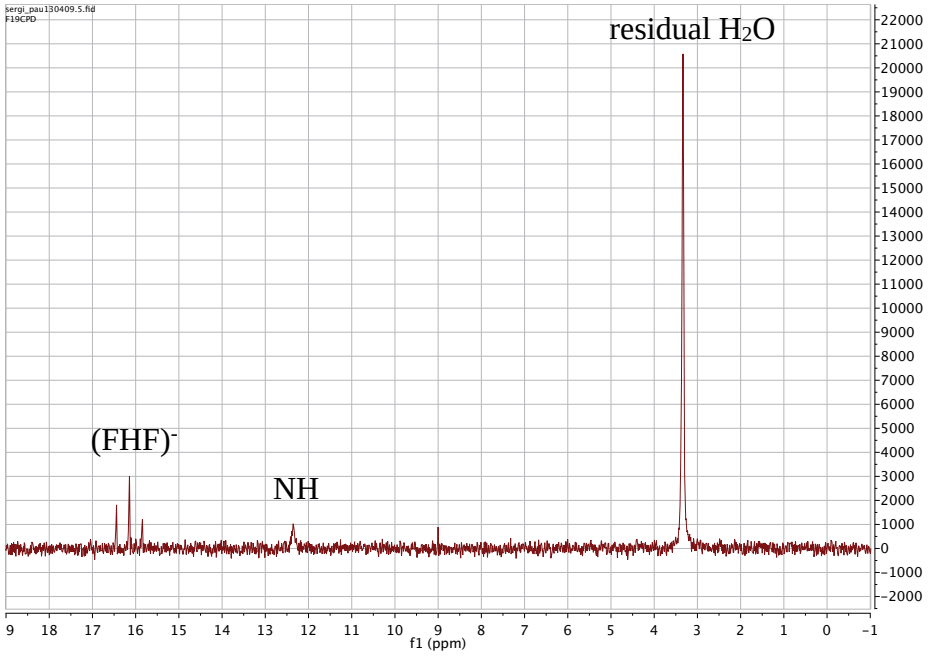

Figure **130**. 1D-selective ^{19}F-^{1}H-NOESY spectrum of **HαOBn** titration with TBAF. DMSO-d_6 (400 MHz).

The spectrum showed correlation between the ^{19}F bifluoride signal and the ^{1}H signal of bifluoride as expected, the residual water due to interchange and with the NH of the host, demonstrating the coordination of bifluoride inside the host.

This particular behaviour was also observed by Shang[314] and Jose,[315] who reported the ^{1}H-NMR experiments of F^- titration in DMSO-d_6 with similar results. The NH signals of their amide and thiourea hosts respectively, disappeared upon 5 equivalents of the TBAF salt. This effect showed that the site at which receptors act with a fluoride anion is a hydrogen atom of an amide bond and its disappearance must be related to the strong interaction towards the anion. Nevertheless, both authors just attributed it to a fact of preference/affinity but not to the basicity of the small F^- anion.

Who attributed this special behaviour of fluoride to its basicity were Jurczak and coworkers[261] whose bishydrazide derivatives of isoindoline showed the disappearance of isoindoline and hydrazide NH signals up to 0.2 and 2.5 equivalents of $TBAPhCO_2$ and $TBAH_2PO_4$, respectively, proving the basicity of benzoate and dihydrogenphosphate towards these hosts.

Nevertheless, there are alternatives for the determination of stoichiometry and K_a if NH signal disappears. Other host signals can be shifted because they are involved in the binding event too.[274]

Since the N-H_3 signal of our host disappeared and H_1 overlapped with TBA^+ counterion signals during the TBAF titration, the stoichiometry and K_a were determined using the H_4 and H_7 signals. They were also shielded due to the strong coordination of fluoride, although direct coordination of such protons was unknown. Chemical shift variation for H_4 and H_7 of **HαOBn** host was calculated in basis of next spectra (Figure **131**).

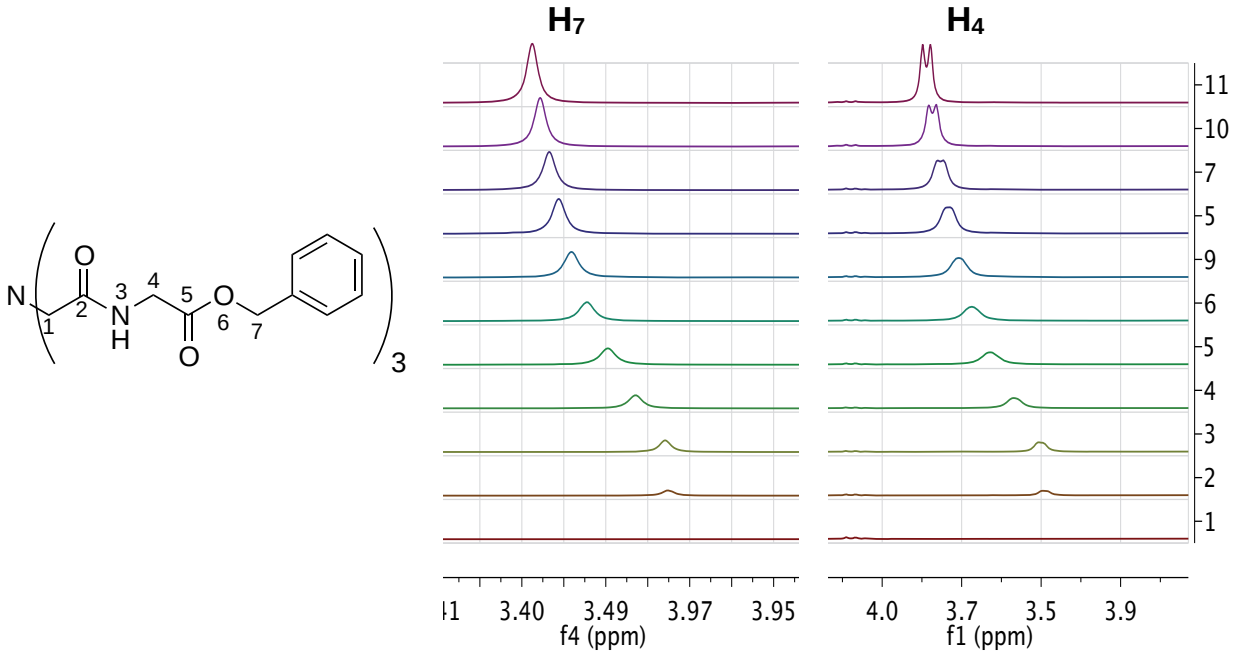

Figure **131**. Zoom of specific signals from the ^{1}H-NMR spectra of **HαOBn** Job's plot experiment. DMSO-d_6 (600 MHz).

Graphical representation of $\Delta\delta \cdot$[Host] *versus* X_{Guest} resulted in the Job's plots shown in Figure **132**.

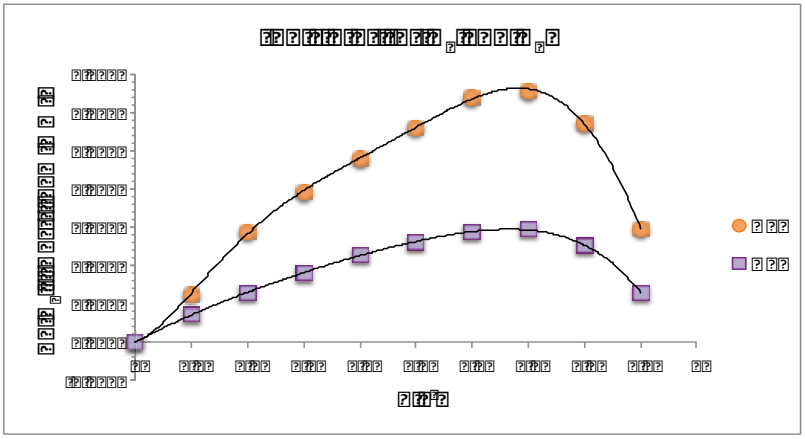

Figure **132**. Job's plot for **[HαOBn][F]** complex.

As it can be observed, the curves presented similar trends for both signals, exhibiting non-symmetric parabolas with the maximum pointing $X_F \simeq 0.7$. This value would be in good agreement with a 1:2 (host:guest) **[HαOBn][F]** complex, because this stoichiometry would imply $X_F = 0.67$.

For this stoichiometry the association constant can not be determined by the linear regression approximation. Hence, WinEQNMR2 program was used to fit data from both signals, corroborating the stoichiometry and providing both thermodynamic constants (β_{11} and β_{12}). Determination of the association constant using both H_4 and H_7 signals for a 1:1 complex, resulted in an average K_a = 11216 M^{-1}, log(K_a) = 4.05 (Annex section **4.5.4.7**). This value was used as initial guide constant for the WinEQNMR2 calculations.

Low temperature experiments were performed in order to make the NH signal to be visible or even split, as observed in literature.[312b,316,317] However, they did not work because the DMSO-d_6 solidifies at relative high temperatures, only allowing to cool it down 5 K to 293 K, at which no significative changes were observed.

On the other hand, it is known that the complexation involving charged species decreases with the polarity of the solvent, so mixtures of DMSO-d_6/water were tested.[318] Water concentrations of 0.05%, 5% and 10% were used for recording stoichiometry experiments and the best results were provided by the highest water-containing mixtures, to our surprise. The N-H_3 signal, although a bit broad, was appreciable during all the titration with TBAF, and H_1 signal was also shifted but in less proportion (Figure **133** and Figure **134**).

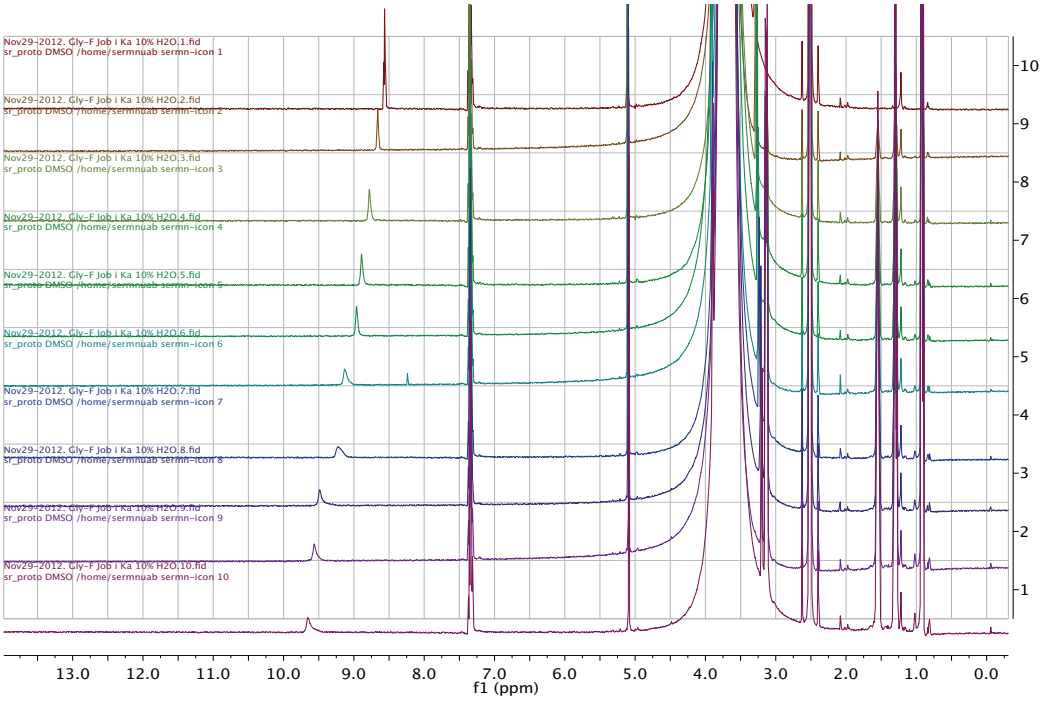

Figure **133**. ^{1}H-NMR spectra of **HαOBn** titration with **TBAF** and 10% of water to determine the stoichiometry of the complex. From X_{Host} = 1 (*top*) to X_{Host} = 0 (*bottom*) in ΔX = 0.1. DMSO-d_6 (600 MHz).

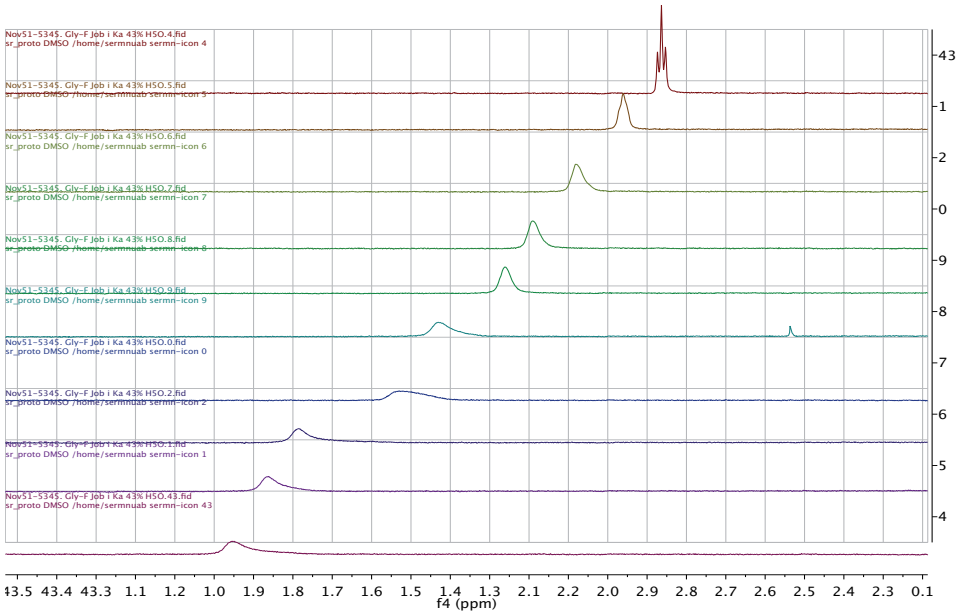

Figure **134**. Zoom of N-H_3 area from the ^{1}H-NMR spectra of **HαOBn** titration with **TBAF** and 10% of water to determine the stoichiometry of the complex. From X_{Host} = 1 (*top*) to X_{Host} = 0 (*bottom*) in ΔX = 0.1. DMSO-d_6 (600 MHz).

In both spectra, the N-H_3 signal did not disappear when 10% (v/v) of deionized water was added. The NH chemical shift just differed 0.029 ppm in the presence or not of 10% of water. In addition, multiplicity (t) was not lost, suggesting the fact that only the F^- ion was significantly coordinated. Water molecules would probably solvate the fluoride ions through hydrogen-bonding, competing with the less acidic NH protons of the host and therefore, decreasing its affinity.

Job's plot of the data from N-H_3 and H_1 signals showed a chemical shift variation not as regular as in other cases, but neither the system was the same (Figure **135** and Figure **136**).

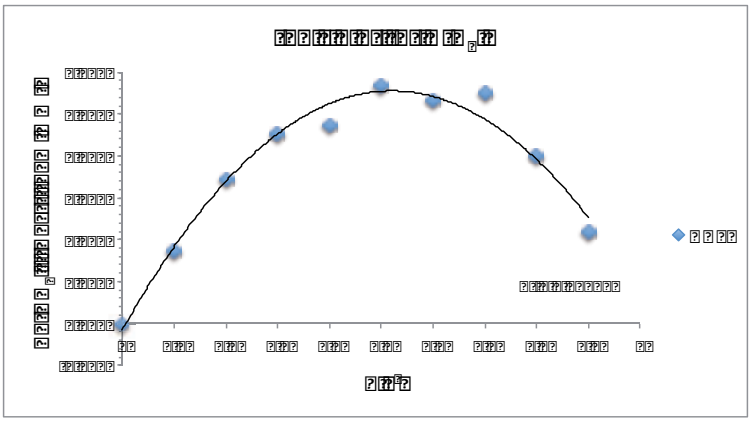

Figure **135**. Job's plot for **[HαOBn][F]** complex with 10% of water.

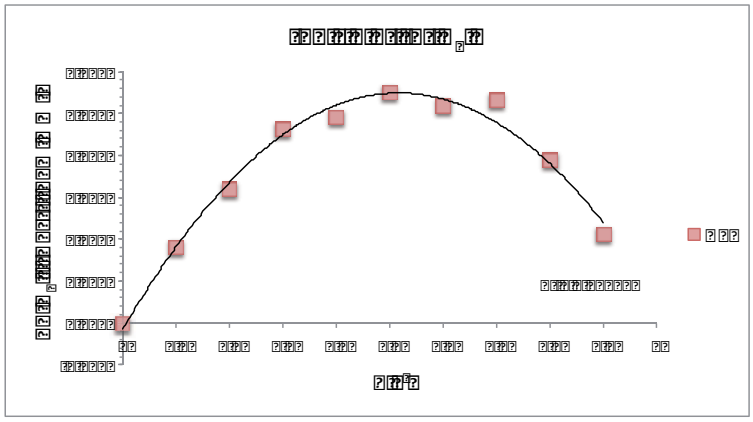

Figure **136**. Job's plot for **[HαOBn][F]** complex with 10% of water.

Nevertheless, R-squared for both parabolas fitted quite well so it could be affirmed that a 1:1 stoichiometry for the **[HαOBn][F]** complex was evidenced when a 10% of water was present in the DMSO-d_6 medium.

Related behaviour has been observed in the literature, where the same host-guest complex showed different stoichiometries depending on the overall polarity of solvent.[303]

The data extracted from them permitted the calculation of the parameters for the linear regression and a good fit was found for the titration experiment. The poor K_a= 7.4 M^{-1} ($\log K_a$ = 0.87) value obtained was in agreement with the competition event for the hydrogen-bonding of fluoride anion, and it was used for the computational calculation (Annex section **4.5.4.7**).

Alternatively, a titration experiment was carried out in MeCN-d_3. DMSO is a very polar solvent that is found to promote basic reaction of F^- even with amide protons[312b] so, acetonitrile was chosen as a less polar aprotic solvent where both host and guest were soluble. It could be observed that the N-H_3 signal disappeared from its initial chemical shift when 0.5 and 1 equivalent of TBAF were added, to reappear at about 12 ppm, showing similar trends as in DMSO. However, bifluoride

$(FHF)^-$ triplet resonance was not observed in the ^{1}H-NMR spectrum although a broad signal with low intensity was appreciable at similar shift.

In parallel, on both ^{1}H-decoupled and -coupled ^{19}F-NMR spectra, a singlet at -150 ppm corresponding to complexed fluoride was observed, corroborating the absence of $(FHF)^-$ (Annex section **4.5.4.7**). This would suggest that MeCN does not promote H abstraction from NH of the host, since it can not solvate fluoride as good as DMSO does. Moreover, $(FDF)^-$ was not either detected, proving that methyl D atoms from MeCN-d_3 are not as acidic as in DMSO-d_6.

Regarding the titration experiment to determine the association constant, H_4 and H_7 signals were also shielded to upfields.

The shifting of these signals was used to perform the program calculations too. Table **21** displays the graphical and computational results for the complexation studies of **[HαOBn][F]** complexes. For the statistics of the data fitting parameters see Annex section **4.5.4.7**.

Table **21**. Logβ and ΔG° values for the complexes formed by **HαOBn** host and fluoride anion.

		Anion sources and methods of determination of association constants[a] (*up*) and free energies[b] (*down*)				
HαOBn		**TBAF**				
		DMSO 99.8%/H_2O 0.2%		**DMSO 90%/H_2O 10%**		**MeCN**
		Graphical	**Win EQNMR2**	**Graphical**	**Win EQNMR2**	**Win EQNMR2**
1:1	**β_{11}**	4.05	1.77 ± 0.30[c]	0.87	1.64 ± 0.46[e]	7.25 ± 0.23[c]
	ΔG	-5.3	-2.3 ± 0.4	-1.1	-2.1 ± 0.6	-9.5 ± 0.3
1:1 1:2	**β_{11} β_{12} ΔG**	--	2.26 ± 0.76 5.86 ± 0.24 -7.6 ± 0.3	--	1.74 ± 4.02 2.42 ± 1.49[d,e] -3.2 ± 195	7.45 ± 0.45 8.82 ± 1.35[d] -11.5 ± 1.8
1:1 2:1	**β_{11} β_{21} ΔG**	--	2.75 ± 0.22 4.41 ± 3.20[c,d] -5.8 ± 4.2	--	1.10 ± 2.63 3.92 ± 3.82[d,e] -5.1 ± 5.0	3.73 ± 3.43 9.06 ± 3.51[d] -11.8 ± 4.6
1:1 1:2 1:3	**β_{11} β_{12} β_{13} ΔG**	--	1.58 ± 1.1 4.87 ± 3.2 7.57 ± 2.1[c,d] -9.9 ± 2.7	--	--	--
1:1 1:2 2:2	**β_{11} β_{12} β_{22} ΔG**	--	1.80 ± 1.0 5.11 ± 0.89 7.20 ± 28[c,d] -9.4 ± 36	--	--	2.81 ± 4.7 6.36 ± 3.74 8.96 ± 2.09[c,d] -11.7 ± 2.7

[a] Logβ: β_{11} (M^{-1}), β_{12} and β_{21} (M^{-2}), β_{13} and β_{22} (M^{-3}). [b] Units: kcal·mol^{-1}. [c] Data does not fit as good as in a 1:2 system. [d] β errors are too big. [e] Regular data fit because some points were random.

Data from H_4 proton did not fit as good as H_7 did, so this one was used to check the possible systems. In DMSO 99.8%, surprisingly, data fitted quite well for a 1:1 system and errors for $\log\beta_{11}$ were acceptable. However, β_{11} value in a 1:1 system was too low to explain the experimental observations. Then, application of the data to a 1:2 system resulted in a better fitting and coherent values for the complexation constants. Taking into account the experimental observations about the presence of coordinated bifluoride and the calculated 1:2 stoichiometry, a possible structure of the complex is suggested in Figure **137**. However, in the literature, the receptors that usually host linear anions are bi- or tricycles with cylindrical shapes.[306,308,312] On the other hand, preliminary theoretical studies would suggest a different complexation event, in which two **HαOBn** hosts encapsulate one bifluoride anion.

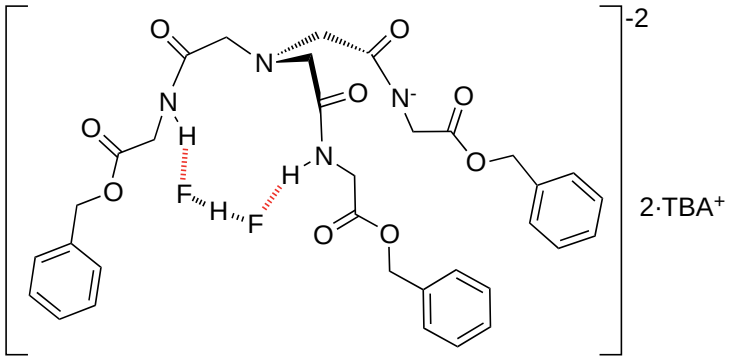

Figure **137**. Suggested structure for the **[HαOBn][FHF]** complex. Red-dashed lines represent normal hydrogen bonds while black-dashed lines represent the strongest hydrogen bonds known in bifluoride anion.

On the other hand, fitting of the data from water-containing experiments did not afford very good statistics because the last points were quite random. Nevertheless, a 1:1 complex was suggested to be formed. In MeCN-d_3, the fitting of the data pointed out to a 1:2 system but error of β_{12} was quite large. Finally, 1:1 system suited better in acetonitrile solvent.

Regarding the association constants, addition of 10% of water into DMSO-d_6 decreased β_{11} at the same level of chloride complexation. This suggested the competition between NH amide protons and the more acidic protons of water for the hydrogen-bonding of fluoride anion. On the contrary, when MeCN-d_3 was employed for the same experiment, the resulting β_{11} of the complex was bigger than the β_{12} in DMSO, as expected for a less polar solvent. However, affinity can not be strictly compared because in acetonitrile the formation of 1:1 complexes was favoured (as in DMSO 90%), evidencing the influence of polarity of the whole solvent in the stoichiometry of complexes. Once more, the constants obtained are beyond the calculation limit by NMR methods too.

These results, taken together, prove a different mode of recognition for F^- in comparison to the other anions. Indeed, given the binding site formed by the three NH amide groups, it seems that only the small fluoride anion can access within deeply and doubly, resulting in bifluoride formation and its corresponding coordination.

Jabin and collaborators,[316] who prepared tripodal calixarene-containing receptors, also suggested a different binding for fluoride anion, although in $CDCl_3$. Moreover, *tren*-based derivatives did not show any affinity towards the anions, fluoride included, while NTA-based one did (Figure **138**).

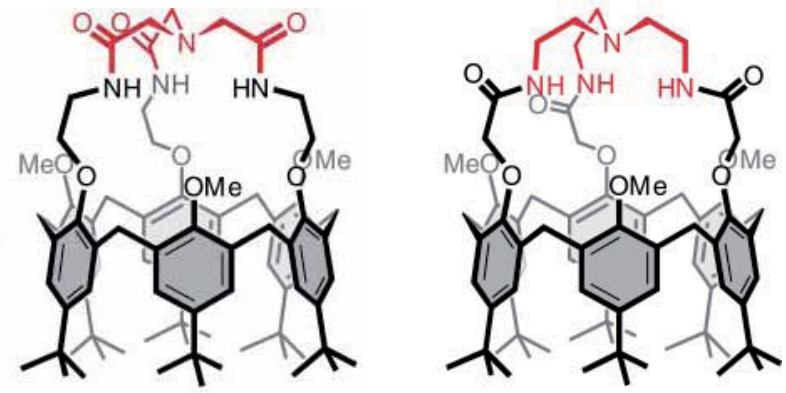

Figure **138**. NTA-based calix[6]cryptamide (*left*) and *tren*-based calix[6]cryptamide (*right*) studied by Jabin.[317]

They proposed that while F^- presents a *endo*-complexation because is the only one which fits in the cryptamide cap, other anions tested (Cl^-, $CH_3CO_2^-$, $CH_3SO_3^-$ and NO_3^-) exhibit a *exo*-complexation characterized by coordination with only one NH proton, what would explain their low affinity. In our case, the host has an open structure which could embrace the anions in variable angles, whereas the cryptamide compound has a limited cavity due to the calixarene cyclic moiety, which requires inclusion of the anion to provide strong interactions. Therefore, our more minimalist host shows better recognition towards acetate and chloride.

On the other hand, Das and co-workers synthesized a *tren*-based host with a comparable structure to ours (Figure **139**).[274]

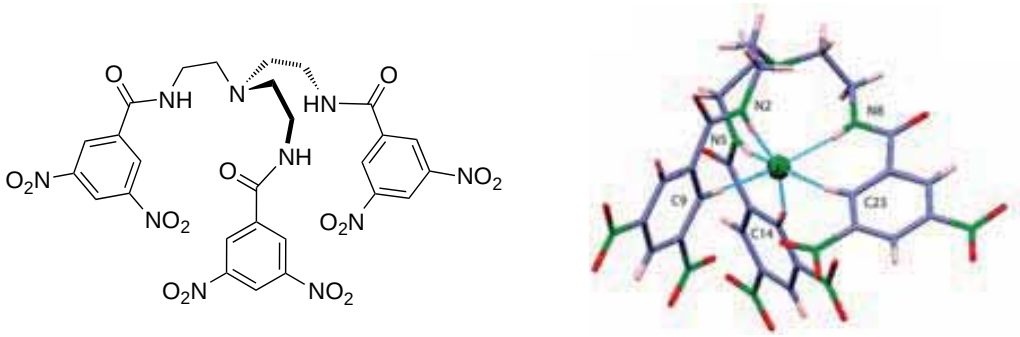

Figure **139**. Molecular structure of *tren*-based host reported by Das (*left*). Crystal structure of the receptor showing coordination of a fluoride ion (*right*).

Their anion recognition studies, using both NMR and UV/vis techniques, concluded that the affinity towards Cl^-, Br^-, I^-, $CH_3CO_2^-$, NO_3^-, $H_2PO_4^-$, HSO_4^- and ClO_4^- was low, while $CH_3CO_2^-$ and $H_2PO_4^-$ have been clearly recognized by our Gly-based receptor. Fluoride anion on the contrary, showed strong affinity too in deuterated DMSO (logK > 7). Their complex exhibited 1:1 stoichiometry, while ours showed 1:2, and $\log\beta_{12} \approx 6$. This comparison nicely illustrates how a slight structural difference at the level of the recognition site can drastically modify the host properties of a receptor. A crystal structure has been also reported from their host solution in polar solvents as MeCN or DMF and TBAF excess, showing a fluoride ion inside the cavity (Figure **139**). The F^- was always coordinated by the three NH protons and the other interactions were provided by the three acidic H_{aryl} protons and the π-electrons of the aromatic rings.

Since dihydrogenphosphate anion gave the highest affinity and a simple 1:1 complex for **HαOBn** host, the study of the chain length effect, through its β-alanine and GABA analogues, was decided to be performed from the point of view of this anion.

4.3.4. HβOBn-H_2PO_4TBA complex

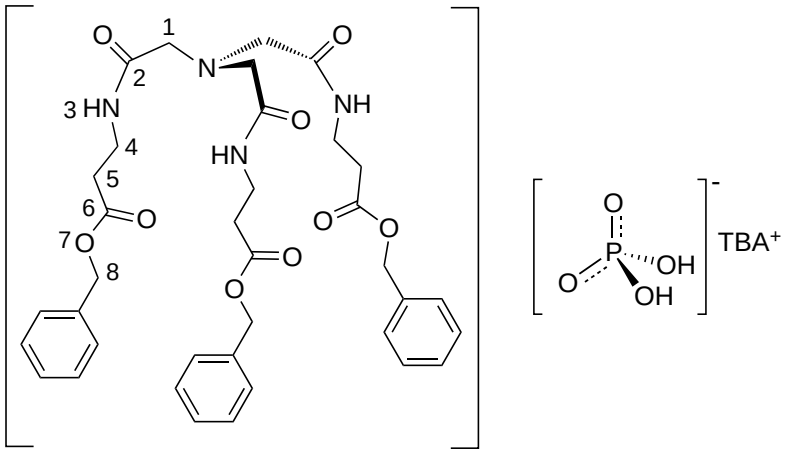

This receptor, a homologated analog of the glycine derivative, was expected to give less affinity for the same anion. Indeed, longer chain would imply more flexibility, causing a loss of preorganization and then decreasing the K_a.

Because no signal was shielded during the experiment, it could be stated that no self-aggregation took place under 4 mM of host concentration (see Annex section **4.5.5**).

Signals corresponding to both β-alanine methylene units did not clearly appear on the spectrum (they are under DMSO and water residual peaks) but other minor signals were observed, concretely for the NH amide proton (N-H_3), the benzylic methylene proton (H_8) and the nitrilo methylene one (H_1) (Figure **140**).

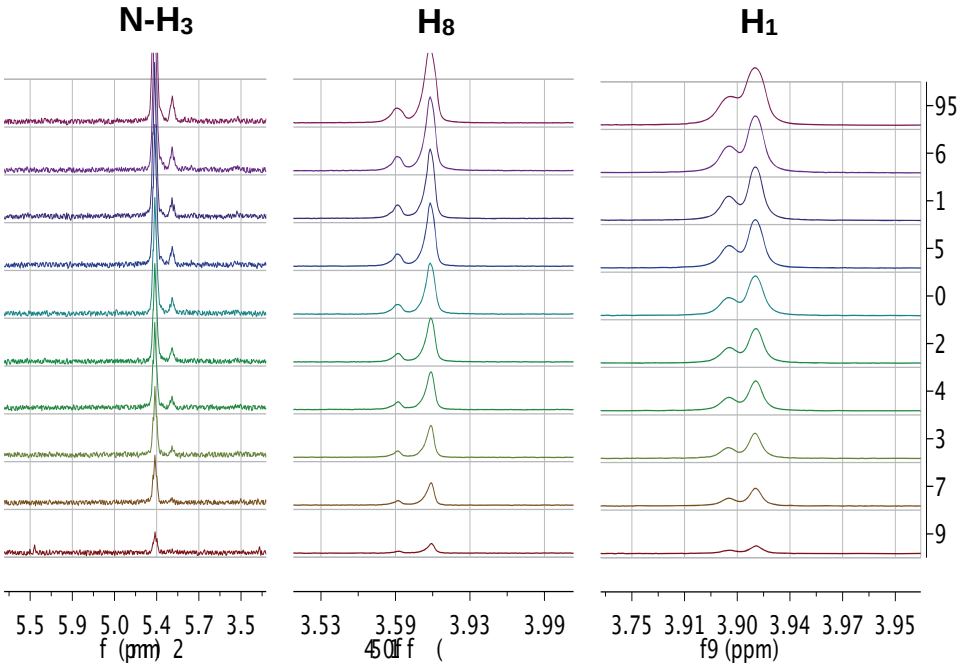

Figure **140**. Zoom of specific signals from the ^{1}H-NMR spectra of **HβOBn** self-aggregation experiment. DMSO-d_6 (600 MHz).

It was supposed that such signals corresponded to minor conformers of the host so the experiment to determine the stoichiometry was performed. It was observed that the minor signals followed different patterns of shielding so we suspected they could be different conformations of the complex. Therefore, variable temperature experiments were carried out and we finally saw that the minor signals were impurities, although they were not appreciated in the previous characterization in $CDCl_3$. Even so, the proportion of the minor signals was less than 10% of the major one.

At this point, it was decided to focus the stoichiometry determination on the major signal and, just to be doubly sure, another Job's plot experiment was carried out (Figure **141** and Annex section **4.5.5**).

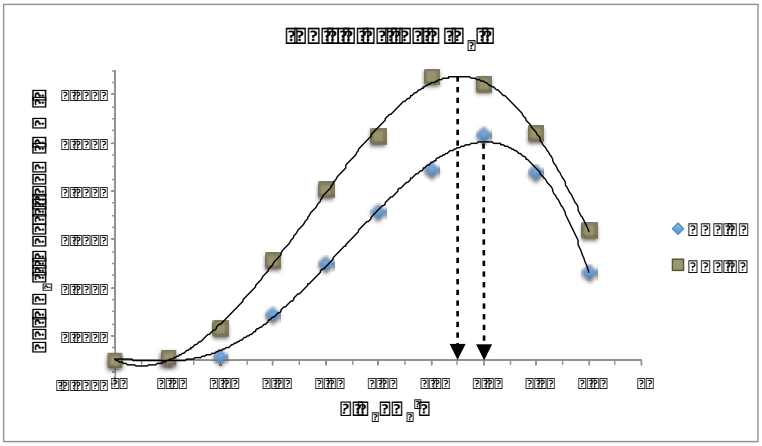

Figure **141**. Job's plot for **[HβOBn][H_2PO_4]** complex. *A* and *B* represent both repetitions of the experiment.

As it can be observed in the Job's plot representation, the maximum values pointed towards X_{Guest} = 0.65-0.7, what suggested a 1:2 stoichiometry for the **[HβOBn][H_2PO_4]** complex. The other shielded signals, H_8 and H_1 seemed to support this 1:2 stoichiometry. Nevertheless, these plots did not exhibit a parabolic profile as in previous cases. The linear regression approximation for a 1:1 system provided a K_a= 105 M^{-1} (logK= 2.02) guide value for the computational calculations.

Opposed preliminary results were obtained with graphical and computational methodologies. This **[HβOBn][H_2PO_4]** complex seemed to be a 1:2 system as deduced by the continuous variation method, but the best results by WinEQNMR2 program led to a 1:1 system (Table **22**). For the statistics of the data fitting parameters see Annex section **4.5.7**.

Table **22**. Logβ and ΔG° values for the complexes formed by **HβOBn** host and dihydrogenphosphate anion in DMSO-d_6.

		Anion sources and methods of determination of association constants[a] (*up*) and free energies[b] (*down*)	
HβOBn		**$TBAH_2PO_4$**	
		Graphical	**Win EQNMR2**
1:1	**β_{11}**	2.02	2.38 ± 0.03
	ΔG	-2.6	-3.1 ± 1.1
1:1 **1:2**	**β_{11}** **β_{12}** **ΔG**	--	2.55 ± 0.32 3.71 ± 3.16[c,d] -4.8 ± 4.1
1:1 **2:1**	**β_{11}** **β_{21}** **ΔG**	--	1.68 ± 0.43 4.07 ± 0.38[c,e] -5.3 ± 0.5
1:1 **1:2** **2:2**	**β_{11}** **β_{12}** **β_{22}** **ΔG**	--	2.76 ± 0.61 3.70 ± 0.86 5.69 ± 12[c,d] -7.4 ± 16

[a] Logβ: β_{11} (M^{-1}), β_{12} and β_{21} (M^{-2}), β_{22} (M^{-3}). [b] Units: kcal·mol^{-1}. [c] Data does not fit as good as in a 1:1 system. [d] β errors are too big. [e] Incoherent chemical shifts and large associated errors.

With this receptor, computational calculations afforded clear preference for a 1:1 system, because the other possibilities resulted in non-acceptable β errors. The Job's plots already exhibited rare curves for a 1:2 systems, what pointed out the little-reliability of this method in this case. On the other hand, linear regression approximation worked well, as it provided similar constant and Gibbs free energy values.

4.3.5. HγOBn-H_2PO_4TBA complex

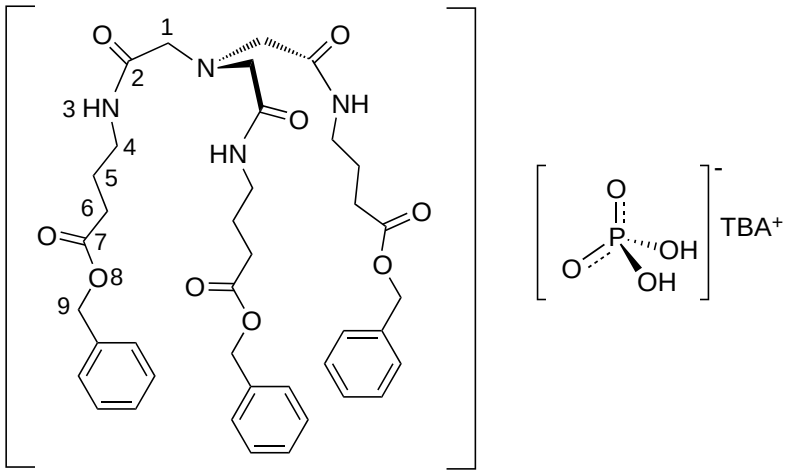

The GABA-containing receptor **HγOBn**, due to its more flexible structure, was expected to give weaker complexes than the rest of the series.

Once more, self-aggregation was not observed (Annex section **4.5.7**). Stoichiometry was shown by Job's plots for the N-H_3 signal (two repetitions), resulting in *a priori* good agreement with 1:2 systems as occurred with the β-alanine derivative. However, the plots deviated from a parabolic profile, what made us suspect from its reliability (Figure **142** and Annex section **4.5.7**).

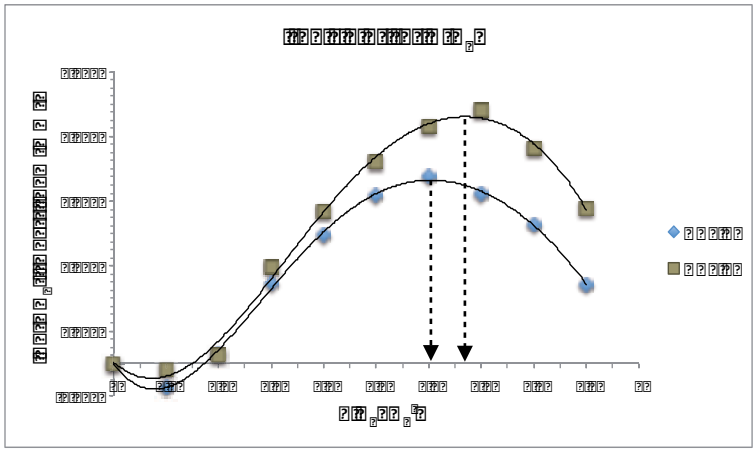

Figure **142**. Job's plot for **[HγOBn][H_2PO_4]** complex. *A* and *B* represent both repetitions of the experiment.

On the contrary, Job's plots using H_1 data from both repetitions were exactly the same and in better agreement with a 1:1 system, although it showed little shielding variation (Figure **143**). This involved little Δδ and led to major errors, so the Job's plots determination would not be so reliable. Anyway, linear approximation supposing a 1:1 system provided a guide value K_a= 2.8 M^{-1}, logK= 0.45. Such constant was less reliable because data used did not fit well with a linear regression and several points has to be omitted so the equation parameters gave real values.

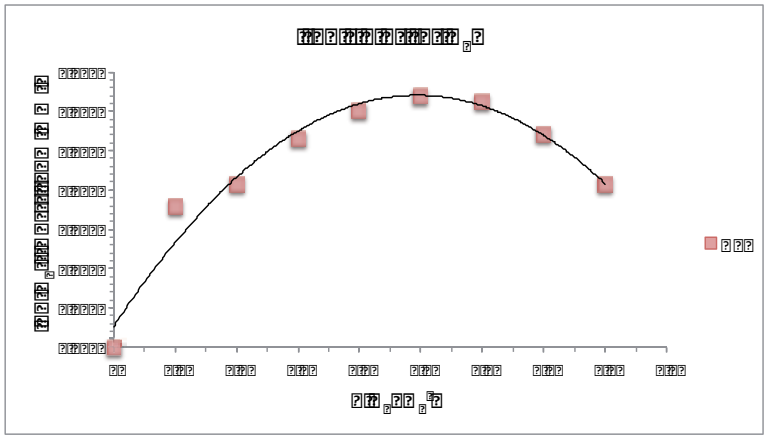

Figure **143**. Job's plot for **[HγOBn][H_2PO_4]** complex.

Finally, WinEQNMR2 calculations led to a 1:1 system (Table **23**).

Table **23**. Logβ and ΔG° values for the complexes formed by **HγOBn** host and dihydrogenphosphate anion in DMSO-*d*6.

		Anion sources and methods of determination of association constants[a] (*up*) and free energies[b] (*down*)	
HγOBn		**$TBAH_2PO_4$**	
		Graphical	**Win EQNMR2**
1:1	**β_{11}**	0.45	2.03 ± 0.22
	ΔG	-0.6	-2.7 ± 0.3
1:1 **1:2**	**β_{11}** **β_{12}** **ΔG**	--	2.27 ± 1.06 3.52 ± 3.70[c,d] -4.6 ± 4.8
1:1 **2:1**	**β_{11}** **β_{21}** **ΔG**	--	1.71 ± 0.87 4.04 ± 2.97[c,d,e] -5.3 ± 3.9
1:1 **1:2** **2:2**	**β_{11}** **β_{12}** **β_{22}** **ΔG**	--	2.12 ± 124 3.28 ± 1613 6.02 ± 311[c,d] -7.8

[a] Logβ: β_{11} (M^{-1}), β_{12} and β_{21} (M^{-2}), β_{22} (M^{-3}). [b] Units: kcal·mol^{-1}. [c] Data does not fit as good as in a 1:1 system. [d] β errors are too big. [e] Incoherent chemical shifts and large associated errors.

Linear approximation did not provide reliable results since it was necessary to discard many data points for a good fitting (Table **23**). Indeed, using this value as guide logβ_{11} in the calculation afforded worst fitting of the data to a 1:1 system, therefore higher values were required. Fitting the data to 1:2 and 2:2 systems, resulted in good statistics but the associated β errors were too big.

4.3.6. HγCbuOBn-FTBA complex

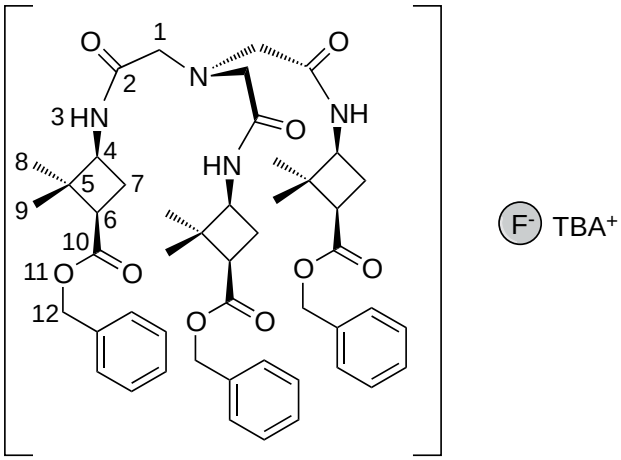

Cyclobutane-containing receptors showed a presumed selectivity towards fluoride anion, as seen in the screening tests. To study its complexation, ^{1}H-NMR and ^{19}F-NMR experiments were carried out in DMSO-d_6. No self-aggregation was neither observed for this host (see Annex section **4.5.8**).

^{1}H-NMR experiment to determine K_a was performed and similar behaviour of N-H_3 proton was observed, as in other hosts under the titration of TBAF (Figure **144**).

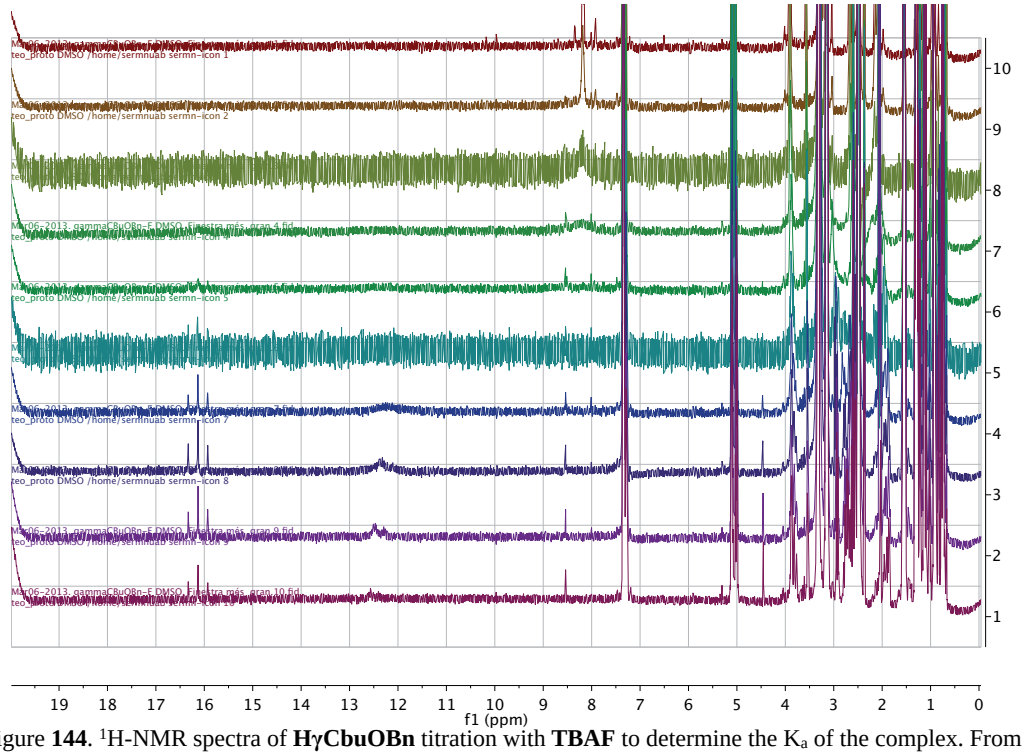

Figure **144**. ^{1}H-NMR spectra of **HγCbuOBn** titration with **TBAF** to determine the K_a of the complex. From Eq. Guest = 0 (*top*) to Eq. Guest = 6 (*bottom*). DMSO-d_6 (600 MHz).

However, the reappearance of N-H_3 signal about 12 ppm after the addition of 3 eq. of TBAF (7th spectrum from above) presented strange multiplicity. Moreover, an additional signal appeared at

about 16 ppm with a defined triplet multiplicity and a coupling constant of J = 120 Hz, corresponding to a complexed bifluoride anion too (Figure **144**).[312]

^{19}F-NMR ^{1}H-coupled and ^{19}F-NMR ^{1}H-decoupled experiments showed two groups of signals (Figure **145**).

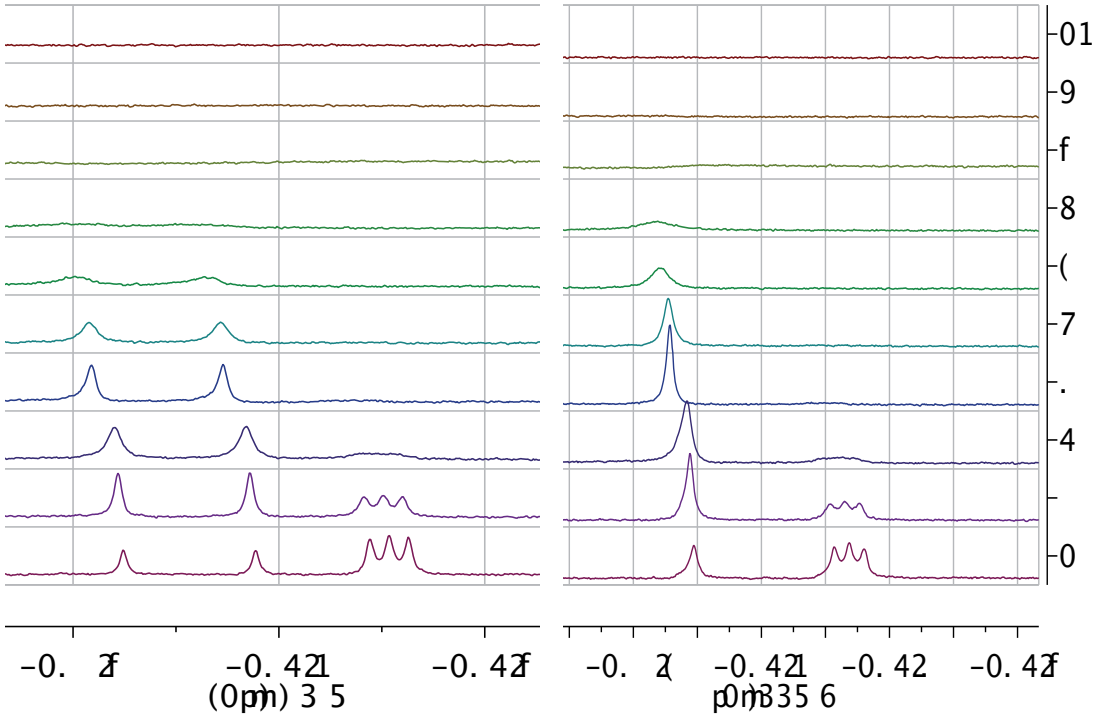

Figure **145**. Zoom of bifluoride area from the ^{19}F-NMR ^{1}H-coupled (*left*) and ^{19}F-NMR ^{1}H-decoupled (*right*) spectra of **HγCbuOBn** titration with **TBAF** to determine the K_a of the complex. From Eq. Guest = 0 (*top*) to Eq. Guest = 6 (*bottom*). DMSO-d_6 (400 MHz).

In the ^{1}H-coupled ^{19}F-NMR spectra, a doublet at about -142.8 ppm, which also presented a coupling constant of J = 120 Hz, supported the presence of bifluoride. Then, a 1:1:1 triplet shifted at about -143.3 ppm also appeared, suggesting the presence of deuterium bifluoride. This fact could be explained because the NH amide proton of **HγCbuOBn** would not be so acidic as in **HαOBn**, since the latter would present a more stable conjugated base due to a stabilizing carbonyl group nearer to the negative charged nitrogen atom. Therefore, there is a competition of fluoride to abstract acidic protons from both the DMSO-d_6[312] in excess and the **HγCbuOBn** host.

The computational calculation by WinEQNMR2 program using the experimental data of the ^{1}H-NMR experiment only fitted well for a 1:2 system (Table **24**). This would suggest the presence of two fluoride anions in the binding site, which would be provided by the bifluoride anion, as explained for the **HαOBn** receptor.

Table **24**. Logβ and ΔG° values for the complexes formed by **HγCbuOBn** host and dihydrogenphosphate anion.

		Anion sources and methods of determination of association constants[a] (*up*) and free energies[b] (*down*)	
HγCbuOBn		**TBAF**	
		Graphical	**Win EQNMR2**
1:1	**β_{11}**	No linear regression could be obtained from any of the H_6 and H_{10} signals employed	2.94 ± 0.33[c]
	ΔG		-3.8 ± 0.4
1:1 **1:2**	**β_{11}** **β_{12}** **ΔG**	--	3.88 ± 0.36 8.22 ± 0.18 -10.7 ± 0.2
1:1 **2:1**	**β_{11}** **β_{21}** **ΔG**	--	3.54 ± 2.08 7.85 ± 1.63[c,d] -10.2 ± 2.1
1:1 **1:2** **2:2**	**β_{11}** **β_{12}** **β_{22}** **ΔG**	--	2.60 ± 1.65 5.06 ± 3.62 8.70 ± 2.40[d] -11.3 ± 3.1

[a] Logβ: β_{11} (M^{-1}), β_{12} and β_{21} (M^{-2}), β_{22} (M^{-3}). [b] Units: kcal·mol^{-1}. [c] Data does not fit well. [d] β errors are too big.

The resulting association constants, $\beta_{12} = 1.6 \cdot 10^8$ M^{-1} for instance, made sense empirically although it is known that it is out of the calculation limit for NMR ($0 < \log\beta < 4$). For the statistics of the data fitting parameters see Annex section **4.5.8**.

Linear regression approximation using H_6 and H_{10a} could not be represented, since their shift data did not fit a linear equation. Hence, the guide values for the calculation were introduced with regards to other related experiments.

Calculations showed good fitting of the data for H_{10a} proton, one of the benzylic methylene protons, which were clearly distinguishable for this host. Statistic parameters exhibited lower errors, whereas for H_6 these values were not so good. Even though, the best result for H_6 fitting gave very similar stability constants β_{11} and β_{12} as for H_{10a}, despite the large associated error for β_{11}. This was supposed to happen because some points were dismissed for the fitting.

4.3.7. Comparative study of HαOBn receptor

Host **HαOBn**, since it resulted to be sensitive to several anions, has been compared to amide-based clip hosts, the structure of which also contain three NH groups, one of them usually provided by a central pyrrole moiety (Figure **146**).[300,319,320]

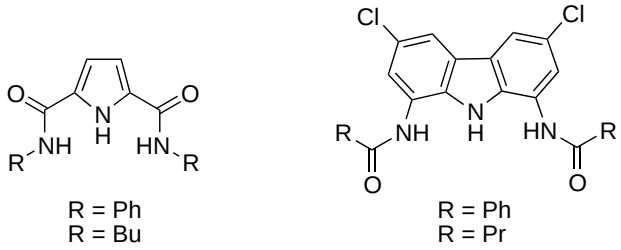

Figure **146**. Amide-based clip receptors showing variable preorganization of the NHs.[300,319]

In general, and taking into account stability constants in DMSO 99.5%, our gly-based receptor showed less affinity to acetate although recognition of benzoate was in the same order, probably because of steric hindrance. The reason is that planar disposition of three NHs enhances affinity towards planar anions as carboxylates. Dihydrogenphosphate and chloride anions showed lower affinity for clip receptors than for **HαOBn**, what supported that a tripodal binding site fits better for tetrahedral and spherical anions, in this case. Nevertheless, when three-rings-system aromatic clip receptors are employed, stability increases because preorganization is enhanced.

HαOBn host has been compared with tripodal amide analogues too, in order to state which chemo-structural little differences can rationalize their affinity towards specific anions (Figure **147**).

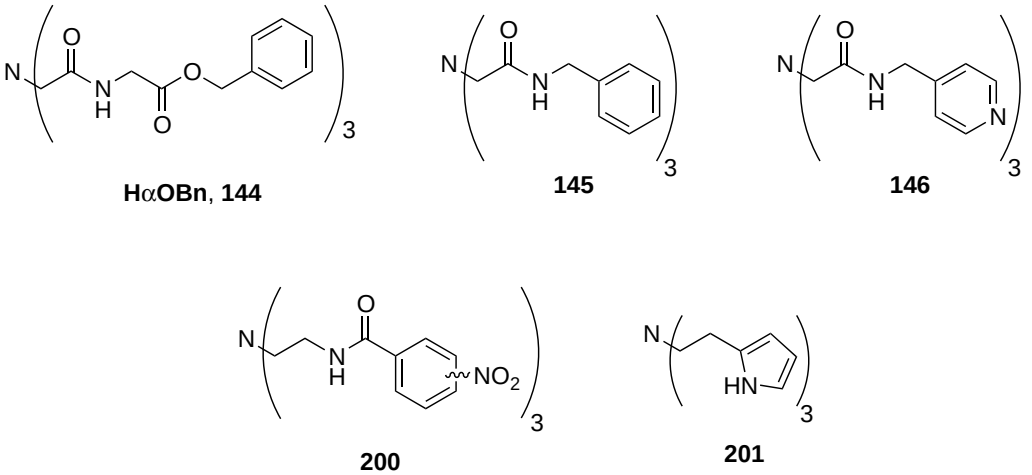

Figure **147**. Structural formula of NTA-based (*top*) and tren-based (*bottom*) tripodal amide receptors synthesized in the current thesis (**144**, **HαOBn**) **a**nd by Togrul[284] (**145**, **146**), Ghosh[321] (**200**) and Cheng[322] (**201**).

Regarding the **145** and **146** hosts reported by Togrul,[284] we realized that ester group influenced significantly in the affinity of dihydrogenphosphate and benzoate anions. It seems that the presence

of donor atoms in the pendant arms specially improved the complexation of dihydrogenphosphate, maybe by hydrogen-bonding of acidic protons. In fact, when a pyridine ring was placed in **146**, the stability of complexes increased with respect to **145**. However, the position of the donor atom is not as good as in our host **144**, nearer to the binding site. Hence, it was suggested that multidentate hosts favour the stabilization of the anions with hydrogen atoms susceptible of being hydrogen-bonded. Our host recognised $H_2PO_4^-$ with β_{11} constant about 9-fold larger than their phenyl-containing host **145**, and about 3-fold larger for the aniline-containing **146**. Complexation of BzO^- exhibited a stability constant between the ones showed by their both receptors (Table **25**).

Concerning the *tren*-based hosts, interesting remarks could be extracted from halide complexation. Nitro-aromatic hosts **200** can bind fluoride and chloride with relative high constants, partly due to the electrowithdrawing effect of the nitro groups in the aryl moieties.[321] This would explain the lower affinity of our host towards chloride. On the other hand, there is a positional isomeric effect, which provides different bulkiness around the binding cavity. So, the *ortho*-**200** derivative only bound fluoride because the nitro groups provoke a steric hindrance for the bigger chloride anion. These motif could explain the fact that our host **144** was able to coordinate two fluoride anions but it would not explain the 1:1 stoichiometry for the *meta*-**200** and *para*-**200** receptors. **HαOBn** recognised two fluoride atoms more selectively than the other hosts, but chloride was weakly bound due to the absence of electrowithdrawing groups.

Table **25**. Comparison of the binding constants[a] for 1:1 complexes in DMSO-d_6 >99.5%, of amide-based tripodal receptors with **HαOBn** host, respectively, at 298 K. Data extracted from references 284, 321 and 322.

		Anions							
Hosts		**$H_2PO_4^-$**	**$C_6H_5CO_2^-$**	**HSO_4^-**	**ClO_4^-**	**PF_6^-**	**F^-**	**Cl^-**	**Br^-**
HαOBn, 144		2046	156	--[c]	✗[d]	✗	724436[e]	45	--[c]
145[b]		241	110	43	--	--	--	✗	--
146[b]		810	286	39	59	73	--	✗	--
200	***orto***	✗	✗	--	--	✗	426580	--	--
	meta						5754	2089	
	para						11482	195	
201		240	✗	<10	✗	✗	187	29	✗

[a] Units: β_{11} (M^{-1}), β_{12} (M^{-2}).
[b] K_a were graphically determined as the average of three experiments, errors were ±10%.
[c] The spectra showed little or no change with the addition of anion so the K_a could not be determined.
[d] Anions not tested. [e] β_{12} constant for a 1:2 complex.

4.4. SUMMARY AND CONCLUSIONS

The synthesis of seven tripodal amide receptors, containing linear or chiral dimethylcyclobutane amino acids, has been accomplished following both divergent and convergent strategies. Better yields and purer compounds were afforded by the convergent route despite more steps were necessary. During their preparation, several derivatives from (-)-verbenone and (-)-pinene have been synthesized and characterized for the first time (Figure **148**).

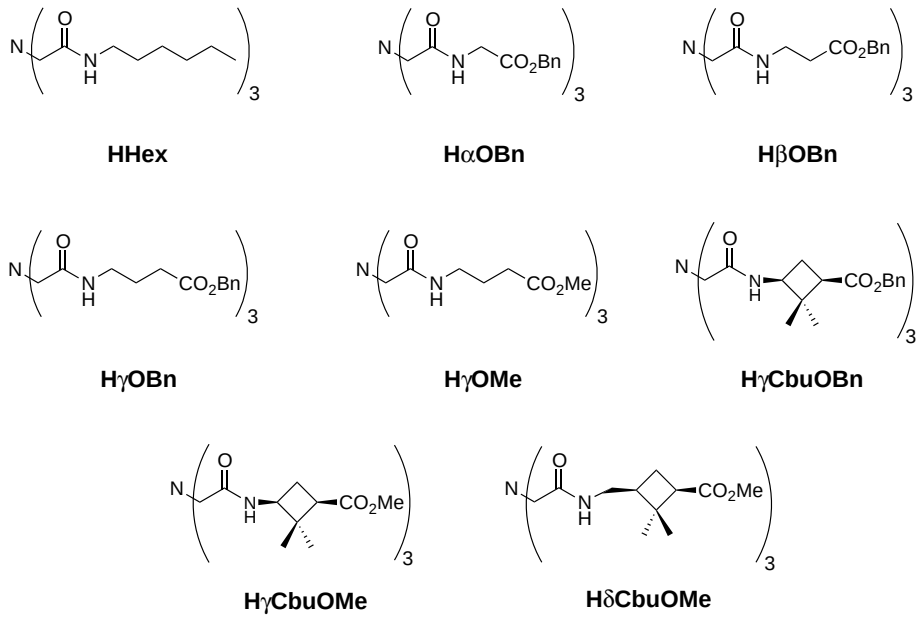

Figure **148**. Anion receptors synthesized and studied in the present thesis.

Comparative screening tests with eleven monovalent anions comprising different geometries and nature showed, for all the receptors, some affinity towards basic oxoanions and a clear preference for fluoride anion. The tripodal binding site of three convergent NHs and the strong basicity and little size of fluoride make all of them to be potential hosts for fluoride sensing. Specially hosts **HγCbuOBn** and **HγCbuOMe**, derived from (-)-verbenone, exhibited excellent selectivity towards it, pointing out the steric key role of the dimethylcyclobutyl moiety. When a methylene unit directly attached to the amide bond was introduced as in **HδCbuOBn**, the binding site became more accessible and therefore, selectivity decreased.

Stability constants and stoichiometries of some selected complexes have been fully calculated using experimental data from the anion titrations applied to WinEQNMR2 program, sometimes supported by the graphical method (Table **26**). The high sensitivity of **HγCbuOBn** with respect to fluoride was translated into the formation and complexation of bifluoride, resulting in a surprising stability constant of $\log\beta_{12} = 8.22$ ($\beta_{12} = 1.7 \cdot 10^8$ M^{-2}), in a 1:2 **[HγCbuOBn][FHF]$_2$** complex. In addition, NH resonance disappearance reflected this strong affinity.

The affinity of **HαOBn** towards the five anions studied in detail resulted in this order: F^- >>> $H_2PO_4^-$ >> $CH_3CO_2^-$ > $PhCO_2^-$ > Cl^-. All the stoichiometries were 1:1 in 99.8% DMSO-d_6 except for fluoride. Since it tended to form a 1:2 (host:anion) complex in DMSO 99.8% and constants were determined by protons different from the NHs, it could not be strictly compared. However, bifluoride was also *in situ* formed and its complexation showed large stability constant, $\log\beta_{12}$ = 8.22 ($\beta_{12} = 7.2 \cdot 10^5$ M^{-2}). Regarding the 1:1 systems in DMSO 99.8%, **HαOBn** presented more sensitivity against selectivity and with $H_2PO_4^-$ and F^- the stability of the complexes was so high that the interaction of the anion with the host was even noticed by hydrogen atoms different from the NHs. If compared with β-alanine and GABA derivatives for the same anion, the chain length effect was clear: as longer and more flexible the chain was the lower stability of the complex.

Table **26**. Stability constants (as logβ) for the four studied hosts with TBAX anions by WinEQNMR2 program.

HOST	Anions and solvents used in the determination of stability constants[a]							
	F			**H_2PO_4**		**CH_3CO_2**	**$PhCO_2$**	**Cl**
	DMSO 99.8%	**DMSO 90%**	**ACN**	**DMSO 99.8%**	**$CDCl_3$**	**DMSO 99.8%**		
HαOBn	β_1= 2.26[c] β_2= 5.86	β_1= 1.64[c]	7.25	3.31	3.75[c] 8.47	2.37	2.19	1.65
HβOBn	ND[b]	ND	ND	2.38	ND	ND	ND	ND
HγOBn	ND	ND	ND	2.03	ND	ND	ND	ND
HγCbuOBn	3.88[c] 8.22	ND	ND	ND	ND	ND	ND	ND

[a] Units logβ: M^{-1} for 1.1 systems (β_1) and M^{-2} for 1:2 systems (β_1 and β_2) with associated errors < 5%.
[b] ND: not determined. [c] 10% < Errors < 30%.

On the other hand, **HγOBn** and **HγOMe** did not show significant changes in the affinity with respect to the different end-group functionalization, even when compared to the **HHex**, as seen in the anion screening tests. We conclude that the chain length effect is more determinant than the end-group effect when this linear chain comprises from 1 to 3 carbons.

Influence of the polarity of the solvent in the stoichiometry and stability constants of the complexes was also proved. Affinity decreased with the polarity of the solvent, as performed in an experiment with 10% of water in DMSO-d_6 to make the disappeared NH signal to recover its resonance. However, the variation of the stoichiometry did not follow any defined pattern.

GENERAL CONCLUSIONS

GENERAL CONCLUSIONS

Several families of peptidomimetics have been synthesized employing cyclobutane and short-linear amino acids. Among the rigid scaffolds, 1,2- and 2,2-dimethyl-1,3-cyclobutane amino acids have been used as conformational restriction elements whereas the linear residues have contributed with flexibility, in order to induce singular and defined properties with interesting applications in supramolecular chemistry.

While the *cis*-β-cyclobutane amino acids adopt a 6-membered hydrogen-bond conformation which leads to an extended ribbon structure, the *trans*-residues present an 8-membered hydrogen-bonding which favours a twisted arrangement. Thus, the design of short cyclobutane β-peptides with a specific folding can be tuned by the strategic combination of its constituting units, like in a lego game where the assembly of its pieces gives a particular structure.

The introduction of linear spacers between the cyclobutane residues also modulates the ribbon folding shown in homochiral short β-peptides. The intercalation of glycine and GABA units changes the hydrogen-bonded pattern into β-sheets while β-alanine amino acid makes the peptide to fold into a 14-helical structure. The intercalation of more rigid spacers as cyclobutene ring is, instead, does not change the ribbon folding at all.

Some of these hybrid peptides show better capacity to gelate most of the common organic solvents than their homo-cyclobutane analogues, at very low concentrations in solvents like toluene, where *mgc* = 7-12 mM for the three tetrapeptides and the pseudotetrapeptide. The supramolecular structure of the gels from hybrid tetrapeptides in toluene is fibrillar except for the globular-arranged β-alanine derivative, exhibiting the translation of different self-assembly from the molecular to the supramolecular scale. These observations prove the influence of the length of the linear spacers and their combination with *cis*-1,2-cyclobutane amino acids.

This influence has been also identified in the recognition capacity of NTA-based tripodal amide hosts. Glycine have enhanced the sensitivity of the host to benzoate, acetate and specially towards dihydrogenphosphate, affinity that decreases with the length of the spacer, except for fluoride anion, towards which they exhibited great recognition. 1,3-Cyclobutane-containing hosts selectively recognized fluoride, one of them showing the formation and complexation of bifluoride with a very high stability constant in the order of 10^8 M^{-2} in DMSO-d_6.

EXPERIMENTAL PART

5.1. GENERAL METHODOLOGY

5.1.1. Spectroscopy and spectrometry

‣ **^{1}H-NMR** (50, 360, 400, 500 or 600 MHz) and **^{13}C-NMR** (62.5, 90, 100, 125 or 150 MHz) were recorded at *Servei de Ressonància Magnètica Nuclear de la Universitat Autònoma de Barcelona*.

The spectrometers used were:

• AC 250 Bruker for ^{1}H at 250 MHz and ^{13}C at 62.5 MHz.

• AVANCE360 Bruker for ^{1}H at 360 MHz and ^{13}C at 90 MHz.

• ARX 400 Bruker for ^{1}H at 400 MHz and ^{13}C at 100 MHz.

• AVANCE500 Bruker for ^{1}H at 500 MHz and ^{13}C at 125 MHz.

• AV600 Bruker for ^{1}H at 600 MHz and ^{13}C at 150 MHz.

Chemical shifts of signals are given in ppm, using as reference the following values:

• Acetone-d_6: δ 2.05 and 29.84, 206.26 for ^{1}H and ^{13}C respectively.

• $CDCl_3$: δ 7.26 and 77.16 for ^{1}H and ^{13}C respectively.

• DMSO-d_6 (H_2O): δ 3.33 (2.50) and 39.52 for ^{1}H and ^{13}C respectively.

• D_2O: δ 4.79 for ^{1}H.

• MeOD-d_4: δ 3.31 (4.87) and 49.00 for ^{1}H and ^{13}C respectively.

The abbreviations used to describe multiplicity of signals are:

s	singlet	q	quartet
m	multiplet	p	pentet
d	doublet	c.a.	complex absorption
dd	double doublet	broad s	broad singlet
ddd	double double doublet	broad d	broad doublet
t	triplet		

NMR signals were assigned with the help of DEPT, NOESY, ROESY, COSY, TOCSY, HMBC and HSQC experiments.

‣ **Infrared** (**IR**) spectra in solid state were recorded on a Sapphire-ATR spectrophotometer and peaks are reported in cm^{-1}. Infrared spectra (**FT-IR**) in solution were recorded on a Perkin Elmer, Spectrum One FT-IR spectrometer, being the signal an average of 16 scans.

‣ **High Resolution Mass Spectra (HRMS)** were mostly recorded at *Servei d'Ànalisi Química de la Universitat Autònoma de Barcelona* in a Bruker Squire 3000 micrOTOFQ spectrometer using ESI-MS (QTOF) and at *RIAIDT de la Universidade de Santiago de Compostela* using a micrOTOF instrument, ESI-TOF injection.

‣ **Circular Dichroism (CD)** spectra were recorded with JASCO-715 spectropolarimeter and were processed using the associated software. Table **27** shows the experimental conditions used for the analysis.

Table **27**. Experimental conditions for the analysis[a] of xerogels by solid CD.

Parameter	Value
Range	190 to 400 nm
Data pitch	0.5 nm
Scanning mode	continuous
Scanning speed	100 nm/min
Response	2 sec.
Band width	5 nm[b]
Accumulation	2

[a] Data recording was repeated 3 times, rotating the pill 60º in each one to obtain representative data.
[b] Thickness of the pills at this band width provide good HT voltage about 200 V.

Figure **149** shows the press and instruments used for the preparation and analysis of film pills.

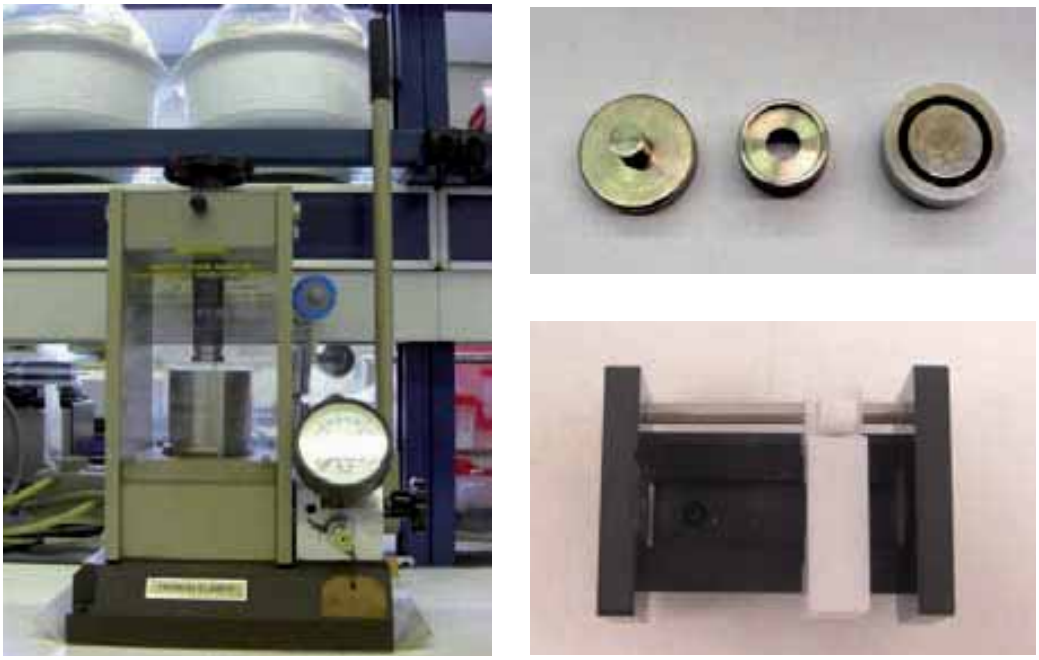

Figure **149**. Perkin-Elmer® 15.011 press used for the preparation of xerogel/KBr pills (*left*). Disc support where the pill is prepared (*right-top*) and top view of support where the disc is placed to register CD (*right-bottom*).

5.1.2. Chromatography

Column chromatography was always performed with Baker® silica gel for flash chromatography (mean pore: 60 Å; particle size: 0.04-0.06 mm, 230-400 mesh ASTM), using nitrogen as driving gas.

All reactions were monitored by thin-layer chromatography (TLC) using ALUGRAM® SIL G/ UV_{254} pre-coated aluminium sheets. Layers of 0.20 mm of thickness covered with silica gel 60 with fluorescent indicator UV_{254}.

Several methods were used to visualise the spots:

- Irradiation under a LED UV-light (UV_{254}), using a VILBER LOURMAT® lamp, VL-4LC model.
- Staining thin-layers under acid solution of *para*-anisaldehyde or vanillin in ethanol 96%.
- Staining thin-layers under basic solution of $KMnO_4$ in water.

5.1.3. Microscopy

‣ **Transmission Electron Microscopy (TEM)** images were acquired with Hitachi H-7000 microscope on samples stained with 2% uranyl acetate in the *Servei de Microscòpia de la Universitat Autònoma de Barcelona*. Carbon-film-coated copper grids were used.

‣ **Scanning Electron Microscopy (SEM)** images were acquired with Quanta FEI 200 apparatus equipped with a field-emission gun (FEG) in the *Institut de Ciència dels Materials de Barcelona (ICMAB)*. To obtain data from xerogels (dry gels), wet gels were disposed on a carbon-film-coated copper grid and were dried standing for 10 minutes on the grid before being introduced into the microscope, working under a pressure of 70 Pa.

5.1.4. General tools

‣ **Optical rotations, $[\alpha]_D$**, were measured using an automatic polarimeter PROPOL™, Dr. Wolfgang Kernchen model, at 22±2 ºC and using a JASCO-715 spectropolarimeter and determined by the associated software.

‣ **Melting points** were determined on a hot stage using a Kofler apparatus, REICHERT AUSTRIA™ model, and are uncorrected.

‣ **Micro-distillations** were carried out in a BÜCHI™ distiller, GKR-51 model.

‣ **Lyophilization** of samples were done using a POLYSCIENCE™ lyophilizator, KR-80A model and a TELSTAR™ lyophilizator, LyoQuest-85 model.

‣ **Hydrogenations** were carried out in an autoclave hydrogenation T-reactor Swagelok™, with a pressure capacity from 1 to 20 at (kg/cm^2).

‣ **Photochemical reactions** were performed in a pyrex T-shaped photochemical reactor from TRALLERO&SCHLEE™. Irradiation is emitted from a mercury lamp of 125 W medium pressure PHILLIPS® and a mercury lamp of 400 W medium pressure ELECTRO DH™. Refrigeration at -40 ºC comes from a C40P TERMO SCIENTIFIC™ refrigerator, Phoenix II model.

‣ **Reagents** were used directly from commercial sources and **Solvents** were directly used due to their high quality. If necessary, reagents were conveniently purified and the solvents were distilled under nitrogen atmosphere using standard procedures described at Vogel's, *Textbook of practical Organic Chemistry*, Ed. Logman Scientific and Technical, UK, **1989**.

- Acetone: $CaCl_2$
- CH_2Cl_2: CaH_2
- THF: Na/benzophenone
- Toluene: Na/benzophenone

‣ **Deuterated solvents** were used directly from commercial source Eurisotop™.

5.1.5. Gelation studies

The preparation of the gels was achieved by the following procedure:

i) A small amount (5.0 ± 0.1 mg) of peptide is weighted in a 2 mL transparent-glass vial with septum screw-on cap. When the 5 mg amount of peptide is soluble in a specific solvent, a new vial containing 10 ± 0.1 mg is prepared and the solubility-gelification checked again. At that point, if the peptide is still soluble, the compound is considered not to be an organogelator because the amount of material needed is too high, in other words, the solution is too concentrated (c = 10 mg/0.5 mL = 20 mg/mL).

ii) In a second step, a certain volume of solvent to be tested is added and the vial closed. The minimum volume added is 0.05 mL. Then the mixture is heated under the boiling point of the solvent using a balloon system in order to avoid solvent pressure and, once a solution is obtained the mixture is sonicated for 1 to 5 minutes. For high concentrations and also in some solvents, previous sonication is needed for a good solubilization during heating and sonication time is usually shorter than for diluted gels. Then, the mixture is left to stabilize and to reach room temperature.

iii) To state that the mixture is a gel the *tube inversion test* is done just by turning the vial upside down. If the sample is a gel it does not drop and if it drops a little it can be classified as gel-like mixture. The mixtures can also be stated as solutions or insoluble systems. In order to determine the minimum gelation concentration (*mgc*), a new volume of solvent is added to the gel and the process is repeated until no gel is formed: the last volume added determines the *mgc*.

5.1.6. Host-guest complexation studies

The high-resolution NMR experiments for the complexation study of the hosts have to be carried out following the same empirical conditions, in order to make the results comparable and reproducible. These conditions are:

‣Anions as their tetrabutylammonium (TBA) salts: F^-, Cl^-, Br^-, I^-, BF_4^-, IO_4^-, HSO_4^-, $H_2PO_4^-$, $CH_3CO_2^-$, $PhCO_2^-$, PhS^- (TBA fluoride salt is hydrated).

The selection of the anions was done taking into account the results of similar tripodal receptors found in the literature[76,89] and others were chosen because of their relationship with those reported, in terms of geometry, basicity, etc.

The reason why such salts were used with TBA counterions is because cations can also be hosted by the receptors and in this case it was expected that the relative big size of such cations would avoid their entrapping in the binding cavities.

‣ Deuterated dimethylsulfoxide (DMSO-d_6) was used as the common solvent for all the studies. The selection of such solvent was done because it was found to be the tendency in this kind of host-guest studies, which main objective is focused on the application of such complexes to biological or environmental fields, where water is the common solvent. Therefore, when water can not be applied because of solubility, DMSO is the solvent usually employed. Its high polarity, miscibility with water and its non expensive availability as deuterated solvent with different % water, make it useful. Moreover, it solubilizes most of organic compounds, including organic and some inorganic salts. TBA salts are supposed to be completely dissociated. Obviously, the more polar the solvent is the more it competes with anions for the binding sites of the host, but good results in such solvent make the conclusions to be more significant in terms of higher affinities.

‣ Host-guest ^{1}H-NMR analysis were carried out using the 600 MHz spectrometer with automatic programming of the experiments, with the aim of having reproducible and comparable spectra. No spinning was used in order to avoid that spinning forces influence the host-guest event. The NMR was successfully and widely used for these kind of complexation studies with the only limitation on the maximum reliable value for the association constants, that had to be $K_a < 10^4$ M^{-1}.[90]

‣ All the experiments described were performed at the same temperature, 25 ± 0.1 ºC, except when indicated.

5.1.7. Computational calculations

For the conformational search based on NMR data, NOE enhancements and *J* coupling constants were used to define distance and torsion angle constraints to be used in conformational searchs. These calculations were carried out using the MMFF force field implemented in the Macromodel 7.0 program. The $CHCl_3$ solvent effect was included through the GB/SA method. ^1H NMR chemical shifts were computed using the gauge independent atomic orbital (GIAO) method at the B3LYP/ 6-311+G(2d,p) level of calculation.

For structure prediction, most of the computations were carried out using the Gaussian 03 software package. All structures optimized at the B3LYP/6-31G(d) level of calculation were fully characterized through the calculation of harmonic vibrational frequencies. The energies were recalculated in chloroform solution using the B3LYP/6-31G(d) basis and PCM solvation model.

5.2. EXPERIMENTAL PROCEDURES

Only the new compounds or compounds we consider as more relevant have been described. For the rest of reported compounds, the experimental descriptions of which has not been included, bibliographic references are given as a number in parentheses next to the number of the compound.

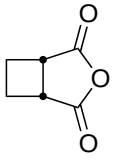

58 (323)

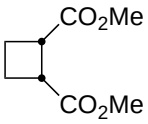

56 (9c)

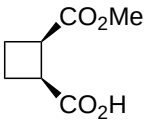

(*S*,*R*)-**8** (65)

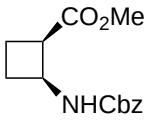

(*S*,*R*)-**17** (62)

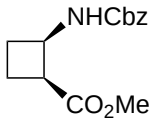

(*R*,*S*)-**17** (62)

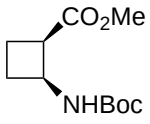

(*S*,*R*)-1**8** (9a)

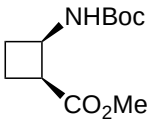

(*R*,*S*)-1**8** (9a)

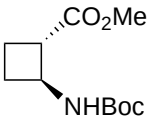

(*S*,*S*)-1**8** (71)

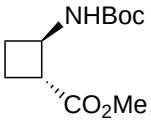

(*R*,*R*)-1**8** (71)

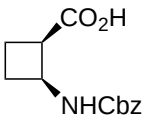

(*S*,*R*)-**16** (62)

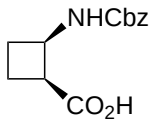

(*R*,*S*)-**16** (324)

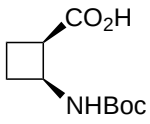

(*S*,*R*)-**15** (9a)

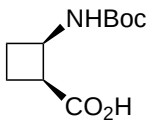

(*R*,*S*)-**15** (71)

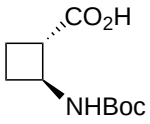

(*S*,*S*)-**15** (72)

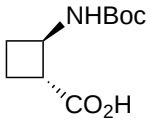

(*R*,*R*)-**15** (71)

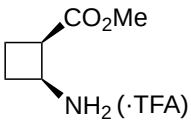

(*S*,*R*)-**59** (9a)

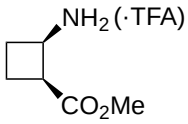

(*R*,*S*)-**59** (9a)

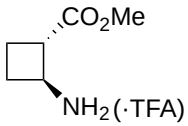

(*S*,*S*)-**59** (10)

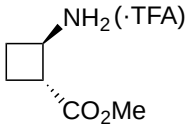

(*R*,*R*)-**59** (84)

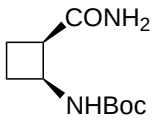

(*S*,*R*)-**66** (72)

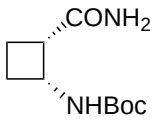

(*R*,*S*)-**66** (72)

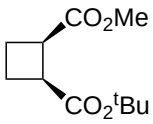

(*S*,*R*)-**9** (324)

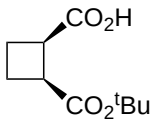

(*S*,*R*)-**63** (324)

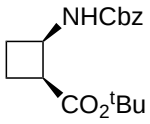

(*R*,*S*)-**64** (324)

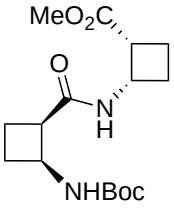

(*S*,*R*,*S*,*R*)-**6** (9a)

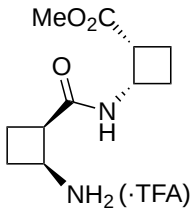

(*S*,*R*,*S*,*R*)-**46** (9a)

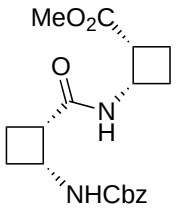

(*R*,*S*,*S*,*R*)-**1** (9a)

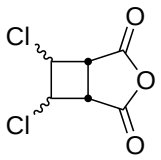

88 (176)

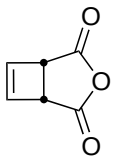

89 (176)

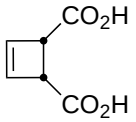

85 (185)

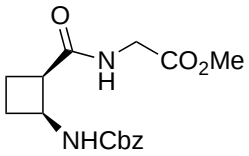

40 (19)

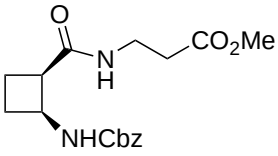

41 (62)

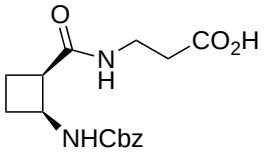

113 (11)

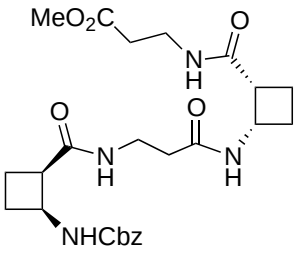

7 (11)

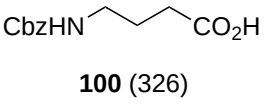

100 (326)

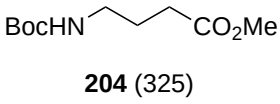

204 (325)

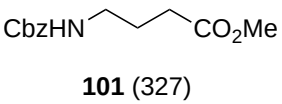

101 (327)

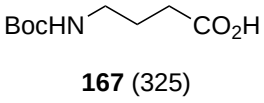

167 (325)

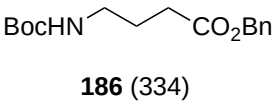

186 (334)

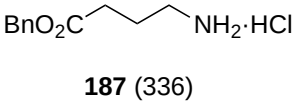

187 (336)

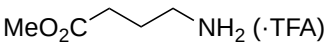

102 (325)

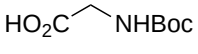

173 (294)

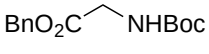

174 (331)

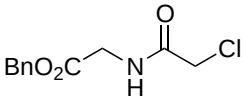

177 (332)

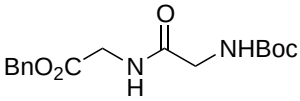

176 (333)

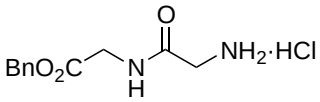

178 (333)

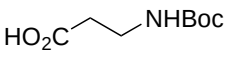

180 (334)

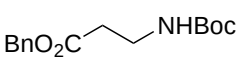

181 (334)

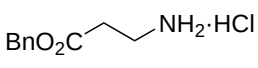

182 (335)

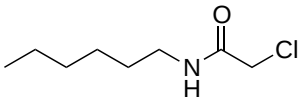

192 (329)

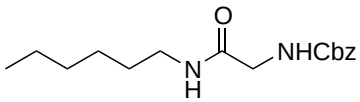

193 (330)

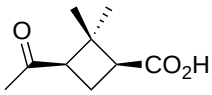

32 (290)

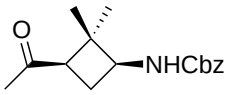

158 (16a)

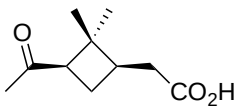

168 (328)

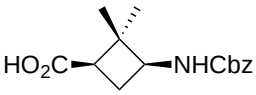

159 (16a)

33 (16a)

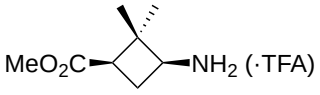

160 (16a)

161 (337)

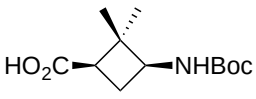

162 (290)

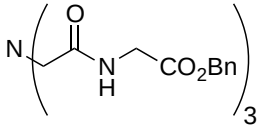

144 (283)

5.2.1. 1,2-Cyclobutane derivatives

_N_-(Boc)Cbz-(_R,S_)-βCbu-OMe 65:

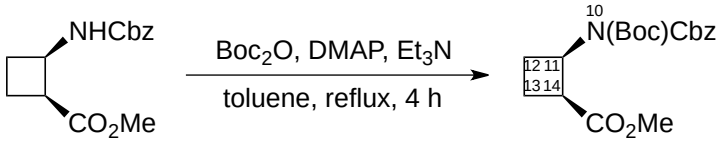

(*R,S*)-**17** (*R,S*)-**65**

Boc_2O (3.9 mL, 0.17 mmol), DMAP (21 mg, 0.17 mmol) and Et_3N (3.6 mL, 0.26 mmol) were added to a solution of amino acid (*R,S*)-**17**[62] (45 mg, 0.17 mmol) in toluene (15 mL). The mixture was stirred under reflux for 4 h. Solvent was removed *in vacuo* and the resulting crude was solved in EtOAc (X mL). The aqueous layer was extracted with EtOAc (3 x 30 mL) and the organic layer was dried over anhydrous $MgSO_4$, filtered and evaporated under reduced pressure. The resulting crude was purified by silica gel chromatography using hexane/EtOAc (2:1) as eluent to afford compound (*R,S*)-**65** (60 mg, 38%) as a yellow oil.

Spectroscopic data and physical constants of compound (*R,S*)-65:

$[\alpha]_D$= -52 (*c*= 1.07, CH_2Cl_2)

IR (cm^{-1}) ν 2978, 2952, 2856, 1787, 1732, 1704.

^{1}H NMR (360 MHz, $CDCl_3$) δ 1.43 (s, 9H, $H_{1'-3'}$), 1.92 (m, 1H, H_{13}), 2.22 (m, 1H, H_{13}), 2.31 (m, 1H, H_{12}), 2.63 (p, $^3J_{H-H}$= 10.3 Hz, 1H, H_{12}), 3.40 (m, 1H, H_{14}), 3.58 (s, 3H, H_{17}), 4.67 (q, $^3J_{H-H}$= 9.2 Hz, 1H, H_{11}), 5.18 (s, 2H, H_7), 7.28-7.41 (c.a., 5H, H_{1-5}).

^{13}C NMR (90 MHz, $CDCl_3$) δ 18.6 (C_{13}), 27.0 (C_{12}), 27.9 ($C_{1'-3'}$), 44.4 (C_{14}), 51.7 (C_{11}, C_{17}), 68.5 (C_7), 83.2 ($C_{4'}$), 128.5, 128.6 (C_{1-5}), 135.5 (C_6), 152.0, 153.8 ($C_{6'}$, C_9), 173.1 (C_{15}).

HRMS: Calculated for $C_{19}H_{25}NO_6Na$ $(M+Na)^+$: 386.1574. Found $(M+Na)^+$: 386.1578.

_N_-Cbz-(_R,S_)-βCbu-(_S,R_)-βCbu 202:

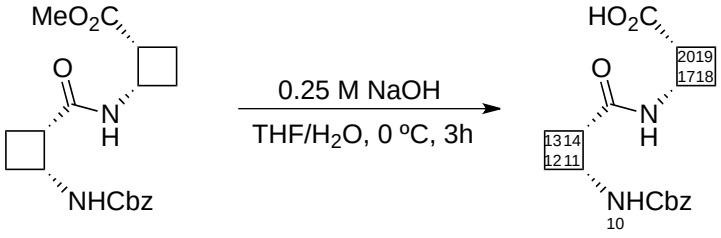

(*R,S,S,R*)-**1** (*R,S,S,R*)-**202**

To an ice-cooled solution of amino acid (*R*,*S*,*S*,*R*)-**1**[9a] (0.20 g, 0.55 mmol) in a 1:10 mixture of THF/ H_2O (60 mL), 0.25 M aqueous NaOH solution (6.0 mL) was added. The mixture was stirred at 0 ºC for 3 h. The mixture was washed with CH_2Cl_2 (1 x 40 mL) before being acidified to pH 2 with 2 M HCl. The aqueous layer was extracted with EtOAc (4 x 30 mL) and the organic layer was dried over anhydrous $MgSO_4$, filtered and evaporated under reduced pressure to afford the corresponding carboxylic acid (*R*,*S*,*S*,*R*)-**202** (0.19 g, quantitative yield) as a white solid. This compound was used directly in next step without further purification.

Spectroscopic data of compound (*R,S,S,R*)-202:

^{1}H NMR (250 MHz, $CDCl_3$) δ 1.86-2.13 (c.a., 4H, H_{12S}, H_{13R}, H_{18R}, H_{19S}), 2.26-2.48 (c.a., 4H, H_{12R}, H_{13S}, H_{18S}, H_{19R}), 3.37-3-55 (c.a., 2H, H_{14}, H_{20}), 4.47 (m, 1H, H_{11}), 4.90 (m, 1H, H_{17}), 5.08 (d, $^2J_{H\text{-}H}$= 12 Hz, 1H, H_7), 5.18 (d, $^2J_{H\text{-}H}$= 12 Hz, 1H, H_7), 5.72 (d, $^3J_{H\text{-}H}$= 9.2 Hz, 1H, NH_{10}), 7.17 (d, $^3J_{H\text{-}H}$= 8.2 Hz, 1H, NH_{16}), 7.35 (s, 5H, $H_{1\text{-}5}$).

***N*-Cbz-(*R*,*S*)-βCbu-(*S*,*R*)-βCbu-NHMe 70:**

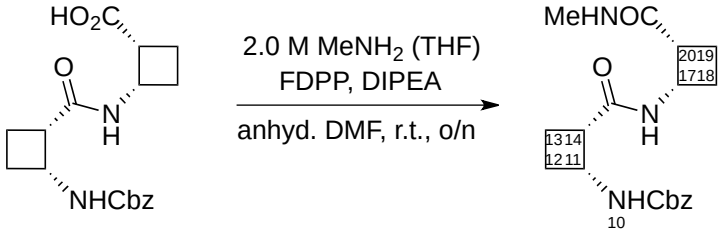

(*R*,*S*,*S*,*R*)-**202** (*R*,*S*,*S*,*R*)-**70**

2.0 M $MeNH_2$ solution in THF (0.13 mL, 0.26 mmol), FDPP (80 mg, 0.21 mmol) and DIPEA (0.09 mL, 0.52 mmol) were added to a solution of acid (*R*,*S*,*S*,*R*)-**202** (60 mg, 0.17 mmol) in anhydrous DMF (10 mL). The mixture was stirred at room temperature overnight. EtOAc (20 mL) was added and the solution was washed with saturated aqueous $NaHCO_3$ solution (3 x 10 mL). The organic layer was dried over anhydrous $MgSO_4$, filtered and the solvent was evaporated *in vacuo*. The resulting residue was purified by silica gel chromatography using EtOAc as eluent to afford (*R*,*S*,*S*,*R*)-**70** (130 mg, quantitative yield) as white solid.

Spectroscopic data and physical constants of compound (*R,S,S,R*)-70:

$[\alpha]_D$= -73 (*c*= 0.6, CH_2Cl_2)

M. p.: 184-186 ºC (EtOAc)

IR (cm^{-1}) ν 3419, 3314, 2970, 1726, 1643.

IR solution (cm^{-1}, $CDCl_3$) ν 3460, 3425, 2953, 1714, 1661.

^{1}H NMR (600 MHz, $CDCl_3$) δ 1.90-2.10 (c.a., 4H, H_{12S}, H_{13R}, H_{18R}, H_{19S}), 2.21-2.39 (c.a., 4H, H_{12R}, H_{13S}, H_{18S}, H_{19R}), 2.69 (d, $^3J_{H\text{-}H}$= 4.2 Hz, 3H, H_{23}), 3.00-3-19 (c.a., 2H, H_{14}, H_{20}), 4.47 (m, 1H, H_{11}), 4.66 (m, 1H, H_{17}), 5.07 (s, 2H, H_7), 5.34 (broad s, 1H, NH_{22}), 6.17 (d, $^3J_{H\text{-}H}$= 8.2 Hz, 1H, NH_{10}), 6.58 (d, $^3J_{H\text{-}H}$= 7.3 Hz, 1H, NH_{16}), 7.35 (s, 5H, $H_{1\text{-}5}$).

^{13}C NMR (150 MHz, $CDCl_3$) δ 19.3, 19.6, 29.3, 30.6 (C_{12}, C_{13}, $C_{18,}$ C_{19}), 26.3 (C_{20}), 44.8, 45.9, 46.0, 46.3 (C_{11}, C_{14}, C_{17}, C_{20}), 66.6 (C_7), 128.1, 128.6 ($C_{1\text{-}5}$), 136.8 (C_6), 155.6 (C_9), 173.1, 173.8 (C_{15}, C_{21}).

HRMS: Calculated for $C_{19}H_{25}N_3O_4Na$ $(M+Na)^+$: 382.1737. Found $(M+Na)^+$: 382.1736.

N-Boc-(*R,S*)-βCbu-(*S,S*)-βCbu-OMe 6:

Amine (*S,S*)-**59**[10] (0.59 g, 2.4 mmol), DIPEA (1.25 mL, 7.29 mmol) and FDPP (1.12 g, 2.92 mmol) were added to a solution of acid (*R,S*)-**15**[71] (0.52 g, 2.43 mmol) in anhydrous DMF (15 mL). The mixture was stirred at room temperature overnight. EtOAc (20 mL) was added and the solution was washed with saturated aqueous $NaHCO_3$ solution (3 x 15 mL). The organic layer was dried over anhydrous $MgSO_4$, filtered and the solvent was evaporated *in vacuo*. The resulting residue was purified by silica gel chromatography using hexane/EtOAc (2:3) as eluent to afford (*R,S,S,S*)-**6** (0.41 g, 52%) as white solid.

Spectroscopic data and physical constants of compound (*R,S,S,S*)-6:

$[\alpha]_D$= +121 (*c*= 0.9, CH_2Cl_2)

M. p.: 125-127 ºC (EtOAc-hexane)

IR (cm^{-1}) ν 3352, 3324, 2982, 1731, 1681, 1651.

IR solution (cm^{-1}, $CDCl_3$) ν 3439, 2984, 1731, 1705, 1670.

^{1}H NMR (600 MHz, $CDCl_3$) δ 1.45 (s, 9H, $H_{1\text{-}3}$), 1.82-1.97 (c.a., 2H, H_{10S}, H_{15R}), 1.97-2.04 (c.a., 2H, H_{16}), 2.08 (m, 1H, H_{9S}), 2.18-2.37 (c.a., 3H, H_{9R}, H_{10R}, H_{15S}), 3.02 (q, $^3J_{H\text{-}H}$= 8.8 Hz, 1H, H_{17}), 3.15 (m, 1H, H_{11}), 3.73 (s, 3H, H_{20}), 4.42 (p, $^3J_{H\text{-}H}$= 8.2 Hz, 1H, H_8), 4.50 (p, $^3J_{H\text{-}H}$= 8.7 Hz, 1H, H_{14}), 5.38 (d, $^3J_{H\text{-}H}$= 9.6 Hz, 1H, NH_7), 5.76 (broad s, 1H, NH_{13}).

^{13}C NMR (150 MHz, $CDCl_3$) δ 17.7 (C_{10}), 18.3 (C_{16}), 26.4 (C_{15}), 28.2 ($C_{1\text{-}3}$), 29.1 (C_9), 46.1 (C_8), 46.2 (C_{11}), 46.8 (C_{17}), 47.6 (C_{14}), 51.6 (C_{20}), 79.2 (C_4), 155.1 (C_6), 172.1 (C_{12}), 173.2 (C_{18}).

HRMS: Calculated for $C_{16}H_{26}N_2O_5Na$ $(M+Na)^+$: 349.1734. Found $(M+Na)^+$: 349.1737.

N-Boc-(*R,S*)-βCbu-(*S,S*)-βCbu 203:

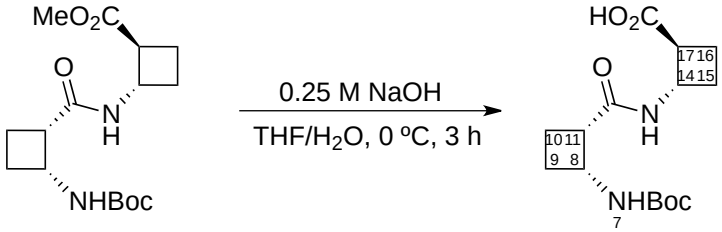

(*R,S,S,S*)-**6** (*R,S,S,S*)-**203**

To an ice-cooled solution of amino acid (*R,S,S,S*)-**6** (210 mg, 0.64 mmol) in a 1:10 mixture of THF/ H_2O (44 mL), 0.25 M aqueous NaOH solution (6.4 mL) was added. The mixture was stirred at 0 ºC for 3 h. The mixture was washed with CH_2Cl_2 (1 x 30 mL) before being acidified to pH 2 with 2 M HCl. The aqueous layer was extracted with EtOAc (4 x 50 mL) and the organic layer was dried over anhydrous $MgSO_4$, filtered and evaporated under reduced pressure to afford the corresponding carboxylic acid (*R,S,S,S*)-**203** (200 mg, quantitative yield) as a white solid. This compound was used directly in next step without further purification.

Spectroscopic data of compound (*R,S,S,S*)-203:

^{1}H NMR (250 MHz, $CDCl_3$) δ 1.45 (s, 9H, $H_{1\text{-}3}$), 1.79-2.37 (c.a., 8H, H_9, H_{10}, H_{15}, H_{16}), 3.08 (m, 1H, H_{17}), 3.30 (m, 1H, H_{11}), 4.24 (m, 1H, H_8), 4.40 (m, 1H, H_{14}), 5.13 (broad s, 1H, NH_7), 6.63 (broad s, 1H, NH_{13}).

_N_-Boc-(_R,S_)-βCbu-(_S,S_)-βCbu-NHMe 69:

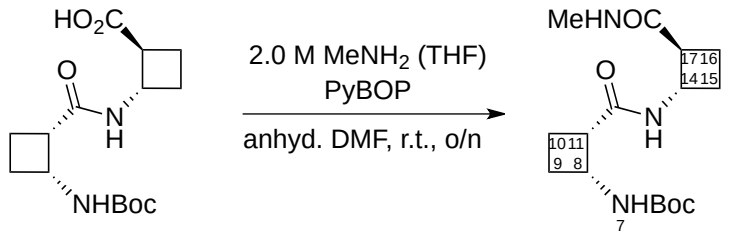

(_R,S,S,S_)-**203** (_R,S,S,S_)-**69**

2.0 M $MeNH_2$ solution in THF (1.6 mL, 3.2 mmol) and PyBOP (0.41 g, 0.77 mmol) were added to a solution of acid (_R,S,S,S_)-**203** (0.20 g, 0.64 mmol) in anhydrous DMF (5 mL). The mixture was stirred at room temperature overnight. EtOAc (25 mL) was added and the solution was washed with saturated aqueous $NaHCO_3$ solution (3 x 10 mL). The organic layer was dried over anhydrous $MgSO_4$, filtered and the solvent was evaporated *in vacuo*. The resulting residue was purified by silica gel chromatography using CH_2Cl_2/MeOH (19:1) as eluent to afford (_R,S,S,S_)-**69** (0.16 g, 77%) as white solid.

Spectroscopic data and physical constants of compound (_R,S,S,S_)-69:

$[\alpha]_D$= +91 (_c_= 1.2, CH_2Cl_2)

M. p.: 163-166 ºC (EtOAc-pentane)

IR (cm^{-1}) ν 3311, 2978, 1682, 1649.

IR solution (cm^{-1}, $CDCl_3$) ν 3442, 3303, 2984, 1706, 1652.

^{1}H NMR (600 MHz, $CDCl_3$) δ 1.44 (s, 9H, $H_{1\text{-}3}$), 1.76 (m, 1H, H_{15R}), 1.93 (m, 1H, H_{10S}), 2.01 (m, 1H, H_{16S}), 2.10-2.22 (c.a., 4H, H_{9R}, H_{10R}, H_{15S}, H_{16R}), 2.35 (m, 1H, H_{9S}), 2.84 (d, $^3J_{H\text{-}H}$= 4.6 Hz, 3H, H_{20}), 3.24 (m, 1H, H_{17}), 4.32 (m, 1H, H_{14}), 4.39 (m, 1H, H_8), 5.03 (d, $^3J_{H\text{-}H}$= 6.7 Hz, 1H, NH_7), 6.11 (broad s, 1H, NH_{13}), 8.38 (broad s, 1H, NH_{19}).

^{13}C NMR (150 MHz, $CDCl_3$) δ 18.0, 19.0, 24.5 (C_9, C_{10}, C_{15}, C_{16}), 26.4 (C_{20}), 28.5 ($C_{1\text{-}3}$), 46.1, 47.0, 48.3, 50.0 (C_8, C_{11}, C_{14}, C_{17}), 80.3 (C_4), 155.8 (C_6), 173.7 (C_{12}, C_{18}).

HRMS: Calculated for $C_{16}H_{27}N_3O_4Na$ $(M+Na)^+$: 348.1894. Found $(M+Na)^+$: 348.1899.

_N_-Boc-(_S,S_)-βCbu-(_R,S_)-βCbu-OMe 6:

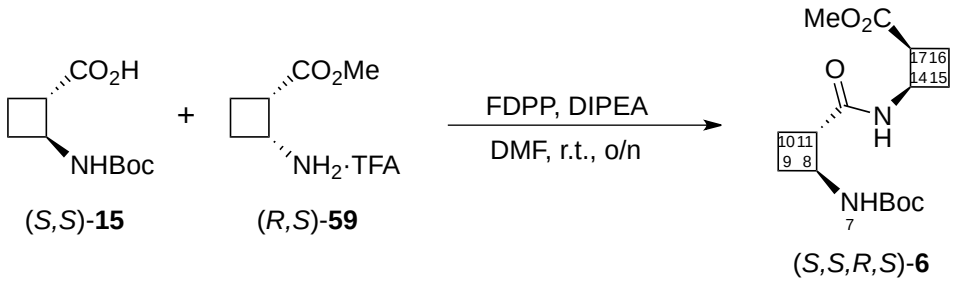

Amine (_R,S_)-**59**[9a] (0.41 g, 1.7 mmol), DIPEA (0.86 mL, 5.0 mmol) and FDPP (0.77 g, 2.0 mmol) were added to a solution of acid (_S,S_)-**15**[72] (0.36 g, 1.7 mmol) in anhydrous DMF (15 mL). The mixture was stirred at room temperature overnight. EtOAc (20 mL) was added and the solution was washed with saturated aqueous $NaHCO_3$ solution (3 x 15 mL). The organic layer was dried over anhydrous $MgSO_4$, filtered and the solvent was evaporated *in vacuo*. The resulting residue was purified by silica gel chromatography using hexane/EtOAc (2:3) as eluent to afford (_S,S,R,S_)-**6** (0.21 g, 39%) as white solid.

Spectroscopic data and physical constants of compound (_S,S,R,S_)-6:

$[\alpha]_D$= +125 (_c_= 0.6, MeOH)

M. p.: 129-131 ºC (EtOAc-pentane)

IR (cm^{-1}) ν 3341, 2970, 1738, 1683, 1650.

IR solution (cm^{-1}, $CDCl_3$) ν 3448, 3279, 2984, 1726, 1699, 1655.

^{1}H NMR (600 MHz, $CDCl_3$) δ 1.47 (s, 9H, $H_{1\text{-}3}$), 1.75 (p, $^3J_{H\text{-}H}$= 9.8 Hz, 1H, H_{9S}), 1.87-2.20 (c.a., 5H, H_{9R}, H_{10}, H_{16}), 2.27-2.39 (c.a., 2H, H_{15}), 2.83 (m, 1H, H_{11}), 3.41 (m, 1H, H_{17}), 3.64 (s, 3H, H_{20}), 4.09 (m, 1H, H_8), 4.71 (m, 1H, H_{14}), 4.85 (broad s, 1H, NH_7), 7.88 (broad s, 1H, NH_{13}).

^{13}C NMR (150 MHz, $CDCl_3$) δ 18.2 (C_{10}), 19.0 (C_{16}), 25.3 (C_9), 28.1 (C_{15}), 28.5 ($C_{1\text{-}3}$), 45.0 (C_{17}), 45.3 (C_{14}), 49.0 (C_8), 49.6 (C_{11}), 51.6 (C_{20}), 80.4 (C_4), 155.9 (C_6), 172.5 (C_{12}), 173.8 (C_{18}).

HRMS: Calculated for $C_{16}H_{26}N_2O_5Na$ $(M+Na)^+$: 349.1734. Found $(M+Na)^+$: 349.1732.

***N*-Boc-(*S*,*S*)-βCbu-(*R*,*S*)-βCbu 203:**

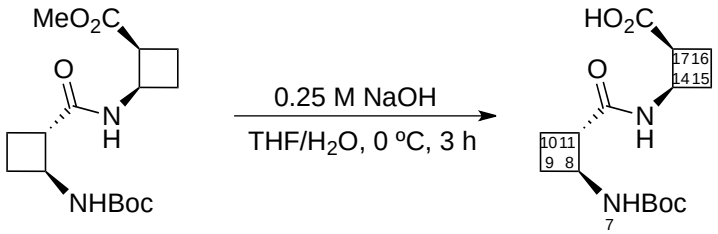

(*S*,*S*,*R*,*S*)-**6** (*S*,*S*,*R*,*S*)-**203**

To an ice-cooled solution of amino acid (*S*,*S*,*R*,*S*)-**6** (90 mg, 0.28 mmol) in a 1:10 mixture of THF/ H_2O (60 mL), 0.25 M aqueous NaOH solution (4 mL) was added. The mixture was stirred at 0 ºC for 3 h. The mixture was washed with CH_2Cl_2 (1 x 40 mL) before being acidified to pH 2 with 2 M HCl. The aqueous layer was extracted with EtOAc (4 x 65 mL) and the organic layer was dried over anhydrous $MgSO_4$, filtered and evaporated under reduced pressure to afford the corresponding carboxylic acid (*S*,*S*,*R*,*S*)-**203** (90 mg, quantitative yield) as a white solid. This compound was used directly in next step without further purification.

Spectroscopic data of compound (*S*,*S*,*R*,*S*)-203:

^{1}H NMR (250 MHz, $CDCl_3$) δ 1.45 (s, 9H, $H_{1\text{-}3}$), 1.79-2.48 (c.a., 8H, H_9, H_{10}, H_{15}, H_{16}), 3.05 (m, 1H, H_{11}), 3.36 (m, 1H, H_{17}), 4.22 (m, 1H, H_8), 4.65 (m, 1H, H_{14}), 5.06 (broad s, 1H, NH_7), 8.01 (broad s, 1H, NH_{13}).

***N*-Boc-(*S*,*S*)-βCbu-(*R*,*S*)-βCbu-NHMe 69:**

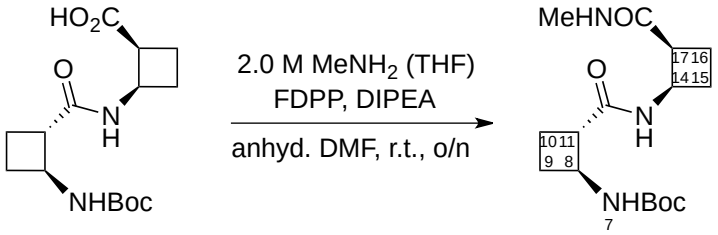

(*S*,*S*,*R*,*S*)-**203** (*S*,*S*,*R*,*S*)-**69**

2.0 M $MeNH_2$ solution in THF (0.22 mL, 0.43 mmol), FDPP (0.13 g, 0.35 mmol) and DIPEA (0.15 mL, 0.86 mmol) were added to a solution of acid (*S*,*S*,*R*,*S*)-**203** (90 mg, 0.28 mmol) in anhydrous DMF (10 mL). The mixture was stirred at room temperature overnight. EtOAc (25 mL) was added and the solution was washed with saturated aqueous $NaHCO_3$ solution (3 x 10 mL). The organic layer was dried over anhydrous $MgSO_4$, filtered and the solvent was evaporated *in vacuo*. The resulting residue was purified by silica gel chromatography using EtOAc as eluent to afford (*S*,*S*,*R*,*S*)-**69** (35.3 mg, 38%) as white solid.

Spectroscopic data and physical constants of compound (*S,S,R,S*)-69:

$[\alpha]_D$= +74 (*c* = 0.5, MeOH)

M. p.: 207-210 ºC (polymorphism: 160 ºC) (EtOAc-pentane)

IR (cm^{-1}) ν 3317, 2975, 1684, 1645.

IR solution (cm^{-1}, $CDCl_3$) ν 3695, 3608, 3450, 3279, 2960, 1690-1650 (broad signal).

^{1}H NMR (600 MHz, $CDCl_3$) δ 1.46 (s, 9H, $H_{1\text{-}3}$), 1.76 (m, 1H, H_{9R}), 1.86 (m, 1H, H_{10R}), 1.93 (m, 1H, H_{16S}), 2.01 (m, 1H, H_{10S}), 2.19-2.36 (c.a., 4H, H_{9S}, H_{15}, H_{16R}), 2.73 (d, $^3J_{H\text{-}H}$= 4.7 Hz, 3H, H_{20}), 2.81 (m, 1H, H_{11}), 3.26 (m, 1H, H_{17}), 4.11 (m, 1H, H_{14}), 4.54 (m, 1H, H_8), 4.88 (broad s, 1H, NH_7), 5.72 (broad s, 1H, NH_{19}), 7.82 (broad s, 1H, NH_{13}).

^{13}C NMR (150 MHz, $CDCl_3$) δ 18.3, 18.7, 25.6, 27.2 (C_9, C_{10}, C_{15}, C_{16}), 26.3 (C_{20}), 28.6 ($C_{1\text{-}3}$), 46.1, 46.4, 48.9, 49.7 (C_8, C_{11}, C_{14}, C_{17}), 80.7 (C_4), 156.0 (C_6), 172.8, 173.6 (C_{12}, C_{18}).

HRMS: Calculated for $C_{16}H_{27}N_3O_4Na$ $(M+Na)^+$: 348.1894. Found $(M+Na)^+$: 348.1901.

N-Boc-(*S,S*)-βCbu-(*R,R*)-βCbu-OMe 6:

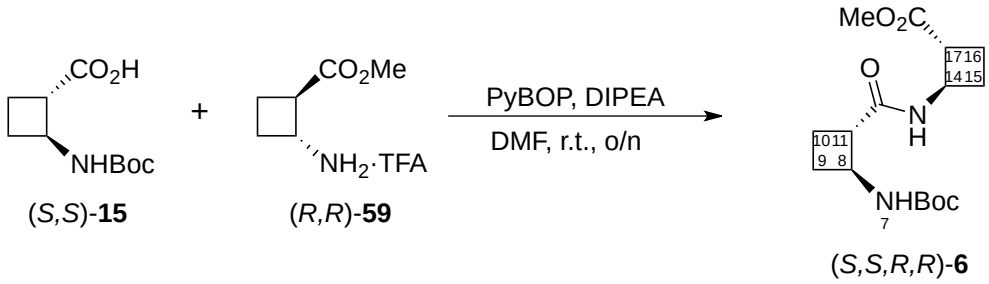

Amine (*R,R*)-**59**[84] (0.13 g, 0.56 mmol), DIPEA (0.30 mL, 1.8 mmol) and PyBOP (0.44 g, 0.84 mmol) were added to a solution of acid (*S,S*)-**15**[72] (0.12 g, 0.56 mmol) in anhydrous DMF (5 mL). The mixture was stirred at room temperature overnight. EtOAc (10 mL) was added and the solution was washed with saturated aqueous $NaHCO_3$ solution (3 x 10 mL). The organic layer was dried over anhydrous $MgSO_4$, filtered and the solvent was evaporated *in vacuo*. The resulting residue was purified by silica gel chromatography using EtOAc as eluent to afford (*S,S,R,R*)-**6** (0.13 g, 71%) as white solid.

Spectroscopic data and physical constants of compound (*S,S,R,R*)-6:

$[\alpha]_D$= -34 (*c* = 0.9, CH_2Cl_2)

M. p.: 174-178 ºC (polymorphism: 153 ºC) (EtOAc-pentane)

IR (cm^{-1}) ν 3352, 3311, 2981, 1724, 1681, 1648.

IR solution (cm^{-1}, $CDCl_3$) ν 3448, 3288, 2985, 1731, 1694, 1656.

^{1}H NMR (600 MHz, $CDCl_3$) δ 1.46 (s, 9H, $H_{1\text{-}3}$), 1.71 (m, 1H, H_{9R}), 1.85-2.05 (c.a., 4H, H_{10R}, H_{15S}, H_{16}), 2.10 (m, 1H, H_{10S}), 2.17 (m, 1H, H_{9S}), 2.31 (m, 1H, H_{15R}), 2.88 (dd, $^3J_{H\text{-}H}$= 9.4 Hz, $^3J_{H\text{-}H}$= 18.3 Hz, 1H, H_{11}), 2.99 (dd, $^3J_{H\text{-}H}$= 8.7 Hz, $^3J_{H\text{-}H}$= 18.2 Hz, 1H, H_{17}), 3.66 (s, 3H, H_{20}), 4.10 (m, 1H, H_8), 4.49 (m, 1H, H_{14}), 4.90 (d, $^3J_{H\text{-}H}$= 6.2 Hz, 1H, NH_7), 8.47 (d, $^3J_{H\text{-}H}$= 5.1 Hz, 1H, NH_{13}).

^{13}C NMR (150 MHz, $CDCl_3$) δ 18.4 (C_{10}), 18.8 (C_{16}), 24.6 (C_9), 27.1 (C_{15}), 28.3 ($C_{1\text{-}3}$), 46.4 (C_{17}), 47.4 (C_{14}), 48.6 (C_8), 50.3 (C_{11}), 51.7 (C_{20}), 80.7 (C_4), 156.5 (C_6), 172.3 (C_{12}), 173.6 (C_{18}).

HRMS: Calculated for $C_{16}H_{26}N_2O_5Na$ $(M+Na)^+$: 349.1735. Found $(M+Na)^+$: 349.1734.

***N*-Boc-(*S,S*)-βCbu-(*R,R*)-βCbu 203:**

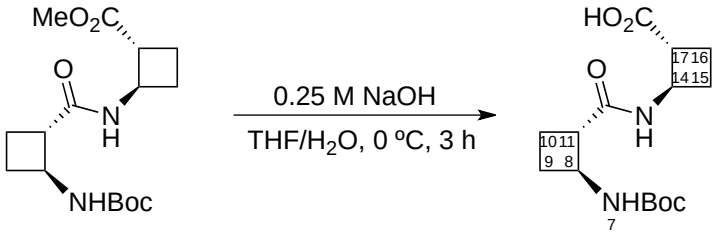

(*S,S,R,R*)-**6** (*S,S,R,R*)-**203**

To an ice-cooled solution of amino acid (*S,S,R,R*)-**6** (70 mg, 0.21 mmol) in a 1:10 mixture of THF/ H_2O (15 mL), 0.25 M aqueous NaOH solution (2.0 mL) was added. The mixture was stirred at 0 ºC for 3 h. The mixture was washed with CH_2Cl_2 (1 x 10 mL) before being acidified to pH 2 with 2 M HCl. The aqueous layer was extracted with EtOAc (4 x 25 mL) and the organic layer was dried over anhydrous $MgSO_4$, filtered and evaporated under reduced pressure to afford the corresponding carboxylic acid (*S,S,R,R*)-**203** (70 mg, quantitative yield) as a white solid. This compound was used directly in next step without further purification.

Spectroscopic data of compound (*S,S,R,R*)-203:

^{1}H NMR (250 MHz, $CDCl_3$) δ 1.47 (s, 9H, $H_{1\text{-}3}$), 1.71-2.32 (c.a., 8H, H_9, H_{10}, H_{15}, H_{16}), 2.99 (m, 1H, H_{11}), 3.11 (m, 1H, H_{17}), 4.07 (m, 1H, H_8), 4.16 (m, 1H, H_{14}), 4.95 (broad s, 1H, NH_7), 9.42 (broad s, 1H, NH_{13}).

_N_-Boc-(_S,S_)-βCbu-(_R,R_)-βCbu-NHMe 69:

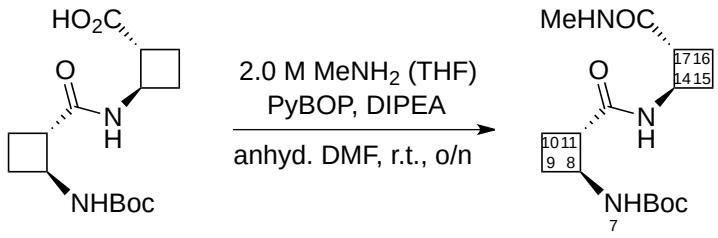

(_S,S,R,R_)-**203** (_S,S,R,R_)-**69**

2.0 M $MeNH_2$ solution in THF (0.14 mL, 0.29 mmol), PyBOP (0.12 g, 0.23 mmol) and DIPEA (0.10 mL, 0.57 mmol) were added to a solution of acid (_S,S,R,R_)-**203** (60 mg, 0.19 mmol) in anhydrous DMF (5 mL). The mixture was stirred at room temperature overnight. EtOAc (15 mL) was added and the solution was washed with saturated aqueous $NaHCO_3$ solution (3 x 10 mL). The organic layer was dried over anhydrous $MgSO_4$, filtered and the solvent was evaporated *in vacuo*. The resulting residue was purified by silica gel chromatography using EtOAc as eluent to afford (_S,S,R,R_)-**69** (30.7 mg, 49%) as white solid.

Spectroscopic data and physical constants of compound (_S,S,R,R_)-69:

$[\alpha]_D$= -58 (_c_ = 0.3, MeOH)

M. p.: 72-75 ºC (EtOAc-pentane)

IR (cm^{-1}) ν 3334, 3286, 2923, 1689, 1660, 1646.

IR solution (cm^{-1}, $CDCl_3$) ν 3448, 3275, 3450, 2984, 1728, 1692, 1651.

^{1}H NMR (600 MHz, $CDCl_3$) δ 1.46 (s, 9H, $H_{1\text{-}3}$), 1.76 (m, 1H, H_{9S}), 1.88 (m, 1H, H_{10R}), 1.93-2.01 (c.a., 2H, H_{15S}, H_{16S}), 2.13-2.27 (c.a., 4H, H_{9R}, H_{10S}, H_{15R}, H_{16R}), 2.78 (d, $^3J_{H\text{-}H}$= 4.7 Hz, 3H, H_{20}), 2.85 (dd, $^3J_{H\text{-}H}$= 9.2 Hz, $^3J_{H\text{-}H}$= 17.9 Hz, 1H, H_{17}), 2.91 (dd, $^3J_{H\text{-}H}$= 9.4 Hz, $^3J_{H\text{-}H}$= 18.4 Hz, 1H, H_{11}), 4.10 (m, 1H, H_8), 4.26 (m, 1H, H_{14}), 4.95 (d, $^3J_{H\text{-}H}$= 6.4 Hz, 1H, NH_7), 8.49 (broad s, 1H, NH_{19}), 8.92 (broad s, 1H, NH_{13}).

^{13}C NMR (150 MHz, $CDCl_3$) δ 18.6, 19.1, 23.5, 24.4 (C_9, C_{10}, $C_{15,}$ C_{16}), 26.1 (C_{20}), 28.3 ($C_{1\text{-}3}$), 48.0, 48.7, 49.7, 50.0 (C_8, C_{11}, C_{14}, C_{17}), 81.0 (C_4), 156.6 (C_6), 174.0, 174.3 (C_{12}, C_{18}).

HRMS: Calculated for $C_{16}H_{27}N_3O_4Na$ $(M+Na)^+$: 348.1894. Found $(M+Na)^+$: 348.1897.

MeO-(*S*,*R*)-βCbu-βdehydroCbu-(*S*,*R*)-βCbu-OMe 97:

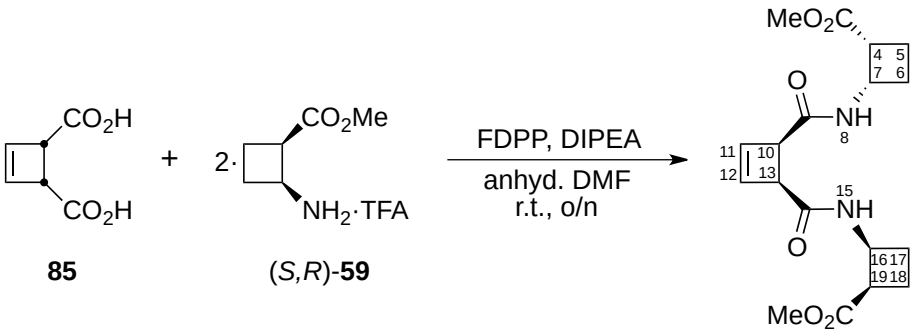

85 (*S*,*R*)-**59** **97**

Diacid **85**[185] (640 mg, 4.5 mmol), FDPP (3.5 g, 9.1 mmol) and DIPEA (5.3 mL, 13.5 mmol) were dissolved in anhydrous DMF (5 mL) under nitrogen atmosphere. In another flask, monomer (*S*,*R*)-**59**[9a] (2.17 g, 8.9 mmol) and DIPEA (4.6 mL, 27 mmol) were dissolved in anhydrous DMF (3 mL) . This solution was transferred to the first flask with the use of a cannula. The mixture was stirred overnight at room temperature. EtOAc (15 mL) was added and the solution was washed with saturated aqueous $NaHCO_3$ solution (3 x 15 mL). The organic layer was dried over anhydrous $MgSO_4$, filtered and the solvent was evaporated *in vacuo*. The resulting residue was purified by silica gel chromatography using CH_2Cl_2 /MeOH (15:1) as eluent to afford **97** (260 mg, 20%) as a pale white solid.

Spectroscopic data and physical constants of compound 97:

$[\alpha]_D$= -65 (*c* = 0.40, CH_2Cl_2)

M. p.: 107-109 ºC (CH_2Cl_2)

IR (cm^{-1}) ν 3293, 2942, 1718, 1648, 1523, 1433.

^{1}H NMR (360 MHz, $CDCl_3$) δ 1.92-2.04 (c.a., 4H, H_5, H_{18}), 2.14-2.33 (c.a., 4H, H_6, H_{17}), 3.29-3.37 (c.a., 2H, H_4, H_{19}), 3.71 (s, 6H, H_1, H_{22}), 3.76-3.80 (c.a., 2H, H_{10}, H_{13}), 4.67 (p, $^3J_{H\text{-}H}$= 8.6 Hz, 2H, H_7, H_{16}), 6.26 (d, $^3J_{H\text{-}H}$= 2.9 Hz, 1H, H_{12}), 6.38 (d, $^3J_{H\text{-}H}$= 2.9 Hz, 1H, H_{11}), 6.77 (broad d, $^3J_{H\text{-}H}$= 8.9 Hz, 1H, NH_8), 6.85 (broad d, $^3J_{H\text{-}H}$= 8.9 Hz, 1H, NH_{15}).

^{13}C NMR (90 MHz, $CDCl_3$) δ 19.3, 19.4 (C_5, C_{18}), 29.3, 29.4 (C_6, C_{17}), 44.0 (C_7, C_{16}), 44.2, 44.3 (C_4, C_{11}), 51.0, 51.5 (C_{10}, C_{13}), 51.8 (C_1, C_{22}), 136.8 (C_{12}), 138.8 (C_{11}), 169.1 (C_9), 169.5 (C_{14}), 174.6 (C_3, C_{20}).

HRMS: Calculated for $C_{18}H_{24}N_2O_6Na$ $(M+Na)^+$: 387.3798. Found $(M+Na)^+$: 387.1529.

MeO-[(*S*,*R*)-βCbu]$_2$-βdehydroCbu-[(*S*,*R*)-βCbu]$_2$-OMe 98:

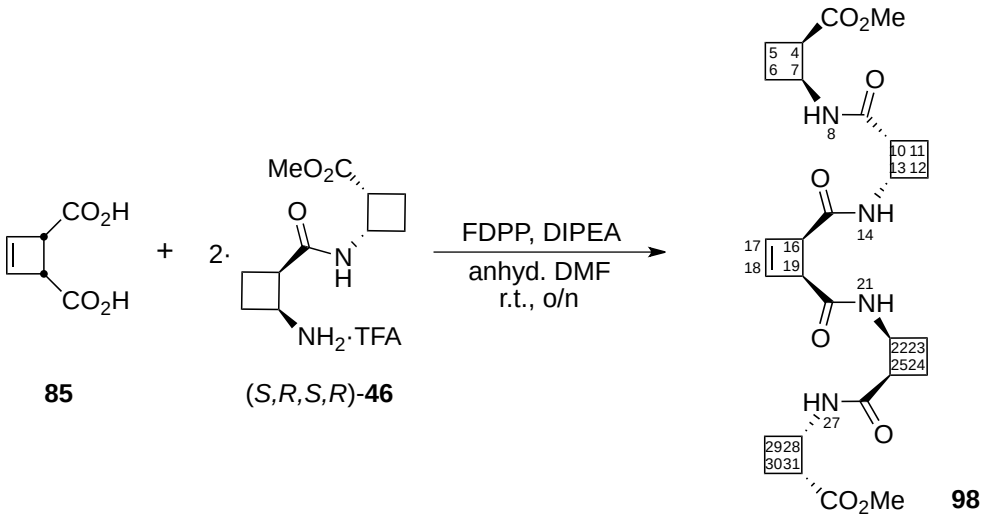

85 (*S*,*R*,*S*,*R*)-**46** **98**

Diacid **85**[185] (72.2 mg, 0.51 mmol), FDPP (0.43 g, 1.1 mmol) and DIPEA (0.65 mL, 1.7 mmol) were dissolved in anhydrous DMF (5 mL) under nitrogen atmosphere. After ten minutes stirring, dipeptide (*S*,*R*,*S*,*R*)-**46**[9a] (334 mg, 0.98 mmol) was added and the mixture was stirred at room temperature overnight. DMF was lyophilized and the resulting residue was dissolved in EtOAc (50 mL). The solution was washed with saturated aqueous $NaHCO_3$ solution (4 x 20 mL) and the organic layer was dried over anhydrous $MgSO_4$, filtered and the solvent was evaporated. The resulting residue was purified by silica gel chromatography using EtOAc and then MeOH as eluents to afford **98** (40 mg, 14%) as a white solid.

Spectroscopic data and physical constants of compound 98:

$[\alpha]_D$= -158 (*c* = 0.96, CH_2Cl_2)

M. p.: 65-69 ºC (CH_2Cl_2)

IR (cm^{-1}) ν 3282, 2949, 1724, 1642, 1512, 1436.

^{1}H NMR (360 MHz, $CDCl_3$) δ 1.83-2.40 (c.a., 16H, H_5, H_6, H_{11}, H_{12}, H_{23}, H_{24}, H_{29}, H_{30}), 3.07-3.23 (c.a., 2H, H_{10}, H_{25}), 3.33-3.47 (c.a., 2H, H_4, H_{31}), 3.67-3.76 (c.a., 2H, H_{16}, H_{19}), 3.69 (s, 6H, H_1, H_{34}), 4.49-4.81 (c.a., 4H, H_7, H_{13}, H_{22}, H_{28}), 6.20 (d, $^3J_{H\text{-}H}$= 2.8 Hz, 1H), 6.36 (d, $^3J_{H\text{-}H}$= 2.8 Hz, 1H), 6.67 (broad d, $^3J_{H\text{-}H}$= 8.6 Hz, 1H, NH), 6.76 (broad d, $^3J_{H\text{-}H}$= 8.5 Hz, 1H, NH), 7.04 (broad d, $^3J_{H\text{-}H}$= 8.7 Hz, 1H, NH_{14}), 7.10 (broad d, $^3J_{H\text{-}H}$= 8.5 Hz, 1H, NH_{21}).

^{13}C NMR (90 MHz, $CDCl_3$) δ 19.0, 19.1, 19.2 (C_5, C_{11}, C_{24}, C_{30}), 28.7, 28.9, 29.1, 29.3 (C_6, C_{12}, C_{23}, C_{29}), 44.6, 44.7, 44.8 (C_4, C_7, C_{13}, C_{22}, C_{28}, C_{31}), 45.6 (C_{10}, C_{25}), 51.0, 51.8 (C_{16}, C_{19}), 51.9 (C_1, C_{34}), 137.0 (C_{18}), 138.4 (C_{17}), 169.7 (C_{15}), 170.2 (C_{20}), 172.3, 172.4 (C_9, C_{26}), 174.6, 174.7 (C_3, C_{32}).

HRMS: Calculated for $C_{28}H_{39}N_4O_8Na$ $(M+Na)^+$: 559.4431. Found $(M+Na)^+$: 559.2755.

_N_-Cbz-(_S_,_R_)-βCbu-Gly 104:

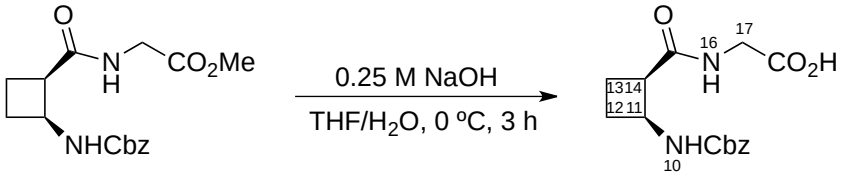

40 **104**

To an ice-cooled solution of dipeptide **40**[19] (120 mg, 0.37 mmol) in a 1:2 mixture of THF/water (21 mL), 0.25 M aqueous NaOH solution (3.5 mL) was added. The mixture was stirred at 0 ºC for 3 h. The mixture was washed with CH_2Cl_2 (1 x 20 mL) before being acidified to pH 2 with 2M HCl. The aqueous layer was extracted with EtOAc (3 x 20 mL) and the organic layer was dried over anhydrous $MgSO_4$, filtered and evaporated under reduced pressure to afford the corresponding carboxylic acid **104** (110 mg, 96% yield) as a white solid. This compound was used directly in next step without further purification.

Spectroscopic data and physical constants of compound 104:

$[\alpha]_D$= -44 (*c* = 0.40, EtOAc)

M. p.: 124-128 ºC (EtOAc)

IR (cm^{-1}) ν 3316, 2951, 1695, 1650, 1537.

^{1}H NMR (250 MHz, $CDCl_3$) 1.90 (m, 1H), 2.10 (m, 1H), 2.15–2.35 (c.a., 2H), 3.32 (m, 1H, H_{14}), 3.61–4.30 (c.a., 2H, H_{17}), 4.49 (p, $^3J_{H\text{-}H}$ = 8.5 Hz, 1H, H_{11}), 5.02 (d, $^2J_{H\text{-}H}$ = 12.2 Hz, 1H, H_7), 5.08 (d, $^2J_{H\text{-}H}$ = 12.2 Hz, 1H, H_7), 5.89 (d, $^3J_{H\text{-}H}$ = 8.5 Hz, 1H, NH_{10}), 6.35 (broad s, 1H, NH_{16}), 7.27–7.41 (broad s, 5H, $H_{1\text{-}5}$).

^{13}C NMR (62.5 MHz, $CDCl_3$) 18.2 (C_{13}), 29.1 (C_{12}), 41.4 (C_{17}), 46.3 (C_{14}), 46.7 (C_{11}), 66.9 (C_7), 128.2, 128.3, 128.6 ($C_{1\text{-}5}$), 136.6 (C_6), 157.9 (C_9), 171.4, 172.4 (C_{15}, C_{18}).

HRMS: Calculated for $C_{15}H_{18}N_2O_5Na$ $(M+Na)^+$: 329.1108. Found $(M+Na)^+$: 329.1115.

TFA·(_S_,_R_)-βCbu-Gly-OMe 105:

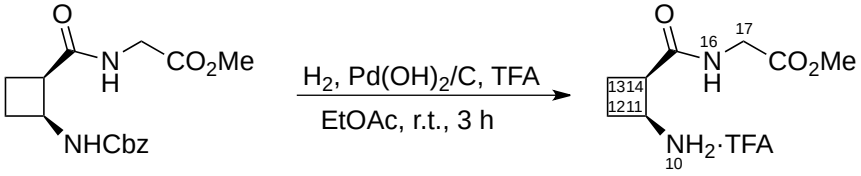

40 **105**

TFA (0.07 mL, 0.93 mmol) was added to a solution of dipeptide **40**[19] (230 mg, 0.72 mmol) in EtOAc (20 mL). The mixture was hydrogenated over 10% $Pd(OH)_2/C$ (84 mg) at room temperature at 6-7 atm for 3 h. The catalyst was removed by filtration through Celite® and washed successively with EtOAc and MeOH. The filtrate was evaporated *in vacuo* to provide **105** (216 mg, quantitative yield) as yellow oil. This compound was used in next step without further purification.

Spectroscopic data of compound 105:

^{1}H NMR (250 MHz, MeOD-d_4) δ 2.15–2.48 (c.a., 4H, H_{12}, H_{13}), 3.43 (m, 1H, H_{14}), 3.71 (s, 3H, H_{20}), 3.96 (broad s, 2H, H_{17}), 4.01 (m, 1H, H_{11}).

^{13}C NMR (62.5 MHz, MeOD-d_4) δ 22.5 (C_{13}), 27.5 (C_{12}), 42.5 (C_{14}, C_{17}), 48.2 (C_{11}), 53.6 (C_{20}), 173.0 (C_{15}), 176.0 (C_{18}).

N-Cbz-[(*S*,*R*)-βCbu-Gly]$_2$-OMe 106:

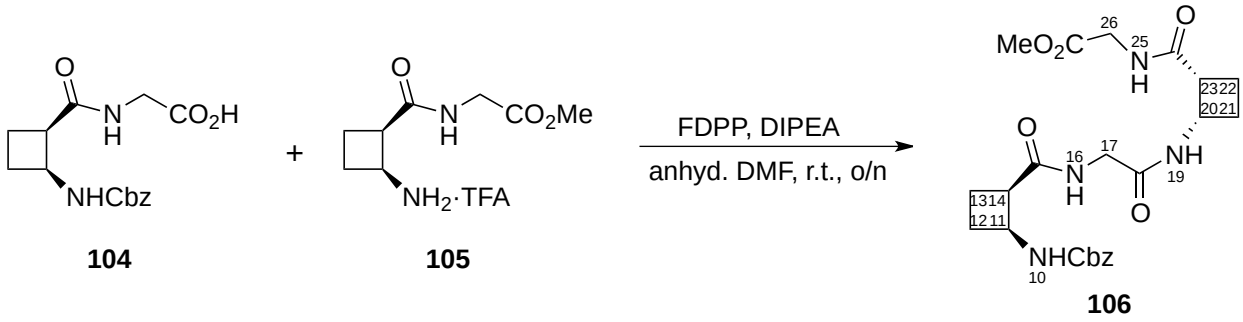

DIPEA (0.4 mL, 2.3 mmol) and FDPP (0.21 g, 0.55 mmol) were added to a solution of acid **104** (150 mg, 0.49 mmol) in a 20:1 mixture of anhydrous CH_2Cl_2/DMF (21 mL). After five minutes stirring dipeptide **105** (147 mg, 0.49 mmol) was added and the mixture was stirred at room temperature overnight. The solvent was removed under reduced pressure and DMF lyophilized. The crude was dissolved in EtOAc (20 mL) and the resulting solution was washed with saturated aqueous $NaHCO_3$ solution (1 x 15 mL) and H_2O (1 x 15 mL). The organic layer was dried over anhydrous $MgSO_4$, filtered and the solvent removed *in vacuo*. The resulting residue was then purified by Et_2O washes, stirring and disaggregating the solid to provide **106** (120 mg, 52%) as a white solid.

Spectroscopic data and physical constants of compound 106:

$[\alpha]_D$= -124 (*c* = 0.29, CH_2Cl_2)

M. p.: 175-179 ºC (Et_2O-pentane)

IR (cm^{-1}) ν 3307, 3067, 2950, 1703, 1650, 1536.

^{1}H NMR (600 MHz, $CDCl_3$) 1.83-1.93 (c.a., 2H, H_{13}, H_{22}), 2.06 (m, 1H, H_{13}), 2.12 (m, 1H, H_{22}), 2.19-2.29 (c.a., 3H, H_{12}, H_{21}), 2.33 (m, 1H, H_{12}), 3.19 (m, 1H, H_{23}), 3.28 (m, 1H, H_{14}), 3.67 (dd, $^2J_{H\text{-}H}$= 17 Hz, $^3J_{H\text{-}H}$= 4.8 Hz, 1H, H_{17}), 3.74 (s, 3H, H_{29}), 3.76 (dd, $^2J_{H\text{-}H}$= 18 Hz, $^3J_{H\text{-}H}$= 5.0 Hz, 1H, H_{26}), 4.01 (dd, $^2J_{H\text{-}H}$= 17 Hz, $^3J_{H\text{-}H}$= 6.0 Hz, 1H, H_{17}), 4.20 (dd, $^2J_{H\text{-}H}$= 18 Hz, $^3J_{H\text{-}H}$= 6.2 Hz, 1H, H_{26}), 4.49 (p, $^3J_{H\text{-}H}$= 8.5 Hz, 1H, H_{11}), 4.67 (p, $^3J_{H\text{-}H}$= 8.5 Hz, 1H, H_{20}), 5.01 (d, $^2J_{H\text{-}H}$= 12 Hz, 1H, H_7), 5.06 (d, $^2J_{H\text{-}H}$= 12 Hz, 1H, H_7), 6.28-6.35 (c.a., 2H, NH_{10}, NH_{25}), 6.50 (broad s, 1H, NH_{16}), 7.15 (d, $^3J_{H\text{-}H}$= 8.5 Hz, 1H, NH_{19}), 7.28-7.37 (c.a., 5H, $H_{1\text{-}5}$).

^{13}C NMR (150 MHz, $CDCl_3$) δ 18.1 (C_{22}), 18.3 (C_{13}), 28.8 (C_{21}), 29.6 (C_{12}), 41.4 (C_{26}), 43.1 (C_{17}), 44.9 (C_{20}), 45.6 (C_{23}), 46.0 (C_{14}), 46.6 (C_{11}), 52.7 (C_{29}), 66.7 (C_7), 128.1, 128.2, 128.6 ($C_{1\text{-}5}$), 136.4 (C_6), 156.0 (C_9), 169.3 (C_{18}), 171.3 (C_{27}), 173.2 (C_{24}), 173.5 (C_{15}).

HRMS: Calculated for $C_{23}H_{30}N_4O_7Na$ $(M+Na)^+$: 497.2007. Found $(M+Na)^+$: 497.2007.

N-Cbz-[(*S*,*R*)-βCbu-Gly]$_2$ 107:

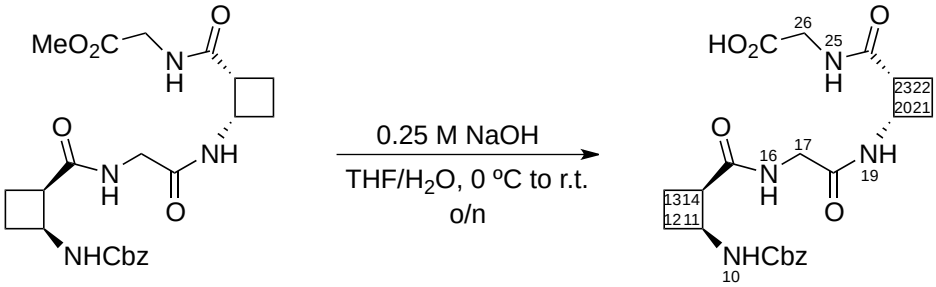

106 **107**

To an ice-cooled solution of tetrapeptide **106** (130 mg, 0.27 mmol) in a 1:1 mixture of THF/water (100 mL), 0.25 M aqueous NaOH solution (3 mL, 0.75 mmol) was added. The mixture was stirred from 0 ºC to room temperature overnight. The mixture was washed with CH_2Cl_2 (1 x 40 mL) before being acidified to pH 2 with 2 M HCl. The aqueous layer was extracted with EtOAc (3 x 50 mL) and the organic layer was dried over anhydrous $MgSO_4$, filtered and evaporated under reduced pressure to afford the corresponding carboxylic acid **107** (100 mg, 79%) as a white solid. This compound was used directly in next step without further purification.

Spectroscopic data and physical constants of compound 107:

$[\alpha]_D$= -53 (*c* = 0.63, DMSO)

M. p.: 143-146 ºC (EtOAc)

IR (cm^{-1}) ν 3328, 2950, 1750, 1687, 1650, 1626, 1561, 1535.

^{1}H NMR (250 MHz, DMSO-d_6) δ 1.75-2.02 (c.a., 4H, H_{13}, H_{22}), 2.03-2.28 (c.a., 4H, H_{12}, H_{21}), 3.21-3.34 (c.a., 2H, H_{14}, H_{23}), 3.56-3.85 (c.a., 4H, H_{17}, H_{26}), 4.33 (p, $^3J_{H\text{-}H}$= 8.2 Hz, 1H, H_{11}), 4.56 (p, $^3J_{H\text{-}H}$= 8.2 Hz, 1H, H_{20}), 5.02 (broad s, 2H, H_7), 7.28 (m, 1H, NH_{10}), 7.30-7.44 (c.a., 5H, $H_{1\text{-}5}$), 7.86-7.96 (c.a., 2H, NH_{16}, NH_{25}), 8.03 (m, 1H, NH_{19}).

^{13}C NMR (62.5 MHz, DMSO-d_6) δ 17.8 (C_{13}, C_{22}), 28.7, 28.8 (C_{12}, C_{21}), 40.9 (C_{26}), 41.9 (C_{17}), 44.4, 44.7, 44.9 (C_{14}, C_{20}, C_{23}), 46.6 (C_{11}), 65.2 (C_7), 127.5, 127.7, 128.4 ($C_{1\text{-}5}$), 137.2 (C_6), 155.2 (C_9), 168.4 (C_{18}), 171.9, 172.1, 172.3 (C_{15}, C_{24}, C_{27}).

HRMS: Calculated for $C_{22}H_{28}N_4O_7Na$ $(M+Na)^+$: 483.1850. Found $(M+Na)^+$: 483.1852.

[(*S*,*R*)-βCbu-Gly]$_2$-OMe 108:

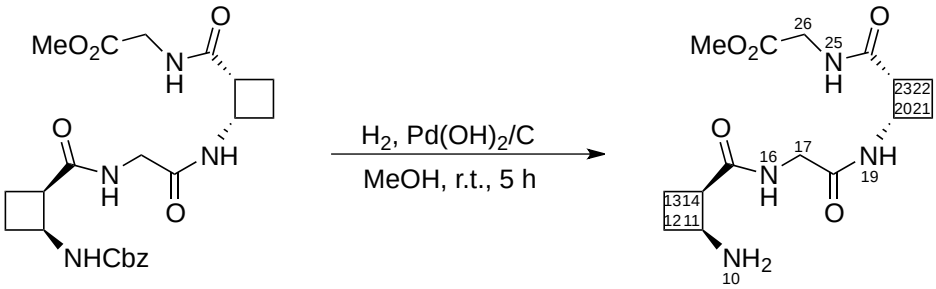

106 **108**

A solution of tetrapeptide **106** (130 mg, 0.27 mmol) in MeOH (20 mL) was hydrogenated over 10% $Pd(OH)_2/C$ (40 mg) at room temperature at 7-8 atm for 5 h. The catalyst was removed by filtration through Celite® and washed successively with CH_2Cl_2 and MeOH. The filtrate was evaporated *in vacuo* to provide **108** (94 mg, quantitative yield) as yellow oil. This compound was used in next step without further purification.

Spectroscopic data of compound 108:

^{1}H NMR (250 MHz, MeOD-d_4) δ 1.91-2.44 (c.a., 8H, H_{12}, H_{13}, H_{21}, H_{22}), 3.34-3.53 (c.a., 2H, H_{14}, H_{23}), 3.75 (s, 3H, H_{29}), 3.79-4.06 (c.a., 5H, H_{11}, H_{17}, H_{26}), 4.67 (q, $^3J_{H\text{-}H}$= 8.5 Hz, 1H, H_{20}).

_N_-Cbz-[(_S_,_R_)-βCbu-Gly]$_3$-OMe 109:

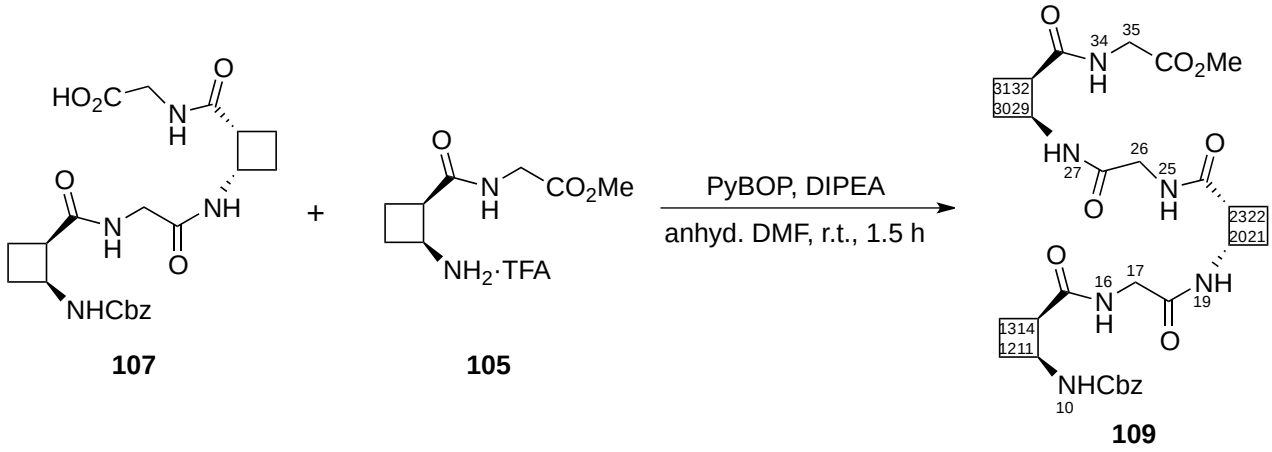

DIPEA (0.36 mL, 2.1 mmol) and PyBOP (0.15 g, 0.29 mmol) were added to a solution of acid **107** (100 mg, 0.22 mmol) in anhydrous DMF (3 mL). After five minutes stirring dipeptide **105** (66 mg, 0.22 mmol) was added and the mixture was stirred at room temperature for 1.5 h. DMF was lyophilized and the resulting crude was dissolved in EtOAc (20 mL). The solution was washed with H_2O (1 x 15 mL) and the organic layer was dried over anhydrous $MgSO_4$, filtered and the solvent removed *in vacuo*. The resulting residue was then purified by Et_2O washes, stirring and disaggregating the solid and by silica gel chromatography using CH_2Cl_2/MeOH (20:1) as eluent to provide **109** (40 mg, 30% yield) as a pale yellow solid.

Spectroscopic data and physical constants of compound 109:

$[\alpha]_D$= -60 (*c* = 0.59, DMSO)

M. p.: 163-166 ºC (Et_2O)

IR (cm^{-1}) ν 3294, 3068, 2947, 1731, 1687, 1633, 1529.

^{1}H NMR (250 MHz, DMSO-d_6) δ 1.70-2.00 (c.a., 6H, H_{13}, H_{22}, H_{31}), 2.03-2.26 (c.a., 6H, H_{12}, H_{21}, H_{30}), 3.02-3.27 (c.a., 3H, H_{14}, H_{23}, H_{32}), 3.54-4.06 (c.a., 6H, H_{17}, H_{26}, H_{35}), 3.64 (s, 3H, H_{38}), 4.30 (p, $^3J_{H\text{-}H}$= 8.5 Hz, 1H, H_{11}), 4.43-4.64 (c.a., 2H, H_{20}, H_{29}), 5.00 (broad s, 2H, H_7), 7.23 (m, 1H, NH_{10}), 7.29-7.41 (c.a., 5H, H_1-H_5), 7.81-7.95 (c.a., 3H, NH), 8.04-8.10 (c.a., 2H, NH).

^{13}C NMR (62.5 MHz, DMSO-d_6) δ 17.7, 17.9 (C_{13}, C_{22}, C_{31}), 28.3, 28.6, 28.9 (C_{12}, C_{21}, C_{30}), 40.4 (C_{35}), 41.9 (C_{17}, C_{26}), 44.3, 44.4, 44.6, 44.7, 44.8 (C_{14}, C_{20}, C_{23}, C_{29}, C_{32}), 46.5 (C_{11}), 51.7 (C_{38}), 65.1 (C_7), 127.4, 127.6, 128.3 ($C_{1\text{-}5}$), 137.1 (C_6), 152.4 (C_9), 168.3, 168.5, 170.6, 172.0, 172.4, (C_{15}, C_{18}, C_{24}, C_{27}, C_{33}, C_{36}).

HRMS: Calculated for $C_{30}H_{40}N_6O_9Na$ $(M+Na)^+$: 651.2749. Found $(M+Na)^+$: 651.2755.

_N_-Cbz-[(_S_,_R_)-βCbu-Gly]$_4$-OMe 110:

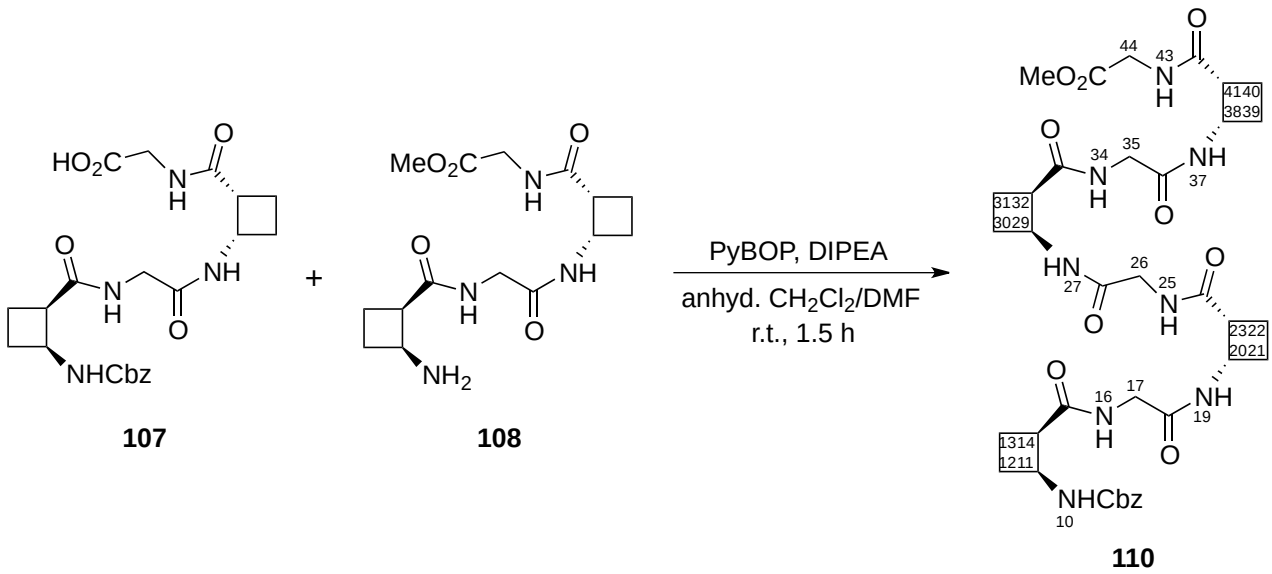

107 **108** **110**

DIPEA (0.14 mL, 0.82 mmol) and PyBOP (0.18 g, 0.35 mmol) were added to a solution of acid **107** (130 mg, 0.29 mmol) in a 12:1 mixture of anhydrous CH_2Cl_2/DMF (19.5 mL). After five minutes stirring amine **108** (99 mg, 0.29 mmol) was added and the mixture was stirred at room temperature for 1.5 h. The solvent was removed *in vacuo* and DMF was lyophilized. The resulting crude was purified by Et_2O washes, stirring and disaggregating the to provide **110** (70 mg, 32%) as a pale yellow solid.

Spectroscopic data and physical constants of compound 110:

$[\alpha]_D$= -226 (*c* = 0.245, DMSO)

M. p.: 182-185 ºC (Et_2O)

IR (cm^{-1}) ν 3294, 3066, 2947, 1726, 1688, 1635, 1533.

^{1}H NMR (360 MHz, DMSO-d_6) δ 1.73-2.00 (c.a., 8H, H_{13}, H_{22}, H_{31}, H_{40}), 2.04-2.22 (c.a., 8H, H_{12}, H_{21}, H_{30}, H_{39}), 3.18-3.30 (c.a., 4H, H_{14}, H_{23}, H_{32}, H_{41}), 3.56-4.05 (c.a., 8H, H_{17}, H_{26}, H_{35}, H_{44}), 3.64 (s, 3H, H_{47}), 4.30 (m, 1H, H_{11}), 4.45-4.62 (c.a., 3H, H_{20}, H_{29}, H_{38}), 4.99 (broad s, 2H, H_7), 7.24-7.39 (c.a., 6H, $H_{1\text{-}5}$, NH_{10}), 7.83-7.98 (c.a., 4H, NH), 8.04-8.10 (c.a., 3H, NH).

^{13}C NMR (90 MHz, DMSO-d_6) δ 17.7, 17.9 (C_{13}, C_{22}, C_{31}, C_{40}), 28.3, 28.6, 28.8, 29.0 (C_{12}, C_{21}, C_{30}, C_{39}), 40.7 (C_{44}), 41.8, 41.9 (C_{17}, C_{26}, C_{35}), 44.3, 44.5, 44.7, 44.7, 44.9 (C_{14}, C_{20}, C_{23}, C_{29}, C_{32}, C_{38}, C_{41}), 46.5 (C_{11}), 51.7 (C_{47}), 65.1 (C_7), 127.4, 127.6, 128.3 ($C_{1\text{-}5}$), 137.2 (C_6), 155.1 (C_9), 168.3, 168.5, 168.6, 170.6, 172.0, 172.5, 174.4 (C_{15}, C_{18}, C_{24}, C_{27}, C_{33}, C_{36}, C_{42}, C_{45}).

HRMS: Calculated for $C_{37}H_{50}N_8O_{11}Na$ $(M+Na)^+$: 805.3491. Found $(M+Na)^+$: 805.3480.

***N*-Boc-(*S*,*R*)-βCbu-βAla-OMe 112:**

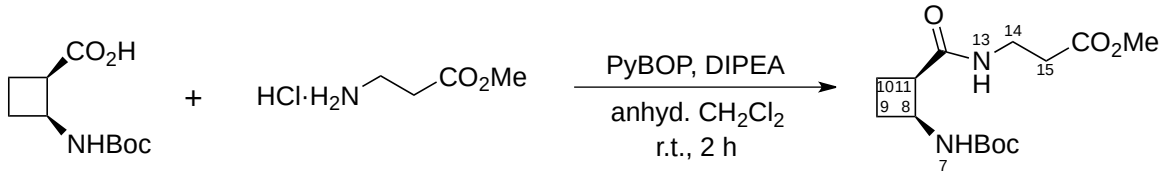

(*S*,*R*)-**16** **111** **112**

DIPEA (2.9 mL, 17.4 mmol) and PyBOP (2.52 g, 4.82 mmol) were added to a solution of acid (*S*,*R*)-**16**[62] (650 mg, 3.02 mmol) in anhydrous CH_2Cl_2 (20 mL). After five minutes stirring, methyl β-alanine hydrochloride **111** (450 mg, 3.09 mmol) was added and the mixture was stirred at room temperature for 2 h. The solvent was removed *in vacuo*, EtOAc (100 mL) was added and the solution was washed with saturated aqueous $NaHCO_3$ solution (1 x 100 mL), saturated aqueous NaCl solution (1 x 100 mL) and H_2O (1 x 100 mL). The organic layer was dried over anhydrous $MgSO_4$, filtered and the solvent was evaporated. The residue was purified by silica gel chromatography using EtOAc as eluent to afford **112** (630 mg, 69%) as a white solid.

Spectroscopic data and physical constants of compound 112:

$[\alpha]_D$= -106 (*c* = 0.59, CH_2Cl_2)

M. p.: 117-119 ºC (CH_2Cl_2)

IR (cm^{-1}) ν 3343, 2988, 2951, 1736, 1674, 1644, 1537, 1510.

^{1}H NMR (250 MHz, $CDCl_3$) δ 1.35 (s, 9H, $H_{1\text{-}3}$), 1.84 (m, 1H, H_{10}), 1.97 (m, 1H, H_{10}), 2.11-2.32 (c.a., 2H, H_9), 2.32-2.57 (c.a., 2H, H_{15}), 3.11 (m, 1H, H_{11}), 3.35-3.57 (c.a., 2H, H_{14}), 3.63 (s, 3H, H_{18}), 4.32 (broad s, 1H, H_8), 5.44 (broad s, 1H, NH_7), 6.21 (broad s, 1H, NH_{13}).

^{13}C NMR (90 MHz, $CDCl_3$) δ 17.9 (C_{10}), 27.9 ($C_{1\text{-}3}$), 28.8 (C_9), 33.8 (C_{15}), 34.6 (C_{14}), 45.8 (C_8, C_{11}), 51.3 (C_{18}), 78.6 (C_4), 154.8 (C_6), 172.1, 172.9 (C_{12}, C_{16}).

HRMS: Calculated for $C_{14}H_{24}N_2O_5Na$ $(M+Na)^+$: 323.1577. Found $(M+Na)^+$: 323.1583.

(HCl or TFA·)(*S*,*R*)-βCbu-βAla-OMe 114:

Method A:

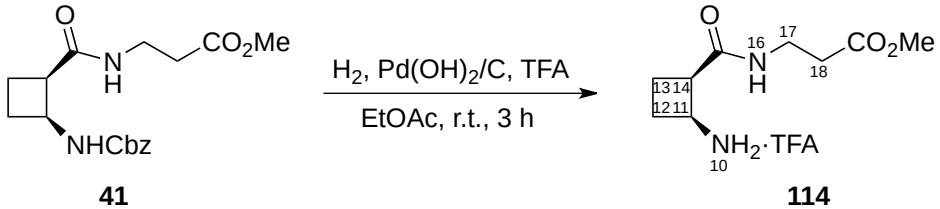

41 **114**

TFA (0.12 mL, 1.6 mmol) was added to a solution of dipeptide **41** (530 mg, 1.6 mmol) in EtOAc (20 mL). The mixture was hydrogenated over 10% $Pd(OH)_2/C$ (160 mg) at room temperature at 6-7 atm for 3 h. The catalyst was removed by filtration through Celite® and washed successively with EtOAc and MeOH. The filtrate was evaporated *in vacuo* to provide **114** (498 mg, quantitative yield) as a yellow oil. This compound was used in next step without further purification.

Method B:

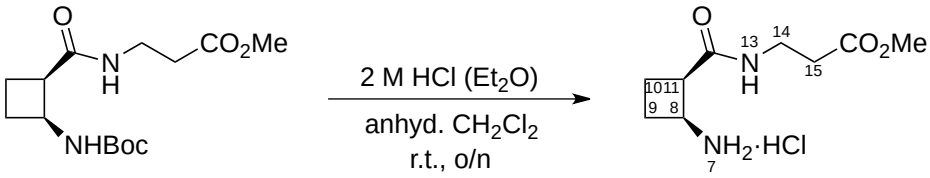

112 **114**

2 M HCl in Et_2O (7.9 mL, 16 mmol) was added to a solution of compound **112** (315 mg, 1.05 mmol) in anhydrous CH_2Cl_2 (20 mL). The mixture was stirred at room temperature overnight. The solvent was removed under reduced pressure to provide salt **114** (249 mg, quantitative yield) as white solid.

Spectroscopic data of compound 114:

^{1}H NMR (250 MHz, $CDCl_3$) δ 2.21 (broad s, 2H), 2.45 (broad s, 2H), 2.61 (broad s, 2H, H_{15}), 3.35-3.61 (c.a., 3H, H_{11}, H_{14}), 3.68 (s, 3H, H_{18}), 4.19 (broad s, 1H, H_8), 7.69 (broad s, 1H, NH_{13}), 8.35 (broad s, 3H, NH_2·HCl).

^{13}C NMR (62.5 MHz, $CDCl_3$) δ 21.0 (C_{10}), 29.9 (C_9), 34.1 (C_{15}), 35.5 (C_{14}), 41.3 (C_{11}), 46.3 (C_8), 52.2 (C_{18}), 173.3 (C_{10}, C_{12}).

N-Cbz-[(*S*,*R*)-βCbu-βAla]$_2$-OMe 7

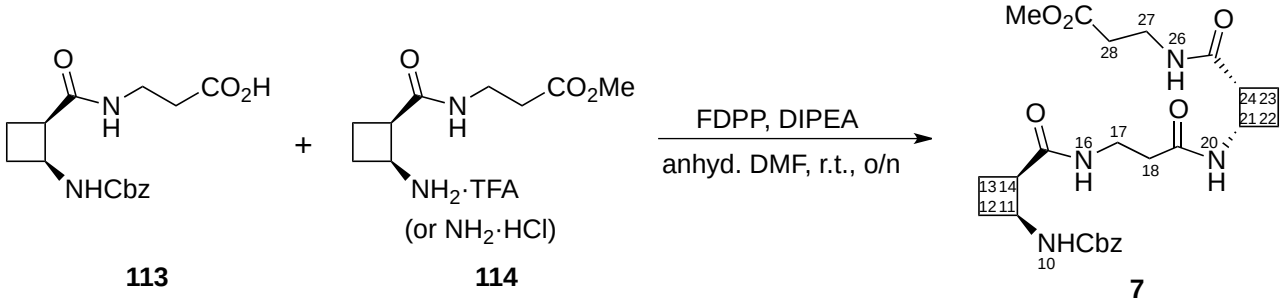

113 **114** **7**

DIPEA (1.3 mL, 7.6 mmol) and FDPP (2.2 g, 5.7 mmol) were added to a solution of acid **113** (460 mg, 1.44 mmol) in anhydrous DMF (5 mL). After five minutes stirring dipeptide **114** (453 mg, 1.44 mmol) was added and the mixture was stirred at room temperature overnight. The solvent was

removed *in vacuo*, EtOAc (30 mL) was added and the solution was washed with saturated aqueous $NaHCO_3$ solution (4 x 30 mL). The organic layer was dried over anhydrous $MgSO_4$, filtered and the solvent was evaporated and the remaining DMF was lyophilized. The resulting residue was purified by silica gel chromatography using CH_2Cl_2/MeOH (15:1) as eluent to afford **7**[11] (430 mg, 60%) as white solid.

Same reaction using the chloride salt provided the tetrapeptide **7** with 48% of yield.

Spectroscopic data of compound 7:

^{1}H NMR (250 MHz, $CDCl_3$) δ 1.80-2.41 (c.a., 10H, H_{12}, H_{13}, H_{18}, H_{22}, H_{23}), 2.45-2.54 (c.a., 2H, H_{28}), 3.17 (m, 1H, H_{24}), 3.21-3.36 (c.a., 2H), 3.40-3.55 (c.a., 2H), 3.61 (m, 1H, H_{14}), 3.69 (s, 3H, H_{31}), 4.47 (m, 1H, H_{11}), 4.61 (m, 1H, H_{21}), 4.97-5.15 (c.a., 2H, H_7), 6.02 (broad s, 1H, NH_{10}) 6.18 (broad s, 1H, NH_{26}), 6.67 (broad s, 1H, NH_{16}), 6.99 (broad s, 1H, NH_{20}), 7.27-7.40 (broad s, 5H, $H_{1\text{-}5}$).

Spectroscopic data are consistent with those reported in reference:

Izquierdo, S.; Kogan, M.J.; Parella, T.; Moglioni, A.G.; Branchadell, V.; Giralt, E.; Ortuño, R.M. *J. Org. Chem.* **2004**, *69*, 5093-5099.

***N*-Cbz-[(*S*,*R*)-βCbu-βAla]$_2$ 115:**

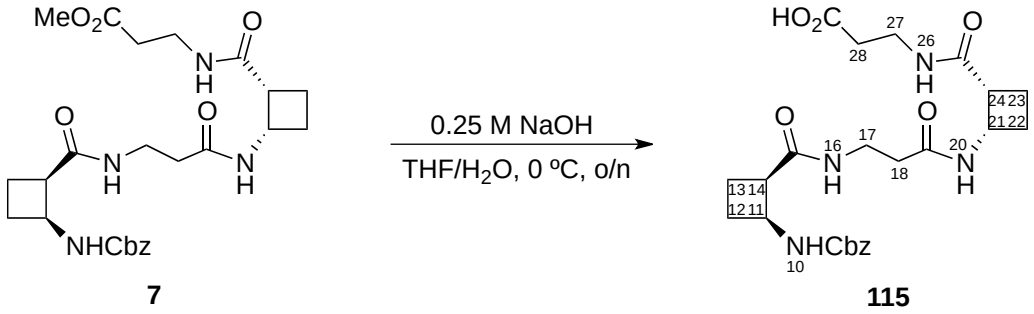

7 **115**

To an ice-cooled solution of tetrapeptide **7**[11] (200 mg, 0.40 mmol) in a 1:1 mixture of THF/water (100 mL), 0.25 M aqueous NaOH solution (4.0 mL, 1.0 mmol) was added. The mixture was stirred from 0 ºC to room temperature overnight. The mixture was washed with CH_2Cl_2 (1 x 40 mL) before being acidified to pH 2 with 2 M HCl. The aqueous layer was extracted with EtOAc (3 x 50 mL) and the organic layer was dried over anhydrous $MgSO_4$, filtered and evaporated under reduced pressure to afford the corresponding tetrapeptide **115** (180 mg, 94%) as a white solid. This compound was used directly in next step without further purification.

Spectroscopic data and physical constants of compound 115:

$[\alpha]_D$= -68 (*c* = 0.29, DMSO)

M. p.: 167-170 ºC (EtOAc)

IR (cm^{-1}) ν 3310, 3030, 2950, 1693, 1648, 1522.

^{1}H NMR (250 MHz, DMSO-d_6) δ 1.67-1.84 (c.a., 2H, H_{13}, H_{23}), 1.85-2.01 (c.a., 2H, H_{13}, H_{23}), 2.06-2.24 (c.a., 6H, H_{12}, H_{22}, H_{18}), 2.28-2.43 (c.a., 2H, H_{28}), 3.07-3.31 (c.a., 6H, H_{14}, H_{17}, H_{24}, H_{27}), 4.25 (p, $^3J_{H\text{-}H}$= 8.25 Hz, 1H, H_{11}), 4.46 (p, $^3J_{H\text{-}H}$= 8.25 Hz, 1H, H_{21}), 5.00 (broad s, 1H, H_7), 7.18 (broad d, $^3J_{H\text{-}H}$= 8.25 Hz, 1H, NH_{10}), 7.24-7.40 (c.a., 5H, H_1-H_5), 7.54-7.67 (c.a., 2H, NH_{16}, NH_{26}), 7.91 (broad d, $^3J_{H\text{-}H}$= 8.15 Hz, 1H, NH_{20}).

^{13}C NMR (62.5 MHz, DMSO-d_6) δ 17.8, 17.9 (C_{13}, C_{23}), 27.3, 27.7 (C_{12}, C_{22}), 34.1, 34.7, 35.3 (C_{17}, C_{18}, C_{27}, C_{28}), 44.8, 44.9, 45.1 (C_{14}, C_{21}, C_{24}), 46.6 (C_{11}), 65.2 (C_7), 127.6, 127.7, 128.3 ($C_{1\text{-}5}$), 137.1 (C_6), 155.1 (C_9), 169.7, 171.6, 172.9 (C_{15}, C_{19}, C_{25}, C_{29}).

HRMS: Calculated for $C_{24}H_{32}N_4O_7Na$ $(M+Na)^+$: 511.2163. Found $(M+Na)^+$: 511.2167.

[(*S*,*R*)-βCbu-βAla]$_2$-OMe 116:

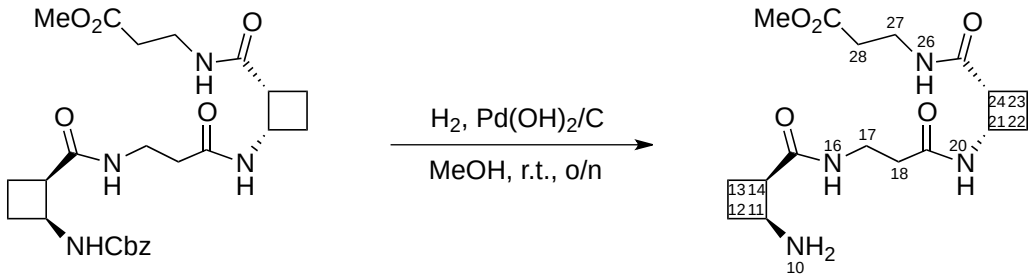

7 **116**

A solution of tetrapeptide **7**[11] (200 mg, 0.40 mmol) in MeOH (40 mL) was hydrogenated over 10% $Pd(OH)_2$/C (60 mg) at room temperature at 7-8 atm overnight. The catalyst was removed by filtration through Celite® and washed successively with CH_2Cl_2 and MeOH. The filtrate was evaporated *in vacuo* to provide **116** (147 mg, quantitative yield) as yellow oil. This compound was used in next step without further purification.

Spectroscopic data of compound 116:

^{1}H NMR (250 MHz, $CDCl_3$) δ 1.85-2.44 (c.a., 10H, H_{12}, H_{13}, H_{18}, H_{22}, H_{23}), 2.52 (t, $^3J_{H\text{-}H}$= 6.1 Hz, 2H, H_{28}), 3.13-3.64 (c.a., 6H, H_{14}, H_{17}, H_{24}, H_{27}), 3.69 (s, 3H, H_{31}), 3.79 (m, 1H, H_{11}), 4.62 (m, 1H, H_{21}).

_N_-Cbz-[(_S_,_R_)-βCbu-βAla]$_4$-OMe 117:

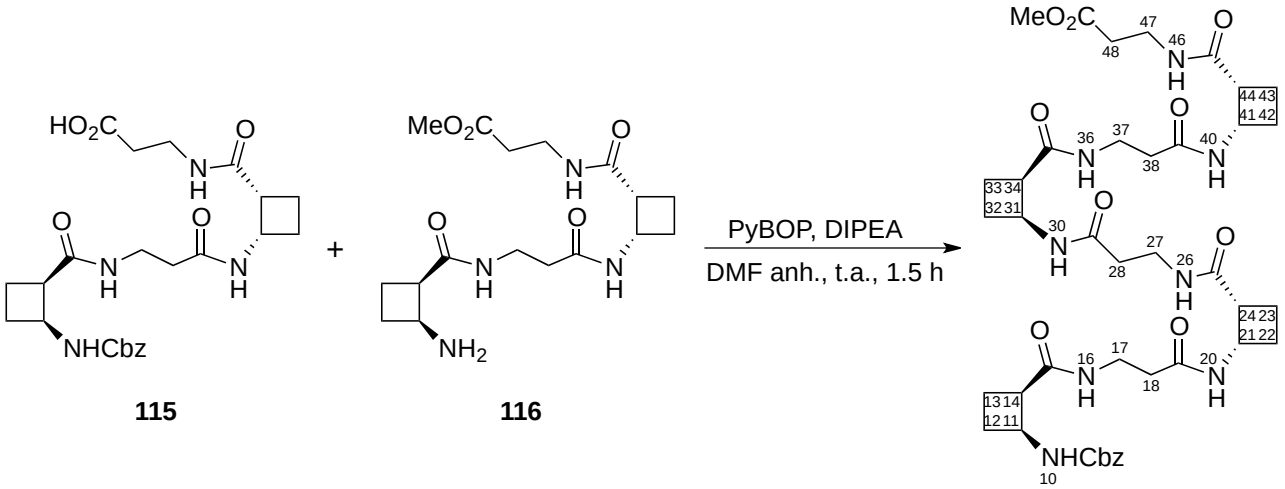

115 **116** **117**

DIPEA (0.90 mL, 5.3 mmol) and PyBOP (0.40 g, 0.77 mmol) were added to a solution of acid **115** (180 mg, 0.37 mmol) in anhydrous DMF (5 mL). After five minutes stirring amine **116** (167 mg, 0.37 mmol) was added and the mixture was stirred at room temperature for 1.5 h. The solvent was removed *in vacuo* and DMF was lyophilized. The resulting crude was purified by Et_2O washes, stirring and disaggregating the solid and by silica gel chromatography using CH_2Cl_2/MeOH (15:1) as eluent to afford octapeptide **117** (190 mg, 27%) as a white solid.

Spectroscopic data and physical constants of compound 117:

$[\alpha]_D$= -73 (*c* = 0.22, DMSO)

M. p.: 242-247 ºC (Et_2O)

IR (cm^{-1}) ν 3298, 3067, 2949, 1647, 1545.

^{1}H NMR (360 MHz, DMSO-d_6) δ 1.67-2.25 (c.a., 22H, H_{12}, H_{13}, H_{18}, H_{22}, H_{23}, H_{28}, H_{32}, H_{33}, H_{38}, H_{42}, H_{43}), 2.35-2.46 (c.a., 2H, H_{48}), 3.07-3.26 (c.a., 12H, H_{14}, H_{17}, H_{24}, H_{28}, H_{34}, H_{38}, H_{44}, H_{47}), 3.58 (s, 3H, H_{51}), 4.26 (p, $^3J_{H\text{-}H}$= 8.5 Hz, 1H, H_{11}), 4.38-4.54 (c.a., 3H, H_{21}, H_{31}, H_{41}), 5.00 (c.a., 2H, H_7), 7.21 (m, 1H, NH_{10}), 7.26-7.37 (c.a., 5H, $H_{1\text{-}5}$), 7.53-7.77 (c.a., 4H, NH), 7.87-8.01 (c.a., 3H, NH).

^{13}C NMR (90 MHz, DMSO-d_6) δ 17.7, 17.9 (C_{13}, C_{23}, C_{33}, C_{43}), 27.3, 27.8, 28.6, 29.0 (C_{12}, C_{22}, C_{32}, C_{42}), 33.8, 34.6, 35.2, 35.4, (C_{17}, C_{18}, C_{27}, C_{28}, C_{37}, C_{38}, C_{47}, C_{48}), 44.8, 45.3 (C_{14}, C_{21}, C_{24}, C_{31}, C_{34}, C_{41}, C_{44}), 46.6 (C_{11}), 51.4 (CH_3), 65.2 (C_7), 127.6, 127.7, 128.3 ($C_{1\text{-}5}$), 137.1 ($C_{6\ ipso}$), 155.1 (C_9), 169.7, 171.5, 171.6, 171.8 (C_{15}, C_{19}, C_{25}, C_{29}, C_{35}, C_{39}, C_{45}, C_{49}).

HRMS: Calculated for $C_{37}H_{50}N_8O_{11}Na$ $(M+Na)^+$: 861.4117. Found $(M+Na)^+$: 861.4123.

N-Cbz-(*S*,*R*)-βCbu-GABA-OMe 118:

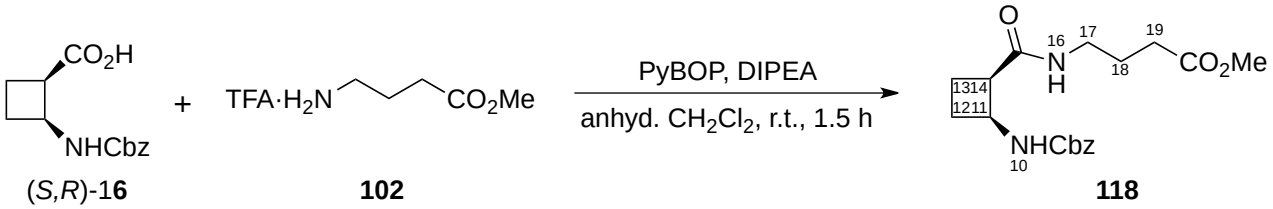

DIPEA (7.0 mL, 41 mmol) and PyBOP (3.5 g, 6.8 mmol) were added to a solution of acid (*S*,*R*)-**16**[62] (1.61 g, 6.5 mmol) in anhydrous CH_2Cl_2 (20 mL). After five minutes stirring, **102**[325] (1.50 g, 6.5 mmol) was added and the mixture was stirred at room temperature for 1.5 h. The solvent was removed *in vacuo*, EtOAc (50 mL) was added and the solution was washed with saturated aqueous $NaHCO_3$ solution (1 x 20 mL), saturated aqueous NaCl solution (1 x 20 mL) and H_2O (1 x 20 mL). The organic layer was dried over anhydrous $MgSO_4$, filtered and the solvent was evaporated. The residue was purified by silica gel chromatography using hexane/EtOAc (1:5) as eluent to afford **118** (1.80 g, 80%) as a white solid.

Spectroscopic data and physical constants of compound 118:

$[\alpha]_D$= -174 (*c* = 0.38, CH_2Cl_2)

M. p.: 82-86 ºC (hexane-EtOAc)

IR (cm^{-1}) ν 3323, 2951, 1733, 1689, 1645, 1526.

^{1}H NMR (400 MHz, $CDCl_3$) δ 1.70- 1.80 (c.a., 2H, H_{18}), 1.91 (m, 1H), 2.05 (m, 1H), 2.22-2.38 (c.a., 4H, H_{12S}, H_{13R}, H_{19}), 3.08-3.29 (c.a., 3H, H_{14}, H_{17}), 3.65 (s, 3H, H_{22}), 4.46 (p, $^3J_{H\text{-}H}$= 8.5 Hz, 1H, H_{11}), 4.98-5.12 (c.a., 2H, H_7), 5.64-5.79 (broad s, 2H, NH_{10}, NH_{16}), 7.33 (broad s, 5H, $H_{1\text{-}5}$).

^{13}C NMR (100 MHz, $CDCl_3$) δ 18.7 (C_{13}), 24.9 (C_{18}), 29.6, 31.6 (C_{12}, C_{19}), 39.0 (C_{14}), 46.6, 46.7 (C_{17}, C_{11}), 51.9 (C_{22}), 66.8 (C_7), 128.2, 128.3, 128.7 ($C_{1\text{-}5}$), 136.7 (C_6), 155.9 (C_9), 173.2, 173.9 (C_{15}, C_{20}).

HRMS: Calculated for $C_{18}H_{24}N_2O_5Na$ $(M+Na)^+$: 371.1577. Found $(M+Na)^+$: 371.1579.

N-Cbz-(*S*,*R*)-βCbu-GABA 119:

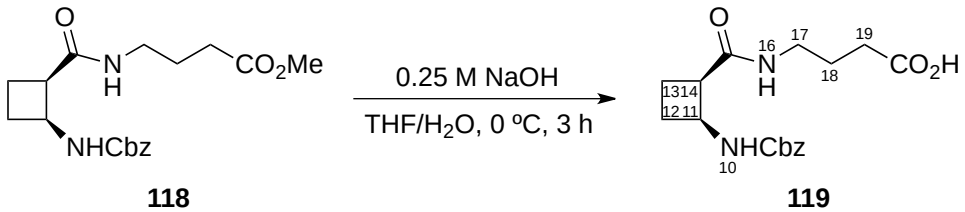

To an ice-cooled solution of dipeptide **118** (640 mg, 1.9 mmol) in a 1:2 mixture of THF/water (105 mL), 0.25 M aqueous NaOH solution (20 mL) was added. The mixture was stirred at 0 ºC for 3 h. The mixture was washed with CH_2Cl_2 (1 x 40 mL) before being acidified to pH 2 with 2 M HCl. The aqueous layer was extracted with EtOAc (3 x 60 mL) and the organic layer was dried over anhydrous $MgSO_4$, filtered and evaporated under reduced pressure to afford the corresponding carboxylic acid **119** (560 mg, 91%) as a white solid. This compound was used directly in next step without further purification.

Spectroscopic data and physical constants of compound 119:

$[\alpha]_D$= -31 (*c* = 0.31, MeOH)

M. p.: 138-141 ºC (CH_2Cl_2)

IR (cm^{-1}) ν 3306, 2947, 1684, 1639, 1526.

^{1}H NMR (360 MHz, $CDCl_3$) δ 1.61-1.79 (c.a., 2H, H_{18}), 1.86 (m, 1H), 2.07 (m, 1H), 2.23-2.35 (c.a., 4H, H_{12}, H_{13}, H_{19}), 3.12-3.28 (c.a., 3H, H_{14}, H_{17}), 4.43 (p, $^3J_{H\text{-}H}$= 8.5 Hz, 1H, H_{11}), 5.01 (d, $^2J_{H\text{-}H}$= 12.3 Hz, 1H, H_7), 5.06 (d, $^2J_{H\text{-}H}$= 12.3 Hz, 1H, H_7), 6.08 (broad d, $^3J_{H\text{-}H}$= 8.5 Hz, 1H, NH_{10}), 6.36 (broad s, 1H, NH_{16}), 7.24-7.36 (broad s, 5H, $H_{1\text{-}5}$), 8.75 (broad s, 1H, CO_2H).

^{13}C NMR (90 MHz, $CDCl_3$) δ 18.2 (C_{13}), 24.8 (C_{18}), 28.9, 31.4 (C_{12}, C_{19}), 38.9 (C_{14}), 46.6, 47.0 (C_{17}, C_{11}), 66.9 (C_7), 128.2, 128.3, 128.7 ($C_{1\text{-}5}$), 136.5 (C_6), 156.3 (C_9), 173.6a, 177.9 (C_{15}, C_{20}).

HRMS: Calculated for $C_{17}H_{22}N_2O_5Na$ $(M+Na)^+$: 357.1421. Found $(M+Na)^+$: 357.1419.

TFA·(*S*,*R*)-βCbu-GABA-OMe 120:

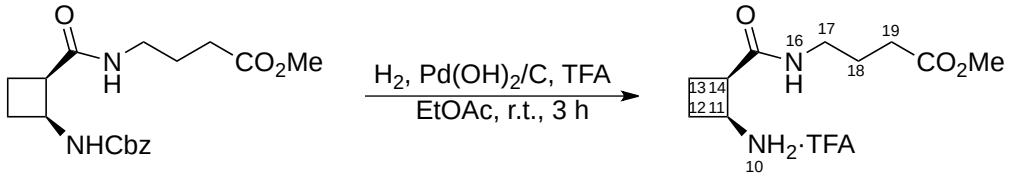

118 **120**

TFA (0.18 mL, 2.3 mmol) was added to a solution of dipeptide **118** (640 mg, 1.8 mmol) in EtOAc (20 mL). The mixture was hydrogenated over 10% $Pd(OH)_2/C$ (200 mg) at room temperature at 6-7 atm for 3 h. The catalyst was removed by filtration through Celite® and washed successively with EtOAc and MeOH. The filtrate was evaporated *in vacuo* to provide **120** (603 mg, quantitative yield) as yellow oil. This compound was used in next step without further purification.

Spectroscopic data of compound 120:

^{1}H NMR (250 MHz, MeOD-d_4) δ 1.81 (p, $^3J_{H\text{-}H}$= 7.3 Hz, 2H), 2.14 (m, 1H), 2.22-2.47 (c.a., 5H), 3.23 (t, $^3J_{H\text{-}H}$= 6.8 Hz, 1H, H_{17}), 3.24 (t, $^3J_{H\text{-}H}$= 6.9 Hz, 1H, H_{17}), signal for H_{14} under MeOH residual peak, 3.67 (s, 3H, H_{22}), 3.98 (m, 1H, H_{11}).

N-Cbz-[(*S*,*R*)-βCbu-GABA]$_2$-OMe 121:

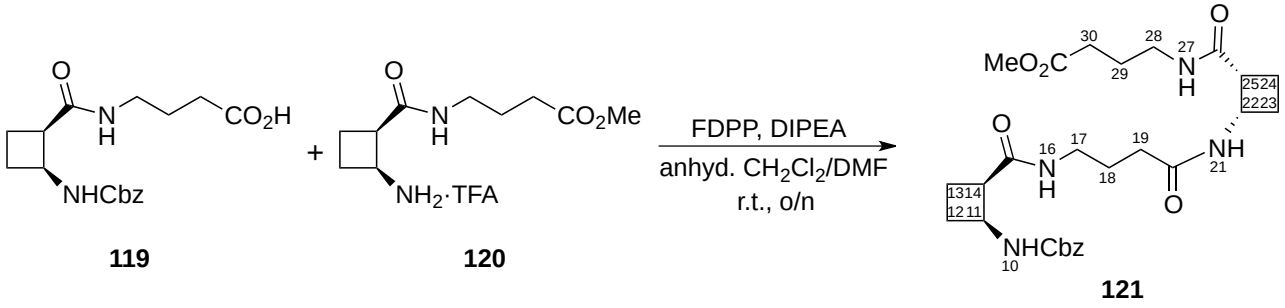

DIPEA (1.85 mL, 10.8 mmol) and FDPP (1.0 g, 2.6 mmol) were added to a solution of acid **119** (710 mg, 2.1 mmol) in anhydrous CH_2Cl_2 (15 mL). After five minutes stirring dipeptide **120** (494 mg, 2.1 mmol) was added and the mixture was stirred at room temperature overnight. The solvent was removed *in vacuo*. EtOAc (20 mL) was added and the solution was washed with saturated aqueous $NaHCO_3$ solution (1 x 20 mL), saturated aqueous NaCl solution (1 x 20 mL) and H_2O (1 x 20 mL). The organic layer was dried over anhydrous $MgSO_4$, filtered and the solvent was evaporated. The resulting residue was purified by Et_2O and pentane washes, stirring and disaggregating the solid to afford **121** (680 mg, 60%) as a white solid.

Spectroscopic data and physical constants of compound 121:

$[\alpha]_D$= -84 (*c* = 1.4, CH_2Cl_2)

M. p.: 146-150 ºC (Et_2O-pentane)

IR (cm^{-1}) ν 3308, 3067, 2948, 1735, 1688, 1639, 1527.

^{1}H NMR (600 MHz, $CDCl_3$) δ 1.62-1.81 (c.a., 4H, H_{18}, H_{29}), 1.85-1.96 (c.a., 2H, H_{13}, H_{24}), 2.01 (m, 1H, H_{13}), 2.05-2.16 (c.a., 3H, H_{19}, H_{24}), 2.23-2.39 (c.a., 6H, H_{12}, H_{23}, H_{30}), 3.04-3.29 (c.a., 6H, H_{14}, H_{17}, H_{25}, H_{28}), 3.64 (s, 3H, H_{33}), 4.44 (p, $^3J_{H\text{-}H}$= 8.4 Hz, 1H, H_{11}), 4.62 (p, $^3J_{H\text{-}H}$= 8.4 Hz, 1H, H_{22}), 4.99 (d, $^2J_{H\text{-}H}$= 12.2 Hz, 1H, H_7), 5.05 (d, $^2J_{H\text{-}H}$= 12.2 Hz, 1H, H_7), 6.14 (broad s, 1H, NH_{27}), 6.23 (d, $^3J_{H\text{-}H}$= 8.4 Hz, 1H, NH_{10}), 6.53 (broad s, 1H, NH_{16}), 7.19 (d, $^3J_{H\text{-}H}$= 8.4 Hz, 1H, NH_{21}), 7.26-7.36 (c.a., 5H, $H_{1\text{-}5}$).

^{13}C NMR (150 MHz, $CDCl_3$) δ 18.5 (C_{13}), 19.1 (C_{24}), 24.6 (C_{29}), 25.2 (C_{18}), 28.5 (C_{23}), 29.1 (C_{12}), 31.3 (C_{30}), 33.5 (C_{19}), 38.6 (C_{28}), 38.7 (C_{17}), 44.9 (C_{22}), 45.9 (C_{25}), 46.2 (C_{14}), 46.6 (C_{11}), 52.0 (C_{33}), 66.6 (C_7), 128.1, 128.2, 128.6 ($C_{1\text{-}5}$), 136.3 (C_6), 155.9 (C_9), 172.5 (C_{20}), 173.4 (C_{15}, C_{26}), 174.0 (C_{29}).

HRMS: Calculated for $C_{27}H_{38}N_4O_7Na$ $(M+Na)^+$: 553.2633. Found $(M+Na)^+$: 553.2629.

N-Cbz-[(*S*,*R*)-βCbu-GABA]$_2$ 122:

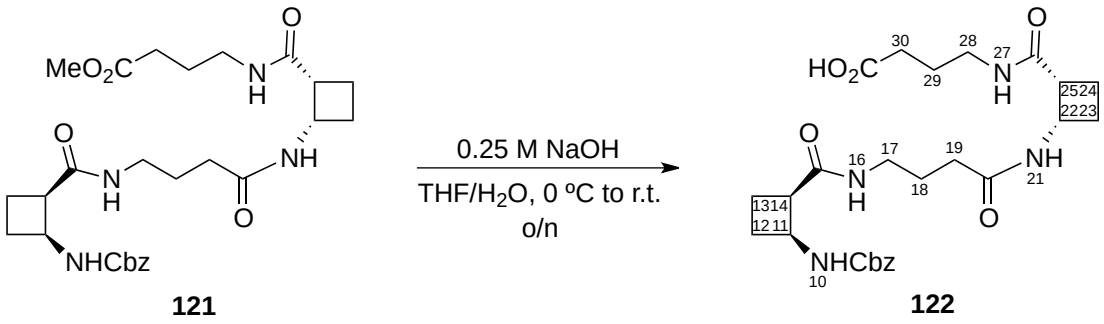

121 **122**

To an ice-cooled solution of tetrapeptide **121** (450 mg, 0.85 mmol) in a 1:1 mixture of THF/H_2O (200 mL), 0.25 M aqueous NaOH solution (11.0 mL, 2.75 mmol) was added. The mixture was stirred from 0 ºC to room temperature overnight. The mixture was washed with CH_2Cl_2 (1 x 100 mL) before being acidified to pH 2 with 2 M HCl. The aqueous layer was extracted with EtOAc (3 x 30 mL) and the organic layer was dried over anhydrous $MgSO_4$, filtered and evaporated under reduced pressure to afford the corresponding carboxylic acid **122** (450 mg, quantitative yield) as a white solid. This compound was used directly in next step without further purification.

Spectroscopic data and physical constants of compound 122:

$[\alpha]_D$= -45 (*c* = 0.31, DMSO)

M. p.: 133-137 ºC (EtOAc)

IR (cm^{-1}) ν 3307, 3065, 2946, 1688, 1639, 1544, 1527.

^{1}H NMR (250 MHz, DMSO-d_6) δ 1.47-1.64 (c.a., 4H), 1.71-2.05 (c.a., 6H), 2.08-2.24 (c.a., 6H), 2.92-3.08 (c.a., 4H, H_{17}, H_{28}), 3.10-3.19 (c.a., 2H, H_{14}, H_{25}), 4.25 (p, $^3J_{H-H}$= 8.5 Hz, 1H, H_{11}), 4.47 (p, $^3J_{H-H}$= 8.5 Hz, 1H, H_{22}), 4.97 (s, 2H, H_7), 7.16 (broad d, $^3J_{H-H}$= 8.5 Hz, 1H, NH), 7.26-7.38 (c.a., 5H, H_{1-5}), 7.57-7.66 (c.a., 2H, NH), 7.82 (broad d, $^3J_{H-H}$= 8.5 Hz, 1H, NH).

^{13}C NMR (62.5 MHz, DMSO-d_6) δ 17.8, 17.9, 24.7, 25.5, 27.5 , 27.7, 31.1, 32.6, 37.8, 38.1, 44.7, 45.1, 45.4, 46.6 (C_{11}), 65.2 (C_7), 127.6, 127.7, 128.3 (C_1-C_5), 137.2 (C_6), 155.1 (C_9), 171.2, 171.6, 171.7, 174.3.

HRMS: Calculated for $C_{26}H_{36}N_4O_7Na$ $(M+Na)^+$: 539.2476. Found $(M+Na)^+$: 539.2479.

[(*S*,*R*)-βCbu-GABA]$_2$-OMe 123:

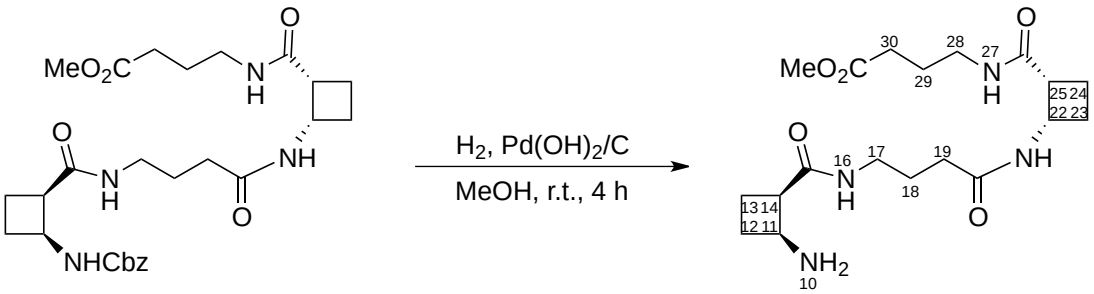

121 **123**

A solution of tetrapeptide **121** (260 mg, 0.49 mmol) in MeOH (25 mL) was hydrogenated over 10% $Pd(OH)_2$/C (80 mg) at room temperature at 7-8 atm for 4 h. The catalyst was removed by filtration through Celite® and washed successively with CH_2Cl_2 and MeOH. The filtrate was evaporated *in vacuo* to provide **123** (190 mg, 98%) as yellow oil. This compound was used in next step without further purification.

Spectroscopic data of compound 123:

^{1}H NMR (250 MHz, MeOD-d_4) δ 1.67-2.39 (c.a., 16H, H_{12}, H_{13}, H_{18}, H_{19}, H_{23}, H_{24}, H_{29}, H_{30}), 3.10-3.27 (c.a., 6H, H_{14}, H_{17}, H_{25}, H_{28}), 3.66 (s, 3H, H_{33}), 3.71 (m, 1H, H_{11}), 4.57 (q, $^3J_{H-H}$= 8.5 Hz, 1H, H_{22}).

_N_-Cbz-[(_S_,_R_)-βCbu-GABA]$_3$-OMe 124:

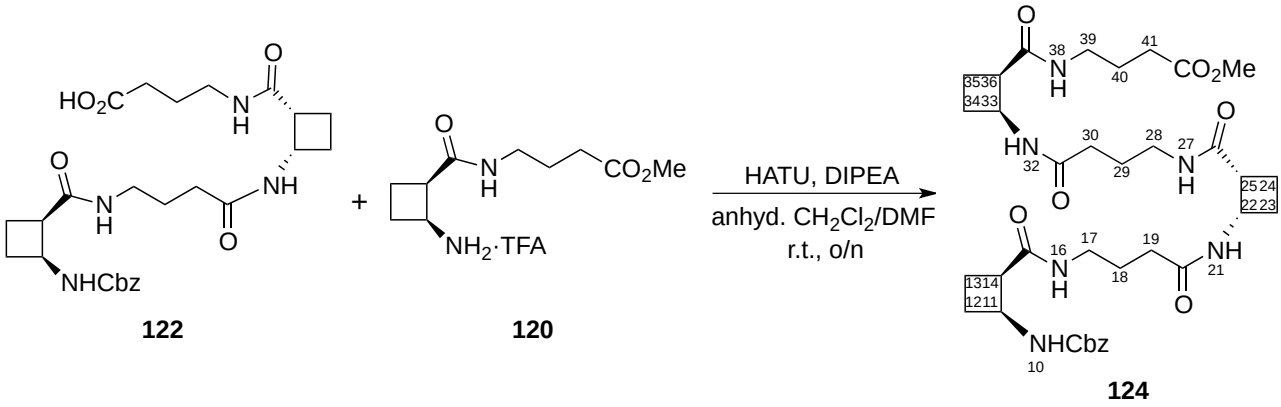

DIPEA (0.40 mL, 2.3 mmol) and HATU (135 mg, 0.36 mmol) were added to a solution of acid **122** (152 mg, 0.29 mmol) in a 25:1 mixture of anhydrous CH_2Cl_2/DMF (26 mL). After five minutes stirring dipeptide **120** (95 mg, 0.29 mmol) was added and the mixture was stirred at room temperature overnight. The solvent was removed *in vacuo* and the DMF was lyophilized. The resulting residue was then purified by H_2O, Et_2O and pentane washes, stirring and disaggregating the solid to provide **124** (75 mg, 36%) as a pale yellow solid.

Spectroscopic data and physical constants of compound 124:

$[\alpha]_D$= -106 (*c* = 0.42, DMSO)

M. p.: 172-175 ºC (Et_2O-pentane)

IR (cm^{-1}) ν 3304, 3068, 2946, 1735, 1688, 1641, 1530.

^{1}H NMR (250 MHz, DMSO-d_6) δ 1.45-1.66 (c.a., 6H, H_{18}, H_{29}, H_{40}), 1.72-2.08 (c.a., 10H), 2.08-2.32 (c.a., 8H), 2.91-3.07 (c.a., 6H, H_{17}, H_{28}, H_{39}), 3.07-3.21 (c.a., 3H, H_{14}, H_{25}, H_{36}), 3.57 (s, 3H, H_{44}), 4.26 (p, $^3J_{H\text{-}H}$= 8.4 Hz, 1H, H_{11}), 4.37-4.55 (c.a., 2H, H_{22}, H_{33}), 4.98 (s, 2H, H_7), 7.16 (d, $^3J_{H\text{-}H}$= 8.2 Hz, 1H, NH_{10}), 7.25-7.39 (c.a., 5H, $H_{1\text{-}5}$), 7.53-7.65 (c.a., 3H, NH), 7.74-7.86 (c.a., 2H, NH).

^{13}C NMR (62.5 MHz, DMSO-d_6) δ 17.8, 17.9, 24.6, 25.5, 27.4, 27.5, 27.7, 30.7 (C_{41}), 32.6 (C_{19}, C_{30}), 37.7, 38.1 (C_{17}, C_{28}, C_{39}), 44.6, 45.0, 45.3 (C_{14}, C_{22}, C_{25}, C_{33}, C_{36}), 46.6 (C_{11}), 51.2 (C_{44}), 65.1 (C_7), 127.5, 127.7, 128.3 ($C_{1\text{-}5}$), 137.1 (C_6), 155.0 (C_9), 171.1, 171.2, 171.5, 173.1, (C_{15}, C_{20}, C_{27}, C_{31}, C_{37}, C_{42}).

HRMS: Calculated for $C_{36}H_{52}N_6O_9Na$ $(M+Na)^+$: 735.3688. Found $(M+Na)^+$: 735.3689.

_N_-Cbz-[(_S_,_R_)-βCbu-GABA]$_4$-OMe 125:

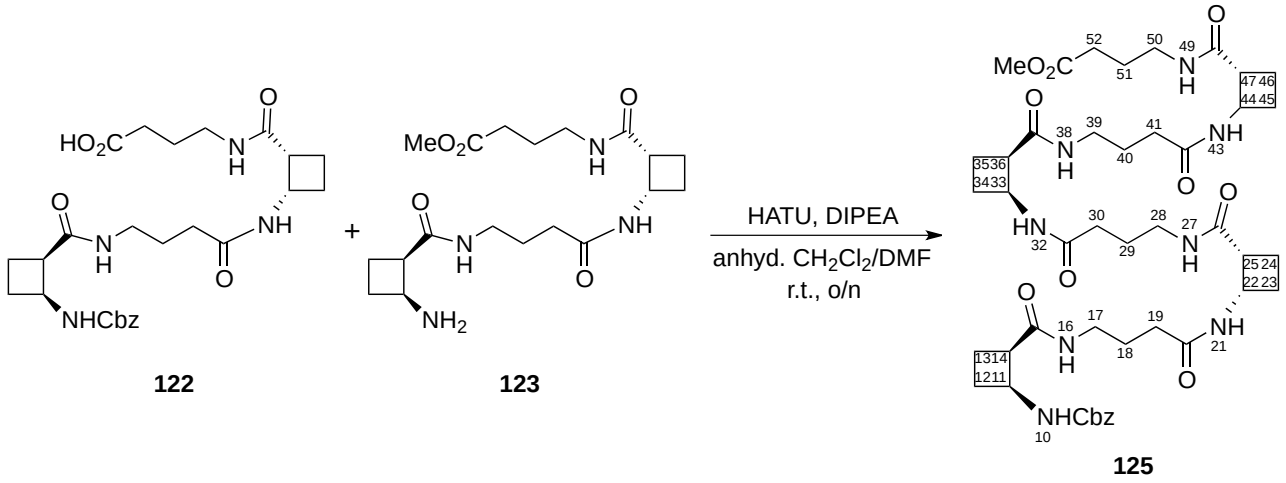

122 **123** **125**

DIPEA (0.26 mL, 1.5 mmol) and HATU (0.28 g, 0.75 mmol) were added to a solution of acid **122** (260 mg, 0.50 mmol) in a 20:1 mixture of anhydrous CH_2Cl_2/DMF (21 mL). After fifteen minutes stirring amine **123** (198 mg, 0.50 mmol) was added and the mixture was stirred at room temperature overnight. The solvent was removed *in vacuo* and the DMF was lyophilized. The resulting residue was then purified by H_2O, Et_2O, pentane and CH_2Cl_2 washes, stirring and disaggregating the solid to provide **125** (280 mg, 62%) as a pale yellow solid.

Spectroscopic data and physical constants of compound 125:

$[\alpha]_D$= -154 (*c* = 0.34, DMSO)

M. p.: 230-234 ºC (Et_2O)

IR (cm^{-1}) ν 3230, 3063, 2945, 1735, 1688, 1639, 1528.

^{1}H NMR (360 MHz, DMSO-d_6) δ 1.46-1.66 (c.a., 8H, H_{18}, H_{29}, H_{40}, H_{51}), 1.71-1.84 (c.a., 4H), 1.84-2.05 (c.a., 10H), 2.05-2.23 (c.a., 8H), 2.23-2.32 (c.a., 2H, H_{52}), 2.89-3.07 (c.a., 8H, H_{17}, H_{28}, H_{39}, H_{50}), 3.08-3.21 (c.a., 4H, H_{14}, H_{25}, H_{36}, H_{47}), 3.57 (s, 3H, H_{55}), 4.25 (p, $^3J_{H\text{-}H}$= 8.3 Hz, 1H, H_{11}), 4.40-4.52 (c.a., 3H, H_{22}, H_{33}, H_{44}), 4.98 (s, 2H, H_7), 7.19 (broad d, $^3J_{H\text{-}H}$= 8.3 Hz , 1H, NH_{10}), 7.26-7.38 (c.a., 5H, $H_{1\text{-}5}$), 7.52-7.67 (c.a., 4H, NH), 7.77-7.89 (c.a., 3H, NH).

^{13}C NMR (90 MHz, DMSO-d_6) δ 17.8, 17.9 (C_{13}, C_{24}, C_{35}, C_{46}), 24.6 (C_{51}), 25.5, 25.6, 25.7 (C_{18}, C_{29}, C_{40}), 27.4, 27.5, 27.7 (C_{12}, C_{23}, C_{34}, C_{45}), 30.7 (C_{52}), 32.6, 32.7 (C_{19}, C_{30}, C_{41}), 37.7, 38.1 (C_{17}, C_{28}, C_{39}, C_{50}), 44.6, 44.7, 45.1, 45.3, 45.4 (C_{14}, C_{22}, C_{25}, C_{33}, C_{36}, C_{44}, C_{47}), 46.6 (C_{11}), 51.2 (CH_3), 65.1 (C_7), 127.5, 127.7, 128.3 ($C_{1\text{-}5}$), 137.2 (C_6), 155.0 (C_9), 171.2, 171.5, 171.6, 173.1 (C_{15}, C_{20}, C_{26}, C_{31}, C_{37}, C_{42}, C_{48}, C_{53}).

HRMS: Calculated for $C_{45}H_{66}N_8O_{11}Na$ $(M+Na)^+$: 917.4743. Found $(M+Na)^+$: 917.4753.

_N_-Cbz-(_S_,_R_)-βCbu-NHHex 127:

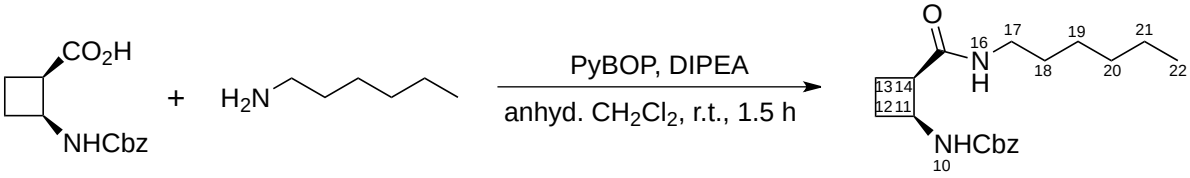

(_S_,_R_)-**16** **127**

DIPEA (1.1 mL, 6.4 mmol) and PyBOP (1.1 g, 2.2 mmol) were added to a solution of acid (_S_,_R_)-**16**[62] (0.44 g, 1.8 mmol) in anhydrous CH_2Cl_2 (20 mL). After five minutes stirring, *n*-hexylamine (0.35 mL, 2.6 mmol) was added and the mixture was stirred at room temperature for 1.5 h. The solvent was removed *in vacuo*, EtOAc (50 mL) was added and the solution was washed with saturated aqueous $NaHCO_3$ solution (1 x 20 mL), saturated aqueous NaCl solution (2 x 20 mL) and H_2O (1 x 20 mL). The organic layer was dried over anhydrous $MgSO_4$, filtered and the solvent was evaporated. The residue was purified by silica gel chromatography using hexane/EtOAc (1:3) as eluent to afford compound **127** (500 mg, 85%) as a white solid.

Spectroscopic data and physical constants of compound 127:

$[\alpha]_D$= -43 (*c* = 0.51, CH_2Cl_2)

M. p.: 83-86 ºC (hexane-EtOAc)

IR (cm^{-1}) ν 3316, 2927, 2856, 1688, 1642, 1545, 1524.

^{1}H NMR (360 MHz, $CDCl_3$) δ 0.86 (broad s, 3H, H_{22}), 1.25 (broad s, 6H, $H_{19\text{-}21}$), 1.34-1.48 (c.a., 2H, H_{18}), 1.90 (m, 1H), 2.05 (m, 1H), 2.23-2.38 (c.a., 2H), 3.15 (broad s, 3H, H_{14}, H_{17}), 4.45 (m, 1H, H_{11}), 4.98-5.12 (c.a., 2H, H_7), 5.55 (broad s, 1H, NH_{10}), 5.75 (broad s, 1H, NH_{16}), 7.32 (broad s, 5H, $H_{1\text{-}5}$).

^{13}C NMR (62.5 MHz, $CDCl_3$) δ 13.9 (C_{22}), 18.3 (C_{13}), 22.5 (C_{21}), 26.5 (C_{19}), 29.0, 29.6 (C_{12}, C_{18}), 31.4 (C_{20}), 39.4 (C_{17}), 46.1, 46.5 (C_{11}, C_{14}), 66.4 (C_7), 127.8, 127.9, 128.3 ($C_{1\text{-}5}$), 136.4 (C_6), 155.7 (C_9), 172.7 (C_{15}).

HRMS: Calculated for $C_{27}H_{38}N_4O_7Na$ $(M+Na)^+$: 553.2633. Found $(M+Na)^+$: 553.2629.

(TFA·)HCl·(_S_,_R_)-βCbu-NHHex 128:

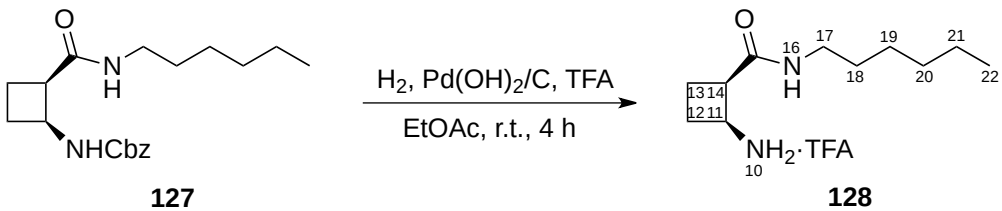

127 **128**

1.25 M HCl in EtOH (0.46 mL, 0.58 mmol) was added to a solution of compound **127** (190 mg, 0.57 mmol) in MeOH (20 mL). The mixture was hydrogenated over 20% $Pd(OH)_2/C$ (60 mg) at room temperature at 6-7 atm overnight. The catalyst was removed by filtration through Celite® and washed successively with CH_2Cl_2 and MeOH. The filtrate was evaporated *in vacuo* to provide **128** (178 mg, quantitative yield) as pale yellow oil. This reaction can also be performed in the presence of TFA.

Spectroscopic data of compound 128:

^{1}H NMR (250 MHz, MeOD-d_4) δ 0.88 (s, 3H, H_{22}), 1.29 (broad s, 6H, $H_{19\text{-}21}$), 1.39-1.55 (c.a., 2H, H_{18}), 2.16-2.45 (c.a., 4H, $H_{12\text{-}13}$), 3.05-3.20 (c.a., 2H, H_{17}), 3.35 (m, 1H, H_{14}), 3.97 (m, 1H, H_{11}).

^{13}C NMR (62.5 MHz, MeOD-d_4) δ 14.4 (C_{22}), 22.3 (C_{13}), 23.6 (C_{21}), 26.8, 27.7 (C_{12}, C_{19}), 30.3, 32.6 (C_{18}, C_{20}), 40.3, 41.5 (C_{14}, C_{17}), 47.3 (C_{11}), 174.7 (C_{15}).

***N*-Cbz-(*S*,*R*)-βCbu-GABA-(*S*,*R*)-βCbu-NHHex 126:**

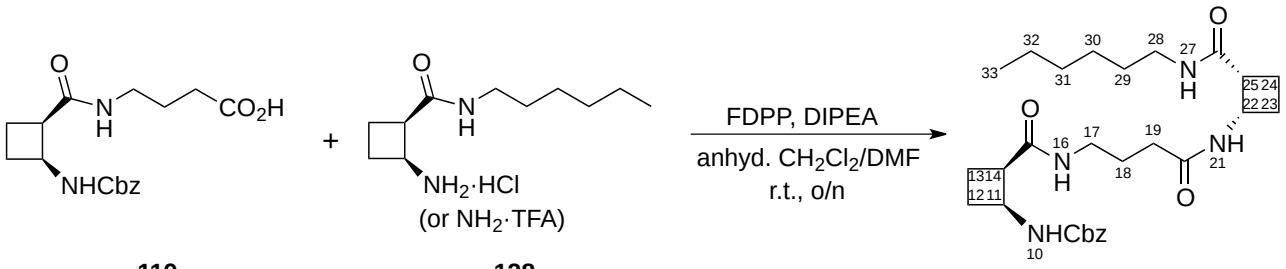

119 **128** **126**

DIPEA (0.3 mL, 1.7 mmol) and FDPP (300 mg, 0.80 mmol) were added to a solution of acid **119** (190 mg, 0.56 mmol) in a 20:1 mixture of anhydrous CH_2Cl_2/DMF (10.5 mL). After ten minutes stirring compound **128** (178 mg, 0.57 mmol) was added with anhydrous CH_2Cl_2 (10 mL) and anhydrous DMF (1 mL) and the mixture was stirred at room temperature overnight. The solvent was removed *in vacuo*, EtOAc (20 mL) was added and the solution was washed with saturated aqueous $NaHCO_3$ solution (1 x 20 mL), saturated aqueous NaCl solution (1 x 20 mL) and H_2O (1 x 20 mL). The organic layer was dried over anhydrous $MgSO_4$, filtered and the solvent was evaporated. The resulting residue was purified by Et_2O and pentane washes, stirring and disaggregating the solid to afford **126** (180 mg, 62%) as a white solid.

Spectroscopic data and physical constants of compound 126:

$[\alpha]_D$= +166.7 (*c* = 0.58, CH_2Cl_2)

M. p.: 148-152 ºC (Et_2O)

IR (cm^{-1}) ν 3305, 2934, 2858, 1688, 1639, 1530, 1454.

^{1}H NMR (360 MHz, $CDCl_3$) δ 0.90 (c.a., 3H, H_{33}), 1.22-1.37 (broad s, 6H, $H_{30\text{-}32}$), 1.39-1.51 (c.a., 2H, H_{29}), 1.64-1.87 (c.a., 2H), 1.87-2.22 (c.a., 6H), 2.25-2.41 (c.a., 4H), 3.05-3.43 (c.a., 6H, H_{14}, H_{17}, H_{25}, H_{28}), 4.49 (m, 1H, H_{11}), 4.67 (m, 1H, H_{22}), 4.99-5.15 (c.a., 2H, H_7), 5.71 (broad s, 1H, NH_{10}), 6.06 (broad s, 1H, NH), 6.35 (broad s, 1H, NH), 7.08 (broad s, 1H, NH), 7.35 (broad s, 5H, $H_{1\text{-}5}$).

^{13}C NMR (62.5 MHz, $CDCl_3$) δ 14.2 (C_{33}), 18.8, 19.6 (C_{13}, C_{24}), 22.7 (C_{32}), 25.1 (C_{30}), 26.8 (C_{18}), 28.8, 29.4 (C_{12}, C_{23}), 29.8 (C_{29}), 31.6 (C_{31}), 33.8 (C_{19}), 38.9 (C_{17}), 39.7 (C_{28}), 45.2 (C_{14}), 45.9, 46.4, 46.9 (C_{11}, C_{22}, C_{25}), 66.8 (C_7), 128.3, 128.7 ($C_{1\text{-}5}$), 136.7 (C_6), 156.0 (C_9), 172.4 (C_{20}), 173.4 (C_{15}, C_{26}).

HRMS: Calculated for $C_{27}H_{38}N_4O_7Na$ $(M+Na)^+$: 553.2633. Found $(M+Na)^+$: 553.2629.

5.2.2. 1,3-Cyclobutane derivatives

Benzyl (1*S*,3*R*)-3-acetyl-2,2-dimethylcyclobutylmethylcarbamate 169:

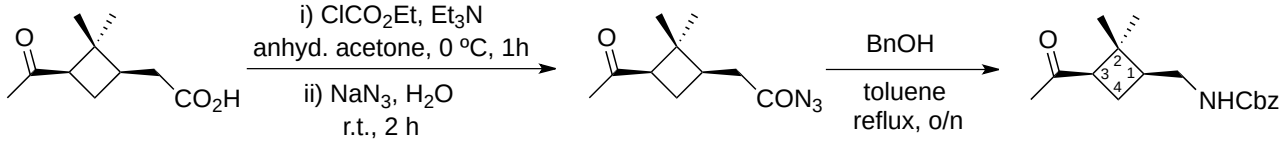

168 **169**

To an ice-cooled solution of acid **168**[328] (2.95 g, 16.0 mmol) in anhydrous acetone (50 mL), Et_3N (3.8 mL, 28 mmol) and $ClCO_2Et$ (2.6 mL, 27 mmol) were added. The mixture was stirred at 0 ºC for 1 h. A solution of NaN_3 (1.5 g, 23 mmol) in H_2O (60 mL) was then added and the mixture was stirred at room temperature for 2 h. The aqueous layer was extracted with CH_2Cl_2 (3 x 90 mL) and the organic layer was dried over anhydrous $MgSO_4$, filtered and evaporated under reduced pressure at a temperature lower than 40 ºC to afford the corresponding acylazide. Immediately afterwards the acylazide was dissolved in ^{t}BuOH (30 mL). The mixture was stirred under reflux overnight. The solvent was removed *in vacuo* and the residue was purified by silica gel chromatography using hexane/EtOAc (2:1) as eluent to afford compound **169** (1.98 g, 48%) as pale yellow oil.

Spectroscopic data and physical constants of compound 169:

$[\alpha]_D$= -4.9 (*c* = 1.21, CH_2Cl_2)

IR (cm^{-1}) ν 3342, 2952, 1701, 1534.

^{1}H NMR (360 MHz, $CDCl_3$) δ 0.89 (s, 3H, Me_{trans}), 1.31 (s, 3H, Me_{cis}), 1.83 (m, 1H, H_4), 1.95 (q, $^3J_{H\text{-}H}$= 10.6 Hz, 1H, H_4), 2.02 (s, 3H, COMe), 2.12 (m, 1H, H_1), 2.81 (dd, $^3J_{H\text{-}H}$= 7.5 Hz, $^3J_{H\text{-}H}$= 10.0 Hz, 1H, H_3), 3.08 (m, 1H, C*H*$_2$NHCbz), 3.18 (m, 1H, C*H*$_2$NHCbz), 4.72 (broad s, 1H, N*H*Cbz), 5.04-5.12 (c.a., 2H, C*H*$_2$Ph), 7.28-7.39 (c.a., 5H, CH_2*Ph*).

^{13}C NMR (90 MHz, $CDCl_3$) δ 17.3 (C_4), 21.1 (Me_{cis}), 30.3 (CO*Me*), 30.9 (Me_{trans}), 41.3 (C_1), 41.7 (*C*H_2NHCbz), 42.7 (C_2), 53.7 (C_3), 66.8 (*C*H_2Ph), 128.2, 128.6 (CH_2*Ph*), 136.6 (C_{ipso} Ph), 156.3 ($CO_{carbamate}$), 207.6 (CO_{acetyl}).

HRMS: Calculated for $C_{17}H_{23}NO_3Na$ $(M+Na)^+$: 312.1570. Found $(M+Na)^+$: 312.1570.

^{t}Butyl-(1*S*,3*R*)-3-acetyl-2,2-dimethylcyclobutylmethylcarbamate 205:

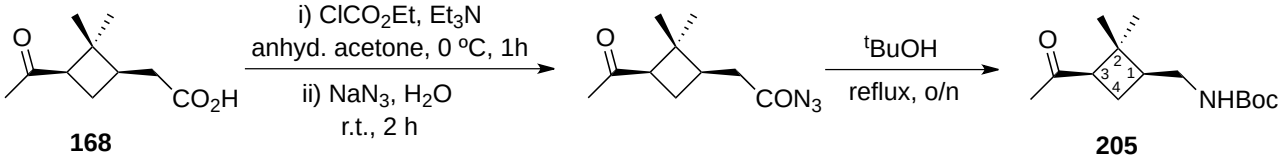

To an ice-cooled solution of acid **168**[328] (2.95 g, 16.0 mmol) in anhydrous acetone (50 mL), Et_3N (3.8 mL, 28 mmol) and $ClCO_2Et$ (2.6 mL, 27 mmol) were added. The mixture was stirred at 0 ºC for 1 h. A solution of NaN_3 (1.5 g, 23 mmol) in H_2O (60 mL) was then added and the mixture was stirred at room temperature for 2 h. The aqueous layer was extracted with CH_2Cl_2 (3 x 90 mL) and the organic layer was dried over anhydrous $MgSO_4$, filtered and evaporated under reduced pressure at a temperature lower than 40 ºC to afford the corresponding acylazide. Immediately afterwards the acylazide was dissolved in ^{t}BuOH (30 mL). The mixture was stirred under reflux overnight. The solvent was removed *in vacuo* and the residue was purified by silica gel chromatography using hexane/EtOAc (2:1) as eluent to afford compound **205** (1.98 g, 48%) as pale yellow oil.

Spectroscopic data and physical constants of compound 205:

$[\alpha]_D$= -44.6 (*c* = 1.02, CH_2Cl_2)

IR (cm^{-1}) ν 3351, 2954, 2926, 1695, 1518.

^{1}H NMR (250 MHz, $CDCl_3$) δ 0.81 (s, 3H, Me_{trans}), 1.24 (s, 3H, Me_{cis}), 1.34 (s, 9H, CMe_3), 1.74 (m, 1H, H_4), 1.86 (q, $^3J_{H\text{-}H}$= 10.7 Hz, 1H, H_4), 1.95 (s, 3H, COMe), 2.03 (m, 1H, H_1), 2.74 (dd, $^3J_{H\text{-}H}$= 7.6 Hz, $^3J_{H\text{-}H}$= 10.0 Hz, 1H, H_3), 2.91 (m, 1H, C*H*$_2$NHBoc), 3.02 (m, 1H, C*H*$_2$NHBoc), 4.52 (broad s, 1H, N*H*Cbz).

^{13}C NMR (62.5 MHz, $CDCl_3$) δ 17.1 (Me_{trans}), 21.1 (C_4), 28.4 (C*Me*$_3$), 30.2 (CO*Me*), 30.7 (Me_{cis}), 41.0 (*C*H_2NHBoc), 41.3 (C_1), 42.7 (C_2), 53.6 (C_3), 79.0 (*C*Me_3), 155.8 ($CO_{carbamate}$), 207.6 (CO_{acetyl}).

HRMS: Calculated for $C_{14}H_{25}NO_3Na$, $(M+Na)^+$: 278.1727. Found $(M+Na)^+$: 278.1732.

N-Cbz-δCbu 170:

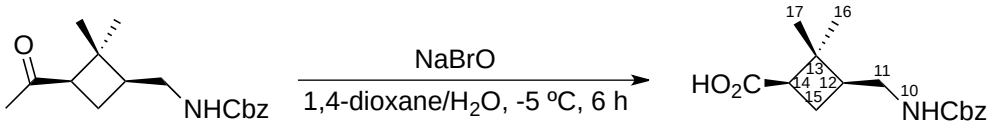

169 **170**

To an ice/NaCl-cooled solution of **169** (1.50 g, 5.18 mmol) in a 3:1 mixture of 1,4-dioxane/H_2O (70 mL), a solution of Br_2 (3 mL, 117 mmol) and aqueous NaOH solution (9.3 g, 233 mmol) in H_2O (200 mL) NaBrO (7.4 mL, 54 mmol) was added. The mixture was stirred at -5 ºC for 6 h. An aqueous solution of $NaHSO_3$ was added until the mixture became white before being acidified to pH 2 with 2 M HCl. The aqueous layer was extracted with CH_2Cl_2 (3 x 120 mL) and the organic layer was dried over anhydrous $MgSO_4$, filtered and evaporated under reduced pressure to afford the corresponding carboxylic acid **170** (1.51 g, quantitative yield) as a transparent oil. This compound was used directly in next step without further purification.

Spectroscopic data and physical constants of compound 170:

$[\alpha]_D$= +14.4 (*c* = 1.33, CH_2Cl_2)

IR (cm^{-1}) ν 3340, 2950, 1701, 1542.

^{1}H NMR (250 MHz, $CDCl_3$) δ 0.94 (s, 3H, H_{16}), 1.14 (s, 3H, H_{17}), 1.70-2.11 (c.a., 3H, $H_{15,}$ H_{12}), 2.63 (dd, $^3J_{H\text{-}H}$= 7.9 Hz, $^3J_{H\text{-}H}$= 10.3 Hz, 1H, H_{14}), 2.95-3.23 (c.a., 2H, H_{11}), 4.60 and 5.80 (broad s, 1H, NH_{10}), 4.99 (s, 2H, H_7), 7.25 (s, 5H, $H_{1\text{-}5}$), 8.86 (broad s, 1H, CO_2H).

^{13}C NMR (62.5 MHz, $CDCl_3$) δ 17.6 (C_{16}), 22.4 (C_{15}), 30.6 (C_{17}), 41.7 (C_{12}), 41.9 (C_{11}), 42.3 (C_{13}), 45.7 (C_{14}), 66.9 (C_7), 128.2, 128.3, 128.76($C_{1\text{-}5}$), 136.6 (C_6), 156.4 (C_9), 178.1 (C_{18}).

HRMS: Calculated for $C_{45}H_{66}N_8O_{11}Na$ $(M+Na)^+$: 314.1363. Found $(M+Na)^+$: 314.1358.

***N*-Cbz-δCbu-OMe 156:**

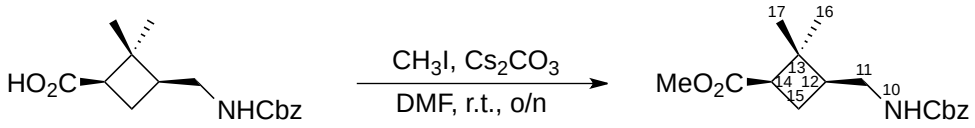

170 **156**

MeI (0.45 mL, 7.2 mmol) and Cs_2CO_3 (2.4 g, 7.4 mmol) were added to a solution of acid **170** (1.34 g, 4.60 mmol) in DMF (20 mL). The mixture was stirred at room temperature overnight. CH_3I excess was removed *in vacuo* and EtOAc (30 mL) was added. The solution was washed with saturated aqueous $NaHCO_3$ solution (3 x 30 mL), saturated aqueous NaCl solution (1 x 30 mL) and with H_2O (1 x 30 mL). The resulting organic layer was then dried over anhydrous $MgSO_4$, filtered and solvents removed under reduced pressure. The solid was purified by silica gel chromatography using EtOAc/hexane (1:3) to afford **156** (1.17 g, 84%) as pale yellow oil.

Spectroscopic data and physical constants of compound 156:

$[\alpha]_D$= +9.2 (*c* = 4.45, CH_2Cl_2)

IR (cm^{-1}) ν 3351, 2952, 1720 (wide peak), 1534.

^{1}H NMR (360 MHz, $CDCl_3$) δ 0.86 (s, 3H, H_{16}), 1.12 (s, 3H, H_{17}), 1.77-1.97 (c.a., 2H, H_{15}), 2.03 (m, 1H, H_{12}), 2.60 (dd, $^3J_{H\text{-}H}$= 8.4 Hz, $^3J_{H\text{-}H}$= 10.2 Hz, 1H, H_{14}), 3.05 (m, 1H, H_{11}), 3.13 (m, 1H, H_{11}), 3.56 (s, 3H, H_{20}), 4.49 (broad s, 1H, NH_{10}), 4.99 (s, 2H, H_7), 7.25 (s, 5H, $H_{1\text{-}5}$).

^{13}C NMR (90 MHz, $CDCl_3$) δ 17.6 (C_{16}), 22.6 (C_{15}), 30.5 (C_{17}), 41.6 (C_{12}), 41.8 (C_{11}), 42.1 (C_{13}), 45.7 (C_{14}), 51.3 (C_{20}), 66.7 (C_7), 128.1, 128.6 ($C_{1\text{-}5}$), 136.7 (C_6), 156.4 (C_9), 173.3 (C_{18}).

HRMS: Calculated for $C_{45}H_{66}N_8O_{11}Na$ $(M+Na)^+$: 328.1519. Found $(M+Na)^+$: 328.1518.

(TFA·)δCbu-OMe 171:

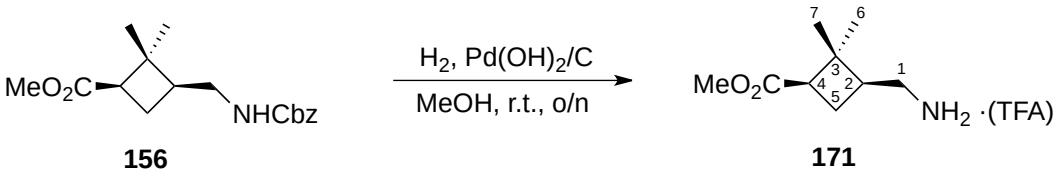

156 **171**

A solution of **156** (1.79 g, 5.86 mmol) in MeOH (60 mL) was hydrogenated over 20% $Pd(OH)_2/C$ (540 mg) at room temperature at 6-7 atm overnight. The catalyst was removed by filtration through Celite® and washed successively with CH_2Cl_2 and MeOH. The filtrate was evaporated *in vacuo* to provide **171** (1.0 g, quantitative yield) as yellow oil. This compound was used in next step without further purification. This reaction can be also performed in the presence of TFA.

Spectroscopic data of compound 171:

^{1}H NMR (250 MHz, MeOD-d_4) δ 0.99 (s, 3H, H_6), 1.23 (s, 3H, H_7), 1.87-2.11 (c.a., 2H, H_5), 2.28 (m, 1H, H_2), 2.78 (dd, $^3J_{H\text{-}H}$= 10.2 Hz, $^3J_{H\text{-}H}$= 7.9 Hz, 1H, H_4), 3.14-3.42 (c.a., 2H, H_1), 3.67 (s, 3H, H_{10}).

^{13}C NMR (90 MHz, $CDCl_3$) δ 17.8 (C_6), 22.6 (C_5), 30.5 (C_7), 40.7, 40.8, 42.1 ($C_{1\text{-}3}$), 45.7 (C_4), 51.5 (C_{21}), 173.2 (C_8).

***N*-Boc-GABA-γCbu-OMe 165:**

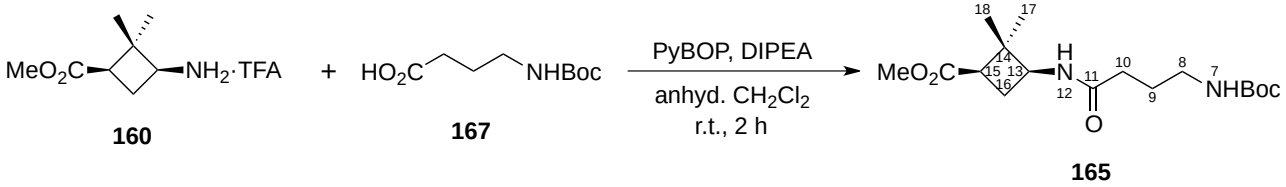

160 **167** **165**

DIPEA (1.56 mL, 8.9 mmol) and PyBOP (1.4 g, 2.7 mmol) were added to a solution of acid **167**[325] (430 mg, 2.12 mmol) in anhydrous CH_2Cl_2 (25 mL). After five minutes stirring, amino acid salt **160**[16a] (575 mg, 2.12 mmol) was added and the mixture was stirred at room temperature for 2 h. EtOAc (40 mL) was added and the solution was washed with saturated aqueous $NaHCO_3$ solution (3 x 30 mL) and saturated aqueous NaCl solution (1 x 40 mL). The organic layer was dried over anhydrous $MgSO_4$, filtered and the solvent was evaporated *in vacuo*. The resulting residue was purified by silica gel chromatography using hexane/EtOAc (1:2) as eluent to afford **165** (600 mg, 84%) as white solid.

Spectroscopic data of compound 165:

^{1}H NMR (360 MHz, $CDCl_3$) δ 0.87 (s, 3H, H_{17}), 1.27 (s, 3H, H_{18}), 1.40 (s, 9H, $H_{1\text{-}3}$), 1.76 (p, $^{3}J_{H\text{-}H}$= 6.8 Hz, 2H, H_9), 2.13 (m, 1H, H_{16}), 2.19 (t, $^{3}J_{H\text{-}H}$= 7.0 Hz, 2H, H_{13}), 2.30 (dd, $^{3}J_{H\text{-}H}$= 12 Hz, $^{3}J_{H\text{-}H}$= 8.0 Hz, 1H, H_{16}), 2.58 (dd, $^{3}J_{H\text{-}H}$= 7.7 Hz, $^{3}J_{H\text{-}H}$= 10.0 Hz, 1H, H_{15}), 3.12 (q, $^{3}J_{H\text{-}H}$= 6.1 Hz, 2H, H_8), 3.65 (s, 3H, H_{21}), 4.08 (q, $^{3}J_{H\text{-}H}$= 8.2 Hz, 1H, H_{13}), 4.87 (broad s, 1H, NH_7), 6.53 (broad s, 1H, NH_{12}).

^{13}C NMR (90 MHz, $CDCl_3$) δ 17.4 (C_{17}), 26.1 (C_{16}), 26.5 (C_9), 28.5 ($C_{1\text{-}3}$), 29.1 (C_{18}), 33.5 (C_{10}), 39.9 (C_8), 43.3 (C_{15}), 46.2 (C_{14}), 50.1 (C_{13}), 51.6 (C_{21}), 79.5 (C_4), 156.7 (C_6), 172.8 (C_{11}), 173.4 (C_{19}).

N-Cbz-GABA-γCbu-OMe 164:

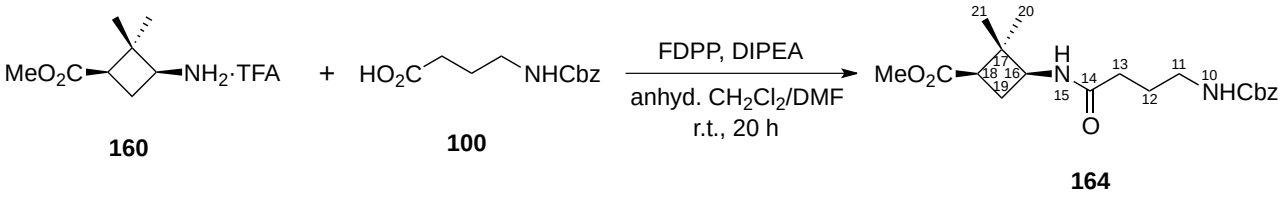

160 **100** **164**

DIPEA (3.0 mL, 17 mmol) and FDPP (2.22 g, 5.81 mmol) were added to a solution of acid **100**[326] (1.14 g, 4.81 mmol) in anhydrous CH_2Cl_2 (30 mL). After five minutes stirring, amino acid salt **160**[16a] (1.30 g, 4.79 mmol) was added and the mixture was stirred at room temperature for 20 h. EtOAc (60 mL) was added and the solution was washed with saturated aqueous $NaHCO_3$ solution (2 x 50 mL) and saturated aqueous NaCl solution (1 x 40 mL). The organic layer was dried over anhydrous $MgSO_4$, filtered and the solvent was evaporated *in vacuo*. The resulting residue was purified by silica gel chromatography using hexane/EtOAc (1:2) as eluent to afford **164** (1.08 g, 60%) as white solid.

Spectroscopic data and physical constants of compound 164:

$[\alpha]_D$= -35.1 (*c* = 0.57, CH_2Cl_2)

M. p.: 105-108 ºC (EtOAc-hexane)

IR (cm^{-1}) ν 3390, 3315, 3035, 2953, 1721, 1708, 1696, 1661, 1536.

^{1}H NMR (250 MHz, $CDCl_3$) δ 0.79 (s, 3H, H_{20}), 1.20 (s, 3H, H_{21}), 1.72 (p, $^3J_{H-H}$= 7.1 Hz, 2H, H_{12}), 2.03 (p, $^3J_{H-H}$= 12.1 Hz, 1H, H_{19}), 2.12 (t, $^3J_{H-H}$= 7.0 Hz, 2H, H_{13}), 2.24 (dd, $^3J_{H-H}$= 12 Hz, $^3J_{H-H}$= 8.0 Hz, 1H, H_{19}), 2.51 (dd, $^3J_{H-H}$= 8.2 Hz, $^3J_{H-H}$= 10.2 Hz, 1H, H_{18}), 3.14 (q, $^3J_{H-H}$= 7.0 Hz, 2H, H_{11}), 3.58 (s, 3H, H_{24}), 4.00 (q, $^3J_{H-H}$= 8.1 Hz, 1H, H_{16}), 4.93 (broad s, 1H, NH_{10}), 5.00 (s, 2H, H_7), 5.97 (broad d, $^3J_{H-H}$= 8.0 Hz, 1H, NH_{15}), 7.25 (broad s, 5H, H_{1-5}).

^{13}C NMR (62.5 MHz, $CDCl_3$) δ 17.0 (C_{20}), 25.2 (C_{13}), 25.9 (C_{12}), 28.8 (C_{21}), 33.1 (C_{19}), 40.2 (C_{11}), 42.8 (C_{18}), 46.0 (C_{17}), 49.7 (C_{16}), 51.2 (C_{24}), 66.3 (C_7), 127.8, 128.3 (C_{1-5}), 136.5 (C_6), 156.7 (C_9), 172.7 (C_{14}), 173.1 (C_{22}).

HRMS: Calculated for $C_{20}H_{28}N_2O_5Na$ $(M+Na)^+$: 399.1890. Found $(M+Na)^+$: 399.1894.

(TFA·)GABA-γCbu-OMe 166:

Method A:

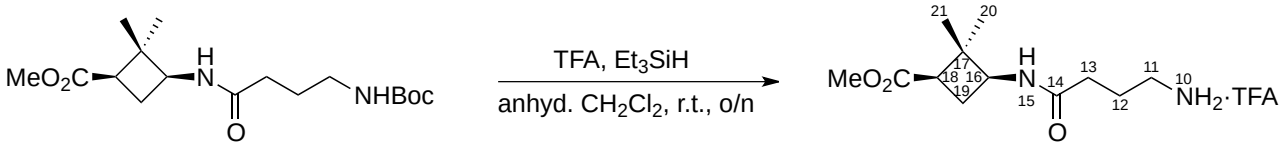

165 **166**

Et_3SiH (0.35 mL, 2.2 mmol) and TFA (0.90 mL, 12 mmol) were added to a solution of amino acid **165** (330 mg, 0.88 mmol) in anhydrous CH_2Cl_2 (40 mL). The mixture was stirred at room temperature overnight. The solvent was removed *in vacuo* and excess of TFA was lyophilized to provide salt **166** (312 mg, quantitative yield) as white doughy solid. This compound was used in next step without further purification.

Method B:

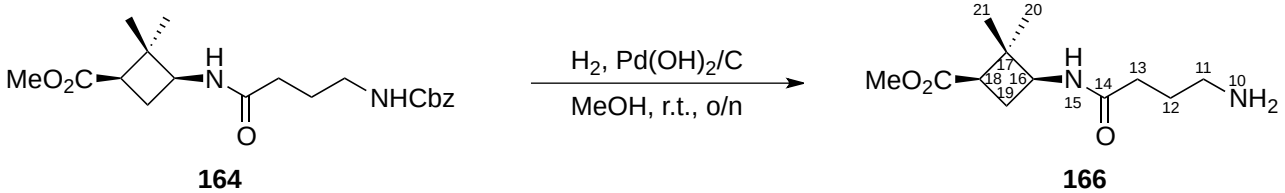

164 **166**

A solution of **164** (560 mg, 1.49 mmol) in MeOH (30 mL) was hydrogenated over 20% $Pd(OH)_2/C$

(170 mg) at room temperature at 6 atm overnight. The catalyst was removed by filtration through Celite® and washed successively with CH_2Cl_2 and MeOH. The filtrate was evaporated *in vacuo* to provide **166** (360 mg, quantitative yield) as yellow oil. This compound was used in next step without further purification.

Spectroscopic data of compound 166:

^{1}H NMR (250 MHz, MeOD-d_4) δ 0.87 (s, 3H, H_{20}), 1.26 (s, 3H, H_{21}), 1.83 (p, $^3J_{H\text{-}H}$= 7.0 Hz, 2H, H_{12}), 2.21 (t, $^3J_{H\text{-}H}$= 9.0 Hz, 2H, H_{19}), 2.29 (t, $^3J_{H\text{-}H}$= 7.0 Hz, 2H, H_{13}), 2.66 (t, $^3J_{H\text{-}H}$= 9.7 Hz, $^3J_{H\text{-}H}$= 8.5 Hz, 1H, H_{18}), 2.80 (t, $^3J_{H\text{-}H}$= 7.1 Hz, 2H, H_{11}), 3.66 (s, 3H, H_{24}), 4.01 (t, $^3J_{H\text{-}H}$= 9.0 Hz, 1H, H_{16}).

^{13}C NMR (62.5 MHz, MeOD-d_4) δ 17.6 (C_{20}), 25.8 (C_{13}), 27.2 (C_{12}), 29.5 (C_{21}), 33.8 (C_{19}), 41.2 (C_{11}), 44.0 (C_{18}), 47.4 (C_{17}), 51.2 (C_{16}), 51.9 (C_{24}), 174.6, 175.1 (C_{14}, C_{22}).

Gly-NHHex 194:

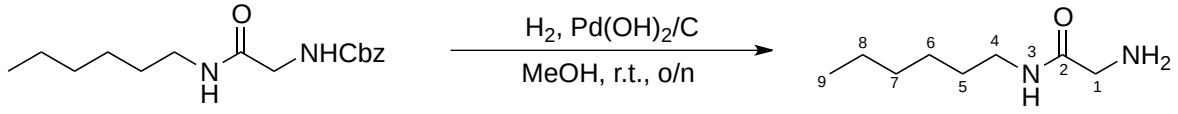

193 **194**

A solution of **193**[330] (140 mg, 0.48 mmol) in MeOH (20 mL) was hydrogenated over 20% $Pd(OH)_2$/C (50 mg) at room temperature at 7-8 atm overnight. The catalyst was removed by filtration through Celite® and washed successively with CH_2Cl_2 and MeOH. The filtrate was evaporated *in vacuo* to provide **194** (76 mg, quantitative yield) as yellow oil. This compound was used in next step without further purification.

Spectroscopic data of compound 194:

^{1}H NMR (360 MHz, $CDCl_3$) δ 0.84 (t, $^3J_{H\text{-}H}$= 6.6 Hz, 3H, H_9), 1.22-1.31 (c.a., 6H, H_6, H_7, H_8), 1.40-1.52 (c.a., 2H, H_5), 3.02 (m, 1H, H_1), 3.13-3.26 (c.a., 2H, H_4), 3.36 (broad s, 1H, H_1), 7.15 (broad s, 2H, NH_2).

^{13}C NMR (90 MHz, $CDCl_3$) δ 14.1 (C_9), 22.6 (C_8), 26.7 (C_6), 29.6 (C_5), 31.6 (C_7), 39.4 (C_4), 49.9 (C_1), 171.9 (C_2).

N(CH_2CO-NHHex)$_3$ 147:

Method A:

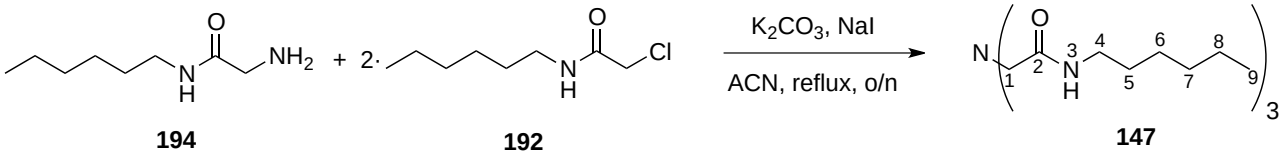

194 **192** **147**

Amine **194** (78 mg, 0.49 mmol), chloride derivative **192**[329] (170 mg, 0.96 mmol), K_2CO_3 (0.27g, 1.96 mmol) and NaI (0.15 g, 0.98 mmol) were mixed in ACN (20 mL). The mixture was stirred under reflux overnight. The solvent was removed *in vacuo* and EtOAc (40 mL) was added and the solution was washed with saturated aqueous NaCl solution (2 x 40 mL) and water (1 x 30 mL). The organic layer was dried over anhydrous $MgSO_4$, filtered and the solvent was evaporated *in vacuo*. The resulting residue was purified by dissolving it again in EtOAc (50 mL) and washing with 2 M HCl solution (3 x 20 mL) and pentane-ether to afford **147** (470 mg, 95%) as white solid.

Method B:

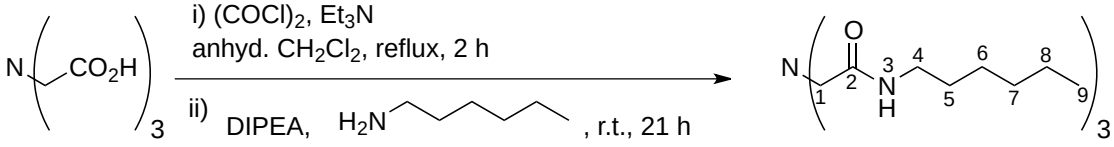

157 **147**

2 M solution of oxalyl chloride in CH_2Cl_2 (0.82 mL, 1.6 mmol) was added to a suspension of triacid **157** (101.3 mg, 0.53 mmol) in anhydrous CH_2Cl_2 (20 mL). Few drops of anhydrous DMF were added and the mixture was stirred under reflux for 2 h. *n*-Hexylamine (0.24 mL, 1.8 mmol) was added, the mixture was left to reach room temperature and Et_3N (0.26 mL, 1.9 mmol) was added. The mixture was stirred at room temperature for 21 h. The solvent was removed under reduced pressure, EtOAc (20 mL) was added and the solution was washed with saturated aqueous $NaHCO_3$ solution (2 x 20 mL), saturated aqueous NaCl solution (1 x 20 mL) and water (1 x 20 mL). The organic layer was dried over anhydrous $MgSO_4$, filtered and evaporated *in vacuo* to provide 210 mg of pale brown solid. The crude was later purified by precipitation using Et_2O and pentane to afford triamide **147** (140 mg, 60%) as white solid.

Spectroscopic data and physical constants of compound 147:

M. p.: 82-85 ºC (Et_2O-pentane)

IR (cm^{-1}) ν 3283, 3082, 2928, 2858, 1648, 1545

^{1}H NMR (360 MHz, $CDCl_3$) δ 0.87 (s, 3H, H_9), 1.28 (broad s, 6H, H_6, H_7, H_8), 1.44-1.55 (c.a., 2H, H_5), 3.24 (q, $^3J_{H\text{-}H}$= 6.7 Hz, 2H, H_4), 3.27 (s, 2H, H_1), 7.35 (broad s, 1H, N-H_3).

^{13}C NMR (90 MHz, $CDCl_3$) δ 14.1 (C_9), 22.7 (C_8), 26.8 (C_6), 29.6 (C_5), 31.6 (C_7), 39.7 (C_4), 60.9 (C_1), 170.4 (C_2).

HRMS: Calculated for $C_{24}H_{48}N_4O_3Na$ $(M+Na)^+$: 463.3619. Found $(M+Na)^+$: 463.3620.

HCl·Gly-OBn 175:

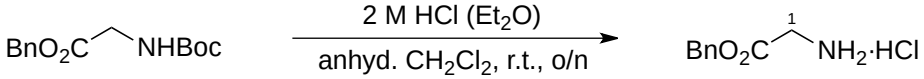

174 **175**

2 M HCl in Et_2O (30 mL, 60 mmol) was added to a solution of compound **174**[331] (1.23 g, 4.64 mmol) in anhydrous CH_2Cl_2 (30 mL). The mixture was stirred at room temperature overnight. The solvent was removed under reduced pressure to provide **175** (935 mg, quantitative yield) as an oil.

Spectroscopic data of compound 175:

^{1}H NMR (360 MHz, MeOD-d_4) δ 3.89 (s, 2H, H_1), 5.30 (s, 2H, H_4), 7.28-7.44 (c.a., 5H, $H_{6\text{-}10}$), 7.349 (c.a., 3H, NH_2·HCl).

N(CH_2CO-Gly-OBn)$_3$ 144:

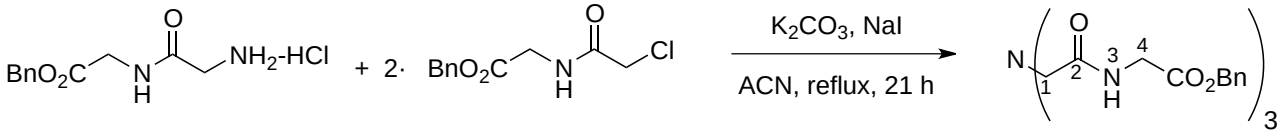

178 **177** **144**

Salt **178**[333] (317 mg, 1.23 mmol), chloride derivative **177**[332] (590 mg, 2.44 mmol), K_2CO_3 (0.68 g, 4.94 mmol) and NaI (0.50 g, 3.27 mmol) were mixed in ACN (50 mL). The mixture was stirred under reflux for 21 h. The solvent was removed *in vacuo* and EtOAc (40 mL) was added and the solution was washed with saturated aqueous $NaHCO_3$ solution (1 x 40 mL), saturated aqueous NaCl solution (2 x 40 mL) and water (1 x 30 mL). The organic layer was dried over anhydrous $MgSO_4$, filtered and the solvent was evaporated *in vacuo*. The resulting residue was purified by y silica gel chromatography using EtOAc and MeOH/CH_2Cl_2 (1:20) as eluents to provide a sticky grey solid. It was later purified by Et_2O digestion at 0 ºC to afford **144**[283] (300 mg, 39%) as white solid.

Spectroscopic data and physical constants of compound 144:

M. p.: 104-106 ºC (Et_2O-pentane)

IR (cm^{-1}) ν 3290, 3066, 3035, 2919, 2849, 1746, 1662, 1540.

^{1}H NMR (360 MHz, $CDCl_3$) δ 3.44 (s, 2H, H_1), 4.07 (d, $^3J_{H\text{-}H}$= 4.3 Hz, 2H, H_4), 5.13 (s, 2H, H_7), 7.33 (s, 5H, $H_{9\text{-}13}$), 7.73 (broad s, 1H, N-H_3).

^{13}C NMR (90 MHz, $CDCl_3$) δ 41.2 (C_4), 58.7 (C_1), 67.5 (C_7), 128.5, 128.7, 128.8 ($C_{9\text{-}13}$), 135.2 (C_8), 170.8 (C_2, C_5).

HRMS: Calculated for $C_{33}H_{36}N_4O_9Na$ $(M+Na)^+$: 655.2374. Found $(M+Na)^+$: 655.2365.

ClCH$_2$CO-Gly-βAla-OBn 184:

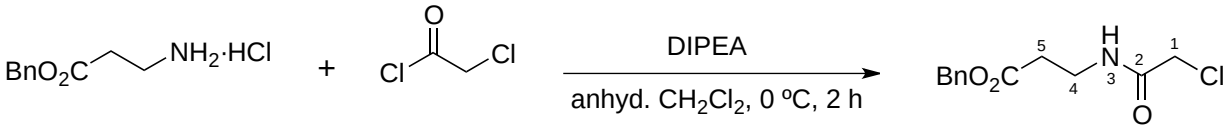

182 **184**

DIPEA (1.0 mL, 5.7 mmol) was added to an ice-cooled solution of salt **182**[335] (1.235 g, 5.73 mmol) in anhydrous CH_2Cl_2 (50 mL). Chloroacetyl chloride (0.55 mL, 6.8 mmol) and DIPEA (1.0 mL, 5.7 mmol) were slowly added and the mixture was stirred for 2 h. The solvent was removed under reduced pressure, EtOAc (50 mL) was added and the solution was washed with saturated aqueous $NaHCO_3$ solution (2 x 50 mL) and saturated aqueous NaCl solution (1 x 50 mL). The organic layer was dried over anhydrous $MgSO_4$, filtered and evaporated *in vacuo*. The resulting residue was purified by silica gel chromatography using hexane/EtOAc (1:2) as eluent to afford **184** (800 mg, 55%) a pale brown oil.

Spectroscopic data and physical constants of compound 184:

$[\alpha]_D$= -9.8 (*c* = 0.81, CH_2Cl_2)

IR (cm^{-1}) ν 3307, 3034, 2950, 1728, 1658, 1533.

^{1}H NMR (360 MHz, $CDCl_3$) δ 2.53 (t, $^3J_{H\text{-}H}$= 6.2 Hz, 2H, H_5), 3.50 (q, $^3J_{H\text{-}H}$= 6.2 Hz, 2H, H_4), 3.92 (s, 2H, H_1), 5.06 (s, 2H, H_8), 7.04 (broad s, 1H, N-H_3), 7.27 (s, 5H, $H_{10\text{-}14}$).

^{13}C NMR (90 MHz, $CDCl_3$) δ 33.8 (C_5), 35.2 (C_4), 42.5 (C_1), 66.7 (C_8), 128.3, 128.4, 128.6 ($C_{10\text{-}14}$), 135.5 (C_9), 166.1 (C_2), 172.9 (C_6).

HRMS: Calculated for $C_{12}H_{14}ClNO_3Na$ $(M+Na)^+$: 278.0554. Found $(M+Na)^+$: 278.0560.

***N*-Boc-Gly-βAla-OBn 183:**

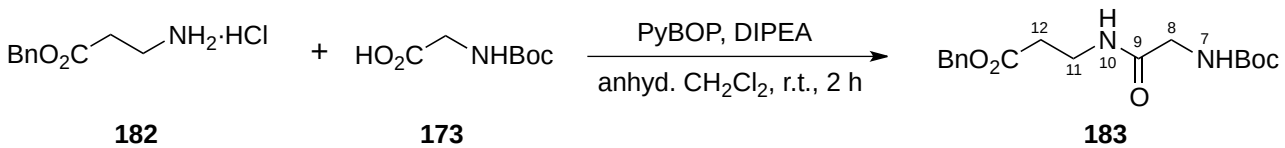

182 **173** **183**

DIPEA (1.5 mL, 8.6 mmol) and PyBOP (2.0 g, 3.9 mmol) were added to a solution of acid **173**[294] (500 mg, 2.4 mmol) in anhydrous CH_2Cl_2 (20 mL). After five minutes stirring, salt **182**[335] (618 mg, 2.9 mmol) was added and the mixture was stirred at room temperature for 2 h. EtOAc (50 mL) was added and the solution was washed with saturated aqueous $NaHCO_3$ solution (2 x 40 mL) and saturated aqueous NaCl solution (1 x 40 mL). The organic layer was dried over anhydrous $MgSO_4$,

filtered and the solvent was evaporated *in vacuo*. The resulting residue was purified by silica gel chromatography using hexane/EtOAc (1:2) as eluent to afford **183** (760 mg, 79%) as dense oil.

Spectroscopic data and physical constants of compound 183:

$[\alpha]_D$= -9.8 (*c* = 0.81, EtOAc)

IR (cm^{-1}) ν 3306, 2943, 1732, 1662, 1539.

^{1}H NMR (250 MHz, $CDCl_3$) δ 1.44 (s, 9H, ,$H_{1\text{-}3}$), 2.59 (t, $^3J_{H\text{-}H}$= 6.1 Hz, 2H, H_{12}), 3.55 (q, $^3J_{H\text{-}H}$= 6.1 Hz, 2H, H_{11}), 3.74 (broad s, 2H, H_8), 5.12 (s, 2H, H_{15}), 5.16 (broad s, 1H, NH_7), 6.69 (broad s, 1H, NH_{10}), 7.34 (s, 5H, $H_{17\text{-}21}$).

^{13}C NMR (62.5 MHz, $CDCl_3$) δ 28.4 ($C_{1\text{-}3}$), 33.9 (C_{12}), 35.2 (C_{11}), 44.4 (C_8), 66.8 (C_{15}), 80.6 (C_4), 128.5, 128.6, 128.8 ($C_{17\text{-}21}$), 135.6 (C_{16}), 156.2 (C_6), 172.3 (C_9 , C_{13}).

HRMS: Calculated for $C_{17}H_{24}N_2O_5Na$ $(M+Na)^+$: 359.1577. Found $(M+Na)^+$: 359.1584.

HCl·Gly-βAla-OBn 185:

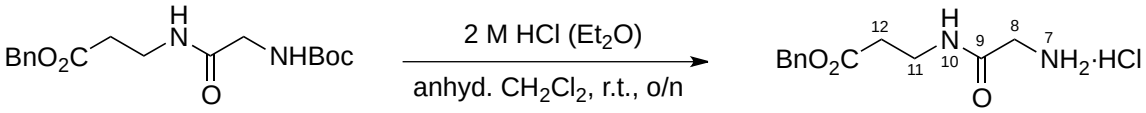

183 **185**

2 M HCl in Et_2O (8 mL, 16 mmol) was added to a solution of compound **183** (480 mg, 1.43 mmol) in anhydrous CH_2Cl_2 (20 mL). The mixture was stirred at room temperature overnight. The solvent was removed under reduced pressure to provide salt **185** (310 mg, 90%) as white solid.

Spectroscopic data of compound 185:

^{1}H NMR (360 MHz, MeOD-d_4) δ 2.57 (broad s, 2H, H_{12}), 3.52 (broad s, 2H, H_{11}), 3.67 (broad s, 2H, H_8), 5.15 (s, 2H, H_{15}), 7.35 (s, 5H, $H_{17\text{-}21}$).

N(CH_2CO-βAla-OBn)$_3$ 148:

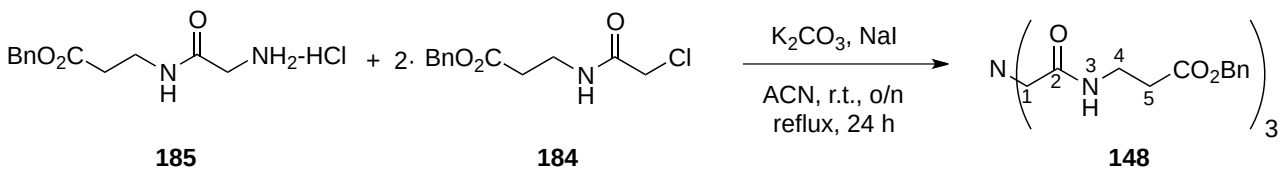

185 **184** **148**

Amine **185** (310 mg, 1.14 mmol), chloride derivative **184** (600 mg, 2.35 mmol), K_2CO_3 (0.81 g, 5.88 mmol) and NaI (0.39 g, 2.54 mmol) were mixed in ACN (30 mL). The mixture was stirred at room temperature overnight and then under reflux for 24 h. The solvent was removed *in vacuo* and EtOAc (30 mL) was added and the solution was washed with saturated aqueous $NaHCO_3$ solution (1 x 30 mL) and saturated aqueous NaCl solution (1 x 20 mL). The organic layer was dried over anhydrous $MgSO_4$, filtered and the solvent was evaporated *in vacuo*. The resulting residue was purified by silica gel chromatography using EtOAc, CH_2Cl_2 and CH_2Cl_2/MeOH (30:1) as eluents to afford **148** (330 mg, 43%) as a dense oil.

Spectroscopic data of compound 148:

IR (cm^{-1}) ν 3291, 3066, 2947, 1731, 1655, 1543.

^{1}H NMR (250 MHz, $CDCl_3$) δ 2.60 (t, $^3J_{H\text{-}H}$= 6.2 Hz, 2H, H_5), 3.18 (d, $^3J_{H\text{-}H}$= 6.2 Hz, 2H, H_1), 3.54 (q, $^3J_{H\text{-}H}$= 6.2 Hz, 2H, H_4), 5.10 (s, 2H, H_8), 7.33 (s, 5H, $H_{10\text{-}14}$), 7.47-7.65 (m, 1H, N-H_3).

^{13}C NMR (62.5 MHz, $CDCl_3$) δ 34.0 (C_5), 35.1 (C_4), 59.8 (C_1), 66.7 (C_8), 128.3, 128.5, 128.7 ($C_{10\text{-}14}$), 135.7 (C_9), 170.3 (C_2), 172.2 (C_6).

HRMS: Calculated for $C_{36}H_{42}N_4O_9Na$ $(M+Na)^+$: 697.2849. Found $(M+Na)^+$: 697.2845.

ClCH$_2$CO-GABA-OBn 189:

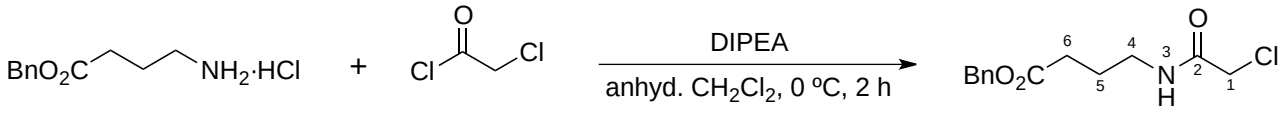

187 **189**

DIPEA (1.00 mL, 5.7 mmol) was added to an ice-cooled solution of salt **187**[336] (1.15 g, 5.01 mmol) in anhydrous CH_2Cl_2 (70 mL). Chloroacetyl chloride (0.52 mL, 6.5 mmol) and DIPEA (1.00 mL, 5.7 mmol) were slowly added and the mixture was stirred for 2 h. The solvent was removed under reduced pressure, EtOAc (60 mL) was added and the solution was washed with saturated aqueous $NaHCO_3$ solution (2 x 50 mL) and saturated aqueous NaCl solution (1 x 50 mL). The organic layer was dried over anhydrous $MgSO_4$, filtered and evaporated *in vacuo*. The resulting residue was purified by silica gel chromatography using hexane/EtOAc (1:2) as eluent to afford **189** (1.04 g, 77%) a yellow oil.

Spectroscopic data and physical constants of compound 189:

$[\alpha]_D$= +12.6 (*c* = 1.09, CH_2Cl_2)

IR (cm^{-1}) ν 3306, 2943, 1732, 1662, 1539.

^{1}H NMR (360 MHz, $CDCl_3$) δ 1.89 (p, $^3J_{H-H}$= 6.9 Hz, 2H, ,H_5), 2.42 (t, $^3J_{H-H}$= 7.0 Hz, 2H, H_6), 3.34 (q, $^3J_{H-H}$= 6.4 Hz, 2H, H_4), 4.00 (s, 2H, H_1), 5.12 (s, 2H, H_9), 6.81 (broad s, 1H, N-H_3), 7.34 (s, 5H, $H_{11\text{-}15}$).

^{13}C NMR (90 MHz, $CDCl_3$) δ 24.4 (C_5), 31.6 (C_6), 39.3 (C_4), 42.6 (C_1), 66.5 (C_9), 128.3, 128.6 ($C_{11\text{-}15}$), 135.8 (C_{10}), 166.1 (C_2), 172.9 (C_7).

HRMS: Calculated for $C_{13}H_{16}ClNO_3Na$ $(M+Na)^+$: 292.0705. Found $(M+Na)^+$: 292.0708

N-Boc-Gly-GABA-OBn 188:

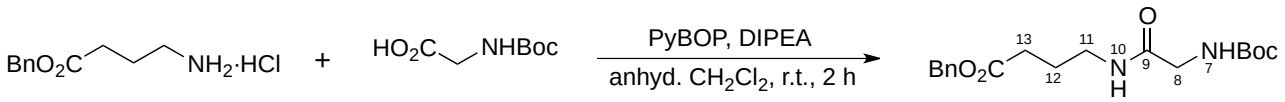

187 **173** **188**

DIPEA (1.2 mL, 6.8 mmol) and PyBOP (2.2 g, 4.3 mmol) were added to a solution of acid **173**[294] (600 mg, 2.9 mmol) in anhydrous CH_2Cl_2 (20 mL). After five minutes stirring, salt **187**[336] (457 mg, 2.9 mmol) was added and the mixture was stirred at room temperature for 2 h. EtOAc (50 mL) was added and the solution was washed with saturated aqueous $NaHCO_3$ solution (3 x 40 mL) and saturated aqueous NaCl solution (1 x 40 mL). The organic layer was dried over anhydrous $MgSO_4$, filtered and the solvent was evaporated *in vacuo*. The resulting residue was purified by silica gel chromatography using hexane/EtOAc (1:3) as eluent to afford **188** (580 mg, 83%) as white solid.

Spectroscopic data and physical constants of compound 188:

$[\alpha]_D$= +12 (*c* = 0.87, EtOAc)

M. p.: 65-68 ºC (EtOAc-hexane)

IR (cm^{-1}) ν 3309, 2977, 1718, 1665, 1536.

^{1}H NMR (360 MHz, $CDCl_3$) δ 1.42 (s, 9H, $H_{1\text{-}3}$), 1.84 (p, $^3J_{H\text{-}H}$= 7.1 Hz, 2H, H_{12}), 2.39 (t, $^3J_{H\text{-}H}$= 7.2 Hz, 2H, H_{13}), 3.29 (q, $^3J_{H\text{-}H}$= 6.6 Hz, 2H, H_{11}), 3.73 (broad s, 1H, H_8), 5.10 (s, 2H, H_{16}), 5.30 (broad s, 1H, NH_7), 6.60 (broad s, 1H, NH_{10}), 7.28-7.39 (c.a., 5H, $H_{18\text{-}22}$).

^{13}C NMR (90 MHz, $CDCl_3$) δ 24.6 (C_{12}), 28.4 ($C_{1\text{-}3}$), 31.7 (C_{13}), 38.9 (C_{11}), 44.3 (C_8), 66.5 (C_{16}), 80.4 (C_4), 128.3, 128.7 ($C_{18\text{-}22}$), 135.9 (C_{17}), 156.2 (C_6), 170.0 (C_9), 173.3 (C_{14}).

HRMS: Calculated for $C_{18}H_{26}N_2O_5Na$ $(M+Na)^+$: 373.1734. Found $(M+Na)^+$: 373.1734.

HCl·Gly-GABA-OBn 190:

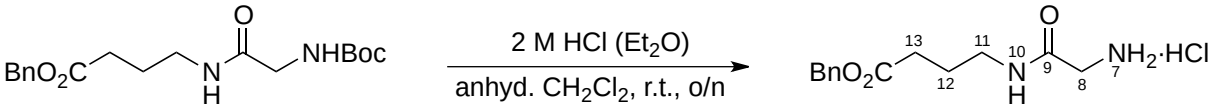

188 **190**

2 M HCl in Et_2O (7.0 mL, 14 mmol) was added to a solution of compound **188** (325 mg, 0.93 mmol) in anhydrous CH_2Cl_2 (20 mL). The mixture was stirred at room temperature overnight. The solvent was removed under reduced pressure to provide salt **190** (266 mg, quantitative yield) as oil.

Spectroscopic data of compound 190:

^{1}H NMR (250 MHz, $CDCl_3$) δ 1.84 (broad s, 2H, H_{12}), 2.37 (broad s, 2H, H_{13}), 3.25 (broad s, 2H, H_{11}), 3.99 (broad s, 2H, H_8), 5.04 (s, 2H, H_{16}), 7.28 (s, 5H, $H_{18\text{-}22}$), 7.73-8.37 (c.a., 3H, NH_7).

^{13}C NMR (62.5 MHz, $CDCl_3$) δ 24.4 (C_{12}), 31.4 (C_{13}), 39.1 (C_{11}), 41.5 (C_8), 66.4 (C_{16}), 128.1, 128.2, 128.5 ($C_{18\text{-}22}$), 135.9 (C_{17}), 166.6 (C_9), 173.4 (C_{14}).

N(CH_2CO-GABA-OBn)$_3$ 149:

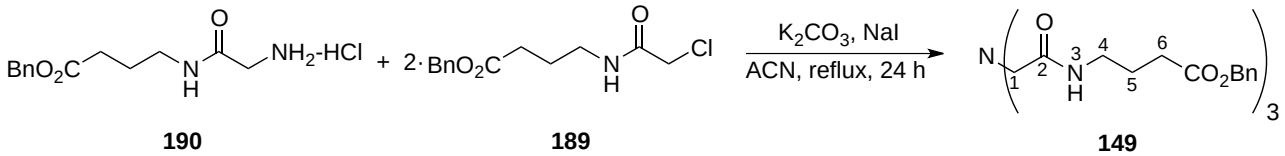

190 **189** **149**

Amine **190** (360 mg, 1.26 mmol), chloride derivative **189** (677 mg, 2.51 mmol), K_2CO_3 (0.9 g, 6.53 mmol) and NaI (0.4 g, 2.61 mmol) were mixed in ACN (70 mL). The mixture was stirred under reflux for 24 h. The solvent was removed *in vacuo* and EtOAc (50 mL) was added and the solution was washed with saturated aqueous $NaHCO_3$ solution (1 x 50 mL) and saturated aqueous NaCl solution (2 x 40 mL). The organic layer was dried over anhydrous $MgSO_4$, filtered and the solvent was evaporated *in vacuo*. The resulting residue was purified by silica gel chromatography using EtOAc and CH_2Cl_2/MeOH (10:1) as eluents to afford **149** (310 mg, 34%) as thick oil.

Spectroscopic data of compound 149:

IR (cm^{-1}) ν 3282, 3066, 2939, 1731, 1655, 1544.

^{1}H NMR (250 MHz, $CDCl_3$) δ 1.83 (p, $^3J_{H-H}$= 7.0 Hz, 2H, ,H_5), 2.37 (t, $^3J_{H-H}$= 7.3 Hz, 2H, H_6), 3.23 (s, 2H, H_1), 3.27 (q, $^3J_{H-H}$= 6.5 Hz, 2H, H_4), 5.09 (s, 2H, H_9), 7.33 (s, 5H, $H_{11\text{-}15}$), 7.47 (broad s, 1H, N-H_3).

^{13}C NMR (62.5 MHz, $CDCl_3$) δ 24.4 (C_5), 31.4 (C_6), 38.6 (C_4), 60.2 (C_1), 66.1 (C_9), 127.9, 128.1, 128.4 ($C_{11\text{-}15}$), 135.7 (C_{10}), 170.6 (C_2), 172.7 (C_7).

HRMS: Calculated for $C_{39}H_{48}N_4O_9Na$ $(M+Na)^+$: 739.3314. Found $(M+Na)^+$: 739.3313.

***N*-Boc-γCbu-OBn 155:**

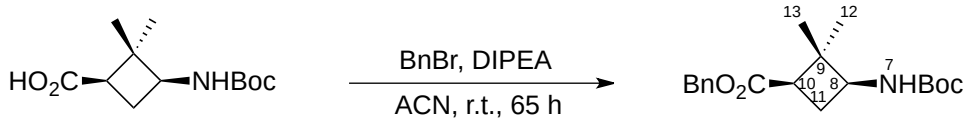

162 **155**

DIPEA (1.00 mL, 5.7 mmol) was added to a solution of acid **162**[290] (1.08 g, 4.44 mmol) in ACN (90 mL). After five minutes stirring, BnBr (0.80 mL, 6.7 mmol) was added drop-wise during 1 hour and the mixture was stirred at room temperature for 65 h. The solvent was removed under reduced pressure and EtOAc (40 mL) was added. The solution was washed with saturated aqueous $NaHCO_3$ solution (2 x 40 mL) and saturated aqueous NaCl solution (1 x 40 mL). The organic layer was dried over anhydrous $MgSO_4$, filtered and the solvent was evaporated *in vacuo*. The resulting residue was purified by silica gel chromatography using hexane/EtOAc (4:1) as eluent to afford **155** (1.41 g, 95%) as white solid.

Spectroscopic data and physical constants of compound 155:

$[\alpha]_D$= -5.2 (*c* = 0.84, CH_2Cl_2)

M. p.: 91-94 ºC (polymorphism: 63-66 ºC) (EtOAc-hexane)

IR (cm^{-1}) ν 3383, 2958, 2869, 1704 (wide peak), 1519.

^{1}H NMR (360 MHz, $CDCl_3$) δ 0.86 (s, 3H, H_{12}), 1.27 (s, 3H, H_{13}), 1.43 (s, 9H, $H_{1\text{-}3}$), 2.05 (m, 1H, H_{11}), 2.30 (m, 1H, H_{11}), 2.60 (m, 1H, H_{10}), 3.81 (m, 1H, H_8), 4.67 (broad s, 1H, NH_7), 5.11 (s, 2H, H_{16}), 7.34 (s, 5H, $H_{18\text{-}22}$).

^{13}C NMR (90 MHz, $CDCl_3$) δ 17.0 (C_{12}), 26.6 (C_{11}), 28.4 ($C_{1\text{-}3}$), 29.1 (C_{13}), 43.0 (C_{10}), 46.4 (C_9), 51.2 (C_8), 66.2 (C_{16}), 79.4 (C_4), 128.3, 128.6 ($C_{18\text{-}22}$), 136.2 (C_{17}), 155.4 (C_6), 172.6 (C_{14}).

HRMS: Calculated for $C_{19}H_{27}NO_4Na$ $(M+Na)^+$: 356.1832. Found $(M+Na)^+$: 356.1839.

HCl·γCbu-OBn 163:

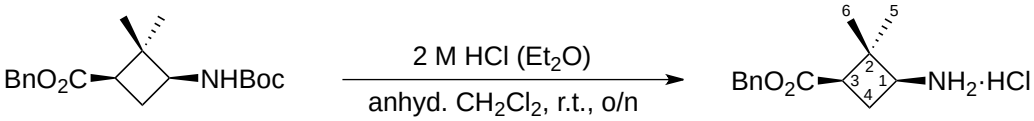

155 **163**

2 M HCl in Et_2O (8.5 mL, 17 mmol) was added to a solution of compound **155** (350 mg, 1.05 mmol) in anhydrous CH_2Cl_2 (20 mL). The mixture was stirred at room temperature overnight. The solvent was removed under reduced pressure to provide salt **163** (283 mg, quantitative yield) as pale yellow oil.

Spectroscopic data of compound 163:

^{1}H NMR (360 MHz, $CDCl_3$) δ 1.16 (s, 3H, H_5), 1.33 (s, 3H, H_6), 2.41 (m, 1H, H_4), 2.53 (m, 1H, H_4), 2.70 (m, 1H, H_3), 3.51 (broad s, 1H, H_1), 5.08 (d, $^2J_{H\text{-}H}$= 12.3 Hz, 1H, H_9), 5.14 (d, $^2J_{H\text{-}H}$= 12.3 Hz, 1H, H_9), 7.32 (s, 5H, $H_{11\text{-}15}$), 8.33 (broad s, 3H, NH_2·HCl).

^{13}C NMR (90 MHz, $CDCl_3$) δ 17.1 (C_5), 28.4 (C_4), 29.6 (C_6), 43.3 (C_3), 43.9 (C_2), 51.3 (C_1), 66.6 (C_9), 128.2, 128.3, 128.5 ($C_{11\text{-}15}$), 135.6 (C_{10}), 171.6 (C_7).

ClCH₂CO-γCbu-OBn 196:

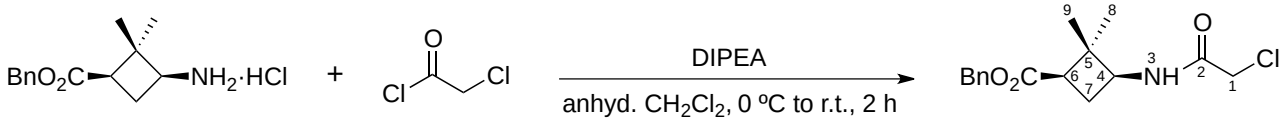

163 **196**

DIPEA (0.10 mL, 0.6 mmol) was added to an ice-cooled solution of salt **163** (146 mg, 0.54 mmol) in anhydrous CH_2Cl_2 (20 mL). Chloroacetyl chloride (0.06 mL, 0.8 mmol) and DIPEA (0.10 mL, 0.6 mmol) were slowly added and the mixture was stirred for 2 h. The solvent was removed under reduced pressure, EtOAc (20 mL) was added and the solution was washed with saturated aqueous $NaHCO_3$ solution (2 x 15 mL) and saturated aqueous NaCl solution (1 x 20 mL). The organic layer was dried over anhydrous $MgSO_4$, filtered and evaporated *in vacuo*. The resulting residue was purified by silica gel chromatography using hexane/EtOAc (1:3) as eluent to afford **196** (140 mg, 84%) as yellow solid.

Spectroscopic data and physical constants of compound 196:

$[\alpha]_D$= -6.6 (*c* = 0.47, CH_2Cl_2)

M. p.: 76-79 ºC (CH_2Cl_2)

IR (cm^{-1}) ν 3305, 2957, 2924, 2852, 1730, 1663, 1539.

^{1}H NMR (250 MHz, $CDCl_3$) δ 0.89 (s, 3H, H_8), 1.31 (s, 3H, H_9), 2.20 (m, 1H, H_7), 2.38 (m, 1H, H_7), 2.70 (dd, $^3J_{H\text{-}H}$= 9.7 Hz, $^3J_{H\text{-}H}$= 7.8 Hz, 1H, H_6), 4.03 (s, 2H, H_1), 4.14 (q, $^3J_{H\text{-}H}$= 8.7 Hz, 1H, H_4), 5.10 (d, $^2J_{H\text{-}H}$= 12.3 Hz, 1H, H_{12}), 5.17 (d, $^2J_{H\text{-}H}$= 12.3 Hz, 1H, H_{12}), 6.71 (broad d, $^3J_{H\text{-}H}$= 6.9 Hz, 1H, N-H_3), 7.36 (s, 5H, $H_{14\text{-}18}$).

^{13}C NMR (62.5 MHz, $CDCl_3$) δ 17.1 (C_8), 26.2 (C_7), 29.1 (C_9), 42.6 (C_1), 43.4 (C_6), 46.1 (C_5), 50.3 (C_4), 66.4 (C_{12}), 128.4, 128.7 ($C_{14\text{-}18}$), 136.0 (C_{13}), 165.8 (C_2), 172.5 (C_{10}).

HRMS: Calculated for $C_{16}H_{20}ClNO_3Na$ $(M+Na)^{+:}$ 332.1024. Found $(M+Na)^+$: 332.1029.

N-Boc-Gly-γCbu-OBn 197:

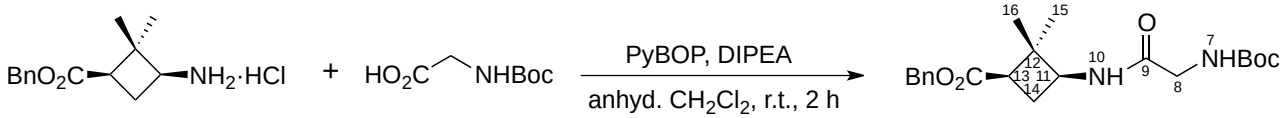

163 **173** **197**

DIPEA (0.51 mL, 2.9 mmol) and PyBOP (530 mg, 1.04 mmol) were added to a solution of acid **173** (166 mg, 0.80 mmol) in anhydrous CH_2Cl_2 (20 mL). After five minutes stirring, amino acid salt **163** (255 mg, 2.9 mmol) was added and the mixture was stirred at room temperature for 2 h. EtOAc (40 mL) was added and the solution was washed with saturated aqueous $NaHCO_3$ solution (2 x 40 mL) and saturated aqueous NaCl solution (1 x 40 mL). The organic layer was dried over anhydrous $MgSO_4$, filtered and the solvent was evaporated *in vacuo*. The resulting residue was purified by

silica gel chromatography using hexane/EtOAc (2:1) as eluent to afford **197** (270 mg, 73%) as a dense oil.

Spectroscopic data and physical constants of compound 197:

$[\alpha]_D$= -20 (*c* = 0.47, CH_2Cl_2)

IR (cm^{-1}) ν 3309, 3068, 3036, 2961, 2932, 1717, 1661, 1523.

^{1}H NMR (360 MHz, $CDCl_3$) δ 0.84 (s, 3H, H_{15}), 1.27 (s, 3H, H_{16}), 1.43 (s, 9H, $H_{1\text{-}3}$), 2.13 (m, 1H, H_{14}), 2.31 (m, 1H, H_{14}), 2.66 (dd, $^3J_{H\text{-}H}$= 9.9 Hz, $^3J_{H\text{-}H}$= 7.8 Hz, 1H, H_{13}), 3.75 (d, $^3J_{H\text{-}H}$= 5.0 Hz, 2H, H_8), 4.11 (dd, $^3J_{H\text{-}H}$= 8.3 Hz, $^3J_{H\text{-}H}$= 17.9 Hz, 1H, H_{11}), 5.04-5.15 (c.a., 2H, H_{19}), 5.38 (broad s, 1H, NH_7), 6.59 (broad s, 1H, NH_{10}), 7.33 (s, 5H, $H_{21\text{-}25}$).

^{13}C NMR (90 MHz, $CDCl_3$) δ 17.1 (C_{15}), 26.1 (C_{14}), 28.4 ($C_{1\text{-}3}$), 29.0 (C_{16}), 43.2 (C_{13}), 44.4 (C_8), 46.3 (C_{12}), 49.8 (C_{11}), 66.3 (C_{19}), 80.3 (C_4), 128.3, 128.6 ($C_{21\text{-}25}$), 136.0 (C_{20}), 156.2 (C_6), 169.5 (C_9), 172.6 (C_{17}).

HRMS: Calculated for $C_{21}H_{30}N_2O_5Na$ $(M+Na)^+$: 413.2047. Found $(M+Na)^+$: 413.2048.

HCl·Gly-γCbu-OBn 198:

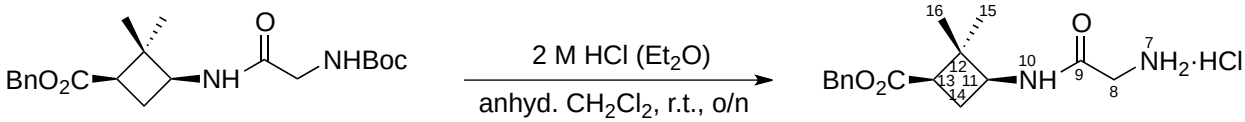

197 **198**

2 M HCl in Et_2O (3.5 mL, 7 mmol) was added to a solution of compound **197** (170 mg, 0.44 mmol) in anhydrous CH_2Cl_2 (20 mL). The mixture was stirred at room temperature overnight. The solvent was removed under reduced pressure to provide salt **198** (144 mg, quantitative yield) as pale yellow oil.

Spectroscopic data of compound 198:

^{1}H NMR (250 MHz, $CDCl_3$) δ 1.05 (s, 3H, H_{15}), 1.34 (s, 3H, H_{16}), 2.35 (m, 1H, H_{14}), 2.46 (m, 1H, H_{14}), 2.76 (m, 1H, H_{13}), 3.99-4.38 (c.a., 3H, H_8, H_{11}), 5.16 (d, $^2J_{H\text{-}H}$= 12.5 Hz, 1H, H_{19}), 5.24 (d, $^2J_{H\text{-}H}$= 12.5 Hz, 1H, H_{19}), 5.47 (broad s, 1H, NH_{10}), 7.27-7.55 (c.a., 5H, $H_{21\text{-}25}$), 8.37 (broad s, 3H, NH_7),), 8.66 (broad d, $^3J_{H\text{-}H}$= 7.0 Hz, 1H, NH_{10}).

^{13}C NMR (62.5 MHz, $CDCl_3$) δ 18.0 (C_{15}), 26.0 (C_{14}), 29.4 (C_{16}), 42.0 (C_8), 43.5 (C_{13}), 47.3 (C_{12}), 51.0 (C_{11}), 66.4 (C_{19}), 128.8, 129.2 ($C_{21\text{-}26}$), 137.5 (C_{20}), 167.3 (C_9), 172.7 (C_{17}).

N(CH$_2$CO-γCbu-OBn)$_3$ 151:

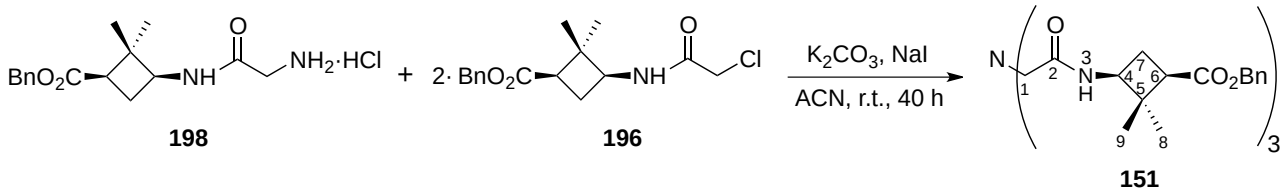

K_2CO_3 (195 mg, 1.42 mmol) and NaI (90 mg, 0.59 mmol) were added to an ice-cooled solution of amine **198** (142 mg, 0.43 mmol) in ACN (10 mL). A solution of chloride derivative **196** (270 mg, 0.87 mmol) in ACN (10 mL) was slowly added and the mixture was stirred at room temperature for 40 h. The solvent was removed *in vacuo* and EtOAc (40 mL) was added and the solution was washed with 2 M HCl solution (1 x 30 mL), water (1 x 30 mL), saturated aqueous $NaHCO_3$ solution (1 x 30 mL) and saturated aqueous NaCl solution (1 x 30 mL). The organic layer was dried over anhydrous $MgSO_4$, filtered and the solvent was evaporated *in vacuo*. The resulting residue was purified by silica gel chromatography using a gradient of CH_2Cl_2/MeOH (from 30:1, 15:1 and to 1.1) to afford **151** (200 mg, 54%) as transparent solid.

Spectroscopic data and physical constants of compound 151:

M. p.: 47-50 ºC (Et_2O/pentane)

IR (cm^{-1}) ν 3274, 2955, 2924, 2870, 1727, 1649, 1534.

^{1}H NMR (360 MHz, $CDCl_3$) δ 0.83 (s, 3H, H_8), 1.27 (s, 3H, H_9), 2.26 (broad s, 2H, H_7), 2.65 (m, 1H, H_6), 3.14-3.38 (c.a., 2H, H_1), 4.11 (broad s, 1H, H_4), 5.12 (broad s, 2H, H_{12}), 7.35 (broad s, 5H, $H_{14\text{-}18}$), 7.60 (m, 1H, N-H_3).

^{13}C NMR (90 MHz, $CDCl_3$) δ 17.3 (C_8), 25.5 (C_7), 29.0 (C_9), 43.2 (C_6), 46.4 (C_5), 50.0 (C_4), 60.2 (C_1), 66.3 (C_{12}), 128.2, 128.6 ($C_{14\text{-}18}$), 136.0 (C_{13}), 170.3 (C_2), 172.5 (C_{10}).

HRMS: Calculated for $C_{48}H_{60}N_4O_9Na$ $(M+Na)^+$: 859.4253. Found $(M+Na)^+$: 859.4274.

N(CH$_2$CO-γCbu-OMe)$_3$ 152:

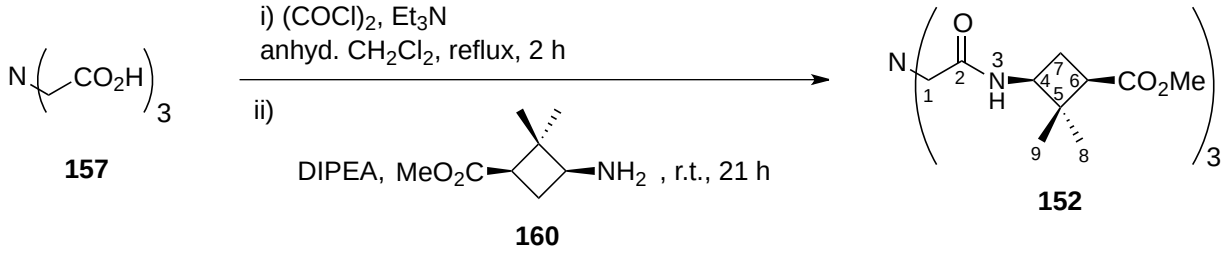

2 M solution of oxalyl chloride in CH_2Cl_2 (2.40 mL, 4.7 mmol) was added to a solution of triacid **157** (270 mg, 1.41 mmol) in anhydrous CH_2Cl_2 (60 mL). Few drops of anhydrous DMF were added

and the mixture was stirred under reflux for 2 h. Amino acid **160** (1.08 g, 6.9 mmol) and DIPEA (2.2 mL, 13 mmol) were added and the mixture was stirred under reflux for 21 h. The solvent was removed under reduced pressure, EtOAc (50 mL) was added and the solution was washed with saturated aqueous $NaHCO_3$ solution (2 x 40 mL) and saturated aqueous NaCl solution (1 x 50 mL). The organic layer was dried over anhydrous $MgSO_4$, filtered and evaporated *in vacuo* to provide 770 mg of dark brown solid. The crude was first purified by silica gel chromatography using EtOAc and CH_2Cl_2/MeOH (20:1) as eluents and later by precipitation using ether and pentane to afford triamide **152** (300 mg, 35%) as pale yellow solid.

Spectroscopic data and physical constants of compound 152:

M. p.: 87-90 ºC (Et_2O/pentane).

IR (cm^{-1}) ν 3271, 2956, 1732, 1653, 1547.

^{1}H NMR (250 MHz, $CDCl_3$) δ 0.80 (s, 3H, H_8), 1.22 (s, 3H, H_9), 2.02-2.34 (c.a., 2H, H_7), 2.55 (m, 1H, H_6), 3.07-3.46 (c.a., 2H, H_1), 3.60 (s, 3H, H_{12}), 4.03 (m, 1H, H_4), 7.26 (broad s, 1H, N-H_3).

^{13}C NMR (62.5 MHz, $CDCl_3$) δ 17.5 (C_8), 25.7 (C_7), 29.1 (C_9), 43.3 (C_6), 46.3 (C_5), 50.2 (C_4), 51.7 (C_{12}), 60.2 (C_1), 170.6 (C_2), 173.2 (C_{10}).

HRMS: Calculated for $C_{30}H_{48}N_4O_9Na$ $(M+Na)^+$: 631.3314. Found $(M+Na)^+$: 631.3322.

N(CH_2CO-δCbu-OMe)$_3$ 153:

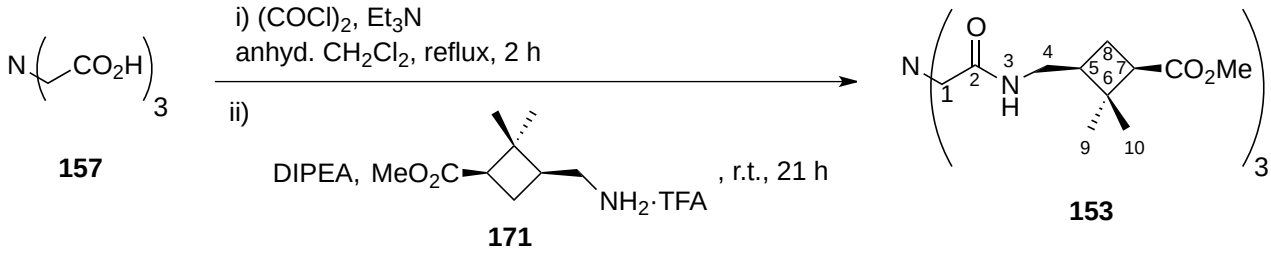

2 M solution of oxalyl chloride in CH_2Cl_2 (2.00 mL, 3.9 mmol) was added to a solution of triacid **157** (105 mg, 0.55 mmol) in anhydrous CH_2Cl_2 (20 mL). Few drops of anhydrous DMF were added and the mixture was stirred under reflux for 2 h. Amino acid salt **171** (0.47 g, 1.6 mmol) and DIPEA (2.0 mL, 12 mmol) were added and the mixture was stirred under reflux for 21 h. The solvent was removed under reduced pressure, EtOAc (20 mL) was added and the solution was washed with saturated aqueous $NaHCO_3$ solution (2 x 20 mL) and saturated aqueous NaCl solution (1 x 20 mL). The organic layer was dried over anhydrous $MgSO_4$, filtered and evaporated *in vacuo*

to provide a dark brown crude. The crude was first purified by silica gel chromatography using EtOAc and CH_2Cl_2/MeOH (20:1) as eluents and later by recrystallization using CH_2Cl_2 and pentane to afford triamide **153** (72 mg, 20%) as pale brown oil.

Spectroscopic data of compound 153:

^{1}H NMR (250 MHz, $CDCl_3$) δ 0.96 (s, 3H, H_9), 1.21 (s, 3H, H_{10}), 1.82-2.30 (c.a., 3H, H_5, H_8), 2.69 (t, $^3J_{H\text{-}H}$= 8.3 Hz, 1H, H_7), 2.83-3.56 (c.a., 4H, H_1, H_4), 3.65 (s, 3H, H_{13}), 8.12 (broad s, 1H, N-H_3).

^{13}C NMR (62.5 MHz, $CDCl_3$) δ 17.8 (C_9), 23.0 (C_8), 30.5 (C_{10}), 41.2 (C_5), 42.2 (C_4, C_6), 45.8 (C_7), 51.4 (C_{13}), 60.4 (C_1), 173.4 (C_2, C_{11}).

HRMS: Calculated for $C_{33}H_{54}N_4O_9Na$ $(M+Na)^+$: 673.3783. Found $(M+Na)^+$: 673.3768.

N(CH$_2$CO-GABA-OMe)$_3$ 150:

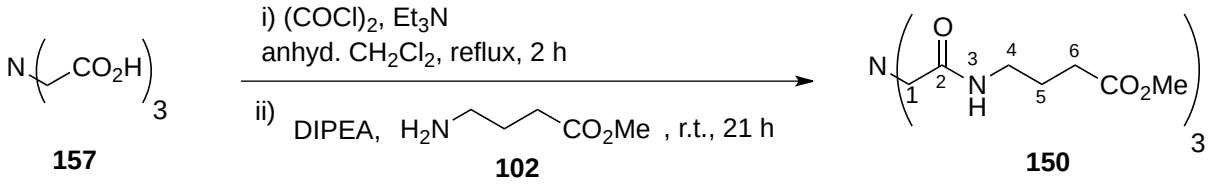

2 M solution of oxalyl chloride in CH_2Cl_2 (1.70 mL, 3.3 mmol) was added to a solution of triacid **157** (200 mg, 1.05 mmol) in anhydrous CH_2Cl_2 (40 mL). Few drops of anhydrous DMF were added and the mixture was stirred under reflux for 2 h. The mixture was left to reach room temperature and Et_3N (0.88 mL, 6.4 mmol) and amino acid **102** (0.37 g, 3.2 mmol) were added. The mixture was stirred at room temperature for 21 h. The solvent was removed under reduced pressure and the resulting residue was purified by precipitation using Et_2O in CH_2Cl_2 to provide 310 mg of pale brown solid. The crude was purified by silica gel chromatography using EtOAc and CH_2Cl_2/MeOH (20:1) as eluents to afford triamide **150** (20 mg, 4%) as pale brown oil.

Spectroscopic data of compound 150:

IR (cm^{-1}) ν 3275, 3056, 2925, 2853, 1734, 1658, 1549.

^{1}H NMR (250 MHz, $CDCl_3$) δ 1.84 (p, $^3J_{H\text{-}H}$= 7.2 Hz, 2H, H_5), 2.36 (t, $^3J_{H\text{-}H}$= 7.2 Hz, 2H, H_6), 3.30 (q, $^3J_{H\text{-}H}$= 7.2 Hz, 2H, H_4), 3.34 (broad s, 2H, H_1), 3.66 (s, 3H, H_9), 7.61 (broad s, 1H, N-H_3).

^{13}C NMR (62.5 MHz, $CDCl_3$) δ 24.7 (C_5), 31.7 (C_6), 39.1 (C_4), 51.9 (C_9), 60.4 (C_1), 170.4 (C_2), 173.9 (C_7).

HRMS: Calculated for $C_{21}H_{36}N_4O_9Na$ $(M+Na)^+$: 511.2374. Found $(M+Na)^+$: 511.2383.

BIBLIOGRAPHY

BIBLIOGRAPHY

1. Kendrew, J. C.; Dickerson, R. E.; Strandberg, B. E.; Hart, R. G.; Davies, D. R.; Phillips, D. C.; Shore, V. C. *Nature* **1960,** *185*, 422-427.
2. Seebach, D.; Beck, A. K.; Bierbaum, D. J. *Chem. Biodiversity* **2004,** *1*, 1111-1239.
3. Kimmerlin, T.; Seebach, D. *J. Pept. Res.* **2005,** *65*, 229-260.
4. Seebach, D.; Hook, D. F.; Glattli, A. *Biopolymers* **2006,** *84*, 23-37.
5. Lelais, G.; Seebach, D. *Biopolymers* **2004,** *76*, 206-243.
6. Gellman, S. H. *Acc. Chem. Res.* **1998,** *31*, 173-180.
7. Cheng, R. P.; Gellman, S. H.; DeGrado, W. F. *Chem. Rev.* **2001,**101, 3219-3232.
8. Martín-Vilà, M.; Minguillón, C.; Ortuño, R. M. *Tetrahedron: Asymmetry* **1998,** *9*, 4291-4294.
9. a) Izquierdo, S.; Rúa, F.; Sbai, A.; Parella, T.; Álvarez-Larena, Á.; Branchadell, V.; Ortuño, R. M. *J. Org. Chem.* **2005**, *70*, 7963-7971. b) Rúa, F.; Boussert, S.; Diez-Pérez, I.; Branchadell, V.; Giralt, E.; Ortuño, R. M. *Org. Lett.* **2007**, *9*, 3643-3645. c) Torres, E.; Gorrea, E.; Burusco, K. K.; Da Silva, E.; Nolis, P.; Rúa, F.; Boussert, S.; Díez-Pérez, I.; Dannenberg, S.; Izquierdo, S.; Giralt, E.; Jaime, C.; Branchadell, V.; Ortuño, R. M. *Org. Biomol. Chem.* **2010**, *8*, 564-575.
10. Torres, E.; Gorrea, E.; Da Silva, E.; Nolis, P.; Branchadell, V.; Ortuño, R. M. *Org. Lett.* **2009**, *11*, 2301-2304.
11. Izquierdo, S.; Kogan, M. J.; Parella, T.; Moglioni, A. G.; Branchadell, V.; Giralt, E.; Ortuño, R. M. *J. Org. Chem.* **2004**, *69*, 5093-5099.
12. Gorrea, E.; Nolis, P.; Álvarez-Larena, A.; Da Silva, E.; Branchadell, V.; Ortuño, R. M. *Tetrahedron:Asymmetry* **2010**, *21*, 339-345.
13. Mayans, E.; Gargallo, A.; Álvarez-Larena, Á.; Illa, O.; Ortuño, R. M. *Eur. J. Org. Chem.* **2013**, *8*, 1425-1433.
14. Gorrea, E.; Nolis, P.; Torres, E.; Da Silva, E.; Amabilino, D. B.; Branchadell, V.; Ortuño, R. M. *Chem. Eur. J.* **2011**, *17*, 4588-4597.
15. Aguilera, J.; Gutiérrez-Abad, R.; Mor, À.; Moglioni, A. G.; Moltrasio, G. Y.; Ortuño, R- M. *Tetrahedron:Asymmetry* **2008**, *19*, 2864-2869.
16. a) Aguilera, J.; Moglioni, A. G.; Moltrasio, G. Y.; Ortuño, R. M. *Tetrahedron:Asymmetry* **2008**, *20*, 302-308. b) Aguilera, J.; Cobos, J. A.; Ortuño, R. M. *Eur. J. Org. Chem.* **2013**. DOI: 10.1002/ejoc.201300066.
17. Gutiérrez-Abad, R.; Carbajo, D.; Nolis, P.; Acosta-Silva, C.; Cobos, J. A.; Illa, O.; Royo, M.; Ortuño, R. M. *Amino Acids* **2011**, *41*, 673-686.

18. Gorrea, E.; Carbajo, D.; Gutiérrez-Abad, R.; Illa, O.; Ortuño, R. M. *Org. Biomol. Chem.* **2012**, *10*, 4050-4057.
19. Fernández, D.; Torres, E.; Avilés, F. X.; Ortuño, R. M.; Vendrell, J. *Bioorg. Med. Chem*. **2009**, *17*, 3824-3828.
20. Torres, E.; Puigmartí-Luis, J.; Pérez del Pino, Á.; Ortuño, R. M.; Amabilino, D. B. *Org. Biomol. Chem.* **2010**, *8*, 1661-1665.
21. Raguse, T. L.; Lai, J. R.; Gellman, S. H. *J. Am. Chem. Soc.* **2003**, *125*, 5592-5593.
22. Seebach, D.; Mahajan, Y. R.; Senthilkumar, R.; Rueping, M.; Jaun, B. *Chem. Commun.* **2002**, 1598-1599.
23. Hanessian, S.; Luo, X.; Schaum, R.; Michnick, S. *J. Am. Chem. Soc.* **1998**, *120*, 8659-8570.
24. Seebach, D.; Abele, S.; Gademann, K.; Guichard, G.; Hintermann, T.; Jaun, B.; Matthews, J. L.; Schreiber, J. V.; Oberer, L.; Hommel, U.; Widmer, H. *Helv. Chim. Acta* **1998**, *81*, 932-982.
25. Appella, D. H.; Christianson, L. A.; Karle, I. L.; Powell, D. R.; Gellman, S. H. *J. Am. Chem. Soc.* **1999**, *121*, 6206-6212.
26. Peelen, T. J.; Chi, Y.; English, E. P.; Gellman, S. H. *Org. Lett.* **2004**, *6*, 4411-4414.
27. Park, J.-S.; Lee, H.-S.; Lai, J. R.; Kim, B. M.; Gellman, S. H. *J. Am. Chem. Soc.* **2003**, *125*, 8539-8545.
28. Appella, D. H.; Christianson, L. A.; Klein, D. A.; Richards, M. R.; Powell, D. R.; Gellman, S. H. *J. Am. Chem. Soc.* **1999**, *121*, 7574-7581.
29. Sharma, G. V. M.; Reddy, K. R.; Krishna, P. R.; Sankar, A. R.; Jayaprakash, P.; Jagannadh, B.; Kunwar, A. C. *Angew. Chem. Int. Ed.* **2004**, *43*, 3961-3965; *Angew. Chem.* **2004**, *116*, 4051-4055.
30. Gruner, S. A. W.; Truffault, V.; Voll, G.; Locardi, W.; Stöckle, M.; Kessler, H. *Chem. Eur. J.* **2002**, *8*, 4365-4376.
31. Seebach, D.; Gademann, K.; Schreiber, J. V.; Matthews, J. L.; Hintermann, T.; Jaun, B.; Oberer, L.; Hommel, U.; Widmer, H. *Helv. Chim. Acta* **1997**, *80*, 2033-2038.
32. Claridge, T. D. W.; Goodman, J. M.; Moreno, A.; Angus, D.; Barker, S. F.; Taillefumier, C.; Watterson, M. P.; Fleet, G. W. J. *Tetrahedron Lett.* **2001**, *42*, 4251-4255.
33. Hetényi, A.; Mándity, I. M.; Martinek, T. A.; Tóth,G. K.; Fülöp, F. *J. Am. Chem. Soc.* **2005**, *127*, 547-553.
34. Doerksen, R. J.; Chen, B.; Yuan, J.; Winkler, J. D.; Klein, M. L. *Chem. Commun.* **2003**, 2534-2535.

35. Gademann, K.; Häne, A.; Rueping, M.; Jaun, B.; Seebach, D. *Angew. Chem. Int. Ed.* **2003**, *42*, 1534-1537; *Angew. Chem.* **2003**, *115*, 1573-1575.

36. Roy, R. S.; Balaram, P. *J. Peptide Res*. **2004**, *63*, 279-289.

37. Bestian, H. *Angew. Chem. Int. Ed*. **1968**, *7*, 278-285.

38. Masamoto, J.; Sasaguri, K.; Ohizumi, C.; Kobayashi, H. *J. Polym. Sci. A-2* **1970**, *8*, 1703-1711.

39. Chen, F.; Lepore, G.; Goodman, M. *Macromolecules* **1974**, *7*, 779-783.

40. Yuki, H.; Okamoto, Y.; Taketani, Y.; Tsubota, T.; Marubayashi, Y. *J. Polym. Sci. Polym. Chem.* **1978**, *16*, 2237-2251.

41. Langenhan, J. M.; Gellman, S. H. *Org. Lett.* **2004**, *6*, 937-940.

42. Langenhan, J. M.; Guzei, I. A.; Gellman, S. H. *Angew. Chem. Int. Ed.* **2003**, *42*, 2402-2405; *Angew. Chem.* **2003**, *115*, 2504-2507.

43. Daura, X.; Gademann, K.; Schafer, H.; Jaun, B.;Seebach, D.; van Gunsteren, W. F. *J. Am. Chem. Soc*. **2001**, *123*, 2393-2404.

44. Seebach, D.; Abele, S.; Gademann, K.; Jaun, B. *Angew. Chem. Int. Ed.* **1999**, *38*, 1595-1597; *Angew. Chem.* **1999**, *111*, 1700-1703.

45. I. Daidone. Cartoon representation of the beta hairpin of the syrian hamster prion protein. 29th Aug 2006. University de L'Aquila. Jan 2013.http://en.wikipedia.org/wiki/File:Beta_hairpin.png.

46. Nano news net. Discovered the secret of the strength and elasticity of the web. 23rd Mar 2010. Russia. http://www.nanonewsnet.ru/news/2010/raskryt-sekret-prochnosti-elastichnosti-pautiny.

47. Baldwin, J. E.; Adlington, R. M.; Parisi, M. F.; Ting, H.-H. *Tetrahedron* **1986**, *42*, 2575-2586.

48. English, E. P.; Chumanov, R. S.; Gellman, S. H.; Compton, T. *J. Bio. Chem.* **2006**, *281*, 2661-2667.

49. Imamura, Y.; Watanabe, N.; Umezawa, N.; Iwatsubo, T.; Kato, N.; Tomita, T.; Higuchi, T.; *J. Am. Chem. Soc*. **2009**, *131*, 7353-7359.

50. Gershonov, E.; Granoth, R.; Tzehoval, E.; Gaoni, Y.; Fridkin, M. *J. Med. Chem.* **1996,** *30*, 4833-4843.

51. Beumer, R.; Reiser, O. *Tetrahedron* **2001,** *57*, 6497-6503.

52. Hibbs, D. E.; Hursthouse, M. B.; Jones, I. G.; Jones, W.; Malik, K. M. A.; North, M. *Tetrahedron* **1997,** *53*, 17417-17424.

53. Porter, E. A.; Wang, X.; Lee, H. -S.; Weisblum, B.; Gellman, S. H. *Nature* (London) **2000,** *404*, 565.

54. Barchi Jr., J. J.; Huang, X.; Appella, D. H.; Christianson, L.; Durell, S. R.; Gellman, S. H. *J. Am. Chem. Soc.* **2000,** *122*, 2711-2718.

55. Appella, D. H.; Christianson, L. A.; Klein, D. A.; Huang, X.; Barchi, J. J.; Powell, D. R.; Gellman, S. H. *Nature* (London) **1997,** *387*, 381-384.

56. Fülöp, F. *Stud. Nat. Prod. Chem.* **2000,** 22, 273–306.

57. Appella, D. H.; Christianson, L. A.; Karle, I. L.; Powell, D. R.; Gellman, S. H. *J. Am. Chem. Soc.* **1999,** *121*, 6206-6212.

58. Fülöp, F. *Chem. Rev.* **2001**, *101*, 2181-2204.

59. Kuhl, A.; Hahn, M. G.; Dumić, M.; Mittendorf, J. *Amino Acids* **2005**, *29*, 89-100.

60. Gnad, F.; Reiser, O. *Chem. Rev.* **2003**, *103*, 1603-1623.

61. Kennewell, P. D.; Matharu, S. S.; Taylor, J. B.; Westwood, R.; Sammes, P. G. *J. Chem. Soc., Perkin Trans.* 1 **1982,** 2563-2570.

62. Martín-Vilà, M.; Muray, E.; Aguado, G. P.; Álvarez-Larena, A.; Branchadell, V.; Minguillón, C.; Giralt, E.; Ortuño, R. M. *Tetrahedron: Asymmetry* **2000,** *11*, 3569-3584.

63. Bolm, C.; Schiffers, I.; Atodiresei, I.; Hackenberger, P. R. *Tetrahedron:Asymmetry* **2003**, *14*, 3455-3467.

64. Bolm, C.; Schiffers, I.; Dinter, C. L.; Defrere, L.; Gerlach, A.; Raabe, G. *Synthesis* **2001**, *14*, 1719-1730.

65. Sabbioni, G.; Jones, J. B. *J. Org. Chem.* **1987**, *52*, 4565-4570.

66. Declerck, V.; Aitken, D. J. *Amino Acids* **2011**, *41*, 587-595.

67. Aitken, D. J.; Gauzy, C.; Pereira, E. *Tetrahedron Lett.* **2002**, *43*, 6177-6179.

68. Aitken, D. J.; Gauzy, C.; Pereira, E. *Tetrahedron Lett.* **2004**, *45*, 2359-2361.

69. Gauzy, C.; Pereira, E.; Faure, S.; Aitken, D. J. *Tetrahedron Lett.* **2004**, *45*, 7095-7097.

70. Gauzy, C.; Saby, B.; Pereira, E.; Faure, S.; Aitken, D. J. *Synlett* **2006**, *9*, 1394-1398.

71. Fernandes, C.; Gauzy, C.; Yang, Y.; Roy, O.; Pereira, E.; Faure, S.; Aitken, D. J. *Synthesis* **2007**, *14*, 2222-2232.

72. Fernandes, C.; Pereira, E.; Faure, S.; Aitken, D. J. *J. Org. Chem.* **2009**, *74*, 3217-3220.

73. Hetényi, A.; Mándity, I. M.; Martinek, T. A.; Tóth, G. K.; Fülöp, F. *J. Am. Chem. Soc*. **2005**, *127*, 547-553. (repetida. és la 13)

74. Martinek, T. A.; Tóth, G. K.; Vass, E.; Hollósi, M.; Fülöp, F. *Angew. Chem. Int. Ed*. **2002**, *41*, 1718-1721.

75. Mangelinckx, S.; De Kimpe, N. *Tetrahedron Lett.* **2003**, *44*, 1771-1774.

76. Roy, O.; Faure, S.; Aitken, D. J. *Tetrahedron Lett.* **2006**, *47*, 5981-5984.

77. Pomerantz, W. C.; Yuwono, V. M.; Pizzey, C. L.; Hartgerink, J. D.; Abbott, N. L.; Gellman, S. H. *Angew. Chem. Int. Ed.* **2008**, *47*, 1241-1244.

78. Hetényi, A.; Tóth, G. K.; Somlai, C.; Vass, E.; Martinek, T. A.; Fülöp, F. *Chem. Eur. J.* **2009**, *15*, 10736-10741.

79. Dutot, L.; Gaucher, A.; Elkassimi, K.; Drapeau, J.; Wakselman, M.; Mazaleyrat, J. -P.; Peggion, C.; Formaggio, F.; Toniolo, C. *Chem. Eur. J.* **2008**, *14*, 3154-3163.

80. Raguse, T. L.; Porter, E. A.; Weisblum, B.; Gellman, S. H. *J. Am. Chem. Soc.* **2002**, *124*, 12774-12785.

81. Horne, W. S.; Gellman, S. H. *Acc. Chem. Res.* **2008**, *41*, 1399-1408.

82. Lee, E. F.; Sadowsky, J. D.; Smith, B. J.; Czabotar, P. E.; Peterson-Kaufman, K. J.; Colman, P. M.; Gellman, S. H.; Fairlie, W. D. *Angew. Chem. Int. Ed. Engl*. **2009**, *48*, 4318-4322.

83. Choi, S. S.; Guzei, I. A.; Spencer, L. C.; Gellman, S. H. *J. Am. Chem. Soc.* **2010**, *132*, 13879-13885.

84. Fernandes, C.; Faure, S.; Pereira, E.; Théry, V.; Declerck, V.; Guillot, R.; Aitken, D. J. *Org. Lett.* **2010**, *12*, 3606-3609.

85. Beke, T.; Somlai, C.; Perczel, A. *J. Comput. Chem.* **2006**, *27*, 20-38.

86. Torres, E. (2009). *Cyclobutane beta-peptides: Synthesis, structure and possible applications*. PhD Thesis. Universitat Autònoma de Barcelona, Spain.

87. Ludvigsen, S.; Andersen, K. V.; Poulsen, F. M. *J. Mol. Biol.* **1991**, *217*, 731-736.

88. Aguilar, M.-I.; Purcell, A. W.; Devi, R.; Lew, R.; Rossjohn, J.; Smith, A. I.; Perlmutter, P. *Org. Biomol. Chem.* **2007**, *5*, 2884-2890.

89. Roy, R. S.; Karle, I. L.; Raghothama, S.; Balaram, P. *PNAS* **2004**, *101*, 16478-16482.

90. Karle, I. L.; Pramanik, A.; Banerjee, A.; Bhattacharjya, S.; Balaram, P. *J. Am. Chem. Soc.* **1997** *119*, 9087-9095.

91. Krauthauser, S.; Christianson, L. A.; Powell, D. R.; Gellman, S. H. *J. Am. Chem. Soc.* **1997,** *119*, 11719-11720.

92. Sengupta, A.; Roy, R. S.; Sabareesh, S.; Shamala, N.; Balaram, P. *Org. Biomol. Chem.* **2006,** *4*, 1166-1173.

93. Woll, M. G.; Lai, J. R.; Guzei, I. A.; Taylor, S. J. C.; Smith, M. E. B.; Gellman, S. H. *J. Am. Chem. Soc.* **2001,** *123*, 11077-11078.

94. Vasudev, P. G.; Chatterjee, S.; Shamala, N.; Balaram, P. *Chem. Rev*. **2011**, *111*, 657-687.

95. Chatterjee, S.; Roy, R. S.; Balaram, P. *J. R. Soc. Interface* **2007**, *4*, 587-606.

96. Chou, K.-C. *Anal. Biochem.* **2000**, *286*, 1-16.

97. *Colloid Chemistry*, vol. 1. D. Jordan-Lloyd. Chemical Catalogue Company, New York (USA).

98. Dastidar, P. *Chem. Soc. Rev.* **2008**, *37*, 2699-2715.

99. Abdallah, D.; Weiss, R. *Adv. Mater.* **2000**, *12*, 1237-1247.

100. Hanabusa, K.; Kawakami, A.; Kimura, M.; Shirai, H. *Chemistry Letters* **1997**, 191-192.

101.Friggeri, A.; van der Pol, C.; van Bommel, K. J. C.; Heeres, A.; Stuart, M. C. A.; Feringa, B. L.; van Esch, J. *Chem. Eur. J.* **2005**, *11*, 5353-5361.

102. Edwards, W.; Lagadec, C. A.; Smith, D. K. *Soft Matter*, **2011**, *7*, 110-117.

103. Pal, ; Dey, J. *Langmuir* **2011**, *27*, 3401-3408;

104. Mallia, V. A.; George, M.; Blair, D. L.; Weiss, R. G. *Langmuir* **2009**, *25*, 8615-8625.

105. Wang, G.-T.; Cheuk, S.; Yang, H.; Goyal, N.; Reddy, P. V. N.; Hopkinson, B. *Langmuir* **2009**, *25*, 8696-8705.

106. Jung, J. H.; John, J. G.; Masuda, M.; Yoshida, K.; Shinkai, S.; Shimizu, T. *Langmuir* **2001**, *17*, 7229-7232.

107. Wang, G.-T.; Jiang, J.; Liu, Y.; Li, Z.; Liu, M. *Langmuir* **2010**, *26*, 18694-18700.

108. Komatsu, H.; Matsumoto, S.; Tamaru, S.-I.; Kaneko, K.; Ikeda, M.; Hamachi, I. *J. Am. Chem. Soc*. **2009**, *131*, 5580-5585.

109. Duan, P.; Liu, M. *Langmuir*, **2009**, *25*, 8706-8713.

110. Rodríguez-Llansola, F.; Miravet, J. F.; Escuder, B. *Chem. Commun.* **2011**, 4706-4708.

111. Piepenbrock, M.-O. M.; Clarke, N.; Steed, J. W. *Soft Matter*, **2011**, *7*, 2412-2418.

112. Pinault, T.; Cannizzo, C.; Andrioletti, B.; Ducouret, G.; Lequeux, F.; Bouteiller, L. *Langmuir* **2009**, *25*, 8404-8407.

113. Zweep, N.; Hopkinson, A.; Meetsma, A.; Browne, W. R.; Feringa, B. L.; van Esch, J. H. *Langmuir* **2009**, *25*, 8802-8809.

114. Nonappa, M.; Lahtinen, M.; Behera, B.; Kolehmainen, E.; Maitra, U. *Soft Matter* **2010**, *6*, 1748-1757.

115. Wu, J.; Yi, T.; Xia, Q.; Zou, Y.; Liu, F.; Dong, J.; Shu, T.; Li, F.; Huang, C. *Chem. Eur. J*. **2009**, *15*, 6234-6243.

116. Wang, G.-T.; Lin, J.-B.; Jiang, X.-K.; Li, Z.-T. *Langmuir* **2009**, *25*, 8414-8418.

117. Suzuki, M.; Saito, H.; Hanabusa, K. *Langmui*r **2009**, *25*, 8579-8585.

118. Moffat, J. R.; Smith, D. K. *Chem. Commun*. **2009**, 316-318.

119. Saha, A.; Manna, S.; Nandi, A. K. *Chem. Commun.*, **2008**, 3732-3734.

120. Basit, H.; Pal, A.; Sen, S.; Bhattacharya, S. *Chem. Eur. J.* **2008**, *14*, 6534-6545.

121. Wang, D.; Hao, J. *Langmuir* **2011**, *27*, 1713-1717.

122. Lin, Y.; Qiao, Y.; Tang, P.; Li, Z.; Huang, J. *Soft Matter* **2011**, *7*, 2762-2769.

123. Buerkle, L. E.; Li, Z.; Jamieson, A. M.; Rowan, S. J. *Langmuir* **2009**, *25*, 8833-8840.

124. Lin, Y.-C.; Weiss, R. G. *Liq. Cryst*. **1989**, *4*, 367-384.

125. Lin, Y.-C.; Weiss, R. G. *Macromolecules* **1987,** *20*, 414-417.

126. Partridge, K. S.; Smith, D. K.; Dykes, G. M.; McGrail, P. T. *Chem. Commun.* **2001**, 319-320.

127. Hirst, A. R.; Smith, D. K.; Feiters, M. C.; Geurts, H. P. M.; Wright, A. C. *J. Am. Chem. Soc.* **2003**, *125*, 9010-9011.

128. Shirakawa, M.; Kawano, S.; Fujita, N.; Sada, K.; Shinkai, S. *J. Org. Chem.* **2003**, 5037-5044.

129. Becerril, J.; Burguete, M. I.; Escuder, B.; Galindo, F.; Gavara, R.; Miravet, J. F.; Luis, S. V.; Peris, G. *Chem. Eur. J.* **2004**, *10*, 3879-3880.

130. Tachibana, T.; Mori, T.; Hori, K.; *Bull. Chem. Soc. Jpn.* **1980**, *53*, 1714-1719.

131. Yoza K.; Amanokura, N.; Ono, Y.; Akao, T.; Shinmori, H.; Takeuchi, M.; Shinkai, S.; Reinhoudt, D. N. *Chem. Eur. J.* **1999**, *5*, 2722-2729.

132. Gronwald, O.; Shinkai, S. *Chem. Eur. J.* **2001**, *7*, 4329-4334.

133. Luboradzki, R.; Gronwald, O.; Ikeda, M.; Shinkai, S.; Reinhoudt, D. N. *Tetrahedron* **2000**, *56*, 9595-9599.

134. Hanabusa, K.; Matsumoto, Y.; Miki, T.; Koyama, T.; Shirai, H. J. Chem. Soc., *Chem. Commun*. **1994**, 1401-1402.

135. Van Esch, J. H.; Feringa, B. L. *Angew. Chem. Int. Ed.* **2000**, *39*, 2263-2266.

136. Maitra, U.; Mukhopadhyay, S.; Sarkar, A.; Rao, P.; Indi, S. S. *Angew. Chem. Int. Ed.* **2001**, *40*, 2281-2283.

137. Aakeröy, C. B.; Seddon, K. R. *Chem. Soc. Rev.* **1993**, *22*, 397-407.

138. Ballabh, A.; Trivedi, D. R.; Dastidar, P. *Chem. Mater.* **2006**, *18*, 3795-3800.

139. Zhang, J.; Wang, X.; He, L.; Chen, L.; Su, C.-H.; James, S. L. *New J. Chem.* **2009**, *33*, 1070-1075.

140. Escuder, B.; Rodríguez-Llansola, F.; Miravet, J. F. *New J. Chem.* **2010**, *34*, 1044-1054.

141. Suzuki, M.; Waraksa, C. C.; Mallouk, T. E.; Nakayama, H.; Hanabusa, K. *J. Phys. Chem. B* **2002**, *106*, 4227-4231.

142. Doig, A. J.; Williams, D. H.; *J. Am. Chem. Soc.* **1992**, *114*, 338-343.

143. DiCapua, F. M.; Swaminathan, S.; Beveridge, D. L. *J. Am. Chem. Soc.* **1991**, *113*, 6145-6155.

144. Ellis-Behnke, R. G.; Liang, Y.-X.; You, S.-W.; Tay, D. K. C.; Zhang, S.; So, K.-F.; Schneider, G. E. *Proc. Natl. Acad. Sci. U.S.A.* **2006,** *103*, 5054-5059.

145. Silva, G. A.; Czeisler, C.; Niece, K. L.; Beniash, E.; Harrington, D. A.; Kessler, J. A.; Stupp, S. I. *Science* **2004,** *303*, 1352-1355.

146. Yang, Z.; Liang, G.; Ma, M.; Abbah, A. S.; Lu, W. W.; Xu, B. *Chem. Commun.* **2007,** 843-845.

147. Fukushima, T.; Asaka, K.; Kosaka, A.; Aida, T. *Angew. Chem. Int. Ed.* **2005,** *44*, 2410-2413.

148. Puigmartí-Luis, J.; Laukhin, V.; Pérez del Pino, Á.; Vidal-Gancedo, J.; Rovira, C.; Laukhina, E.; Amabilino, D. B. *Angew. Chem. Int. Ed.* **2007,** *46*, 238-241.

149. Couffin-Hoarau, A.-C.; Motulsky, A.; Delmas, P.; Leroux, J.-C. *Pharm. Res*. **2004**, *21*, 454-457.

150. Hanabusa, K.; Tanaka, R.; Suzuki, M.; Kimura, M.; Shirai, H. *Adv. Mater.* **1997**, *9*, 1095-1097.

151. Iqbal, S.; Miravet, J. F.; Escuder, B. *Eur. J. Org. Chem.* **2008,** 4580-4590.

152. Escuder, B.; Martí, S.; Miravet, J. F. *Langmuir* **2005**, *21*, 6776-6787.

153. Jung, J. P.; Gasiorowski, J. Z.; Collier, J. H. Biopolymers **2010**, *94*, 49-59.

154. Lagadec, C.; Smith, D. K. *Chem. Commun.* **2011**, 340-342.

155. Tomasini, C.; Castellucci, N. *Chem. Soc. Rev.* **2013**, *42*, 156-172.

156. Hirst, A. R.; Coates, I. A.; Boucheteau, T. R.; Miravet, J. F.; Escuder, B.; Castelletto, V; Hamley, I. W.; Smith, D. K. *J. Am. Chem. Soc.* **2008**, *130*, 9113-9121.

157. Huang, X.; Terech, P.; Raghavan, S. R.; Weiss, R. G. *J. Am. Chem. Soc.* **2005,** *127*, 4336-4344.

158. Ballabh, A.; Adalder, T. K.; Dastidar, P. *Cryst. Growth Des.* **2008**, *8*, 4144-4149.

159. Beginn, U.; Sheiko, S.; Moeller, M. *Macromol. Chem. Phys.* **2000**, *201*, 1008-1015.

160. Mieden-Gundert, G.; Klein, L.; Fischer, M.; Vögtle, F.; Heuze, K.; Pozzo, J. L.; Vallier, M.; Fages, F. *Angew. Chem. Int. Ed*. **2001**, *40*, 3164-3166.

161. Yasuda, Y.; Iishi, E.; Inada, H.; Shirota, Y. *Chem. Lett.* **1996**, 575-576.

162. Hanabusa, K.; Koto, C.; Kimura, M.; Shirai, H.; Kakehi, A. *Chem. Lett.* **1997**, 429-430.

163. Heeres, A.; van der Pol, C.; Stuart, M.; Friggeri, A.; Feringa, B. L.; van Esch, J. *J. Am. Chem. Soc.* **2003**, *125*, 14252-14253.

164. Van Bommel, K. J. C.; van der Pol, C.; Muizebelt, I.; Friggeri, A.; Heeres, A.; Metsma, A.; Feringa, B. L.; van Esch, J. *Angew. Chem. Int. Ed*. **2004**, *43*, 1663-1667.

165. Menger, F. M.; Caran, K. L. *J. Am. Chem. Soc.* **2000**, *122*, 11679-11691.

166. Suzuki, M.; Owa, S.; Yumoto, M.; Kimura, M.; Shirai, H.; Hanabusa, K. *Tetrahedron Lett.* **2004**, *45*, 5399-5402.

167. Jokic, M.; Makarevic, J., Zinic, M. *Chem. Commun.* **1995**, 1723-1724.

168. Becerril, J.; Burguete, M. I.; Escuder, B.; Luis, S. V.; Miravet, J. F.; Querol, M. *Chem. Commun*. **2002**, 738-739.

169. Maji, S. K.; Malik, S.; Drew, M. G. B.; Nandi, A. K.; Banerjee, A. *Tetrahedron Lett.* **2003**, *44*, 4103-4107.

170. Escuder, B.; Miravet, J. F. *Langmuir* **2006**, *22,* 7793-7797.

171. Ariga, K.; Kikuchi, J.; Naito, M.; Koyama, E.; Yamada, N. *Langmuir* **2000**, *16*, 4929-4939.

172. Yamada, N.; Ariga, K. *Synlett* **2000**, 575-586.

173. Lyon, R. P.; Atkins, W. M. *J. Am. Chem. Soc*. **2001**, *123*, 4408-4413.

174. Trivedi, D. R.; Dastidar, P. *Cryst.Growth Des.* **2006**, *6*, 2114-2121.

175. Gorrea, E. (2012). *Cyclobutane peptides and ureas: synthesis, folding, self-assembling and some biological properties*. PhD Thesis. Universitat Autònoma de Barcelona, Spain.

176. Gauvry, N.; Comoy, C.; Lescop, C.; Huet, F. *Synthesis* **1999**, *4*, 574-576.

177. Foulger, B. E.; Grevels, F. W.; Hess, D.; Koerner von Gustorf, E. A.; Leitich, J. *J. Chem. Soc. Dalton Trans.* **1979**, *10*, 1451-1459.

178. Karl-Ludwig. Procedure for the preparation of cyclobutene lactones. DE363312, **1987** 10 22

179. Dolbier, W.; Koroniak, H.; Houk, K.; Sheu, C. *Acc Chem. Res*. **1996**, *29*, 471-477.

180. Niwayama, S.; Kallel, E.; Spellmeyer, D.; Sheu, C.; Houk, K. *J. Org. Chem.* **1996**, *61*, 2813-2825.

181. Gourdel-Martin, M.-E.; Planchenault, D.; Huet, F. *Tetrahedron* **1995**, *51*, 4985-4990.

182. Harvey, I.; Crout, D. *Tetrahedron: Asymmetry* **1993**, *4*, 807-812.

183. Gourdel-Martin, M.-E.; Huet, F. *J. Org. Chem.* **1997**, *62*, 2166-2172.

184. Gauvry, N.; Huet, F. *J. Org. Chem.* **2001**, *66*, 583-588.

185. Perrott, M.; Novak, B. *Macromolecules* **1996**, *29*, 1817-1823.

186. Coste, J.; Le-Nguyen, D.; Castro, B. *Tetrahedron Lett.* **1990**, *31*, 205-208.

187. Castro, B.; Dormoy, J. R.; Evin, G.; Selve, C. *Tetrahedron Lett.* **1975**, *14*, 1219-1222.

188. Han, S.-Y.; Kim, Y.-A. *Tetrahedron* **2004**, *60*, 2447-2467.

189. Doig, A. J.; Baldwin, R. L. *Protein Sci.* **1995**, *4*, 1325-1236.

190. Rohl, C. A.; Charkrabartty, A.; Baldwin, R. L. *Protein Sci.* **1996**, *5*, 2623-2637.

191. Scholtz, J. M.; Baldwin, R. L. *Peptides* **1995**, 171-192.

192. López de la Paz, M.; Lacroix, E.; Ramírez-Alvarado, M.; Serrano, L. *J. Mol. Biol.* **2001**, *312*, 229-246.

193. Smith, A. M.; Williams, R. J.; Tang, C.; Coppo, P.; Collins, R. F.; Turner, M. L.; Saiani, A.; Ulijn, R. V. *Adv. Mater.* **2008**, *20*, 37-41.

194. Fernández-Escamilla, M.; Ventura, S.; Serrano, L.; Jiménez, M. A. *Protein Sci.* **2006**, *15*, 2278-2289.

195. Chen, L.; Morris, K.; Laybourn, A.; Elias, D.; Hicks, M. R.; Rodger, A.; Serpell, L.; Adams, D. J. *Langmuir* **2010**, *26*, 5232-5242.

196. Baxter, N. J.; Williamson, M. P. *J. Biomol. NMR* **1997**, *9*, 359-369.

197. Chang, G.; Guida, W. C.; Still, W. C. *J. Am. Chem. Soc.* **1989**, *111*, 4379-4386.

198. Chang, G.; Guida, W. C.; Still, W. C. *J. Am. Chem. Soc.* **1990**, *111*, 1419-1427.

199. Kolossváry, I.; Guida, W. C. *J. Am. Chem. Soc.* **1996**, *118*, 5011-5019.

200. Kolossváry, I.; Guida, W. C. *J. Comput. Chem.* **1999**, *20*, 1671-1684.

201. Halgren, T. A. *J. Comput. Chem.* **1996**, *17*, 490-519.

202. Mohamadi, F.; Richards, N. G. H. W.; Guida, W. C.; Liskamp, R.; Lipton, M.; Caufield, C.; Chang, G.; Qiu, D.; Shenkin, P. S.; Hollinger, F. P.; Still, W. C. *J. Phys. Chem. A,* **1990**, *11*, 440-467; MacroModel 9.0. http://www.schrodinger.com.

203. MacroModel 9.8 **2010**, Schrodinger, LLC, New York, NY.

204. Qiu, D.; Shenkin, P. S.; Hollinger, F. P.; Still, W. C. *J. Phys. Chem. A.* **1997**, *101*, 3005-3014.

205. Becke, A. D. *J. Chem. Phys.* **1993**, 98, 5648-5652.

206. Frisch, M. J.; Trucks, G. W.; Schlegel, H. B.; Scuseria, G. E.; Robb, M. A.; Cheeseman, J. R.; Scalmani, G.; Barone, V.; Mennucci, B.; Petersson, G. A.; Nakatsuji, H.; Caricato, M.; Li, X.; Hratchian, H. P.; Izmaylov, A. F.; Bloino, J.; Zheng, G.; Sonnenberg, J. L.; Hada, M.; Ehara, M.; Toyota, K.; Fukuda, R.; Hasegawa, J.; Ishida, M.; Nakajima, T.; Honda, Y.; Kitao, O.; Nakai, H.; Vreven Jr., T.; Montgomery, J. A.; Peralta, J. E.; Ogliaro, F.; Bearpark, M.; Heyd, J. J.; Brothers, E.; Kudin, K. N.; Staroverov, V. N.; Kobayashi, R.; Normand, J.; Raghavachari, K.; Rendell, A.; Burant, J. C.; Iyengar, S. S.; Tomasi, J.; Cossi, M.; Rega, N.; Millam, N. J.; Klene, M.; Knox, J. E.; Cross, J. B.; Bakken, V.; Adamo, C.; Jaramillo, J.; Gomperts, R.; Stratmann, R. E.; Yazyev, O.; Austin, A. J.; Cammi, R.; Pomelli, C.; Ochterski, J. W.; Martin, R. L.; Morokuma, K.; Zakrzewski, V. G.; Voth, G. A.; Salvador, P.; Dannenberg, J. J.; Dapprich, S.; Daniels, A. D.; Farkas, Ö.; Foresman, J. B.; Ortiz, J. V.; Cioslowski, J.; Fox, D. J. **2009** Gaussian 09, Revision B.01. Gaussian, Inc., Wallingford CT.

207. Sulzbach, H. M.; Schleyer, P. v. R.; Schaefer, H. F. *J. Am. Chem. Soc.* **1994**, *116*, 3967-3972.

208. Hoeben, F. J. M.; Wolffs, M.; Zhiang, J.; de Feyter, S.; Leclère, P.; Schenning, A. P. H. J.; Meijer, W. E. *J. Am. Chem. Soc.* **2007**, *129*, 9819-9828.

209. Nam, S. R.; Lee, H. Y.; Hong, J.-I. *Chem. Eur. J.* **2008**, *14*, 6040-6043.

210. Iavicoli, P.; Xu, H.; Feldborg, L. N.; Linares, M.; Paradinas, M.; Stafstrçm, S.; Ocal, C.; Nieto-Ortega, B.; Casado, J.; López-Navarrete, J. T.; Lazzaroni, R.; de Feyter, S.; Amabilino, D. B. *J. Am. Chem. Soc.* **2010**, *132*, 9350-9362.

211. Zhao, Y.; Truhlar, D. G. *Theor. Chem. Acc.*, **2008**, *120*, 215-241.

212. Marenich, A. V.; Cramer, C. J.; Truhlar, D. G. *J. Phys. Chem. B* **2009**, *113*, 6378-6396.

213. Seebach, D.; Jaun, B.; Sebesta, R.; Mathad, R. I.; Flögel, O.; Limbach, M.; Sellner, H.; Cottens, S. *Helv. Chim. Acta* **2006**, *89*, 1801-1825.

214. De Pol, S.; Zorn, C.; Klein, C. D.; Zerbe, O.; Reiser, O. *Angew. Chem. Int. Ed.* **2004**, *43*, 511-514.

215. Horne, W: S.; Johnson, L. M.; Ketas, T.; Thomas, J.; Klasse, P. J.; Lu, M.; Moore, J. P.; Gellman, S. H. *Proc. Nat. Acad. Sci. USA* **2009**, *106*, 14751-14756.

216. Giuliano, M. W.; Horne, W. S.; Gellman, S. H. *J. Am. Chem. Soc.* **2009**, *131*, 9860-9861.

217. *Supramolecular chemistry of anions*. A. Bianchi, K. Bowman-James, E.García-España. 1st edition, 1997. John Wiley & Sons, USA.

218. *Supramolecular chemistry*. J. W. Steed, J. L. Atwood. 2nd edition, 2009. John Wiley & Sons, USA.

219. *Anion Receptor Chemistry*, J. L. Sessler, P. A. Gale, W. S. Cho. 2006. Royal Society of Chemistry, Cambridge.

220. J. Bardi, R. Graham. Blasting antibodies with lasers provides direct way of measuring their flexibilities. 16th Dec 2002. University of California. Oct 2012. http://ucsdnews.ucsd.edu/newsrel/science/romesberg.htm

221. Steed, J. W.; Juneja, R. K.; Atwood, J. L. *Angew. Chem.* **1994**, *106*, 2571-2573.

222. Lehn, J. -M.; Méric, R.; Vigneeron, J. -P.; Bkouche-Waksman, I.; Pascard, C. *J. Chem. Soc. Chem. Commun.* **1991**, *2*, 62-64.

223. Cram, D. J.; Karbach, S.; Kim, Y. H.; Baczynskyj, L.; Kalleymeyn, G. W. *J. Am. Chem. Soc.* **1985,** *107*, 2575-2576.

224. Fairchild, R. M.; Holman, K. T. *J. Am. Chem. Soc.* **2005**, *127*, 16364-16365.

225. Steed, J. W. *Chem. Soc. Rev.* **2009**, *38*, 506-519.

226. Weber, E.; Hosel, H.-P. *J. Incl. Phenom.* **1983**, *1*, 79-85.

227. Vögtle, F.; Weber, E. *Inorg. Chim. Acta* **1980**, *45*, L65-L67.

228. Vögtle, F.; Weber, E. *Angew. Chem. Int. Ed. Engl.* **1979**, *18*, 753-776.

229. Vögtle, F.; Weber, E. *Angew. Chem. Int. Ed. Engl.* **1979**, *91*, 813-837.

230. *Encyclopedia of Supramolecular Chemistry*, J. L. Atwood, J. W. Steed. 2004. Marcel Dekker, Inc., USA.

231. Dietrich, B.; Lehn, J. -M.; Guilhem, J.; Pascard, C. *Tetrahedron Lett.* **1989**, *30*, 4125-4128.

232. Graf, E.; Lehn, J. -M. *J. Am. Chem. Soc.* **1976**, *98*, 6403-6405.

233. Jung, M. E.; Xia, H. *Tetrahedron Lett.* **1988**, *29*, 297-300.

234. Newcomb, M.; Madonik, A. M.; Blanda, M. T.; Judice, J. K. *Organometallics* **1987**, *6*, 145-150.

235. Lehn, J. -M.; Sonveaux, E.; Willard, A. K. *J. Am. Chem. Soc.* **1978**, *100*, 4914-4916.

236. Heyer, D.; Lehn, J. -M. *Tetrahedron Lett.* **1986**, 27, 5869-5872.

237. a) Schmidtchen, F. P.; Gleich, A.; Schummer, A. *Pure Appl. Chem.* **1989**, *61*, 1535-1546. b) Seel, C.; Galan, A.; de Mendoza, J. *Top. Curr. Chem.* **1995**, *175*, 101-132.

238. Dietrich, B.; Fyles, T. M.; Lehn, J. -M.; Pease, L- G.; Fyles, D. L. *J. Chem. Soc. Chem. Commun.* **1978**, 934-936.

239. Gross, R.; Bats, J. W.; Göbel, M. W. *Liebigs Ann. Chem.* **1994**, 205-210.

240. Gelb, R. I.; Schwartz, L. M.; Zompa, L. J. *Inorg. Chem.* **1986**, *25*, 1527-1535.

241. Morgan, G.; MacKee, V.; Nelson, J. *J. Chem. Soc. Chem. Commun.* **1995**, 1649-1652.

242. Bencini, A.; Bianchi, A.; Dapporto, P.; García-España, E.; Micheloni, M.; Paoletti, P.; Paoli, P. *J. Chem. Soc. Chem. Commun.* **1990**, 753-755.

243. Dietrich, B.; Hosseini, M. W.; Lehn, J. -M.; Sessions, R. B. *J. Am. Chem. Soc.* **1981**, *103*, 1282-1283.

244. a) Hosseini, M. W.; Ruppert, R.; Schaeffer, P.; De Cian, A.; Kyritsaka, N.; Fishcer, J. *J. Chem. Soc. Chem. Commun.* **1994**, 2135-2136. b) Brand, G.; Hosseini, M. W.; Rupert, R.; De Cian, A.; Fischer, J.; Kyritsaka, N. *New J. Chem.* **1995**, *19*, 9-13.

245. Smith, P. J.; Reddington, M. V.; Wilcox, C. S. *Tetrahedron Lett.* **1992**, *33*, 6085-6088.

246. Fan, E.; Van Arman, S. A.; Kincaid, S.; Hamilton, A. D. *J. Am. Chem. Soc.* **1993**, *115*, 369-370.

247. Pascal, R. A.; Spergel, J.; Van Eggen Jr., D. *Tetrahedron Lett.* **1986**, *27*, 4099-4102.

248. Valiyaveettil, S.; Engbersen, J. F. J.; Verboom, W.; Reinhoudt, D. N. *Angew. Chem. Int. Ed. Engl.* **1993**, *32*, 900-901.

249. Inoue, Y.; Kanbara, T.; Yamamoto, T. *Tetrahedron Lett.* **2003**, *44*, 5167-5169.

250. Hossain, M. A.; Llinares, J. M.; Powell, D.; Bowman-James, K. *Inorg. Chem.* **2003**, *42*, 5043-5045.

251. Kavallieratos, K.; Gala, S. R.; Austin, D. J.; Crabtree, R. H. *J. Am. Chem. Soc.* **1997**, *119*, 2325-2326.

252. Beer, P. D.; Chen, Z.; Goulden, A. J., *et al. J. Chem. Soc. Chem. Commun.* **1993**, 1834-1836.

253. Danby, A.; Seib, L.; Alcock, N. W.; Bowman-James, K. *Chem. Commun.* **2000**, 973-974.

254. Lakshminarayanan, P. S.; Suresh, E.; Ghosh, P. *Inorg. Chem.* **2006**, *45*, 4372-4380.

255. *Supramolecular Chemistry: From Molecules to Nanomaterials*, P. A. Gale, J. W. Steed. 2012. John Wiley & Sons, USA.

256. Bordwell, F. G.; Algrim, D. J.; Harrelson Jr., J. A. *J. Am. Chem. Soc.* **1988**, *110*, 5903-5904.

257. Bordwell, F. G. *Acc. Chem. Res.* **1988**, *21*, 456-463.

258. Zielinsky, T.; Jurczak, J. *Tetrahedron,* **2005**, *61,* 4081-4089.

259. *Industrial Organic Chemistry*. K. Weissermel, H. -J. Arpe. 3rd edition, 1997. VCH, Germany.

260. *Macrocyclic polyether syntheses*, G. W. Gokel, S. H. Korzeniowski. 1982. Springer-Verlag, Germany.

261. Dydio, P.; Zielinski, T.; Jurczak, J. *J. Org. Chem.* **2009**, *74*, 1525–1530.

262. Leska, B.; Pankiewicz, R.; Schroeder, G.; Gierczyk, B.; Maciejewski, H.; Marciniec, B. *Catal. Commun.*, **2008**, *9*, 821-825.

263. Leska, B.; Pankiewicz, R.; Schroeder, G.; Maia, A. *J. Mol. Catal. A-Chem.* **2007**, *269*, 141-148.

264. Praveen, L.; Ganga, V. B.; Thirumalai, R.; Sreeja, T.; Reddy, M. L. P.; Varma, R. L. *Inorg. Chem.* **2007**, *46*, 6277-6282.

265. Valik, M.; Kral, V,; Herdtweck, E.; Schmidtchen, F.P. *New J. Chem*., **2007**, *31*, 703-710.

266. Seganish, J- L.; Santacroce, P. V.; Salimian, K. J.; Fettinger, J. C.; Zavalij, P. Y.; Davis, J. T. *Angew. Chem., Int. Ed.*, **2006**, *45*, 3334-3338.

267. Christofi, A. M.; Garratt, P. J.; Hogarth, G.; Ibbett, A. J., Ng, Y-F.; Steed, J. W. *Tetrahedron*, **2002**, *58*, 4543-4549.

268. Kohl, S. W.; Heinemann, F. W.; Hummert, M.; Weisshoff, H.; Grohmann, A. *Eur. J. Inorg. Chem.* **2006**, 3901-3910.

269. Coyle, J. L.; Fuller, A.; McKee, V.; Nelson, J. *Acta Crystallogr. C*, **2006**, *62*, 472-476.

270. Jäntti, A.; Wagner, M.; Suontamo, R.; Kolehmainen, E.; Rissanen, K. *Eur. J. Inorg. Chem.* **1998**, 1555-1562.

271. Singh, A. S.; Sun, S-S. *J. Org. Chem.* **2012**, *77*, 1880-1890.

272. Dey, S. K.; Pramanik, A.; Das, G. *CrystEngComm.* **2011**, *13*, 1664-1675.

273. Koeller, S.; Bernardinelli, G.; Piguet, C. *Dalton Trans.* **2003**, 2395-2404.

274. Dey, A. K.; Das, G. *Chem. Commun.* **2011**, *47*, 4983-4985.

275. Ortuño, J. A.; Expósito, R.; Sánchez-Pedreño, C.; Albero, M. A.; Espinosa, A. *Anal. Chim. Acta* **2004**, *525*, 231-237.

276. Mukherjee, J.; Lucas, R. L.; Zart, M. K.; Powell, D. R:; Day, V. W.; Borovik, A. S. *Inorg. Chem.* **2008,** *47*, 5780-5786.

277. Tang, K-Z.; Li, Y-F.; Tang, Y.; Liu, W-S.; Tang, N.; Tan, M-Y. *Spectrochim. Acta, Part A* **2007**, *67*, 858-863.

278. Ibrahim, M. M.; Mersal, G. A. M. *J. Inorg. Biochem.* **2010**, *104*, 1195-1204.

279. Ray, M.; Golombek, A. P.; Hendrich, M. P.; Yap, G. P. A.; Liable-Sands, L. M.; Rheingold, A. L.; Borovik, A. S. *Inorg. Chem.* **1999**, *38*, 3110-3115.

280. Hammes, B. S.; Ramos-Maldonado, D.; Yap, G. P. A.; Liable-Sands, L.; Rheingold, A. L.; Young, V. G.; Borovik, A. S. *Inorg. Chem.* **1997**, *36*, 3210-3211.

281. Popovski, E.; Klisarova, L.; Vikic-Topic, D. *Molecules* **2000**, *5*, 927-936.

282. Nishiyama, K.; Mikuni, H.; Harada, M. *Bull. Chem. Soc. Jpn.* **1985**, *58*, 3381-3382.

283. Schultz, M.; Kulis, J.; Murison, J.; Andrews, G. W. *Aust. J. Chem.* **2008**, *61*, 297-302.

284. Öztürk, G.; Çolak, M.; Togrul, M. *J. Incl. Phenom. Macrocyclic Chem.* **2010**, *68*, 49-54.

285. Wang, Q.; Tang, K.; Jin, X.; Huang, X.; Liu, W.; Yao, X.; Tang, Y. *Dalton Trans.* **2012**, *41*, 3431-3438.

286. Kang, D.; Lee, J. Y.; Lee, J. -E.; Lee, S. Y.; Choi, K. S.; Lee, S. S. *Inorg. Chem. Commun.* **2007**, *10*, 1105-1108.

287. Moglioni, A. G.; Muray, E.; Castillo, J. A.; Álvarez-Larena, Á.; Moltrasio, G. Y.; Branchadell, V.; Ortuño, R. M. *J. Org. Chem.* **2002**, *67*, 2402-2410.

288. Aguado, G. P.; Moglioni, A. G.; García-Expósito, E.; Branchadell, V.; Ortuño, R. M. *J. Org. Chem.* **2004**, *69*, 7971-7918.

289. Ortuño, R. M.; Moglioni, A. G.; Moltrasio, *G. Curr. Org. Chem*. **2005**, *9*, 237-259.

290. Burgess, K.; Li, S.; Rebenspies, J. *Tetrahedron Lett.* **1997**, *38*, 1681-1684.

291. Brough, P.; Klumpp, C. *J. Org. Chem.* **2006**, *71*, 2014-2020.

292. Han, S.-Y.; Kim, Y.-A. *Tetrahedron*, **2004**, *60*, 2447-2467.

293. Iqbal, M.; Huskens, J.; Sypula, M.; Modolo, G.; Verboom, W. *New J. Chem.*, **2011**, *35*, 2591-2600.

294. Huang, Z.; Park, J. I.; Watson, D. S.; Hwang, P.; Szoka Jr., F. C. *Bioconjugate Chem.* **2006**, *17*, 1592-1600.

295. Muller, P. *PAC* **1994**, *66*, 1077-1184.

296. Bordwell, F. G.; Algrim, D. *J. Org. Chem.* **1976**, *41*, 2507-2508.

297. Olmstead, W. N.; Bordwell, F. G. *J. Org. Chem.* **1980**, *45*, 3299-3305.

298. Werner, F.; Schneider, H. -J. *Helv. Chim Acta*, **2000**, *83*, 465-478.

299. Chmielewski, M. J.; Zielinski, T.; Jurczak, J. *Chem. Eur. J*. **2005**, *11*, 6080-6094.

300. Bates, G. W.; Triyanti; Light, M. E.; Albrecht, M.; Gale, P. A.; *J. Org. Chem.* **2007**, *72*, 8921-8927.

301. Yang, D.; Li, X.; Sha, Y.; Wu, Y. -D. *Chem. Eur. J.* **2005**, *11*, 3005-3009.

302. Kaewtong, C.; Fuangswasdi, S.; Muangsin, N.; Chaichit, N.; Vicens, J.; Pulpoka, B. *Org. Lett*. **2006**, *8*, 1561-1564.

303. Bondy, C. R.; Loeb, S. J. *Coord. Chem. Rev.* **2003**, *240*, 77-99.

304. Murphy, V. J.; Hascall, T.; Chen, J. Y.; Parkin, G. *J. Am. Chem. Soc.* **1996**, *118*, 7428-7429.

305. Perera, S. A.; Bartlett, R. J. *J. Am. Chem. Soc.* **2000,** *122*, 1231-1232.

306. Kang, S. O.; Powell, D.; Day, V. W.; Bowman-James, K. *Angew. Chem. Int. Ed.* **2006**, *45*, 1921-1925.

307. Costere, A. M.; Bañuls, M. J.; Aurell, M. J.; Ward, M. D.; Argent, S. *Tetrahedron* **2004**, *60*, 9471-9478.

308. a) Kang, S. O.; Llinares, J. M.; Powell, D.; VanderVelde, D.; Bowman-James, K. *J. Am. Chem. Soc*. **2003**, *125*, 10152-10153; b) Kang, S. O.; VanderVelde, D.; Powell, D.; Bowman-James, K. *J. Am. Chem. Soc.* **2004**, *126*, 12272-12273; c) Kang, S. O.; Powell, D.; Bowman-James, K. *J. Am. Chem. Soc*. **2005**, *127*, 13478-13479.

309. a) Esteban-Gómez, D.; Fabbrizzi, L.; Licchelli, M. *J. Org. Chem.* **2005**, *70*, 5717-5720 ; b) Boiocchi, M.; Boca, L. D.; Gómez, D. E.; Fabbrizzi, L.; Licchelli, M.; Monzani, E.; *J. Am. Chem. Soc.* **2004**, *126*, 16507-16514.

310. a) Gunnlaugsson, T.; Kruger, P. E.; Jensen, P.; Pfeffer, F. M.; Hussey, G. M. *Tetrahedron Lett.* **2003**, *44*, 8909–8913; b) Pfeffer, F. M.; Gunnlaugsson, T.; Jensen, P.; Kruger, P. E. *Org. Lett.* **2005**, *7*, 5357–5360; c) Gunnlaugsson, T.; Kruger, P. E.; Jensen, P.; Tierney, J.; Ali, H. D. P.; Hussey, G. M. *J. Org. Chem.* **2005**, *70*, 10875–10878.

311. a) Camiolo, S.; Gale, P. A.; Hursthouse, M. B.; Light, M. E.; Shi, A. J. *Chem. Commun.* **2002**, 758-759. b) Gale, P. A.; Navakhun, K.; Camiolo, S.; Light, M. E.; Hursthouse, M. B. *J. Am. Chem. Soc.* **2002**, *124*, 11228-11229. c) Camiolo, S.; Gale, P. A.; Hursthouse, M. B.; Light, M. E. *Org. Biomol. Chem.* **2003**, *1*, 741-744.

312. a) Kang, S. O.; Day, V. W.; Bowman-James, K. *Inorg. Chem.* **2010**, *49*, 8629-8636. b) Kang, S. O.; Day, V. W.; Bowman-James, K. *J. Org. Chem.* **2010**, *75*, 277-283.

313. Kang, S. O.; Begum, R. A.; Bowman-James, K. *Angew. Chem. Int. Ed.* **2006**, *45*, 7882-7894.

314. Shang, X. -F.; Xu, X. -F.; Lin, H.; Shao, J.; Lin, H. -K. *J. Mol. Recognit.* **2007**, *20*, 139-144.

315. Jose, D. A.; Kumar, D. K.; Ganguly, B.; Das, A. Org. Lett. **2004**, *6*, 3445-3448.

316. Lascaux, A.; Le Gac, S.; Wouters, J.; Luhmerd, M.; Jabin, I. *Org. Biomol. Chem.* **2010**, *8*, 4607-4616.

317. Woods, C. J.; Camiolo, S.; Light, M. E.; Coles, S. J.; Hursthouse, M. B.; King, M. A.; Gale, P. A.; Essex, J. W. *J. Am. Chem. Soc.* **2002**, *124*, 8644-8652.

318. Bates, G. W.; Gale, P. A.; Light, M. E. *Chem. Commun.* **2007**, 2171-2173.

319. Chmielewski, M. J.; Charon, M.; Jurczak, J. *Org. Lett.* **2004**, *6*, 3501-3504.

320. Li, R.; Evans, L. S.; Larsen, D. S.; Gale, P. A.; Brooker, S. *New J. Chem.* **2004**, *28*, 1340-1343.

321. Ravikumar, I.; Lakshminarayanan, P. S.; Ghosh, P. *Inorg. Chim. Acta* **2010**, *363*, 2886-2895.

322. Yin, Z.; Zhang, Y.; Hea, J.; Cheng, J. -P. *Tetrahedron* **2006**, *62*, 765-770.

323. Tufariello, J. J.; Milowsky, A. S.; Al-Nuri, M.; Goldstein, S. *Tetrahedron Lett.* **1987**, *28*, 267-270.

324. Izquierdo, S.; Martin-Vilà, M.; Moglioni, A. G.; Branchadell, V.; Ortuño, R. M. *Tetrahedron: Asymmetry* **2002**, *13*, 2403-2405.

325. Zhao, L-X.; Park, J.G.; Moon, Y-S.; Basnet, A.; Choi, J.; Kim, E-K.; Jeong, T.C.; Jahng, Y.: Lee, E-S. *Il Farmaco* **2004**, *59*, 381-387.

326. Tegoni, M.; Ferretti, L.; Sansone, F.; Remelli, M.; Bertolasi, V.; Dallavalle, F. *Chem. Eur. J.* **2007,** *13*, 1300-1308.

327. García-Álvarez, I.; Garrido, L.; Fernández-Mayoralas, A. *ChemMedChem* **2007,** *2*, 496-504.

328. Muscio, O.J.; Paulter, C.D. *J.Org. Chem*. **1974**, *39*, 3288-3291.

329. Tomapatanaget, B.; Tuntulani, T.; Wisner J. A.; Beer, P. D.*Tetrahedron Lett.* **2004**, *45*, 663-666.

330. Zeng, H.; Xiaowu, Y.; Flowers, R. A.; Gong, B. *J. Am. Chem. Soc.* **2002**, *124*, 2903-2910.

331. Matsoukas, J.; Moharir, Y. E.; Findlay, J. A. *J. Nat. Products* **1983**, *46*, 582-585.

332. Ranganathan, R. S.; Fan, H.; Tweedle, M. F., inventors; 2007 Jan. 9. Conjugates of antioxidants with metal chelating ligands for use in diagnostic and therapeutics (page 22). United States patent US 7,160,535.

333. Boger, D. L.; Zhou, J.; Winter, B.; Kitos, P. A. *Bioorg. Med. Chem.* **1995**, *3*, 1579-1593.

334. Ham, P. B., inventor; 1989 Dec. 21. Compounds having a renin-inhibitory activity (page 39). European patent EP 0 375 451.

335. Tietze, L. F.; Panknin, O.; Krewer, B.; Major, F.; Schuberth, I. *Int. J. Mol. Sci.* **2008**, *9*, 821-837.

336. DeVita, R. J.; Frontier, A. J.; Schoen, W. R.; Wyvratt, M. J.; Fisher, M. H.; Cheng, K.; Chan, W. W.-S.; Butler, B. S.; Smith, R. G. *Helv. Chim. Acta* **1997**, *80*, 1244-1259.

337. Parthasardhi B.; Vamsi, B.; Manohar, V.; Rathnakar, K.; Madhanmohan, M., inventors; 2011 Jul. 7. Novel aza-peptides containing 2,2-disubstituted cyclobutyl and/or substituted alkoxy benzyl derivatives as antivirals (page 32). International patent WO 2011/080562.

ANNEXES

ANNEX CHAPTER II

2.5.1. Structural study in solution of β -dipeptides (*S*,*R*,*S*,*S*)-69, (*S*,*S*,*R*,*R*)-69, (*R*,*S*,*S*,*S*)-69 and (*R*,*S*,*S*,*R*)-70

Through 1D selective TOCSY experiments, the isolated selection of NH_4, NH_{10} and NH_{16} protons and posterior magnetization to the whole spin system permitted the edition of ^{1}H-NMR spectrum of each residue into separated subspectra (Figure **150**). Such spectra give the information of which signals correspond to the protons belonging to the same residue as the NH_i irradiated, because the magnetization is transferred through a chain link, without exceeding carbonyl groups.

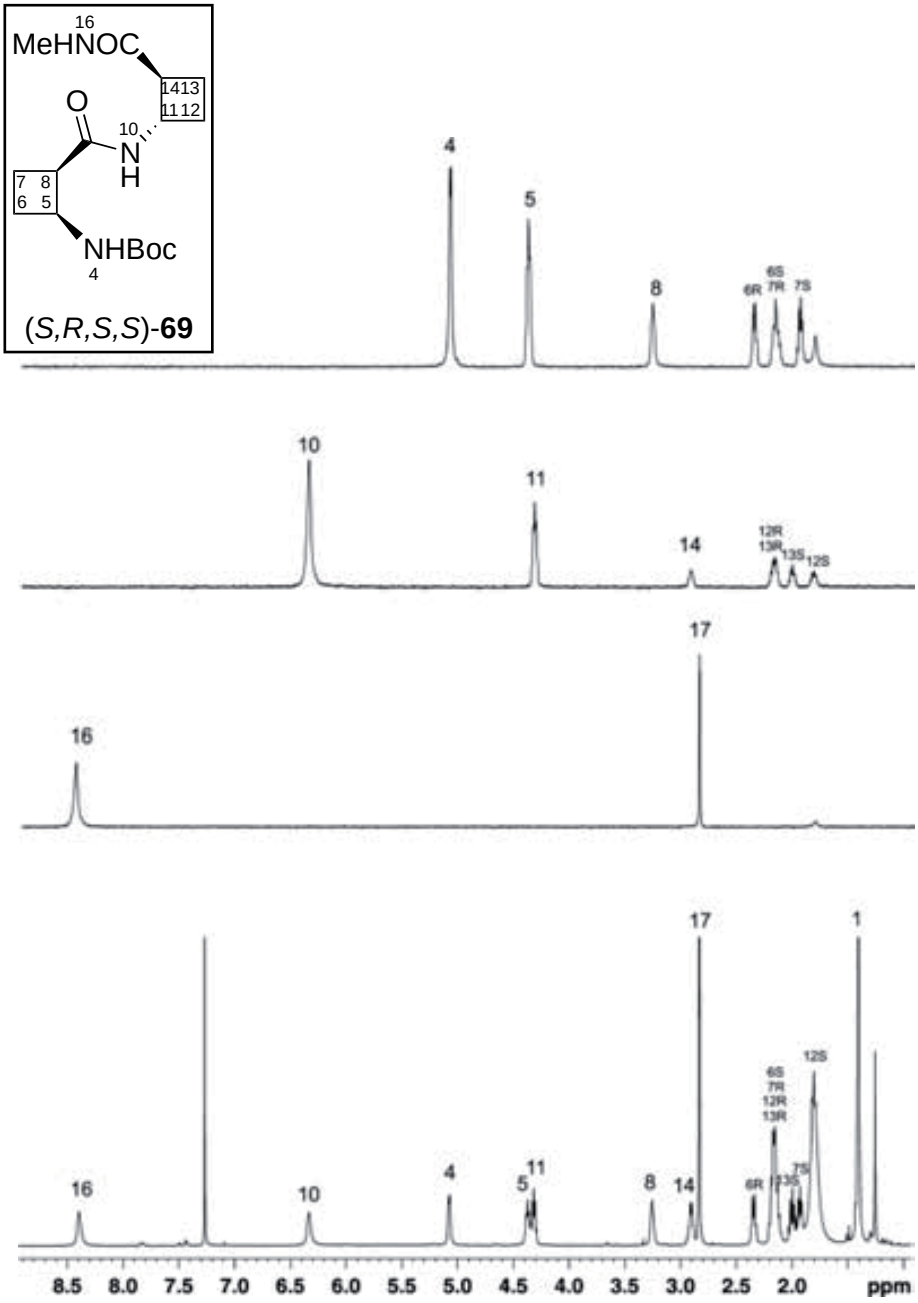

Figure **150**. 1D selective TOCSY experiments on NHs of (*S*,*R*,*S*,*S*)-**69** used for characterization purposes. TOCSY mixing time was 60 ms at 298 K in $CDCl_3$ (600 MHz); ^{1}H-NMR at the bottom for visual comparison.

On the other hand, spatial disposition of the residues was disclosed with the inspection of 1D selective NOE experiments on the same NH protons (Figure **151**).

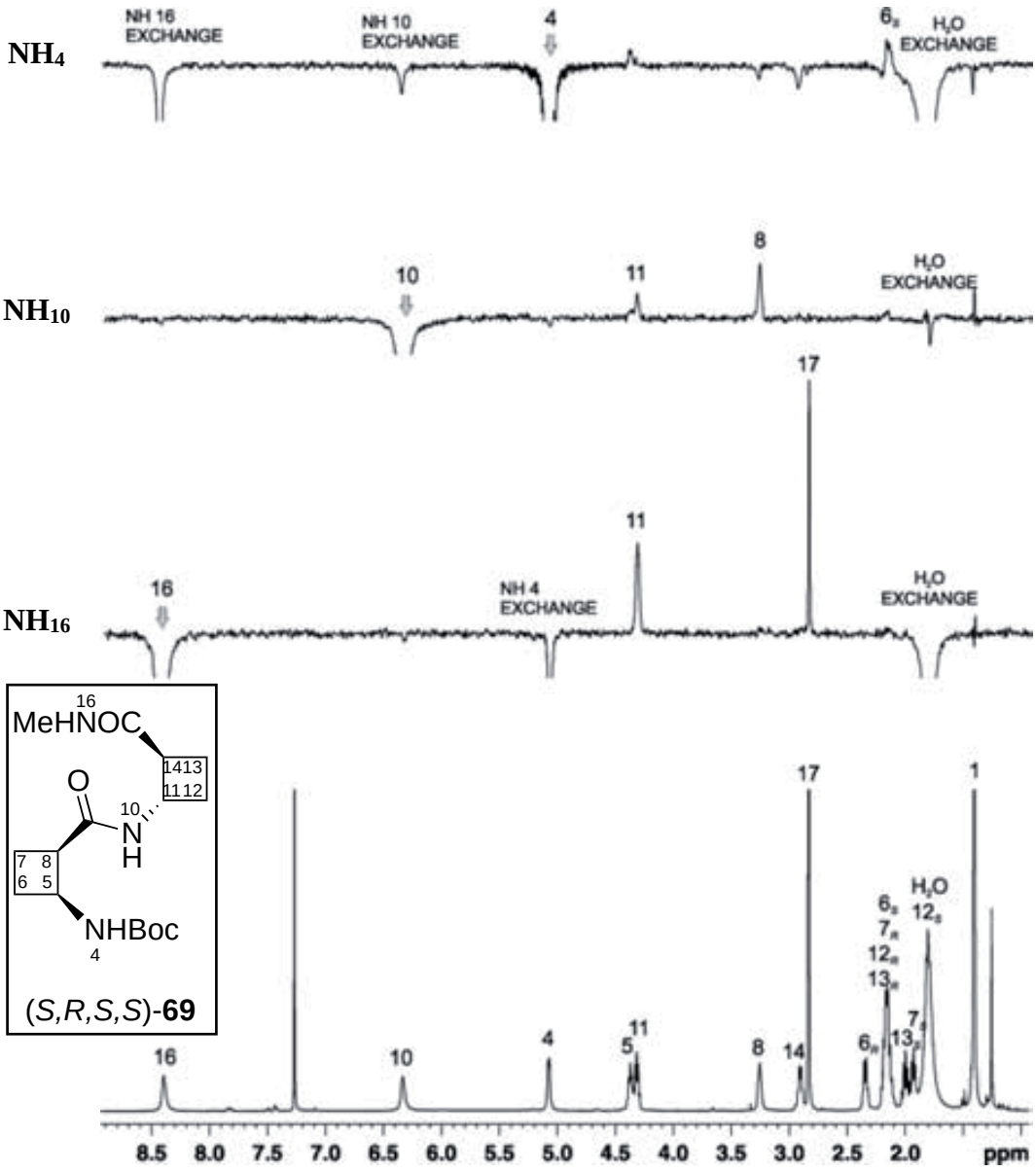

Figure **151**. 1D selective NOESY experiments on NHs of (*S*,*R*,*S*,*S*)-**69** used for characterization and conformational elucidation. NOESY mixing time was 500 ms at 298 K in $CDCl_3$ (600 MHz); ^{1}H-NMR at the bottom for visual comparison.

As it is observed in the spectra, each of the irradiated NH signals showed to have intra and/or inter-residual interactions. This suggested that some hydrogen bonds could be possibly shared between neighbour cyclobutane residues. Moreover, the presence of different secondary structures depending on the chirality of the peptides could be directly detected when registering ^{1}H-NMR

spectra (Figure **152**). It is noteworthy that each secondary structure(s) led to distinct shifts on NH signals.

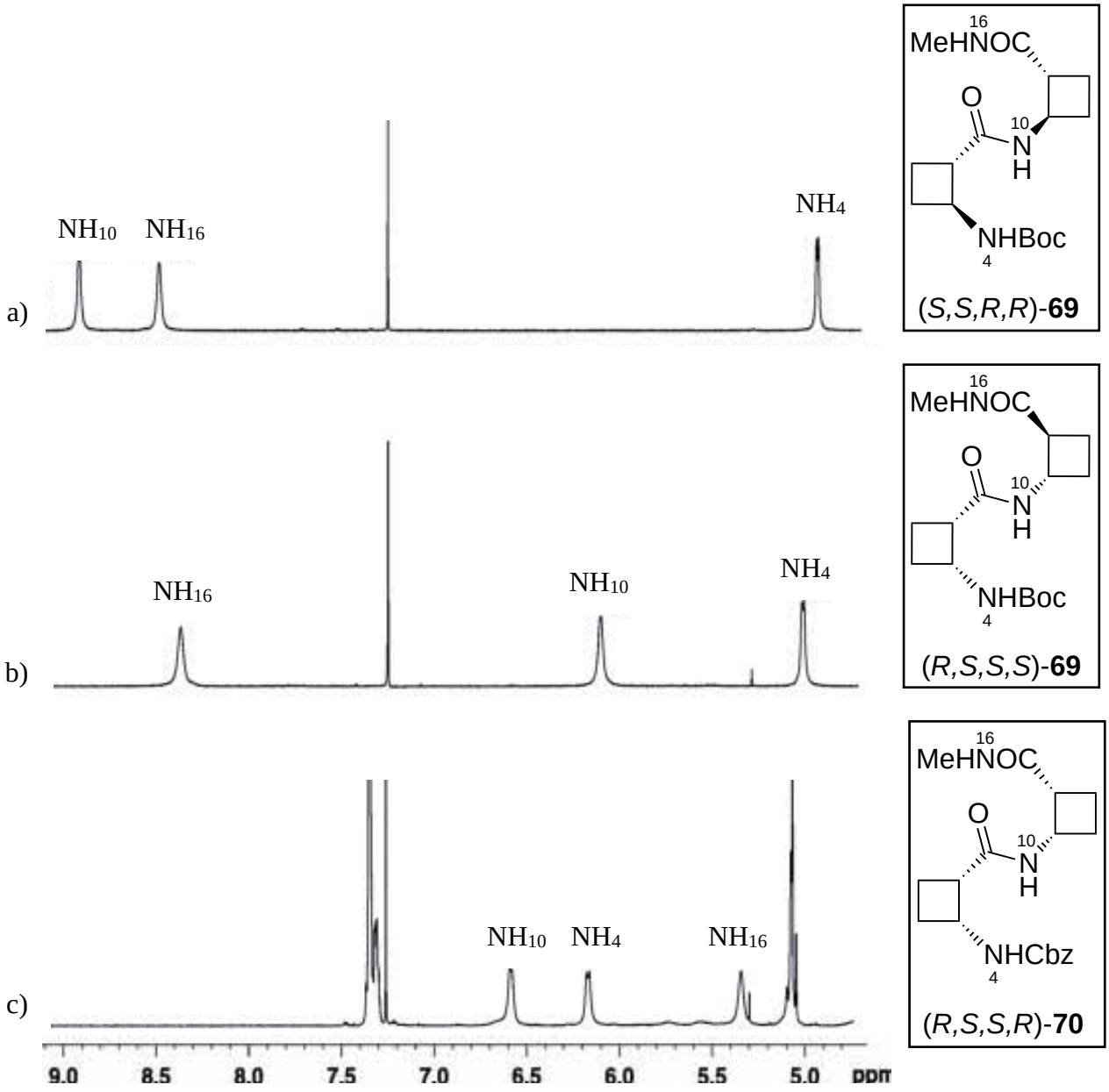

Figure **152**. NH pattern of pseudotripeptides: a) (*S*,*S*,*R*,*R*)-**69** corresponding to $H8_PH8_M$ structure. b) (*R*,*S*,*S*,*S*)-**69** corresponding to $Z6_MH8_P$-$Z8_MH8_P$ equilibrium. c) (*R*,*S*,*S*,*R*)-**70** corresponding to $Z6_MZ6_P$ structure. 600 MHz in $CDCl_3$ at 298 K. Note that numbering of the NHs is done equally so they can be easily compared, despite it does not follows the real order of the atoms.

ANNEX CHAPTER III

3.5.1. Structural study in solution of pseudopeptides

3.5.1.1. Pseudodipeptide 97

1D Selective TOCSY experiments on both NH_8 and NH_{15} protons were primarily carried out, showing same ^1H-^1H correlation (Figure **153**).

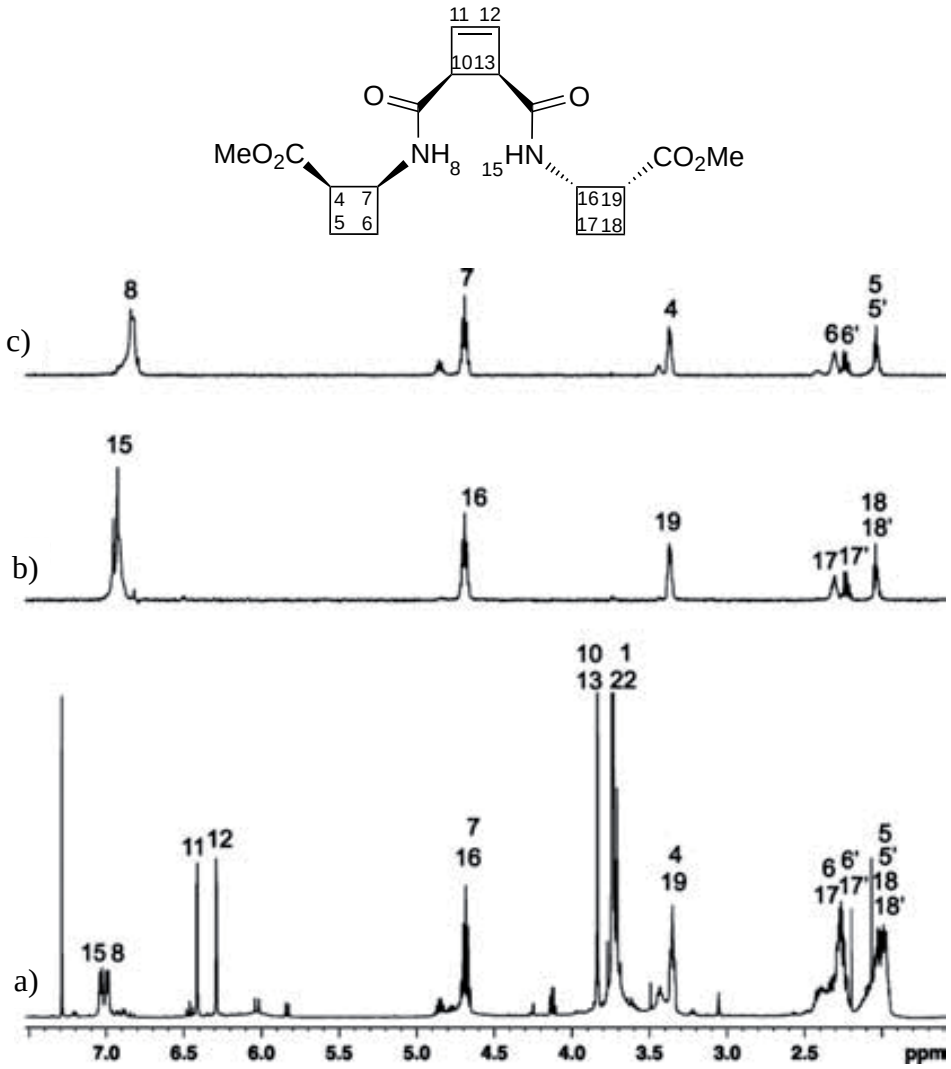

Figure **153**. 1D selective TOCSY NMR experiments used for product characterization of pseudodipeptide **97**. TOCSY mixing time was set to 60 ms in all the experiments. Experiments were performed at 298 K in $CDCl_3$ (600 MHz). a) ^1H-NMR for visual comparison purposes. b) NH_{15} selective TOCSY. c) NH_8 selective TOCSY.

1D Selective NOESY also showed similar intra-residue patterns (Figure **154**).

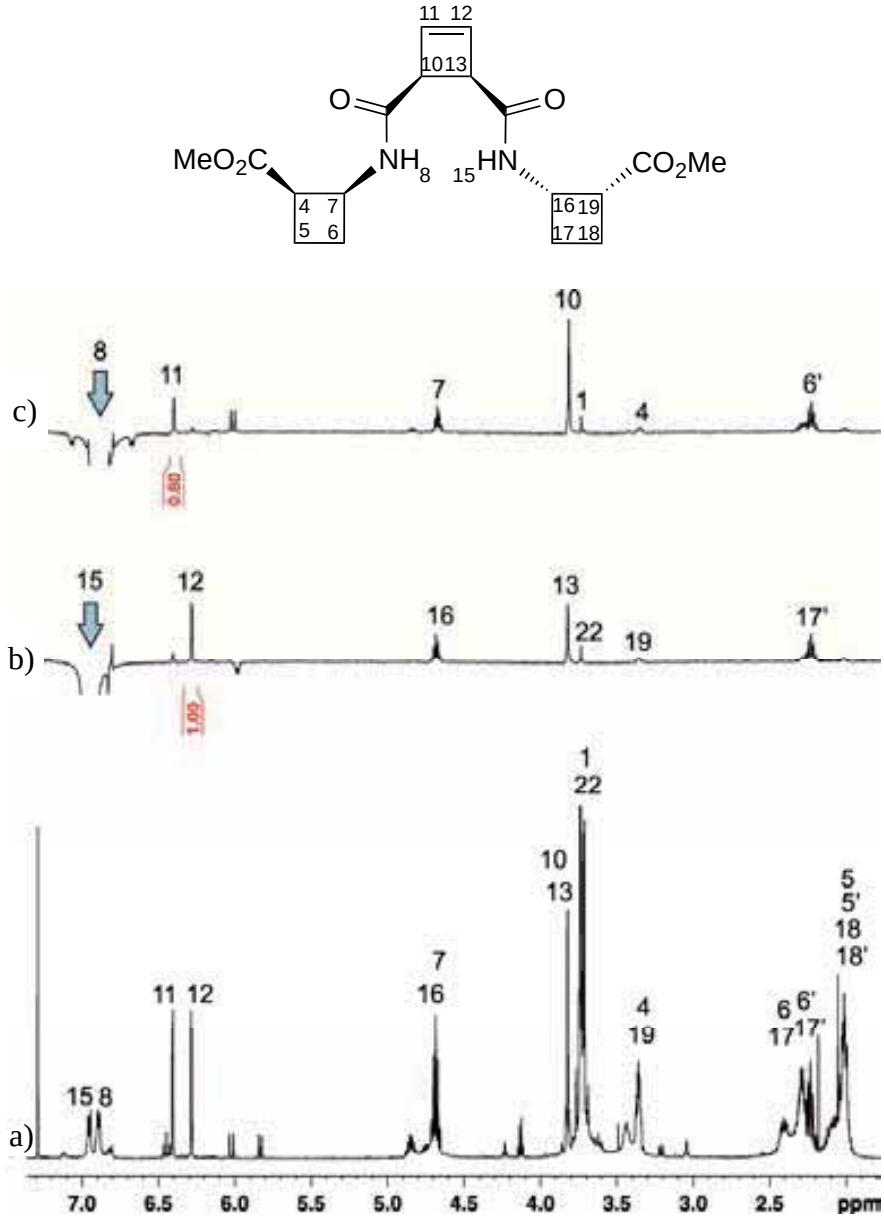

Figure **154**. a) ^{1}H-NMR of pseudodipeptide **97** in $CDCl_3$ recorded at 298 K (600 MHz) . b) 1D-selective NOE experiment when irradiating NH_{15} proton. c) 1D-selective NOE experiment when irradiating NH_8 proton. All NOE experiments were performed in a Bruker 600 MHz spectrometer in $CDCl_3$ at 298 K and using a NOE mixing time of 500 ms.

As preliminary result, TOCSY data and NOE contacts suggested the formation of similar six-membered hydrogen-bonded rings in every residue, as in the isolated monomers. Therefore, the structural effect of the intercalated cyclobutene unit seemed to be negligible.

3.5.1.2. Pseudotetrapeptide 98

1D selective TOCSY experiments showed two different pairs of NH-cyclobutane residues, but signals were not completely distinguishable because of their overlapping (Figure **155**).

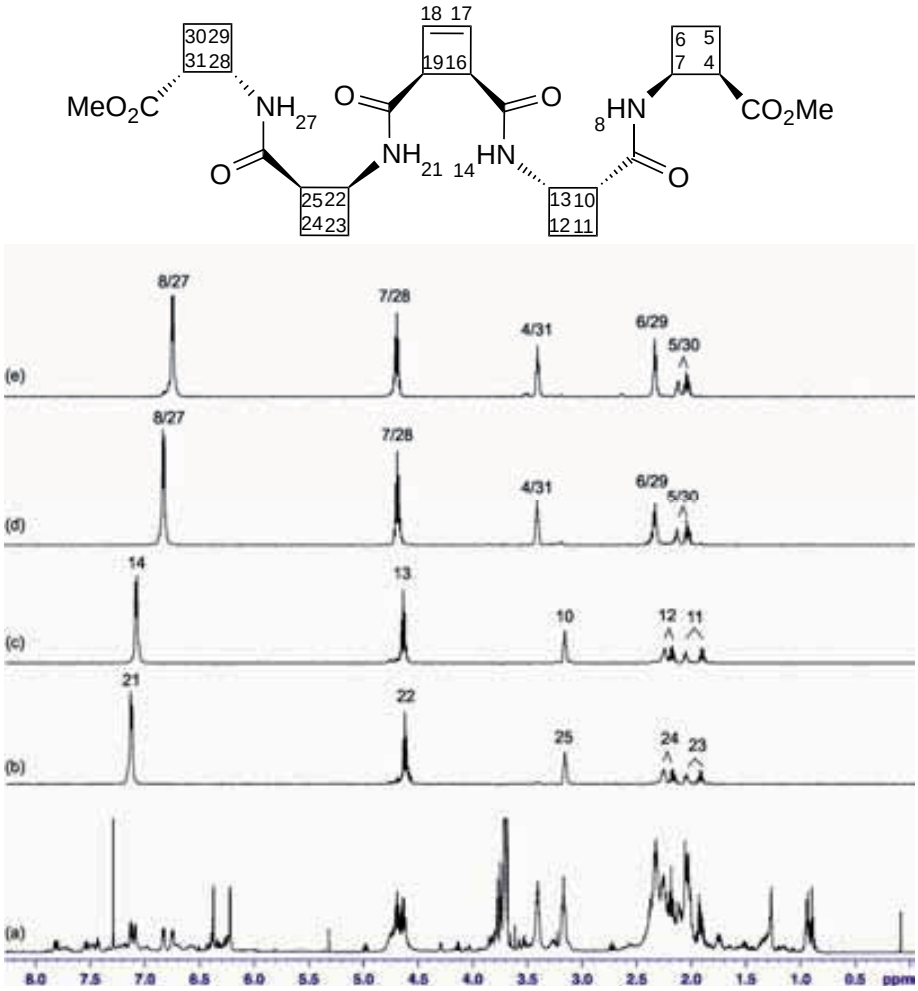

Figure **155**. 1D selective TOCSY NMR experiments used for product characterization of pseudotetrapeptide **98**. a) ^{1}H-NMR for visual comparison purposes. (b) NH_{21} selective TOCSY. (c) NH_{14} selective TOCSY. d) and e) $NH_{8/27}$ selective TOCSY. TOCSY mixing time was set to 60 ms in all the experiments. Experiments were performed at 298 K in $CDCl_3$ (600 MHz).

ROESY experiments exhibited strong inter-residue ROE contacts between $H\alpha_{(i)}$ and $NH_{(i\pm1)}$ protons (Figure **156)**.

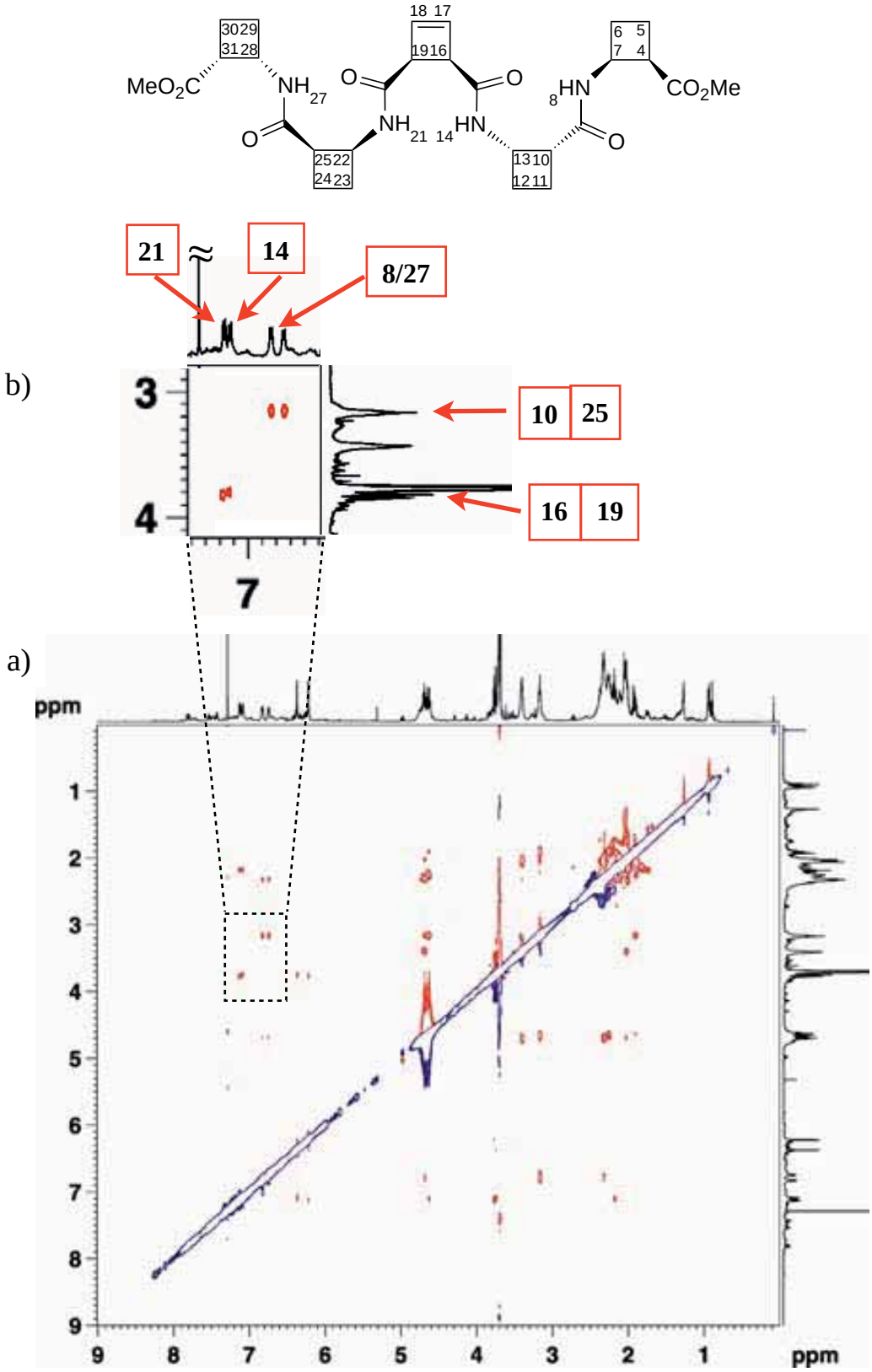

Figure **156**. a) ROESY NMR spectrum of pseudopeptide **98** in $CDCl_3$ recorded at 298 K (600 MHz). b) ROESY NMR spectrum enlargement showing the strong inter-residue contacts.

3.5.2. Gelation properties of linear AA-containing hybrid peptides

- When **121** and **126** were mixed with CH_2Cl_2 or EtOH 96% and acetone or MeCN, respectively, some gel or gel-like material spontaneously appeared in the mixtures after 1-2 hours at room temperature, before heating or sonication (Figure **157**). Although they were not as homogeneous as the prepared gels and some supernatant solvent was observed, this fact revealed the intrinsic capacity of both compounds to gelate different types of solvents.

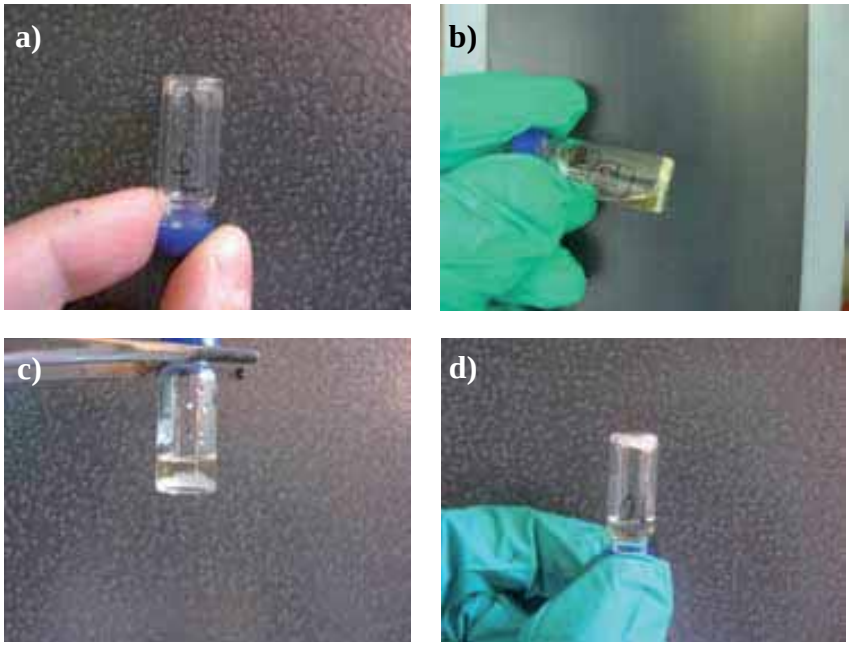

Figure **157**. Spontaneous gel formation when solvent and organogelator were mixed and they were left for 1-2 hours at room temperature. a) Tetrapeptide **121** in CH_2Cl_2 (200 mg/mL). b) **121** in EtOH 96% (200 mg/mL). c) Pseudotetrapeptide **126** in acetone (17 mg/mL). d) **126** in ACN (11 mg/mL).

- Table **28** shows gelation tests with GABA-containing hexapeptide and octapeptide.

Table **28**. Gelation behaviour of compounds **124** and **125** in common alcohols.[a]

Compound	**Solvent and minimum gelation concentration**[b,c]			
	***iso*-PrOH**	**Ethanol**	**Methanol**	**Ethylene glycol**
124	7 9	8 11	6 8	S[d]
125	S[e]	S[f]	S[e]	S[e]

[a] Dielectric constant increases from left to right.
[b] Units: *mgc* in mg/mL (*top*) and mM (*bottom*).
[c] S: soluble.
[d] Soluble at 27 mg/mL concentration, 37 mM.
[e] Soluble at 50 mg/mL concentration, 56 mM.
[f] Soluble at 10 mg/mL concentration, 11 mM.

- Table **29** shows hydrogelation tests with GABA-containing hexapeptide.

Table **29**. Hydrogelation behaviour tests of compound **124** (5 mg) in common alcohols.

Vial	Alcohol	V alcohol (mL)	V H_2O (mL)	H_2O content (% v/v)
1	*iso*-PrOH	0.45	0.05	10
2		0.40	0.02	4.8
3		0.35	0.05	12.5
4	Ethanol	0.30	0.02	6.3

3.5.3. Supramolecular study of gels from tetrapeptides 106 and 121 in toluene

3.5.3.1. High-resolution NMR experiments for tetrapeptide 106

Graphical representations of of some selected signals for the gelation process.

H_{26R}/H_{26S} pair exhibited similar behaviour to H_7 pair.

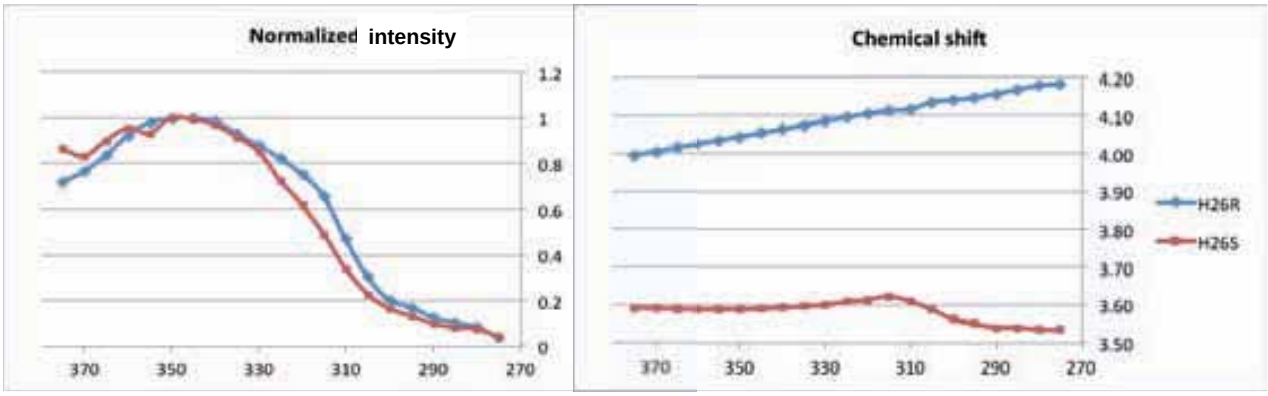

Figure **158**. Variation of chemical shift and normalized intensity of H_{26R}/H_{26S} with respect to the temperature (K).

H_{17R}/H_{17S} pair exhibited similar behaviour to H_7 pair.

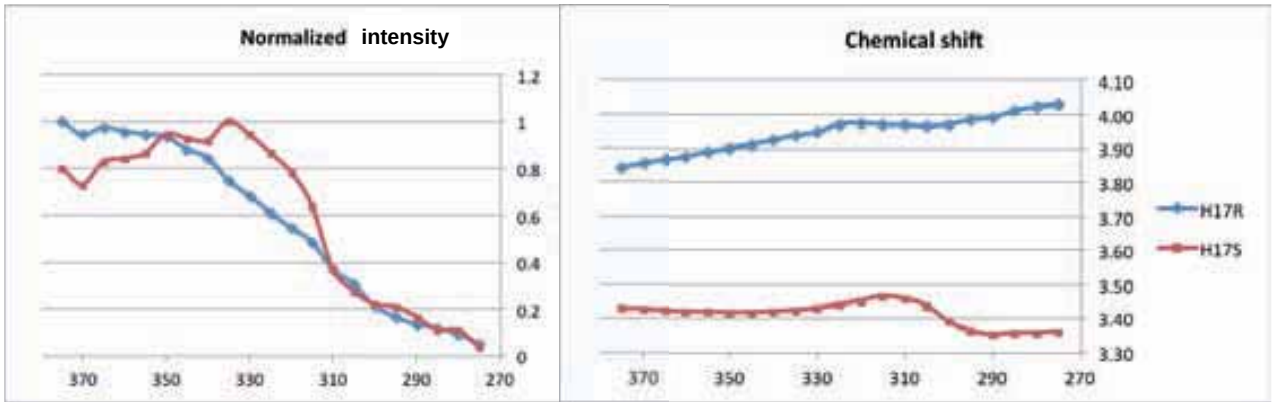

Figure **159**. Variation of chemical shift and normalized intensity of H_{17R}/H_{17S} with respect to the temperature (K).

H_{20}/H_{11}pair (analog protons): In this case, H_{11} starts gelation much more earlier than its analog H_{20} (365 K *vs.* 335 K), which is a quite big difference, indicating that NH_{10} is earlier involved in intermolecular hydrogen bonding formation than NH_{19} is.

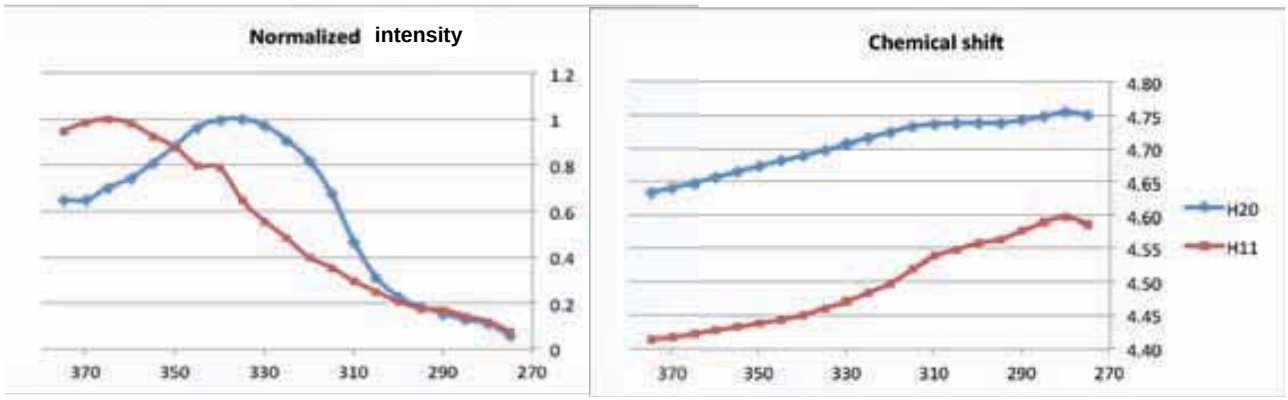

Figure **160**. Variation of chemical shift and normalized intensity of H_{20}/H_{11} with respect to the temperature (K).

NH_{19}: curve is cut by overlapping with toluene signals.

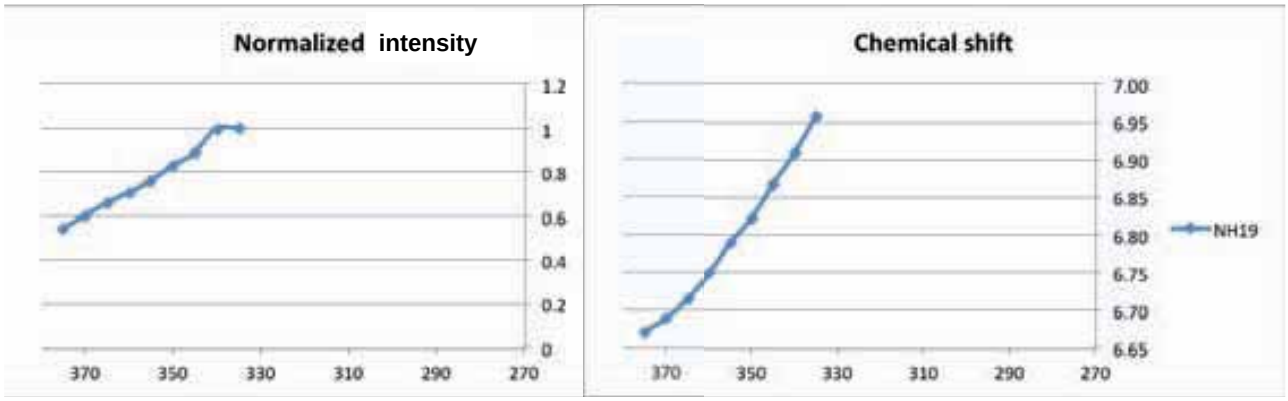

Figure **161**. Variation of chemical shift and normalized intensity of NH_{19} with respect to the temperature (K).

NH_{16}: gel formation starts at 345 K.

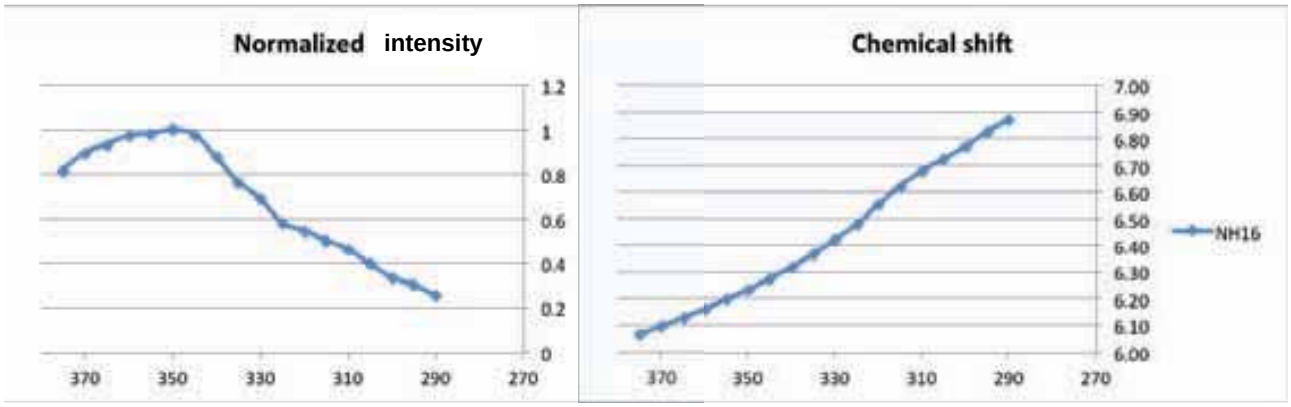

Figure **162**. Variation of chemical shift and normalized intensity of NH_{16} with respect to the temperature (K).

NH_{10} and NH_{25}: gel formation starts at 345 K.

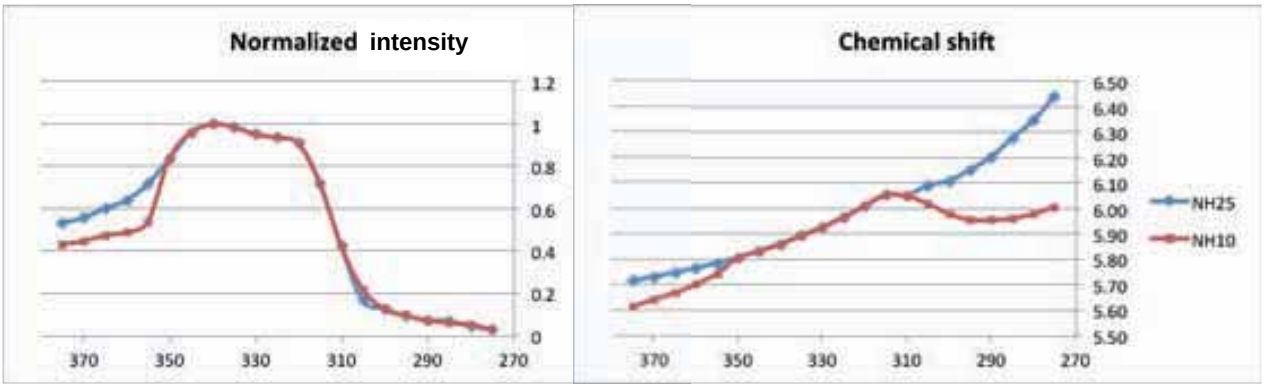

Figure **163**. Variation of chemical shift and normalized intensity of NH_{10} and NH_{25} with respect to the temperature (K).

3.5.3.2. Theoretical calculations

Hybrid Tetrapeptide 106

In Figure **164**, the structure of cyclobutane-glycine hybrid tetrapeptide **106** is shown with numbering in some selected atoms:

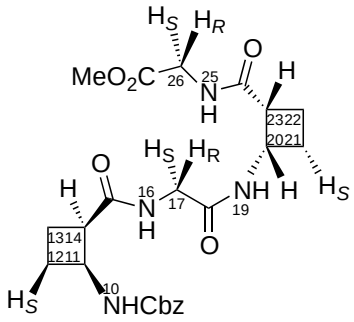

Figure **164**. Numbering of glycine tetrapeptide **106**.

The computational method was applied following three steps:

1. Correlation between ROE contacts and ^{1}H-^{1}H distances is displayed in Table **30**.

Table **30**. Distances extracted from 2D ^{1}H-^{1}H ROESY spectrum of tetrapeptide **106**.

	Strong	**Medium**	**Weak**
ROE restrictions	NH_{16}-H_{14}	NH_{25}-H_{23}	NH_{10}-H_{14}
	NH_{25}-H_{26R}	NH_{16}-H_{17R}	NH_{10}-H_{12S}
		NH_{19}-H_{20}	
		NH_{19}-H_{17R}	
		NH_{19}-H_{17S}	
		NH_{19}-H_{21S}	
Distance (Å)	3 ± 0.5	4 ± 0.5	5 ± 0.5

Apart from the ROE data, *J* coupling values were used to extract dihedral angles. ^{3}J NH_{10}-H_{11} is 9.5 Hz, so applying the Karplus equation,[87] the dihedral angle for H_{10}-N_{10}-C_{11}-H_{11} is 180º. ^{3}J NH_{19}-H_{20} is 8.5 Hz so the dihedral angle (H_{19}-N_{19}-C_{20}-H_{20}) associated is ± 158º. ^{3}J NH_{16}-H_{17S} is 6.0 Hz, that is consistent with four dihedral angles (H_{16}-N_{16}-C_{17}-H_{17}): ± 23º and ± 137º whereas ^{3}J NH_{16}-H_{17R} is 4.7 Hz, which represents dihedral angles of ± 37º and ± 127º. Another dihedral restriction due to glycine CH_2 protons diastereotopicity was considered for the calculations: N_{16}-C_{17}-C_{18}-N_{19}: ± 120º. In all cases a margin of ± 20º was allowed. The possibilities arisen from these values which have a reasonable geometric sense are summarized in Table **31**.

Table **31**. Possible combinations of dihedral angles and resulting structure possibilities for tetrapeptide **106**.

	Structure possibilities							
Dihedral angles	**1**	**2**	**3**	**4**	**5**	**6**	**7**	**8**
H_{10}-N_{10}-C_{11}-H_{11}	180	180	180	180	180	180	180	180
H_{19}-N_{19}-C_{20}-H_{20}	158	-158	158	-158	158	-158	158	-158
H_{16}-N_{16}-C_{17}-H_{17S}	23	23	23	23	-23	-23	-23	-23
H_{16}-N_{16}-C_{17}-H_{17R}	127	127	127	127	127	127	127	127
N_{16}-C_{17}-C_{18}-N_{19}	120	120	-120	-120	120	120	-120	-120

	Structure possibilities							
Dihedral angles	**1**	**2**	**3**	**4**	**5**	**6**	**7**	**8**
H_{10}-N_{10}-C_{11}-H_{11}	180	180	180	180	180	180	180	180
H_{19}-N_{19}-C_{20}-H_{20}	158	-158	158	-158	158	-158	158	-158
H_{16}-N_{16}-C_{17}-H_{17S}	-137	-137	-137	-137	137	137	137	137
H_{16}-N_{16}-C_{17}-H_{17R}	-37	-37	-37	-37	-127	-127	-127	-127
N_{16}-C_{17}-C_{18}-N_{19}	120	120	-120	-120	120	120	-120	-120

These 16 possibilities, each of them with the distance restrictions shown in Table **34**, were submitted to a conformational search, resulting in 8 different groups. Such groups were organized with the criteria of distinct NH···OC interactions, so all the structures obtained from the conformational search were classified into the 8 families.

2. The most stable structure (lowest energy) of each of these families was optimized at the B3LYP/6-31G(d) level of calculation in the gas phase. Table **32** summarizes these results.

Table **32**. Number of conformers within 1 kcal/mol for each structure possibility and number of optimized conformers in each group for tetrapeptide **106**.

Structure possibilities	**1**	**2**	**3**	**4**	**5**	**6**	**7**	**8**
Conformers within 1 kcal/mol	14	23	38	9	8	7	7	1 (4)[b]
Optimized conformers at B3LYP/6-31G(d)	1	1	0[c]	2	2	0[c]	1	1

Structure possibilities	**9**	**10**	**11**	**12**	**13**	**14**	**15**	**16**
Conformers within 1 kcal/mol	10	4	17	1 (4)[b]	5	2 (3)[b]	13	22
Optimized conformers at B3LYP/6-31G(d)	1	1	3	1	1	1	2	2

[a] Conformational search with angle variation of ± 10º.
[b] Number of conformers within 1 kcal/mol too small, so conformers within 2 kcal/mol were taken.
[c] Not optimized at the B3LYP/6-31G(d) level of theory because the conformers found are very similar to others of different groups.

The energies of all the computed structures were compared in terms of ΔG and finally structure A, resulting from the starting structure 8, was the most stable one.

3. Frequency calculations were carried out for this structure A and the three following most stable ones B, C and D. Structures and relative energies of these four conformers are shown in Figure **72** in section **3.3.2.2.**

Hybrid Tetrapeptide 121

In Figure **165**, the structure of cyclobutane-GABA hybrid tetrapeptide **121** is shown with numbering in some selected atoms:

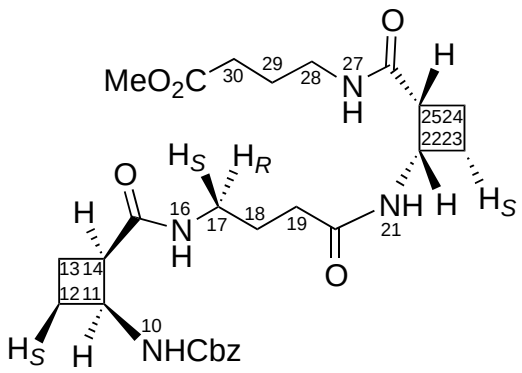

Figure **165**. Numbering of GABA tetrapeptide **121**.

The computational method was applied following three steps:

1. Correlation between ROE contacts and ^{1}H-^{1}H distances is displayed in Table **33**.

Table **33**. Distances extracted from 2D ^{1}H-^{1}H ROESY spectrum of tetrapeptide **121**.

	Strong	**Medium**	**Weak**
ROE restrictions	NH_{16}-H_{17R}	NH_{21}-H_{22}	NH_{16}-H_{18}
	NH_{27}-H_{28}	NH_{21}-H_{19}	NH_{16}-H_{17S}
		NH_{21}-H_{23S}	NH_{27}-H_{30}
		NH_{10}-H_{12}	NH_{27}-H_{29}
			NH_{21}-H_{25}
Distance (Å)	3 ± 0.5	4 ± 0.5	5 ± 0.5

Apart from the ROE data, *J* coupling values were used to extract dihedral angles. ^{3}J NH_{10}-H_{11} is 8.3 Hz, so applying the equation from Karplus,[87] the dihedral angle for H_{10}-N_{10}-C_{11}-H_{11} is ± 156º. ^{3}J NH_{19}-H_{20} is 8.5 Hz so the dihedral angle (H_{19}-N_{19}-C_{20}-H_{20}) associated is ± 160º. ^{3}J NH_{16}-H_{17S} is 4.7 Hz, that is consistent with four dihedral angles (H_{16}-N_{16}-C_{17}-H_{17}): ± 29º and ± 133º and ^{3}J NH_{16}-H_{17R} is 6.0 Hz, which represents dihedral angles of approximately ± 29º and ± 133º, also. These last two values represent 9 possible combinations which together with the other 4 dihedral angles make a total of 36 possible combinations. In view of this situation another approximation was used to obtain starting dihedral angles for H_{16}-N_{16}-C_{17}-H_{17}. Based on a work done with a glycine amide,[207] the difference of chemical shift in ppm of two diastereotopic protons was correlated with an associated dihedral angle. The difference in ppm for protons H_{17} is 0.15 ppm and for protons H_{28} is 0.06 ppm. These values correlate with dihedral angles of 75º (N_{16}-C_{17}-C_{18}-C_{19}) and 85º (N_{27}-C_{28}-C_{29}-C_{30}), respectively (Figure **166**).

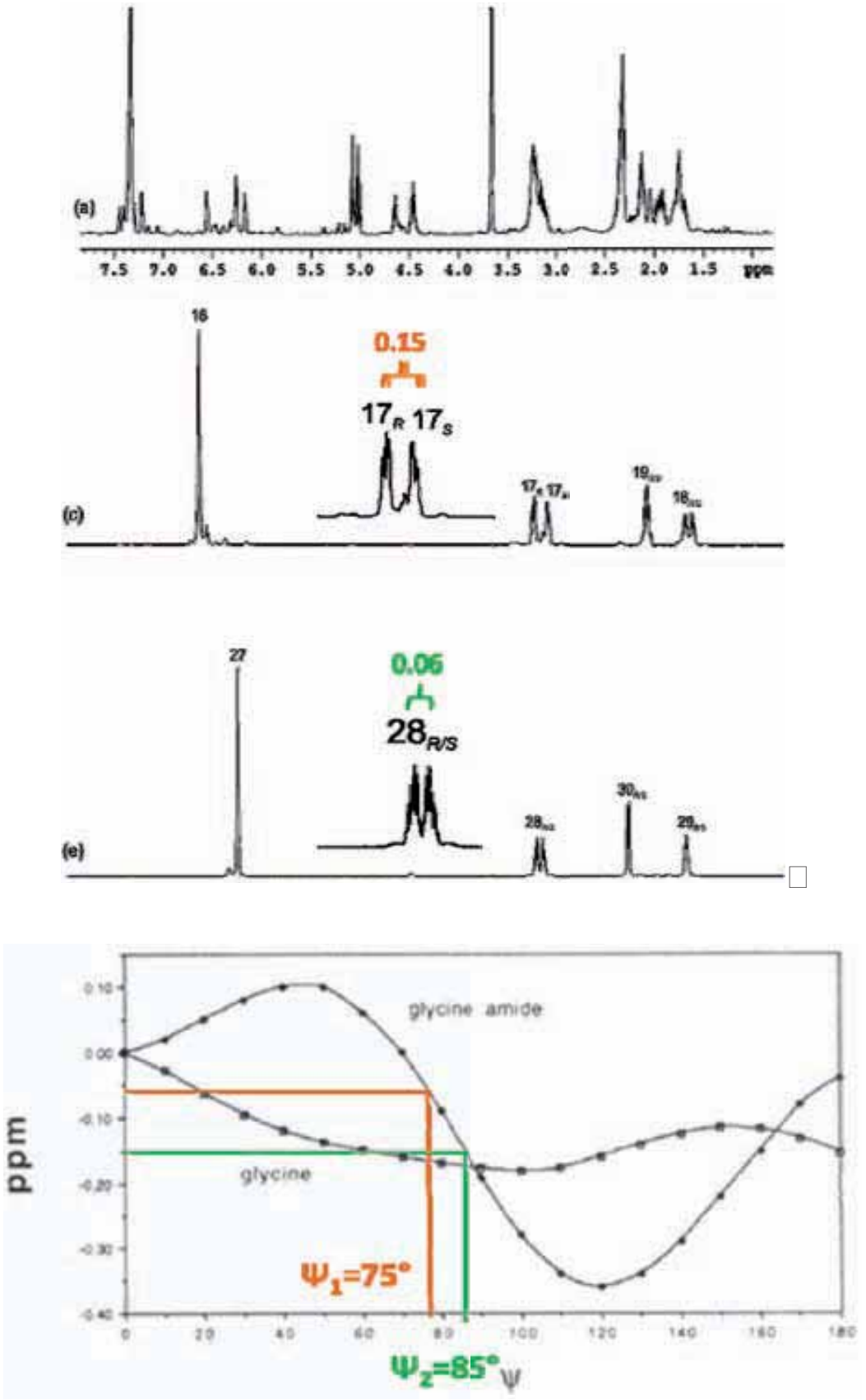

Figure **166**. Differences in the chemical shifts for protons H_{17} and H_{28} of tetrapeptide **121**. Correlation with dihedral angles (figure extracted from reference 207).

The possibilities arisen from these values which have a reasonable sense are summarized in Table **34**. In all cases a margin of ± 20º was allowed.

Table **34**. Possible combinations of dihedral angles and resulting structure possibilities for tetrapeptide **121**.

	Structure possibilities			
Dihedral angles	**1**	**2**	**3**	**4**
H_{10}-N_{10}-C_{11}-H_{11}	156	-156	156	-156
H_{16}-N_{16}-C_{17}-$H_{17R/S}$	85	85	85	85
H_{16}-N_{16}-C_{17}-$H_{17R/S}$	75	75	75	75
H_{21}-N_{21}-C_{22}-N_{22}	160	160	-160	-160

2. The most stable structure (lowest energy) of each of these four families was optimized at the B3LYP/6-31G(d) level of calculation in the gas phase, together with prior distance restrictions. Results are summarized in Table **35**.

Table **35**. Number of conformers within 1 kcal/mol for each structure possibility and number of optimized conformers in each group for tetrapeptide **121**.

Structure possibilities	**1**	**2**	**3**	**4**
Conformers within 1 kcal/mol	48	46	39 (104)[a]	68
Optimized conformers at B3LYP/6-31G(d)	2	4	3	4

[a] Number of conformers within 1 kcal/mol too small, so conformers within 2 kcal/mol were taken.

The energies of all the computed structures were compared in terms of ΔG and finally structure E, resulting from the starting structure 4, was the most stable one.

3. Frequency calculations were carried out for this structure A and the three following most stable ones B, C and D. Structures and relative energies of these four conformers are shown in Figure **74** in section **3.3.2.2.**

Head-to-tail disposition of tetrapeptide 106

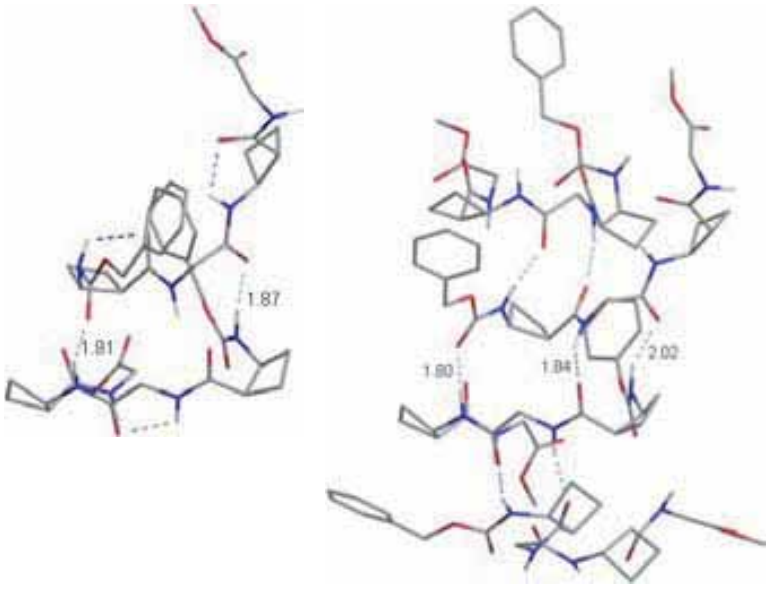

D' **T'**

Figure **167**. Structures of dimeric (D') and tetrameric (T') aggregates of peptide **106** optimized at the M06-2X/6-31G(d) level of calculation. Selected interatomic distances are in Å. Non polar hydrogen bonds were omitted for clarity.

Table **36**. Aggregation energies[a] computed for tetrapeptide **121**.

Structure	ΔE	ΔE/n
D	-22.1	-11.0
D'	-11.1	-5.6
T	-76.9	-19.2
T'	-35.4	-8.8

[a] In kcal/mol. ΔE corresponds to the n **121** → (**121**)$_n$ process.
[b] M06-2X/6-31G(d) level of calculation.

Intermolecular distances in the D, T and H aggregates of tetrapeptide 106

- Intermolecular distances (below 2.200 Å) in the D, T and H aggregates were measured.

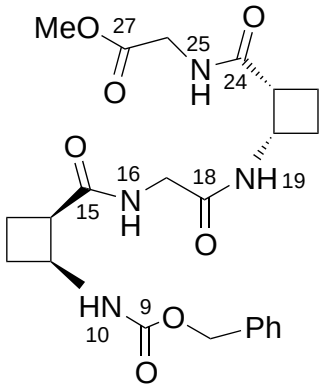

Figure **168**. Structure of hybrid α,β-tetrapeptide **106** showing some selected atom numeration.

Dimeric D aggregate, optimized at the M06-2X[210]/6-31G(d) level of calculation (Figure **169**), shows four inter-molecular hydrogen bonds (Table **37**).

Figure **169**. Optimized structure calculated for the D aggregate.

Table **37**. Distances of hydrogen bonds between molecules in the calculated D aggregate.

Hydrogen bond		**Distance (Å)**
molecule *n*	**molecule *n+1***	**1····2**
NH10	**OC9**	2.049
CO15	**NH16**	1.919
NH19	**OC18**	1.958
CO24	**NH25**	2.175
Average		2.025

Tetrameric T aggregate, optimized at the M06-2X[210]/6-31G(d) level of calculation (Figure **170**), shows the inter-molecular hydrogen bonds displayed in Table **38**.

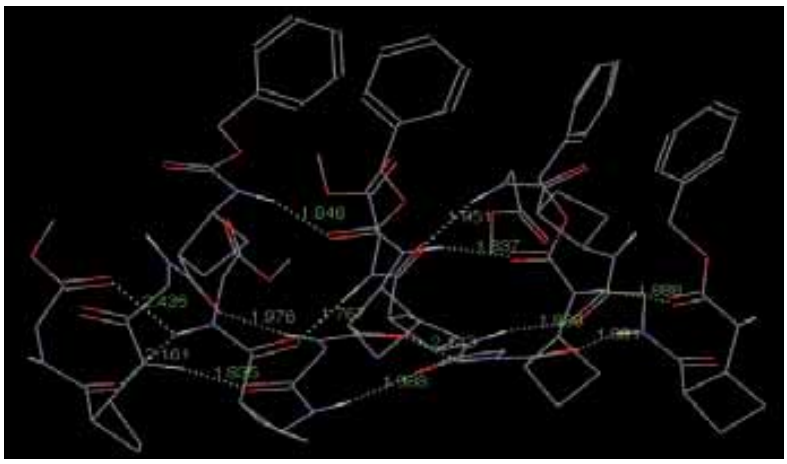

Figure **170**. Optimized structure calculated for the T aggregate.

Table **38**. Distances of hydrogen bonds between molecules in the calculated T aggregate.

Hydrogen bond		**Distance (Å)**		
molecule *n*	**molecule *n+1***	**1····2**	**2····3**	**3····4**
NH10	**OC9**	1.846	1.837	1.888
CO15	**NH16**	1.976	2.143	1.881
NH19	**OC18**	1.835	1.767	1.83
CO24	**NH25**	2.161[a]	1.988	1.951
Average		1.955	1.934	1.889

[a] Bifurcated hydrogen bond. CO_{27} also interacts with NH_{25} with distance 2.435 Å but it is not considered.

Hexameric H aggregate, optimized at the M06-2X[210]/6-31G(d) level of calculation (Figure **171**), shows the inter-molecular hydrogen bonds displayed in Table **39**.

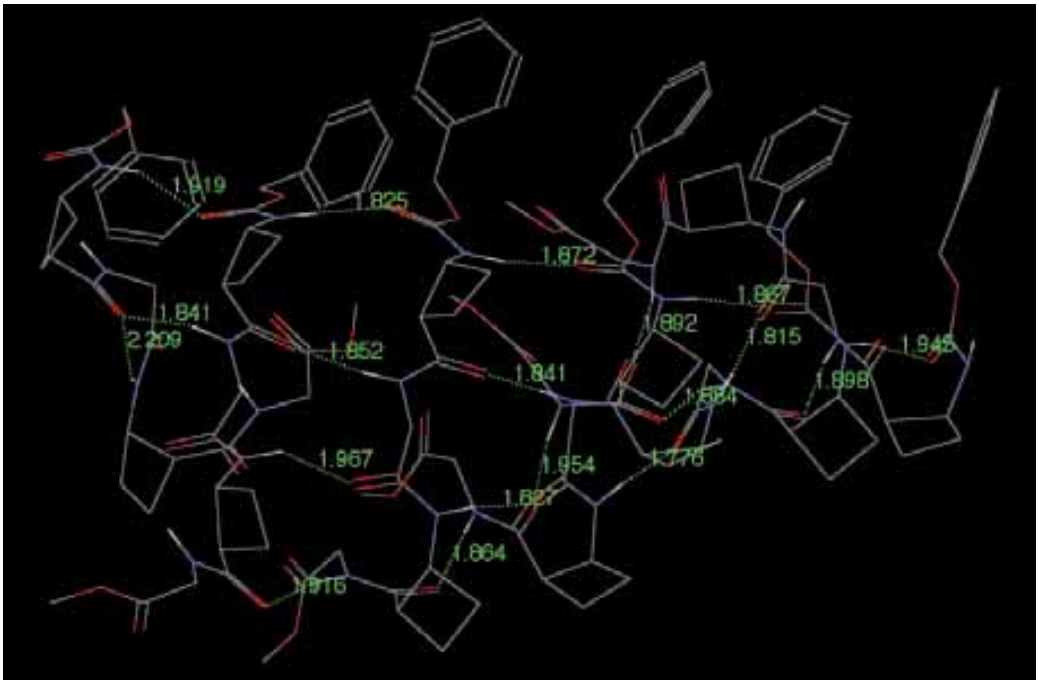

Figure **171**. Optimized structure calculated for the H aggregate.

Table **39**. Distances of hydrogen bonds between molecules in the calculated T aggregate.

Hydrogen bond		**Distance (Å)**				
molecule *n*	**molecule *n+1***	**1····2**	**2····3**	**3····4**	**4····5**	**5····6**
NH10	**OC9**	1.919	1.825	1.872	1.867	1.945
CO15	**NH16**	1.841[a]	1.852	1.841	1.884	1.898
NH19	**OC18**		1.967	1.827	1.776	1.815
CO24	**NH25**		1.916	1.864	1.954	1.892
Average		--	1.890	1.851	1.870	1.889

[a] Bifurcated hydrogen bond. CO_{15} also interacts with NH_{19} in a inter-residue of the same molecule.

Average distance of all the intermolecular bonds for D is about 2.03 Å, for T about 1.91 Å and for hexamer is about 1.87 Å. These values corroborate the cooperative effect in the aggregation event. $E_{agg.}$= [E(aggregate *n*) - *n* x E(monomer)]/*n* calculated for aggregates from 2 to 6 monomers increases with its size.

Determination of the helical axis in the HD aggregate of tetrapeptide 106

Trying to determine the axis of helical folding we realized that the monomers were not parallel between them, indeed, they moved in the three dimensions between adjacent units. Angles of deviation were approximated using fake atoms situated in strategic positions between C15-C19 of consecutive monomers (Figure **172**).

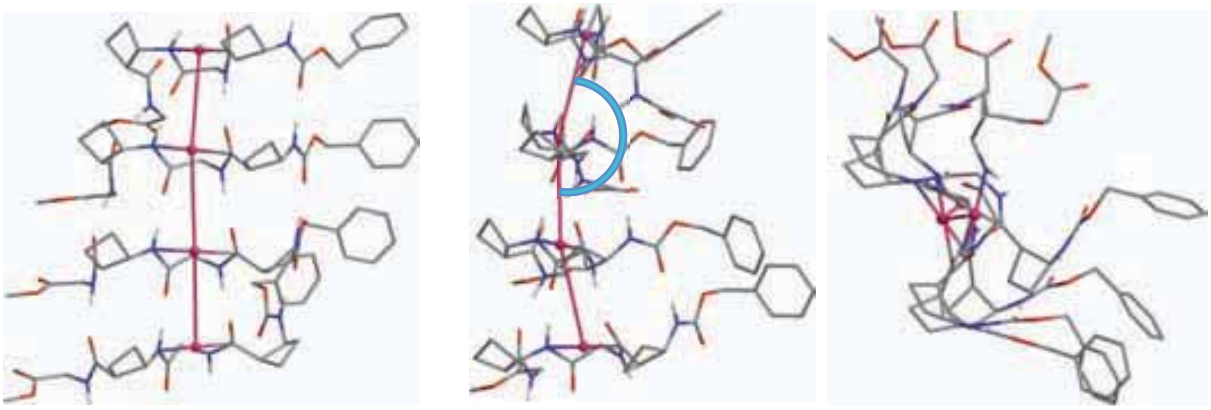

Frontal view
Angle= -25º

Side view
Folding Angle= 165º

Top view
Torsion Angle= -28º

Figure **172**. Different views of the central tetramer of the hexadecameric aggregate, showing angles of deviation from a straight axis.

It has been also done with the centres of mass of 4 consecutive monomers, and in the Figure **173** can be seen that they are not on a straight line. That is also caused by the folding and torsion of the monomers respect each other and the real axis.

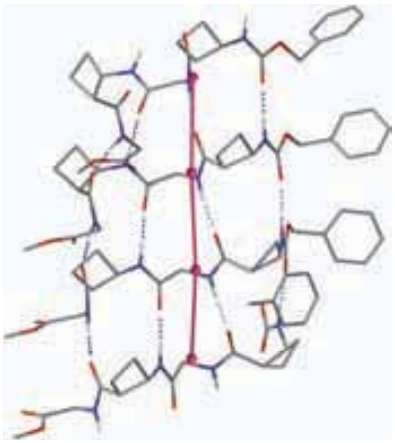

Figure **173**. Frontal view of the central tetramer of the hexadecameric aggregate showing centres of mass, near C17.

In Figure **174** the real axis of the helical aggregate is represented in two views with the corresponding angles of deviation.

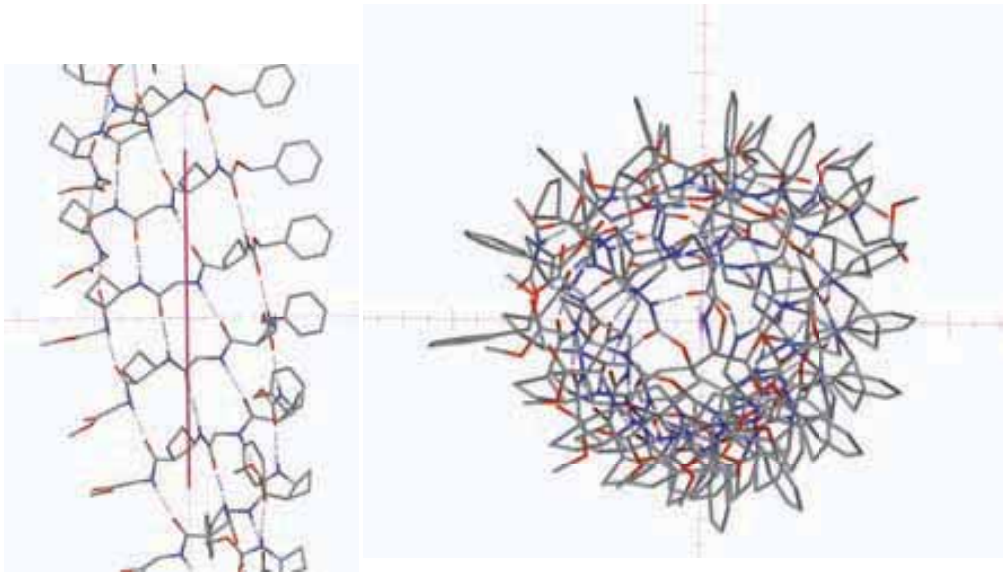

Frontal view
Angle= -25º

Top view
Torsion Angle= -20º

Figure **174**. Frontal and top views of the determined helical axis for a 1D fibril of tetrapeptide **106** in a toluene gel.

Taking in account both angles of deviation in the top views of both approximations, one can calculate the number of molecules for a complete turn of the helical aggregate. For an angle of -28º, 13 monomers are necessary whereas for an angle of -20º, 18 units are required. Then about 16 monomers is the average number to complete a turn.

ANNEX CHAPTER IV

4.5.1. Determination of stoichiometry and association constant

The anion binding properties of the receptors were studied at three different levels:

- Screening analysis to determine the anion scope for all receptors.
- Self-aggregation tests for some selected receptors.
- Stoichiometry and association constant determination of some selected complexes.

The quantitative study was performed following some general reported criteria for the study of similar host-guest events.[A1] This methodology consists in a graphical approximation of the equilibrium by a linear regression.[A2] Nevertheless, the use of graphical methods is successfully applicable when such equilibriums are simple. For more complicated systems, and because nowadays the existence of calculation programs is affordable, computational resolution is a must, and actually more accurate method, to be used when work on this field is accomplished. Therefore, the WinEQNMR2 software developed by Michael Haynes was also used;[A3] indeed, comparison of both methods showed the drawbacks of employing the graphical one.

Within the program many systems can be considered, with the presence of up to 4 complexed species, and the general procedure consists in fitting the data of the NMR experiment with the systems (1:1, 2:1, 1:2,...) suspected to take place (Table **40** and Table **41**). WinEQNMR2 works on the basis of overall stability constants β_{nm}, where K_{nm} are the stepwise constants. The best statistic results and the logical values of constants and their corresponding errors determine the appropriate system.

Table **40**. Host-Guest systems considered in the supramolecular study of anion receptors.

		Systems		
		1:1	**1:2**	**2:2**
Equilibria	1:1	$H + G \rightleftharpoons HG$	$H + G \rightleftharpoons HG$	$H + G \rightleftharpoons HG$
	1:2		$HG + G \rightleftharpoons HG_2$	$HG + G \rightleftharpoons HG_2$
	2:2			$HG_2 + H \rightleftharpoons (HG)_2$
Constants	1:1	$\beta_{11} = K_{11} = K_a$	$\beta_{11} = K_{11} = K_a$	$\beta_{11} = K_{11} = K_a$
	1:2		$\beta_{12} = K_{11} \cdot K_{12}$	$\beta_{12} = K_{11} \cdot K_{12}$
	2:2			$\beta_{2\,2} = K_{11} \cdot K_{12} \cdot K_{22}$

Table **41**. 2:1 Host-Guest system considered in the supramolecular study of anion receptors.

		Systems	
		1:1	**2:1**
Equilibria	1:1	$H + G \rightleftharpoons HG$	$H + G \rightleftharpoons HG$
	2:1		$HG + H \rightleftharpoons H_2G$
Constants	1:1	$\beta_{11} = K_{11} = K_a$	$\beta_{11} = K_{11} = K_a$
	2:1		$\beta_{21} = K_{11} \cdot K_{21}$

Anyhow, before applying any method, self-aggregation of the host must be studied to assure that the changes observed by NMR can be attributed to anion complexation. Next, determination of the stoichiometry and K_a using graphical and/or computational methods can be performed.

i) **Anion scope screening experiments:** because of the *a priori* unknown relationship between a positive anion recognition and host nature, a series of comparative experiments to find out the anion scope of the amide-based tripodands were performed. On the grounds of positive but weak recognition observed in preliminary studies, these experiments were designed with an excess (10 eq.) of the anions in their tetrabutylammonium salt form. Screening tests of each and every one of the hosts separately with each anion showed a first conclusion of which anions interacted stronger with their respective same host and allowed to compare the binding properties between different receptors in a qualitative manner.

Twelve NMR tubes, one tube for each one of the eleven anions to test and the twelfth one for the host only, were arranged to contain 0.6 mL of a solution of host:guest in a molar ratio of 1:10 and 100% of host, respectively (Table **42**).

Table **42**. Composition of each experiment (NMR tube) for a given host an a concrete anion.

Compound	**[Stock solution] (mM)**	**$V_{Stock\ solution}$ (µL)**	***n*** **(mmol)**	**V_{DMSO} (µL)**	**V_{total} (µL)**	**[Total] = molar ratio (mM)**
Host[a]	4	150	$6 \cdot 10^{-4}$	50	600	1
Guest	15	400	$6 \cdot 10^{-3}$			10

[a]The twelfth NMR tube containing 100% of host is prepared also with 150 µL of the same stock solution of host and then 450 µL of DMSO-d_6 to reach the final volume of 0.6 mL.

It must be reminded that the NH signal after addition of the anion, in case of a positive recognition, is an average of the free and the complexed host because the host:guest event is an equilibrium. Notwithstanding, it is expected that the addition of 10 equivalents of the anions may simulate the maximum displacement of the equilibrium to the formation of the complex. In the next section, this premise was proved when the experiment for the K_a determination was performed. In there, 6 eq. of the anion moved the NH signal to the same chemical shift as 10 eq. did. However, screening tests do not take into account the stoichiometry of the complexes formed and the intensity of the NH signals may vary depending on the specific interactions. Normally, the more anion recognition takes place, the more shift to downfield and the more broadening and less intensity of the signal can be observed.

ii) **Self-aggregation experiments:** since the hosts to be studied are amide-based compounds, self-assembling of such molecules can occur through intermolecular interactions. In this case the matter is related to the possible formation of dimers or host-host higher aggregates. Two of the the main factors involved in the self-aggregation are the solvent and the concentration. So, in order to test auto-aggregation process a first experiment to check this behaviour will be necessary: ^{1}H-NMR spectrum recording from a series of solutions containing the host to be studied in a gradient of concentrations, which must cover both minimum and maximum values of total concentration of the host in the host:guest experiments.

Since the host:guest experiments had been designed with total concentrations of hosts from 1 to 2 mM, the gradient of concentrations to check self-aggregation of the host was decided to be in 0 to 4 mM range. In practice, auto-aggregation of the current tripodal amide-based receptors must be reflected in the NH proton shielding with the concentration variation.

Table **43** shows the data for the preparation of ten different concentrations for the experiments, which resulted in no self-aggregation for any of the hosts tested. These results justified that the following host-guest experiments were performed under 4 mM total concentration of the host. Total volume of the solutions summed 0.5 mL.

Table **43**. Data for preparing self-aggregation experiment in eleven NMR tubes. Total volume reaches 0.5 mL

Tube	**1**	**2**	**3**	**4**	**5**	**6**	**7**	**8**	**9**	**10**
V_{Host} 4mM (µL)	50	100	150	200	250	300	350	400	450	500
V_{DMSO} (µL)	450	400	350	300	250	200	150	100	50	0
***n* Host (10^{-3} mmol)**	0.2	0.4	0.6	0.8	1	1.2	1.4	1.6	1.8	2
[Host] (mM)	0.4	0.8	1.2	1.6	2	2.4	2.8	3.2	3.6	4

4.5.1.1. Graphical method

iii) **Determination of the complex stoichiometry. Job's plot:**[A4] before quantifying the association strength of a complex, it is necessary to find out which binding event takes place. That is saying which stoichiometry the complex has, and depending on it, one model or another have to be applied. The usual methodology which easily affords the stoichiometry of a complex is the Job's plot method, or method of continuous variation, where molar ratio of the host:guest complex is determined graphically. In solutions where a host may bind a guest, the method is based in a constant total molar concentration but the mole fractions of each species are continuously varied ($X_{Host} + X_{Guest} = 1$).

The *x*-parameter, concerning the variation of the chemical shift, is plotted *versus* the mole fraction of the guest normally (*y*-parameter). From this Job's plot representation, graphic must be shown as a parabola and when its maximum points at $X_{Guest} = 0.5$, a 1:1 stoichiometry of the host:guest complex is supposed. For complexes with 1:2 or 2:1 stoichiometry, the maximum would be at mole fractions of the guest $X_{Guest} = 0.33$ and $X_{Guest} = 0.67$, respectively (Figure **175**). It is worth saying that Job's method, in practice, is useful for simple complexes, complexes with a molar ratio under 0.25, which corresponds to a 1:4 or 4:1 stoichiometry. For instance, complexes with 1:5, 1:6 or 1:7 stoichiometry would suppose to have a molar ratio of 0.20, 0.17 and 0.14 what would mean very poor difference on the *x* axis values and they could be in the error range of the procedure.

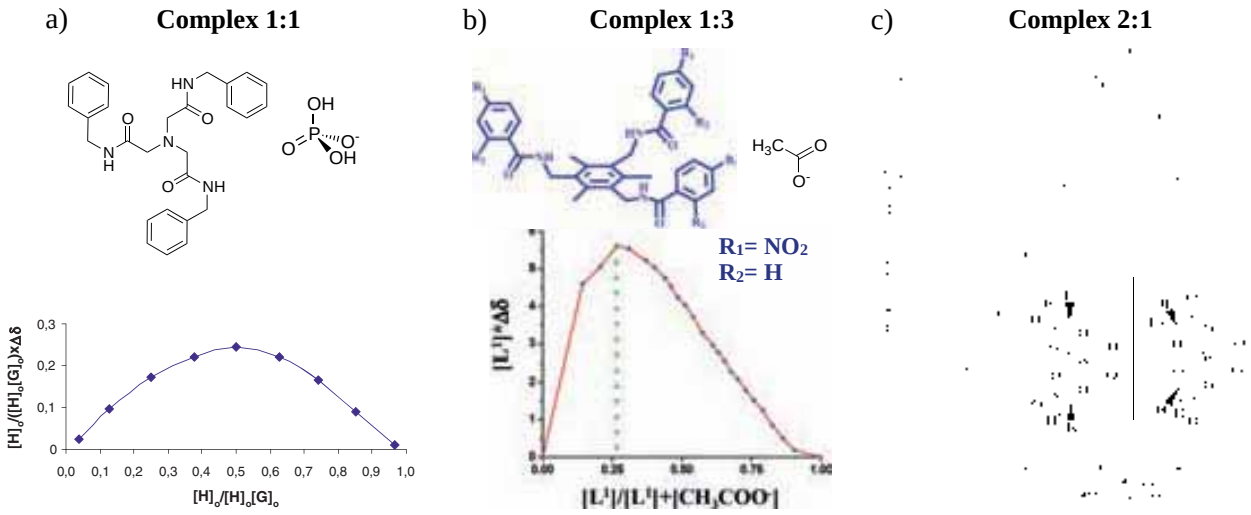

Figure **175.** a) Job's plot for the 1:1 X:H_2PO_4TBA complex in DMSO-d_6.[A1] b) Job's plot for the 1:3 L:CH_3CO_2TBA complex in DMSO-d_6.[A5] c) Both possible structures of a 2:1 complex of glycolic acid with W(IV) in D_2O.[A6]

Table **44** contains the data to complete Table **46**, in order to prepare Job's plot experiments recycling sample from the previous NMR tubes used for self-aggregation test. Therefore, the total volume of the solutions became 1 mL and the new total concentration of host was recalculated.

Table **44**. Data for completing Job's plot experiment adding the indicated volumes in to the previous NMR tubes from self-aggregation experiment. Total volume reaches 1 mL.

Tube	**1**	**2**	**3**	**4**	**5**	**6**	**7**	**8**	**9**	**10**	**11**
V_{Guest} 4 mM (µL)	500	450	400	350	300	250	200	150	100	50	0
V_{DMSO} (µL)	500	50	100	150	200	250	300	350	400	450	500
***n* Host (10^{-3} mmol)**	0	0.2	0.4	0.6	0.8	1	1.2	1.4	1.6	1.8	2
***n* Guest (10^{-3} mmol)**	2	1.8	1.6	1.4	1.2	1	0.8	0.6	0.4	0.2	0
[Host] (mM)	0	0.2	0.4	0.6	0.8	1	1.2	1.4	1.6	1.8	2
[Guest] (mM)	2	1.8	1.6	1.4	1.2	1	0.8	0.6	0.4	0.2	0
X_{Host}	0	0.1	0.2	0.3	0.4	0.5	0.6	0.7	0.8	0.9	1
X_{Guest}	1	0.9	0.8	0.7	0.6	0.5	0.4	0.3	0.2	0.1	0

For the rest of the anions, within the same host and keeping the initial conditions, new NMR tubes were prepared using the following data in 0.5 mL solutions (Table **45**).

Table **45**. Data for preparing Job's plot experiment using 0.5 mL of total volume.

Tube	**1**	**2**	**3**	**4**	**5**	**6**	**7**	**8**	**9**	**10**	**11**
V_{DMSO} (µL)	250	250	250	250	250	250	250	250	250	250	250
V_{Host} 4 mM (µL)	0	25	50	75	100	125	150	175	200	225	250
V_{Guest} 4 mM (µL)	250	225	200	175	150	125	100	75	50	25	0
***n* Host (10^{-3} mmol)**	0	0.1	0.2	0.3	0.4	0.5	0.6	0.7	0.8	0.9	1
***n* Guest (10^{-3} mmol)**	1	0.9	0.8	0.7	0.6	0.5	0.4	0.3	0.2	0.1	0
[Host] (mM)	0	0.2	0.4	0.6	0.8	1	1.2	1.4	1.6	1.8	2
[Guest] (mM)	2	1.8	1.6	1.4	1.2	1	0.8	0.6	0.4	0.2	0
X_{Host}	0	0.1	0.2	0.3	0.4	0.5	0.6	0.7	0.8	0.9	1
X_{Guest}	1	0.9	0.8	0.7	0.6	0.5	0.4	0.3	0.2	0.1	0

Once the spectra were recorded, they were piled up and, if there was a positive and quantifiable anion recognition, the proton shift differences between each concentration (δ_n) with respect to the initial (when X_{Host} = 1, δ_{Host}) were calculated ($\Delta\delta = \delta_n - \delta_{Host}$). This difference with respect to the signal of the non-complexed host can be to higher or lower fields so, the variation can be a positive

or negative value respectively; in the present thesis all variations are expressed as absolute values except when both upfield and downfields shifts were calculated.

Then, discrete values of $\Delta\delta \cdot$[Host] *vs.* X_{Guest} were plotted and Job's plot was obtained.

iv) **Determination of the association constant (K_a) for a 1:1 complex:** once the stoichiometry of the complex is established, the appropriate model can be applied. The general expression for the association constant between a host (H) and a guest (G) for a 1:1 molar ratio is described below (Equation 2).[A7]

$$H + G \rightleftharpoons HG \tag{2}$$

To simplify the discussion, activity coefficients will be avoided. Then, the association constant can be expressed as:

$$K_a = \frac{[HG]}{[H][G]} \tag{3}$$

If only a single signal is observed in the ^{1}H-NMR spectrum for the equilibrium between free host (H) and complexed host (HG), it means that the interchange between them is faster than the resonance frequency of the ^{1}H-NMR experiment. The slow exchange limit usually implies a lifetime of the complex much longer than 10^{-2} s, so different signals for each species H and HG are observed. Therefore, the chemical shift observed (δ_{obs}) will be an average of both signals:

$$\delta_{obs} = X_H \cdot \delta_H + X_{HG} \cdot \delta_{HG} \tag{4}$$

where δ_H is the shift of free host and δ_{HG} the shift of pure complex. X_H and X_{HG} are the mole fractions which are defined by the expressions:

$$X_H = \frac{n_H}{n_H + n_{HG}} \tag{5.1}$$

$$X_{HG} = \frac{n_{HG}}{n_H + n_{HG}} \tag{5.2}$$

and the sum of both mole fractions for the total concentration of host in the solution is:

$$X_H + X_{HG} = 1 \tag{6}$$

With equation (6), equation (4) can be reformulated only as a function of the mole fraction of the complex:

$$\delta_{obs} = \delta_H + X_{HG} \cdot (\delta_{HG} - \delta_H) \tag{7}$$

Defining chemical shift differences:

$$\Delta\delta_{max} = \delta_{obs} - \delta_H \quad (8.1)$$

$$\Delta\delta = \delta_{HG} - \delta_H \quad (8.2)$$

allows to express equation (7) related to the physical chemical variable property and the concentration of guest:

$$\Delta\delta = \frac{\Delta_{HG} K_a [G]}{1 + K_a [G]} \quad (9)$$

This equation is the binding isotherm that graphically shows a rectangular hyperbola. Linearization is possible by a non-logarithmic linear plotting, so it is finally obtained the Benesi-Hildebrand equation or the double-reciprocal plot which allows to plot $1/\Delta\delta$ *vs.* $1/[G]$ as known values to afford K_a:

$$\frac{1}{\Delta\delta} = \frac{1}{K_a \Delta\delta_{max} [G]} + \frac{1}{\Delta\delta_{max}} \quad (10)$$

The experiments to determine association constant were performed with a constant concentration of the host [H] and a variable concentration (titration) of the guest [G] ([G] = 0 to 6 mM). Table **46** summarizes the data used for preparing the NMR tubes in order to determine the K_a values using the linear binding isotherm.

Table **46**. Data for preparing experiment for determining association constants using 0.5 mL of total volume.

Tube	**1**	**2**	**3**	**4**	**5**	**6**	**7**	**8**	**9**	**10**
V_{DMSO} (µL)	375	343.75	312.5	281.25	250	218.75	187.5	125	62.5	0
V_{Host} 4 mM (µL)	125	125	125	125	125	125	125	125	125	125
V_{Guest} 8 mM (µL)	0	31.25	62.5	93.75	125	156.25	187.5	250	312.5	375
***n* Host (10^{-3} mmol)**	0.5	0.5	0.5	0.5	0.5	0.5	0.5	0.5	0.5	0.5
***n* Guest (10^{-3} mmol)**	0	0.25	0.5	0.75	1	1.25	1.75	2	2.5	3
[Host] (mM)	1	1	1	1	1	1	1	1	1	1
[Guest] (mM)	0	0.5	1	1.5	2	2.5	3	4	5	6

After plotting $1/\Delta\delta$ *vs.* $1/[G]$, the best linear regression is fitted taking into account the value of correlation squared ($r^2 > 0.995$). The linear equation is defined as:

$$\frac{1}{\Delta\delta} = \text{slope}\frac{1}{[G]} + A \tag{11}$$

with the following graphical representation:

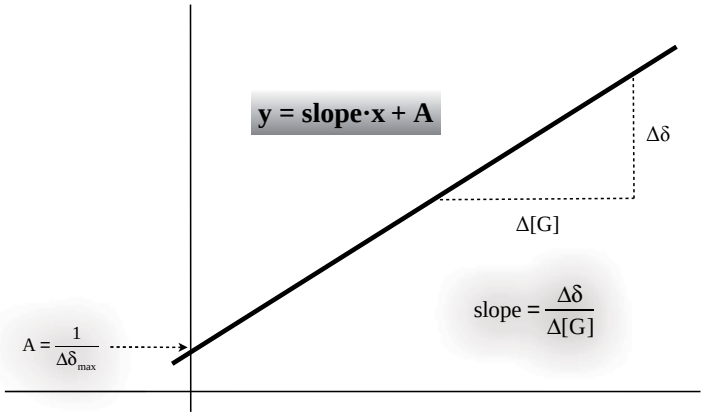

Association constant can be approximately calculated from the slope of the linear fitted equation and the value of $\Delta\delta_{max}$, deduced as the $1/\Delta\delta$ value when $1/[G] = 0$. So, K_a is calculated as:

$$K_a = \frac{1}{\Delta\delta_{max} \cdot \text{slope}} = \frac{A}{\text{slope}} \tag{12}$$

Association constants, since they can cover several orders of magnitude, are usually given as the decimal logarithm, $\log_{10}(K_a)$. In any case, as it is being used the NMR, the limits of the association constants will be $0 < \log_{10}(K_a) < 4$.

This approximated values would be useful for carrying out the computational method, as guide values for the constants are required to run it.

4.5.1.2. Computational method (WinEQNMR2 program)[A3]

This software presents four modules, through which whom can deal with the data. The experimental data needed comprise the chemical shifts of the complexed signals during an anion titration in which one of the concentrations (normally the [Host]) is kept constant.

To prepare input files, *PrepareFile2* module allows to introduce all the characteristics of the equilibrium system one want to study, defining the number of uncomplexed (only one) and complexed species (up to four), the presence or not of proton or metal equilibria, the guide values of association constants and chemical shift parameters.

Module *WinEQNMR2* is the program that calculates the statistic values, providing residuals squared and R-factor, and the association constants. *FitPlot2* module produces a plot of experimental and

calculated data together with a residuals plot, where the fitting of the system can be visually checked. Finally, *ConcPlot2* module provides a plot of species distribution in the system during the titration.

NMR is not a very sensitive technique, this is why NMR titrations are only suitable for relatively simple systems. Ideally, one should have data in the range of 10% to 90% complex formation but, this is an ideal not always achievable in practice. When an equilibrium system has very low stability the experiment would have to be performed using impossible high concentrations to achieve even 50% complex formation. Fortunately, programs such as WinEQNMR still give acceptable results even when the degree of complex formation is less than 50%.

Some examples of input and output files, and *fitplots* and *concplots*, are displayed in Annex section **4.5.4.6.**

4.5.2. Synthesis of tripodal amides

4.5.2.1. Optimization of the benzylation reaction

The first attempt to test the benzylation reaction was carried out on *N*-Cbz-δCbu **170** (Table **47**, entry 1) and it was performed by a previous activation of the carboxylic acid by oxalyl chloride followed by the addition of benzyl alcohol. *N*-Boc-GABA substrate was also employed with the same purpose and with similar results (Table **X**, entry 1 and 2). As the yield was moderate, probably because the poor nucleophilicity of the benzyl alcohol, a second strategy was attempted: a simple substitution reaction with benzyl bromide and an organic base of moderate strength.[A8] Following the procedure described by Brough and Klumpp, but using DIPEA instead of DBU, we obtained better yields (entry 3 and 5) and we realized the importance of reaction time, because shorter times (t < 60 h) led to uncompleted reactions (entry 4). Purification of the desired products could be performed by distillation under reduced pressure using microdistillator or by flash chromatography using neutral silica-gel and proper eluent mixture. Because of the high boiling point of benzyl bromide (198-199 ºC) and because the purification could not be monitored, flash chromatography was used from then on.

Table **47**. Testing conditions employed to afford the synthesis of benzyl ester derivatives during the set up of the reaction. Equivalents are equimolar except when indicated.

Entry	Reactant	Conditions	Product	Yield
1	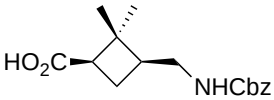	i) $(ClCO)_2$, Et_3N, anhyd. DMF drops, anhyd. CH_2Cl_2, r.t., 1 h ii) BnOH, r.t., **o/n**	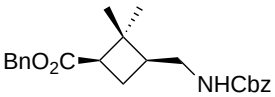	53%[a]
2	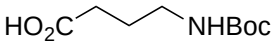	i) $(ClCO)_2$, Et_3N, anhyd. DMF drops, anhyd. CH_2Cl_2, r.t., 1 h ii) BnOH, r.t., **40 h**	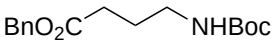	50%[b]
3	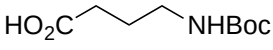	DIPEA, BnBr, MeCN, r.t., **65 h**	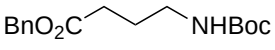	79%[a]
4	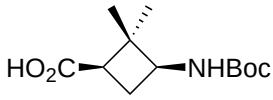	DIPEA, BnBr, MeCN, r.t., **o/n**		56%[b]
5	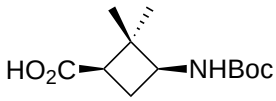	DIPEA, BnBr, MeCN, r.t., **65 h**		95%[c]

[a]Yield after distillation and flash chromatography purifications.
[b]Yield after distillation purification.
[c]Yield after flash chromatography purification.

4.5.2.2. Synthesis of the $N(CH_2CO\text{-}\delta Cbu\text{-}OMe)_3$ tripodal amide 153

Table **48** shows all the trials performed in Scheme **48**:

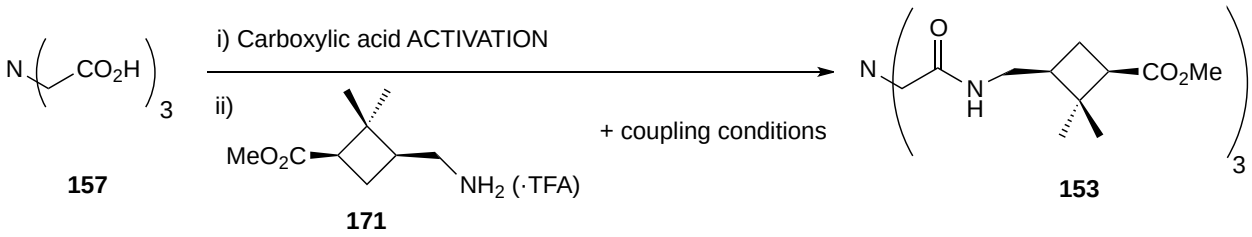

Scheme **48**. Coupling reaction to synthesize compound **153** by divergent approach.

Table **48**. Testing conditions used for the synthesis of **153** by divergent approach. Entries 2 and 3 were repeated using recovered amine from entries 1 and 2 respectively**.** Equivalents are equimolar except when indicated.

Entry	NTA acid activation	Reactant (amine)	Coupling conditions	Product	Comments	Yield[a]
1	$(ClCO)_2$ anhyd. DMF drops anhyd. CH_2Cl_2 r.t., 1 h	R-NH_2·TFA	r.t., 2 h	✗	R-NH_2 from starting reactant was recovered	63%
2		R-NH_2	r.t., 20 h + reflux, 4 h	✗	R-NH_2 from starting reactant was recovered	71%
3		R-NH_2	reflux, 24 h	✗	R-NH_2 from starting reactant was recovered	100%
4		R-NH_2·TFA	reflux, 24 h	✓	Tripodal amide was obtained	20%
5	PyBOP, DIPEA anhyd. CH_2Cl_2 and DMF, reflux, 1 h	R-NH_2·TFA	r.t., o/n + reflux, o/n	✗	No clear product was observed	--

[a] Isolated yield after purification.

4.5.2.3. Synthesis of the N(CH_2CO-γCbu-GABA-OMe)$_3$ tripodal amide 191

Through the acyl chloride activation (Entry 1, Table **49**) it was possible to obtain a fraction after flash chromatography, the proton (Figure **178**) and carbon (Figure **179**) spectra of which suggested uncompleted reaction (Table **49**).

Table **49**. Testing conditions employed to achieve the synthesis of **191** by divergent approach. Equivalents are equimolar except when indicated.

Entry	Acid activation	Reactant (γ,γ-dipeptide)	Coupling conditions	Product	Comments
1	$(ClCO)_2$, Et_3N anhyd. DMF drops anhyd. CH_2Cl_2 reflux, 1 h	R-NH_2·TFA	reflux, 30 h	✓	Desired product was observed in a mixture with trailing compounds
2	PyBOP, DIPEA anhyd. DMF, r.t., 15 min.	R-NH_2	r.t., 6 h	✗	No product was clearly observed

Besides the assigned proton signal of amide NH proton (δ ≃ 7.90 ppm), a second NH proton signal was observed (δ ≃ 6.85 ppm), corresponding to the disubstituted intermediate; on the ^{13}C-NMR spectrum two signals of the methylene nitrilo carbon atom (C_1) could be detected although the difference in the chemical shift was too little to be determinant.

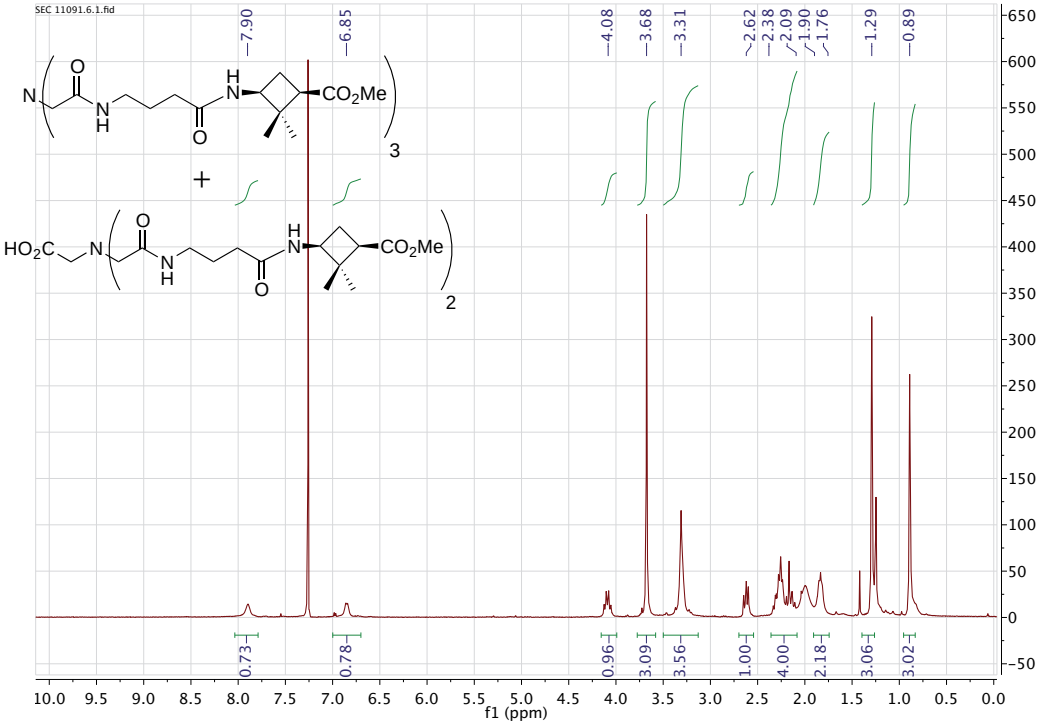

Figure **178**. ^{1}H-NMR spectrum of entry 1 from Table **49** in $CDCl_3$ (360 MHz).

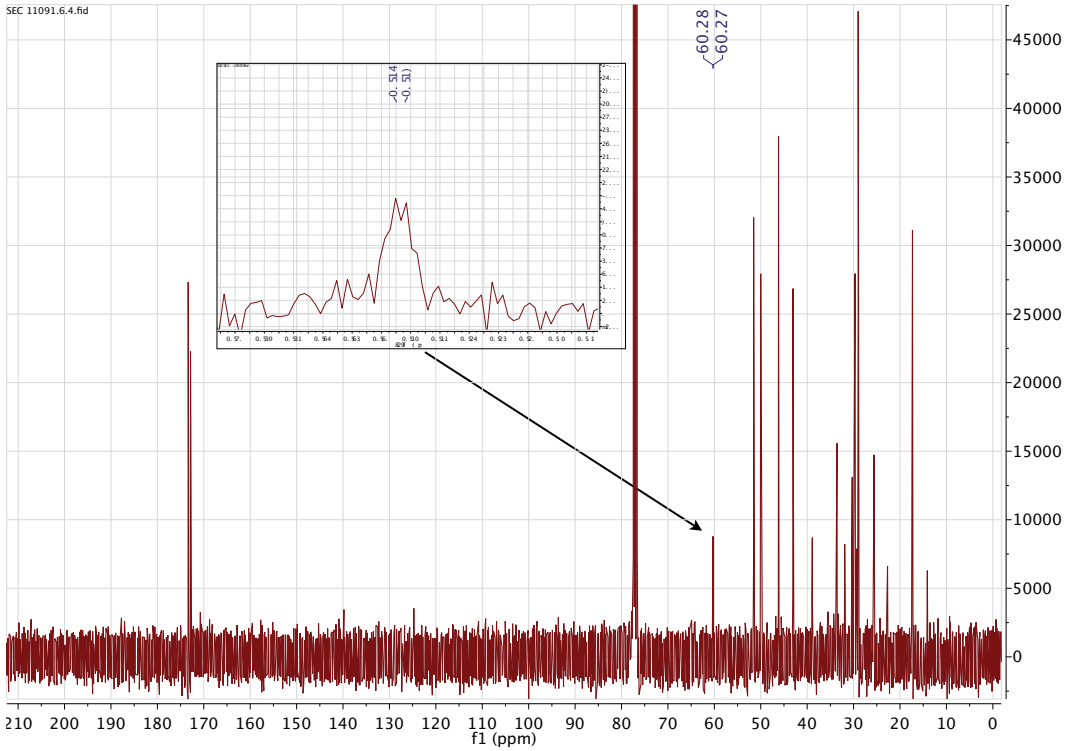

Figure **179**. ^{13}C-NMR spectrum of entry 1 from Table **49** in $CDCl_3$ (360 MHz).

Figure **180** shows LRMS for the isolated fraction:

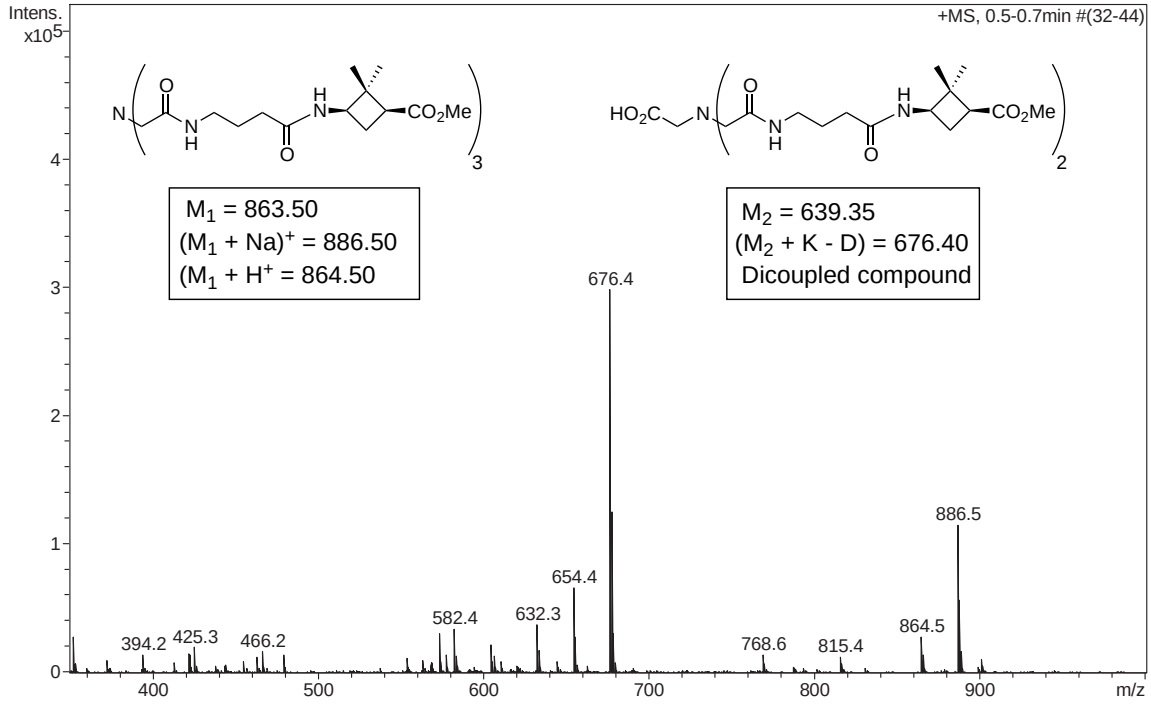

Figure **180**. LRMS of a sample containing tripodand **191** and other impurities. Entry 1 of Table **27**. Molecular peak corresponds to the neutral species (M_2 + K - D).

Note that the molecular peak primarily corresponds to the dicoupled trailing compound (M_2) but the LRMS was carried out with ESI+, so only positive and neutral species can be detected. Assignation of the mass with the loss of two acidic protons (one from de carboxylic acid and another from NH of amide bonds), it would suppose a negative charge on the molecule. It was concluded that, as the compound had been in contact with deuterated solvents ($CDCl_3$ for the NMR analysis), acidic ^{1}H-^{2}D were presumably interchanged in the carboxylic acid moiety. Then, the loss of only the deuterium atom would match with the loss of two units of mass with only loss of one positive charge, counteracted by a potassium cation.

4.5.2.4. Synthesis of bromo-derivatives

- Table **50** shows all the trials performed in this reaction (Scheme **49**):

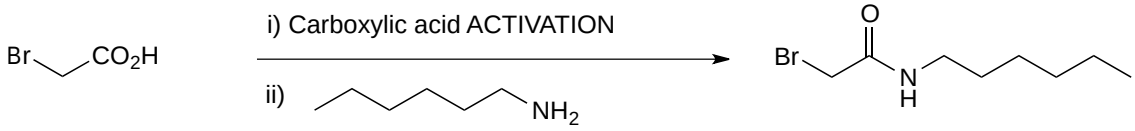

Scheme **49**. Coupling reaction to synthesize 2-bromo-*N*-hexylacetamide.

Table **50**. Testing conditions employed to afford the synthesis of compound 2-bromo-*N*-hexylacetamide during the set up of the reaction. Equivalents are equimolar except when indicated.

Entry	Acid activation	Coupling conditions	Product	Comments
1	EDAC (suspension), DIPEA, anhyd. CH_2Cl_2	r.t., 20 h	✗	--
2	$(COCl)_2$, anhyd. CH_2Cl_2 anhyd. DMF drops reflux, 2 h	r.t., o/n DIPEA	✓	After flash chrom. some product was obtained (20% yield) but HRMS did not match.
3	$ClCO_2Et$, Et_3N anhyd. acetone, 0 ºC, 30 min.	r.t., 2 h	✓	Product from flash chrom. was isolated with impurities
4	PyBOP, DIPEA, anhyd. CH_2Cl_2	r.t., 2 h	✗	--
5	DCC (suspension), DIPEA anhyd. CH_2Cl_2	r.t., 24 h	✗	--
6	HATU, DIPEA, anhyd. CH_2Cl_2	r.t., o/n	✗	--

- Failed attempts were tried before the convenient conditions were at last set up. For the synthesis of the nucleophile by coupling HCl·γCbu-OBn **163** with *N*-Boc-Gly **173** using PyBOP coupling agent no problems were encountered and the yield was satisfactory. However, the electrophile species approach was also primarily designed as a bromide derivative instead of a chloride (Scheme **50**).

Scheme **50**. Coupling reaction to synthesize of γ-cyclobutane-bromide derivatives.

The attempts were performed using the methyl ester derivative and no desired product was observed. In all cases starting amino acid was recovered in its free amine form or no clear product could be described. A possible problem under the tested conditions was a competition between both reactive sites of the bromoacetic acid (Table **51**).

Table **51**. Testing conditions employed to achieve the synthesis of γ-cyclobutane-bromide derivative. Equivalents are equimolar except when indicated.

Entry	Acid activation	Reactant (γ-AA)	Coupling conditions	Product
1	FDPP, DIPEA, anhyd. DMF and CH_2Cl_2, r.t., 5 min.	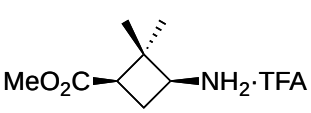	DIPEA r.t., o/n	✗
2	EDAC, DIPEA, anhyd. DMF and CH_2Cl_2, r.t., 5 min.		DIPEA r.t., 3 days	✗

4.5.2.5. Synthesis of the *n*-hexyl tripodal amide 147

After the basic aqueous and NaCl washes work up, evaporation of solvents afforded a crude of two compounds. ^{13}C-NMR spectrum of this sample revealed two signals at about 60 ppm which was a suspicion of the presence of trailing compounds and it was attributed to the secondary amine intermediate (Figure **176**).

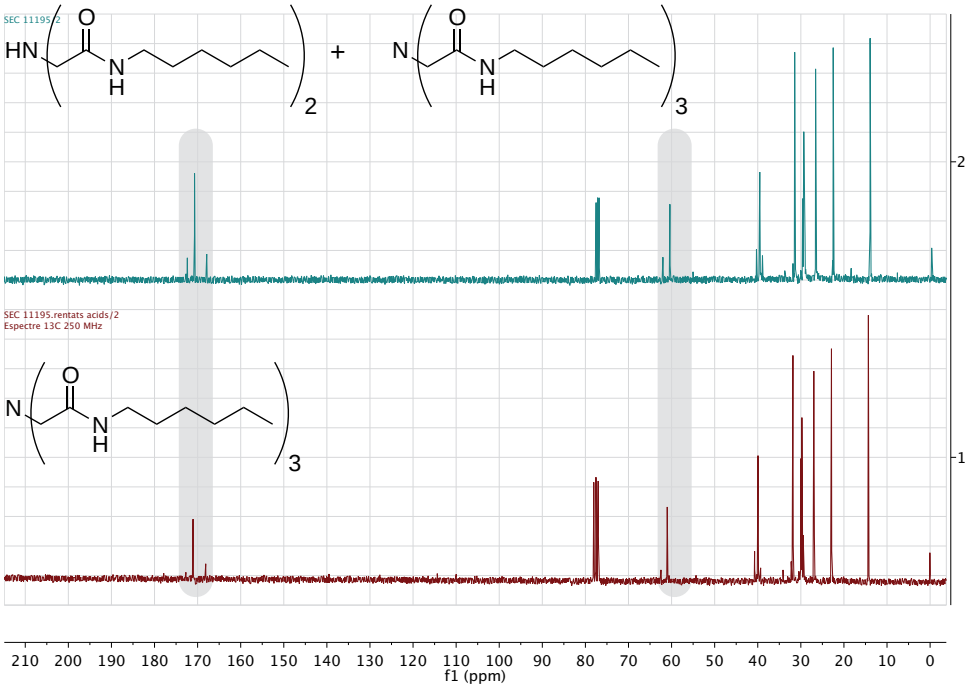

Figure **176**. ^{13}C-NMR spectra of a reaction mixture recorded at 360 MHz (*top*) and 250 MHz (*bottom*) in $CDCl_3$. From the *top* to the *bottom* spectra is possible to observe the purification by acid washes.

4.5.2.6. Synthesis of chloride-derivatives

In order to deal with chloroacetyl derivatives two chloride-containing reagents were tested (Scheme **51**).

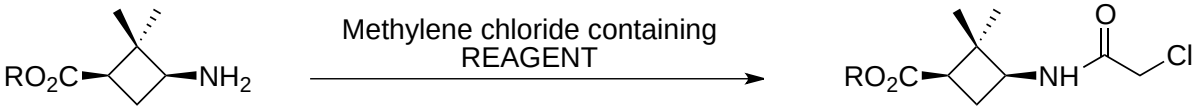

Scheme **51**. Coupling reaction to synthesize of γ-cyclobutane-chloride derivatives.

Table **52** summarizes some of the attempts to synthesize **196** (R= OBn) and its methyl ester derivative. Finally, the best results were obtained: by adding acyl chloride reagent slowly and at low temperature to a solution of the amine.

Table **52**. Testing conditions employed to achieve the synthesis of γ-cyclobutane-chloride derivatives. Equivalents are equimolar except when indicated.

Entry	R	Cl containing reagent	Conditions	Product	Comments	Yield[a]
1	OMe	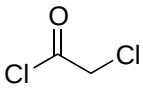	Et_3N, anhyd. CH_2Cl_2 r.t., 2 h	✗	R-NH_2 from starting reactant is recovered	71%
3			1.5 eq. of $ClCOCH_2Cl$ DIPEA (2 eq.) anhyd. THF reflux, o/n	✓	Mixed crude with both starting and final compounds	--
4			1.5 eq. of $ClCOCH_2Cl$ DIPEA (1.3 eq.) anhyd. THF reflux, 40 h	✓	Same as entry **3** but some progress was observed	--
5	OBn	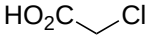	PyBOP, DIPEA anhyd. CH_2Cl_2 r.t., 2 h	✓	Flash chromatography purification	40%
6		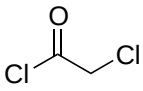	DIPEA, anhyd. CH_2Cl_2 0 ºC to r.t., 2 h	✓	Flash chromatography purification	84%

[a] Isolated yield after purification.

In Figure **177** the evolution of the reactions in entries 2 to 4 is shown, where some advances in the chemical conversion were achieved. Top spectrum is of the free amine recovered and then, next spectrum, evolution to the final product (chloride derivative) could be observed. Signal corresponding to methylene-Cl carbon atom (δ ≃ 60 ppm) and to the carbonyl of new amide bond formed (δ ≃ 167 ppm) appeared, whereas two signals corresponding to free amine (δ ≃ 52 ppm; maybe the C atom adjacent to the free amine) became smaller.

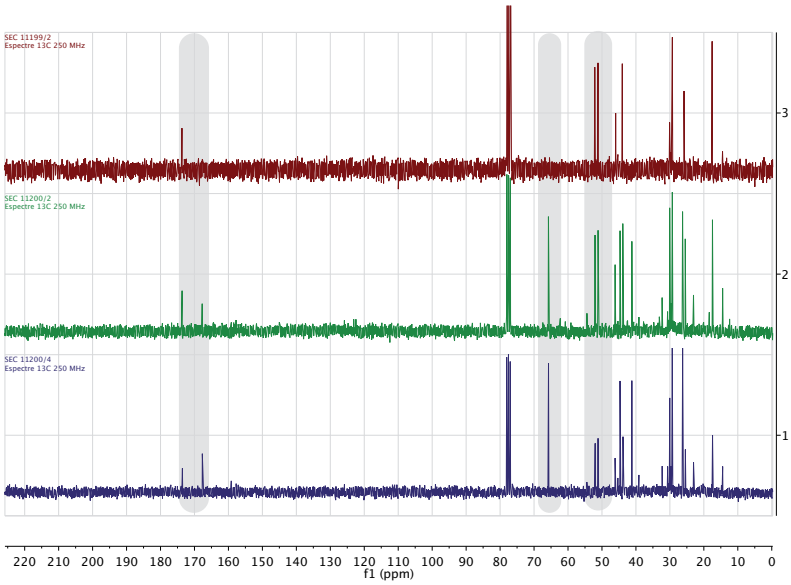

Figure **177**. ^{13}C-NMR spectra of entries 2, 3 and 4 (from *top* to *bottom*) recorded at 250 MHz in $CDCl_3$.

4.5.3. Screening tests to determine anion scope of receptors

Spectra and tables of the screening analysis are displayed from 100% host (*top*) to TBAF (*bottom*):

▸ **HHex:**

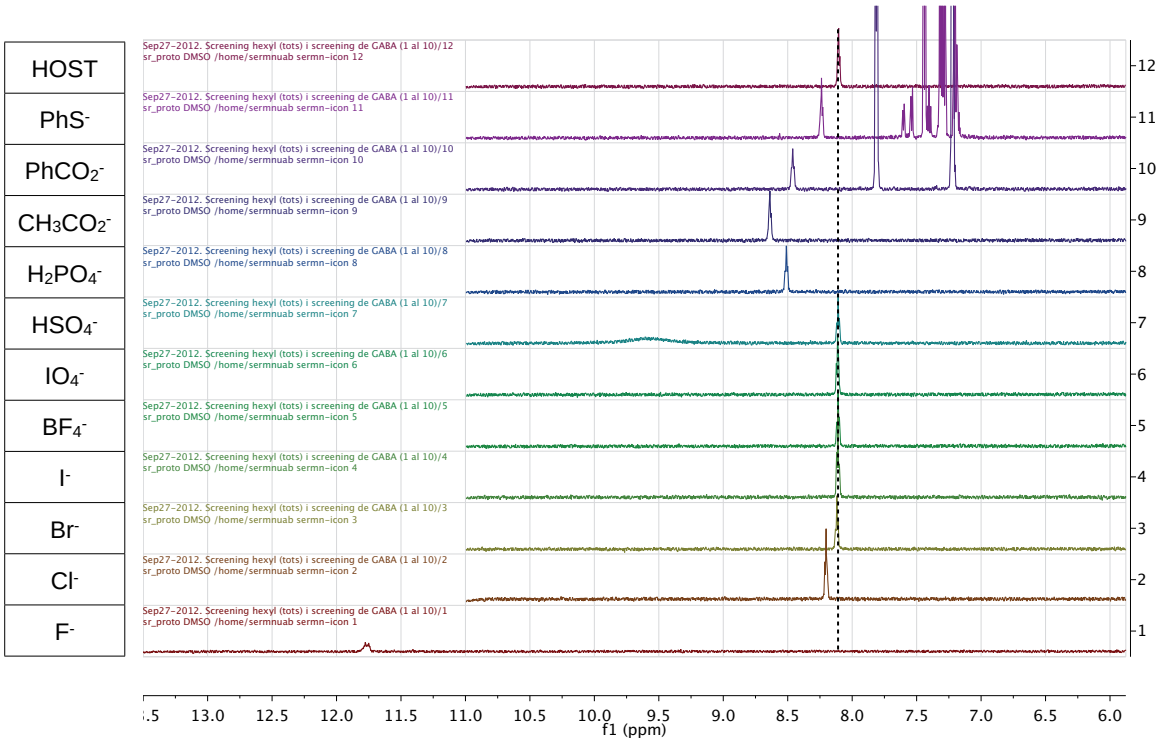

Figure **181**. ^{1}H-NMR anion screening of **HHex** in DMSO-d_6 (600 MHz).

Table **53**. Chemical shift shielding and relative affinity of **HHex** host towards several anions.

	δ NH (ppm)	**Δδ NH (ppm)**	**Relative Δδ (%)**
Free H	8.105	0.000	0.0
PhS^-	8.238	0.133	3.6
$PhCO_2^-$	8.461	0.356	9.7
$CH_3CO_2^-$	8.638	0.533	14.6
$H_2PO_4^-$	8.510	0.405	11.1
HSO_4^-	8.109	0.004	0.1
IO_4^-	8.113	0.008	0.2
BF_4^-	8.109	0.004	0.1
I^-	8.111	0.006	0.2
Br^-	8.119	0.014	0.4
Cl^-	8.202	0.097	2.7
F^-	11.762	3.657	100.0

HαOBn:

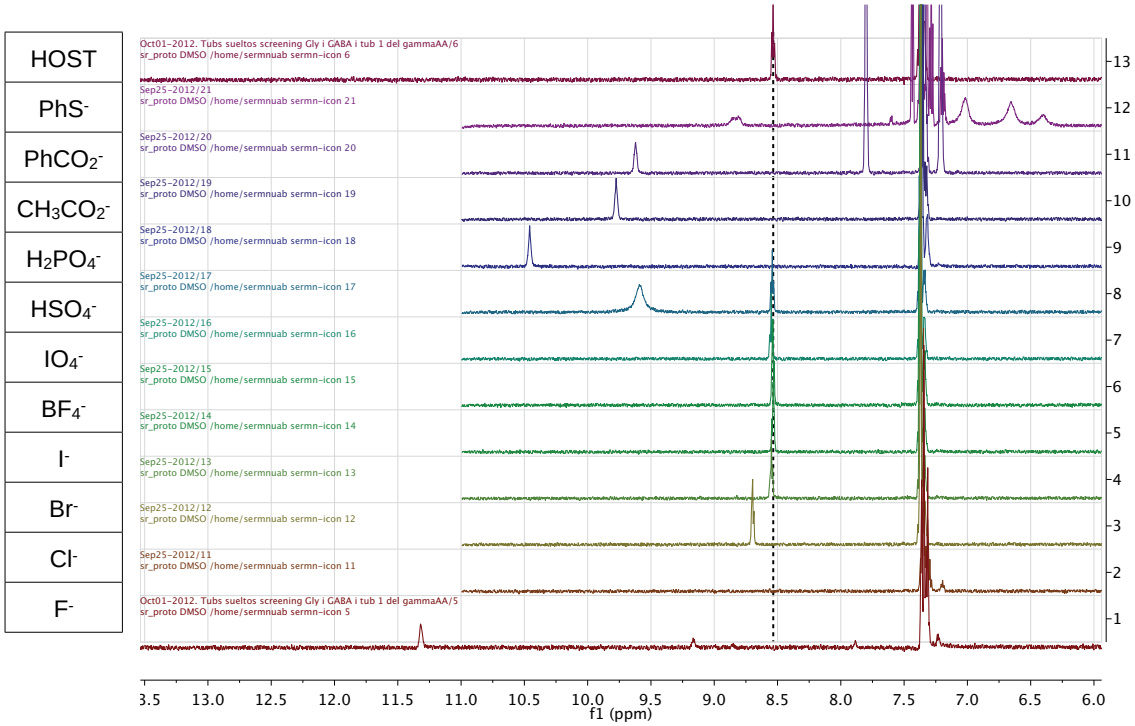

Figure **182**. ^{1}H-NMR anion screening of **HαOBn** in DMSO-d_6 (600 MHz).

Table **54**. Chemical shift shielding and relative affinity of **HαOBn** host towards several anions.

	δ NH (ppm)	Δδ NH (ppm)	Relative Δδ (%)
Free H	8.535	0.000	0.0
PhS^-	8.826	0.291	10.5
$PhCO_2^-$	9.621	1.086	39.1
$CH_3CO_2^-$	9.775	1.240	44.6
$H_2PO_4^-$	10.458	1.923	69.1
HSO_4^-	8.541	0.006	0.2
IO_4^-	8.550	0.015	0.5
BF_4^-	8.536	0.001	0.0
I^-	8.535	0.000	0.0
Br^-	8.548	0.013	0.5
Cl^-	8.696	0.161	5.8
F^-	11.316	2.781	100.0

▸HβOBn:

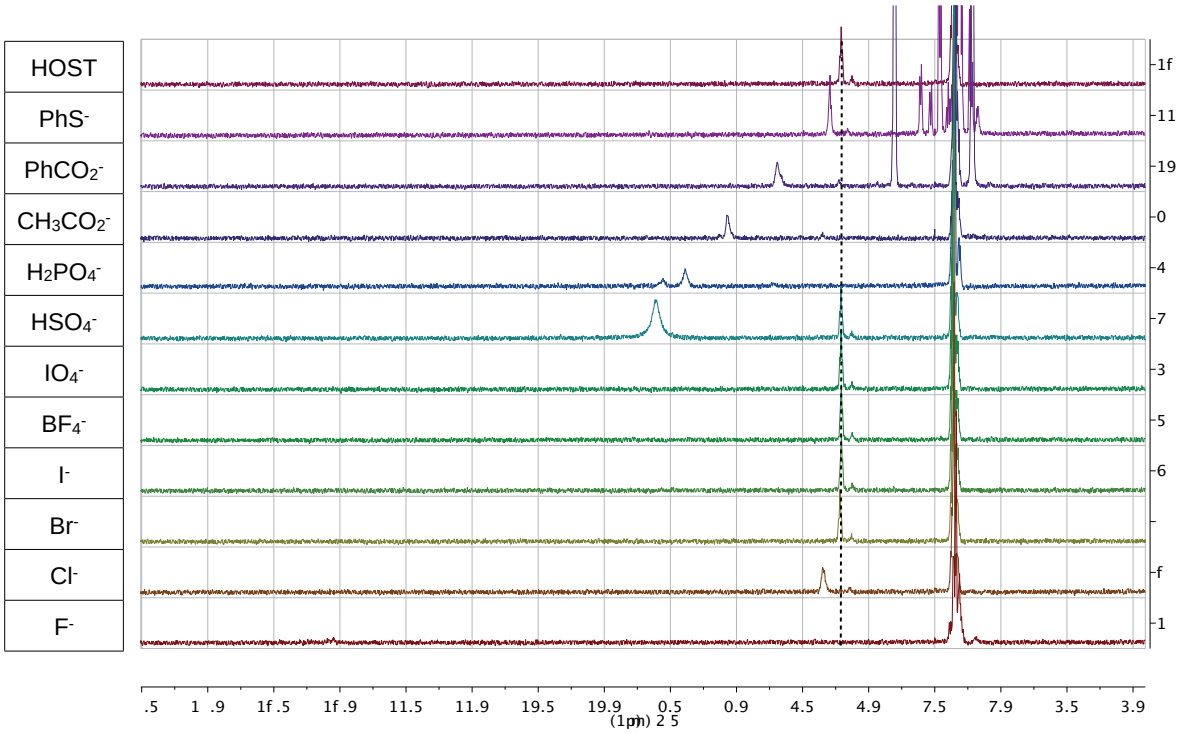

Figure **183**. ^{1}H-NMR anion screening of **HβOBn** in DMSO-d_6 (600 MHz).

Table **55**. Chemical shift shielding and relative affinity of **HβOBn** host towards several anions.

	δ NH (ppm)	**Δδ NH (ppm)**	**Relative Δδ (%)**
Free H	8.208	0.000	0.0
PhS^-	8.292	0.084	2.2
$PhCO_2^-$	8.688	0.480	12.5
$CH_3CO_2^-$	9.063	0.855	22.3
$H_2PO_4^-$	9.388	1.180	30.7
HSO_4^-	8.210	0.002	0.1
IO_4^-	8.209	0.001	0.0
BF_4^-	8.207	-0.001	0.0
I^-	8.207	-0.001	0.0
Br^-	8.217	0.009	0.2
Cl^-	8.342	0.134	3.5
F^-	12.047*	3.839	100.0

* No clear signal is observed: broad peak at 12 ppm with very low intensity can be hardly seen.

▸HγOBn:

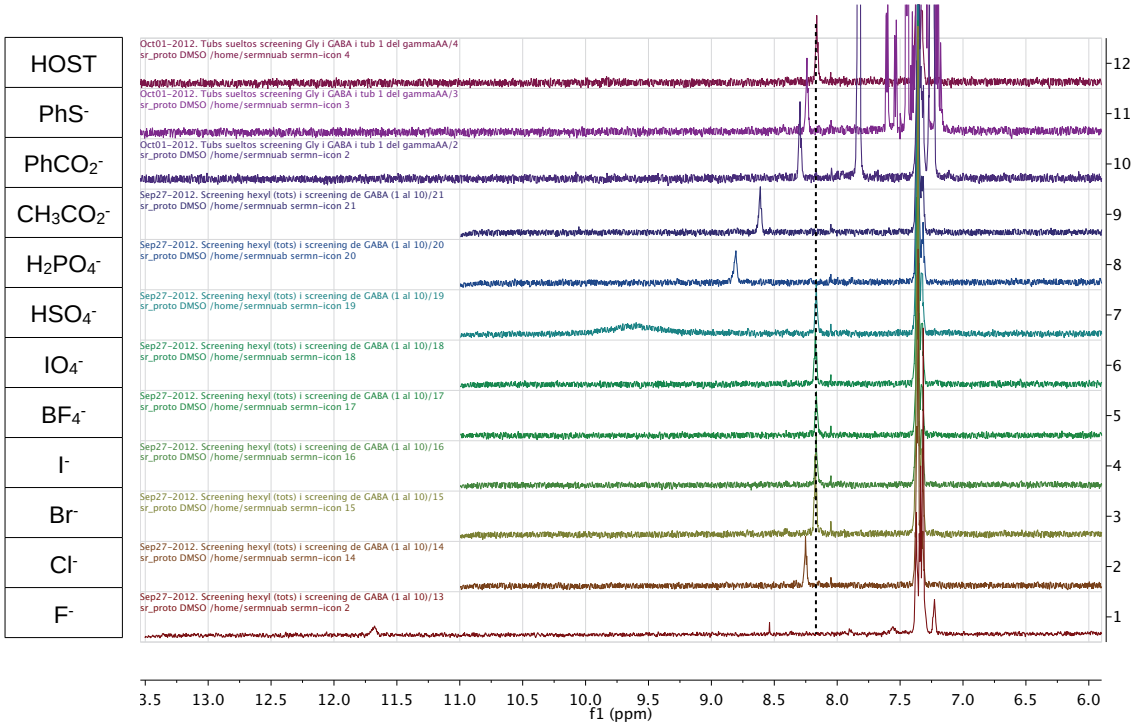

Figure **184**. ^{1}H-NMR anion screening of **HγOBn** in DMSO-d_6 (600 MHz).

Table **56**. Chemical shift shielding and relative affinity of **HγOBn** host towards several anions.

	δ NH (ppm)	**Δδ NH (ppm)**	**Relative Δδ (%)**
Free H	8.163	0.000	0.0
PhS^-	8.241	0.078	2.2
$PhCO_2^-$	8.295	0.132	3.8
$CH_3CO_2^-$	8.611	0.448	12.8
$H_2PO_4^-$	8.804	0.641	18.3
HSO_4^-	8.166	0.003	0.1
IO_4^-	8.173	0.010	0.3
BF_4^-	8.165	0.002	0.1
I^-	8.166	0.003	0.1
Br^-	8.173	0.010	0.3
Cl^-	8.252	0.089	2.5
F^-	11.674	3.511	100.0

▸HγOMe:

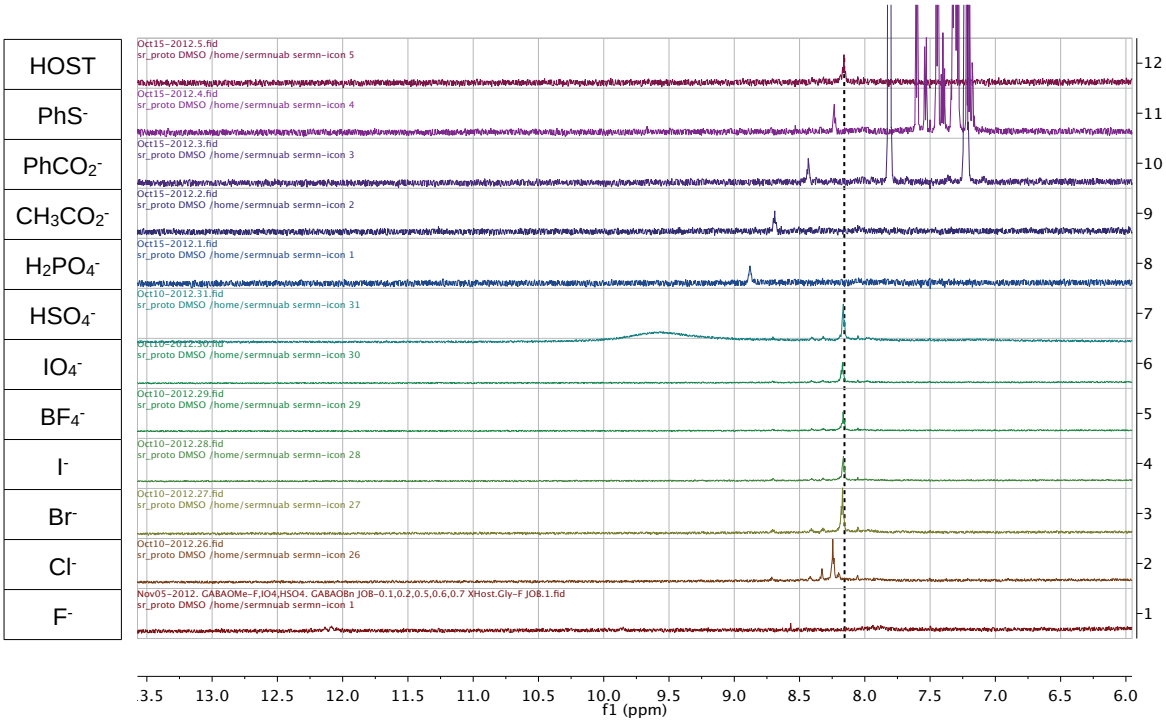

Figure **185**. ^{1}H-NMR anion screening of **HγOMe** in DMSO-d_6 (600 MHz).

Table **57**. Chemical shift shielding and relative affinity of **HγOMe** host towards several anions.

	δ NH (ppm)	**Δδ NH (ppm)**	**Relative Δδ (%)**
Free H	8.160	0.000	0.0
PhS$^-$	8.234	0.074	1.9
PhCO$_2^-$	8.433	0.273	7.0
CH$_3$CO$_2^-$	8.690	0.530	13.5
H$_2$PO$_4^-$	8.880	0.720	18.3
HSO$_4^-$	8.165	0.005	0.1
IO$_4^-$	8.171	0.011	0.3
BF$_4^-$	8.166	0.006	0.2
I$^-$	8.164	0.004	0.1
Br$^-$	8.171	0.011	0.3
Cl$^-$	8.246	0.086	2.2
F$^-$	12.085*	3.925	100.0

* Although low intensity of more than one signal make difficult to assign it the one with the highest intesity is observed at about 12 ppm.

▸HγCbuOBn:

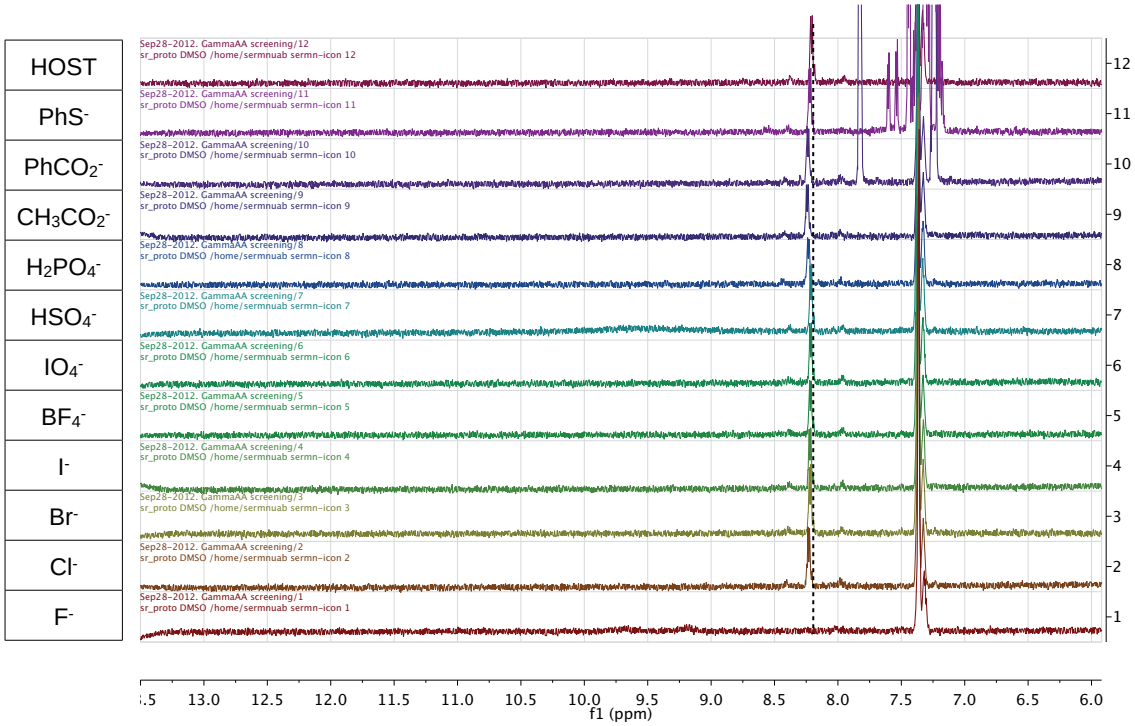

Figure **186**. ^{1}H-NMR anion screening of **HγCbuOBn** in DMSO-d_6 (600 MHz).

Table **58**. Chemical shift shielding and relative affinity of **HγCbuOBn** host towards several anions.

	δ NH (ppm)	**Δδ NH (ppm)**	**Relative Δδ (%)**
Free H	8.207	0.000	0.0
PhS$^-$	8.221	0.014	41.2
PhCO$_2^-$	8.235	0.028	82.4
CH$_3$CO$_2^-$	8.241	0.034	100.0
H$_2$PO$_4^-$	8.232	0.025	73.5
HSO$_4^-$	8.212	0.005	14.7
IO$_4^-$	8.215	0.008	23.5
BF$_4^-$	8.217	0.010	29.4
I$^-$	8.220	0.013	38.2
Br$^-$	8.219	0.012	35.3
Cl$^-$	8.229	0.022	64.7
F$^-$	*	--	--

* No clear signal is observed (below 13 ppm). However, recognition takes place because NH resonance disappears completely.

▸HγCbuOMe:

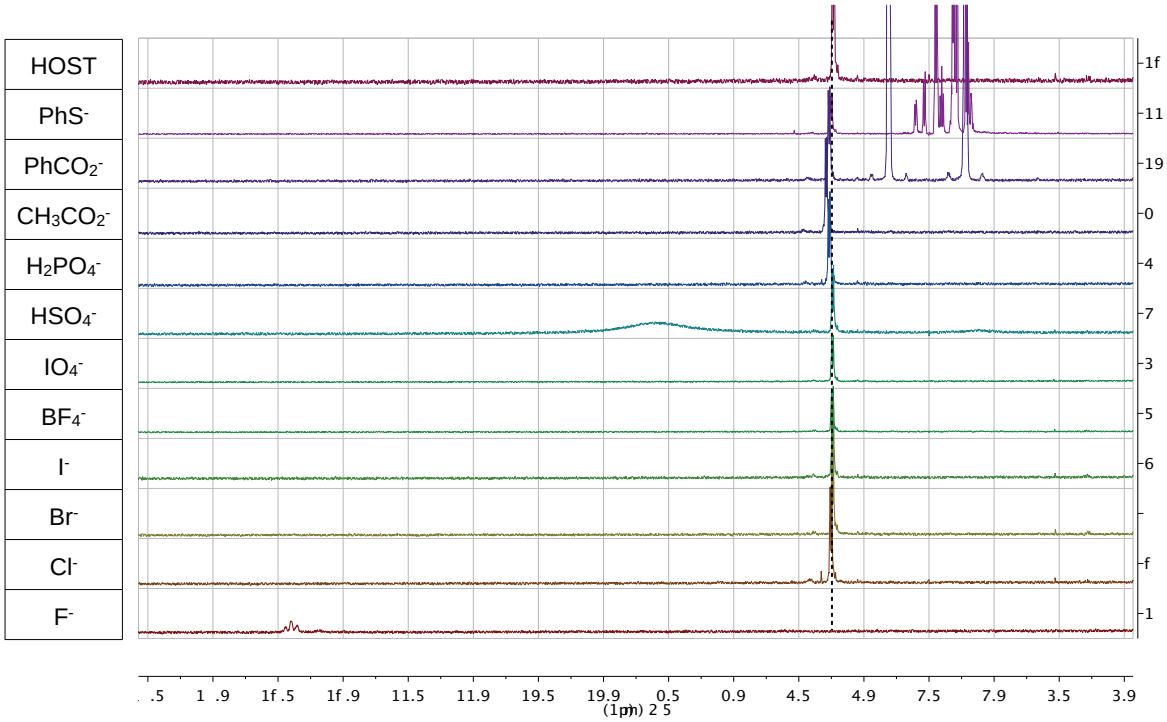

Figure **187**. ^{1}H-NMR anion screening of **HγCbuOMe** in DMSO-d_6 (600 MHz).

Table **59**. Chemical shift shielding and relative affinity of **HγCbuOMe** host towards several anions.

	δ NH (ppm)	**Δδ NH (ppm)**	**Relative Δδ (%)**
Free H	8.235	0.000	0.0
PhS^-	8.250	0.015	0.4
$PhCO_2^-$	8.268	0.033	0.8
$CH_3CO_2^-$	8.290	0.055	1.3
$H_2PO_4^-$	8.267	0.032	0.8
HSO_4^-	8.238	0.003	0.1
IO_4^-	8.240	0.005	0.1
BF_4^-	8.240	0.005	0.1
I^-	8.239	0.004	0.1
Br^-	8.241	0.006	0.1
Cl^-	8.251	0.016	0.4
F^-	12.393	4.158	100.0

‣HδCbuOMe:

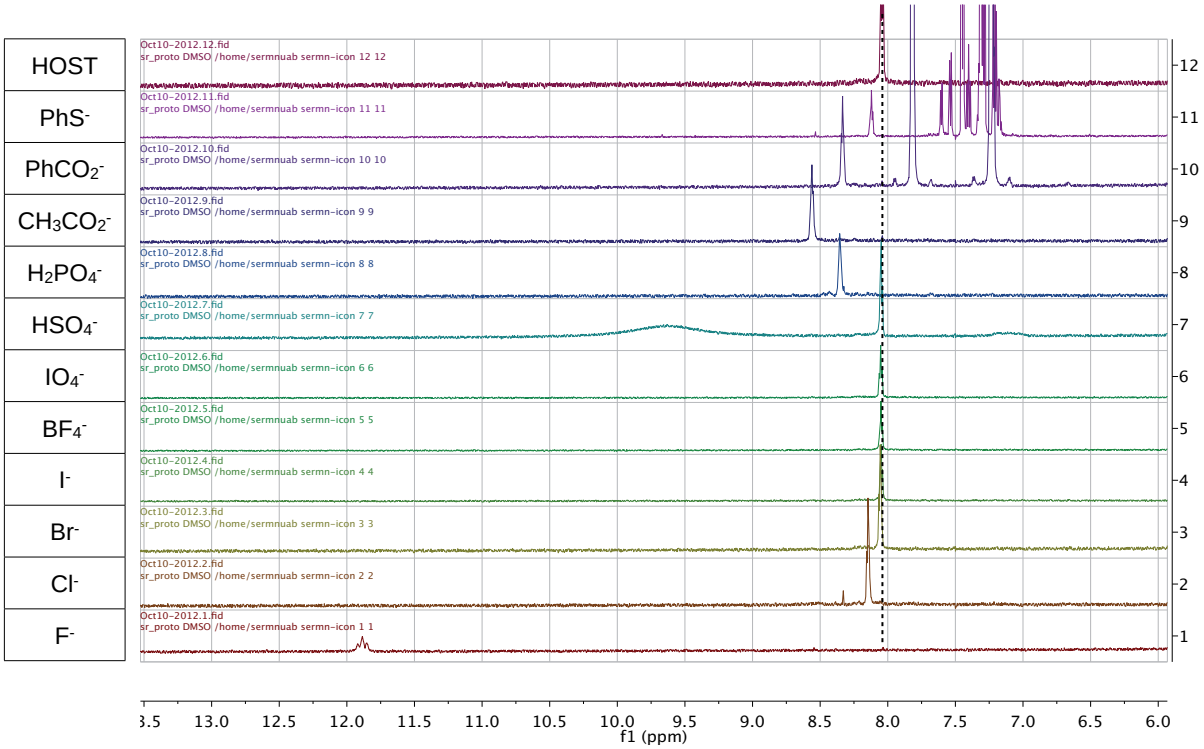

Figure **188**. ^{1}H-NMR anion screening of **HδCbuOMe** in DMSO-d_6 (600 MHz).

Table **60**. Chemical shift shielding and relative affinity of **HδCbuOMe** host towards several anions.

	δ NH (ppm)	**Δδ NH (ppm)**	**Relative Δδ (%)**
Free H	8.042	0.000	0.0
PhS^-	8.121	0.079	2.1
$PhCO_2^-$	8.334	0.292	7.6
$CH_3CO_2^-$	8.561	0.519	13.5
$H_2PO_4^-$	8.356	0.314	8.2
HSO_4^-	8.048	0.006	0.2
IO_4^-	8.052	0.010	0.3
BF_4^-	8.050	0.008	0.2
I^-	8.048	0.006	0.2
Br^-	8.056	0.014	0.4
Cl^-	8.146	0.104	2.7
F^-	11.884	3.842	100.0

4.5.4. HαOBn-AnionTBA complexes

4.5.4.1. HαOBn-H_2PO_4TBA complex

Table **61** and Table **62** show the data used for the Job's plot representations in DMSO-d_6.

Table **61**. ^{1}H-NMR data to determine stoichiometry of the complex [**HαOBn][H_2PO_4]** by Job's plot, represented using the data in light grey columns.

Tube	[Host]	X_{Host}	X_{Guest}	δ N-H_3	Δδ N-H_3	Δδ N-H_3·[Host]
1	2.0	1.0	0.0	8.536	0.000	0.000
2	1.8	0.9	0.1	8.722	0.186	0.335
3	1.6	0.8	0.2	8.951	0.415	0.664
4	1.4	0.7	0.3	9.219	0.683	0.956
5	1.2	0.6	0.4	9.463	0.927	1.112
6	1.0	0.5	0.5	9.683	1.147	1.147
7	0.8	0.4	0.6	9.875	1.339	1.071
8	0.6	0.3	0.7	10.01	1.473	0.884
9	0.4	0.2	0.8	10.11	1.576	0.630
10	0.2	0.1	0.9	10.19	1.652	0.330

Units:[Host] (mM); δ and Δδ (ppm); Δδ·[Host] (ppm·mM)

Table **62**. ^{1}H-NMR data to determine stoichiometry of the complex [**HαOBn][H_2PO_4]** by Job's plot, represented using the data in light grey columns *vs.* X_{Guest}.

Tube	[Host]	δ H_1	Δδ H_1	Δδ H_1·[H]	δ H_4	Δδ H_4	Δδ H_4·[H]	δ P	Δδ[a] P	Δδ P·[H]
1	2.0	3.294[b]	0.000	0.000	3.945	0.000	0.000	0.174	0.000	0.000
2	1.8	3.304	0.010	0.018	3.954	0.009	0.016	0.110	0.064	0.115
3	1.6	3.272	0.022	0.035	3.965	0.020	0.032	0.069	0.105	0.168
4	1.4	3.235	0.059	0.083	3.977	0.032	0.045	0.008	0.166	0.232
5	1.2	3.201	0.093	0.112	3.988	0.043	0.052	-0.082	0.256	0.307
6	1.0	3.171	0.123	0.123	3.997	0.052	0.052	-0.161	0.335	0.335
7	0.8	3.144	0.150	0.120	4.005	0.060	0.048	-0.205	0.379	0.303
8	0.6	3.126	0.168	0.101	4.010	0.065	0.039	-0.257	0.431	0.259
9	0.4	3.112	0.182	0.073	4.014	0.069	0.028	-0.283	0.457	0.183
10	0.2	3.101	0.193	0.039	4.016	0.071	0.014	-0.335	0.509	0.102

[a] Δδ is given as absolute value |Δδ|

[b] H_1 real signal is under the residual peak of water from DMSO-d_6, so a reference value is given according to the shift of similar signals.

Units:[Host] (mM); δ and Δδ (ppm); Δδ·[Host] (ppm·mM)

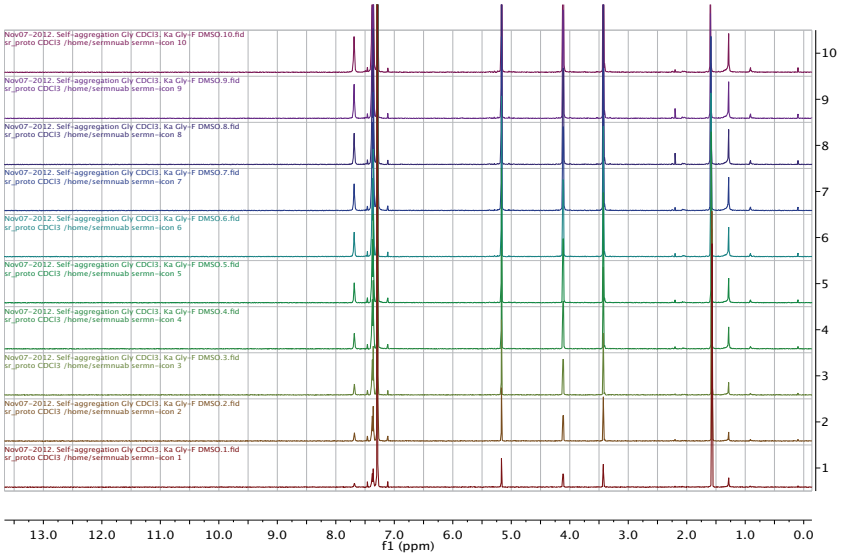

Figure **189**. ^{1}H-NMR spectra of the self-aggregation experiment for **HαOBn** receptor from [Host] = 4 mM (*top*) to [Host] = 0.2 mM (*bottom*). $CDCl_3$ (600 MHz).

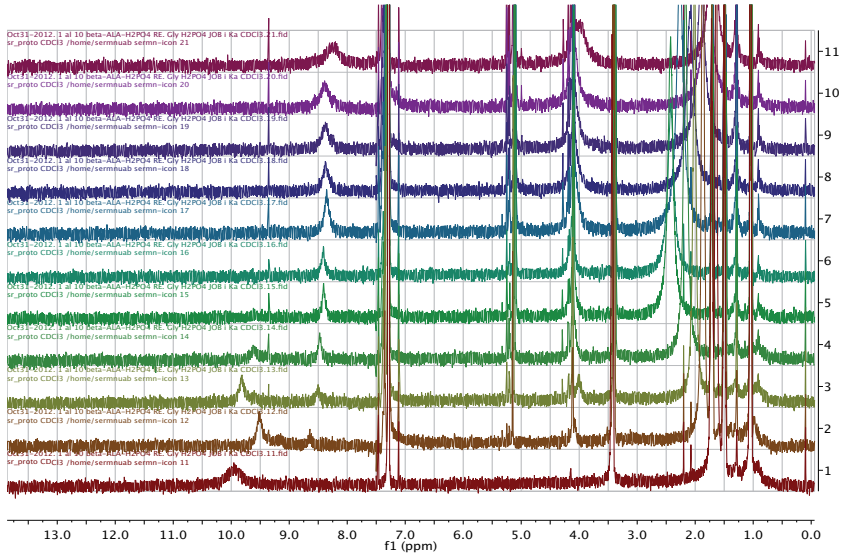

Figure **190**. ^{1}H-NMR spectra of **HαOBn** titration with **$TBAH_2PO_4$** to determine the stoichiometry of the complex. From X_{Host} = 1 (*top*) to X_{Host} = 0 (*bottom*) in ΔX = 0.1. $CDCl_3$ (600 MHz).

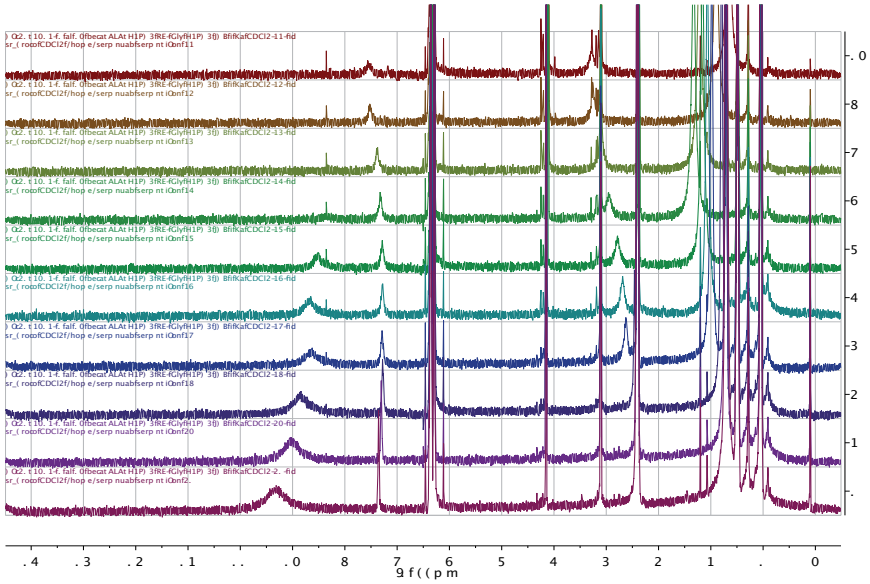

Figure **191**. ^{1}H-NMR spectra of **HαOBn** titration with **$TBAH_2PO_4$** to determine the K_a of the complex. From Eq. Guest = 0 (*top*) to Eq. Guest = 6 (*bottom*). $CDCl_3$ (600 MHz).

WinEQNMR2 program calculations

The statistics through which the data is considered to fit good a system is summarized in Table **63**.

Table **63**. Statistics of the data fitting for the four complexes formed by **HαOBn** host in DMSO-d_6.

		Anion sources and methods of determination of association constants[a,b] (*up*) and free energies[c] (*down*)
HαOBn		**$TBAH_2PO_4$ in $CDCl_3$**
		WinEQNMR2
1:1	**RSS[d]** **R factor**	$3.04 \cdot 10^{-4}$ 0.1133
1:1 **1:2**	**RSS** **R factor**	$1.73 \cdot 10^{-5}$ 0.0270
1:1 **2:1**	**RSS** **R factor**	$1.06 \cdot 10^{-4}$ 0.0670
1:1 **1:2** **2:2**	**RSS** **R factor**	$2.51 \cdot 10^{-4}$ 0.1028

[a] Logβ: β_{11} (M^{-1}), β_{12} and β_{21} (M^{-2}), β_{22} (M^{-3}). [b] Introduced guide values: $\log\beta_{11}=3$, $\log\beta_{12}=7$, $\log\beta_{22}=10$. [c] Units: kcal·mol^{-1}. [d] RSS: Residual Sum of Squares.

4.5.4.2. HαOBn-CH_3CO_2TBA complex

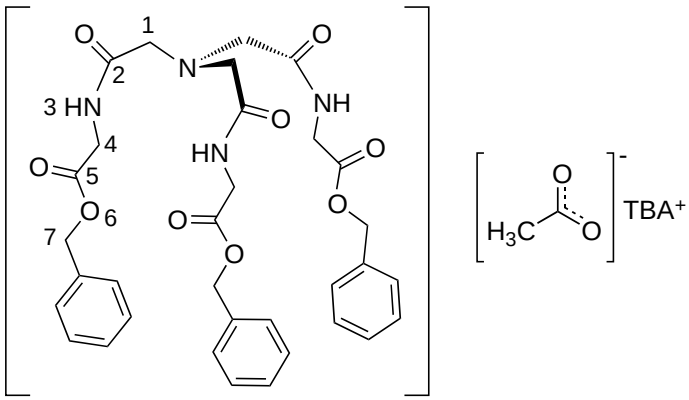

Stoichiometry

The shifting of N-H_3 signal could be followed easily but H_1 signal showed the initial peak, when no anion is added, overlapped by residual water in DMSO-d_6 at about 3 ppm (Figure **192** and Figure **193**).

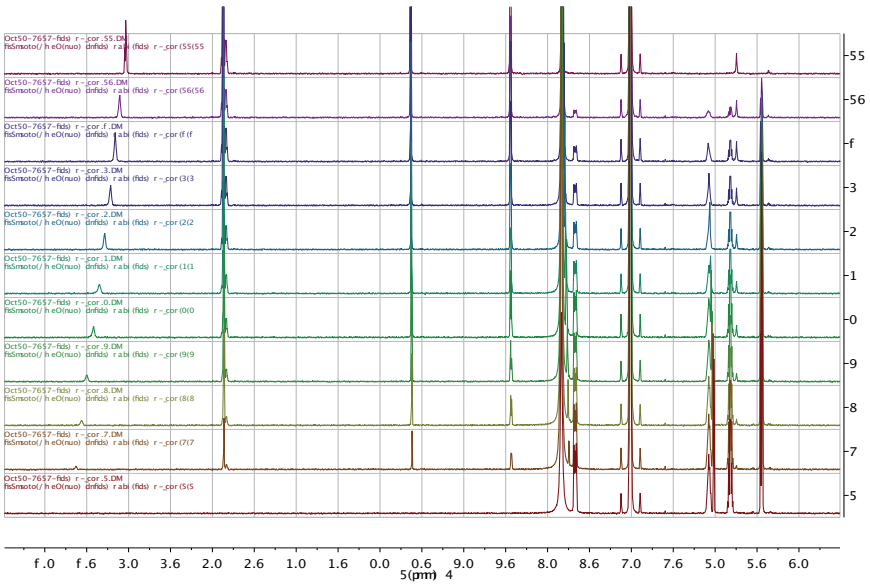

Figure **192**. ^{1}H-NMR spectra of **HαOBn** titration with **TBACH$_3$CO$_2$** to determine the stoichiometry of the complex. From X_{Host} = 1 (*top*) to X_{Host} = 0 (*bottom*) in ΔX = 0.1. DMSO-d_6 (600 MHz).

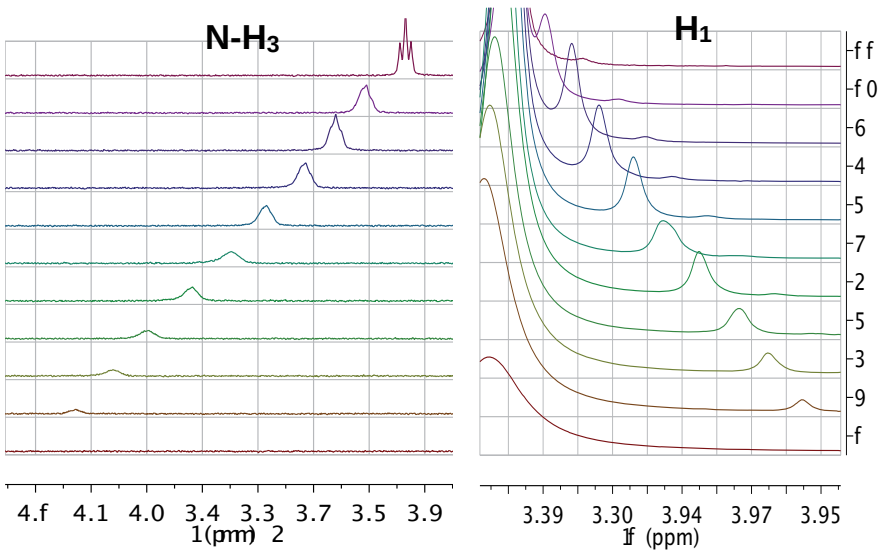

Figure **193**. Zoom of specific signals from the ^{1}H-NMR spectra of **HαOBn** titration with **TBACH$_3$CO$_2$** to determine the stoichiometry of the complex. From X_{Host} = 1 (*top*) to X_{Host} = 0 (*bottom*) in ΔX = 0.1. DMSO-d_6 (600 MHz).

Thus, Δδ H_1 was calculated by subtraction of a reference value (δ = 3.394 ppm), given according to similar shift variations, because neat difference for the second point could not be zero (Table **64**).

Table **64**. ^{1}H-NMR data to determine stoichiometry of the complex [**HαOBn][CH_3CO_2]** by Job's plot, represented using the data in light grey columns.

Tube	[Host]	X_{Host}	X_{Guest}	δ NH_3	Δδ NH_3	Δδ NH_3·[H]	δ H_1	Δδ[a] H_1	Δδ H_1·[H]
1	2.0	1.0	0.0	8.535	0.000	0.000	3.323[b]	0.000	0.000
2	1.8	0.9	0.1	8.605	0.070	0.126	3.319	0.004	0.007
3	1.6	0.8	0.2	8.660	0.125	0.200	3.312	0.011	0.018
4	1.4	0.7	0.3	8.714	0.179	0.251	3.304	0.019	0.027
5	1.2	0.6	0.4	8.785	0.250	0.300	3.294	0.029	0.035
6	1.0	0.5	0.5	8.848	0.313	0.313	3.285	0.038	0.038
7	0.8	0.4	0.6	8.918	0.383	0.306	3.275	0.048	0.038
8	0.6	0.3	0.7	8.998	0.463	0.278	3.264	0.059	0.035
9	0.4	0.2	0.8	9.060	0.525	0.210	3.255	0.068	0.027
10	0.2	0.1	0.9	9.128	0.593	0.119	3.245	0.078	0.016

[a] Δδ is given as absolute value |Δδ|
[b] H_1 real signal is under the residual peak of water from DMSO-d_6, so a reference value is given according to the shift of similar signals.
Units:[Host] (mM); δ and Δδ (ppm); Δδ·[Host] (ppm·mM)

Job's plots showed a 1:1 stoichiometry for the complex **[HαOBn][CH_3CO_2]** (Figure **194** and Figure **195**).

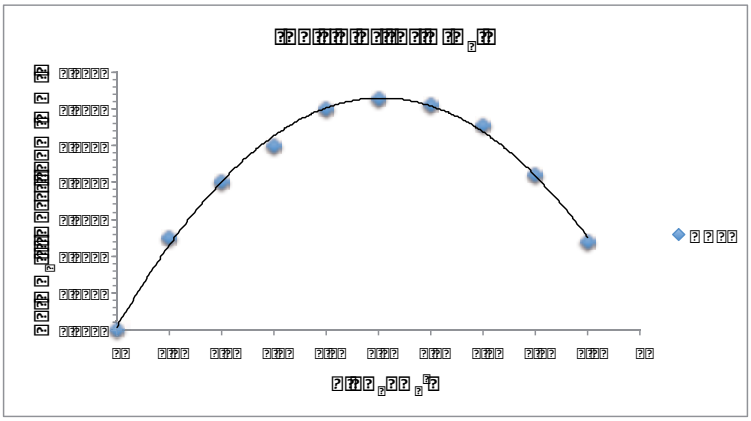

Figure **194**. Job's plot for **[HαOBn][CH_3CO_2]** complex.

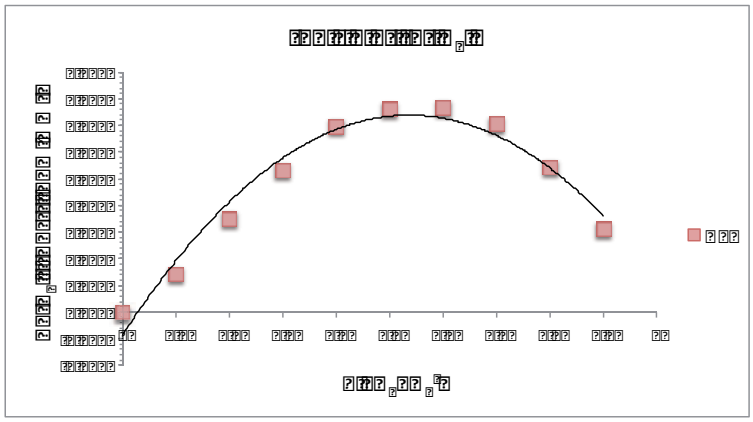

Figure **195**. Job's plot for **[HαOBn][CH_3CO_2]** complex.

Association constant K_a

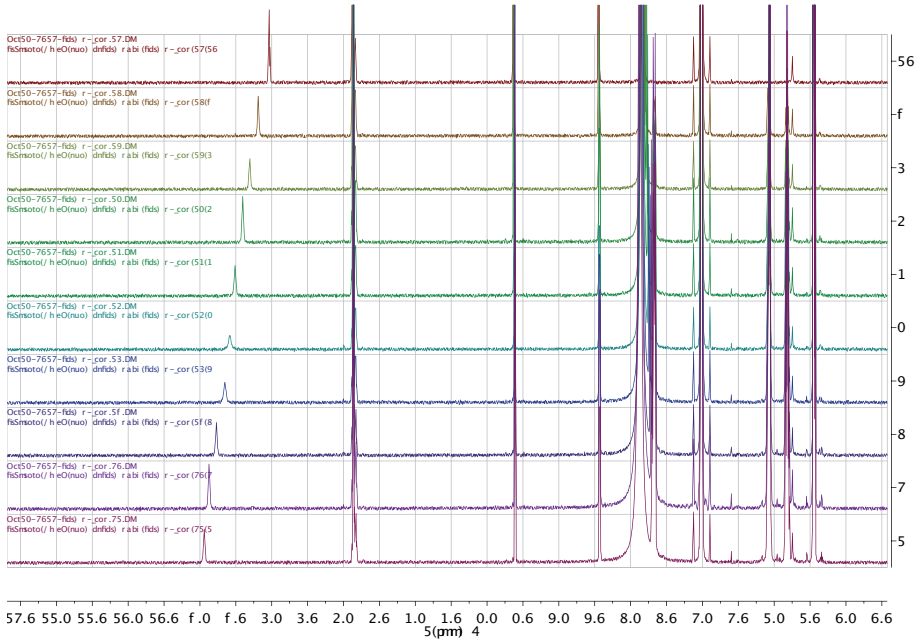

Figure **196**. ^{1}H-NMR spectra of **HαOBn** titration with **TBACH_3CO_2** to determine the K_a of the complex. From Eq. Guest = 0 (*top*) to Eq. Guest = 6 (*bottom*). DMSO-d_6 (600 MHz).

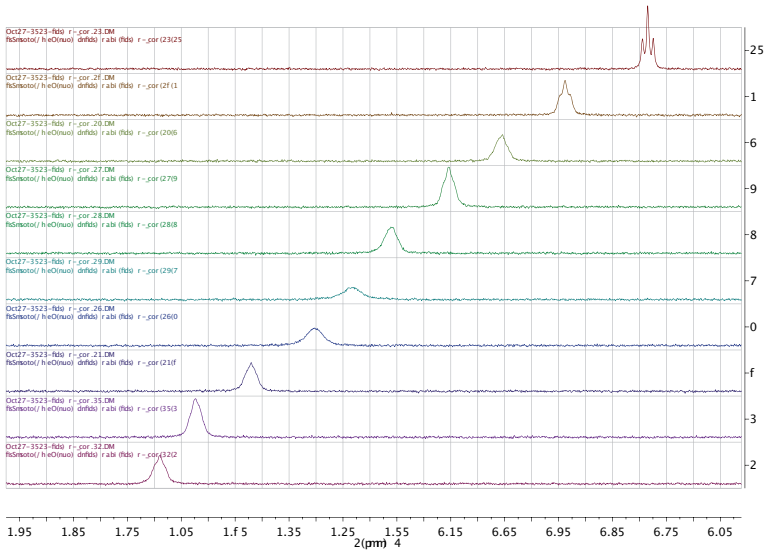

Figure **197**. Zoom of the N-H_3 area from the ^{1}H-NMR spectra of **HαOBn** titration with **TBACH_3CO_2** to determine the K_a of the complex. From Eq. Guest = 0 (*top*) to Eq. Guest = 6 (*bottom*). DMSO-d_6 (600 MHz).

Table **65**. Calculated data to determine K_a of the complex **[HαOBn][CH₃CO₂]** by linear regression of the represented data in light grey columns.

Tube	[Guest] = Eq. Guest	1/[Guest]	δ N-H₃	Δδ N-H₃	1/Δδ
1	0.0	--[a]	8.535	0.000	--[a]
2	0.5	2.00	8.687	0.152	1.692
3	1.0	1.00	8.805	0.270	1.009
4	1.5	0.67	8.902	0.367	0.775
5	2.0	0.50	9.011	0.476	0.682
6	2.5	0.40	9.084	0.549	0.638
7	3.0	0.33	9.152	0.617	0.607
8	4.0	0.25	9.270	0.735	0.576
9	5.0	0.20	9.374	0.839	0.556
10	6.0	0.17	9.439	0.904	0.541

[a] When [Guest] = 0 no useful data can be calculated, so it is not represented on the graphic.
Units:[Guest] (mM); 1/[G] (mM^{-1}); Δδ (ppm); 1/Δδ (ppm^{-1})

Linear regression of the data fitted very well (Figure **198**).

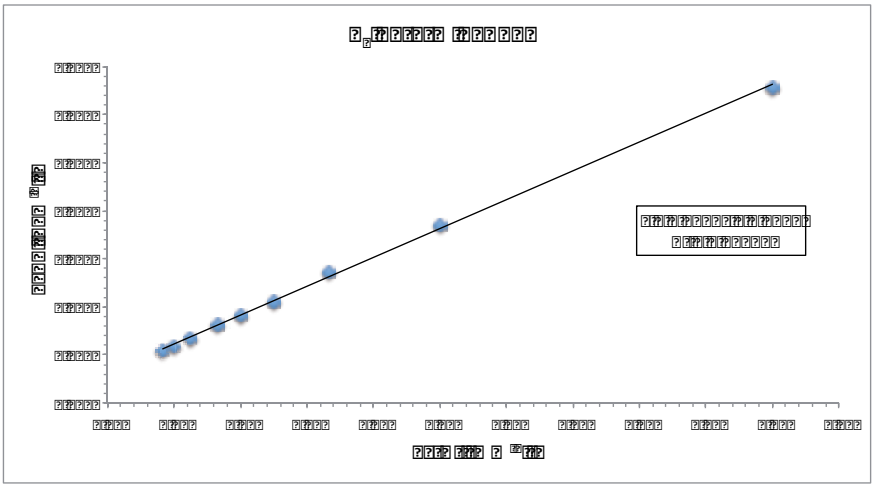

Figure **198**. Linear fitting of the data to determine the K_a of the **[HαOBn][CH₃CO₂]** complex .

Calculation of the association constant revealed a lower value than for the $H_2PO_4^-$ anion (Table **66**).

Table **66**. Thermodynamic parameters Ka and ΔG° determination for the **[HαOBn][CH₃CO₂]** complex.

Equation	Calculation	Results
$K_a = \frac{A}{slope}$	$K_a = \frac{0.6279 ppm^{-1}}{3.0014 mM \cdot ppm^{-1}}$	$K_a = 0.2092 mM^{-1} = 209 M^{-1}$ $\log K_a = 2.32$
$\Delta G^\circ = -RT \ln K_a$	$\Delta G^\circ = -1.9 \frac{cal}{K \cdot mol} \cdot 298 K \cdot \ln(209 M^{-1})$	$\Delta G^\circ = -3025 \frac{cal}{mol} = -3.0 \frac{kcal}{mol}$

4.5.4.3. HαOBn-PhCO$_2$TBA complex

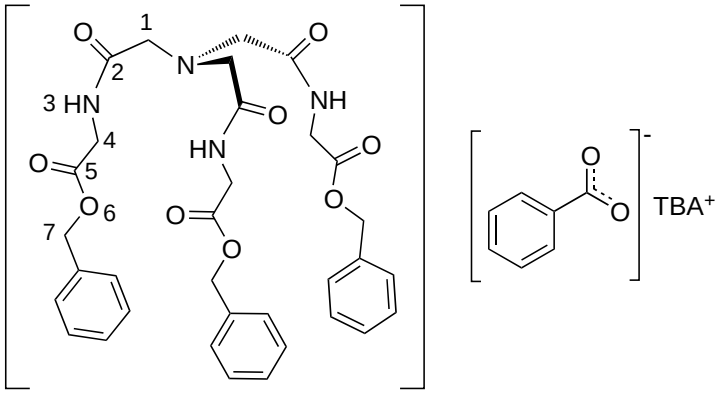

Stoichiometry

In this case, only the N-H$_3$ signal underwent a significant shielding (Figure **199** Figure **200**).

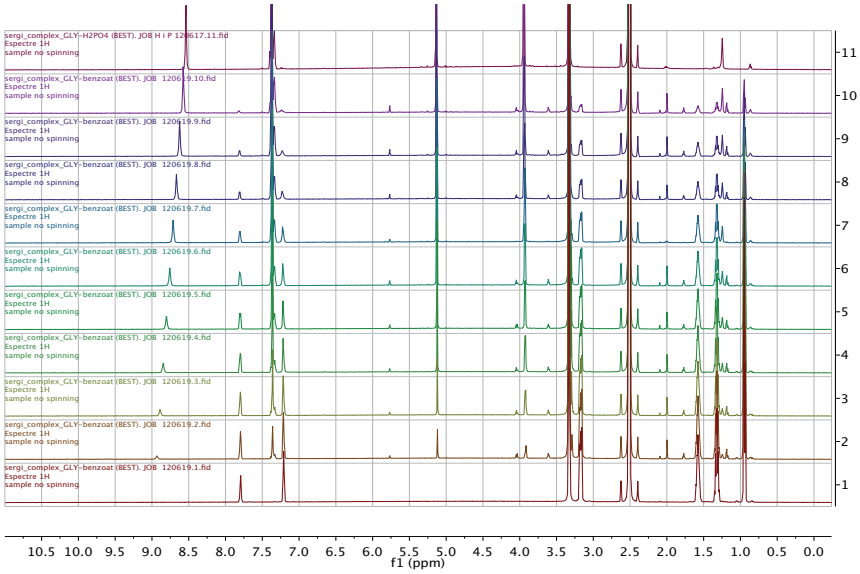

Figure **199**. ^{1}H-NMR spectra of **HαOBn** titration with **TBAPhCO$_2$** to determine the stoichiometry of the complex. From X_{Host} = 1 (*top*) to X_{Host} = 0 (*bottom*) in ΔX = 0.1. DMSO-d_6 (600 MHz).

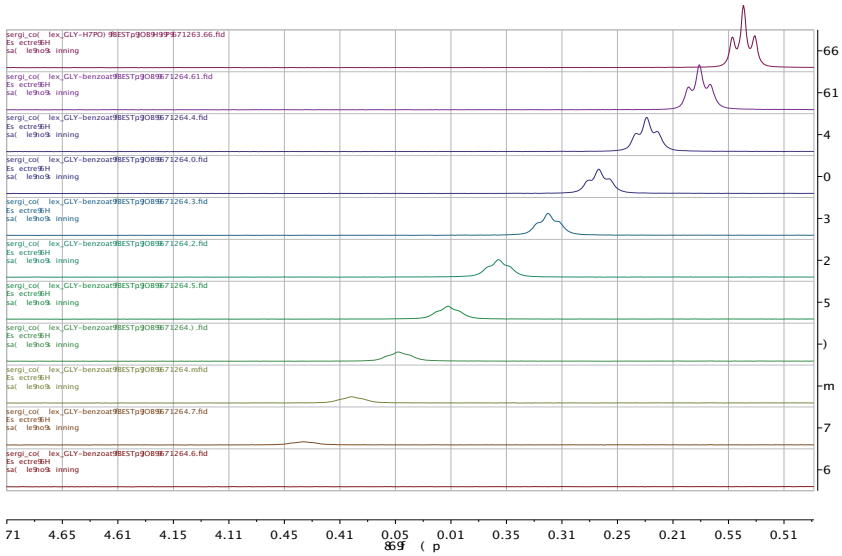

Figure **200**. Zoom of N-H$_3$ area from the ^{1}H-NMR spectra of **HαOBn** titration with **TBAPhCO$_2$** to determine the stoichiometry of the complex. From X_{Host} = 1 (*top*) to X_{Host} = 0 (*bottom*) in ΔX = 0.1. DMSO-d_6 (600 MHz).

Table **67**. ^{1}H-NMR data to determine stoichiometry of the complex [**HαOBn][PhCO$_2$]** by Job's plot, represented using the data in light grey columns.

Tube	[Host]	X_{Host}	X_{Guest}	δ N-H$_3$	Δδ N-H$_3$	Δδ N-H$_3$·[Host]
1	2.0	1.0	0.0	8.536	0.000	0.000
2	1.8	0.9	0.1	8.576	0.040	0.072
3	1.6	0.8	0.2	8.624	0.088	0.141
4	1.4	0.7	0.3	8.667	0.131	0.183
5	1.2	0.6	0.4	8.712	0.176	0.211
6	1.0	0.5	0.5	8.767	0.231	0.231
7	0.8	0.4	0.6	8.803	0.267	0.214
8	0.6	0.3	0.7	8.847	0.311	0.187
9	0.4	0.2	0.8	8.890	0.354	0.142
10	0.2	0.1	0.9	8.933	0.397	0.079

Units:[Host] (mM); δ and Δδ (ppm); Δδ·[Host] (ppm·mM)

The maximum of the Job's plot curve is also obtained at molar fraction value of 0.5, what means a 1:1 stoichiometry for the complex **[HαOBn][PhCO$_2$]** in DMSO-d_6 (Figure **201**).

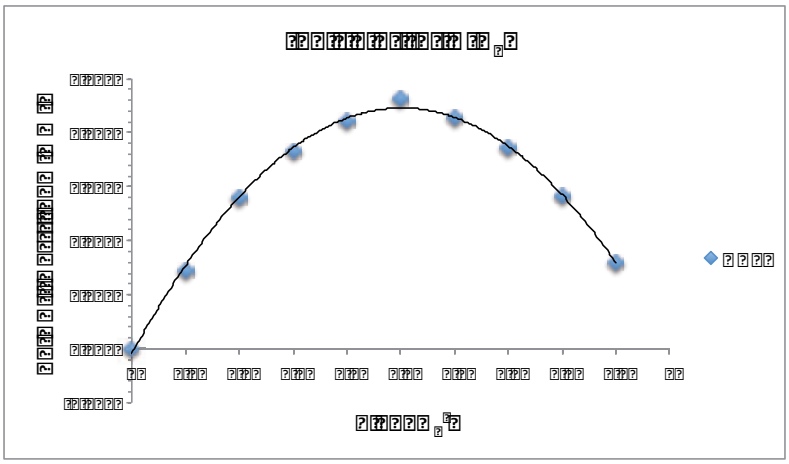

Figure **201**. Job's plot for **[HαOBn][PhCO$_2$]** complex.

Association constant K_a

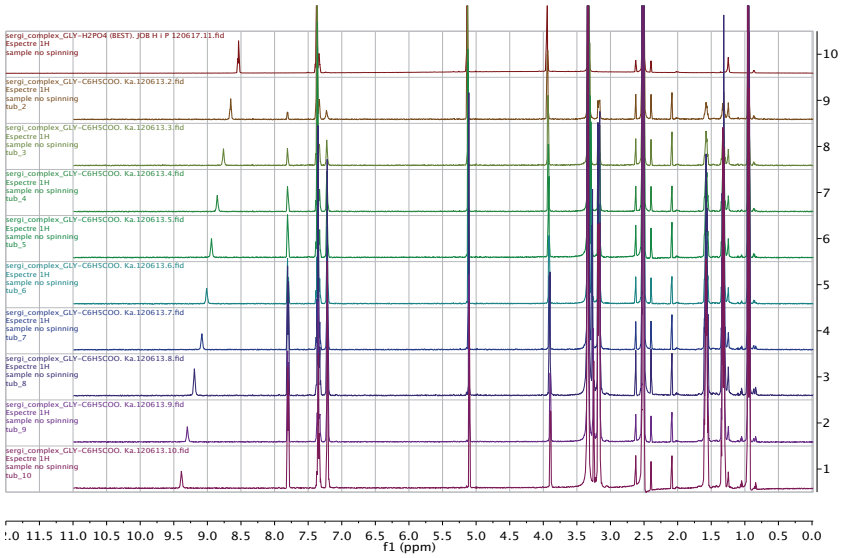

Figure **202**. ^{1}H-NMR spectra of **HαOBn** titration with **TBAPhCO$_2$** to determine the K_a of the complex. From Eq. Guest = 0 (*top*) to Eq. Guest = 6 (*bottom*). DMSO-d_6 (600 MHz).

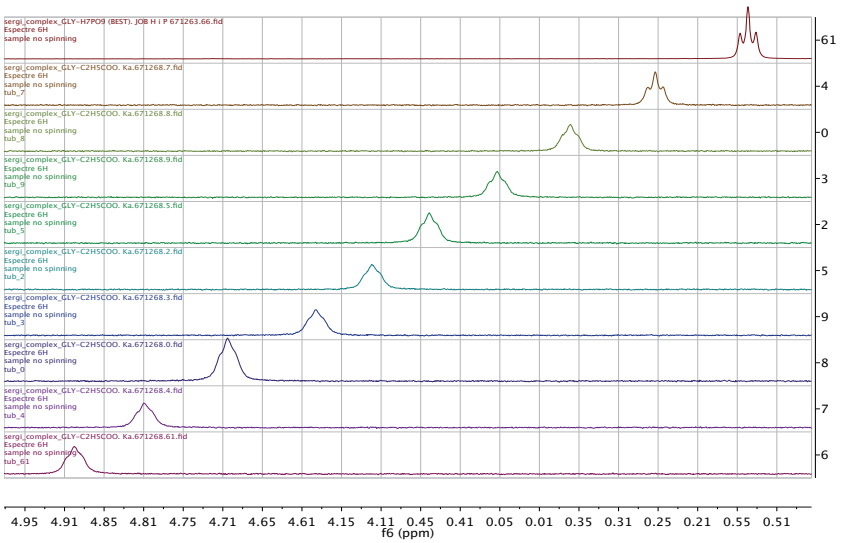

Figure **203**. Zoom of the N-H$_3$ area from the ^{1}H-NMR spectra of **HαOBn** titration with **TBAPhCO$_2$** to determine the K_a of the complex. From Eq. Guest = 0 (*top*) to Eq. Guest = 6 (*bottom*). DMSO-d_6 (600 MHz).

Table **68**. Calculated data to determine K_a of the complex **[HαOBn][PhCO₂]** by linear regression of the represented data in light grey columns.

Tube	[Guest] = Eq. Guest	1/[Guest]	δ N-H₃	Δδ N-H₃	1/Δδ
1	0.0	--[a]	8.536	0.000	--[a]
2	0.5	2.00	8.653	0.117	8.547
3	1.0	1.00	8.761	0.225	4.444
4	1.5	0.67	8.853	0.317	3.155
5	2.0	0.50	8.939	0.403	2.481
6	2.5	0.40	9.012	0.476	2.101
7	3.0	0.33	9.082	0.546	1.832
8	4.0	0.25	9.194	0.658	1.520
9	5.0	0.20	9.299	0.763	1.311
10	6.0	0.17	9.388	0.852	1.174

[a] When [Guest] = 0 no useful data can be calculated, so it is not represented on the graphic.
Units:[Guest] (mM); 1/[G] (mM^{-1}); Δδ (ppm); 1/Δδ (ppm^{-1})

Linear regression of the data fitted very well taking all the points (Figure **204**).

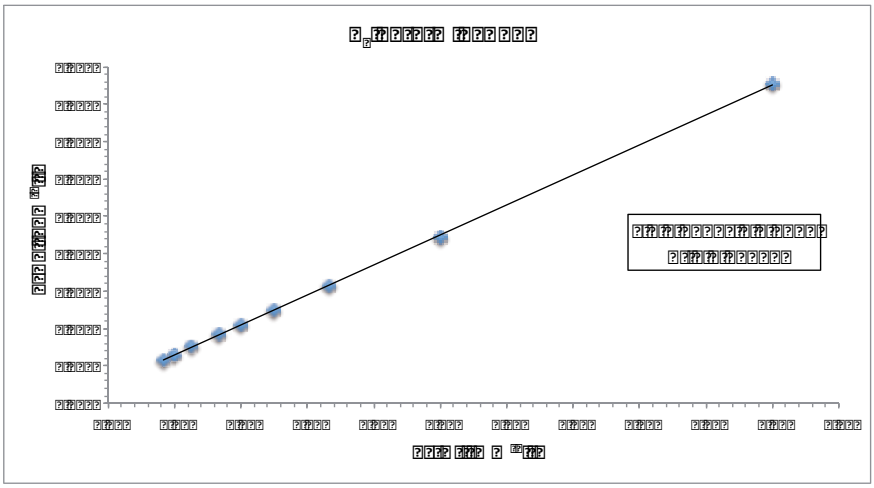

Figure **204**. Linear fitting of the data to determine the K_a of the **[HαOBn][PhCO₂]** complex .

Calculation of the K_a value was in agreement with a weaker 1:1 complex (Table **69**).

Table **69**. Thermodynamic parameters Ka and ΔG° determination for the **[HαOBn][PhCO₂]** complex.

Equation	Calculation	Results
$K_a = \frac{A}{slope}$	$K_a = \frac{0.4927 ppm^{-1}}{4.0113 mM \cdot ppm^{-1}}$	$K_a = 0.1228 mM^{-1} = 123 M^{-1}$ $\log K_a = 2.09$
$\Delta G^\circ = -RT \ln K_a$	$\Delta G^\circ = -1.9 \frac{cal}{K \cdot mol} \cdot 298 K \cdot \ln(123 M^{-1})$	$\Delta G^\circ = -2725 \frac{cal}{mol} = -2.7 \frac{kcal}{mol}$

4.5.4.4. HαOBn-ClTBA complex

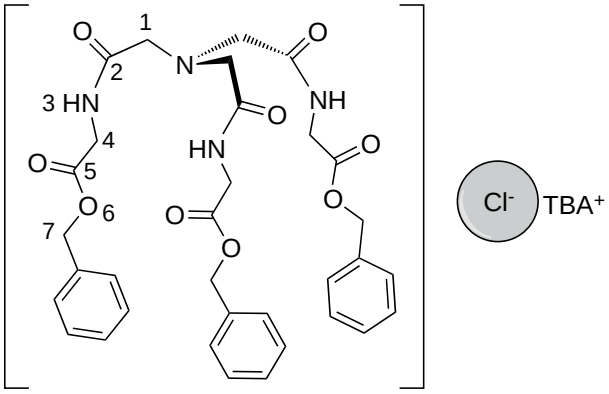

Stoichiometry

Chloride binding was weak and the N-H_3 signal was barely shifted (Figure **205** and Figure **206**).

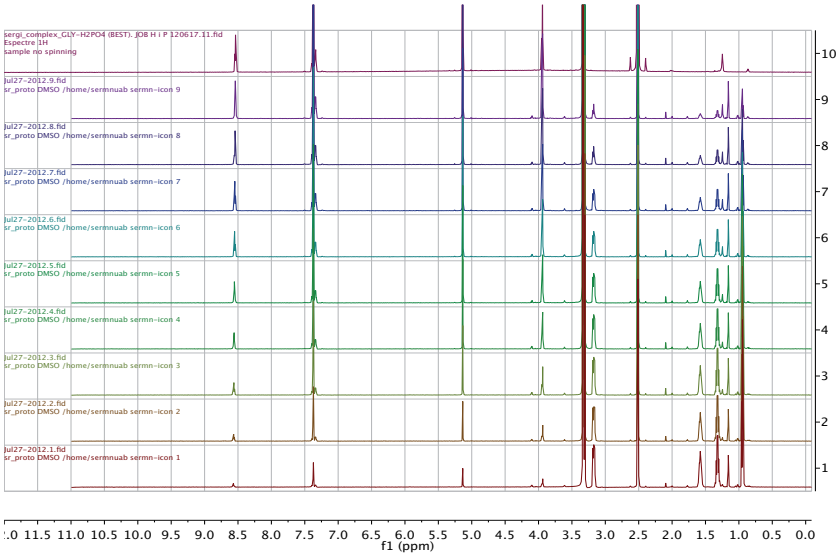

Figure **205**. ^{1}H-NMR spectra of **HαOBn** titration with **TBACl** to determine the stoichiometry of the complex. From X_{Host} = 1 (*top*) to X_{Host} = 0 (*bottom*) in ΔX = 0.1. DMSO-d_6 (600 MHz).

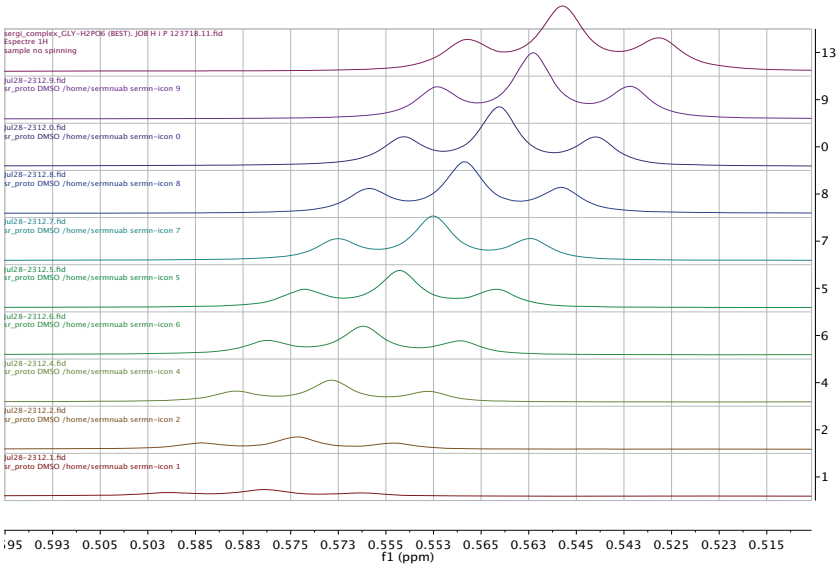

Figure **206**. Zoom of N-H_3 area from the ^{1}H-NMR spectra of **HαOBn** titration with **TBACl** to determine the stoichiometry of the complex. From X_{Host} = 1 (*top*) to X_{Host} = 0 (*bottom*) in ΔX = 0.1. DMSO-d_6 (600 MHz).

Nevertheless, chemical shift variation could be calculated (Table **70**).

Table **70**. ^{1}H-NMR data to determine stoichiometry of the complex [**HαOBn][Cl]** by Job's plot, represented using the data in light grey columns.

Tube	[Host]	X_{Host}	X_{Guest}	δ N-H$_3$	Δδ N-H$_3$	Δδ N-H$_3$·[Host]
1	2.0	1.0	0.0	8.536	0.000	0.000
2	1.8	0.9	0.1	8.540	0.004	0.007
3	1.6	0.8	0.2	8.543	0.007	0.011
4	1.4	0.7	0.3	8.547	0.011	0.015
5	1.2	0.6	0.4	8.550	0.014	0.017
6	1.0	0.5	0.5	8.554	0.018	0.018
7	0.8	0.4	0.6	8.557	0.021	0.017
8	0.6	0.3	0.7	8.561	0.025	0.015
9	0.4	0.2	0.8	8.564	0.028	0.011
10	0.2	0.1	0.9	8.568	0.032	0.006

Units:[Host] (mM); δ and Δδ (ppm); Δδ·[Host] (ppm·mM)

The maximum of the Job's plot curve is also obtained at molar fraction value of 0.5, what means a 1:1 stoichiometry for the complex **[HαOBn][Cl]** (Figure **207**).

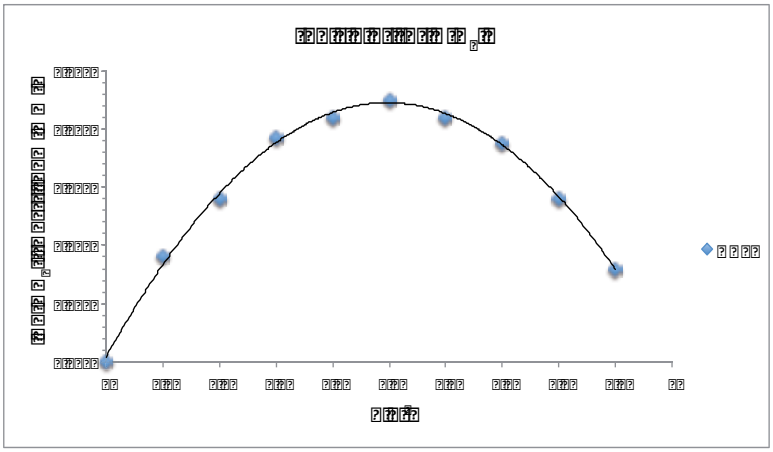

Figure **207**. Job's plot for **[HαOBn][Cl]** complex.

Association constant K_a

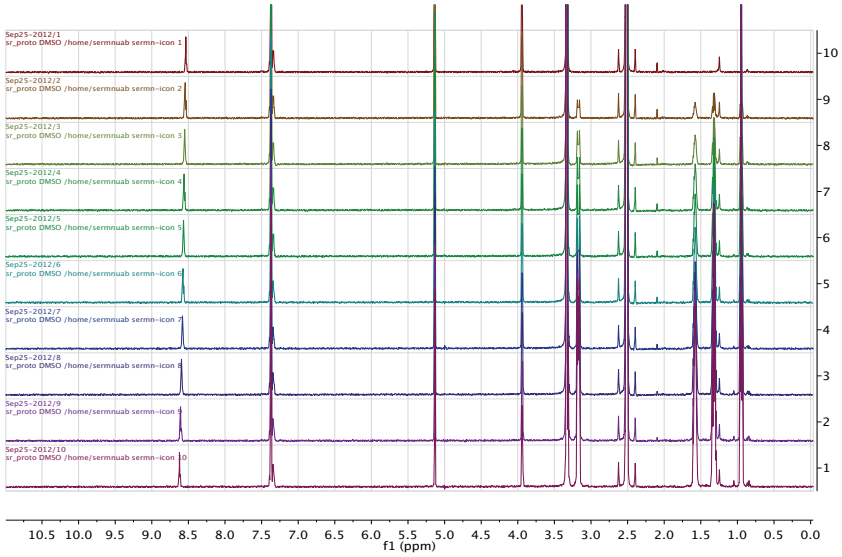

Figure **208**. ^{1}H-NMR spectra of **HαOBn** titration with **TBACl** to determine the K_a of the complex. From Eq. Guest = 0 (*top*) to Eq. Guest = 6 (*bottom*). DMSO-d_6 (600 MHz).

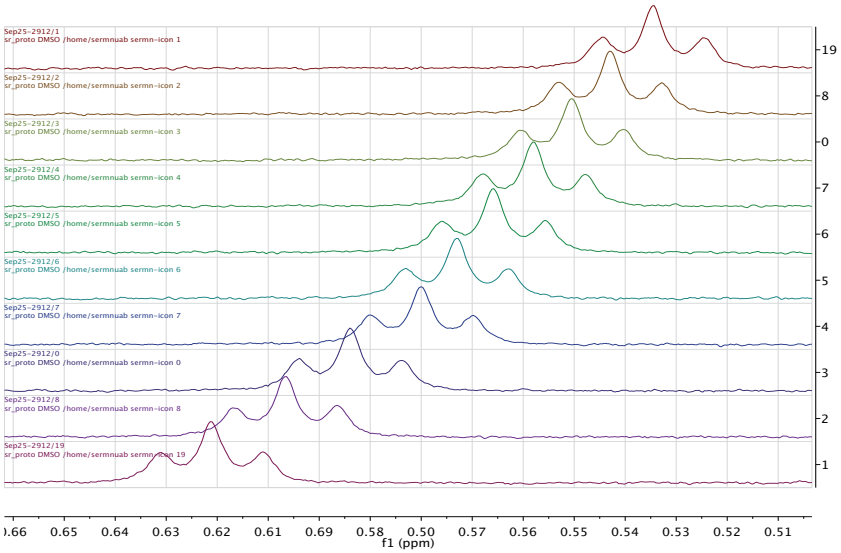

Figure **209**. Zoom of the N-H_3 area from the ^{1}H-NMR spectra of **HαOBn** titration with **TBACl** to determine the K_a of the complex. From Eq. Guest = 0 (*top*) to Eq. Guest = 6 (*bottom*). DMSO-d_6 (600 MHz).

Table **71**. Calculated data to determine K_a of the complex [**HαOBn][Cl]** by linear regression of the represented data in light grey columns.

Tube	[Guest] = Eq. Guest	1/[Guest]	δ N-H$_3$	Δδ N-H$_3$	1/Δδ
1	0.0	--[a]	8.534	0.000	--[a]
2	0.5	2.00	8.543	0.009	111.111
3	1.0	1.00	8.551	0.017	58.824
4	1.5	0.67	8.558	0.024	41.667
5	2.0	0.50	8.566	0.032	31.250
6	2.5	0.40	8.573	0.039	25.641
7	3.0	0.33	8.580	0.046	21.739
8	4.0	0.25	8.594	0.060	16.667
9	5.0	0.20	8.607	0.073	13.699
10	6.0	0.17	8.621	0.087	11.494

[a] When [Guest] = 0 no useful data can be calculated, so it is not represented on the graphic.
Units:[Guest] (mM); 1/[G] (mM^{-1}); Δδ (ppm); 1/Δδ (ppm^{-1})

Chloride anion also provided a good fit for the linear regression of the data (Figure **210**).

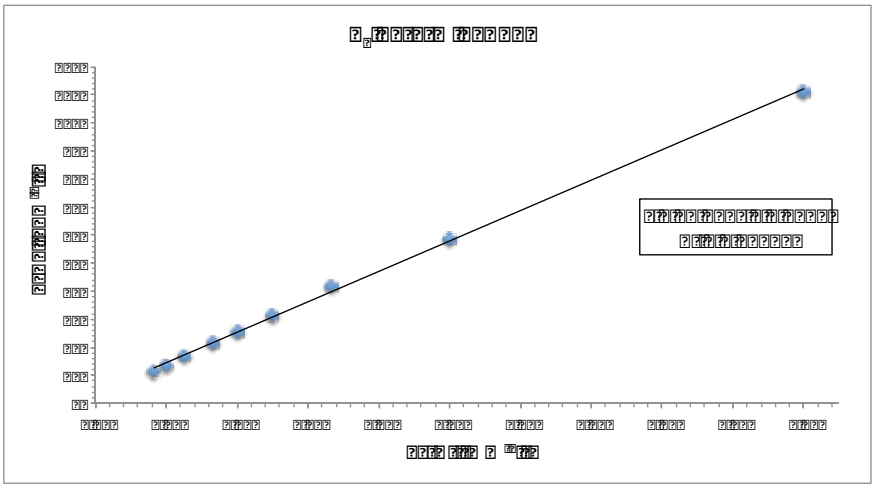

Figure **210**. Linear fitting of the data to determine the K_a of the **[HαOBn][Cl]** complex .

Calculation of the K_a value was in agreement with a weaker 1:1 complex (Table **72**).

Table **72**. Thermodynamic parameters K_a and ΔG^o determination for the **[HαOBn][Cl]** complex.

Equation	Calculation	Results
$K_a = \frac{A}{slope}$	$K_a = \frac{3.6543 ppm^{-1}}{54.236 mM \cdot ppm^{-1}}$	$K_a = 0.0674 mM^{-1} = 67 M^{-1}$ $\log K_a = 1.83$
$\Delta G^\circ = -RT \ln K_a$	$\Delta G^\circ = -1.9 \frac{cal}{K \cdot mol} \cdot 298 K \cdot \ln(67 M^{-1})$	$\Delta G^\circ = -2384 \frac{cal}{mol} = -2.4 \frac{kcal}{mol}$

4.5.4.5. Statistics from WinEQNMR2 calculations of HαOBn-AnionTBA complexes

The statistics by which the data is considered or not to fit good a system is summarized in Table **73**.

Table **73**. Statistics of the data fitting for the four complexes formed by **HαOBn** host in DMSO-d_6.

		Anion sources and methods of determination of association constants[a,b] (*up*) and free energies[c] (*down*)			
HαOBn		**$TBAH_2PO_4$**	**$TBACH_3CO_2$**	**$TBAPhCO_2$**	**TBACl**
		Win EQNMR2	**Win EQNMR2**	**Win EQNMR2**	**Win EQNMR2**
1:1	**RSS[d]**	$7.15 \cdot 10^{-4}$	$2.48 \cdot 10^{-4}$	$6.12 \cdot 10^{-5}$	$7.47 \cdot 10^{-6}$
	R factor	0.0892	0.0578	0.0289	0.0106
1:1 **1:2**	**RSS**	$5.70 \cdot 10^{-4}$	$2.15 \cdot 10^{-4}$	$2.30 \cdot 10^{-5}$	$5.10 \cdot 10^{-7}$
	R factor	0.0797	0.0538	0.0177	0.0028
1:1 **1:2** **2:2**	**RSS**	$6.76 \cdot 10^{-4}$	$2.20 \cdot 10^{-4}$	$2.17 \cdot 10^{-5}$	$7.13 \cdot 10^{-7}$
	R factor	0.0868	0.0544	0.0172	0.0033

[a] Logβ: β_{11} (M^{-1}), β_{12} (M^{-2}), β_{22} (M^{-3}). [b] Introduced guide values: $TBAH_2PO_4$: $\log\beta_{11}=3$, $\log\beta_{12}=5$, $\log\beta_{22}=9$; $TBARCO_2$: $\log\beta_{11}=3$, $\log\beta_{12}=5$, $\log\beta_{22}=9$; TBACl: $\log\beta_{11}=1$, $\log\beta_{12}=3$, $\log\beta_{22}=5$. [c] Units: kcal·mol^{-1}. [d] RSS: Residual Sum of Squares.

4.5.4.6. Input/Output files, *Fitplots* and *Concplots* from [HαOBn][H_2PO_4] complex

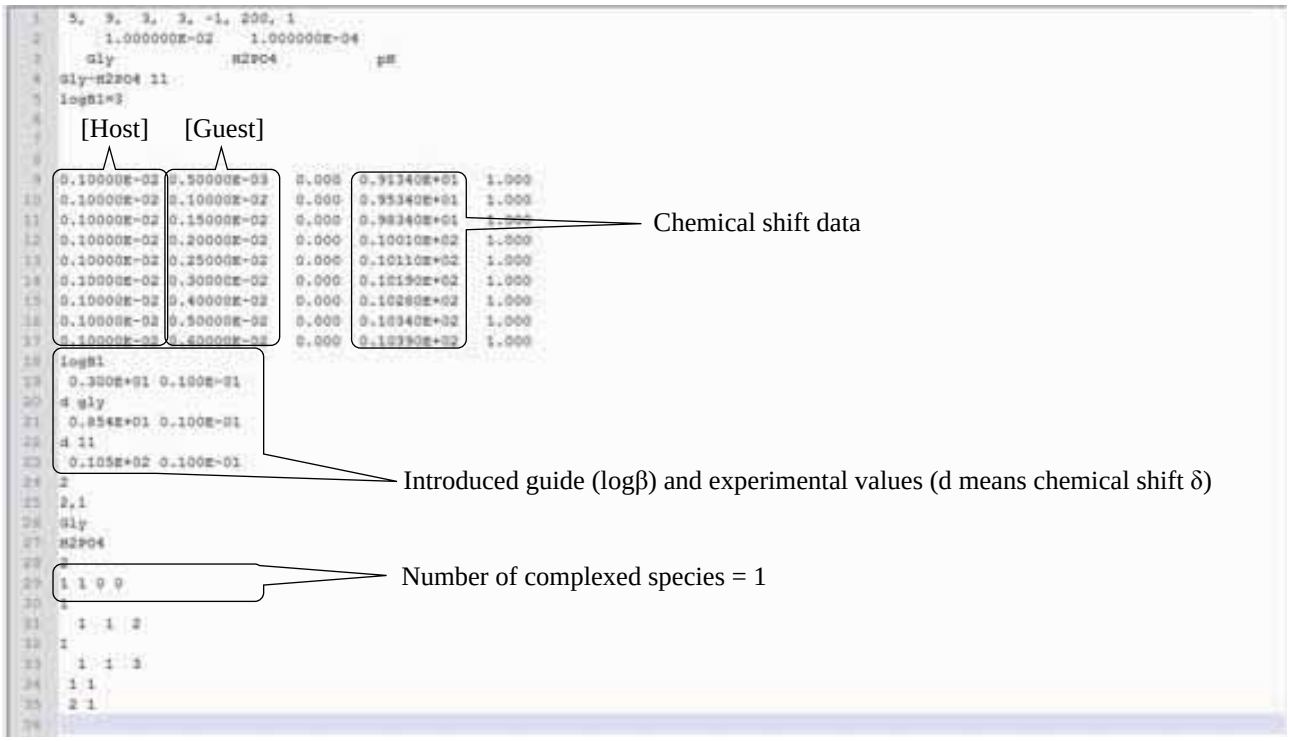


```
5,  9,  3,  3, -1, 200, 1
    1.000000E-02    1.000000E-04
  Gly           H2PO4          pH
Gly-H2PO4 11
logB1=3
0.10000E-02 0.50000E-03  0.000  0.91340E+01  1.000
0.10000E-02 0.10000E-02  0.000  0.95340E+01  1.000
0.10000E-02 0.15000E-02  0.000  0.98340E+01  1.000
0.10000E-02 0.20000E-02  0.000  0.10010E+02  1.000
0.10000E-02 0.25000E-02  0.000  0.10110E+02  1.000
0.10000E-02 0.30000E-02  0.000  0.10190E+02  1.000
0.10000E-02 0.40000E-02  0.000  0.10280E+02  1.000
0.10000E-02 0.50000E-02  0.000  0.10340E+02  1.000
0.10000E-02 0.60000E-02  0.000  0.10390E+02  1.000
logB1
 0.300E+01 0.100E-01
d gly
 0.854E+01 0.100E-01
d 11
 0.105E+02 0.100E-01
2
2,1
Gly
H2PO4
2
1 1 0 0
1
 1  1  2
1
 1  1  3
 1 1
 2 1
```

Figure **211**. Input file used for the data fitting to a 1:1 **[HαOBn][H_2PO_4]** complex.

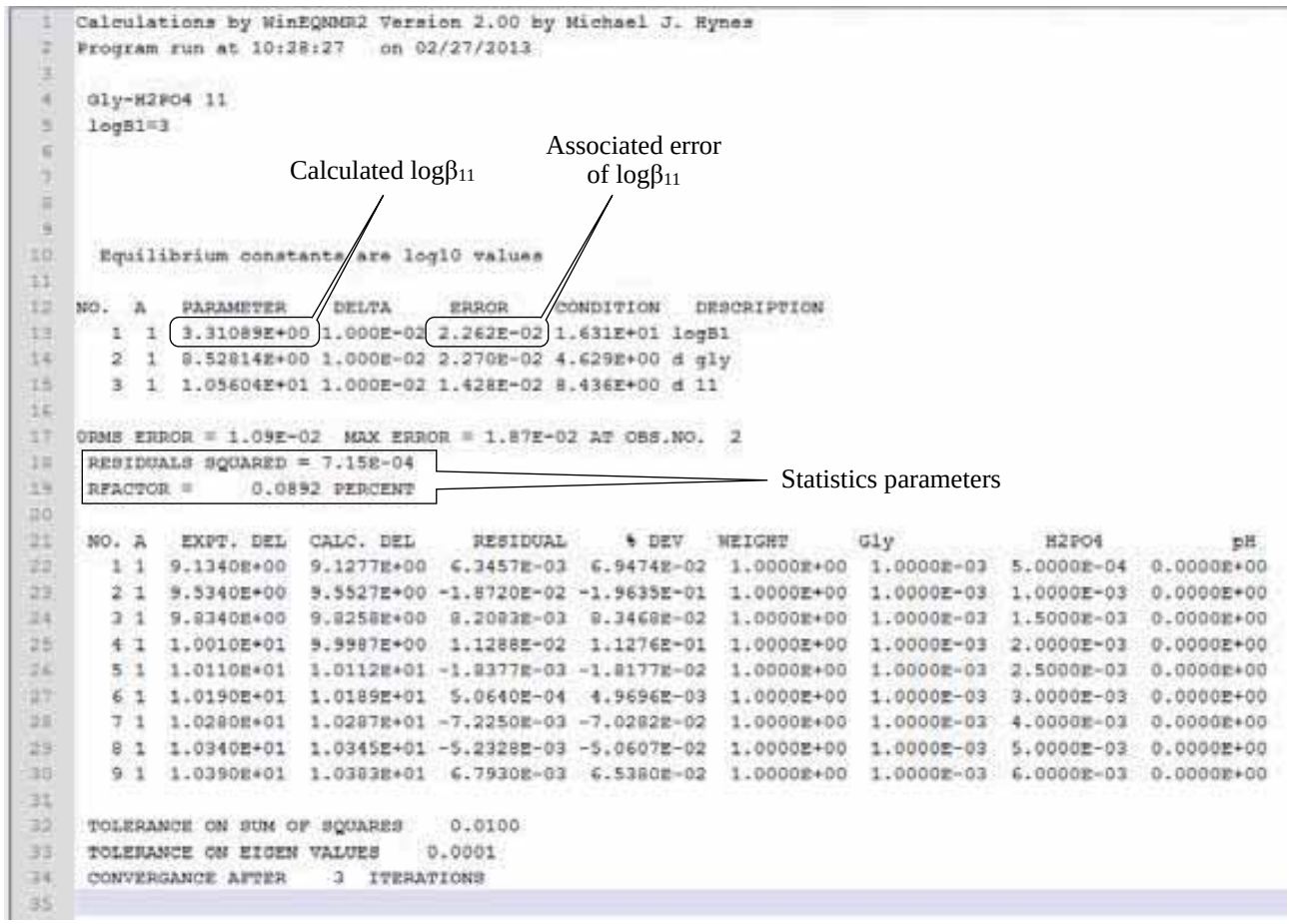


```
Calculations by WinEQNMR2 Version 2.00 by Michael J. Hynes
Program run at 10:28:27   on 02/27/2013

 Gly-H2PO4 11
 logB1=3

  Equilibrium constants are log10 values

NO.  A   PARAMETER    DELTA     ERROR     CONDITION   DESCRIPTION
   1  1  3.31089E+00 1.000E-02 2.262E-02 1.631E+01 logB1
   2  1  8.52814E+00 1.000E-02 2.270E-02 4.629E+00 d gly
   3  1  1.05604E+01 1.000E-02 1.428E-02 8.436E+00 d 11

ORMS ERROR = 1.09E-02  MAX ERROR = 1.87E-02 AT OBS.NO.  2
 RESIDUALS SQUARED = 7.15E-04
 RFACTOR =      0.0892 PERCENT

 NO. A   EXPT. DEL  CALC. DEL     RESIDUAL     % DEV   WEIGHT      Gly           H2PO4          pH
   1 1  9.1340E+00  9.1277E+00  6.3457E-03  6.9474E-02  1.0000E+00  1.0000E-03  5.0000E-04  0.0000E+00
   2 1  9.5340E+00  9.5527E+00 -1.8720E-02 -1.9635E-01  1.0000E+00  1.0000E-03  1.0000E-03  0.0000E+00
   3 1  9.8340E+00  9.8258E+00  8.2083E-03  8.3468E-02  1.0000E+00  1.0000E-03  1.5000E-03  0.0000E+00
   4 1  1.0010E+01  9.9987E+00  1.1288E-02  1.1276E-01  1.0000E+00  1.0000E-03  2.0000E-03  0.0000E+00
   5 1  1.0110E+01  1.0112E+01 -1.8377E-03 -1.8177E-02  1.0000E+00  1.0000E-03  2.5000E-03  0.0000E+00
   6 1  1.0190E+01  1.0189E+01  5.0640E-04  4.9696E-03  1.0000E+00  1.0000E-03  3.0000E-03  0.0000E+00
   7 1  1.0280E+01  1.0287E+01 -7.2250E-03 -7.0282E-02  1.0000E+00  1.0000E-03  4.0000E-03  0.0000E+00
   8 1  1.0340E+01  1.0345E+01 -5.2328E-03 -5.0607E-02  1.0000E+00  1.0000E-03  5.0000E-03  0.0000E+00
   9 1  1.0390E+01  1.0383E+01  6.7930E-03  6.5380E-02  1.0000E+00  1.0000E-03  6.0000E-03  0.0000E+00

 TOLERANCE ON SUM OF SQUARES    0.0100
 TOLERANCE ON EIGEN VALUES    0.0001
 CONVERGANCE AFTER    3  ITERATIONS
```

Figure **212**. Output file obtained for the data fitting to a 1:1 **[HαOBn][H_2PO_4]** complex.

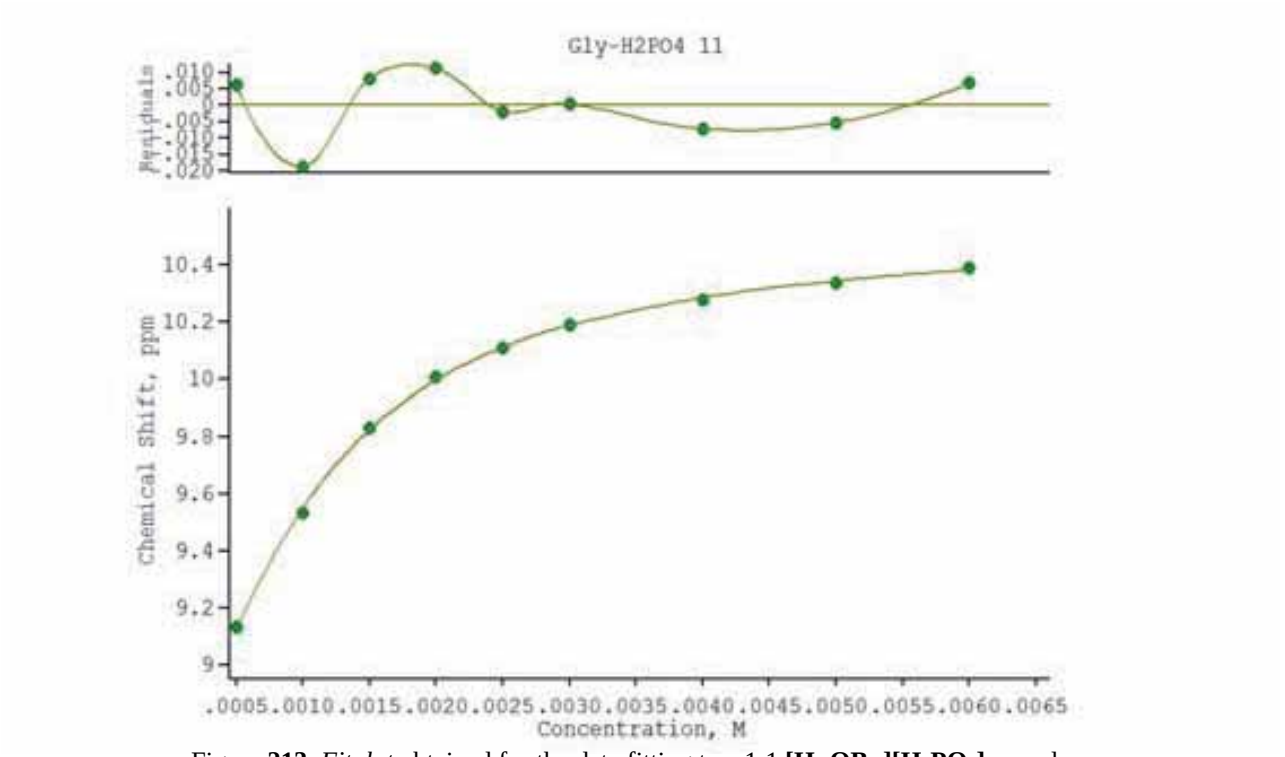

Figure **213**. *Fitplot* obtained for the data fitting to a 1:1 **[HαOBn][H_2PO_4]** complex.

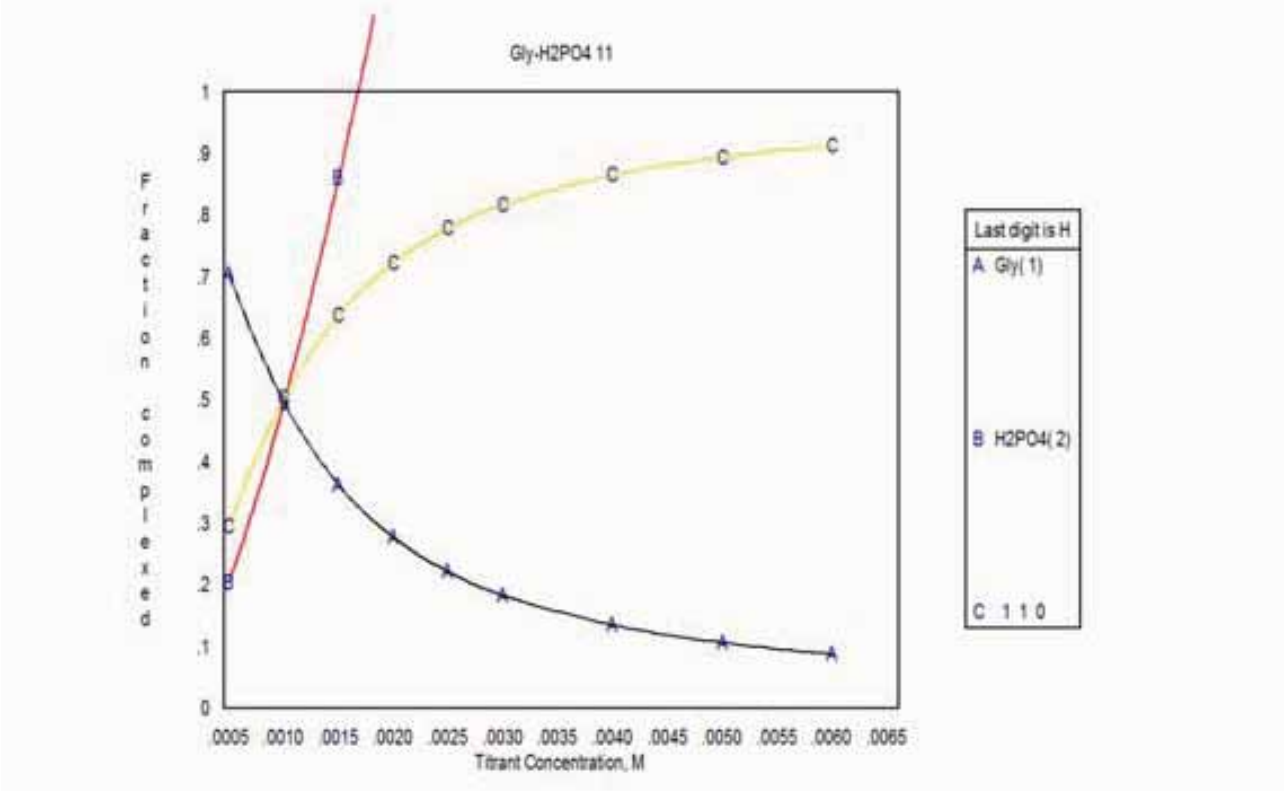

Figure **214**. *Concplot* obtained for the data fitting to a 1:1 **[HαOBn][H_2PO_4]** complex.

```
5,  9,  3,  5, -1, 200, 1
    1.000000E-02    1.000000E-04
  gly           H2PO4          pH
Gly-H2PO4 12 system
logB1=3
logB2=5


0.10000E-02 0.50000E-03   0.000  0.91360E+01   1.000
0.10000E-02 0.10000E-02   0.000  0.95340E+01   1.000
0.10000E-02 0.15000E-02   0.000  0.98340E+01   1.000
0.10000E-02 0.20000E-02   0.000  0.10010E+02   1.000
0.10000E-02 0.25000E-02   0.000  0.10110E+02   1.000
0.10000E-02 0.30000E-02   0.000  0.10190E+02   1.000
0.10000E-02 0.40000E-02   0.000  0.10280E+02   1.000
0.10000E-02 0.50000E-02   0.000  0.10340E+02   1.000
0.10000E-02 0.60000E-02   0.000  0.10390E+02   1.000
logB1
 0.300E+01 0.100E-01
logB2
 0.500E+01 0.100E-01
d gly
 0.854E+01 0.100E-01
d 11
 0.105E+02 0.100E-01
d 12
 0.110E+02 0.100E-01
2
2,2
gly
H2PO4
2
1 1 0 0
1 2 0 0
1
  1  1  3
2
  1  1  4
  1  2  5
 1 1
 2 1
```

Figure **215**. Input file used for the data fitting to a 1:2 **[HαOBn][H_2PO_4]** complex.

```
Calculations by WinEQNMR2 Version 2.00 by Michael J. Hynes
Program run at 10:39:44   on 02/27/2013

 Gly-H2PO4 12 system
 logB1=3
 logB2=5



  Equilibrium constants are log10 values

NO.  A   PARAMETER    DELTA     ERROR    CONDITION   DESCRIPTION
   1  1  3.30668E+00 1.000E-02 4.334E-01 3.975E+03 logB1
   2  1  4.46029E+00 1.000E-02 1.403E+01 3.665E+02 logB2
   3  1  8.53185E+00 1.000E-02 3.178E-02 6.145E+00 d gly
   4  1  1.05629E+01 1.000E-02 6.629E-01 1.097E+04 d 11
   5  1  1.03639E+01 1.000E-02 6.901E+00 4.767E+03 d 12

ORMS ERROR = 1.33E-02  MAX ERROR = 1.73E-02 AT OBS.NO.  2
 RESIDUALS SQUARED = 7.05E-04
 RFACTOR =     0.0889 PERCENT

 NO. A   EXPT. DEL  CALC. DEL     RESIDUAL     % DEV   WEIGHT      gly           H2PO4          pH
   1 1  9.1340E+00  9.1285E+00  5.5227E-03  6.0463E-02  1.0000E+00  1.0000E-03  5.0000E-04  0.0000E+00
   2 1  9.5340E+00  9.5513E+00 -1.7254E-02 -1.8097E-01  1.0000E+00  1.0000E-03  1.0000E-03  0.0000E+00
   3 1  9.8340E+00  9.8248E+00  9.1925E-03  9.3476E-02  1.0000E+00  1.0000E-03  1.5000E-03  0.0000E+00
   4 1  1.0010E+01  9.9984E+00  1.1618E-02  1.1606E-01  1.0000E+00  1.0000E-03  2.0000E-03  0.0000E+00
   5 1  1.0110E+01  1.0112E+01 -2.0094E-03 -1.9875E-02  1.0000E+00  1.0000E-03  2.5000E-03  0.0000E+00
   6 1  1.0190E+01  1.0190E+01 -1.3065E-04 -1.2822E-03  1.0000E+00  1.0000E-03  3.0000E-03  0.0000E+00
   7 1  1.0280E+01  1.0288E+01 -7.5674E-03 -7.3613E-02  1.0000E+00  1.0000E-03  4.0000E-03  0.0000E+00
   8 1  1.0340E+01  1.0344E+01 -4.4765E-03 -4.3293E-02  1.0000E+00  1.0000E-03  5.0000E-03  0.0000E+00
   9 1  1.0390E+01  1.0381E+01  8.9588E-03  8.6225E-02  1.0000E+00  1.0000E-03  6.0000E-03  0.0000E+00

 TOLERANCE ON SUM OF SQUARES     0.0100
 TOLERANCE ON EIGEN VALUES     0.0001
 CONVERGANCE AFTER     4  ITERATIONS
```

Figure **216**. Output file obtained for the data fitting to a 1:2 **[HαOBn][H_2PO_4]** complex.

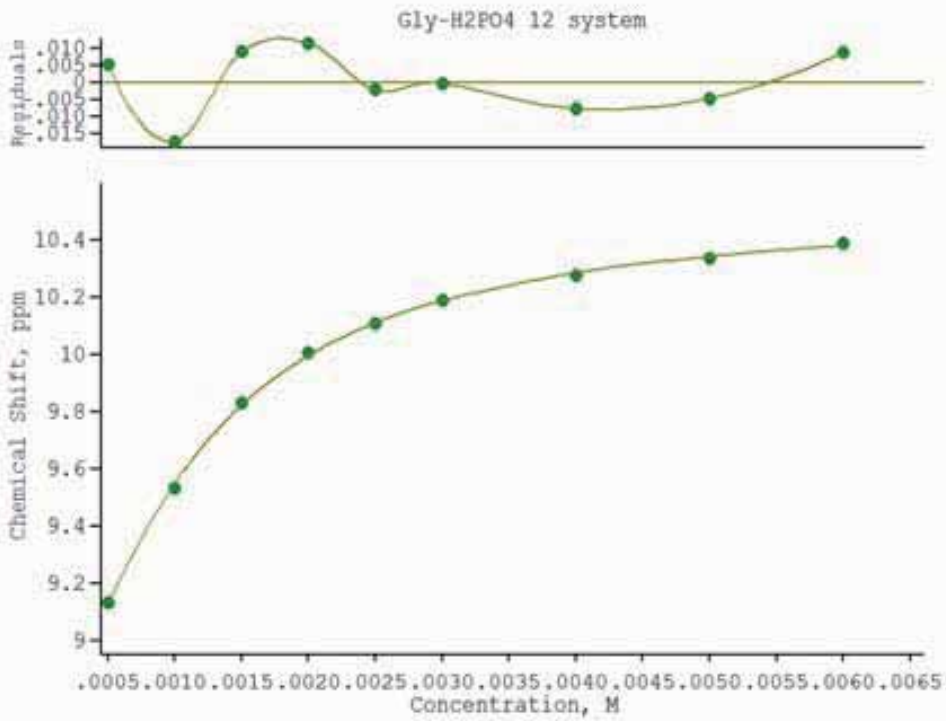

Figure **217**. *Fitplot* obtained for the data fitting to a 1:2 **[HαOBn][H_2PO_4]** complex.

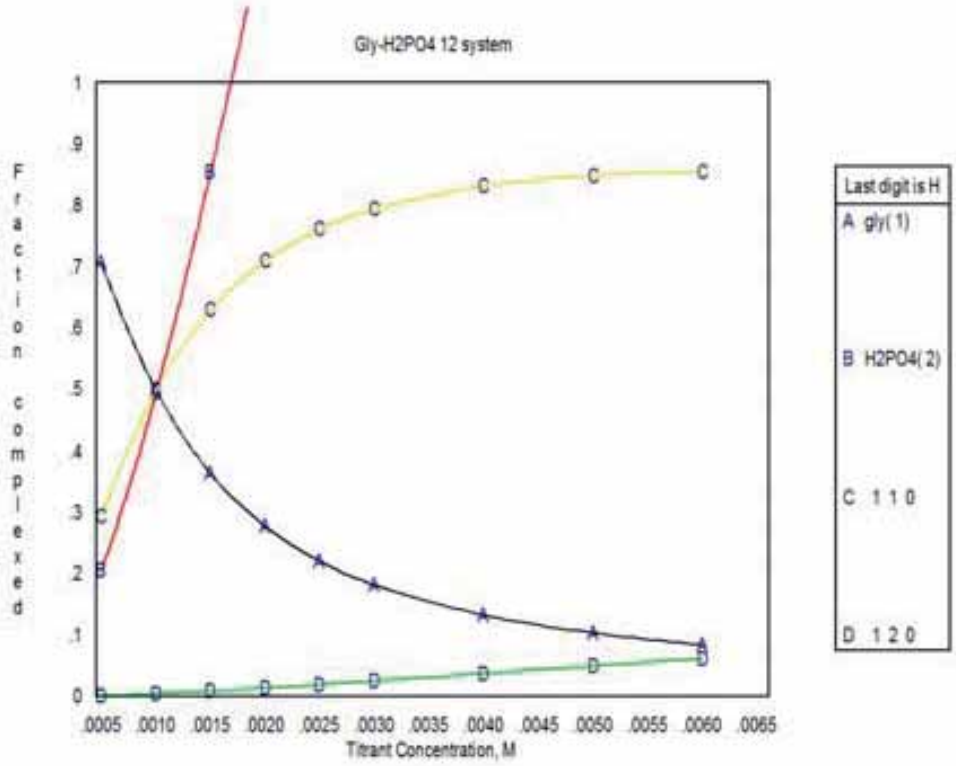

Figure **218**. *Concplot* obtained for the data fitting to a 1:2 **[HαOBn][H_2PO_4]** complex.

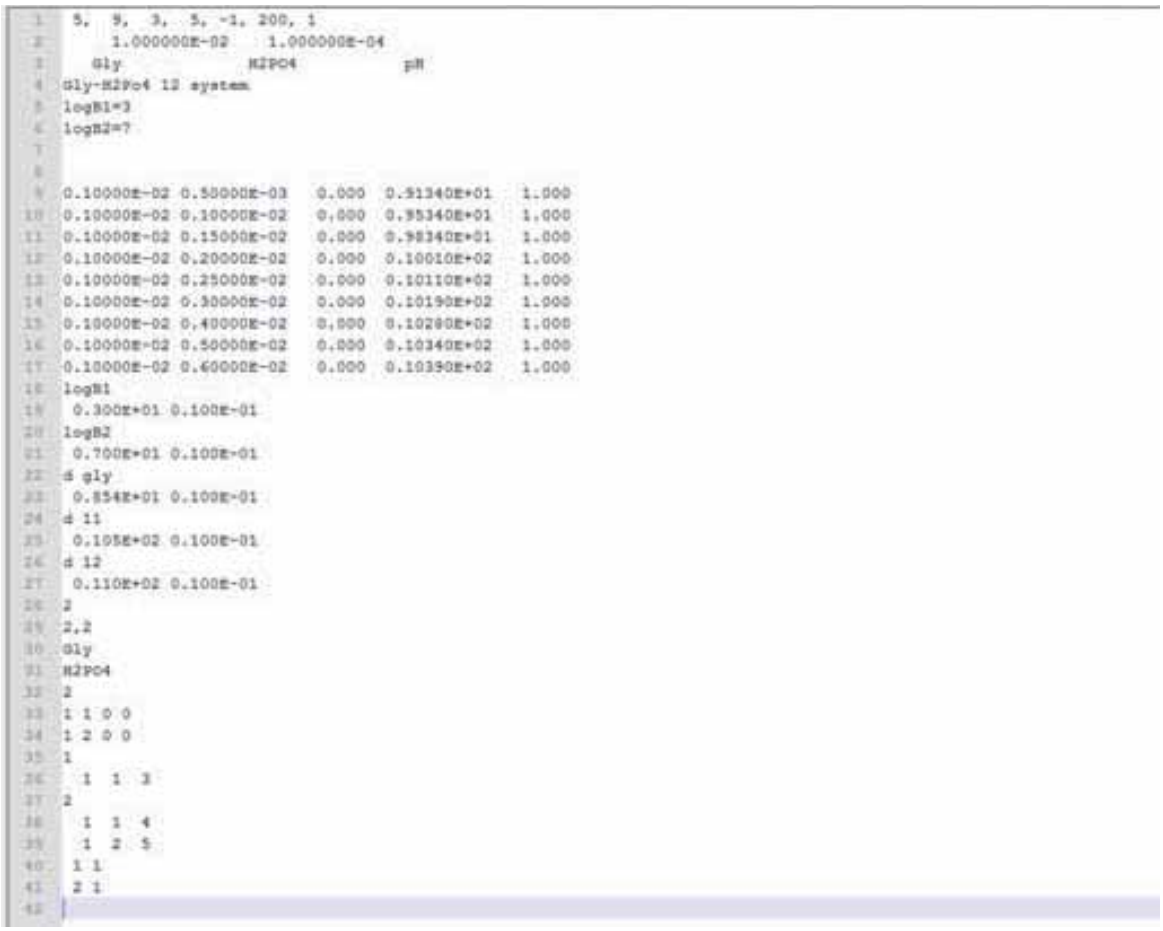

```
 5,  9,  3,  5, -1, 200, 1
     1.000000E-02    1.000000E-04
   Gly           H2PO4          pH
Gly-H2Po4 12 system
logB1=3
logB2=7


0.10000E-02 0.50000E-03   0.000  0.91340E+01   1.000
0.10000E-02 0.10000E-02   0.000  0.95340E+01   1.000
0.10000E-02 0.15000E-02   0.000  0.98340E+01   1.000
0.10000E-02 0.20000E-02   0.000  0.10010E+02   1.000
0.10000E-02 0.25000E-02   0.000  0.10110E+02   1.000
0.10000E-02 0.30000E-02   0.000  0.10190E+02   1.000
0.10000E-02 0.40000E-02   0.000  0.10280E+02   1.000
0.10000E-02 0.50000E-02   0.000  0.10340E+02   1.000
0.10000E-02 0.60000E-02   0.000  0.10390E+02   1.000
logB1
 0.300E+01 0.100E-01
logB2
 0.700E+01 0.100E-01
d gly
 0.854E+01 0.100E-01
d 11
 0.105E+02 0.100E-01
d 12
 0.110E+02 0.100E-01
2
2,2
Gly
H2PO4
2
1 1 0 0
1 2 0 0
1
  1  1  3
2
  1  1  4
  1  2  5
 1 1
 2 1
```

Figure **219**. Input file used for the data fitting to a 1:2 **[HαOBn][H_2PO_4]** complex.

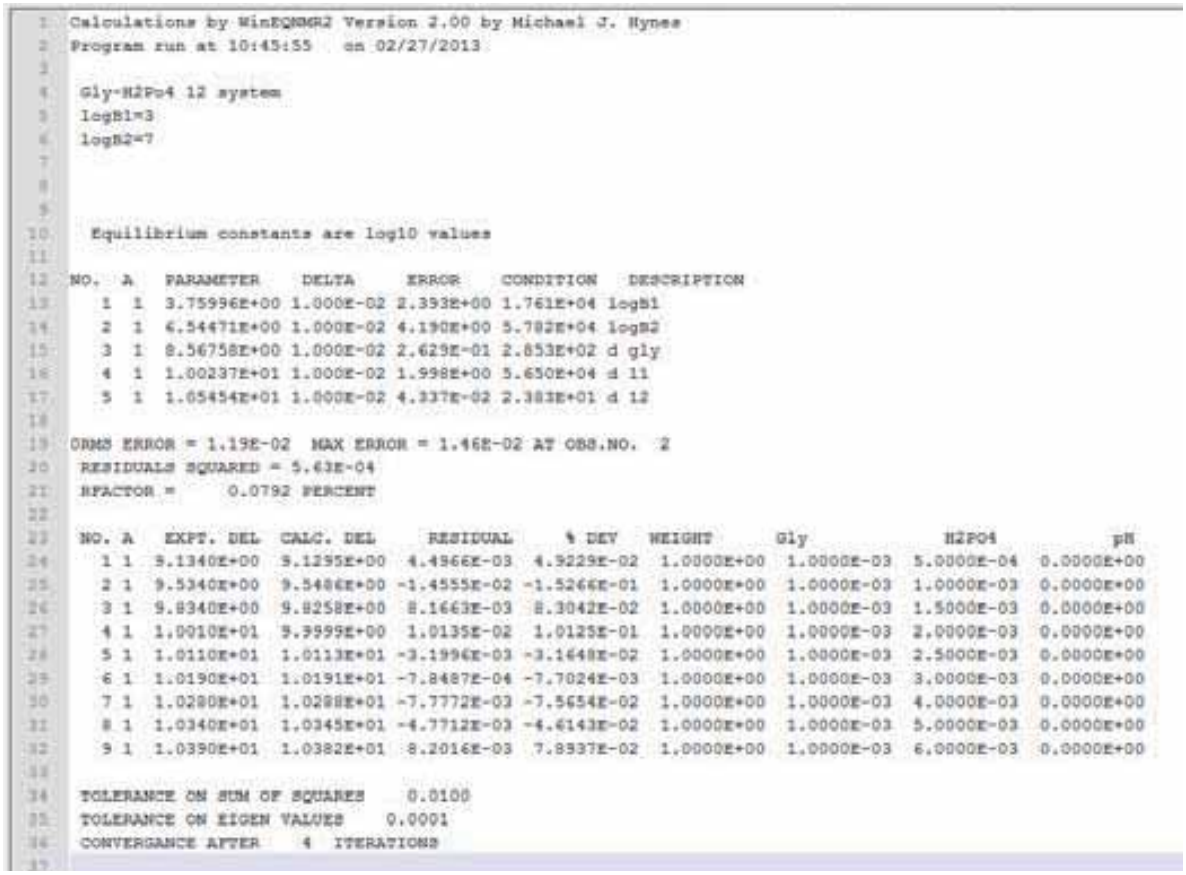

```
Calculations by WinEQNMR2 Version 2.00 by Michael J. Hynes
Program run at 10:45:55   on 02/27/2013

 Gly-H2Po4 12 system
 logB1=3
 logB2=7



  Equilibrium constants are log10 values

NO.  A   PARAMETER    DELTA     ERROR    CONDITION   DESCRIPTION
   1  1  3.75996E+00 1.000E-02 2.393E+00 1.761E+04 logB1
   2  1  6.54471E+00 1.000E-02 4.190E+00 5.782E+04 logB2
   3  1  8.56758E+00 1.000E-02 2.629E-01 2.853E+02 d gly
   4  1  1.00237E+01 1.000E-02 1.998E+00 5.650E+04 d 11
   5  1  1.05454E+01 1.000E-02 4.337E-02 2.383E+01 d 12

ORMS ERROR = 1.19E-02  MAX ERROR = 1.46E-02 AT OBS.NO.  2
 RESIDUALS SQUARED = 5.63E-04
 RFACTOR =     0.0792 PERCENT

 NO. A   EXPT. DEL  CALC. DEL     RESIDUAL     % DEV   WEIGHT      Gly            H2PO4          pH
   1 1  9.1340E+00  9.1295E+00  4.4966E-03  4.9229E-02  1.0000E+00  1.0000E-03  5.0000E-04  0.0000E+00
   2 1  9.5340E+00  9.5486E+00 -1.4555E-02 -1.5266E-01  1.0000E+00  1.0000E-03  1.0000E-03  0.0000E+00
   3 1  9.8340E+00  9.8258E+00  8.1663E-03  8.3042E-02  1.0000E+00  1.0000E-03  1.5000E-03  0.0000E+00
   4 1  1.0010E+01  9.9999E+00  1.0135E-02  1.0125E-01  1.0000E+00  1.0000E-03  2.0000E-03  0.0000E+00
   5 1  1.0110E+01  1.0113E+01 -3.1996E-03 -3.1648E-02  1.0000E+00  1.0000E-03  2.5000E-03  0.0000E+00
   6 1  1.0190E+01  1.0191E+01 -7.8487E-04 -7.7024E-03  1.0000E+00  1.0000E-03  3.0000E-03  0.0000E+00
   7 1  1.0280E+01  1.0288E+01 -7.7772E-03 -7.5654E-02  1.0000E+00  1.0000E-03  4.0000E-03  0.0000E+00
   8 1  1.0340E+01  1.0345E+01 -4.7712E-03 -4.6143E-02  1.0000E+00  1.0000E-03  5.0000E-03  0.0000E+00
   9 1  1.0390E+01  1.0382E+01  8.2016E-03  7.8937E-02  1.0000E+00  1.0000E-03  6.0000E-03  0.0000E+00

 TOLERANCE ON SUM OF SQUARES    0.0100
 TOLERANCE ON EIGEN VALUES    0.0001
 CONVERGANCE AFTER    4  ITERATIONS
```

Figure **220**. Output file obtained for the data fitting to a 1:2 **[HαOBn][H_2PO_4]** complex.

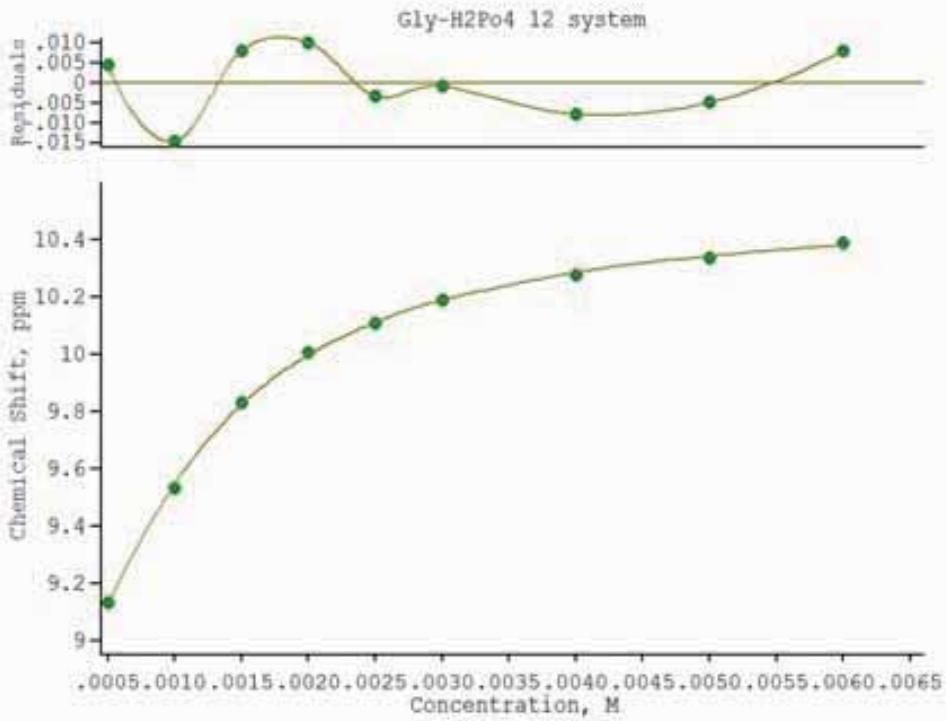

Figure **221**. *Fitplot* obtained for the data fitting to a 1:2 **[HαOBn][H_2PO_4]** complex.

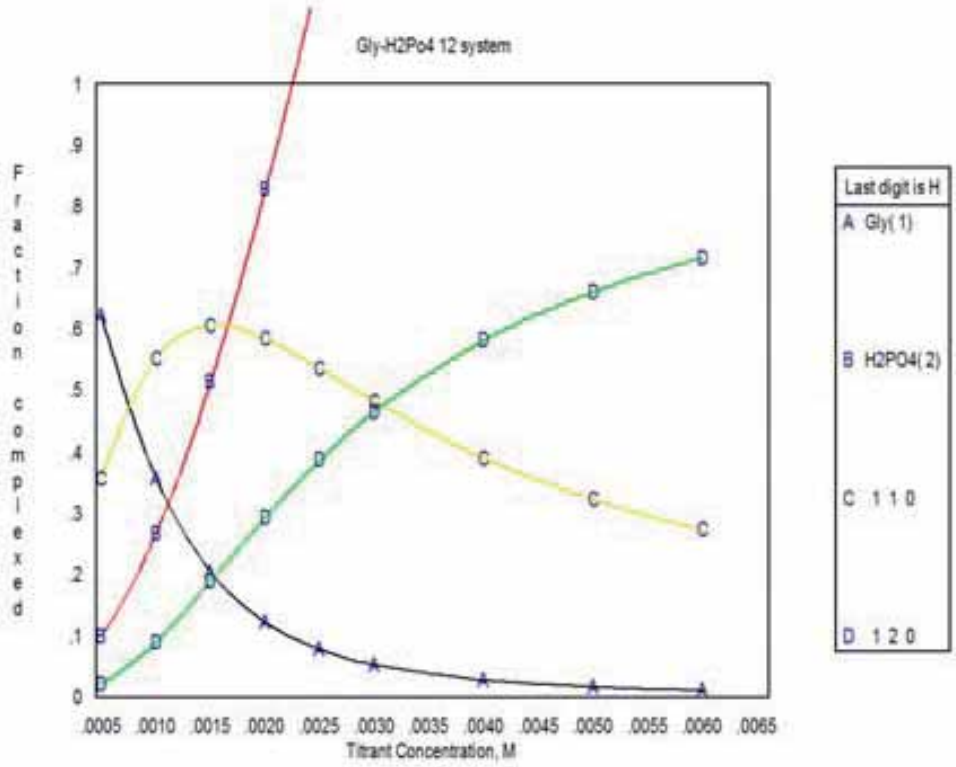

Figure **222**. *Concplot* obtained for the data fitting to a 1:2 **[HαOBn][H_2PO_4]** complex.

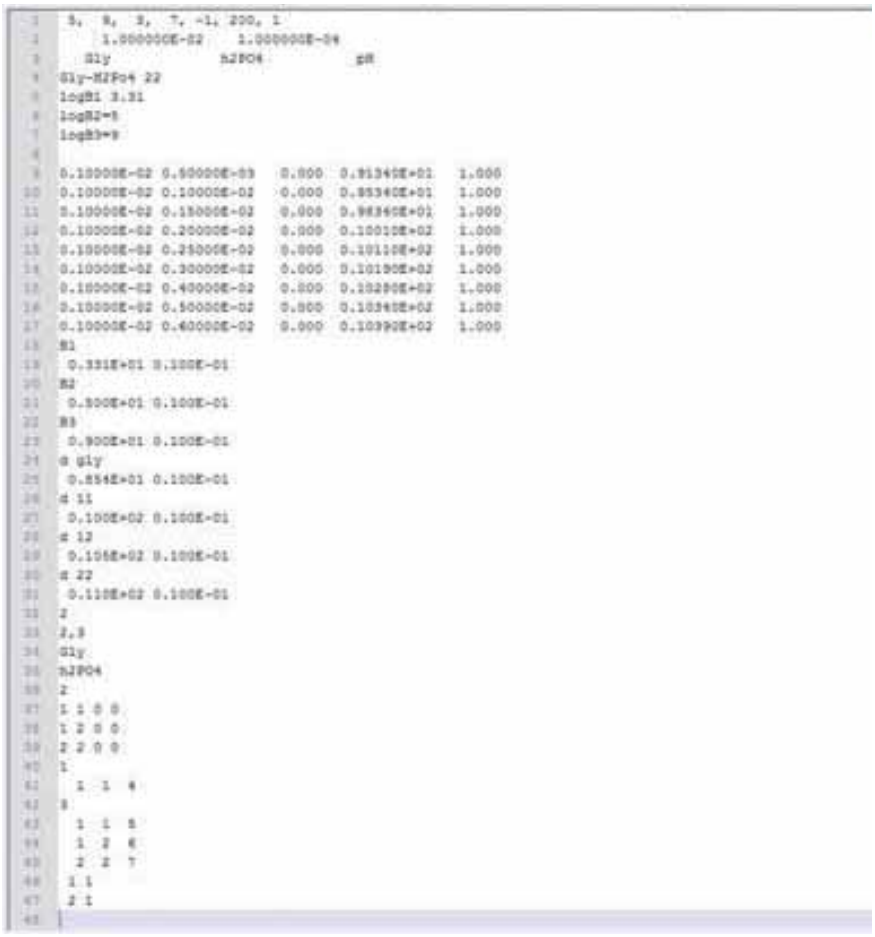

```
 5,  8,  3,  7, -1, 200, 1
    1.000000E-02    1.000000E-04
   Gly            h2PO4          pH
Gly-H2Po4 22
logB1 3.31
logB2=5
logB3=9

0.10000E-02 0.60000E-03   0.000  0.91340E+01   1.000
0.10000E-02 0.10000E-02   0.000  0.85340E+01   1.000
0.10000E-02 0.15000E-02   0.000  0.98360E+01   1.000
0.10000E-02 0.20000E-02   0.000  0.10010E+02   1.000
0.10000E-02 0.25000E-02   0.000  0.10110E+02   1.000
0.10000E-02 0.30000E-02   0.000  0.10190E+02   1.000
0.10000E-02 0.40000E-02   0.000  0.10290E+02   1.000
0.10000E-02 0.50000E-02   0.000  0.10340E+02   1.000
0.10000E-02 0.60000E-02   0.000  0.10390E+02   1.000
B1
 0.331E+01 0.100E-01
B2
 0.500E+01 0.100E-01
B3
 0.900E+01 0.100E-01
d gly
 0.854E+01 0.100E-01
d 11
 0.100E+02 0.100E-01
d 12
 0.105E+02 0.100E-01
d 22
 0.110E+02 0.100E-01
2
2,3
Gly
h2PO4
2
1 1 0 0
1 2 0 0
2 2 0 0
1
  1  1  4
3
  1  1  5
  1  2  6
  2  2  7
 1 1
 2 1
```

Figure **223**. Input file used for the data fitting to a 2:2 **[HαOBn][H_2PO_4]** complex.

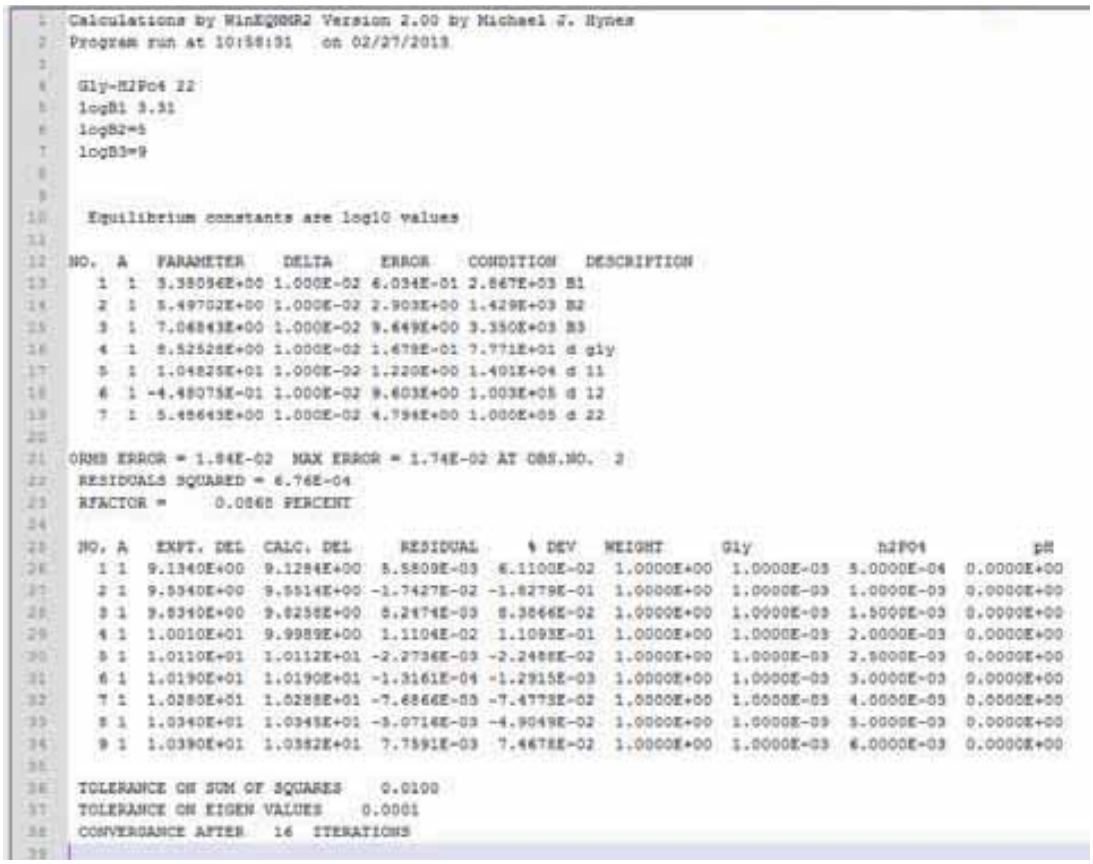

```
Calculations by WinEQNMR2 Version 2.00 by Michael J. Hynes
Program run at 10:58:31   on 02/27/2013

 Gly-H2Po4 22
 logB1 3.31
 logB2=5
 logB3=9


  Equilibrium constants are log10 values

NO.  A   PARAMETER     DELTA     ERROR     CONDITION   DESCRIPTION
   1  1  5.38056E+00 1.000E-02 6.034E-01 2.867E+03 B1
   2  1  5.49702E+00 1.000E-02 2.903E+00 1.429E+03 B2
   3  1  7.04843E+00 1.000E-02 9.649E+00 3.350E+03 B3
   4  1  8.52528E+00 1.000E-02 1.479E-01 7.771E+01 d gly
   5  1  1.04825E+01 1.000E-02 1.220E+00 1.401E+04 d 11
   6  1 -4.48075E-01 1.000E-02 9.603E+00 1.003E+05 d 12
   7  1  5.48643E+00 1.000E-02 4.794E+00 1.000E+05 d 22

ORMS ERROR = 1.84E-02  MAX ERROR = 1.74E-02 AT OBS.NO.  2
 RESIDUALS SQUARED = 6.76E-04
 RFACTOR =     0.0868 PERCENT

 NO. A   EXPT. DEL  CALC. DEL     RESIDUAL     % DEV   WEIGHT      Gly            h2PO4          pH
   1 1  9.1340E+00  9.1294E+00  4.5809E-03  6.1100E-02  1.0000E+00  1.0000E-03  5.0000E-04  0.0000E+00
   2 1  9.5340E+00  9.5514E+00 -1.7427E-02 -1.8279E-01  1.0000E+00  1.0000E-03  1.0000E-03  0.0000E+00
   3 1  9.8360E+00  9.8258E+00  8.2174E-03  8.3566E-02  1.0000E+00  1.0000E-03  1.5000E-03  0.0000E+00
   4 1  1.0010E+01  9.9989E+00  1.1104E-02  1.1093E-01  1.0000E+00  1.0000E-03  2.0000E-03  0.0000E+00
   5 1  1.0110E+01  1.0112E+01 -2.2736E-03 -2.2488E-02  1.0000E+00  1.0000E-03  2.5000E-03  0.0000E+00
   6 1  1.0190E+01  1.0190E+01 -1.3161E-04 -1.2915E-03  1.0000E+00  1.0000E-03  3.0000E-03  0.0000E+00
   7 1  1.0290E+01  1.0288E+01 -7.6866E-05 -7.4773E-02  1.0000E+00  1.0000E-03  4.0000E-03  0.0000E+00
   8 1  1.0340E+01  1.0345E+01 -5.0716E-03 -4.9049E-02  1.0000E+00  1.0000E-03  5.0000E-03  0.0000E+00
   9 1  1.0390E+01  1.0382E+01  7.7591E-03  7.4678E-02  1.0000E+00  1.0000E-03  6.0000E-03  0.0000E+00

 TOLERANCE ON SUM OF SQUARES    0.0100
 TOLERANCE ON EIGEN VALUES    0.0001
 CONVERGANCE AFTER   16  ITERATIONS
```

Figure **224**. Output file obtained for the data fitting to a 2:2 **[HαOBn][H_2PO_4]** complex.

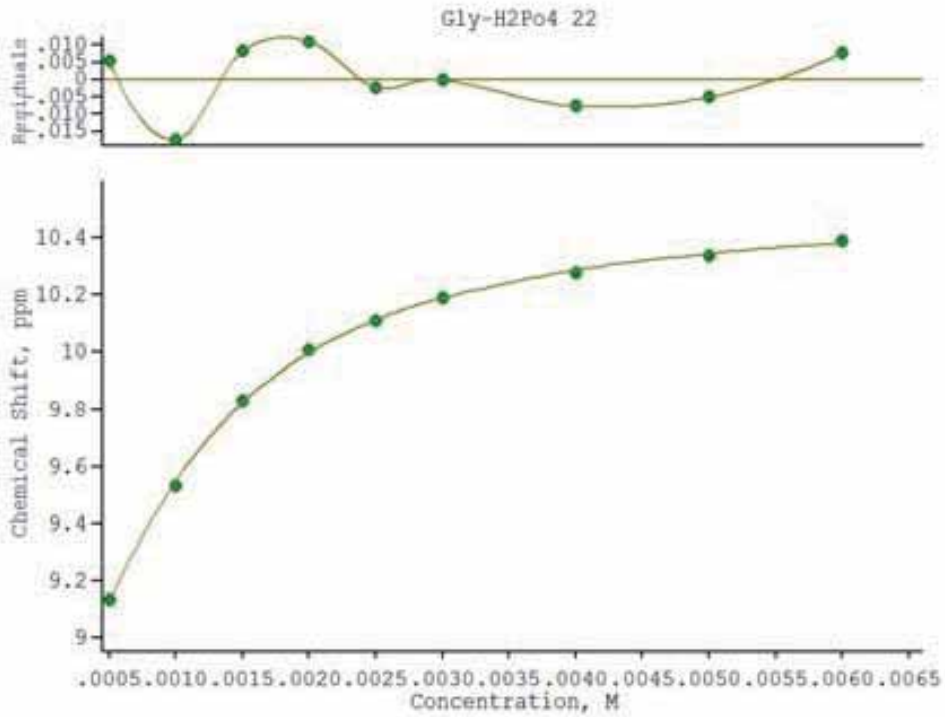

Figure **225**. *Fitplot* obtained for the data fitting to a 2:2 **[HαOBn][H_2PO_4]** complex.

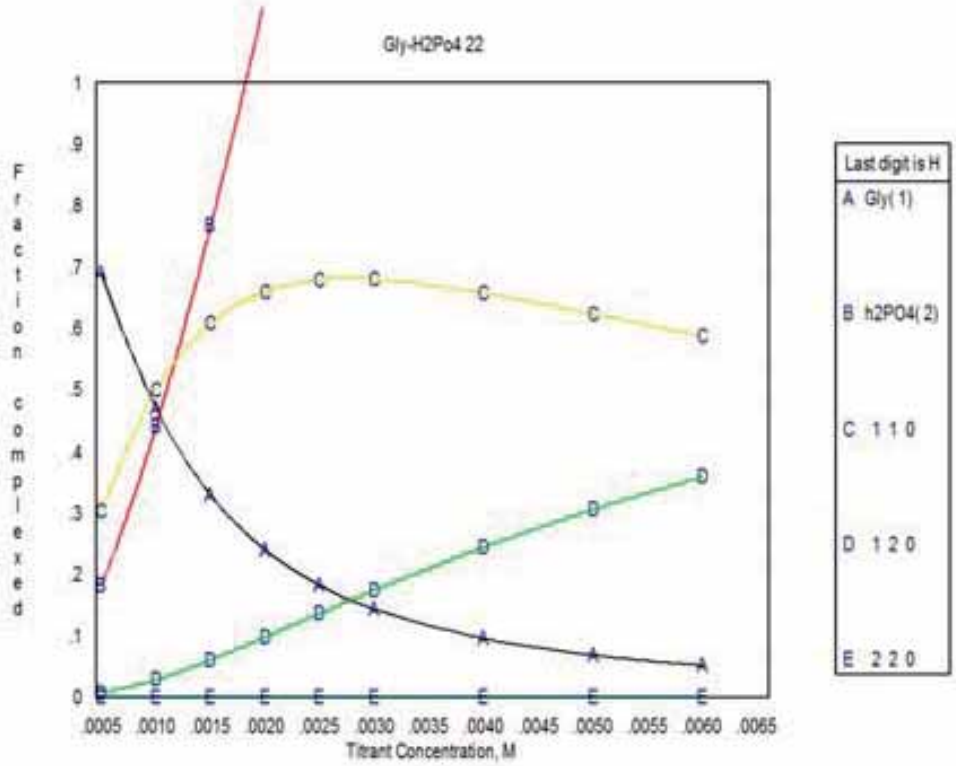

Figure **226**. *Concplot* obtained for the data fitting to a 2:2 **[HαOBn][H_2PO_4]** complex.

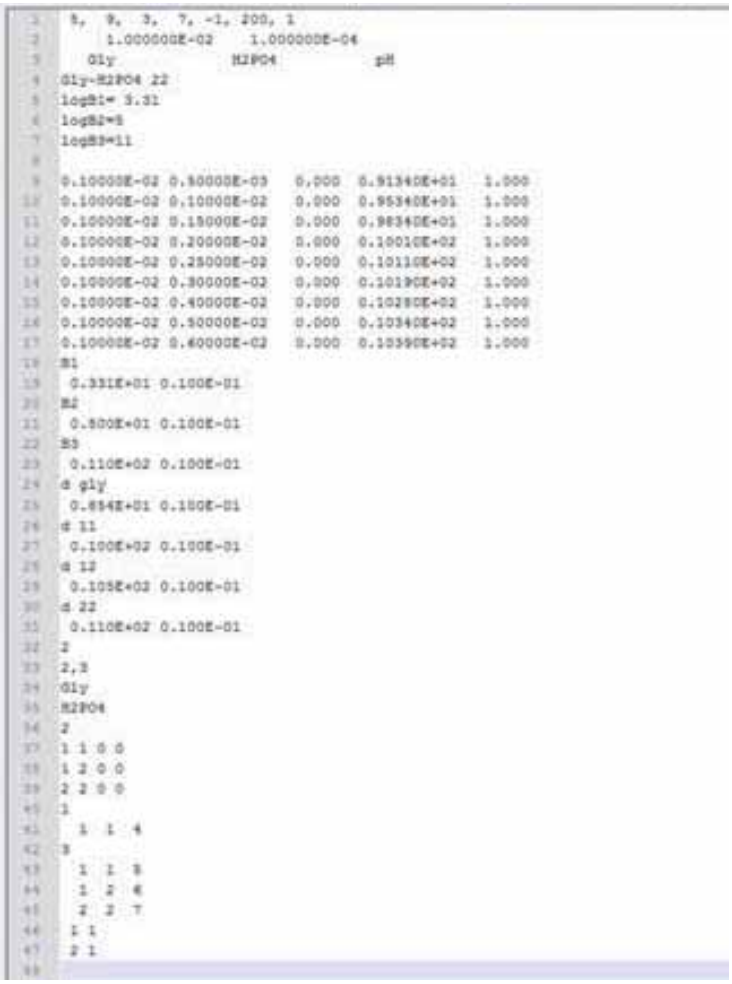

```
 5,  9,  3,  7, -1, 200, 1
     1.000000E-02     1.000000E-04
   Gly            H2PO4          pH
Gly-H2PO4 22
logB1= 3.31
logB2=5
logB3=11

0.10000E-02 0.50000E-03   0.000  0.91340E+01   1.000
0.10000E-02 0.10000E-02   0.000  0.95340E+01   1.000
0.10000E-02 0.15000E-02   0.000  0.98340E+01   1.000
0.10000E-02 0.20000E-02   0.000  0.10010E+02   1.000
0.10000E-02 0.25000E-02   0.000  0.10110E+02   1.000
0.10000E-02 0.30000E-02   0.000  0.10190E+02   1.000
0.10000E-02 0.40000E-02   0.000  0.10280E+02   1.000
0.10000E-02 0.50000E-02   0.000  0.10340E+02   1.000
0.10000E-02 0.60000E-02   0.000  0.10390E+02   1.000
B1
 0.331E+01 0.100E-01
B2
 0.500E+01 0.100E-01
B3
 0.110E+02 0.100E-01
d gly
 0.654E+01 0.100E-01
d 11
 0.100E+02 0.100E-01
d 12
 0.105E+03 0.100E-01
d 22
 0.110E+02 0.100E-01
2
2,3
Gly
H2PO4
2
1 1 0 0
1 2 0 0
2 2 0 0
1
  1  1  4
3
  1  1  3
  1  2  6
  2  2  7
 1 1
 2 1
```

Figure **227**. Input file used for the data fitting to a 2:2 **[HαOBn][H_2PO_4]** complex.

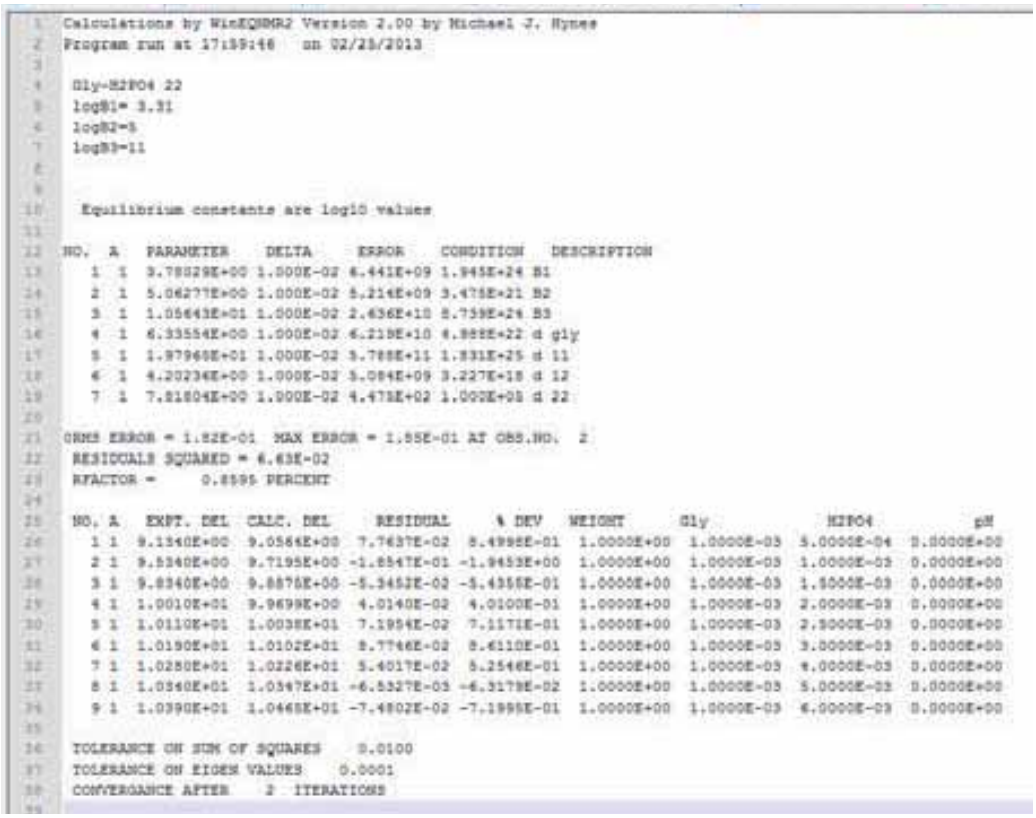

```
Calculations by WinEQNMR2 Version 2.00 by Michael J. Hynes
Program run at 17:59:46   on 02/25/2013

 Gly-H2PO4 22
 logB1= 3.31
 logB2=5
 logB3=11


  Equilibrium constants are log10 values

NO.  A   PARAMETER    DELTA     ERROR    CONDITION   DESCRIPTION
   1  1  9.78029E+00 1.000E-02 6.441E+09 1.945E+24 B1
   2  1  5.06277E+00 1.000E-02 5.214E+09 3.475E+21 B2
   3  1  1.05643E+01 1.000E-02 2.636E+10 8.739E+24 B3
   4  1  6.33554E+00 1.000E-02 6.219E+10 6.988E+22 d gly
   5  1  1.97968E+01 1.000E-02 5.788E+11 1.931E+25 d 11
   6  1  4.20234E+00 1.000E-02 5.084E+09 3.227E+18 d 12
   7  1  7.81804E+00 1.000E-02 4.473E+02 1.000E+08 d 22

ORMS ERROR = 1.82E-01  MAX ERROR = 1.55E-01 AT OBS.NO.  2
 RESIDUALS SQUARED = 6.63E-02
 RFACTOR =     0.8595 PERCENT

 NO. A   EXPT. DEL  CALC. DEL     RESIDUAL     % DEV   WEIGHT      Gly            H2PO4          pH
   1 1  9.1340E+00  9.0564E+00  7.763TE-02  8.4998E-01  1.0000E+00  1.0000E-03  5.0000E-04  0.0000E+00
   2 1  9.5340E+00  9.7195E+00 -1.854TE-01 -1.9453E+00  1.0000E+00  1.0000E-03  1.0000E-03  0.0000E+00
   3 1  9.8340E+00  9.8876E+00 -5.3463E-02 -5.4355E-01  1.0000E+00  1.0000E-03  1.5000E-03  0.0000E+00
   4 1  1.0010E+01  9.9699E+00  4.0140E-02  4.0100E-01  1.0000E+00  1.0000E-03  2.0000E-03  0.0000E+00
   5 1  1.0110E+01  1.0038E+01  7.1954E-02  7.1171E-01  1.0000E+00  1.0000E-03  2.5000E-03  0.0000E+00
   6 1  1.0190E+01  1.0102E+01  8.7746E-02  8.6110E-01  1.0000E+00  1.0000E-03  3.0000E-03  0.0000E+00
   7 1  1.0280E+01  1.0226E+01  5.4017E-02  5.2546E-01  1.0000E+00  1.0000E-03  4.0000E-03  0.0000E+00
   8 1  1.0340E+01  1.0347E+01 -6.5327E-03 -6.3179E-02  1.0000E+00  1.0000E-03  5.0000E-03  0.0000E+00
   9 1  1.0390E+01  1.0465E+01 -7.4802E-02 -7.1995E-01  1.0000E+00  1.0000E-03  6.0000E-03  0.0000E+00

 TOLERANCE ON SUM OF SQUARES    0.0100
 TOLERANCE ON EIGEN VALUES    0.0001
 CONVERGANCE AFTER    2  ITERATIONS
```

Figure **228**. Output file obtained for the data fitting to a 2:2 **[HαOBn][H_2PO_4]** complex.

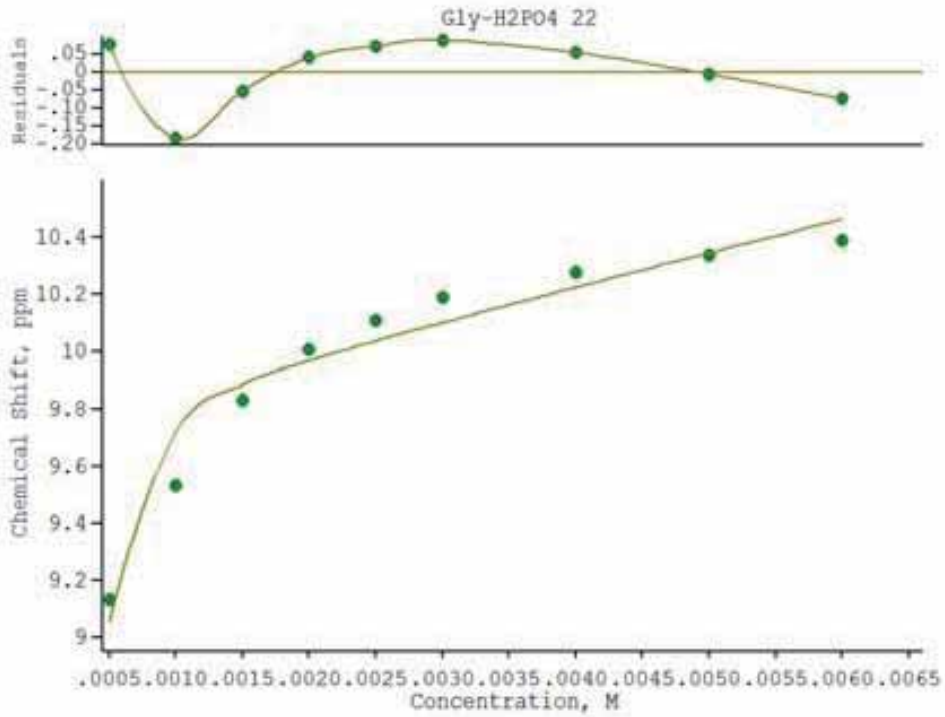

Figure **229**. *Fitplot* obtained for the data fitting to a 2:2 **[HαOBn][H_2PO_4]** complex.

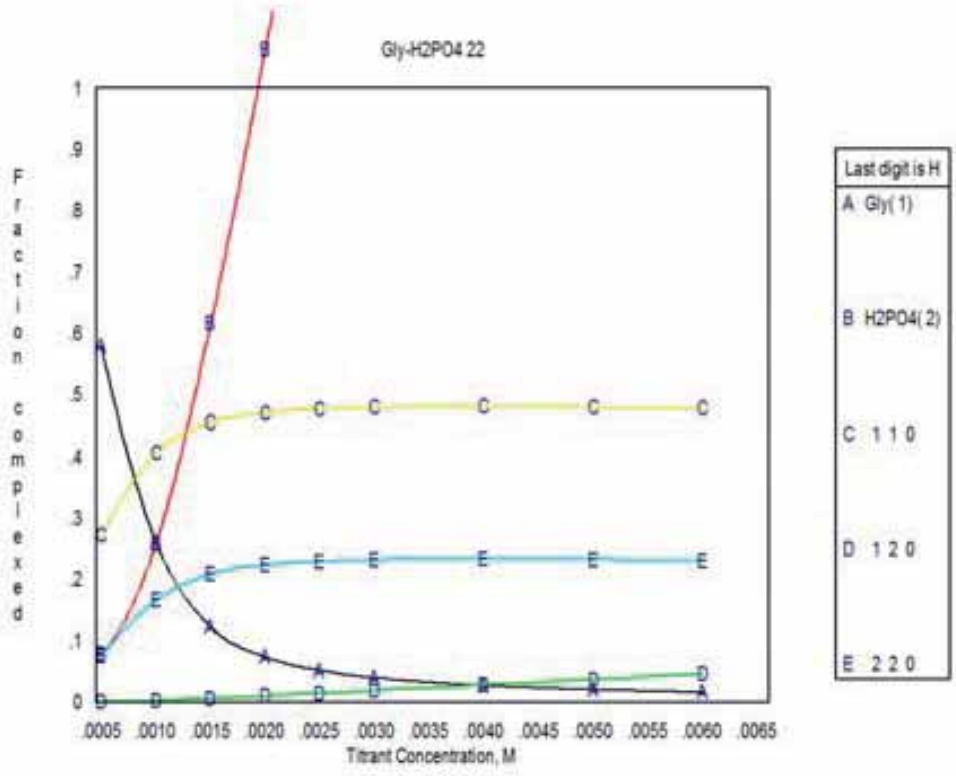

Figure **230**. *Concplot* obtained for the data fitting to a 2:2 **[HαOBn][H_2PO_4]** complex.

4.5.4.7. HαOBn-FTBA complex

TBAF

Spectra of 20 mM of TBAF in DMSO-d_6 99.8%. No bifluoride was observed, but on the ^{19}F-NMR spectra a 1:1:1 triplet appeared about -143.1 ppm. Deuterium bifluoride is suggested to be formed.

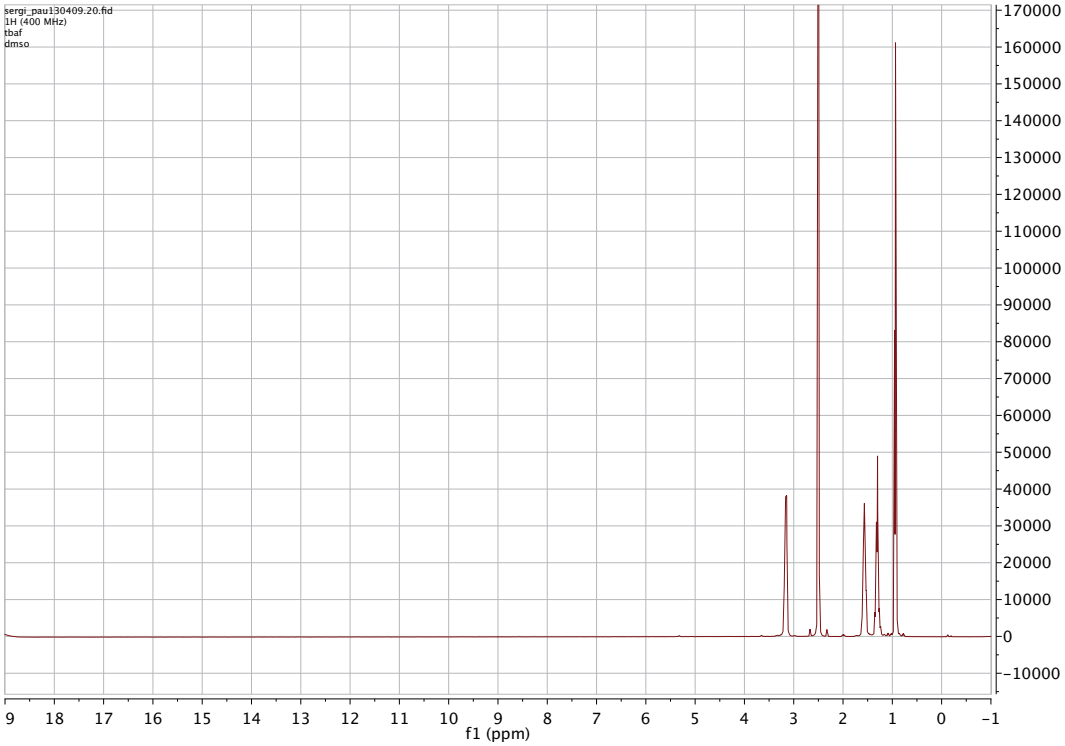

Figure **231**. ^{1}H-NMR spectrum of commercial TBAF hydrated. DMSO-d_6 (400 MHz).

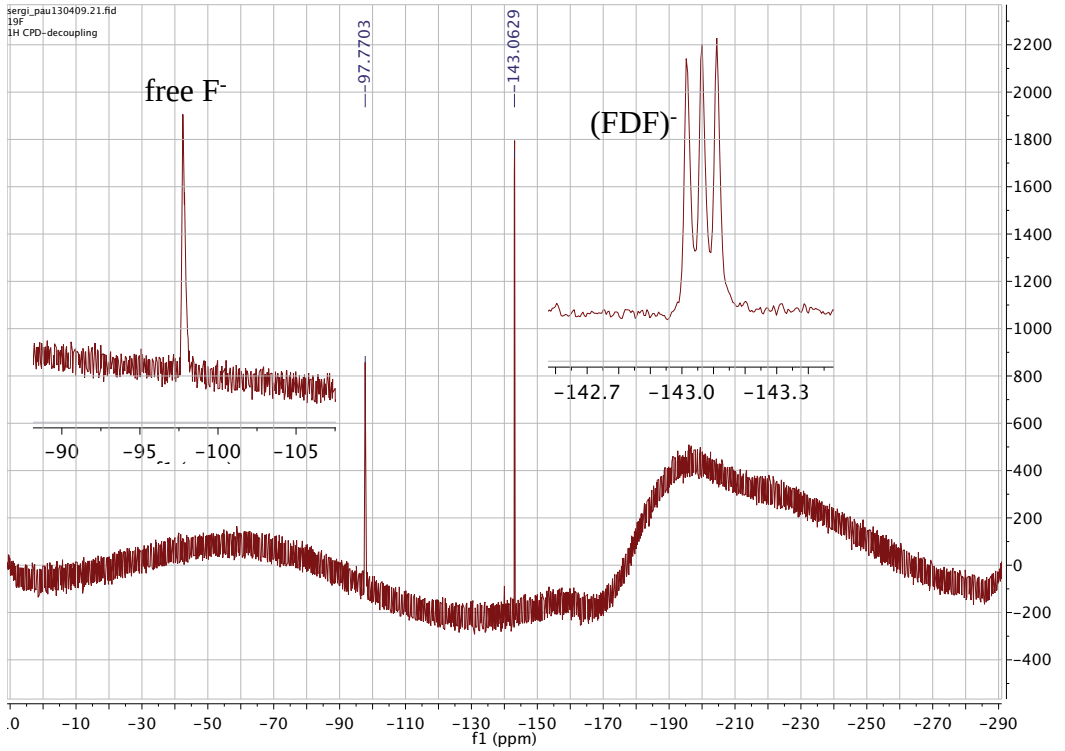

Figure **232**. ^{19}F-NMR H-decoupled spectrum of commercial TBAF hydrated. DMSO-d_6 (400 MHz).

DMSO-d_6 99.8%

Stoichiometry

Table **74** summarizes the calculated data to be represented as Job's plots.

Table **74**. ^{1}H-NMR data to determine stoichiometry of the complex **[HαOBn][F]** by Job's plot, represented using the data in light grey columns *vs*. X_{Guest}.

Tube	[Host]	δ H_4	Δδ H_4	Δδ H_4·[H]	δ H_7	Δδ H_7	Δδ H_7·[H]
1	2.0	3.944	0.000	0.000	5.135	0.000	0.000
2	1.8	3.937	0.007	0.013	5.131	0.004	0.007
3	1.6	3.926	0.018	0.029	5.127	0.008	0.013
4	1.4	3.916	0.028	0.039	5.122	0.013	0.018
5	1.2	3.904	0.040	0.048	5.116	0.019	0.023
6	1.0	3.888	0.056	0.056	5.109	0.026	0.026
7	0.8	3.864	0.080	0.064	5.099	0.036	0.029
8	0.6	3.835	0.109	0.065	5.086	0.049	0.029
9	0.4	3.801	0.143	0.057	5.072	0.063	0.025
10	0.2	3.796	0.148	0.030	5.070	0.065	0.013

Units:[Host] (mM); δ and Δδ (ppm); Δδ·[Host] (ppm·mM)

Association constant K_a

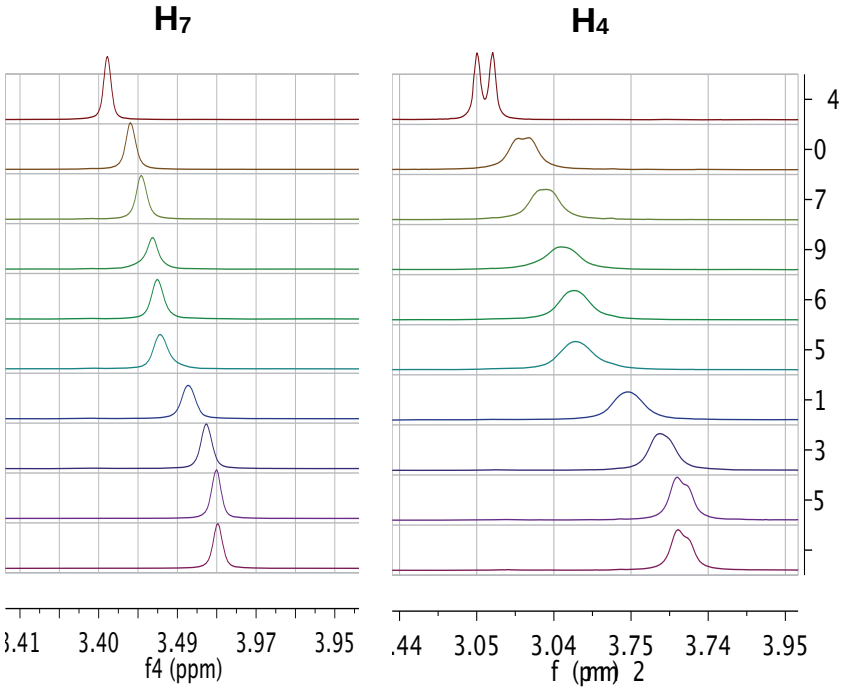

Figure **233**. Zoom of specific signals from the ^{1}H-NMR spectra of **HαOBn** Job's plot experiment. DMSO-d_6 (600 MHz).

Table **75**. Calculated data to determine K_a of the complex [**HαOBn][F]** in DMSO-d_6 by linear regression of the represented data in light grey columns.

Tube	[Guest] = Eq. Guest	1/[Guest]	δ H_4	Δδ H_4	1/ΔδH_4	δ H_7	Δδ H_7	1/ΔδH_7
1	0.0	--[a]	3.944	0.000	--[a]	5.135	0.000	--[a]
2	0.5	2.000	3.937	0.007	142.9	5.131	0.004	250.0
3	1.0	1.000	3.926	0.018	55.56	5.127	0.008	125.0
4	1.5	0.667	3.916	0.028	35.71	5.122	0.013	76.92
5	2.0	0.500	3.904	0.040	25.00	5.116	0.019	52.63
6	2.5	0.400	3.888	0.056	17.86	5.109	0.026	38.46
7	3.0	0.333	3.864	0.080	12.50	5.099	0.036	27.78
8	4.0	0.250	3.835	0.109	9.174	5.086	0.049	20.41
9	5.0	0.200	3.801	0.143	6.993	5.072	0.063	15.87
10	6.0	0.167	3.796	0.148	6.757	5.070	0.065	15.39

[a] When [Guest] = 0 no useful data can be calculated, so it is not represented on the graphic.
Units:[Guest] (mM); 1/[G] (mM^{-1}); Δδ (ppm); 1/Δδ (ppm^{-1})

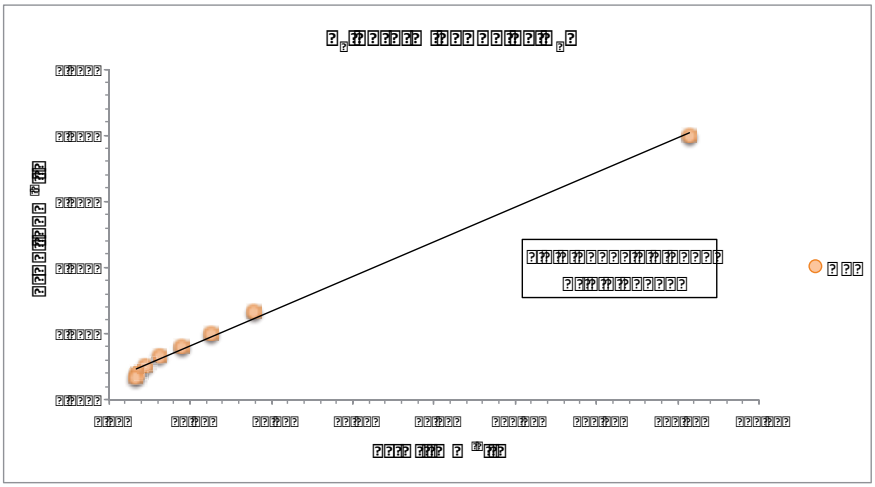

Figure **234**. Linear fitting of the data to determine the K_a of the **[HαOBn][F]** complex.

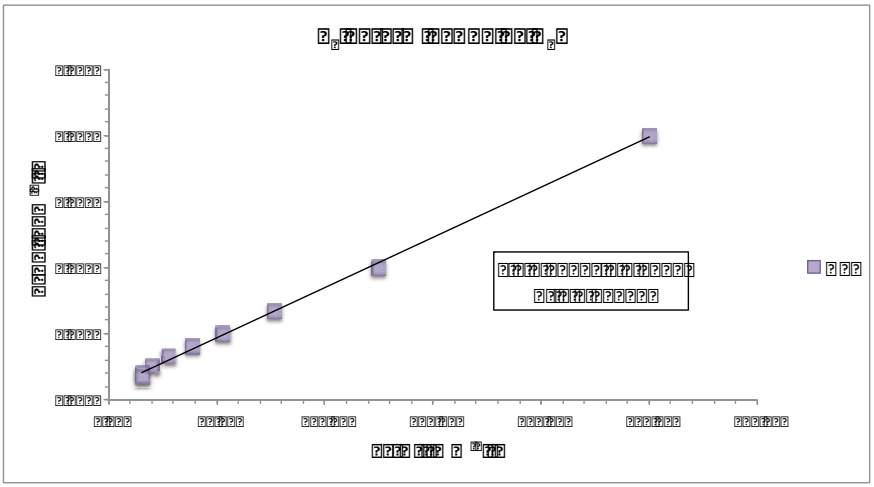

Figure **235**. Linear fitting of the data to determine the K_a of the **[HαOBn][F]** complex.

Table **76** summarizes the graphical results and calculated stability constants.

Table **76**. Thermodynamic parameters K_a and ΔG° determination for the **[HαOBn][F]** complex.

	Equation	Calculation	Results
H4	$K_a = \frac{A}{slope}$	$K_a = \frac{0.1432 ppm^{-1}}{0.0131 mM^{-1} \cdot ppm^{-1}}$	$K_a = 10.931 mM^{-1} = 10931 M^{-1}$ $\log K_a = 4.04$
	$\Delta G^\circ = -RT \ln K_a$	$\Delta G^o = -1.9 \frac{cal}{mol \cdot K} \cdot 298K \cdot \ln(10931 M^{-1})$	$\Delta G^o = -5265 \frac{cal}{mol} = -5.3 \frac{kcal}{mol}$
H7	$K_a = \frac{A}{slope}$	$K_a = \frac{0.0874 ppm^{-1}}{0.0076 mM^{-1} \cdot ppm^{-1}}$	$K_a = 11.5 mM^{-1} = 11500 M^{-1}$ $\log K_a = 4.06$
	$\Delta G^\circ = -RT \ln K_a$	$\Delta G^o = -1.9 \frac{cal}{mol \cdot K} \cdot 298K \cdot \ln(11500 M^{-1})$	$\Delta G^o = -5294 \frac{cal}{mol} = -5.3 \frac{kcal}{mol}$

DMSO-*d*$_6$ 99.8% + 10% H_2O

Stoichiometry

Table **77**. ^{1}H-NMR data to determine stoichiometry of the complex **[HαOBn][F]** with 10% of water by Job's plot, represented using the data in light grey columns *vs*. X_{Guest}.

Tube	[Host]	δ N-H$_3$	Δδ N-H$_3$	Δδ N-H$_3$·[H]	δ H$_1$	Δδ^a H$_1$	Δδ H$_1$·[H]
1	2.0	8.564	0.000	0.000	3.300	0.000	0.000
2	1.8	8.661	0.097	0.175	3.290	0.010	0.018
3	1.6	8.778	0.214	0.342	3.280	0.020	0.032
4	1.4	8.888	0.324	0.454	3.267	0.033	0.046
5	1.2	8.959	0.395	0.474	3.259	0.041	0.049
6	1.0	9.131	0.567	0.567	3.245	0.055	0.055
7	0.8	9.228	0.664	0.531	3.235	0.065	0.052
8	0.6	9.483	0.919	0.551	3.211	0.089	0.053
9	0.4	9.563	0.999	0.400	3.203	0.097	0.039
10	0.2	9.653	1.089	0.218	3.194	0.106	0.021

[a] Δδ is given as absolute value $|\Delta\delta|$
Units:[Host] (mM); δ and Δδ (ppm); Δδ·[Host] (ppm·mM)

Association constant K_a

Table **78**. Calculated data to determine K_a of the complex [**HαOBn][F]** in 10% water-containing DMSO-d_6 by linear regression of the represented data in light grey columns.

Tube	[Guest] = Eq. Guest	1/[Guest]	δ N-H$_3$	Δδ N-H$_3$	1/Δδ
1	0.0	--[a]	8.564	0.000	--[a]
2	0.5	2.000	8.593	0.029	34.483
3	1.0	1.000	8.623	0.059	16.949
4	1.5	0.667	8.654	0.090	11.111
5	2.0	0.500	8.686	0.122	8.197
6	2.5	0.400	8.705	0.141	7.092
7	3.0	0.333	8.743	0.179	5.587
8	4.0	0.250	8.764	0.200	5.000
9	5.0	0.200	8.857	0.293	3.413
10	6.0	0.167	8.863	0.299	3.344

[a] When [Guest] = 0 no useful data can be calculated, so it is not represented on the graphic.
Units:[Guest] (mM); 1/[G] (mM^{-1}); Δδ (ppm); 1/Δδ (ppm^{-1})

Linear regression of the data fitted very well taking all the points (Figure **236**).

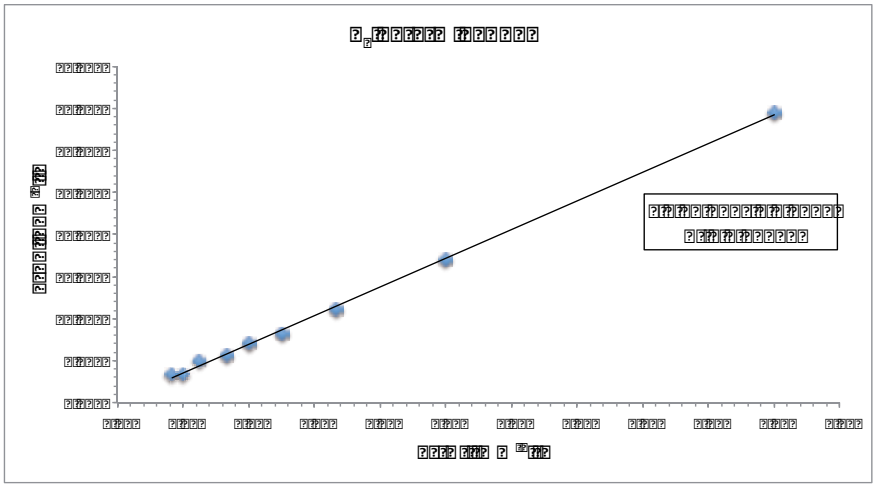

Figure **236**. Linear fitting of the data to determine the K_a of the **[HαOBn][F]** complex .

Table **79** summarizes the graphical results and calculated stability constant.

Table **79**. Thermodynamic parameters K_a and ΔG° determination for the **[HαOBn][F]** complex with 10% of water.

Equation	Calculation	Results
$K_a = \frac{A}{slope}$	$K_a = \frac{0.1261 ppm^{-1}}{17.047 mM^{-1}\cdot ppm^{-1}}$	$K_a = 0.00740 mM^{-1} = 7.4 M^{-1}$ $\log K_a = 0.87$
$\Delta G^{\circ} = -RT \ln K_a$	$\Delta G^{o} = -1.9 \frac{cal}{mol\cdot K} \cdot 298K \cdot \ln(7.4 M^{-1})$	$\Delta G^{o} = -1133 \frac{cal}{mol} = -1.1 \frac{kcal}{mol}$

MeCN-d_3

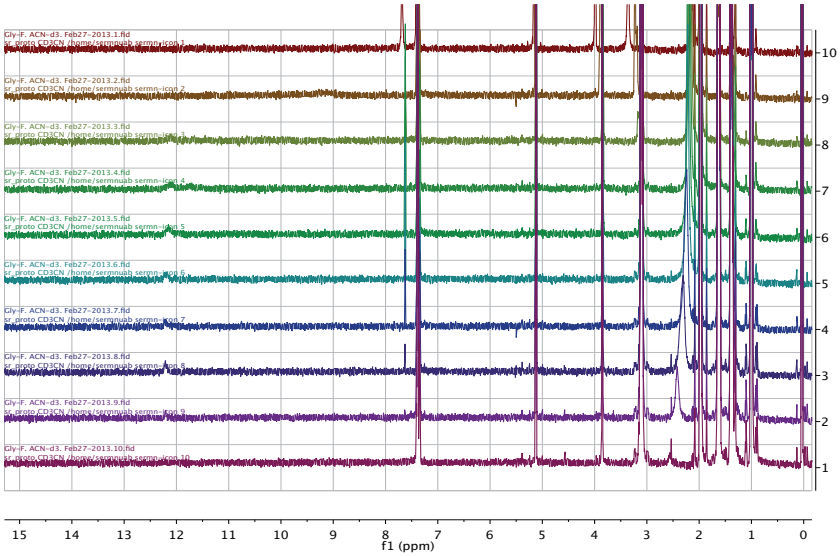

Figure **237**. ^{1}H-NMR spectra of **HαOBn** titration with **TBAF** to determine the K_a of the complex. From Eq. Guest = 0 (*top*) to Eq. Guest = 6 (*bottom*). MeCN-d_3 (600 MHz).

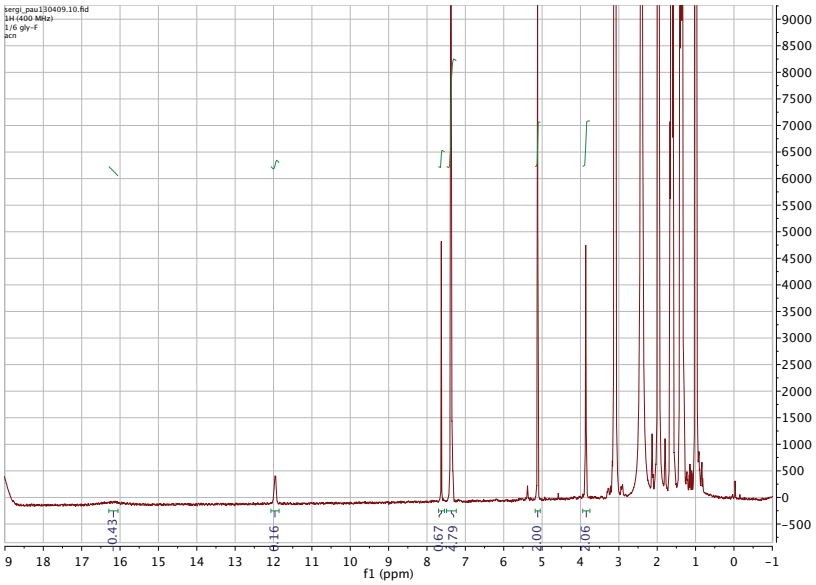

Figure **238**. ^{1}H-NMR spectrum of **HαOBn** titration with TBAF (6 eq.). MeCN-d_3 (400 MHz).

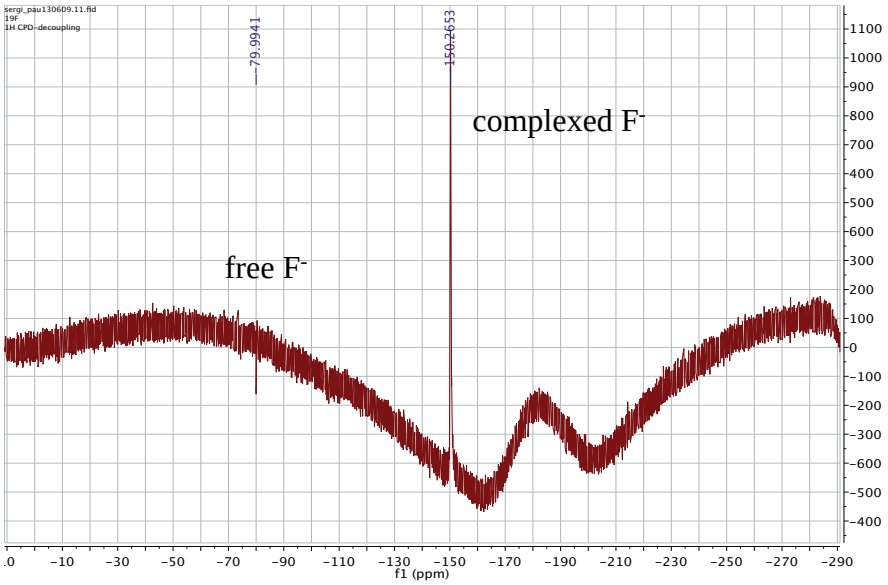

Figure **239**. ^{19}F-NMR H-decoupled spectrum of **HαOBn** titration with TBAF (6 eq.). MeCN-d_3 (400 MHz).

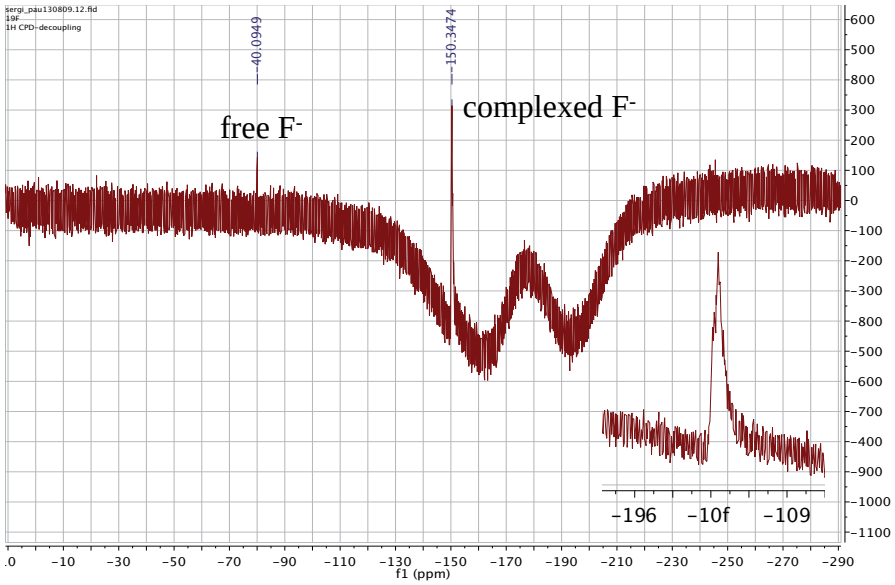

Figure **240**. ^{19}F-NMR H-coupled spectrum of **HαOBn** titration with TBAF (6 eq.). MeCN-d_3 (400 MHz).

Association constant K_a

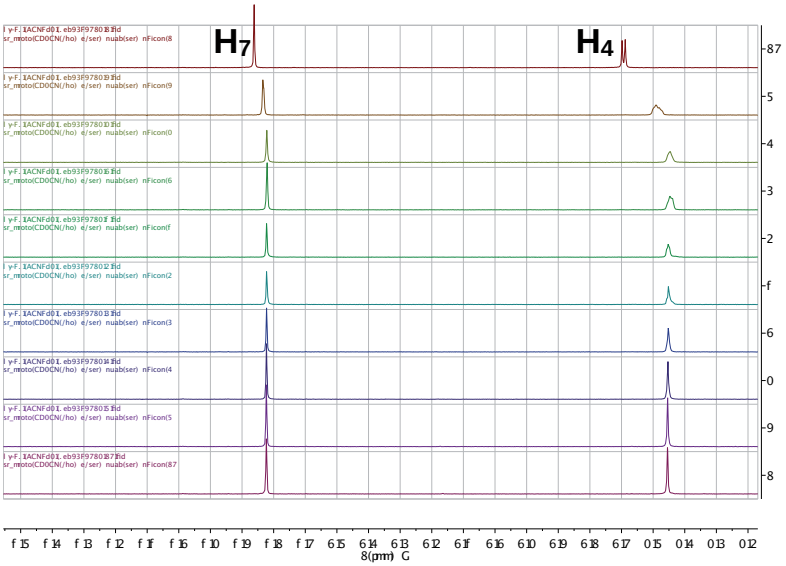

Figure **241**. Zoom of the H_4 and H_7 area from the ^{1}H-NMR spectra of **HαOBn** titration with **TBAF** to determine the K_a of the complex. From Eq. Guest = 0 (*top*) to Eq. Guest = 6 (*bottom*). MeCN-d_3 (600 MHz).

4.5.4.8. Statistics from WinEQNMR2 calculations of HαOBn-FTBA complexes

Table **80**. Statistics of the data fitting for the complexes formed by **HαOBn** host and fluoride anion.

		Anion sources and methods of determination of association constants[a] (*up*) and free energies[b] (*down*)		
HαOBn		**TBAF**		
		DMSO 99.8%/H_2O 0.2%	**DMSO 90%/H_2O 10%**	**MeCN**
		WinEQNMR2	**WinEQNMR2**	**Win EQNMR2**
1:1	**RSS[d] R factor**	$7.41 \cdot 10^{-5}$ 0.0562	$1.32 \cdot 10^{-3}$ 0.1390	$5.12 \cdot 10^{-6}$ 0.0147
1:1 1:2	**RSS[d] R factor**	$1.81 \cdot 10^{-5}$ 0.0278	$1.33 \cdot 10^{-3}$ 0.1391	$2.04 \cdot 10^{-6}$ 0.0093
1:1 2:1	**RSS[d] R factor**	$3.20 \cdot 10^{-5}$ 0.0369	$1.33 \cdot 10^{-3}$ 0.1394	$2.81 \cdot 10^{-6}$ 0.0109
1:1 1:2 1:3	**RSS[d] R factor**	$3.27 \cdot 10^{-5}$ 0.0374	--	--
1:1 1:2 2:2	**RSS[d] R factor**	$2.73 \cdot 10^{-5}$ 0.0341	--	$1.94 \cdot 10^{-5}$ 0.0286

[a] Logβ: β_{11} (M^{-1}), β_{12} and β_{21} (M^{-2}), β_{13} and β_{22} (M^{-3}). [b] Introduced guide values: TBAF DMSO 99.8%: $\log\beta_{11}$=1.88, $\log\beta_{12}$=4/5/7, $\log\beta_{13}$=7, $\log\beta_{21}$=$\log\beta_{22}$=7; TBAF DMSO 90%: $\log\beta_{11}$=0.86/1, $\log\beta_{12}$=2, $\log\beta_{21}$=3. [c] Units: kcal·mol^{-1}. [d] RSS: Residual Sum of Squares.

4.5.5. HβOBn-H_2PO_4TBA complex

Self-aggregation

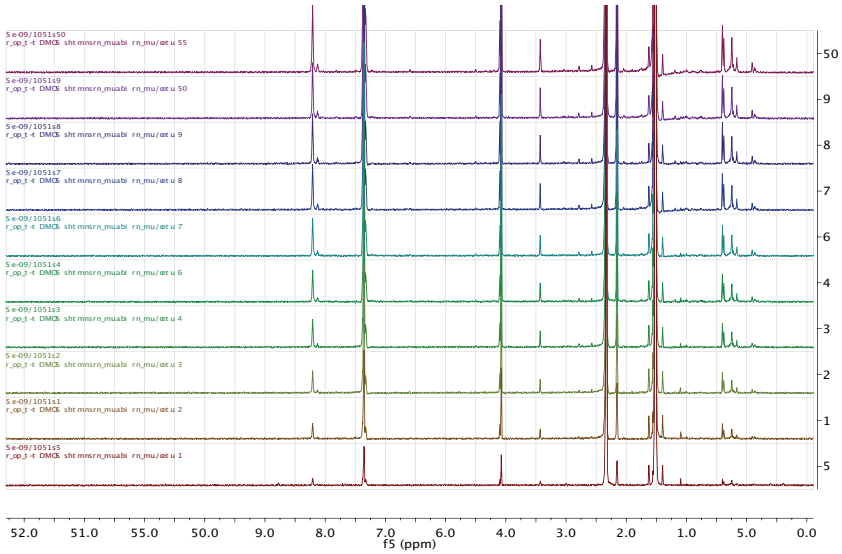

Figure **242**. ^{1}H-NMR spectra of the self-aggregation experiment for **HβOBn** receptor from [Host] = 4 mM (*top*) to [Host] = 0.2 mM (*bottom*). DMSO-d_6 (600 MHz).

Stoichiometry

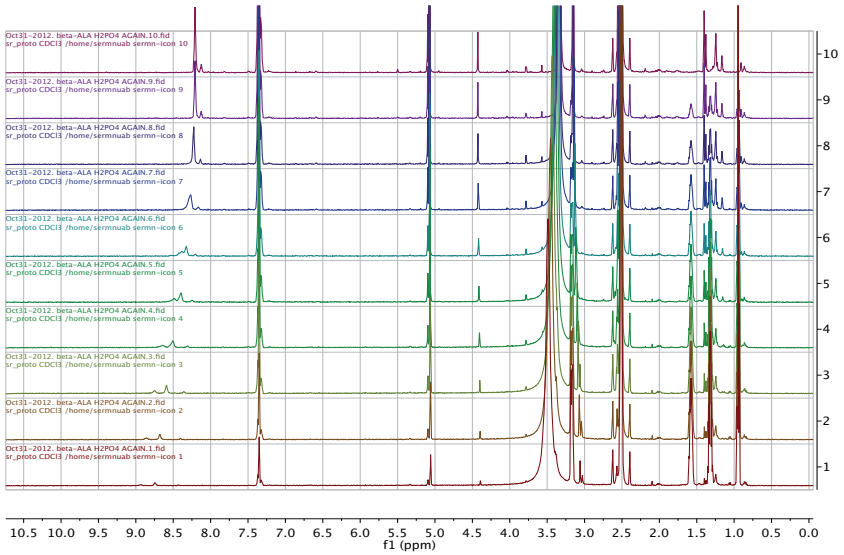

Figure **243**. ^{1}H-NMR spectra of **HβOBn** titration with **TBAH$_2$PO$_4$** to determine the stoichiometry of the complex. From X_{Host} = 1 (*top*) to X_{Host} = 0 (*bottom*) in ΔX = 0.1. DMSO-d_6 (600 MHz).

The NH area of the spectra in DMSO is zoomed in Figure **244**, where three signals can be distinguished showing different patterns of shielding upon the addition of dihydrogenphosphate anion.

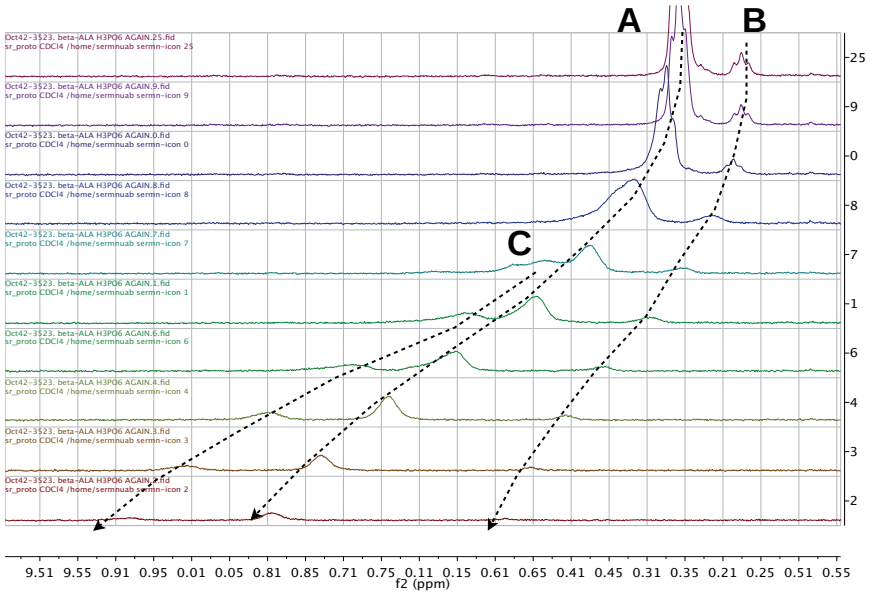

Figure **244**. Zoom of N-H$_3$ area from the ^{1}H-NMR spectra of **HβOBn** titration with **TBAH$_2$PO$_4$** to determine the stoichiometry of the complex. Dashed arrows indicate the shielding direction of NH signals of the three conformers. From X_{Host} = 1 (*top*) to X_{Host} = 0 (*bottom*) in ΔX = 0.1. DMSO-d_6 (600 MHz).

The presence of different conformations of the host and the formation of three different complexes were suspected so, in order to find out the origin of the minor signal, a variable temperature experiment was performed to discern between their nature (Figure **245**).

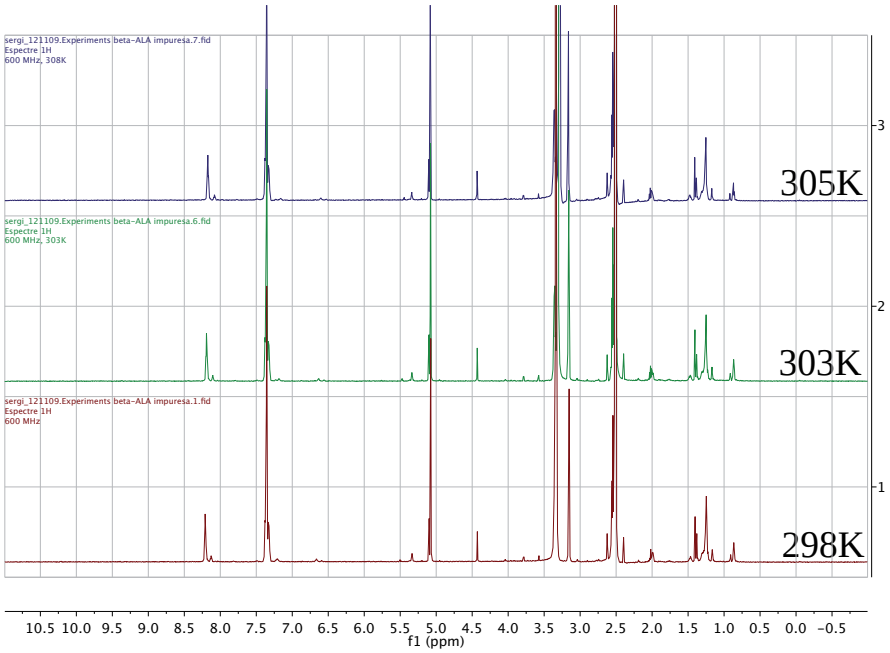

Figure **245**. ^{1}H-NMR spectra of variable temperature experiment of a 1mM sample of **HβOBn** host. DMSO-d_6 (600 MHz).

Variable temperature would make the three signals to collapse in case they were minor conformers but this behaviour was not observed, in fact, both NH signals separated one with respect to the other (Figure **246**). In addition, selective NOESY experiment did not exhibit any correlation between the minor signals and other signals corresponding to the host.

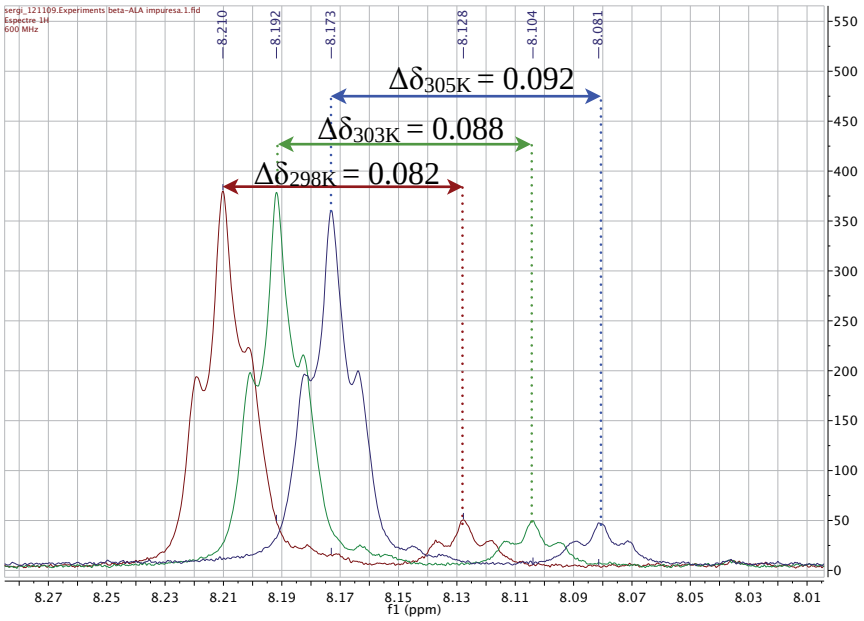

Figure **246**. Zoom of N-H$_3$ area from the ^{1}H-NMR spectra of variable temperature experiment of a 1mM sample of **HβOBn** host. DMSO-d_6 (600 MHz).

Table **81** shows data for the Job's plots of N-H_3.

Table **81**. ^{1}H-NMR data to determine stoichiometry of the complex **[HβOBn][H_2PO_4]** according to the major N-H_3 signal. Job's plot is represented using the data in light grey columns *vs.* X_{Guest}.

Tube	δ NH_A	Δδ NH_A	Δδ NH_A·[H]	δ NH_B	Δδ NH_B	Δδ NH_B·[H]
1	8.208	0.000	0.000	8.208	0.000	0.000
2	8.209	0.001	0.002	8.209	0.001	0.002
3	8.224	0.016	0.026	8.224	0.016	0.026
4	8.267	0.059	0.083	8.267	0.059	0.083
5	8.326	0.118	0.142	8.326	0.118	0.142
6	8.394	0.186	0.186	8.394	0.186	0.186
7	8.501	0.293	0.234	8.501	0.293	0.234
8	8.590	0.382	0.229	8.590	0.382	0.229
9	8.677	0.469	0.188	8.677	0.469	0.188
10	8.743	0.535	0.107	8.743	0.535	0.107

Units:[Host] (mM); δ and Δδ (ppm); Δδ·[Host] (ppm·mM)

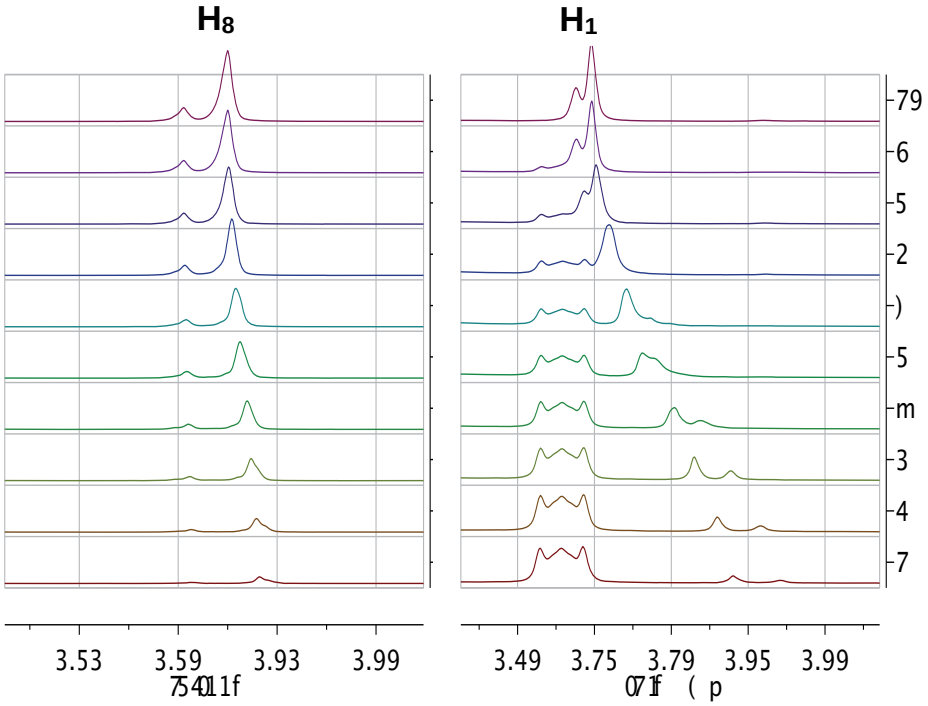

Figure **247**. Zoom of specific signals from the ^{1}H-NMR spectra of **HβOBn** Job's plot experiment. DMSO-d_6 (600 MHz).

Table **82** and Table **83** show data for the Job's plots of H_1 and H_8.

Table **82**. ^{1}H-NMR data to determine stoichiometry of the complex **[HβOBn][H_2PO_4]** by Job's plot, represented using the data in light grey columns *vs*. X_{Guest}.

Tube	[Host]	δ H_{1A}	Δδ[a] H_{1A}	Δδ H_{1A}·[H]	δ H_{1B}	Δδ[a] H_{1B}	Δδ H_{1B}·[H]
1	2.0	3.153	0.000	0.000	3.152	0.000	0.000
2	1.8	3.153	0.000	0.000	3.152	0.000	0.000
3	1.6	3.152	0.001	0.002	3.149	0.003	0.005
4	1.4	3.148	0.005	0.007	3.140	0.012	0.017
5	1.2	3.141	0.012	0.014	3.129	0.023	0.028
6	1.0	3.130	0.023	0.023	3.119	0.033	0.033
7	0.8	3.116	0.037	0.030	3.098	0.054	0.043
8	0.6	3.098	0.055	0.033	3.085	0.067	0.040
9	0.4	3.084	0.069	0.028	3.070	0.082	0.033
10	0.2	3.087	0.066	0.013	3.060	0.092	0.018

[a] Δδ is given as absolute value |Δδ|
Units:[Host] (mM); δ and Δδ (ppm); Δδ·[Host] (ppm·mM)

Table **83**. ^{1}H-NMR data to determine stoichiometry of the complex **[HβOBn][H_2PO_4]** by Job's plot, represented using the data in light grey columns *vs*. X_{Guest}.

Tube	[Host]	δ H_{8A}	Δδ[a] H_{8A}	Δδ H_{8A}·[H]	δ H_{8B}	Δδ[a] H_{8B}	Δδ H_{8B}·[H]
1	2.0	5.076	0.000	0.000	5.075	0.000	0.000
2	1.8	5.076	0.000	0.000	5.075	0.000	0.000
3	1.6	5.076	0.000	0.000	5.074	0.001	0.002
4	1.4	5.075	0.001	0.001	5.073	0.002	0.003
5	1.2	5.073	0.003	0.004	5.071	0.004	0.005
6	1.0	5.072	0.004	0.004	5.069	0.006	0.006
7	0.8	5.069	0.007	0.006	5.065	0.010	0.008
8	0.6	5.066	0.010	0.006	5.063	0.012	0.007
9	0.4	5.063	0.013	0.005	5.060	0.015	0.006
10	0.2	5.063	0.013	0.003	5.059	0.016	0.003

[a] Δδ is given as absolute value |Δδ|
Units:[Host] (mM); δ and Δδ (ppm); Δδ·[Host] (ppm·mM)

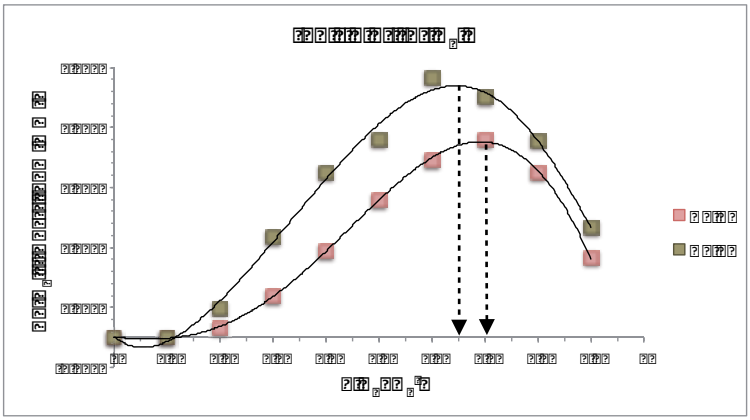

Figure **248**. Job's plot for **[HβOBn][H_2PO_4]** complex. *A* and *B* represent both repetitions of the experiment.

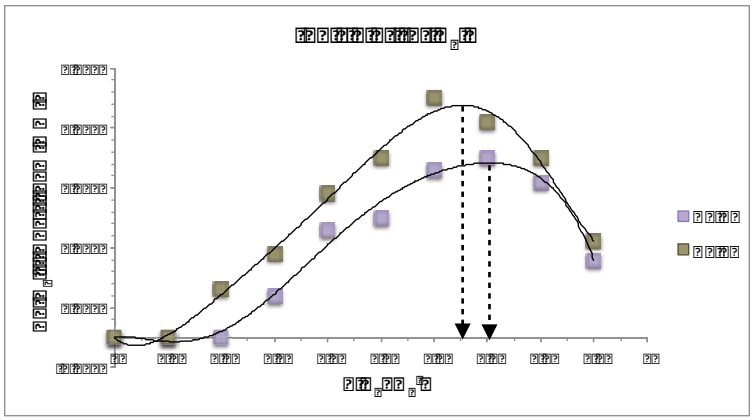

Figure **249**. Job's plot for **[HβOBn][H_2PO_4]** complex. *A* and *B* represent both repetitions of the experiment.

Association constant K_a

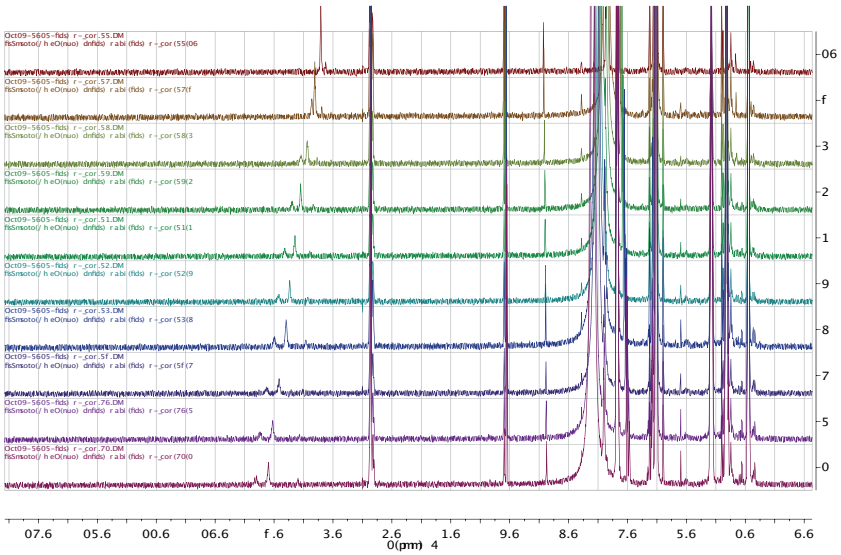

Figure **250**. ^{1}H-NMR spectra of **HβOBn** titration with **TBAH_2PO_4** to determine the K_a of the complex. From Eq. Guest = 0 (*top*) to Eq. Guest = 6 (*bottom*). DMSO-d_6 (600 MHz).

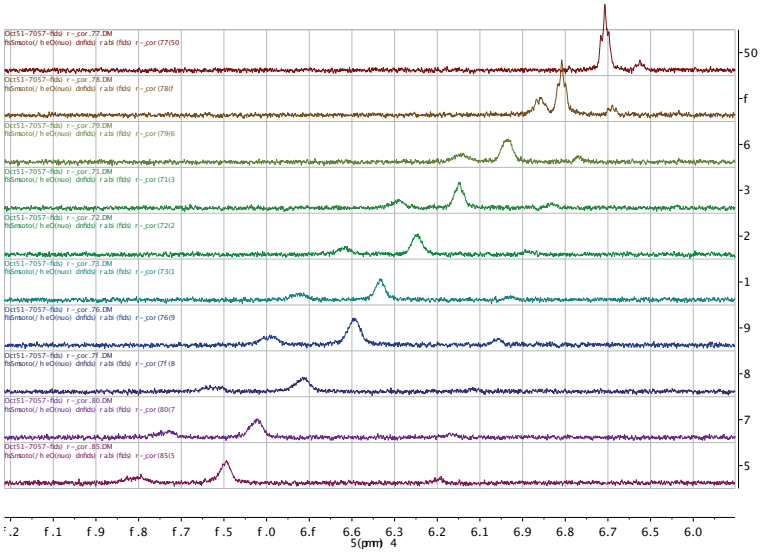

Figure **251**. Zoom of the N-H$_3$ area from the ^{1}H-NMR spectra of **HβOBn** titration with **TBAH$_2$PO$_4$** to determine the K$_a$ of the complex. From Eq. Guest = 0 (*top*) to Eq. Guest = 6 (*bottom*). DMSO-d_6 (600 MHz).

Table **84**. Calculated data to determine K$_a$ of the complex [**HβOBn][H$_2$PO$_4$]** in DMSO-d_6 by linear regression of the represented data in light grey columns.

Tube	[Guest] = Eq. Guest	1/[Guest]	δ N-H$_3$	Δδ N-H$_3$	1/Δδ
1	0.0	--[a]	8.207	0.000	--[a]
2	0.5	2.000	8.308	0.101	9.901
3	1.0	1.000	8.434	0.227	4.405
4	1.5	0.667	8.546	0.339	2.950
5	2.0	0.500	8.645	0.438	2.283
6	2.5	0.400	8.730	0.523	1.912
7	3.0	0.333	8.795	0.588	1.701
8	4.0	0.250	8.912	0.705	1.418
9	5.0	0.200	9.024	0.817	1.224
10	6.0	0.167	9.094	0.887	1.127

[a] When [Guest] = 0 no useful data can be calculated, so it is not represented on the graphic.
Units:[Guest] (mM); 1/[G] (mM^{-1}); Δδ (ppm); 1/Δδ (ppm^{-1})

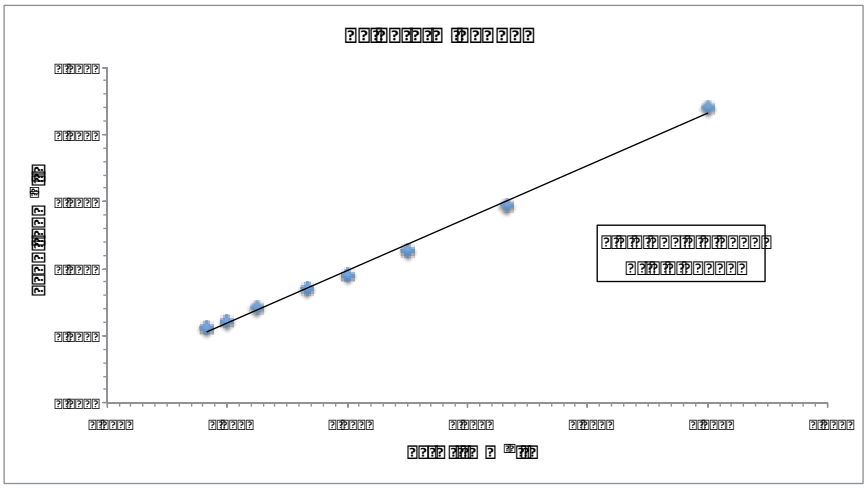

Figure **252**. Linear fitting of the data to determine the K_a of the **[HβOBn][H_2PO_4]** complex.

Table **85** summarizes the graphical results and calculated stability constant.

Table **85**. Thermodynamic parameters K_a and ΔG^o determination for the **[HβOBn][H_2PO_4]** complex.

Equation	Calculation	Results
$K_a = \frac{A}{slope}$	$K_a = \frac{0.4088 ppm^{-1}}{3.91 mM \cdot ppm^{-1}}$	$K_a = 0.1045 mM^{-1} = 105 M^{-1}$ $\log K_a = 2.02$
$\Delta G^\circ = -RT \ln K_a$	$\Delta G^o = -1.9 \frac{cal}{K \cdot mol} \cdot 298 K \cdot \ln(105 M^{-1})$	$\Delta G^o = -2633 \frac{cal}{mol} = -2.6 \frac{kcal}{mol}$

WinEQNMR2 program calculations

The statistics information through which the data fitting is considered to be good for a system is summarized in Table **90**, together with the statistics of **HγOBn** receptor.

4.5.6. HγOBn-H_2PO_4TBA complex

Self-aggregation

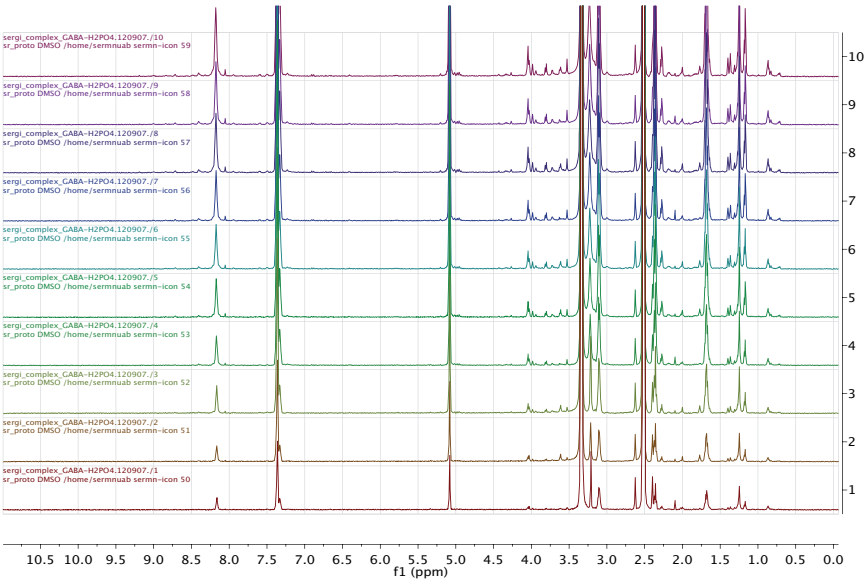

Figure **253**. ^{1}H-NMR spectra of the self-aggregation experiment for **HγOBn** receptor from [Host] = 4 mM (*top*) to [Host] = 0.2 mM (*bottom*). DMSO-d_6 (600 MHz).

Stoichiometry

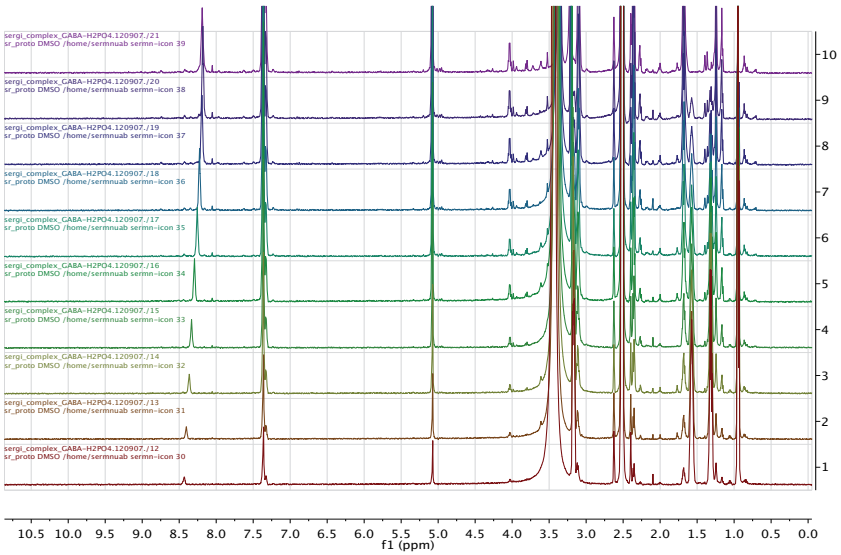

Figure **254**. ^{1}H-NMR spectra of **HγOBn** titration with **$TBAH_2PO_4$** to determine the stoichiometry of the complex. From X_{Host} = 1 (*top*) to X_{Host} = 0 (*bottom*) in ΔX = 0.1. DMSO-d_6 (600 MHz).

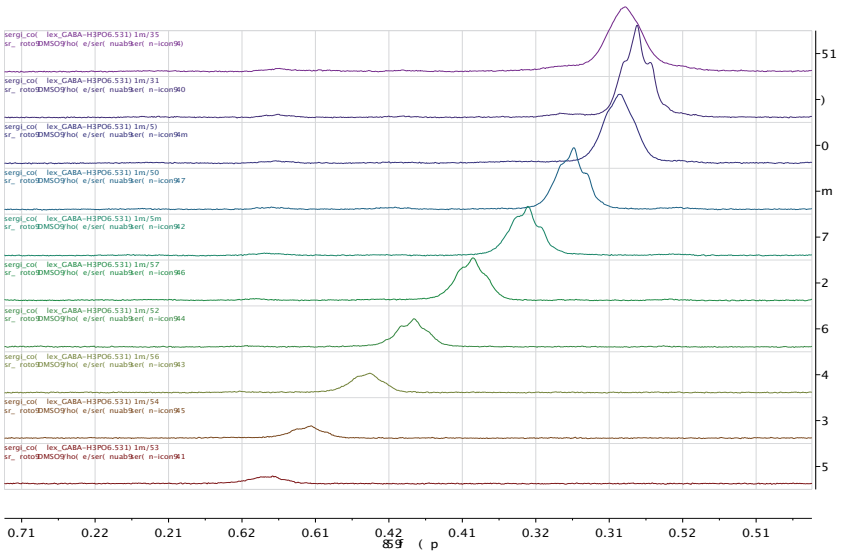

Figure **255**. Zoom of N-H_3 area from the ^{1}H-NMR spectra of **HγOBn** titration with **$TBAH_2PO_4$** to determine the stoichiometry of the complex. From X_{Host} = 1 (*top*) to X_{Host} = 0 (*bottom*) in ΔX = 0.1. DMSO-d_6 (600 MHz).

Table **86**. ^{1}H-NMR data to determine stoichiometry of the complex **[HγOBn][H_2PO_4]** according to the N-H_3 signal. Job's plots are represented using the data in light grey columns *vs*. X_{Guest}.

Tube	δ NH_A	Δδ NH_A	Δδ NH_A·[H]	δ NH_B	Δδ NH_B	Δδ NH_B·[H]
1	8.189	0	0.000	8.190	0.000	0.000
2	8.181	-0.008	-0.014	8.188	-0.002	-0.004
3	8.193	0.004	0.006	8.193	0.003	0.005
4	8.224	0.035	0.049	8.227	0.037	0.059
5	8.255	0.066	0.079	8.257	0.067	0.094
6	8.293	0.104	0.104	8.294	0.104	0.125
7	8.333	0.144	0.115	8.336	0.146	0.146
8	8.363	0.174	0.104	8.385	0.195	0.156
9	8.403	0.214	0.086	8.411	0.221	0.133
10	8.432	0.243	0.049	8.428	0.238	0.095

Units:[Host] (mM); δ and Δδ (ppm); Δδ·[Host] (ppm·mM)

Table **87**. ^{1}H-NMR data to determine stoichiometry of the complex **[HγOBn][H_2PO_4]** according to the H_1 signal. Job's plots are represented using the data in light grey columns.

Tube	[Host]	X_{Guest}	δ H_1	Δδ[a] H_1	Δδ H_1·[H]
1	2.0	0.0	3.300	0.000	0.000
2	1.8	0.1	3.290	0.010	0.018
3	1.6	0.2	3.280	0.020	0.032
4	1.4	0.3	3.267	0.033	0.046
5	1.2	0.4	3.259	0.041	0.049
6	1.0	0.5	3.245	0.055	0.055
7	0.8	0.6	3.235	0.065	0.052
8	0.6	0.7	3.211	0.089	0.053
9	0.4	0.8	3.203	0.097	0.039
10	0.2	0.9	3.194	0.106	0.021

[a] Δδ is given as absolute value |Δδ|
Units:[Host] (mM); δ and Δδ (ppm); Δδ·[Host] (ppm·mM)

Association constant K_a

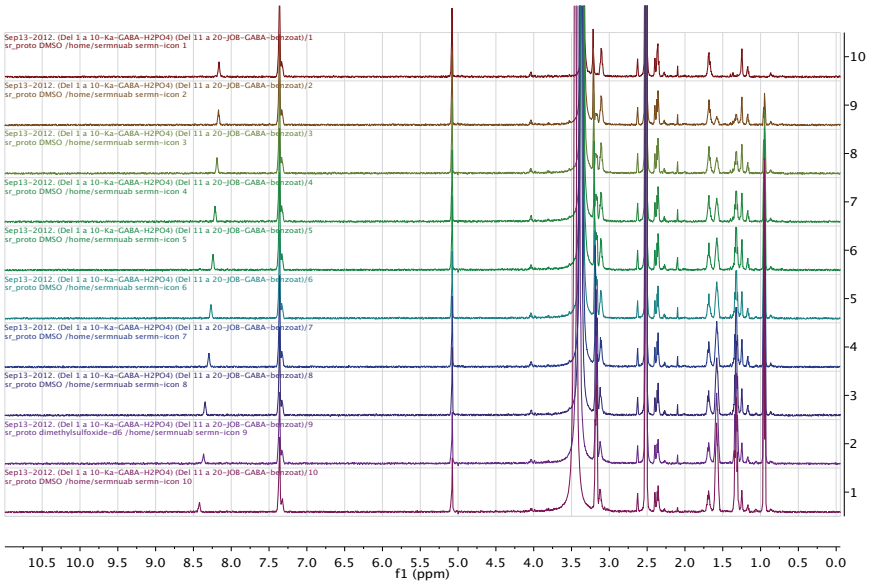

Figure **256**. ^{1}H-NMR spectra of **HγOBn** titration with **TBAH$_2$PO$_4$** to determine the K_a of the complex. From Eq. Guest = 0 (*top*) to Eq. Guest = 6 (*bottom*). DMSO-d_6 (600 MHz).

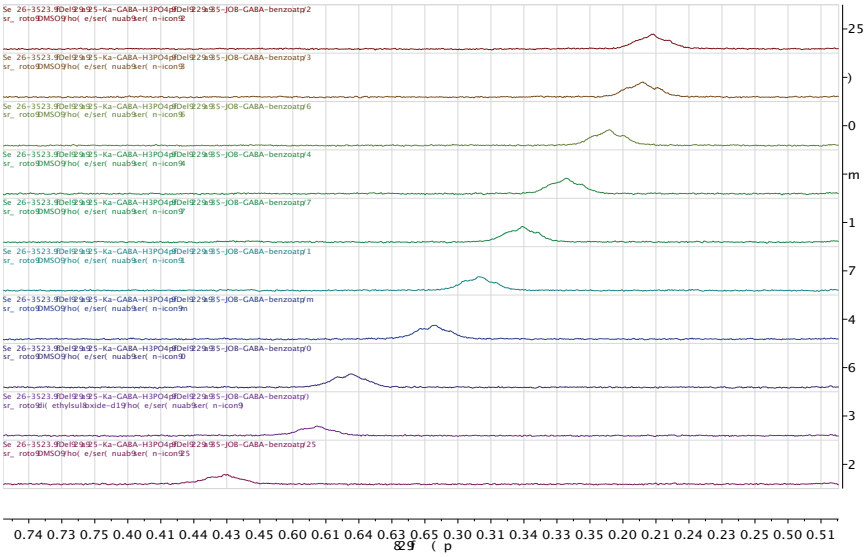

Figure **257**. Zoom of the N-H$_3$ area from the ^{1}H-NMR spectra of **HγOBn** titration with **TBAH$_2$PO$_4$** to determine the K_a of the complex. From Eq. Guest = 0 (*top*) to Eq. Guest = 6 (*bottom*). DMSO-d_6 (600 MHz).

Table **88**. Calculated data to determine K_a of the complex **[HγOBn][H₂PO₄]** in DMSO-d_6 by linear regression of the represented data in light grey columns.

Tube	[Guest] = Eq. Guest	1/[Guest]	δ N-H₃	Δδ N-H₃	1/Δδ
1	0.0	--[a]	8.162	0	--[a]
2	0.5	4.000	8.168	0.006	166.7
3	1.0	2.000	8.188	0.026	38.46
4	1.5	1.333	8.214	0.052	19.23
5	2.0	1.000	8.241	0.079	12.66
6	2.5	0.800	8.268	0.106	9.434
7	3.0	0.667	8.294	0.132	7.576
8	4.0	0.500	8.344	0.182	5.495
9	5.0	0.400	8.365	0.203	4.926
10	6.0	0.333	8.42	0.258	3.876

[a] When [Guest] = 0 no useful data can be calculated, so it is not represented on the graphic.
Units:[Guest] (mM); 1/[G] (mM^{-1}); Δδ (ppm); 1/Δδ (ppm^{-1})

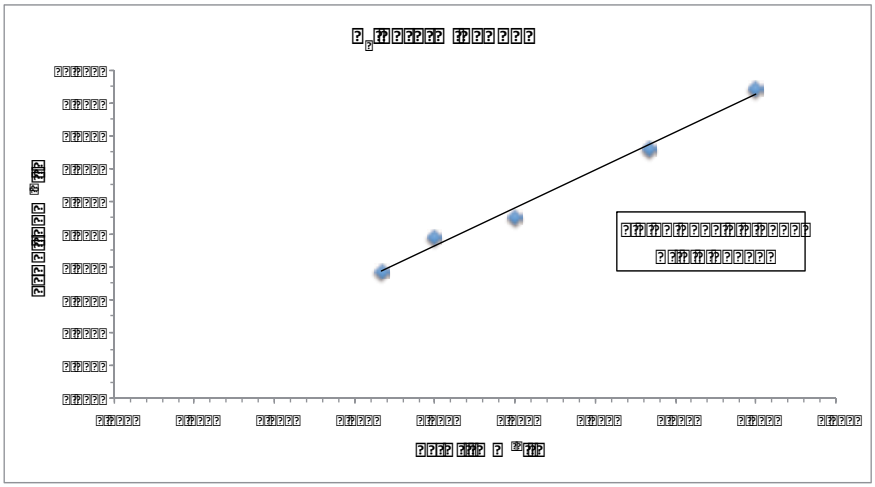

Figure **258**. Linear fitting of the data to determine the K_a of the **[HγOBn][H₂PO₄]** complex.

Table **89** summarizes the graphical results and and calculated stability constant, which was further used for the computational calculation with WinEQNMR2 program.

Table **89**. Thermodynamic parameters K_a and ΔG^o determination for the **[HγOBn][H₂PO₄]** complex.

Equation	Calculation	Results
$K_a = \frac{A}{slope}$	$K_a = \frac{0.0327 ppm^{-1}}{11.534 mM \cdot ppm^{-1}}$	$K_a = 0.00284 mM^{-1} = 2.8 M^{-1}$ $\log K_a = 0.45$
$\Delta G^\circ = -RT \ln K_a$	$\Delta G^o = -1.9 \frac{cal}{K \cdot mol} \cdot 298 K \cdot \ln(2.8 M^{-1})$	$\Delta G^o = -583 \frac{cal}{mol} = -0.6 \frac{kcal}{mol}$

4.5.7. Statistics from WinEQNMR2 calculations of Hβ- and Hγ-H_2PO_4TBA complexes

The statistics by which the data is considered or not to fit good a system is summarized in Table **90**.

Table **90**. Statistics of the data fitting for the complexes formed by **HβOBn** and **HγOBn** hosts and dihydrogenphosphate anion in DMSO-d_6..

		Anion sources and methods of determination of association constants[a] (*up*) and free energies[b] (*down*)	
		$TBAH_2PO_4$	
		HβOBn	**HγOBn**
		WinEQNMR2	**WinEQNMR2**
1:1	**RSS[d]** **R factor**	$1.64 \cdot 10^{-4}$ 0.0490	$2.90 \cdot 10^{-4}$ 0.0686
1:1 **1:2**	**RSS[d]** **R factor**	$1.64 \cdot 10^{-4}$ 0.0490	$2.86 \cdot 10^{-4}$ 0.0681
1:1 **2:1**	**RSS[d]** **R factor**	$2.05 \cdot 10^{-4}$ 0.0547	$2.96 \cdot 10^{-4}$ 0.0693
1:1 **1:2** **2:2**	**RSS[d]** **R factor**	$2.60 \cdot 10^{-4}$ 0.0616	$2.92 \cdot 10^{-4}$ 0.0688

[a] Logβ: β_{11} (M^{-1}), β_{12} and β_{21} (M^{-2}), β_{22} (M^{-3}). [b] Introduced guide values: **HβOBn**: $\log\beta_{11}=1/2$, $\log\beta_{12}=2$, $\log\beta_{21}=3$, $\log\beta_{22}=5$; **HγOBn**: $\log\beta_{11}=1/2$, $\log\beta_{12}=\log\beta_{12}=3$, $\log\beta_{22}=5$. [c] Units: kcal·mol^{-1}. [d] RSS: Residual Sum of Squares.

4.5.8. HγCbuOBn-FTBA complex

Self-aggregation

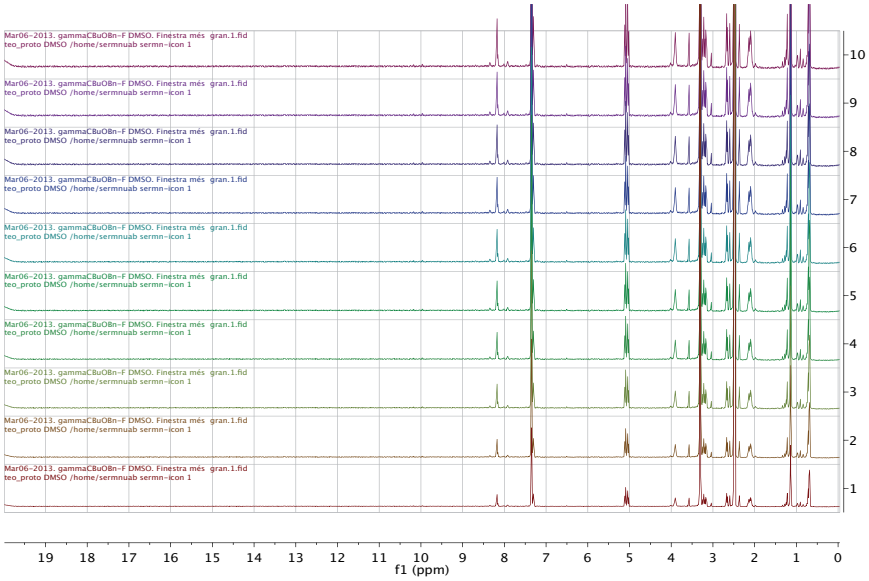

Figure **259**. ^{1}H-NMR spectra of the self-aggregation experiment for **HγCbuOBn** receptor from [Host] = 4 mM (*top*) to [Host] = 0.2 mM (*bottom*). DMSO-d_6 (600 MHz).

WinEQNMR2 program calculations

Table **91**. Statistics of the data fitting for the four complexes formed by **HγCbuOBn** host in DMSO-d_6.

		Anion sources and methods of determination of association constants[a,b] (*up*) and free energies[c] (*down*)
HγCbuOBn		**TBAF**
		WinEQNMR2
1:1	**RSS[d]** **R factor**	$1.40 \cdot 10^{-3}$ 0.4813
1:1 **1:2**	**RSS** **R factor**	$1.56 \cdot 10^{-6}$ 0.0083
1:1 **2:1**	**RSS** **R factor**	$9.16 \cdot 10^{-5}$ 0.0636
1:1 **1:2** **2:2**	**RSS** **R factor**	$2.53 \cdot 10^{-5}$ 0.0334

[a] Logβ: β_{11} (M^{-1}), β_{12} and β_{21} (M^{-2}), β_{22} (M^{-3}). [b] Introduced guide values: $\log\beta_{11}$=2/4/8, $\log\beta_{12}$=5/10, $\log\beta_{21}$=10, $\log\beta_{22}$=9. [c] Units: kcal·mol^{-1}. [d] RSS: Residual Sum of Squares.

BIBLIOGRAPHY ANNEXES

A1. Öztürk, G.; Çolak, M.; Togrul, M. *J. Incl. Phenom. Macrocyclic Chem.* **2010**, *68*, 49-54.

A2. *Binding constants, the measurement of molecular complex stability*. K. A. Connors. 1987. John Wiley & Sons, USA.

A3. Hynes, M. J.; *J. Chem. Soc. Dalton Trans.* **1993**, 311-312.

A4. Job, P. *Ann. Chim. Appl.* **1928**, *9*, 113-203.

A5. Arunachalam, M.; Ghosh, P. *Inorg. Chem.* **2010**, *49*, 943-951.

A6. Caldeira, M. M.; Ramos, M. L.; Gil, V. M. *Can. J. Chem.* **1987**, *65*, 827-832.

A7. *Encyclopedia of Supramolecular Chemistry*, J. L. Atwood, J. W. Steed. 2004. Marcel Dekker, Inc., USA.

A8. Brough, P.; Klumpp, C. *J. Org. Chem.* **2006**, *71*, 2014-2020.